Technical Report Documentation Page

1. Report No. FHWA/TX-16/0-6869-1	2. Government Accession No.	3. Recipient's Catalog No.
4. Title and Subtitle ADVANCING INNOVATIVE HIGH-SPEED REMOTE-SENSING HIGHWAY INFRASTRUCTURE ASSESSMENT USING EMERGING TECHNOLOGIES: TECHNICAL REPORT		5. Report Date February 2017 6. Performing Organization Code
7. Author(s) Paul Carlson, Beverly Storey, Mo Poorsartep, Charles Stevens, Ben Ettelman, Tomas Lindheimer, Maryam Dastgiri, Adel Khodakarami, Jeff Miles, Dezhen Song, Robert Lytton, Xue Luo, Yong Deng, Fan Gu, and Stefan Hurlebaus		8. Performing Organization Report No. Report 0-6869-1
9. Performing Organization Name and Address Texas A&M Transportation Institute College Station, Texas 77843-3135		10. Work Unit No. (TRAIS) 11. Contract or Grant No. Project 0-6869
12. Sponsoring Agency Name and Address Texas Department of Transportation Research and Technology Implementation Office 125 E. 11th Street Austin, Texas 78701-2483		13. Type of Report and Period Covered Technical Report: March 2015–August 2016 14. Sponsoring Agency Code

15. Supplementary Notes
Project performed in cooperation with the Texas Department of Transportation and the Federal Highway Administration.
Project Title: Advancing Innovative High-Speed Remote-Sensing Highway Infrastructure Assessment Using Emerging Technologies
URL: http://tti.tamu.edu/documents/0-6869-1.pdf

16. Abstract
Asset management is a strategic approach to the optimal allocation of resources for the management, operation, maintenance, and preservation of transportation infrastructure. Asset management combines engineering and economic principles with sound business practices to support decision making at the strategic, network, and project levels. One of the key aspects of the development of asset management is data collection. The way in which transportation agencies collect, store, and analyze data has evolved along with advances in technology, such as mobile computing (e.g., laptops, tablets), sensing (e.g., laser and digital cameras), and spatial technologies (e.g., global positioning systems [GPS], geographic information systems [GIS], and spatially enabled database management systems). These technologies have enhanced the data collection and integration procedures necessary to support the comprehensive analyses and evaluation processes needed for asset management.

Data collection is costly. In determining what data to collect, agencies must weigh these costs against the potential benefits from better data. Traditional pavement and bridge management approaches are data intensive, requiring extensive data collection activities of most or all pavement and bridge assets on an annual or biannual basis. These efforts can be justified given the cost of agencies' pavement and bridge programs. However, depending on the level of technology needed and the associated costs, it may be difficult to justify similarly extensive data collection efforts for safety and operation assets.

While many of the technology innovations and improved data collection processes have been in the bridges and pavements area, there are emerging technologies in the safety and operations infrastructure areas that have yet to be applied to the transportation space. These technologies are driving the costs and efficiencies to the point that makes good sense in terms of the tradeoffs between fiscal responsibilities and advantages of having the data. Therefore, while this research covers all highway infrastructure areas, it includes an emphasis on technologies to assess safety and operations infrastructure. Ultimately, through the three-phased approach, the research strives to bundle the best technologies that maximize sensors and computing power in an effort to achieve the vision of one day having an all-in-one data collection system for infrastructure assessment.

17. Key Words Asset Management, LiDAR, Data Collection,	18. Distribution Statement No restrictions. This document is available to the public through NTIS: National Technical Information Service Alexandria, Virginia http://www.ntis.gov		
19. Security Classif. (of this report) Unclassified	20. Security Classif. (of this page) Unclassified	21. No. of Pages 384	22. Price

Form DOT F 1700.7 (8-72) Reproduction of completed page authorized

ADVANCING INNOVATIVE HIGH-SPEED REMOTE-SENSING HIGHWAY INFRASTRUCTURE ASSESSMENT USING EMERGING TECHNOLOGIES: TECHNICAL REPORT

by

Paul Carlson
Senior Research Engineer

Beverly Storey
Associate Research Scientist

Mo Poorsartep
Research Scientist

Charles Stevens
Research Engineer

Ben Ettelman
Associate Transportation Researcher

Tomas Lindheimer
Associate Transportation Researcher

Maryam Dastgiri
Graduate Assistant

Adel Khodakarami

Jeff Miles

Dezhen Song

Robert Lytton
Research Engineer

Xue Luo
Assistant Research Scientist

Yong Deng
Student Technician

Fan Gu
Post Doctoral Research Associate

and

Stefan Hurlebaus
Research Scientist

Report 0-6869-1
Project 0-6869
Project Title: Advancing Innovative High-Speed Remote-Sensing Highway Infrastructure Assessment Using Emerging Technologies

Performed in cooperation with the
Texas Department of Transportation
and the
Federal Highway Administration

February 2017

TEXAS A&M TRANSPORTATION INSTITUTE
College Station, Texas 77843-3135

DISCLAIMER

This research was performed in cooperation with the Texas Department of Transportation (TxDOT) and the Federal Highway Administration (FHWA). The contents of this report reflect the views of the authors, who are responsible for the facts and the accuracy of the data presented herein. The contents do not necessarily reflect the official view or policies of the FHWA or TxDOT. This report does not constitute a standard, specification, or regulation.

This report is not intended for construction, bidding, or permit purposes. The engineer in charge of the project was Paul J. Carlson, P.E. #85402.

The United States Government and the State of Texas do not endorse products or manufacturers. Trade or manufacturers' names appear herein solely because they are considered essential to the object of this report.

ACKNOWLEDGMENTS

This project was conducted in cooperation with TxDOT and FHWA. The authors thank the project director, members of the Project Monitoring Committee.

TABLE OF CONTENTS

Page

LIST OF FIGURES

Page

LIST OF TABLES

Page

CHAPTER 1. IDENTIFY EXISTING AND EMERGING TECHNOLOGIES

INTRODUCTION

Infrastructure asset management is the integrated, multidisciplinary set of strategies used in sustaining public infrastructure assets such as water treatment facilities, sewer lines, roads, utility grids, bridges, and railways. The basic objective of this discipline is to extend the expected service life and, in doing so, maintain asset performance by intervening at strategic points in an asset's normal life cycle. In the context of this project and for the purposes of this section, highway-related assets are the only category considered. Hence, "systematic process that aims to preserve, expand, and operate highway assets in the most cost-effective manner" (*1*) is the working definition pertinent to this investigation.

In order to achieve the objective of highway asset management, data and information need to be captured in the most cost-effective way to enable and create a good understanding of where each asset is in its life cycle and determine if strategic interventions (e.g., maintenance, repair, replacement) are needed. Methods and approaches to collect and monitor highway assets have evolved over the years. Technological advancements in different fields have been adopted and implemented by the road owners and operators in performing tasks related to highway asset management. Most of these efforts related to measuring and monitoring highway assets involve rather time-consuming and resource-intensive activities, such as driving instrumented vehicles (as shown in Figure 1) within the targeted road network and collecting data related to road signs, pavement markings, pavement quality, guardrails, and more. The data collected by these vehicles includes but is not limited to elements such as retroreflectivity, location, size, and height.

Figure 1. Instrumented Van (*2*).

Existing and emerging technologies that use mobile, nondestructive evaluation (NDE)/ nondestructive testing (NDT) techniques for the inspection of infrastructure are becoming more cost-effective and are proving to provide reliable data with decreased risk for workers and minimal or no traffic disruption. The majority of the advanced technologies for transportation use some method of remote sensing that gathers data from a distance without direct contact with the roadway, bridge, sign, or other infrastructure components. These methods include remote sensing data collection systems typically used by transportation agencies, such as photogrammetric methods (i.e., 3D Optics™, Bridgeviewer, GigaPan), electro-optical satellite,

airborne imagery, optical interferometry, thermal infrared, X-ray fluorescence, acoustics, high-speed ultrasonic tomography, ultrasound, digital image correlation, radar (including backscatter and speckle), interferometric synthetic aperture radar (InSAR/IfSAR), passive infrared thermography, Light Detection and Ranging (LiDAR), ultra-wide band imaging of ground penetrating radar (GPR), multispectral satellite imagery, and high-resolution "StreetView-style" digital photography (see Appendix A). Most of these systems incorporate some sort of global positioning systems (GPS), global information system (GIS), global navigation satellite system (GNSS), and/or continuously operating reference station (CORS). These technologies are capable of capturing surface and subsurface conditions at high speeds (*3*, *4*).

A review of the literature indicated an extensive list of data elements relevant to highway (or transportation) asset management. However, monitoring of the physical condition of transportation assets appeared to be the common thread in all practices. Table 1 provides an example of the main asset data that are required for an adequate asset management program (*5*).

Table 1. Asset Data Requirements for Asset Management.

Physical Asset Type	Example Data Types
Pavement	Structural adequacy, distress, serviceability, friction, design details, construction history, maintenance history
Bridges	Structural adequacy, design details, construction history, maintenance history
Signage	Condition, reflectivity, installation and maintenance history
Electronic Signals	Condition, efficacy, installation and maintenance history, energy use
Pavement Markings/ Delineators	Condition, installation and maintenance history
Drainage	Condition, efficacy, design details, environmental impact, construction and maintenance history
Lighting	Condition, efficacy, energy usage, environmental impact, installation and maintenance history
ITS Roadside Equip. and Communications	Condition, efficacy, installation and maintenance history

Many of the data and information presented in Table 1 are currently captured using varying methods. Some information is archived and available if needed, while some is measured on a daily basis (such as weather and environmental conditions), some are measured in scheduled intervals, and others are observed and measured on an as-needed basis. Much of the data and information, including installation, maintenance history, and design detail, are outside the scope of this effort.

Transportation agencies are looking to incorporate emerging and existing sensor sources and technologies to assist in high-speed data collection regarding the condition of pavements, bridges, and other infrastructure. The bundled technologies that connect vehicles, mobile devices, public and private systems, and the transportation facility consist of high-tech sensor

systems that gather real-time data as the user drives. The basic concept is to use the Internet of Things (IoT). The IoT is the "concept of basically connecting any device with an on and off switch to the Internet (and/or to each other). This includes everything from cell phones, coffee makers, washing machines, headphones, lamps, wearable devices and almost anything else you can think of. This also applies to components of machines, for example a jet engine of an airplane or the drill of an oil rig. The IoT is a giant network of connected "things" (which also includes people). The relationship will be between people-people, people-things, and things-things" (*6*). Figure 2 shows a model for the IoT.

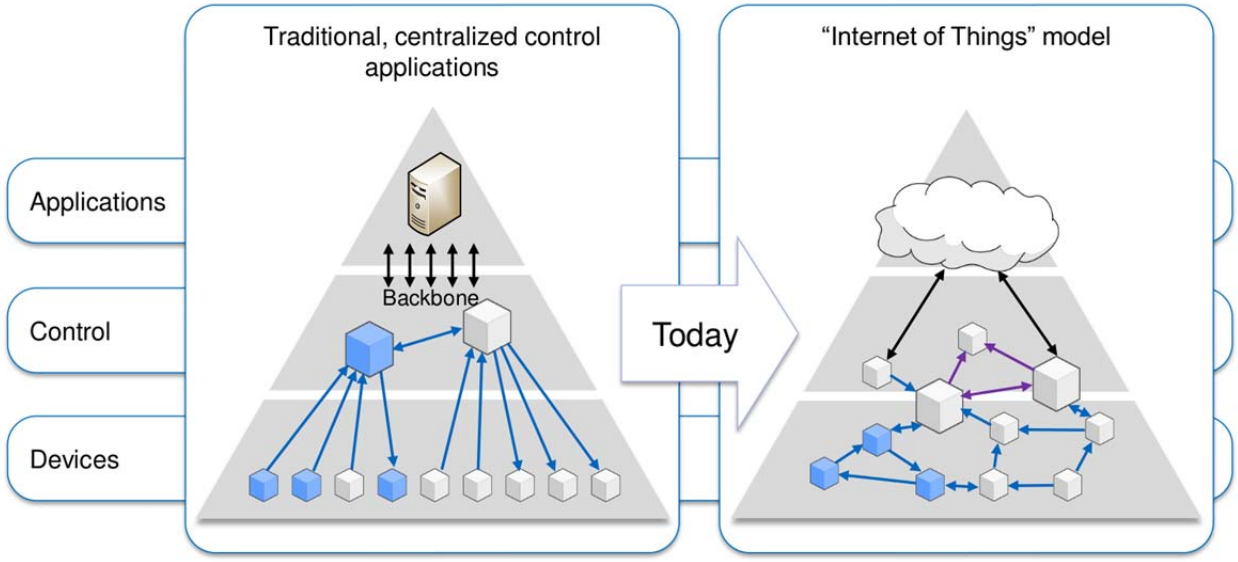

Figure 2. Internet of Things Model (*7*).

The Michigan DOT has investigated several options for using innovative concepts for data acquisition such as cloudsourcing and their data use analysis and processing (DUAP) system, as described below:

- Cloudsourcing.
  - Leverages the combined intelligence, knowledge, or experience of a group of people to answer a question, solve a problem, or manage a process. Transportation data applications include four categories.
    - Third-party Aggregated Crowdsourced Data.
    - Social Media for Public Engagement.
    - The Internet as a Sensor.
    - Dedicated Platforms for Transportation System Management (*8*).
- DUAP system.
  - Collects, aggregates, processes, and provides interactive views of the connected vehicle data.
  - Applications evaluated with data made available to the project included traffic monitoring, pavement defect and condition assessment, and origin-destination studies for planning (*9*).

Data collection systems can be static or affixed to a data collection vehicle. For high-speed data collection, mobile technology is considered the most efficient, safest, and most flexible because data collection can use vehicles operating at posted roadway speeds and/or manned and unmanned aerial vehicles for data capture. Computer technologies and portable convenience now enable high-speed digital recording and processing for storage and interpretation. These advanced survey technologies facilitate automated, nondestructive infrastructure inspection on an accelerated level. A survey conducted in 2013 for the National Cooperative Highway Research Program (NCHRP) queried departments of transportation (DOTs) regarding their adoption of advanced geospatial data tools, technologies, and information. Respondents stated that their respective agencies are proactive in researching new technology to:

- Help modify their standard operating procedures (SOPs) (53 percent).
- Develop their initial SOP (35 percent).
- Adopt technology after their SOP has been developed and proven (13 percent) (*10*).

The technologies widely used by DOTs for infrastructure inspection include photogrammetry, video logging, GPS, GIS, and statewide CORS networks. These mature technologies are integrated into operations, are used across several applications (e.g., planning, right of way, design, construction, and operations), and have a wide support base. Newer technologies such as cloud computing, machine control, electromagnetic imaging, unmanned airborne vehicles (UAVs), and InSAR/IfSAR have not been readily adopted. LiDAR is becoming more common; however, any form of LiDAR is not a standard operating procedure for the majority of the states. The top three barriers to technology adoption are cost, inertia, and technical expertise (*10*). Table 2 shows the percentage of DOTs using various technologies, sorted from most common to least common.

Table 2. Percentage of DOTs Using Technologies (*10*).

Technology	Standard Operating Procedure	Implementing	Investigating	Researching	Not Using	No Interest	Not Sure
Photogrammetry	90%	6%	2%	0%	0%	0%	2%
Video Logging	90%	6%	0%	0%	4%	0%	0%
GPS	88%	10%	0%	2%	0%	0%	0%
GIS	88%	8%	0%	2%	2%	0%	0%
Statewide CORS Network	67%	8%	2%	4%	12%	0%	6%
Online Mapping Service	65%	16%	2%	4%	12%	0%	0%
Statewide GNSS Real Time Networks	56%	13%	8%	2%	13%	2%	6%
Oblique Photography	47%	8%	16%	2%	18%	2%	6%
OPUS (Online Positioning User Service)	45%	8%	6%	2%	20%	2%	16%
Software as a Service	43%	14%	10%	8%	16%	2%	6%
Tablet Computers/Smart Phones	39%	31%	16%	4%	8%	0%	2%
Static 3-D Laser Scanning	38%	10%	8%	13%	25%	0%	6%
Airborne LiDAR	35%	33%	14%	4%	10%	0%	4%
Open Source Software	34%	14%	16%	8%	22%	4%	2%
Ground Penetrating Radar	33%	8%	10%	14%	22%	0%	12%
3-D Model-based Design	29%	23%	19%	10%	15%	2%	2%
Low Distortion Coordinate Systems	28%	14%	8%	4%	26%	2%	18%
Mobile LiDAR	22%	20%	22%	18%	14%	0%	2%
Cloud Computing	22%	20%	24%	14%	18%	0%	2%
Machine Control	20%	24%	6%	18%	14%	0%	16%
Electromagnetic Imaging	6%	4%	8%	8%	45%	0%	29%
UAV	2%	4%	6%	18%	63%	2%	4%
InSAR/IfSAR	2%	2%	6%	10%	50%	2%	27%

IDENTIFY EXISTING AND EMERGING DATA COLLECTION TECHNOLOGIES

The objective of Task 1 was to identify effective mobile data collection technologies and strategies and present their capabilities and limitations. The research team conducted a national and international literature review to identify mobile data collection technologies and strategies that have either recently been deployed or are in the prototype phase of development. The task identified recent and emerging technologies currently in the transportation space, as well as recent and emerging technologies outside the transportation space but with significant potential to be used for highway infrastructure assessments. A list of the subtasks undertaken to achieve the above include:

- Subtask 1.1. State-of-the-Art: Existing Highway Technologies and Systems.
- Subtask 1.2. State-of-the-Art: Advanced Vehicle Technologies.
- Subtask 1.3. Detailed Assessment of Selected Agencies and/or Technologies.

SUBTASK 1.1. STATE-OF-THE-ART: EXISTING HIGHWAY TECHNOLOGIES AND SYSTEMS

The primary objective of this subtask is to conduct a comprehensive literature search to identify recent, emerging, and prototype technologies for remote high-speed infrastructure inspections. The search includes other industries, such as agriculture and defense, to identify technologies that have potential to provide significant benefit to the transportation industry in these four key areas:

- Bridges.
- Pavements.
- Safety and Operation Infrastructure.
- Bundled Technologies.

LiDAR

Description

Light Detection and Ranging integrates lasers, sensors, GNSS, GPS, GIS, inertial navigation systems (INS), and/or inertial measurement units (IMUs) as a range-based imaging tool. A LiDAR scanner measures the distance to an object or surface by calculating the time delay between the initial transmission of individual laser pulses and the returning detection of reflected signals, which is similar to radar or sonar technology (*11*). The scanner uses light pulses (typically, near-infrared [NIR]) and time of flight and intensity levels as light returns to create a dense three-dimensional (3-D) spatial data set (i.e., point cloud). “A point cloud is the basis from which all information and products are processed, analyzed, and derived. Typical point cloud formats include ASCII, LAS, SVY, PTS/PTX, and other proprietary formats. ASCII, American Standard Code for Information Interchange, stores a point cloud as a basic, generic set of XYZ coordinates. The file can then be imported to software as delimited text or database files. LAS

(Log ASCII Standard) is a binary file format based on standard ASCII code" (*11*). LiDAR can be used for just about any structure or roadway application, from bridges to vegetation.

LiDAR Data Collection Methods

The general LiDAR systems most often used by departments of transportation include the following (see Figure 3):

- Static or Fixed Terrestrial Laser Scanning (STLS).
  - Scanner mounts on a stationary surveying tripod at a single location.
  - Does not require GPS or INS for georeferencing but can incorporate, if necessary.
- Mobile Terrestrial Laser Scanning (MLS).
  - Scanner typically mounts onto ground vehicles and travels with traffic flow, but can be used on trains and boats.
  - Collects 1000 points/m^2 using a vehicle-mounted platform (*12*).
  - Provides data collection efficiency up to 50 times that of conventional means.
  - Takes from 10 days to 30 minutes to scan a 20-mile highway segment (*13*).
  - Scans up to 150 miles per day (*14*).
  - Reduces workers' exposure to traffic, the elements, and other hazards in the field because data collection occurs at posted highway speeds.
  - Increases data collection speed and accuracy with integrated survey system, GPS, GNSS, and IMU data, digital cameras, and LiDAR scanners.
  - Delivers product in formats immediately available in computer-aided design (CAD) or other software packages.
  - Minimizes or eliminates need for field collection.
  - Enables accurate and complete 3-D detail capture of infrastructure, roads, etc.
  - Can be used day or night.
- Airborne Laser Scanning (ALS).
  - Scanner mounts to airplanes, helicopters, and UAVs to survey targeted areas.
  - Uses longer wavelengths than terrestrial systems, and are less affected by atmospheric conditions.
  - Determines position and orientation of the aircraft by integrating georeferencing devices. Laser emission vectors collected between the sensors and the ground below are recorded to compute XYZ coordinates of each laser beam (*11*).

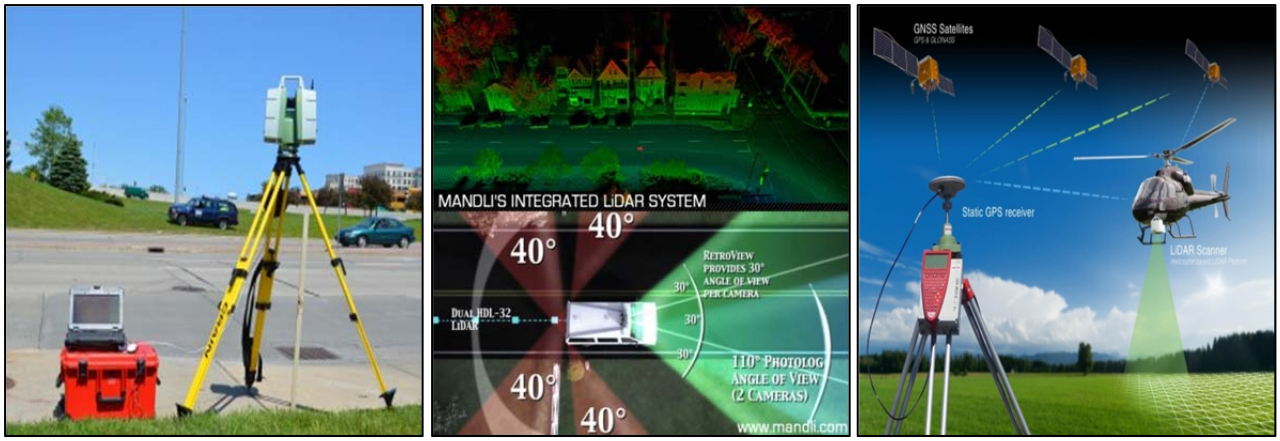

Figure 3. LiDAR Scanner Types – Left, Terrestrial; Middle, Mobile; Right Aerial (*15*, *16*, *17*).

Advantages/Challenges

The advantage to LiDAR for high-speed data collection use is its ability to collect data using ground vehicles (i.e., data collection vehicles move at traffic speeds) and in aerial applications). LiDAR use has enabled transportation agencies to improve worker safety and increase the level of detail and accuracy of data collection. Data are collected once, filtered and extracted to meet agency needs, and then shared with multiple users. Other advantages and challenges of using MLS and ALS for high-speed, nondestructive data collections as listed in the literature (*18, 19, 20*) are as follows:

- Advantages.
  - Useable in areas inaccessible by workers or vehicles.
  - Not constrained by limitations of traditional photography relative to nighttime and certain weather-related issues.
  - Provides millions of 3-D points over the entire survey area, compared with the extraction of elevation and features on discreet locations by stereoscopic photogrammetry.
  - Penetrates vegetated canopy.
  - Is more accurate than photogrammetry in regions with little texture or poor definition (i.e., snow, ice, swamps, wetlands, and sand).
  - Maps linear features and structures – Both large (bridges, etc.) and small (signs, etc.).
  - Offers time and cost savings after initial investment.
- Challenges.
  - Requires georeferenced imagery of the study area.
  - Computationally efficient and less time consuming, but also requires special training.
  - Error/uncertainty – Level of accuracy requires planning.
  - Provides improved data collection perspective (i.e., 900 ft above ground), but may require supplemental ground data verification.
  - Has increased post-processing requirements.
  - Generates large amounts of data (increased data storage).

Infrastructure Data Collection Capabilities

According to the cost-effective data collected by the Washington State DOT (WSDOT) (*14*), renting or contracting for services is an option, while purchasing equipment has long-term benefits. However, technologies are rapidly changing and for short-term use renting/contracting may prove a better choice. Common infrastructure data collected are as follows:

- ADA compliance/inventory.
- Bridges and tunnels.
  - Structural health monitoring.
  - Geometry and clearance measurements.
  - Restoration.
  - As-built drawings.
- Construction inspection documentation.
- Geotechnical engineering.
  - Rock mass and rock fall characterization.
  - Landslide mapping.
  - Tunnel construction and maintenance.
  - Slope stability.
  - Structural health monitoring.
  - Volumetric change.
- Highway design and corridor mapping.
  - Design improvement.
  - Elevation and cross section.
  - Topographic surveying.
- Hydraulics and hydrology.
  - Digital elevation model.
  - Geographic information system.
  - Coastal change.
  - Flood and inundation mapping.
  - High hazard dam.
- Pavement.
  - Grade estimation.
  - Cross slope.
  - Resurface assessment.
  - Crack detection.
- Photogrammetry.
  - Airport obstruction survey.
  - Digital elevation model.
  - Geographic information system.
  - Transmission line survey.
- Historic, natural, and cultural preservation.
- Safety surveys.
  - Guardrail location and height determination.
  - Line-of-sight analysis for safety and engineering studies.
- Power lines and utilities/luminaires/signals (*11, 14*).

The NCHRP Report 748 (*21*) discusses mobile LiDAR usage as it relates to the transportation industry. Data collection methods are contingent upon the required level of accuracy and density of data (resolution). Their recommended data collection category (DDC) for MLS includes level of accuracy (1=high, 2=medium, and 3=low) and point density (A=course, B=intermediate, and C=fine). The data collection cost escalates with the level of accuracy required. The report recommends considering all potential data users when deciding on the level of accuracy and resolution for a specific project. Agencies should coordinate to ascertain data collection needs to determine the maximum cost/benefit ratio for the MLS project. "Obviously, datasets collected at higher accuracies and point densities will be usable for less-demanding applications, but doing so may not be cost-effective. In contrast, data collected at a lower DCC may still be useful for an application requiring a higher DCC. For example, drainage analysis 1A could benefit from 2B data compared to what is available; however, the analysis may be more difficult to perform and less-reliable than if 1A data were collected" (*21*). Table 3 shows the recommended LiDAR accuracy and resolution requirements.

Table 3. Application Matrix and Suggested Accuracy and Resolution (*21*).

Accuracy	High <0.05 m (<0.16 ft)	Medium 0.05 to 0.02 m (0.16 to 0.66 ft)	Low >0.20 m (>0.66 ft)
Density	**1A**	**2A**	**3A**
FINE >100 pts/m^2 (>9 pts/ft^2)	• Engineering surveys • Digital terrain modeling • Construction automation /Machine control • ADA compliance • *Clearances** • *Pavement analysis* • Drainage/Flooding analysis • Virtual, 3-D design • CAD models/Baseline data • BIM/BRIM** • Post construction QC • As built/As is/Repair reports • Structural inspections	• *Forensics/Accident investigation** • *Historical preservation* • Power line clearance	• Roadway condition assessment (general)
	1B	**2B**	**3B**
INTERMEDIATE 30 to 100 pts/m^2 (3 to 9 pts/ft^2)	• Unstable slopes • Landslide assessment	• General mapping • *General measurements* • Driver assistance • Autonomous navigation • Automated/Semi-automatic extraction of signs and other features • Coastal change • *Safety* • Environmental studies	• Asset management • Inventory mapping (e.g., GIS) • Virtual tourism
	1C	**2C**	**3C**

COARSE <30 pts/m^2 (<3 pts/ft^2)	• *Quantities (e.g., earthwork)* • Natural terrain mapping	• *Vegetation management*	• Emergency response planning • Land use/Zoning • Urban modeling • Traffic congestion/Parking utilization • Billboard management

***Network accuracies may be relaxed for applications identified in red italics.**
****BIM/BRIM: BIM = Building Information Modeling; BRIM = Bridge Information Modeling.**

Transportation Agency Experiences/Research/Systems Used

Hawaii Department of Transportation

The Hawaii DOT (HDOT) started using LiDAR in 2009. HDOT contracted with Mandli Communications Inc. (http://mandli.com/) to implement a data collection process based on a combination of digital photography and LiDAR with the objective to develop of a photolog and the 3-D measurement of roadway assets. The LiDAR system used the Velodyne HDL Sensor (http://velodynelidar.com/) and Applanix POS LV 220 GPS hardware (http://www.applanix.com/) to collect data in 2009. Table 4 shows comparison of file format using LAS Version 1.2 and Mandli Format.

Table 4. Hawaii DOT 2009 Data Collection Comparison (*22*).

LAS Version 1.2	Mandli File Format
Public Header – 227 Bytes	More route data set friendly
Variable Length Header – 54 Bytes	Set of 4 files
Point Data – 20 Bytes	Approx. 3.125 Bytes per point total
Complete Route Files – Size a concern	Entire route contained in one file set
Largest File – 125.44 GB	Largest File – 19.6 GB
1,000 miles of Data (2 billion points)	
4,000 GB	650 GB

Mandli works with the Hawaii DOT to develop data management workflows that are efficient, intuitive, and compatible with the end user software, such as Bentley's InRoads and Intergraph's GeoMedia product suite (*22*). The primary objective of the development of an integrated road information system is to facilitate the management and maintenance of roadside assets and facilities throughout the state. The aim is to manage the information of state facilities and assets through their whole life cycle. In addition, the system is designed to achieve zero information leakage, to enable the information to be accessed from anywhere within the DOT, to share information that has been seen and/or heard, and to integrate all this information within a statewide GIS. HDOT added color to the point cloud data collected with pixel data from the photo-log images of the target roads and surrounding structures using the point cloud Photo Processing Extension plug-in (PPE) developed by FORUM8 (http://www.forum8.com/), real-time interactive 3-D virtual reality (VR) simulation, and modeling software. The colored point cloud data were then imported into VR-Design Studio. A 3-D VR simulation environment of the

target area was built using the colored point cloud data along with shapefile information, terrain data, and aerial orthophotography, all of which were imported into VR-Design Studio (*22, 23*).

Illinois Department of Transportation

Different highway inventory data collection methods were examined for the Illinois DOT. The methods included photo/video log, satellite/aerial imagery, MLS, GPS data logger, and robotic total station. Results of the experiments showed that mobile LiDAR scored the highest among the various types when considering data completeness and data quality (*13*).

Kentucky Transportation Cabinet

In a study conducted by the University of Kentucky, mobile laser scanning was used to verify bridge heights on the Western Kentucky Parkway. The LiDAR collected 400,000 points/sec at a driving speed of 30 mph. Results showed less than 1.2 inches difference as compared to manual measurement (*24*).

North Carolina Department of Transportation

According to the report, *Infrastructure Investment Protection with LiDAR,* the North Carolina DOT (NCDOT) used STLS predominantly. At the time of the report, NCDOT was contracting to use MLS on an as-needed basis (*11*).

Michigan Department of Transportation

The Michigan Technological University conducted an assessment report for the Michigan DOT (MDOT) regarding the potential use of remote sensing technologies for bridge inspection. The DOT currently uses visual evaluation as the primary tool for routine inspections. As a result, routine inspections are highly subjective and rely on experience-based expertise that must be developed over the years with practice. The report evaluated GPR, spectra, 3-D optics (including photogrammetry), electro-optical satellite and airborne imagery, optical interferometry, LiDAR, thermal infrared, remote acoustics, DIC, radar (including backscatter and speckle), InSAR, and high-resolution "Street View–style" digital photography. Table 5 compares the performance ratings for the above-listed technologies. The ratings are based, in part, on theoretical sensitivity for measurement technologies (*25*).

Table 5. Performance Rating of Commercial Remote Sensing Technologies (*25*).

Location	Challenges	Indicator	Desired Measurement Sensitivity	GPR	Spectra	3D Photo-grammetry	EO Airborne/ Satellite Imagery	Optical Inter-ferometry	LiDAR	Thermal IR	Acoustics	DIC	Radar (Backscatter/ Speckle)	InSAR	Streetview-Style Photography
Deck Surface	Expansion Joint	Torn/Missing Seal		0	8	14	12	11	13	11	0	0	9	0	13
		Armored Plated Damage		0	0	14	12	11	13	11	0	0	0	0	13
		Cracks within 2 Feet	0.8 mm to 4.8 mm (1/32" to 3/16") width	0	8	14	0	12	12	11	0	0	9	0	13
		Spalls within 2 Feet	6.0 mm to 25.0 mm (1/4" to 1") depth	0	8	14	12	12	12	11	0	0	9	0	13
		Chemical Leaching on Bottom		0	11	0	0	0	0	0	0	0	0	0	0
	Map Cracking	Surface Cracks	0.8 mm to 4.8 mm (1/32" to 3/16") width	0	8	14	12	12	12	11	8	0	9	0	13
	Scaling	Depression in Surface	6.0 mm to 25.0 mm (1/4" to 1") depth	0	8	14	12	12	12	11	0	0	9	0	13
	Spalling	Depression with Parallel Fracture	6.0 mm to 25.0 mm (1/4" to 1") depth	0	8	14	12	12	12	11	0	0	9	0	13
	Delamination	Surface Cracks	0.8 mm to 4.8 mm (1/32" to 3/16") width	0	8	14	0	12	12	11	8	0	0	0	13
Deck Subsurface	Expansion Joint	Material in Joint		0	0	0	0	11	0	0	0	0	0	0	0
	Delamination	Moisture in Cracks	Change in moisture content	11	0	0	0	0	0	11	0	0	0	0	0
		Internal Horizontal Crack	Approximately 0.1 mm (0.004") level	0	0	0	0	0	0	11	8	0	0	0	0
		Hollow Sound		0	0	0	0	0	0	0	8	0	0	0	0
		Fracture Planes / Open Spaces	Change in signal from integrated volume	12	0	0	0	0	0	0	8	0	12	0	0
	Scaling	Depression in Surface	6.0 mm to 25.0 mm (1/4" to 1") depth	12	0	0	0	0	0	11	0	0	0	0	0
	Spalling	Depression with Parallel Fracture	6.0 mm to 25.0 mm (1/4" to 1") depth	12	0	0	0	0	0	11	0	0	0	0	0
	Corrosion	Corrosion Rate (Resistivity)	5 to 20 kΩ-cm	0	0	0	0	0	0	0	0	0	0	0	0
		Change in Cross-Sectional Area	Amplitude of signal from rebar	13	0	0	0	0	0	0	8	0	13	0	0
	Choride Ingress	Choride Content through the Depth	0.4 to 1.0 % chloride by mass of cement	12	0	0	0	0	0	0	0	0	12	0	0
Girder Surface	Steel Structural Cracking	Surface Cracks	< 0.1 mm (.004"), hairline	0	8	11	0	12	0	11	0	0	0	0	0
	Concr. Structural Cracking	Surface Cracks	.1 mm (.004")	0	8	11	0	12	0	11	8	0	0	0	0
	Steel Section Loss	Change in Cross-Sectional Area	Percent thickness of web or flange	0	0	11	12	0	13	11	0	0	11	0	0
	Paint	Paint Condition	Amount of missing paint (X %)	0	9	0	0	0	0	11	0	0	0	0	0
	Concrete Section Loss	Change in Cross-Sectional Area	Percent volume per foot	0	0	11	12	0	13	11	7	0	11	0	0
Girder Subsurface	Concr. Structural Cracking	Internal Cracks (e.g. Box Beam)	Approx 0.8 mm (1/32")	0	0	0	0	0	0	11	8	0	0	0	0
	Concrete Section Loss	Change in Cross-Sectional Area	Percent volume per foot	0	0	0	0	0	0	0	7	0	11	0	0
	Prestress Strand Breakage	Change in Cross-Sectional Area	Wire 2 mm or strand 9.5 mm diameter	9	0	0	0	0	0	0	8	0	9	0	0
	Corrosion	Corrosion Rate (Resistivity)	5 to 20 kΩ-cm	0	0	0	0	0	0	0	0	0	0	0	0
		Change in Cross-Sectional Area	Amplitude of signal from rebar	8	0	0	0	0	0	0	8	0	13	0	0
	Choride Ingress	Choride Content through the Depth	0.4 to 1.0 % Chloride by mass of cement	10	0	0	0	0	0	0	0	0	11	0	0
Global Metrics	Bridge Length	Change in Bridge Length	Accuracy to 30 mm (0.1ft) (smaller)	0	0	15	13	0	0	0	0	9	0	12	0
	Bridge Settlement	Vertical Movement of Bridge	Approximately 6 mm to 12 mm	0	0	12	0	0	12	0	0	9	0	12	0
	Bridge Movement	Transverse Directions	Approximately 6 mm to 12 mm	0	0	12	0	0	12	0	0	9	0	12	0
	Surface Roughness	Surface Roughness	Change over time	0	9	14	13	12	12	0	0	0	11	13	13
	Vibration	Vibration	.5 -20 Hz, amplitude?	0	0	0	0	12	0	0	0	10	12	12	0

Another study conducted for the Michigan DOT compared aerial imagery with LiDAR, mobile imaging/photologging, and manual data collection (*19*). Table 6 shows the results of the study. The research also compared costs per asset inventory type and hours necessary to complete task as shown in Table 7. The hours were project-specific and would decrease based on number of miles involved.

Table 6. Accuracy Comparison of Data Collection Types (*19*).

Asset	Manual	Mobile Imaging	Mobile Imaging w/ LiDAR Correction	Aerial Imaging w/ LiDAR Correction
Attenuators	0	0	2	4
Bituminous Lanes (miles)	10.38	10.07	9.9	10.23
Concrete Lanes (miles)	0	0	0	0
Total Lanes (miles)	10.38	10.07	9.9	10.23
Catch Basin	22	13	33	15
Culverts (each)	88	N/A	N/A	N/A
Curbs (miles)	0.68	0.61	0.65	0.67
Delineators (each)	7	36	6	26
Ditches (miles)	7.82	7.64	7.02	0.61
Guardrails (linear feet)	2,496	2,581	2,472	3,051
Guardrail Endings (each)	5	N/A	10	10
Mowable Acres (acres)	7.53	14.07	12.29	14.73
Gravel Shoulders (miles)	1.35	1.12	2.05	2.64
Paved Shoulders (miles)	7.83	6.32	6.66	7.77
Total Shoulders (miles)	9.18	7.44	8.71	10.41
ROW Fencing (linear feet)	3,405	3,514	3,897	0
Signs (each)	88	100	92	63
Sweepable Approaches (each)	20	9	132	9
Traffic Signals (each)	8	4	2	2

Table 7. Project-Specific Cost per Mile and Hours per Mile Comparison (*19*).

Item	Manual	Mobile Imaging	Mobile Imaging with LiDAR Correction	Aerial Imaging with LiDAR Correction
Cost per Mile	$289	$369	$933	$900
Hours per Mile (project-specific)	9.0	7.4	6.7	10.2

Missouri Department of Transportation

A study conducted for the Missouri DOT (MoDOT) analyzed the state of laser-based technology and its applicability, potential accuracies, and information content for use by MoDOT (*26*). This study involved collection of airborne, static (terrestrial) ,and mobile LiDAR over a known

project area with existing control and check data sets to provide an assessment of accuracy, cost, and feasibility.

The study used an aerial LiDAR system comprised of a Leica ALS50II MPIA system (http://www.leica.com/) and an Applanix DSS 439 medium-format 39-megapixel (mp) digital camera (http://www.applanix.com/products.html). The combination of the LiDAR and camera enabled the DOT to overlay the point cloud with the images to increase the data point identification accuracy.

The mobile LiDAR data collection system used Optech Lynx, consisting of Dual 200 kHz Lasers, two GPS antennas, and an IMU (http://www.teledyneoptech.com/index.php/product/lynx-mg1/). The system was configured to collect at the full 200 kHz per laser head, effectively collecting 400,000 points/sec. Researchers wanted to identify areas where logical breaks for data collection could occur for easier processing. Short segments of approximately <0.5 miles were used to minimize the risk of poor GPS reception and to enable the use of calibration software.

Static LiDAR data were collected using both the Trimble GSX Advanced Terrestrial Scanner and the Optech ILRIS (http://www.teledyneoptech.com/index.php/product/optech-ilris/).

Table 8 shows a project-specific cost analysis of the systems used in the 2010 study. Data processing and feature extraction is based on the road, vegetation, poles, and buildings as per sample data provided for a sample 7-mile corridor. The costs for mobilization and some other charges were not included in the estimates.

Table 8. MoDOT Study LiDAR Cost Analysis (Adapted from *26*).

Method	Hours	Labor Cost	Person Days	$/Mile
Traditional Survey Design	1281	$131,585	160.1	$18,798
Aerial LiDAR	444	$ 58,250	55.5	$ 8,321
Mobile LiDAR	726	$ 81,688	90.8	$ 9,933
Static LiDAR	1700	$204,805	212.5	$29,258

Utah Department of Transportation

The Utah DOT uses Mandli's mobile LiDAR (http://mandli.com/) for data collection to gather, identify, and process its infrastructure and assets on state and Interstate routes. This effort was initiated to collect data on pavements. However, it soon became apparent that UDOT was duplicating data collection across divisions and decided to consolidate efforts to a more cost-effective and efficient method, thereby using an "economies of scale" approach to procurement.

"The UDOT Roadway Imaging and Inventory program requires the vendor to gather no less than a dozen different roadway assets including roadway distress data, surface areas, lane miles, number of signs, ROW images, vertical clearances, and more with each of those categories broken down even further into subcategories ranging from condition data to GPS data, etc. Sensors on the UDOT Mandli flagship vehicle include a Velodyne LiDAR sensor (http://velodynelidar.com/), a laser road imaging system, a laser rut measurement system, a laser

crack measurement system, a road surface profiler, a position orientation system, and more—certainly making it one of Mandli's most advanced asset gathering vehicles in their fleet" (*27*).

Virginia Department of Transportation

A study conducted for Virginia DOT in 2010 examined the use of MLS using Topcon's IP-S2 mobile mapping technology (https://www.topconpositioning.com/). From the experimental data, 96 percent of IP-S2 runs were within a 95 percent confidence level of the manually collected data. Furthermore, when IP-S2 fast and IP-S2 slow were compared, 100 percent were within the 95 percent confidence level. The IP-S2 cannot assess certain failure codes of assets such as missing guardrail bolts, damage to the back of guardrail components, turned signs, and missing object markers (*28*).

According to the VDOT Survey Manual (*29*), airborne LiDAR services are conducted by consultants. VDOT requires consultants to have the necessary hardware, software, and experience that will provide a consistent, accurate, and reliable product that includes appropriate data filtering and editing to eliminate incorrect, non-surface readings and reduce the file to a manageable size. Photogrammetry is used to develop break lines for the digital terrain mapping (DTM) and to provide a means for quality control of the LiDAR data. Photogrammetry provides break lines along all pavement, ditches, ridges, valleys, streams, edges of water, and any other significant surface feature that would require a break line for proper definition (*29*).

Washington State Department of Transportation

The Washington State DOT evaluated a vehicle-mounted mobile LiDAR technology to collect data for the WSDOT Roadside Feature Inventory Program, bridge clearance measurement, and ADA feature inventory. Cost/benefit analyses of seven mobile LiDAR deployment options were conducted. Researchers found that purchasing and operating a survey-grade mobile LiDAR system produced the highest savings of $6.1 million in six years. Although deploying the survey-grade mobile LiDAR system costs more, the benefits and cost savings from the bridge clearance operation and ADA feature inventory outweigh the higher cost and produce higher savings. Mobile LiDAR technology lowers the number of employees, vehicles, and carbon dioxide emissions for data collection. The major intangible benefactors are WSDOT's GeoMetrix Office, Geotechnical Office, Planning Office, Environmental Office, and Attorney General's Office. Results recommended that WSDOT deploy a mobile LiDAR system (*14*).

United Kingdom Highway Agency

The United Kingdom Highway Agency conducted a study to evaluate the use of traffic speed LiDAR using the Velodyne LiDAR system and the TopCon IP-S2 mobile mapping system for assessing barrier height and bridge clearance. They installed the Velodyne LiDAR system on the HARRIS2, an experimental platform for testing innovations in pavement assessment equipped with GPS receivers, a built-in IMU, and a highly accurate Phoenix Laser Scanning system that provides millimeter-level accuracy pavement condition data. HARRIS2 is also used as a reference device for vehicles operating under the Agency's TRACS3 contract. The Velodyne LiDAR outputs were integrated with HARRIS2's GPS and IMU systems to meet traffic speed LiDAR requirements.

The Velodyne LiDAR system was used because its rapidly rotating head can be used to generate a 360-degree 3-D image of a road environment when moving at traffic speed. The researchers installed the Velodyne LiDAR head horizontally. This placement allowed the motion of the vehicle (along the road) to generate a spiral of data. The Velodyne head can spin at up to 900 rpm, which means that it can complete a single revolution in as little as ~66 ms. In this time, a vehicle traveling at a traffic speed of 50 mph will have moved approximately 5 ft. The greater the speed, the farther the distance.

The TopCon IP-S2 mobile mapping system employs three SICK LIDAR systems that scan the ground behind the vehicle and each of the off and near sides with a small gap above the vehicle. The IP-S2 is a self-contained unit consisting of the LiDAR systems, IMU, SLR cameras, and a vehicle wheel-encoder attachment, which can be attached to any suitable vehicle. The system generates point clouds in full color by using images from its cameras to artificially color individual points.

Researchers used a prototype algorithm to detect barriers and estimate their height to better than ±10 cm. The total processing time for 3 km (1 mile) was a few minutes. Accuracy was outside typical requirements for a manual survey (±3 cm); however, this may be sufficient to identify significant problems. As routine manual measurements are only made every 100 m, the more closely spaced measurements provided by the LiDAR may offset some of the absolute accuracy concerns. LiDAR can be used to measure bridge clearances to a suitable level of accuracy, and its use should provide an automated process. Another 200 km (125 miles) survey of barrier clearance took only one day, and a streamlined processing system using LiDAR slices enabled the 250 km dataset to be manually analyzed in a few days (*30*).

Multispectral LiDAR

Description

Multispectral LiDAR combines the structural mapping capabilities of LiDAR with instrumentation that can capture and measure the spectral properties. Current applications of this technology are mostly in the agriculture, atmospheric, environmental, oil and gas, and oceanography disciplines (i.e., forest canopy cover/forest mapping). Multispectral and hyperspectral imagery allows the user to view a greater portion of the light spectrum to include red, green, blue, infrared, etc. This is accomplished in the form of electromagnetic radiation reflected back to a sensor. The light ranges are based on frequency/wavelength (Figure 4):

- Visible light – 380 nm to 700 nm.
- Infrared – 700 nm to 1 nm.
- Ultraviolet – 10 nm to 380 nm.

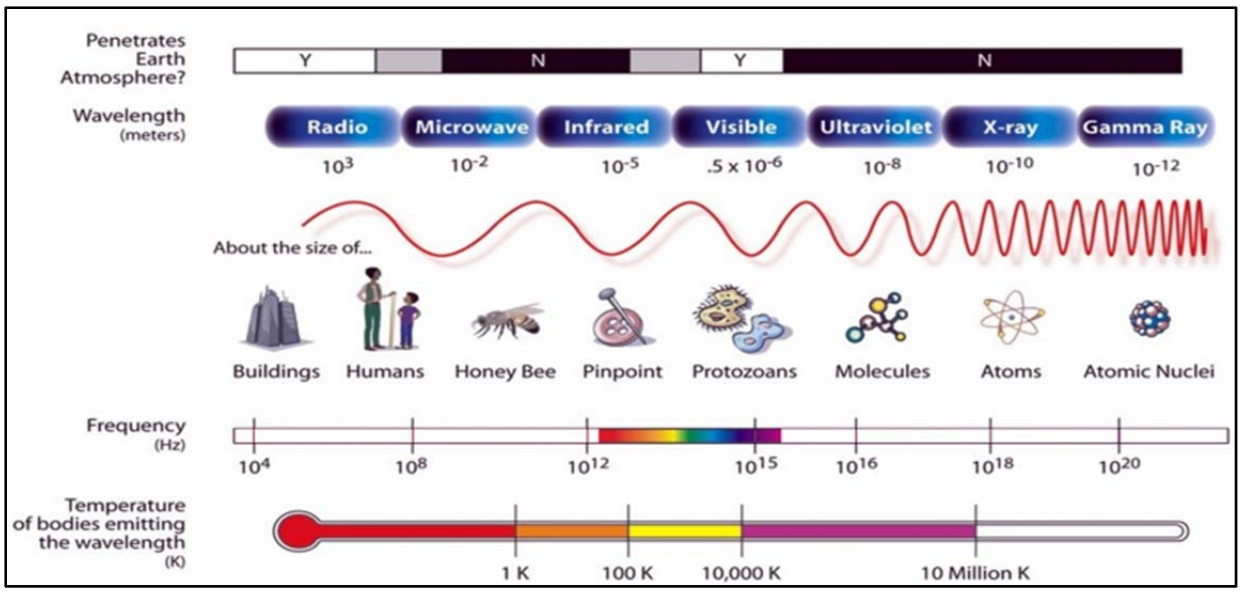

Figure 4. Wavelength, Frequency, and Temperature as Compared to Physical Objects (*31*).

Multispectral imagery generally refers to 3 to 10 bands that are represented in pixels acquired using a remote sensing radiometer (Figure 5) (*32*). This technology may allow the user to view images using the visible near-infrared (NIR), shortwave infrared, broadband microwave infrared, and longwave infrared.

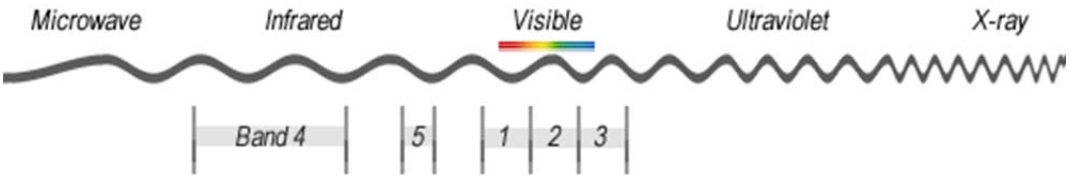

Figure 5. Multispectral Using Five Wide Bands (*32*).

Hyperspectral imagery, obtained with an imaging spectrometer, uses narrower bands (10–20 nm) so images may have hundreds of thousands of bands (Figure 6).

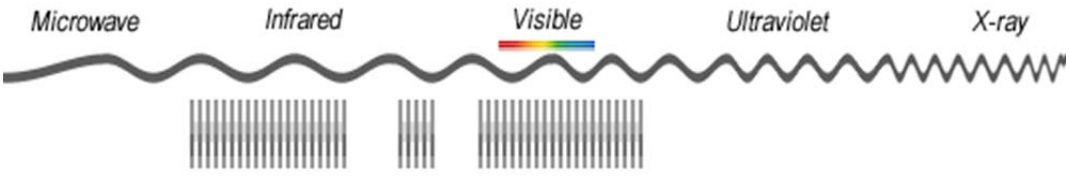

Figure 6. Hyperspectral with Hundreds of Bands (*32*).

Hakala et al. (*33*) used multispectral LiDAR to efficiently map the spatial distributions of tree physiological parameters correlated with reflectance of the foliage (such as chlorophyll a and b). Multispectral LiDAR has the potential to measure other reflectance properties.

Advantages/Challenges

- Advantages.
  - Enables detection of retroreflectivity.
  - Enables capture of broader light spectrum.
  - May enable nighttime data collection.
- Challenges.
  - Spacing of the emitters and receivers creates a near zero observation angle.
  - Existing asset management capabilities may need updating.

Infrastructure Data Collection Capabilities

- Sign and pavement markings.
- Water management.
- Drainage management.
- Vegetation management.
- Post-storm event management (i.e., flooding).

Transportation Agency Experiences/Research/Systems Used

Experiences within transportation agencies are minimal.

Ground Penetrating Radar

Description

Ground penetrating radar transmits short pulses of electromagnetic energy into the ground, and GPR antennas are generally classified as either ground-coupled or air-coupled systems. The reflected images of these pulses are analyzed using one-dimensional electromagnetic wave propagation theory. These pulses are reflected back to the antenna with amplitudes and arrival times that are related to the dielectric constants of the material layers (*34*). Measured arrival times depend on the dielectric constant of the material and lead to information about subsurface anomalies and their depth. Figure 7 shows a vehicle-mounted air-coupled GPR system. Generally, a high-frequency (1 GHz or more) antenna is used for non-contact GPR surveys at highway speeds (*35*). However, recent research at the Texas A&M Transportation Institute (TTI) used a 2.5-GHz system that proved beneficial as an implementable solution for uniformity analysis of asphalt mixture construction (*36*).

Figure 7. Air-Coupled Ground Penetrating Radar System (*37*).

Advantages/Challenges

- Advantages.
  - Has mature technology, used by many DOTs.
  - Offers relatively cost-effective inspection method.
  - Can be used at speeds up to 65 mph.
  - Air-coupled systems – High frequency (≥1 GHz), highway speed, yield better vertical resolution, but low penetration depth.
  - Ground-coupled systems – Low frequency (<1 GHz), penetrate deeper, but lower vertical resolution.
  - Provides continuous data collection.
  - Offers versatile applications.
- Challenges.
  - Newly placed concrete attenuates signal and reduces penetration depth.
  - Accuracy is affected by signal frequency, material properties (e.g., water content), and electromagnetism.
  - Automated data processing and analysis software has not advanced enough.
  - Requires special expertise (*38*).

Infrastructure Data Collection Capabilities

- Bridge decks.
- Asphalt and concrete pavements.
- Vertical concrete structures.
- Pavement thickness measurement.
- Surface, base, and subbase road course assessment.
- Detection of cavities, voids, and delamination.
- Detection of subsurface water-saturated areas.

- Airport runway condition assessment.
- Structural composition of construction elements.

Transportation Agency Experiences/Research/Systems Used

As of the 2013 NCHRP Report 446 (*10*) ground penetrating radar is used by over one-third of state transportation agencies surveyed as an asset management tool with another third in the process of implementing, investigating, or researching GPR usage.

Infrared Imaging/Thermography

Description

Infrared imaging or thermography can detect radiation in the long-infrared range of the electromagnetic spectrum (roughly 9000–14,000 nanometers or 9–14 μm), convert, and produce images of that radiation as a thermal distribution, called thermograms. Since infrared radiation is emitted by all objects with a temperature above absolute zero, according to the black body radiation law, thermography makes it possible to see one's environment with or without visible illumination (see Figure 4). The amount of radiation emitted by an object increases with temperature; therefore, thermography allows one to see variations in temperature (*39*).

Advantages/Challenges

- Advantages.
  - Can capture surface temperature distribution and produce a visible display, and show a visual picture so temperatures over a large area can be compared.
  - Can be conducted in real time.
  - Has the ability to find deteriorating (i.e., higher temperature) components prior to their failure.
  - Can be used to measure or observe in areas inaccessible or hazardous for other methods.
  - Offers a nondestructive test method for various infrastructures.
  - Can be used to detect objects in dark areas (*39, 40*).
- Challenges.
  - Quality cameras with larger pixel arrays are expensive.
  - Must have calibrated equipment capable of capturing the necessary irradiance measurements to construct the output image.
  - Images can be difficult to interpret accurately.
  - Accurate reading can be affected by differing emissivities and reflections from other surfaces.
  - May not be as accurate as contact methods.
  - Only capable of directly detecting surface temperatures.
  - Condition of work, depending on the case, can be drastic: 10 °C of difference between internal/external, 10 km/h of wind maximum, no direct sun, no recent rain, etc. (*39*).

Infrastructure Data Collection Capabilities

- Road and bridge pavement inspection and monitoring.
- Construction monitoring.
- UAV surveillance.
- Nighttime or minimal/no light condition inspection and monitoring.
- Nondestructive testing.
- Utility failure detection (i.e., leaks).
- Water quality/environmental surveillance.
- Location of buried features.
- Environmental surveillance.
- Post-storm event surveillance.

Transportation Agency Experiences/Research/Systems Used

Current Pooled Fund Study

The Missouri DOT is currently leading a Pooled Fund Study (FL, GA, IA, KY, MI, MN, MO, NY, OH, OR, PA, TX, and WisDOT), *Field Testing Hand-Held Thermographic Inspection Technologies Phase II* (*41*), with the objectives of validation of the inspection guidelines, validating the capability and reliability of the technology, and identifying implementation barriers.

Ultrasonic Shear-Wave Tomography

Description

There are numerous methods for assessing the condition of pavements and structures using some variation of sound waves. These methods are very effective, but many use a static measurement method or use handheld instrumentation, making adaption to high-speed data collection difficult. These techniques typically include:

- Ultrasonic pulse velocity.
- Crosshole sonic logging.
- Sonic echo–impulse response.
- Spectral analysis of surface waves.
- Impact echo scanner.

However, the NDT method known as ultrasonic shear-wave tomography (UST) seems to be among the few that are best suited for high-speed data collection. UST uses a low frequency (20 to 100 kHz) multifunctional phased array ultrasonic system (known as MIRA) that is engineered for the detection of reinforcement, voids, cracking, delaminations, overlay debonding, and other anomalies. UST is also capable of producing 3-D models of the pavement's internal structure for a better evaluation of the condition of the pavement, concrete, bridge piers, or foundations (*412*).

Advantages/Challenges

- Advantages.
  - Produces 3-D models of pavement or structure.
  - Measures thickness.
  - Detects reinforcement, voids, cracking, delaminations, overlay debonding, and other anomalies.
  - Capable of evaluating concrete structure to 4 ft thick (*433*).
- Challenges.
  - Congested reinforcement limits usefulness (*433*).
  - Has limited capabilities for detecting incipient distresses.

Infrastructure Data Collection Capabilities

- Internal void and honeycomb.
- Delamination (*433*).

Transportation Agency Experiences/Research/Systems Used

Georgia and Minnesota Departments of Transportation

Nondestructive test methods using an ultrasonic tomography device, MIRA, (http://germann.org/all-products) demonstrated its capabilities for determining concrete pavement thickness, reinforcement location, detection of flaws such as delamination, and degradation at pavement joints. The device comes with powerful data interpretation software that uses the synthetic aperture focusing technique. However, in the study conducted by Hoegh et al., the authors realized the importance of customizing and automating the data interpretation process for the most typical applications to ensure more widespread implementation and reduce the need for specialized user expertise and experience. MIRA can be used as a stand-alone tool, but when combining with other NDT methods will significantly improve the quality of pavement NDT evaluation (*444*).

Photogrammetry for Pavement Deflection Measurements

Description

Photogrammetry is based upon a pinhole imaging principle, as shown in Figure 8, in which the small pinhole (i.e., the perspective center of camera lens, points S or S1), the image points (i.e., points I or I1) on the left image plane (i.e., gray planes in Figure 8), and the objective point P should be collinear. For example, the three points S, I, and P should be collinear in Figure 8.

Therefore, the three lines SP, SS1, and PS1 are coplanar and form the triangle. In photogrammetry, the image plane is depicted at the left of the pinhole, which allows one to work with image geometry as found on a positive photo position rather than that found on a photographic negative.

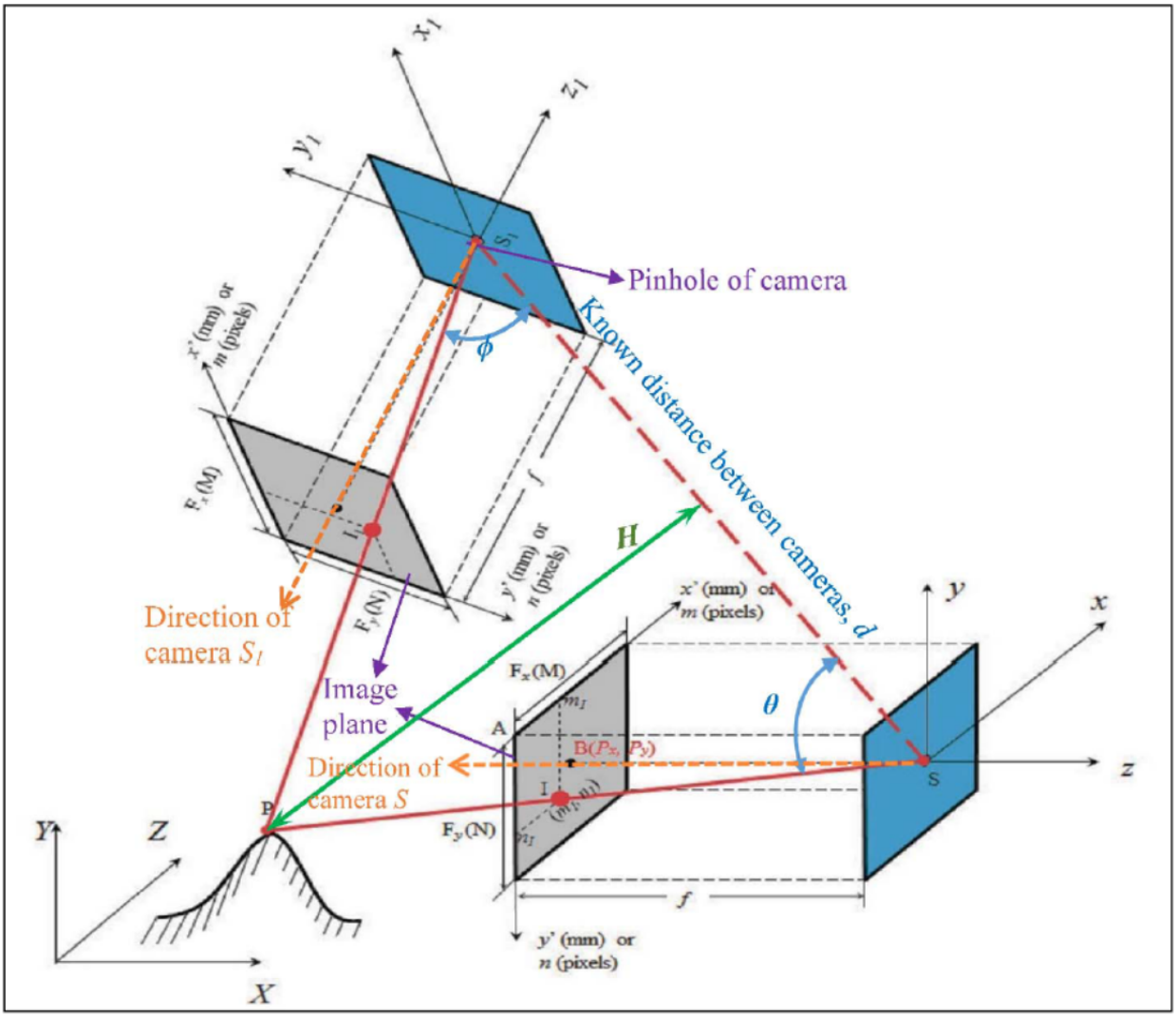

Figure 8. Principle of Photogrammetry.

To ensure a good quality image captured at a highway speed, the camera needs to be able to record the pavement surface at a high speed in terms of frames per second (FPS). Current commercially available high speed cameras can file as quickly as 1 million FPS. That means it takes 1 μs to take one image. Assuming that the test truck travels at a speed of 60 mph on the highway, the laser reference point will move forward about 0.027 mm, which will not influence the quality of the image. A lower speed camera may be used to reduce the project budget while still producing a quality image. In addition, a third camera can be used to calibrate and increase the accuracy of the measurements of the deflection profile.

Advantages/Challenges

The advantages of the photogrammetry-based moving deflection measuring system over the Rolling Wheel Deflectometer (RWD) include:

- Measurements will not be affected by longitudinal tinting on concrete pavement and other rough or open surface textures, by projecting more laser reference points to the pavement surface. RWD cannot work on concrete pavements and flexible pavements with a rough surface and significant cracking.
- The accuracy of a photogrammetry-based deflection measuring system can reach to 2 to 3 μm (0.002 to 0.003 mm) when using a 1.6 million pixel camera, which is sufficient for the typical range of pavement deflections from 0.1 to 1 mm. The accuracy can be even higher when using more cameras with higher resolution.
- The photogrammetry-based moving deflection measuring system can obtain a comprehensive profile for a specific deflection basin as a series of points are measured simultaneously. RWD can only obtain a single measurement for one location.

The challenge for this technology comes from applying this in a high-speed (traffic speed) data collection format.

Unmanned Aerial Vehicle/Unmanned Aircraft Systems

Description

The use of Unmanned Aerial Vehicles/Unmanned Aircraft Systems (UASs) has grown rapidly throughout the United States and the uses are far-reaching and ever expanding. These aircraft are typically known as UAV, drones, radio-controlled aircraft, and remotely piloted aircraft. An unmanned aircraft is a device used or intended to be used for flight in the air that has no onboard pilot, and includes all classes of airplanes, helicopters, airships, and powered-lift aircraft without an onboard pilot (*455*). The terms UAV and UAS are used interchangeably throughout the literature. The U.S. Department of Transportation's Federal Aviation Administration (FAA) refers to systems used to gather data as UAS, such as those used by transportation agencies.

A UAS is the unmanned aircraft (UA) and all of the associated support equipment, control station, data links, telemetry, communications and navigation equipment, etc., necessary to operate the unmanned aircraft. The UA is the flying portion of the system, flown by a pilot via a ground control system, or autonomously through use of an onboard computer, communication links, and any additional equipment that is necessary for the UA to operate safely. FAA issues an experimental airworthiness certificate for the entire system, not just the flying portion of the system (*466*).

UAS operations are generally categorized by size and mission, as shown in Figure 9. Small UAS are those under 55 lb, and large UAS weigh greater than 55 lb. Most UAS in use fall in the small category. UAS missions are categorized as to whether the operator maintains line of sight or operation is beyond the line of sight. The vast majority of UAS flights are piloted by ground-based personnel that use a three-component framework consisting of the UA, the ground control station (GCS), and the communications link between the two. For example, consider a real estate agent taking photographs of a house—the operator relies only on his or her vision to avoid colliding with other objects. Flights that take the UAS out of the line of sight of the pilot require additional satellite control and GCSs (e.g., applications of roadway, rail, or pipeline inspection). Those UAS controlled beyond the line of sight require that FAA segregate the airspace or that

the UAS includes instruments to sense other aircraft and avoid obstacles. Even when flying pre-programmed routes and tasks, real-time pilot intervention is always available (*477*, *488*).

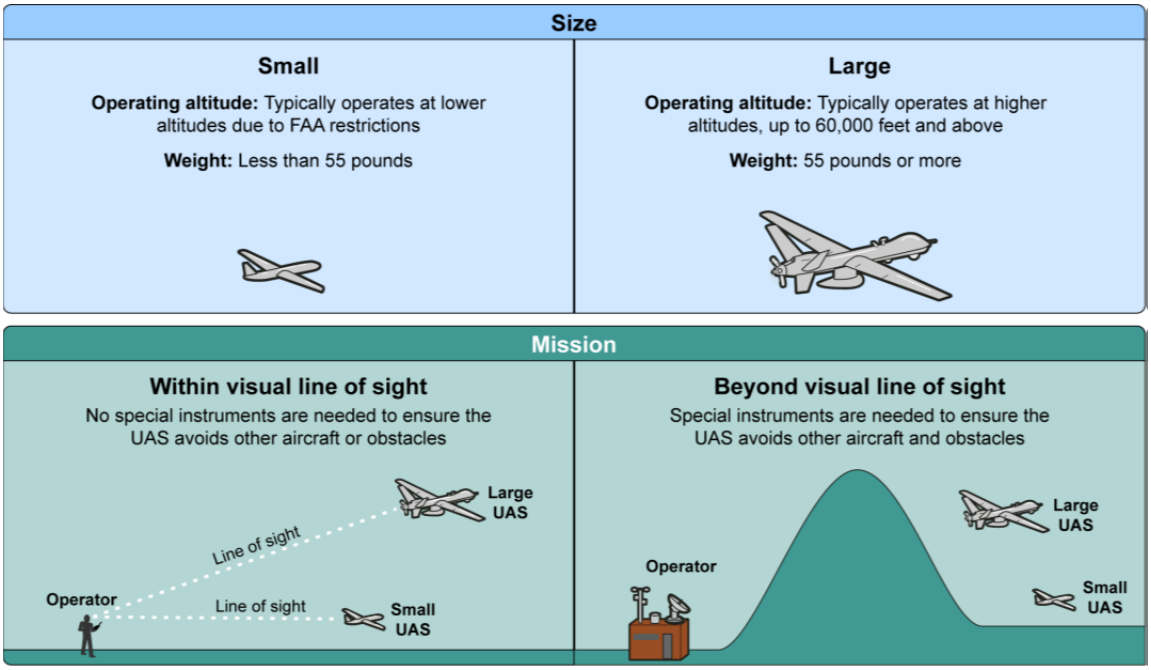

Figure 9. UAV/UAS Size and Categories (*477*).

Advances in technology of the UAS components such as sensors; lighter and stronger aircraft structures; more powerful, lighter, and smaller computers; better aircraft-to-ground communications; and increasingly accurate GPS/GNSS have made them more attractive to transportation agencies for use in infrastructure inspection, avalanche control, search and rescue, crash-scene photography, land-use mapping, surveying, security inspections, hazardous material monitoring, construction data collection, aerial surveillance, and monitoring the condition and congestion of roadways (*499*).

The U.S. Department of Transportation's FAA has proposed a framework of regulations that would allow routine use of certain small UAS in today's aviation system, while maintaining flexibility to accommodate future technological innovations. The FAA proposal offers safety rules for small UAS (under 55 lb) conducting nonrecreational operations. The rule would limit flights to daylight and visual line-of-sight (VLOS) operations. It also addresses height restrictions, operator certification, optional use of a visual observer, aircraft registration and marking, and operational limits (*50*). An overview of the proposed rulemaking is included in Appendix B.

A public aircraft is one that is used only by the United States government or owned and operated by the government of a state, the District of Columbia, or a territory or possession of the United States or a political subdivision. Operators of public aircraft include state/local agencies and qualifying universities. For public aircraft operations, FAA issues a Certificate of Waiver or Authorization (COA) that permits public agencies and organizations to operate a particular aircraft, for a particular purpose, in a particular area. The COA allows an operator to use a

defined block of airspace and includes special safety provisions unique to the proposed operation. COAs usually are issued for a specific period—up to two years in many cases (*50*).

Types of UAV/UAS

There are two basic UAV/UAS types, fixed-wing or rotary-wing, as shown in Figure 10. The micro UAV (MUAV or MAV) is starting to dominate the UAV marketplace for purposes other than recreational. The small, lightweight vehicles have extreme maneuverability and can access and collect data from locations previously deemed too difficult or dangerous. The size of the fixed-wing MUAV typically ranges from 12 inches to 4 ft, while the rotary-wing MUAV are getting as small as the technology will allow. For most transportation agency uses, the size ranges between 2 and 3 ft diametrically (*511*).

There are advantages to both UAV configurations. The fixed-wing UAV has greater speed, is able to carry larger payloads, and can glide to reduce fuel/battery use. The rotary-wing UAV has greater maneuverability, can hover in place, is smaller, and can take off/land in a confined space (*511*).

Figure 10. Fixed-Wing and Rotary-Wing UAV (*511*).

Advantages/Challenges

Some of the advantages to using UAVs for data collection on transportation facilities include:

- Provides non-intrusive methods.
- Reduces the risk for workers.
- Operations are becoming less expensive.
- Mobilizes quickly.
- Requires no pilot on board.
- Can be used in areas dangerous and/or inaccessible (i.e., wildlife habitat, wetlands, bridges, or culverts).
- Can be programmed to complete tasks autonomously even when contact with its GCS is lost (*522*).

The challenges of using UAVs for infrastructure data collections within the highways system are very broad, from public perception to FAA regulations. The pending FAA regulations are the most significant. These include:

- Public perception/privacy/liability issues.
- Potential for vehicle/infrastructure collision.
- FAA restrictions.
- High start-up cost.
- Limited availability of lightweight sensors.

Infrastructure Data Collection Capabilities

The data collection capabilities of using UAV/UAS for highway infrastructure assessment are vast. UAV technology coupled with LiDAR, GPS, GNSS, photogrammetry, and other collection methods can provide data that can be shared throughout agencies.

Transportation Agency Experiences/Research/Systems Used

Several DOT and other state and federal agencies such as the National Oceanic and Atmospheric Administration and the U.S. Geological Survey are increasing their use of UASs for monitoring, surveillance, inspection, and inventory. Transportation agencies using UASs for transportation-related activities has gained momentum as the aircraft have become more capable, smaller, and more affordable. UASs uses range from simple video surveillance to pavement crack detection using LiDAR. Legislation is trying to keep up with the demand for use of UASs for commercial, public, and private use. According to the National Conference of State Legislature, 35 states considered UAS or UAV bill and resolutions, with 10 states enacting new laws in 2014 (*533*). Figure 11 shows the number of states that have introduced, enacted, and adopted UAS legislation.

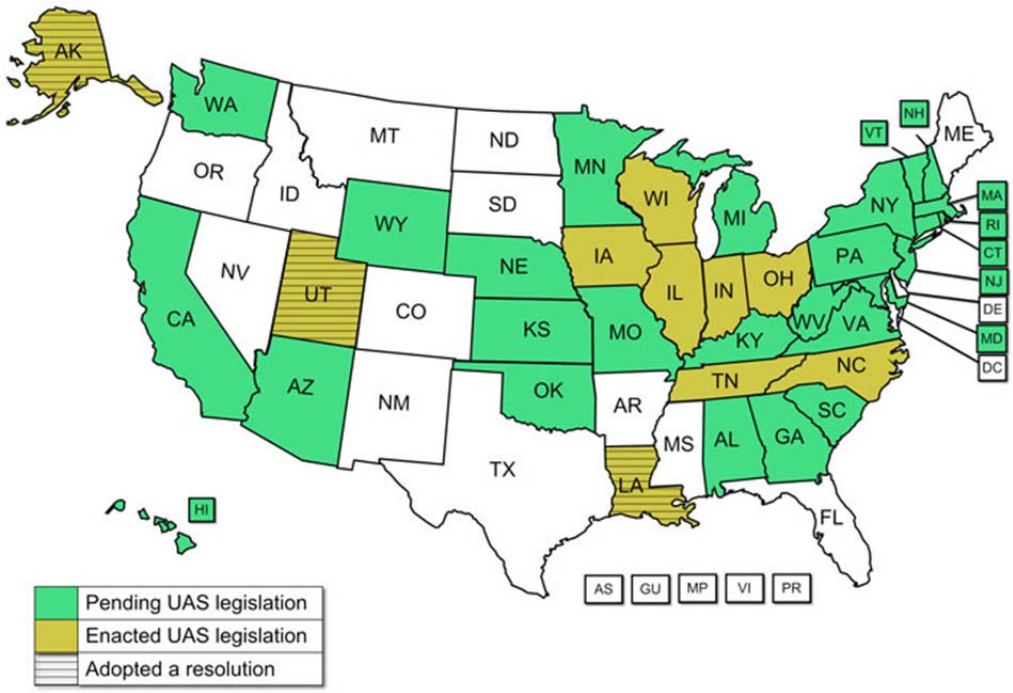

Figure 11. 2014 States with UAS Legislation (*533*).

Not including the current efforts by TxDOT and TTI, 11 DOTs have or are currently investigating UAV applications or are sponsoring UAV research including:

- Arkansas State Highway and Transportation Department (AHTD).
- California Department of Transportation (Caltrans).
- Florida Department of Transportation (FDOT).
- Georgia Department of Transportation (GDOT).
- Michigan Department of Transportation (MDOT).
- North Carolina Department of Transportation.
- Ohio/Indiana Department of Transportation (ODOT).
- Utah Department of Transportation (UDOT).
- Virginia Department of Transportation (VDOT).
- Washington State Department of Transportation.
- West Virginia Division of Highways.

Arkansas State Highway and Transportation Department

AHTD completed a project out of the research section in 2010 that investigated mobile systems to monitor traffic from above. The project compared literature between UAV, a mobile mast mounted camera, and a tethered helium balloon technology for use in collecting HD video and pictures to quantify turning movements, traffic volumes, vehicle headways, queue lengths, and vehicle classification, and for simulation model calibration. Prior to the testing and demonstration phase of the project, AHTD abandoned UAVs as a possible system, citing FAA restrictions and time constraints (*544*).

California Department of Transportation

In August of 2014, Caltrans produced a report on the use of UAVs for steep-terrain investigation. Initial work focused on previous DOT experiences, the role of FAA, UAV applications, and training resources. The report discussed prior Caltrans research for using UAVs for bridge inspection in 2008 but indicated that no additional research has been completed in the state of California. The report indicates future research needs in the areas of proof-of-concept testing and close monitoring of the FAA regulatory environment (*544*).

Florida Department of Transportation

Over a span of four years, the University of Florida completed an airborne traffic surveillance "proof of concept" study for FDOT. After engaging over 50 UAV vendors, the researchers selected the Aerosonde make of UAV (http://www.aerosonde.com/). This project also focused heavily on communication, obtaining the necessary equipment to outfit two microwave towers. Unfortunately, this project was also denied FAA approval of a COA. The specific points of contention were the "see and avoid" and safe-landing issues. Due to these concerns and the denial of the COA, FDOT canceled the project, citing no solution to the see and avoid and safe-landing issues (*555*).

Georgia Department of Transportation

In 2014 the Georgia Institute of Technology completed a feasibility study for GDOT, studying the potential of UAV application for GDOT operations. Researchers developed basic goals and information requirements and proposed five reference systems for the ability to capture real-time data including:

- Flying camera.
- Flying total station.
- Perching camera.
- Medium altitude, long endurance.
- Complex manipulation.

In addition to developing reference systems, the researchers interviewed 24 GDOT staff members and concluded that the primary areas of application included collecting data, providing information, and decision making based on the data. Future research in the areas of economics and intangible benefits were also listed (*566*).

Michigan Department of Transportation

The Michigan DOT tested and evaluated five main UAV platforms with a combination of optical, thermal, and LiDAR sensors to assess critical transportation infrastructure and issues such as bridges, confined spaces, traffic flow, and roadway assets. The research efforts demonstrated that UAVs can help with many transportation issues, including providing flexible low-cost traffic monitoring; helping with needed bridge element inspection data, including identifying spalls with optical images and likely delaminations with thermal data; evaluating the status and safety of confined spaces; and identifying types of "roadway assets" through UAV-based image analysis (*577*). The platforms and sensors used are listed below.

- Bergen Hexacopter (http://www.bergenrc.com/Multi.php).
  - Nikon D800 camera.
    - Bridge deck inspection through 3-D modeling.
  - Hokuyo UTM-30LX-EW LiDAR.
    - Roadway assets.
  - Tau 2 FLIR thermal camera.
    - Delamination detection.
- DJI Phantom 2 Vision (http://www.dji.com/product/phantom-2-vision).
  - Integrated camera.
    - Bridge structure imaging and construction monitoring.
- Blackout Mini H Quadcopter (http://www.minihquad.com/).
  - Integrated camera.
    - Bridge structure imaging, confined space assessment, culvert inspection.
- Heli-Max 1 Si (http://www.helimaxrc.com/helicopters/hmxe0830-1si/).
  - Integrated camera.
    - Confined space assessment.

- Walkera QR 100S (http://www.walkera.com/en/shops.php?id=122).
  - Integrated camera.
    - Confined space assessment.
- FPVfactory Mariner Waterproof Quadcopter (http://www.fpvfactory.com).
  - GoPro camera.
    - Bridge structure imaging – Undersides (for bridges over water).
- Blimp.
  - Samsung 4G camera.
    - Traffic monitoring/operations and maintenance (*577*).

North Carolina Department of Transportation

The State of North Carolina approved a test UAV program at North Carolina State University in August 2013. In March 2014 a report on unmanned aircraft use was presented to the State Legislative Joint Oversight Committee on Information Technology, Joint Legislative Transportation Oversight Committee, and the Fiscal Research Division. The report was in response to the legislative request that included coordination with the Chief Information Officer and Aviation Division Director of NCDOT to develop a proposal for the implementation of a UAV program. The program lists several areas that will benefit from UAV use, including agriculture, surveying, wildlife monitoring, state infrastructure monitoring, migration monitoring, and emergency management. A breakdown of the cost of the UAV program was also provided, estimating a start-up cost of $850,000 and recurring annual costs of $435,250 (*589*).

Ohio/Indiana Departments of Transportation

In 2002 Ohio State University performed field experiments in Columbus to determine the feasibility of collecting data on freeway conditions, intersection movements, network paths, and parking lots (*60*). In 2013, ODOT continued innovation by implementing UASs for more efficient and effective operations. However, it was noted that the biggest challenge was obtaining clearance to fly in the national airspace. Working closely with FAA they have developed a method to streamline the COA process (*60*). In 2013, the governor of Ohio, John R. Kasich, announced a joint initiative with the State of Indiana to develop an Unmanned Aircraft Systems Center to advance the commercialization of the technology and support UAS research. The Center is formally a component of ODOT, and the Ohio legislature passed a declaration supporting the center. The current website offers services including Flight Operations (see Figure 12) and Flight Testing (see Figure 13) including language regarding pay-based services (*61*).

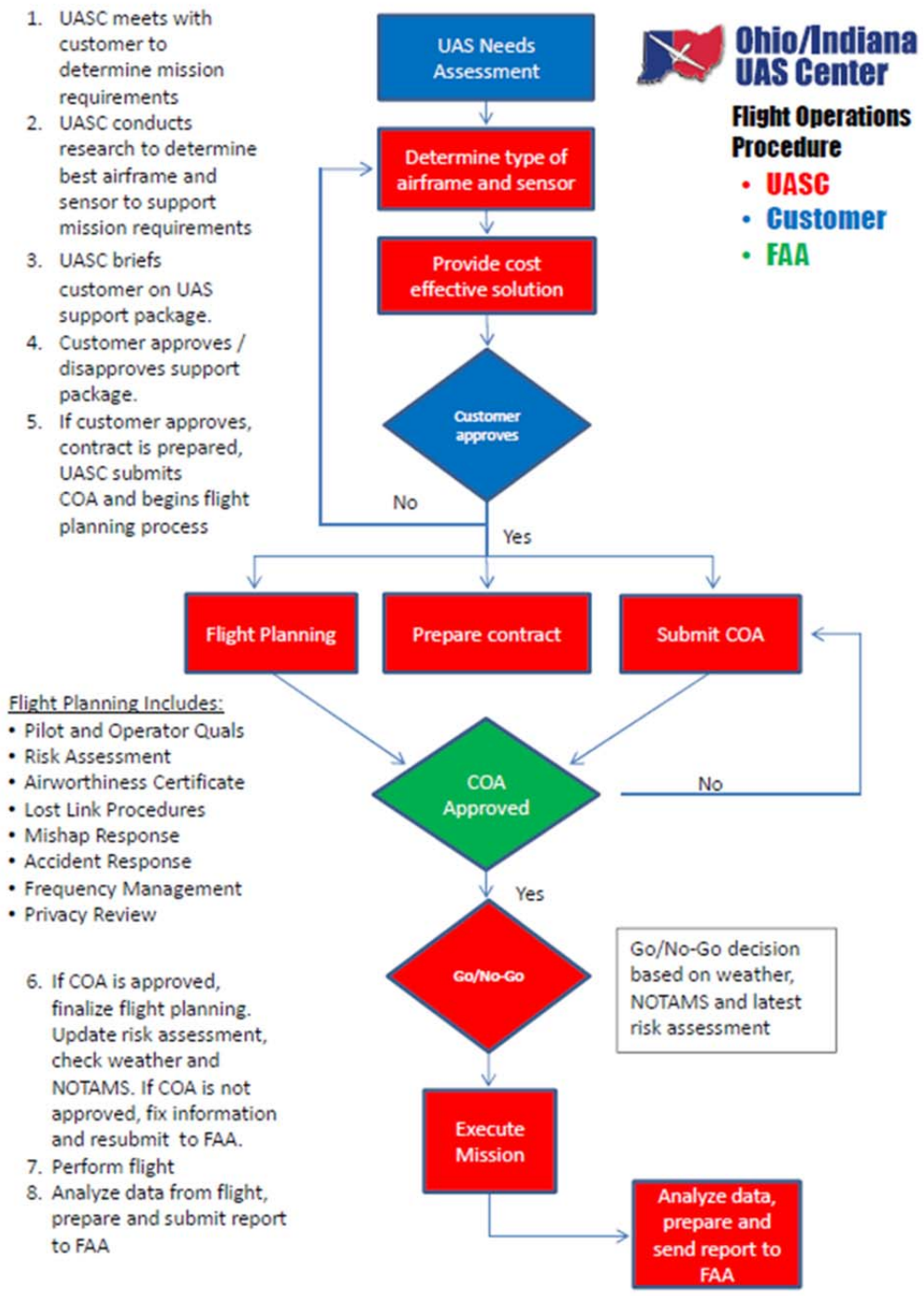

Figure 12. Ohio/Indiana UAS Center Flight Operation Procedures (*611*).

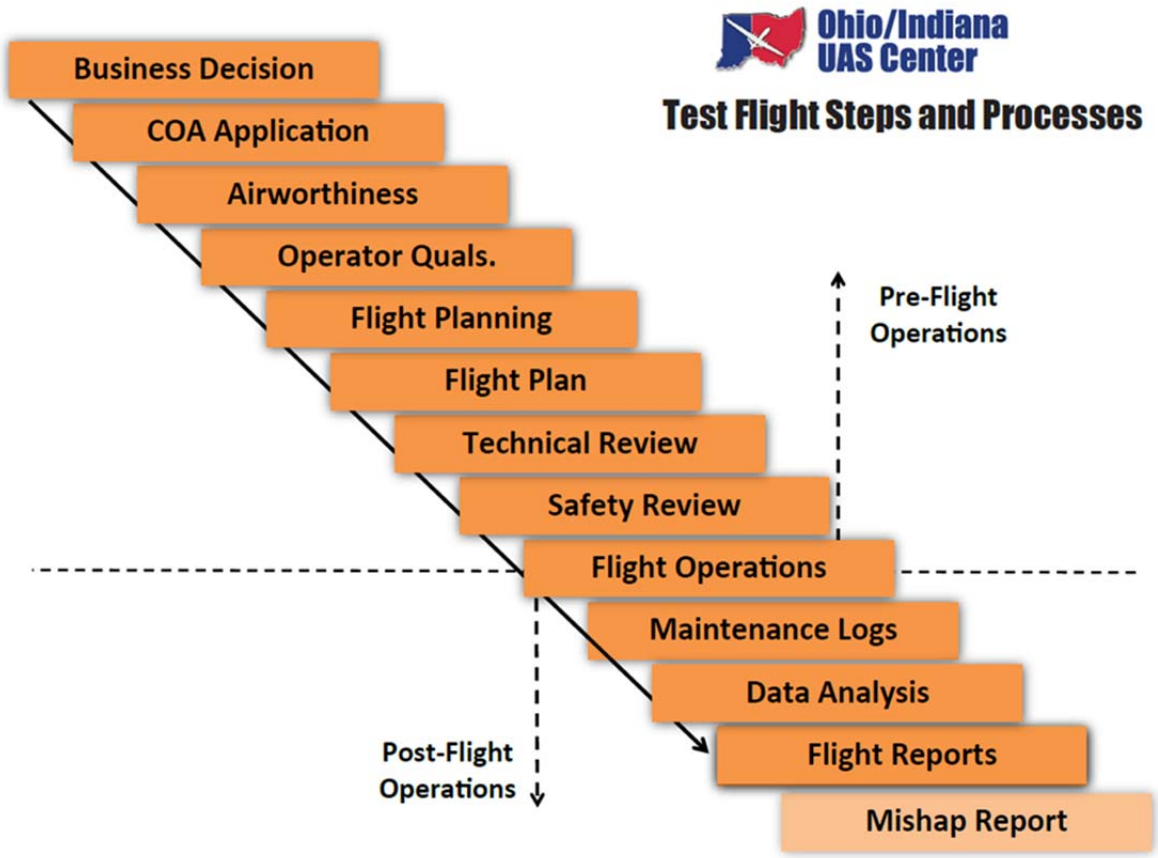

Figure 13. Ohio/Indiana UAS Center Test Flight Steps and Processes (*611*).

Utah Department of Transportation

Utah State University and Utah Water Research Lab completed an evaluation of UAVs for UDOT needs in 2012. The main focus of the project was to document construction as well as classification of wetland plan species. The primary objectives of the project were to use UAVs to capture high-resolution images of construction projects for monitoring and take digital images with the aim to classify wetland plant species. Several flights were conducted. Images were captured before, during, and after the completion of the Southern Parkway Highway, at the Utah Airport and the Utah Lake Wetlands. The results of the project were favorable and researchers concluded that UAVs as a tool had value for digital imagery, including roadway traffic conditions, and for use in wetland monitoring and mitigation permitting (*622*).

Virginia Department of Transportation

The National Consortium on Remote Sensing in Transportation, in cooperation with VDOT, demonstrated Airborne Data Acquisition Systems (ADASs) for real-time traffic surveillance, monitoring traffic incidents and signals, and environmental condition assessment of roadside areas (*633*). In August 2014, Virginia Tech announced that its unmanned aircraft test site was fully operational. UAV demonstrations were carried out on VDOT's Smart Road, a 2.2-mile section of limited access roadway used for testing new technologies (*644*).

Washington State Department of Transportation

WSDOT's collaboration with the University of Washington's Washington State Transportation Center in 2008 completed two test flights of specific UAVs: the MLB BAT (http://martinuav.com/uav-products/) and the Yamaha R-Max (http://rmax.yamaha-motor.com.au/industrial-use) (see Figure 14). The primary purpose of testing UAVs was to determine the feasibility of using UAV technology to control avalanches and capture images including traffic conditions (*499*).

Figure 14. The Yamaha R-Max (*499*).

West Virginia Division of Highways

West Virginia University researchers successfully demonstrated that UAVs can be a low-cost solution to providing a stable aerial platform for transportation use. The project funded jointly by the Mid-Atlantic Universities Transportation Center and the West Virginia Division of Highways utilized a fixed-wing aircraft to capture aerial images and develop georeferencing software (*655*).

SUBTASK 1.2. STATE-OF-THE-ART: ADVANCED VEHICLE TECHNOLOGIES

The primary objective of this subtask was to evaluate how connected and automated vehicle technologies, and highway infrastructure technologies in the connected and automated vehicle space can be leveraged to provide information related to highway infrastructure identification and inspection.

Advanced Vehicle Technologies

Developments in the automotive industry have brought about the introduction of new sensors into vehicles, both passenger and commercial, that could perhaps be used to fulfill at least some of the tasks performed by previously mentioned instrumented vans and provide the data needed by roads owners and operators. Many of these market-available vehicle technologies could potentially be used for asset management–related activities.

Given the main asset data that are required for an adequate asset management program, as shown in Table 1, it becomes apparent that researchers should consider and study only advanced vehicle applications that could detect and track certain assets and generate the required data. As a result, the following discussion investigates the advanced vehicle technologies that are deemed pertinent to this effort.

The automotive industry has witnessed dramatic improvements in recent decades. These advances have come in improved styling and aerodynamics, crashworthiness, power, and more. To a large extent, these improvements are owed to a vehicle's software and electronics that control almost every aspect of the vehicle functions, ranging from door locks, wipers, infotainment units, engine, brakes, lights, and so forth. To demonstrate the role of software and electronic components in today's vehicles, F-22 Raptor, the current U.S. Air Force frontline jet fighter, consists of about 1.7 million lines of software code or Boeing's new 787 Dreamliner requires about 6.5 million lines of software code, whereas an S-class Mercedes-Benz requires over 20 million lines of code (*666*). The same can be said for the number of computers or electronic control units (ECUs) that are in a car.

This increased rate of software and electronics being integrated into vehicles provided the opportunity for the automotive industry to use outward-looking sensors, in addition to many inward-looking sensors that monitor parameters like vehicle load, tire pressure, battery voltage, engine operation, and more. These outward-looking sensors' range (e.g., cameras, ultrasonics, radars, laser scanners, infrared cameras, IMUs, wheel encoders) are used to measure different parameters (e.g., as distance to objects and velocity of other vehicles around the immediate vicinity of the host vehicle) and provide input information for the vehicle to process. Many of these sensors are available today even on mid-priced vehicles, not only as an option, but in certain makes and models as standard equipment. Nevertheless, each sensor has unique strengths and weaknesses. Hence, each sensor (or a combination of) is suitable for certain application(s). Table 9 provides an overview of advantages for the main sensors used for ADAS applications.

Table 9. Advantages for Main Sensors Used for ADAS Applications.

Sensor	Main Advantages
Camera (Vision)	• Variable field of view (FOV), narrow to panoramic • High spatial resolution • Color data • Low unit volume costs • Passive/Non-emitting • Configurable for multiple applications
Radar	• Wide FOV • High range resolution • High reliability in adverse weather conditions • Functions over significant distances
Laser Scanner (LiDAR)	• Wide FOV with angular resolution • Ranging • High accuracy
Ultrasonic	• Suitable for short distances • Low unit volume costs
Thermal Cameras	• Passive/Non-emitting • High temperature resolution

Collectively, and individually, these sensors are used for specific applications. Many of these applications are driven by safety objectives, making the vehicle a safer mode of transportation for driver/passengers and other road users. That said, there are many other applications as well that are mostly concerned with comfort and convenience that use the same set of sensors. For instance, the same camera used for lane departure warning (LDW) can be used to adjust the suspension in a Mercedes-Benz (Magic Body Control), providing a smoother ride as the vehicle goes over obstacles and other road imperfections (see Figure 15).

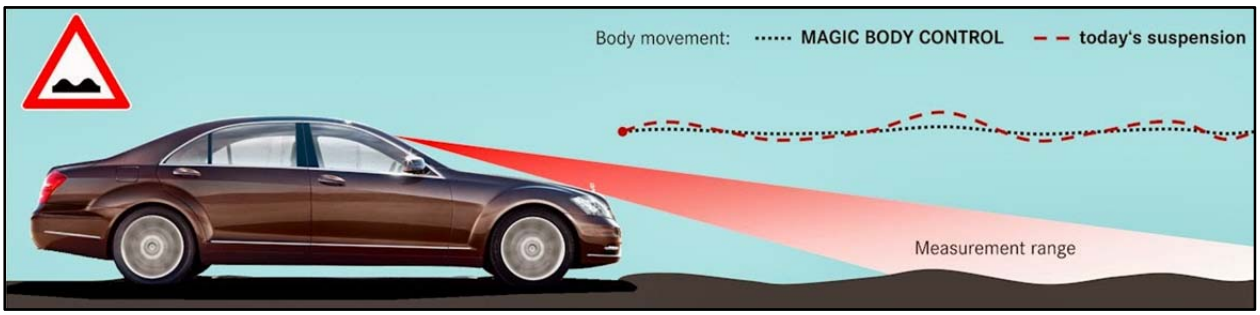

Figure 15. Magic Body Control (*677*).

Pertaining to safety applications, broadly referred to as ADAS, almost all sensors mentioned before are used (see Figure 16) to provide 360-degree awareness to the driver and vehicle system responsible for analyzing traffic situations and providing necessary actions (e.g., alerts and warnings, braking, steering). These sensors capture different information from the environment for processing and it is the objective of this study to evaluate the possibility of using the data/information generated by these sensors for asset management practice. Hence, it is important to distinguish what the highway assets are and what information is usually collected to enable proper maintenance and operation of these assets. Once the assets and pertinent

information are identified, suitable ADAS applications could be identified, fitting the objective of this research.

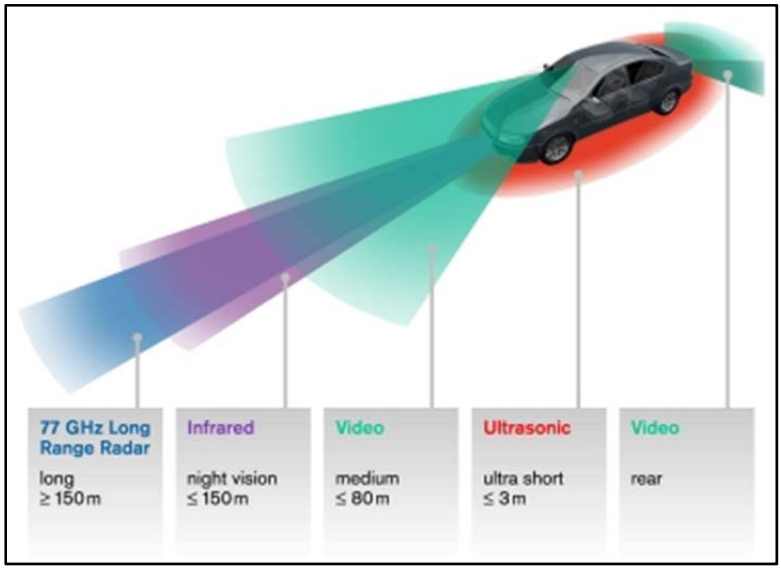

Figure 16. Typical Sensors Used For Environment Sensing (*68*).

Advanced Driver Assistance Systems

ADAS commonly refers to a collection of technologies that provide the driver with essential information and situational awareness, automate certain tasks, and ultimately assist drivers in the driving tasks. ADAS technologies and application are primarily focused on collision avoidance, and many of them have been around for decades with proven results in improving driving experience and better overall road safety.

There are many ADAS applications available in the market that could come as standard or optional on many vehicles. There are certain applications that can be obtained as an aftermarket solution for older model vehicles. Current ADAS applications are many, and the following list provides a rather comprehensive list of existing applications that can be obtained today ranging from mid-priced to luxury vehicles:

- Advanced emergency braking system.
- Collision avoidance system (forward collision warning).
- Lane keeping assist (LKA).
- Lane change assistance.
- Left turn assist.
- Adaptive cruise control.
- Adaptive light control.
- Automatic parallel parking.
- Night vision.
- Blind spot monitor/detection.
- Crosswind stabilization.

- Driver drowsiness detection.
- Driver monitoring system.
- Intersection assistant.
- Hill descent control.
- Intelligent speed adaptation or intelligent speed advice.
- Lane departure warning.
- Pedestrian protection system.
- Traffic sign recognition.
- Wrong-way driving warning.
- Traffic jam assist.

The applications listed above are in addition to technologies that have been in vehicles for decades. These range from anti-lock braking (ABS) and electronic stability control to electronic traction control. All these applications and technologies implemented in vehicles obtain and process data/information from the vehicle's internal sensors and components or the vehicle's surrounding. These data then will be processed internally and used to either perform an action controlling the vehicle (e.g., apply braking forces, provide differential steering, govern transmission) or provide information to the driver (e.g., engine warning light, low tire pressure, lane departure alert) However, except for certain situations, almost all these data/information are lost after necessary actions are performed and desirable outcome achieved.

After reviewing the literature and consulting with experts, the most promising applications that could be used by state DOTs and similar agencies for asset management appeared to be the following:

- Lane departure warning.
- Lane keeping assist.
- Traffic sign detection (TSD).

Researchers selected the above applications based on several criteria, including current availability to consumers, availability of aftermarket solutions, usefulness and value of data for asset management, and ease of transferring data. All three applications met the majority or all of the criteria and hence were selected for further investigation. There are several future applications that could fulfill the above criteria, but they were not selected given that they are not currently available to consumers today.

To distinguish and better understand the differences between the three applications (i.e., LDW, LKA, and TSD), the following descriptions are provided:

- **LDW** is a mechanism designed to warn a driver when the vehicle begins to move out of its lane (unless a turn signal is on in that direction) on freeways and arterial roads.
- **LKA** is a feature that, in addition to the lane departure warning system, can automatically take steps (differential braking or active steering) to ensure the vehicle stays within its lane.
- **TSD** is a driver support function that can be used to notify and warn the driver about restrictions or other information that may be effective on the current stretch of road.

Evident from the above descriptions, LDW and LKA are based on the same platform. The only difference is that after the lanes are detected, the LKA acts upon the information/situations to maintain the vehicle within the lanes. Given that these two applications are based on the same platform and the active interventions of the LKA does not relate to the scope of this project, only LDW is considered hereafter.

Lane Departure Warning and Vehicle Data

As previously mentioned, LDW is a mechanism designed to warn a driver when the vehicle begins to move out of its lane (unless a turn signal is on in that direction) on freeways and arterial roads. It is also deemed, in this effort, as a potential application that could be used in transportation asset management practices. This application (or technology) is enabled by advanced cameras, powerful image processors, and robust algorithms. One of the main reasons that cameras are the preferred sensor by car manufacturers for LDW, as opposed to LiDAR, is the price. Currently LiDARs and Flash LiDARs are not cost-effective to be used for LDW application, in spite of their superior performance in detecting pavement markings in normal and adverse lighting conditions. Table 10 compares the performance of cameras, radars, and LiDARs in adverse lighting conditions.

Table 10. Sensor Performance in Adverse Lighting Conditions.

Case	Camera	Radar	Flash LiDAR
Backlight	X	O	O
Bridge or Tunnel Entrance/Exit	X	O	O
Full Darkness	X	O	O
Reflective Rain Hiding Lane Markings	X	X	O
Dark Shadows or Low Contrast	X	O	O
Lane Detection in Medium Rain (Daylight)	O	X	D
X = Poor, D = Marginal, O = Good			

Given the affordability of cameras and considering that advisory/warning vehicle systems are more easily implemented than fully autonomous (or automated) control functions, machine vision algorithms proved popular in target detection and tracking (*699*). In the case of LDW, these algorithms must not only detect the lane itself, but extract other important data from the detected lanes. Double or continuous line boundaries separate the directions of traffic; discontinuous boundaries separate lane markings in the same direction; and merge-type markings (dense discontinuous markings) separate the road from the road-side parking area—these are only a few examples of such additional information that these algorithms need to provide for proper functionality of an LDW system (*70*). The algorithms should be able to interpret nuances within the region of interest. This includes dealing with strong shadows, misleading lines, obstacles, and more as demonstrated in Figure 17.

Figure 17. Lane Tracking Algorithms Showing the Estimated Lane Boundary against Shadows, Obstacles, and Misleading Markings (*71*).

Yet, as industry introduces more sophisticated ADAS applications with some degrees of autonomous (or automated) control, such as lane keeping/centering, collision avoidance, and overtaking and turning, they need additional information about each lane marking (*72*). Although lane position and type are sufficient for some applications, such as LDW, there are other applications that require lane-curvature information. For example, a collision-warning system can generate false alarms when the lane curvature is not known, as shown in Figure 18 (*73*).

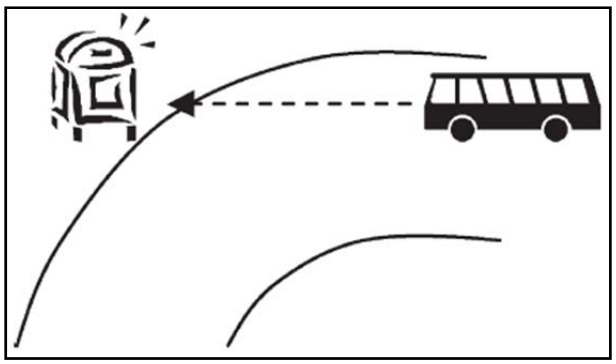

Figure 18. False Alarm Caused due to Lack of Lane-Curvature Data (*73*).

Given the number and complexity of data and information that needs to be detected and interpreted by the LDW system, it demonstrates the importance of processes and algorithms that process and derive this information. Investigating the lowest layer of LDW systems, the algorithms, researchers found that most developments have focused on performance of these algorithms with not much attention paid to the properties of the detected lane markings. Reliability of feature detection as a function of intrinsic marking properties, ambient lighting and weather conditions, and viewing geometry is an equally important aspect of algorithm performance, which must be explored if progress is to continue in this area of research. While detection methods have been shown to be effective in current LDW systems, many have only worked well with particular types of road markings or conditions (*74*).

Even in the testing regiment proposed for verification and validation of LDW, ISO 17361:2007 does not explicitly state the types of road markings that the system has to detect. However, the system has to be able to pass a series of performance tests. These are performed in a test location where the "lane markings are in good condition in accordance with the nationally defined visible lane markings." There are no requirements on the environmental conditions that the system must be capable of operating under. However, the performance testing must be carried out where the visibility range is greater than 1 km (*75*). A very similar approach is found in a National Highway Traffic Safety Administration LDW test procedure document, requiring high contrast and uniform pavement; lane marking specifications adhering to Manual on Uniform Traffic Control Devices (MUTCD) and considered in good conditions; and avoiding tests in inclement weather, including rain, fog, snow, hail, smoke, or ash (*76*).

Nevertheless, the reality of the road infrastructure may not necessarily follow the minimum performance requirements set by the abovementioned guidelines, especially when the tests, developments, and requirements are performed independent of intrinsic properties of lane markings. For example, worn yellow markings often have similar grayscale intensity to the road pixels (*73*), making detection a more challenging task. Or glare, caused by oncoming headlamps, bright sunlight (see Figure 19), or reflections can also cause the system to fail (*74*). Other examples include bright reflections caused by surface water, very faint lane markings, and zigzag lane markings were found to cause inaccurate readings (*74*), or some misdetection was caused by strong shadows created by overpasses, as shown in Figure 20 (*73*).

Figure 19. Challenges in Detecting Faded Lane Markings (*74*).

Figure 20. Misdetection Caused by Strong Shadows (*73*).

The performance of an image processing algorithm to detect road lane markings is also subject to a variety of factors such as (*77*):

- Viewing geometry that defines distance to the target area of the examined scene.
- Viewing angle with respect to horizontal to the target area (i.e., sun location).
- Lighting conditions (e.g., directness of illumination [clear vs. overcast vs. foggy]).
- Physical properties of the feature in the target area (e.g., intrinsic visual properties of the white/yellow stripe such as width and contrast, as described before).
- Environmental conditions (amount, rate, and type of precipitation) (*76*).

The above list is not comprehensive, but it covers the majority of the factors and demonstrates the importance to develop and evaluate the performance of algorithms while considering other criteria. Nevertheless, algorithms, regardless of their robustness, rely on the data they receive from cameras.

Automotive cameras are built to conform to a very stringent set of requirements. These requirements, especially for safety-critical applications such as LDW, have made many of the challenging scenarios mentioned before easier to overcome. The following lists some of these requirements:

- **Wide dynamic range** is a property required to guarantee performance under major disparities in ambient lighting. This requirement translates into the ability to accurately capture visual information in conditions such as approaching headlights, glare from other

vehicles, tunnel entrances and exits, and rising or setting sun. To accomplish this, it is necessary to reduce the exposure response time.

- **Signal to noise ratio** is a requirement to efficiently convert light to signal and produce minimum noise. This sensitivity helps the camera to yield a good signal to noise ratio and, thus, useable images, in environment with less light.
- **Near-infrared** sensitivity is required to provide better performance at night. This becomes especially relevant as NIR can also be projected by special headlights as an additional lighting source since it is invisible to the drivers' eyes.
- **Reliability** is an undeniable characteristic of any automotive part or component in order to withstand the harsh operating environment**.** Automotive parts, including cameras, should be manufactured and delivered under specific standards and guidelines to ensure a high level of product quality and reliability.
- **Competitive prices** are desired for automotive systems. This is accomplished by controlling the cost of the camera component itself, as well as designing the camera to enable lower costs in the overall system while balancing the other requirements mentioned.

Even with these stringent requirements and many advances that have been introduced to the automotive camera systems (e.g., High Dynamic Range CMOS cameras compared to CCD cameras), and improved algorithms for detection and recognition, lane marking detection is still a challenge.

This section provided a summary of how the LDW systems operate and what challenges are present in detecting the lane marking. This establishes adequate background information to determine if the data received from the vehicle's LDW system is sufficiently reliable to be used for asset management purposes. Despite all the challenges portrayed, review of the available literature and interactions with industry experts revealed the data can be sufficiently reliable. However, there is more research to be done to empirically establish the foundation of this statement.

LWD and Vehicle Data

For the purposes of this project in evaluating the possibility of using vehicles' onboard sensors and data for highway asset management, it was deemed necessary to study, at the meta-level, the applications stated above; evaluate different sensors that could fit into the objective of this study; and investigate the data generated by these systems/sensors. These activities resulted in the list of data elements shown in Table 11.

The data elements presented here are not all from the LDW system. Many are available from the vehicle itself (e.g., mileage or outside temperature) and other sensors, independent of the availability of the LDW system. Not all the data listed in this table are available from any given vehicle. These data are not standard in all vehicles, and some vehicle makes or models may have these data available through vehicle network and others may not.

Table 11. List of Potential Data Elements Available.

Data Type	Elements
Vehicle Data	vehicleType
	vehicleLength
	vehicleWidth
	vehicleHeight
	mileageValue
	transmissionMode
	lightState
	lightConditions
	wiperState
	driveWheelReference
	tireSlippageEvent
	crashDetectedEvent
	emergencyBrakingEvent
	electronicStabilityControlEvent
	antiLockBrakingSystemEvent
	externalAirTemperature
	externalAirTemperatureAccuracy_
	precipitation
	speedVector
	speedValue
	accelerationVector
	accelerationValue
	throttlePosition
	brakePosition
	steeringAngle
	yawRate
	pitchRate
	rollRate
Position	timeStamp
	interpolatedPoint
	longitude
	latitude
	altitude
	heading
	speed
	altitudeAccuracy
	horizontalAccuracy
	speedAccuracy
	headingAccuracy
	speedDetectionType
Forward Path and Lane Detection	curvature
	slope
	positionOffset
	laneBoundaryType
	laneBoundaryColor
	laneMarkerWidth

	laneMarkerWidthAccuracy
	laneDeclination
	laneDeclinationAccuracy
	laneBoundaryTypeConfidence
Sensors	sensorType
	sensorOffset
	sensorDirection
	sensorVerticalViewingAngle
	sensorHorizontalViewingAngle

In addition to the data elements in Table 11, which could be available through the vehicle network, there are other data elements that could be generated. These data elements are not necessarily accessible through the vehicle network nor are they always computed. These data are generated after detecting the stripe edges in an image and then computing measures that characterize the visual properties of the stripe. The data elements that can be computed are (*777*):

- Stripe width.
- Mean intensity of pixels inside the stripe edges.
- Standard deviation of the intensity of pixels inside the stripe edges.
- Mean intensity of pixels outside the stripe edge (i.e., pavement pixels).
- Standard deviation of the intensity of pavement pixels.
- Absolute contrast between the stripe and pavement (defined as the difference in means between the stripe pixel intensities and the pavement pixel intensities).
- Relative contrast between the stripe and pavement (defined as the difference in mean intensities of the stripe and pavement divided by the standard deviation of the stripe intensities).

Many of the data presented in the table and discussed above may not be accessible or available outside of the vehicle network; some of these data elements are considered proprietary by the vehicle manufacturers.

Future Technologies

The previous sections investigated the ADAS applications that are currently in the market and available to the consumer. The automotive industry is fast growing and fiercely competitive, which creates the necessity for innovation. To keep pace with ever-growing consumer demands for sophisticated new technologies, the automotive industry spent $102 billion in R&D activities in 2013—almost four times what was spent by the global aerospace and defense industry (i.e., roughly $25.5 billion) in the same year (*788*). Hence, it will not be farfetched to investigate potential technologies that could be introduced into the market in the near future.

Connected Vehicle

The connected vehicle technology refers to the use of two-way wireless communication technology that can be used as a platform in developing applications that address three broad domains: 1) safety, 2) environment, and 3) mobility. The U.S. Department of Transportation has spearheaded and championed this technology in collaboration with the automotive industry for

more than a decade, and the industry is now only a couple of years from a regulatory mandate, requiring all new vehicles to be equipped with this capability.

This technology uses dedicated short range communications (DSRC) in 5.9-GHz band dedicated to the transportation industry by the Federal Communications Commission. The issues, challenges, and opportunities in each of the three abovementioned domains can be addressed by establishing wireless links between vehicles (vehicle-to-vehicle [V2V]) and/or between vehicles and infrastructure (vehicle-to-infrastructure [V2I]). For instance, the majority of safety applications are concerned with V2V to create situational awareness for the driver. This is accomplished by every vehicle broadcasting its location, speed, heading, trajectory, brake status, etc., 10 times per second (10 Hz) so that other vehicles could listen to this broadcasted message and avoid the target vehicle if there is an imminent danger.

Broadcasting these messages, defined as a *basic safety message* or BSM, can also provide the opportunity of using vehicle data for asset management. Part 1 of the BSM contains the data elements (*799*) presented in Table 12. There is an overlap between the data elements presented before and the ones available through the BSM Part 1.

Table 12. Basic Safety Message, Part 1.

Data Type	Elements
Position	Latitude
	Longitude
	Elevation
	Positional accuracy
Motion	Transmission state
	Speed
	Heading
	Steering wheel angle
	Longitudinal acceleration
	Lateral acceleration
	Vertical acceleration
	Yaw rate
Brake System Status	Brake applied status
	Brake status not available
	Traction control state
	Anti-lock brake status
	Stability control status
	Brake boost applied
	Auxiliary brake status
Vehicle Size	Vehicle width
	Vehicle length

University of Michigan Transportation Research Institute, in partnership with the Michigan Department of Transportation, worked on a project with the objective to determine how in-vehicle systems can be leveraged for collecting roadway and weather data, reduce data-collection costs, increase travel information effectiveness, and improve the efficiency of asset management

processes. One aspect of this project involved monitoring onboard accelerometer data to measure road roughness (*80*). Figure 21 shows an example of this application. This effort closely resembles and validates the feasibility of using "position" and "motion" data elements from BSM for asset management purposes. In another effort, MDOT's internal inquiries from another department revealed that connected vehicle data can be used for a variety of practice areas that are of concern to a state DOT. The applications that could be enabled by using connected vehicle data in order to increase the efficiency and accuracy of concerned practice areas are demonstrated in Table 13.

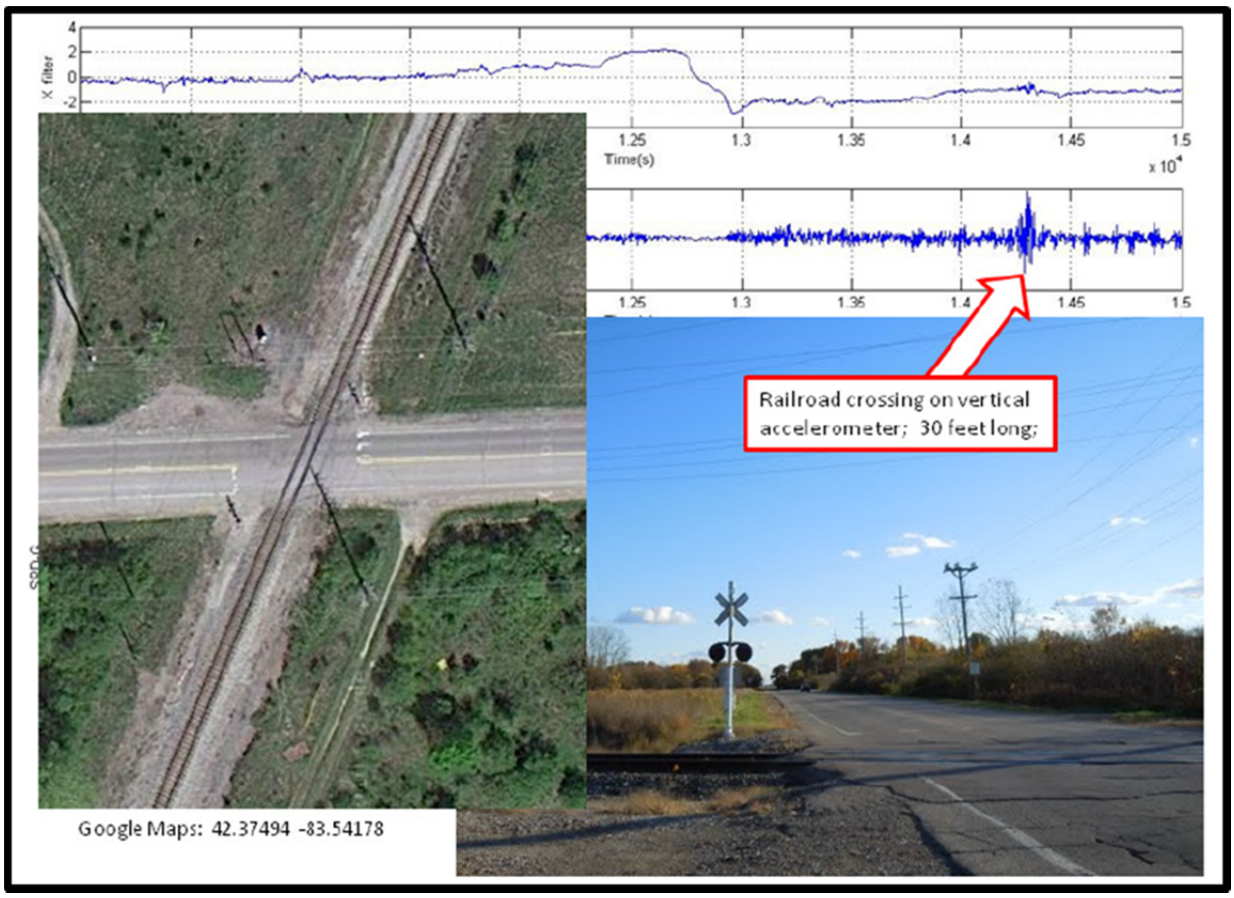

Figure 21. Use of Onboard Accelerometer Data to Measure Road Roughness (*80*).

Though there are some uncertainties as to when and how the connected vehicle technology will be deployed and at what rate (based on a federal mandate or voluntary industry adoption), most in the industry can agree on the implementation of the technology within the next five years. However, the current generation of connected vehicle data does not include data received from cameras and, as a result, does not support applications related to lane marking detection.

Table 13. Potential Applications Enabled by Connected Vehicle Data (*80*).

Planning & Asset Management	Design	Construction	Maintenance	Operations
Potential Applications to Enhance Performance Management and Data Sharing				
Pavement Conditions • **IRI** • **PASER sufficiency ratings** • **Accelerometry**	**Pavement Conditions** • Measure rutting (traction control?) • Pavement roughness vs fuel consumption	**Pavement Performance Correlation with Environment** • Long-term pavement performance and cracking • Tracking pavement conditions for verification of reported vehicle damage • Cure time on environmental conditions • Trending data for cost/benefit analysis	**Pavement Conditions** • Friction • Ride quality • Defect type and location • IRI PASER • Accelerometry	**Pavement Conditions** • Ice forming • Tracking pavement conditions for verification of reported vehicle damage • Friction • Markings • Load restrictions • Subsurface impact
Traffic Planning • **Volume distribution** • **Volume growth** • **Congestion relied** • **Roadway system planning**	**Intelligent Construction** **Probes for Comprehensive As-Builts** • Determine actual subgrade compaction state • Environmental conditions at time of placement	**Weather/Environmental Information** • Monitoring weather parameters • Frost depth • Best paving conditions monitoring • Work conditions monitoring (i.e., rain delays) • Greenhouse gas emissions	**Weather** • Winter weather maintenance o Response times o Analyzing and tracking weather systems o Winter maintenance activities • General year-round maintenance	**Traffic Management** • Volume • Occupancy • Speed • Travel time • Seasonal volume changes • Route guidance • Incident notification • User delay cost
Highway Performance Monitoring System and TMS • **Asset location** • **Current condition** • **System performance**	**Weather Stations** • Ongoing environmental monitoring • Impact on life of pavement • Rate of degradation of pavement • Winter weather maintenance	**Work Zone** • Traffic conditions, i.e., speed, volume, queue lengths • Lane departures • Worker safety • Monitor when active	**Incident Management** • Time of occurrence • Pinpoint locations • Damage tracking on infrastructure • Time to repair • Damage log • High incident locations	**Incident Management** • Incident report • First responders' times • First responders' guidance • Incident locations • High incident locations • User delay cost
Reporting • **Volume** • **Speed** • **Occupancy** • **Classification** • **Travel time** • **Origin and destination planning**	**Mechanistic Empirical Pavement Design** • Weather impact • Fixed station placement	**Site Monitoring** • Real time site monitoring • Utility location for construction equipment (DSRC), i.e., overhead power lines • High precision as-built mapping	**Signals** • Cost to operate • Phase analysis • Volume • Incident analysis o Vehicle location o Signal phasing o Signal delay	**Weather Management** • Treatment status • Driving conditions status
Counts Path • **Pedestrian** • **Bicycle**	**Traffic Monitoring** • Impact of traffic on pavement over time • Classification, load cell	**Contractor Management** • Conditions of temporary pavement (ride quality) • Monitor road/lane closures • Work progress for incentive payments	**Rest Areas** • Vehicles pulling in • Time spent • Parking availability	
Truck Tracking • **Freight** • **Light**		**Topological Analysis** • Channel system migration • Land erosions • Water levels		

LiDAR-Based ADAS Applications

As discussed, advanced driver assistance systems are becoming available on more vehicles, at more affordable prices. This increased rate of adoption is coupled with an increasing level of functionality and complexity of ADAS applications. To reliably perform more complex tasks and maneuvers, ADAS applications coming to the market in the near future need to rely on more sensory information received from their environment and provide redundancy in measuring different factors (e.g., distance). These requirements introduce the need for more robust and accurate sensors, one of which is LiDAR. Though LiDARs are not currently widely adopted by the automotive industry, their use in future ADAS applications and automated driving systems is only a matter of time and affordability.

The LIDAR operates based on the time-of-flight principle and can measure the 3-D structure of the vehicle's surrounding environment. LIDARs can not only provide a good measure of distance, but the majority can also report reflected intensity as well, providing a substitute to a visual camera. LiDAR, however, has the added advantage of being an active light source and, thus, independent of natural light issues. This specifically helps in coping with shadows and darkness and night operations (*811*).

This distinction and ability to perform independent of light source is due to the fact that LiDAR-based lane detection senses the lane markings based on increased reflectivity of the lane markings when compared to the road. Cameras, on the other hand, detect lane markings by distinguishing the edges of the lane markings in the image (*822*).

Though LiDAR provides a robust and accurate measurement of its surrounding, it appears that cameras provide slightly more accurate measurements than LiDARs while having a decrease in detection rate. Also, cameras perform well in the rain, where LiDARs experienced decreased detection rates (*822*). These offsetting properties of LiDARs and cameras, among other reasons, lead to a combined and complementary implementation of these two sensors to increase reliability and robustness of detection tasks. Examples of this complementary strength can be seen in Figure 22 where even the right lane, which is occluded in the video image, is detected by LiDAR (*833*).

While using LiDAR in order to enable ADAS applications or automated driving is not a ubiquitous practice for the automotive consumer yet, the transportation asset management industry has been using mobile mapping units equipped with LiDAR for a while now, making this technology a more familiar topic for the road owners and operators. That in itself validates the feasibility of using future LiDAR units on board passenger or commercial vehicles for asset management purposes, and more specifically monitoring the state and condition of lane markings.

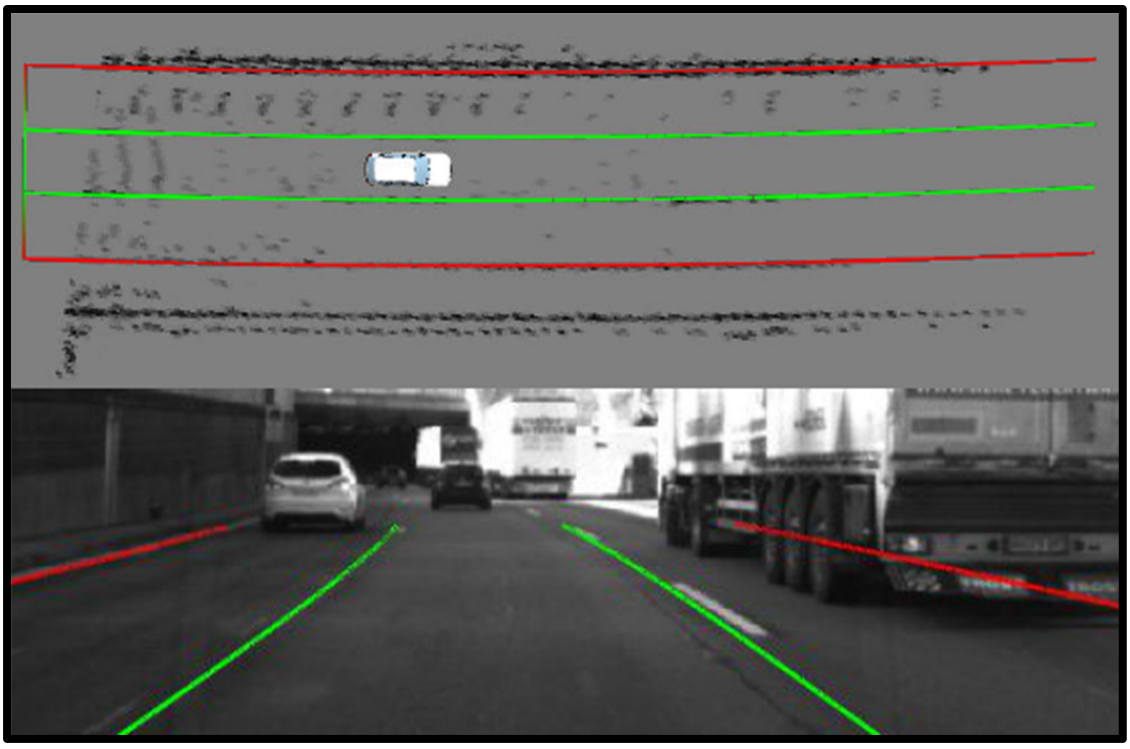

Figure 22. Example of Robust Lane Detection by Using LiDAR (*833*).

SUBTASK 1.3. DETAILED ASSESSMENT OF SELECTED AGENCIES AND/OR TECHNOLOGIES

The primary objective of this subtask was to assess whether information beyond the existing literature needs to be gathered from agencies or technology owners to obtain more detailed data. Researchers on this project attended the Society of Automotive Engineers World Congress & Exhibition 2015. This venue provided the opportunity to exchange ideas and interact with automotive experts from manufacturers such as Honda, Quanergy, Hyundai-Kia, Ricardo, and Bosch. Also, the Automated Vehicles Summit in Ann Arbor was another opportunity where the researchers had the opportunity to chair two breakout sessions and discuss the latest technologies with attendees from both academia and the automotive industry. Most technology was confirmed in the literature. Other information was deemed proprietary and not openly discussed.

CONCLUSIONS

State DOTs and other road owners and operators spend a significant amount of resources to monitor, measure, and manage the condition or road assets every year. This is usually performed by either internal staff or contractors and by driving on the road network—usually thousands of miles—while often visually inspecting the conditions of the road surface, lane markings, etc. As expected, these visual inspections can be fairly subjective as they are based on the opinion of the individual who is performing the inspection task. This task explored many of the challenges that are faced by vision-based LDW systems and the possibility of using the data captured by these systems for tracking and monitoring the conditions of lane markings as vehicles traverse the roads. The premise of this technology for the asset management practice is to not only reduce the

amount of resources required for asset management, but also increase the frequency and reliability of current practices, by providing data streams from many vehicles that travel through any specific stretch of road.

Based on what the researchers learned in this effort, the technical feasibility of using LDW to measure and monitor the conditions of road markings is well within the realm of possibilities. Vehicles equipped with the LDW technology can measure and capture a variety of data elements (e.g., position, time, heading, lighting conditions, weather conditions, confidence in lane detection, and type of lane) that can be combined together and create a map of the road network where the status of lane marking conditions can be displayed (see Figure 23). Should a vehicle have difficulty in detecting lane markings (for instance, lane marking detection confidence of 0.5 or less), it can transmit these data, combined with other pertinent data points, to the relevant authority or a third party where it can be combined with data points received from other vehicles that encountered the same condition.

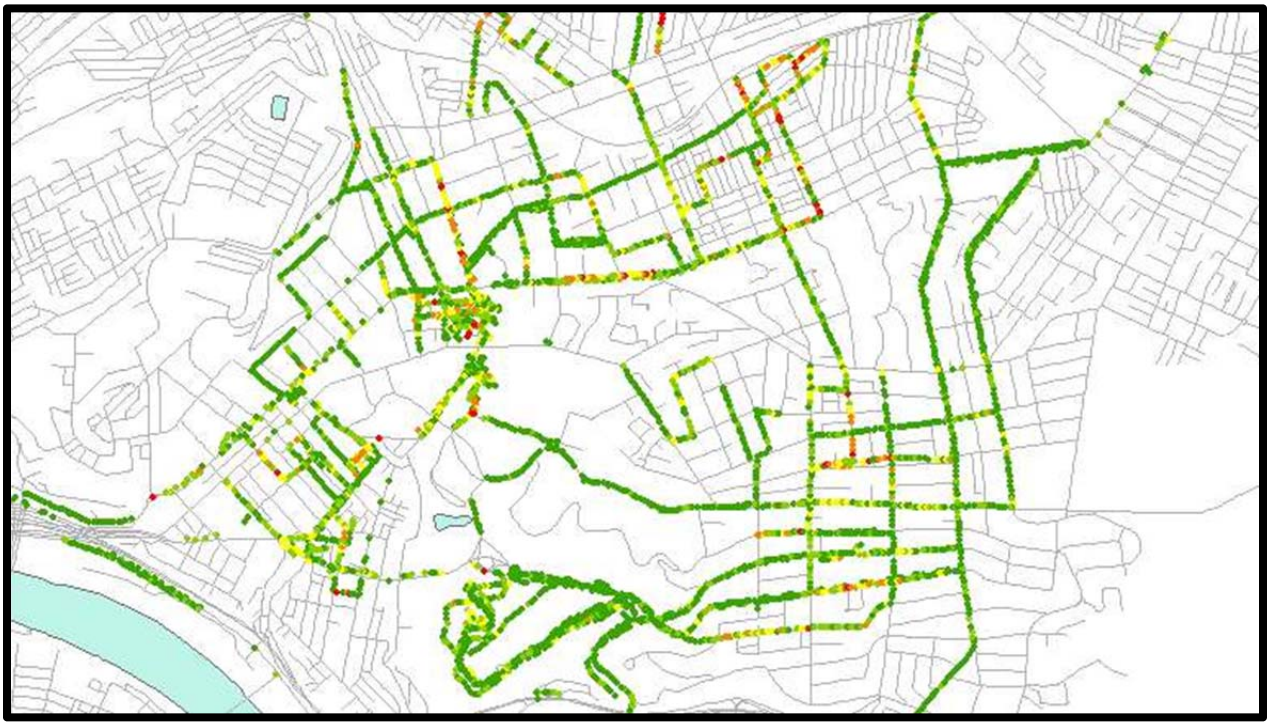

Figure 23. Hypothetical Map of a Road Network with Poor Lane Markings.

However, while this concept is technically feasible there are challenges and questions that needs be further investigated. The list of more critical questions is as follow:

1. **Standards**: OEMs use LDW systems that are developed by different suppliers and developers. While one supplier may use certain criteria to define what an acceptable level of confidence is in detecting a lane, another supplier may use a different criteria or threshold to investigate the same. Hence, there are no standards in defining what is the acceptable threshold in detecting what is lane marking and what is not.

2. **Interoperability**: For a state DOT or other responsible parties to analyze and interpret the data received from the LDW systems, they would need to know different information about what data elements they are receiving, such as data format, measurement unit, and more. Current practices in the automotive industry related to the LDW are not deemed suitable as each developer and OEM may choose a different approach in defining its data elements.

3. **Adoption Rate**: In 2013, only 1 percent of new vehicles had LDW as standard feature and 19 percent of new vehicles had this as an optional feature, and it will not be until 2044 that 95 percent of all registered vehicles will have LDW as standard or optional (*844*). While the current market penetration rate of LDW systems could not be found under this effort, it will be prudent to assume it will be at least a decade before it reaches 50 percent of the U.S. market. Higher market penetration rate can make more data points available at least on roads most travelled and increase the accuracy and reliability of measurements that are based on data received from the LDW systems (see Figure 24).

4. **Consumer Acceptance**: Availability of LDW system, either as standard or optional, does not necessarily translate to user acceptance. For instance, it was found that less than 17 percent of owners driving a 2009 Infiniti model or 2013 Toyota model had always had the system "ON," whereas the rest were using the system only "Sometimes" or "Never" (*855*). In order for such system to be used for asset management, consumers need to keep the system "ON" at all times, otherwise data will not be captured nor transmitted.

5. **Business Case**: Assuming all the above questions are addressed and challenges overcome, transmitting the LDW data requires a business case for the OEMs—and possibly the consumer—in order to justify building and providing the communication infrastructure and other subsystems to reliably make this information available. The business case in conjunction with technical requirements will influence what data, how frequent, and how (among other factors) it should/will be transmitted to benefit all parties involved. Absence of a working business model may lead to resistance from the cost-sensitive automotive industry.

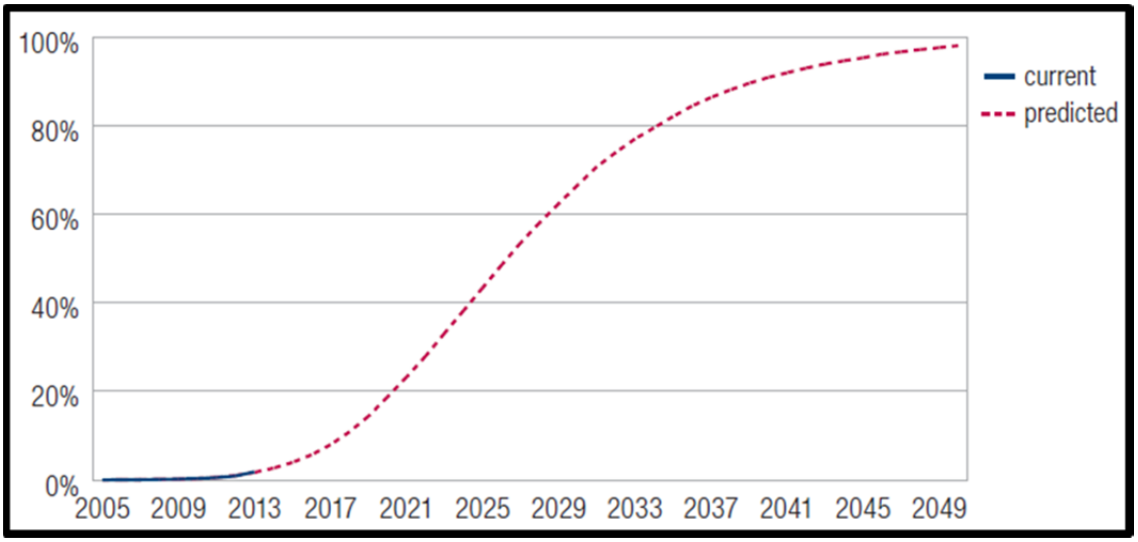

Figure 24. Predicted Percentage of Registered Vehicles with Lane Departure Warning.

Ancillary Findings

Findings from the literature review and interactions with the industry revealed that there is an overall lack of methodologies to evaluate the reliability of vision-based lane detection as a function of environmental conditions in vision-based LDW systems (*776*). Most efforts in evaluating the performance of lane marking detection systems that are available in the public domain have emphasized accuracy of recovered geometry rather than reliability of feature extraction. This is a critical research gap for different groups for the following reasons (*776*):

- Developer Community.
  - To determine performance limitations of an algorithm.
  - To test if solutions to existing known problems actually worked.
- Policy Makers.
  - To determine the suitability to deploy an algorithm.
  - To decide between competing algorithms.
- Infrastructure Owners/Operators.
  - To determine what part of the road needs repainting and to what specifications.

The relatively limited performance of cameras and the lack of reliable evaluation methodologies to detect lane markings in adverse lighting conditions has increased the importance of improving the quality and availability of lane markings. The importance of this proposition is realized by the European Union (EU). They reviewed existing national practices and available research, and also conducted industry discussions that included representatives from consumer associations, safety organizations, vehicle manufacturers, and sign and marking industries. What they found was that the combination of inadequate maintenance of roads and differences in national regulations for road markings and traffic signs across Europe was a major obstacle to the effective implementation of ADAS technologies, specifically LDW/LKA and TSR (*866*).

This effort conducted by the European Road Assessment Programme (EuroRAP) concluded that the road markings on Europe's roads should adopt a simple 150 × 150 standard. This indicates that the lane and edge markings should be a consistent 150 mm wide, and these markings should reflect light at 150 millicandela (formally 150 mcd/lux/m²) under dry conditions (*866*).

Future Work

Given that the background research related to the EuroRAP study has not been made available and there are major differences between road markings in the United States and the EU, a similar research should be carried out to determine minimum width and retroreflectivity properties of lane markings to increase the detection rate by LDW/LKA systems while maintaining (or improving) the detection rate of lane markings by the human driver.

Also, it is highly recommended to study and establish evaluation criteria to measure the reliability of LDW systems to detect the lane markings as a function of environmental conditions (e.g., low angle sun, wet surface, low visibility [e.g., fog], lane width, and worn-out markings,).

REFERENCES

1. L. Zongzhi and K. Sinha. *Multicriteria Highway Programming Incorporating Risk and Uncertainty: A Methodology for Highway Asset Management System.* Indiana Department of Transportation, Indianapolis, 2004.

2. Mandli Communications (Mandli). http://www.mandli.com/. Accessed June 3, 2015.

3. T. Ahlborn, R. Shuchman, L. Sutter, D. Harris, C. Brooks, and J. Burns. *Bridge Condition Assessment Using Remote Sensors, Volume I of II—Main Body*. U.S. Department of Transportation Research and Innovative Technology Administration, Michigan Technological University, Houghton, 2013. http://mtri.org/bridgecondition/VolumeI-MainBody.pdf.

4. K. Maser. Automated Systems for Infrastructure Condition Assessment. *Journal of Infrastructure Systems© ASCE*, Sept. 2005, p. 153.

5. Center for Automotive Research. *Pavement Condition Monitoring with Connected Vehicle Data.* Michigan Department of Transportation, Ann Arbor, 2013.

6. J. Morgan. A Simple Explanation of the 'Internet of Things.' Forbes, May 13, 2014. http://www.forbes.com/sites/jacobmorgan/2014/05/13/simple-explanation-internet-things-that-anyone-can-understand/. Accessed September 29. 2015.

7. A. Kemper, A. Scholz, C. Winkler, and T. Kothmayr. *The "Internet of Things" for Industrial Applications*. Technische Universität München, 2015. http://www-db.in.tum.de/teaching/ws1314/industrialIoT/?lang=en.

8. E. Dennis, R. Wallace, and B. Reed. *Cloudsourcing Transportation Systems Data.* Michigan Department of Transportation, Lansing, 2015.

https://www.michigan.gov/documents/mdot/02-14-2015_Crowd_Sourced_Mobile_Applications_483062_7.pdf.

9. L. Mixon, J. Garrett, and B. Krueger. *Vehicle Infrastructure Integration (VII) Data Use Analysis and Processing—Project Summary Report*. Michigan Department of Transportation, Lansing, 2012. https://www.michigan.gov/documents/mdot/08-31-2012_VII_DUAP_Project_Summary_Report_444701_7.pdf.

10. M. Olsen, J. Raugust, and G. Roe. *NCHRP Report 446: Use of Advanced Geospatial Data, Tools, Technologies, and Information in Department of Transportation Projects.* Transportation Research Board, National Research Council, Washington, D.C., 2013. http://onlinepubs.trb.org/onlinepubs/nchrp/nchrp_syn_446.pdf.

11. J. Chang, M. K. Tsai, D. Findley, and C. Cunningham. *Infrastructure Investment Protection with LiDAR.* Institute for Transportation Research and Education, North Carolina State University, Raleigh, 2012. http://www.ncdot.gov/doh/preconstruct/tpb/research/download/2012-15finalreport.pdf.

12. L. Zhou and G. Vosselman. Mapping Curbstones in Airborne and Mobile Laser Scanning Data. *International Journal of Applied Earth Observation and Geoinformation,* Vol. 18, Aug. 2012, pp. 293–304. https://www.infona.pl/resource/bwmeta1.element.elsevier-5be369e3-0751-3a7b-84df-6cd885c955a0.

13. H. Zhou, M. Jalayer, J. Gong, S. Hu, and M. Grinter. *Investigation of Methods and Approaches for Collecting and Recording Highway Inventory Data*. Research Report FHWA-ICT-13-022. Illinois Center for Transportation, 2013. Accessed at https://apps.ict.illinois.edu/projects/getfile.asp?id=3166.

14. K. Yen, B. Ravani, and T. Lasky. *LiDAR for Data Efficiency*. Research Report WA-RD 778.1. Washington State Department of Transportation, Olympia, 2011. http://www.wsdot.wa.gov/research/reports/fullreports/778.1.pdf.

15. Ayres Associates website. Geospatial Services. http://www.ayresassociates.com/services/geospatial/.

16. Mandli Communications, Inc. website. Mandli's Integrated LiDAR System. Oct. 2011. http://www.mandli.com/mandlis-integrated-lidar-system.

17. NM Group website. Surveying and Mapping. http://www.nmgroup.com/en/services/surveying-and-mapping/.

18. C. B. Young. *Assessing LiDAR Elevation Data for KDOT Applications*. Report No. K-TRAN: KU-10-8. Kansas Department of Transportation, Lawrence, Kansas, 2013. ftp://ftp.mdt.mt.gov/research/OTHER/AERIAL_PHOTO/LITERATURE/YOUNG_ASSESSING_LIDAR_KDOT_2013.PDF.

19. Dye Management Group, Inc. (DMG). *Monitoring Highway Assets with Remote Technology*. Final Report RC-1607. Michigan Department of Transportation, Lansing, 2014. http://www.michigan.gov/documents/mdot/RC-1607_466453_7.pdf.

20. W. Uddin. Transportation Management: LiDAR, Satellite Imagery Expedite Infrastructure Planning. *Earth Imaging Journal*, March 2014. http://eijournal.com/print/articles/lidar-showcase-state-of-the-industry-transportation-management.

21. M. Olsen, G. Roe, C. Glennie, F. Persi, M. Reedy, D. Hurwitz, K. Williams, H. Tuss, A. Squellati, and M. Knodler. *NCHRP Report 748: Guidelines for the Use of Mobile LIDAR in Transportation Applications*. Transportation Research Board of the National Academies, Washington, D.C., 2013. Accessed at http://onlinepubs.trb.org/onlinepubs/nchrp/nchrp_rpt_748.pdf.

22. L. Mattke and G. Sulijoadikusumo. *LiDAR Collection and Integration for the Hawaii DOT*. Mandli Communications, Inc.; GIS-T 2010; Hawaii Department of Transportation, 2010. http://www.gis-t.org/files/B2iCO.pdf.

23. FORUM8. *Integration of Point Cloud Data and Photo-Log Images of Highways within VR-Design Studio (UC-win/Road)*. Users Report, Vol. 107. Hawaii Department of Transportation, Honolulu. http://www.forum8.co.jp/user/user107-e.htm.

24. B. Rister, L. McIntosh, and J. Whelan. *Utilization of Mobile LiDAR to Verify Bridge Clearance Heights on the Western Kentucky Parkway*. Report KTC13-09. University of Kentucky, Kentucky Transportation Cabinet, Lexington, 2013. http://www.ktc.uky.edu/projects/utilization-of-mobile-lidar-to-verify-bridge-clearance-heights-on-the-western-kentucky-parkway/

25. T. Ahlborn, R. Shuchman, L. Sutter, D. Harris, C. Brooks, and J. Burns. *Bridge Condition Assessment Using Remote Sensors, Volume II of II – Appendices*. U.S. Department of Transportation Research and Innovative Technology Administration; Center for Automotive Research, Michigan Department of Transportation; Michigan Technological University, Houghton, 2013. http://mtri.org/bridgecondition/VolumeII-Appendices.pdf.

26. R. Vincent and M. Ecker. *Light Detection and Ranging (LiDAR) Technology Evaluation.* Final Report TR10-007. Missouri Department of Transportation, 2010. ftp://ftp.mdt.mt.gov/research/OTHER/AERIAL_PHOTO/LITERATURE/SANBORN_LIDAR_TECH_EVAL_2010.pdf.

27. P. Ellsworth. *Utah DOT Leveraging LiDAR for Asset Management Leap*. Utah Department of Transportation blog, Feb. 25, 2013. http://blog.udot.utah.gov/2013/02/utah-dot-leveraging-lidar-for-asset-management-leap/.

28. C. G. Howerton and D. Sideris. *A Study of Implementation of IP-S2 Mobile Mapping Technology for Highway Asset Condition Assessment.* MS thesis. Virginia Polytechnic Institute and State University, Blacksburg, 2010. http://www.champs.eng.vt.edu/docs/research/HowertonSideris%20P&R%20Final%20Report.pdf.

29. Location and Design Division. *Commonwealth of Virginia Survey Manual, Chapter 5 Photogrammetric Surveys*. Virginia Department of Transportation, Richmond, 2009 (revised July 2015). http://www.virginiadot.org/business/resources/LocDes/SurveyManual/Chapter_5a-2014x.pdf.

30. D. Wright. *Investigation into the Potential of LiDAR to Support Traffic Speed Asset Measurement and Assessment.* Transport Research Laboratory, UK, 2014. http://www.trl.co.uk/reports-publications/report/?reportid=6994.

31. Oregon State University. *Infrared Thermography*. Marine Mammal Institute, Hatfield Marine Science Center, Newport, 2015. http://mmi.oregonstate.edu/infrared-thermography.

32. GIS Geography. *Multispectral vs Hyperspectral Imagery Explained*. 2015. http://gisgeography.com/multispectral-vs-hyperspectral-imagery-explained/.

33. T. Hakala, O. Nevalainen, S. Kaasalainen, and R. Mäkipää. Technical Note: Multispectral LIDAR Time Series of Pine Canopy Chlorophyll Content. *Biosciences*, Vol. 12, 2015, pp. 1629–1634. http://www.biogeosciences.net/12/1629/2015/.

34. M. Loken. *Use of Ground Penetrating Radar to Evaluate Minnesota Roads*. Report MN/RC-2007-01. Minnesota Department of Transportation, St. Paul, 2007. http://dotapp7.dot.state.mn.us/ResearchTracking/pdf/200701.pdf.

35. W. Uddin. *Ground Penetrating Radar Study—Phase I Technology Review and Evaluation.* University of Mississippi, Center for Advanced Infrastructure Technology, University, Miss., 2006. http://mdot.ms.gov/documents/research/Reports/Interim%20and%20Final%20Reports/State%20Study%20182%20-%20Ground%20Penetrating%20Radar%20Study%20Technology%20Review%20and%20Evaluation%20(Phase%20I).pdf.

36. S. Sebesta, T. Scullion, and T. Saarenketo. *SHRP 2 Report S2-R06C-RR-1: Using Infrared and High-Speed Ground-Penetrating Radar for Uniformity Measurements on New HMA Layers.* Transportation Research Board of the National Academies, 2013. http://onlinepubs.trb.org/onlinepubs/shrp2/SHRP2prepubR06C.pdf.

37. W. Liu and T. Scullion. *PAVECHECK: Integrating Deflection and Ground Penetrating Radar Data for Pavement Evaluation*. Report FHWA/TX-06/0-4495-1. Texas Transportation Institute, College Station, 2006. http://d2dtl5nnlpfr0r.cloudfront.net/tti.tamu.edu/documents/0-4495-1.pdf.

38. A. Nazef. *MIT Scan-T2 A Device for Concrete Pavement Thickness Measurement*. Presented at 2013 Construction Conference, Orlando, Florida, 2013. https://www.kesslerdcp.com/images/phocadownload/PDF-Documents/022013ConstructionConferenceFlorida.pdf

39. Public Works and Government Services Canada. *Thermography-Infrared (IR) Thermographic Investigation.* http://www.tpsgc-pwgsc.gc.ca/biens-property/sngp-npms/bi-rp/tech/ir-eng.html. Accessed September 29, 2015.

40. Nippon Avionics Co., Ltd. What is Infrared Thermography? 2015. http://www.infrared.avio.co.jp/en/products/ir-thermo/what-thermo.html.

41. S. Sharp and C. Ozyildirim. *Nondestructive Measurements Using Mechanical Waves in Reinforced Concrete Structures*. Final Report FHWA/VCTIR 14-R8. Virginia Center for Transportation Innovation and Research, Charlottesville, 2014. http://www.virginiadot.org/vtrc/main/online_reports/pdf/14-r8.pdf.

42. Missouri Department of Transportation. Field Testing Hand-Held Thermographic Inspection Te*chnologies Phase II*. http://www.pooledfund.org/Details/Study/475. Accessed 9-3-2015.

43. M. Lim and H. Cao. Combining Multiple NDT Methods to Improve Testing Effectiveness. *Construction and Building Materials*, Vol. 38, Jan. 2013, pp. 1310–1315. http://www.sciencedirect.com/science/article/pii/S0950061811000274.

44. K. Hoegh, L. Khazanovich, and H. Yu. Ultrasonic Tomography for Evaluation of Concrete Pavements. In *Transportation Research Record: Journal of the Transportation Research Board, No. 2232.* Transportation Research Board of the National Academies, Washington, D.C., pp. 85–94.

45. Federal Aviation Administration. *Integration of Civil Unmanned Aircraft Systems (UAS) in the National Airspace System (NAS) Roadmap*. U.S. Department of Transportation, 2013. https://www.faa.gov/uas/media/UAS_Roadmap_2013.pdf.

46. Federal Aviation Administration. Unmanned Aircraft Systems (UAS) Frequently Asked Questions. 2015. https://www.faa.gov/uas/faq/#qn1.

47. US Government Accountability Office. *Unmanned Aerial Systems: FAA Continues Progress toward Integration into the National Airspace.* Report to Congressional Committees, July 2015. http://www.gao.gov/assets/680/671469.pdf.

48. Aerospace Industries Association. *Unmanned Aircraft Systems: Perceptions & Potential.* 2013. http://www.aia-aerospace.org/assets/AIA_UAS_Report_small.pdf.

49. E. D. McCormack. *The Use of Small Unmanned Aircraft by the Washington State Department of Transportation*. Washington State Department of Transportation, Olympia, 2008. http://www.wsdot.wa.gov/research/reports/fullreports/703.1.pdf.

50. Federal Aviation Administration. *Small UAS Notice of Proposed Rulemaking (NPRM)*. 2015. https://www.faa.gov/uas/nprm/.

51. W. Hart and N. Gharaibeh. *Use of Micro Unmanned Aerial Vehicles for Roadside Condition Assessment.* Southwest Region University Transportation Center, College Station, Texas, 2010.

http://d2dtl5nnlpfr0r.cloudfront.net/swutc.tamu.edu/publications/technicalreports/476660-00019-1.pdf.

52. Unmanned Aerial Vehicle Systems Association. *Advantages of UAS*. 2015. https://www.uavs.org/advantages.

53. R. Williams. *2014 State Unmanned Aircraft Systems (UAS) Legislation.* National Conference of State Legislatures, 2014. http://www.ncsl.org/research/civil-and-criminal-justice/2014-state-unmanned-aircraft-systems-uas-legislation.aspx.

54. Caltrans. *The Use of Unmanned Aerial Systems for Steep Terrain Investigations.* Caltrans Division of Engineering Services, Geotechnical Services, California Department of Transportation, 2014. http://www.dot.ca.gov/newtech/researchreports/preliminary_investigations/docs/unmanned_aerial_systems_preliminary_investigation_rev8-14-14.pdf.

55. H. A. Latchman, T. Wong, J. Shea, J. McNair, M. Fang, K. Courage, D. Bloomquist, and I. Li. *Airborne Traffic Surveillance Systems: Proof of Concept Study.* University of Florida; Florida Department of Transportation, Gainesville, 2005. http://www.dot.state.fl.us/research-center/completed_proj/summary_te/fdot_bc354_86_rpt.pdf.

56. J. Irizarry and E. N. Johnson. *Feasibility Study to Determine the Economic and Operational Benefits of Utilizing Unmanned Aerial Vehicles (UAVs)*. Report No. FHWA-GA-1H-12-38. Georgia Institute of Technology; Georgia Department of Transportation, Forest Park, 2014. https://smartech.gatech.edu/bitstream/handle/1853/52810/FHWA-GA-1H-12-38.pdf.

57. C. Brooks, R. Dobson, D. Banach, D. Dean, T. Oommen, R. Wolf, T. Havens, T. Ahlborn, and B. Hart. *Evaluating the Use of Unmanned Aerial Vehicles for Transportation Purposes*. Final Report, No. RC-1616. Michigan Department of Transportation, Lansing, 2015. http://www.michigan.gov/mdot/0,4616,7-151-9622_11045_24249_52176-353767--,00.html.

58. C. Estes. *Unmanned Aircraft in North Carolina: Report to the Joint Legislative Oversight Committee on Information Technology and Transportation Oversight Committee.* 2014. http://digital.ncdcr.gov/cdm/ref/collection/p16062coll9/id/148633.

59. B. Coifman, M. McCord, R. Mishalani, M. Iswalt, and Y. Ji. Roadway Traffic Monitoring from an Unmanned Aerial Vehicle. *Intelligent Transport Systems, IEEE*, Vol. 153, No. 1, Mar. 2006, pp. 11–20. http://ieeexplore.ieee.org/xpls/abs_all.jsp?arnumber=1618950.

60. F. Judson. The Ohio Department of Transportation and Unmanned Aircraft Systems. *Lidar Magazine*, Vol. 3, No. 5, 2013. Spatial Media. http://www.lidarmag.com/PDF/LiDARMagazine_Judson-ODOTandUAS_Vol3No5.pdf.

61. Ohio/Indiana UAS Center. Ohio Department of Transportation. 2015. http://www.dot.state.oh.us/divisions/uas/Pages/default.aspx.

62. S. L. Barfuss, A. Jensen, and S. Clemens. *Evaluation and Development of Unmanned Aircraft (UAV) for UDOT Needs*. Report No. UT-12.08. Utah Department of Transportation, Salt Lake City, 2012. http://www.udot.utah.gov/main/uconowner.gf?n=10710706202834543.

63. E. A. Carroll and D. B. Rathbone. Using an Unmanned Airborne Data Acquisition System (ADAS) for Traffic Surveillance, Monitoring, and Management. *Proc., 2002 International Mechanical Engineering Congress and Exposition,* New Orleans, Louis., ASME, 2002, pp. 145–157. http://proceedings.asmedigitalcollection.asme.org/proceeding.aspx?articleID=1584571.

64. J. D. Pastor. *Virginia Tech's Unmanned Aircraft Test Site Program 'Fully Operational', FAA Says*. Office of University Relations, August 13, 2014. http://www.vtnews.vt.edu/articles/2014/08/081314-research-faa.html.

65. Research and Innovative Technology Administration. Development of UAV-Based Remote Sensing Capabilities for Highway Applications. *UTC Spotlight.* USDOT RITA, 2012. http://www.rita.dot.gov/utc/sites/rita.dot.gov.utc/files/utc_spotlights/pdf/spotlight_1202.pdf.

66. R. Charette. This Car Runs on Code. IEEE Spectrum, *IEEE*, Jan. 2, 2009. http://spectrum.ieee.org/transportation/systems/this-car-runs-on-code. Accessed Aug. 7, 2015.

67. Mercedes Benz. *ABC Active Body Control/MBC Magic Body Control.* 2015. http://500sec.com/abc-active-body-control-mbc-magic-body-control/.

68. Bosch Software Innovations. 2015. https://www.bosch-si.com/home/homepage.php.

69. J. Rupp and A. King. Autonomous Driving—A Practical Roadmap. *SAE Convergence*. Detroit, Michigan, 2010.

70. V. Popescu, R. Danescu, and S. Nedevschi. On-road Position Estimation by Probabilistic Integration of Visual Cues. *Proc., IEEE Intelligent Vehicles Symposium,* 2012, pp. 583–589.

71. L. Fletcher, N. Apostoloff, L. Petersson, and A. Zelinsky. Vision in and out of Vehicles. *Intelligent Transportation Systems*, IEEE Computer Society, May/June 2003.

72. D. Ding, J. Yoo, J. Jung, S. Jin, and S. Kwon. Various Lane Marking Detection and Classification for Vision-Based Navigation System? *IEEE International Conference on Consumer Electronics (ICCE)*, Las Vegas, Nevada, 2015, pp. 491–492.

73. Z. Kim. Robust Lane Detection and Tracking in Challenging Scenarios. *IEEE Transactions on Intelligent Transportation Systems*, Vol. 9, No. 1, March 2008, pp. 17–26.

74. D. Cualain, M. Glavin, and E. Jones. Multiple-Camera Lane Departure Warning System for the Automotive Environment. *Intelligent Transport Systems*, Vol. 6, No. 3, 2012, pp. 223–234.

75. D. Cualain, C. Hughes, M. Glavin, and E. Jones. Automotive Standards-Grade Lane Departure Warning System. *Intelligent Transport Systems*, Vol. 6, No. 1, 2012, pp. 44–57.

76. National Highway Traffic Safety Administration. *Lane Departure Warning System Confirmation Test and Lane Keeping Support Performance Documentation*. U.S. Department of Transportation, Washington, D.C., 2013.

77. K. Kluge and G. Johnson. Statistical Characterization of the Visual Characteristics of Painted Lane Markings. *Proc., Intelligent Vehicles '95 Symposium*, Detroit, Michigan, 1995, pp. 488–493.

78. B. Jaruzelski, J. Loehr, and R. Holman. *The Global Innovation 1000: Navigating the Digital Future*. Booz & Co., 2013.

79. M. McGurrin. *Vehicle Information Exchange Needs for Mobility Applications.* U.S. Department of Transportation, Research and Innovative Technology Administration, Washington, D.C., 2012.

80. University of Michigan Transportation Research Institute. *Connected Vehicle Update*. Vol. 4, No. 1. 2011. https://www.michigan.gov/documents/mdot/mdot_connected_vehicle_update_v4_n1_369079_7.pdf

81. A. B. Hillel, R. Lerner, D. Levi, and G. Raz. Recent Progress in Road and Lane Detection: A Survey. *Machine Vision and Applications*, Vol. 25, No. 3, pp. 727–745, 2014. (Published first online, Febr. 7, 2012.)

82. J. Britt, C. Rose, and D. Bevly. A Comparative Study of Lidar and Camera-based Lane Departure Warning Systems. *Proc., 24th International Technical Meeting of The Satellite Division of the Institute of Navigation (ION GNSS 2011)*, Portland, Oregon, 2011, pp. 324–332.

83. F. Homm, N. Kaempchen, and D. Burschka. Fusion of Laserscanner and Video Based Lanemarking Detection for Robust Lateral Vehicle Control and Lane Change Maneuvers. *IEEE Intelligent Vehicles Symposium (IV)*, Baden-Baden, Germany, 2011.

84. Highway Loss Data Institute. *Predicted Availability of Safety Features on Registered Vehicles—An Update*, Vol. 31, No. 15, 2014.

85. Insurance Institute for Highway Safety (IIHS). *Advanced Safety Technologies and Other Guideposts on the Road to Vision Zero.* Maastricht, 2014.

86. EuroRAP. *Roads that Cars Can Read.* European Road Assessment Programme, 2013.

APPENDIX A: TECHNOLOGY VENDORS AND SERVICE PROVIDERS

Many of the technology vendors and service providers listed below were identified in the literature as one used by an entity, whether a DOT or in some other application for data collection. This is not considered to be an all-inclusive list of technology vendors or service providers nor an endorsement of any product or service.

LASER SCANNERS

Mandli Communications – http://mandli.com/applications

- Applications.
  - Urban modeling.
  - Asset inventory.
  - RetroView: Sign retroreflectivity.
- High Speed Mobile LiDAR.
  - Collects up to 1.4 million points of data per second to create a three-dimensional model of the environment. This model can be used to inventory and measure a variety of roadway assets, including signs, pavement surface areas, bridge clearances, guardrails, and more.
  - Integration with Mandli's Workstation Software.
  - Fully interactive 360º point cloud.
  - Georeferenced images, GPS, and point cloud data.
  - Compatibility with existing databases.
  - Precise measurements of asset attributes.
  - 5 cm to 100 m range.
- **Utah DOT, Hawaii DOT.**

Sanborn – http://www.sanborn.com/products/mobilemapping

- Mobile LiDAR System delivers better than 5 cm accuracy and a resolution of up to 1 cm, providing 3-D detail from a vehicle moving at speeds up to 60 mph.
  - 2× 200 kHz Lasers.
  - 45° heading, 10° pitch.
  - 2× 5-mp digital cameras.
  - 2× GPS antennas.
  - 1× POS IMU / 1× DMI.
  - 1 TB storage.
  - 360° scanning / 9000 rpm.
  - Range: 200 m.
  - Each unit 200,000 measurements per second.

Teledyne Optech – http://www.teledyneoptech.com/

- Galaxy, Orion, and Pegasus airborne laser mappers for efficient acquisition of high-accuracy spatial data.
- Titan.

    - Commercial multispectral LiDAR, expanding forestry, geologic, bathymetry, and any other spectral mapping applications to high-precision 3-D and day or night operations.
    - Incorporates three independent laser beams at different wavelengths, with a combined ground sampling rate approaching 1 MHz.
    - The sensor includes full gyrostabilization compatibility for predictable point distribution and a fully programmable scanner for significant point density increases at narrower FOVs.
- CZMIL.
    - LiDAR bathymeter with the technology to reach 80 m in clear waters and extract detail in shallow turbid and muddy conditions.
- Lynx Mobile Mapper™ SG1.
    - Has two 600-kHz sensors for survey-grade precision with measurement rates of up to 1.2 million measurements per second from a vehicle at cruising speeds.
- Lynx Mobile Mapper™ MG1.
    - Single 500-kHz sensor head, and is designed as a lower cost solution for projects requiring lower absolute accuracy than design engineering projects.
- ILRIS.
    - Fully portable, laser-based ranging and imaging system for the commercial survey, engineering, mining, and industrial markets.
    - A compact and highly integrated instrument with digital image capture and sophisticated software tools.
    - Field-ready and requires no specialized training for deployment.
    - ILRIS is packaged for several applications, including automated monitoring and long-range scanning.

Trimble – http://www.trimble.com/3d-laser-scanning/tx5.aspx
Though best known for GPS technology, Trimble integrates a wide range of positioning technologies including GPS, laser, optical and inertial technologies with application software, wireless communications, and services to provide complete commercial solutions. Its integrated solutions allow customers to collect, manage, and analyze complex information faster and easier, making them more productive, efficient, and profitable.

Virtual Geomatics SmartLiDAR™ – http://www.virtualgeomatics.com/
- VG4D SmartLiDAR Explorer.
    - Customized process-oriented workflow for mobile, corridor, airborne, and static LiDAR/point cloud datasets.
    - Offers complete end-to-end workflow to handle large strips (billions of points), automatic classification, smart feature extraction, automatic digitization, asset management, project management, and tracking to highlight a few. It provides complete solution for various LiDAR applications.
    - Add-on modules available.
- LiDAR Explorer Lite.
    - Stand-alone tool, designed to help engineers, surveyors, construction, and mining personnel to easily and instantly extract volume information from LiDAR point

cloud data. The software can directly import data from a variety of popular terrestrial and mobile sensors.

Leica – http://www.leica-geosystems.com/

- Leica HDS6000.
  - Compact is an ultra-high-speed laser scanner with scanner, controller, data storage, and battery in a single instrument.
  - Users can operate the scanner from a simple, side touch panel.
  - An optional PDA or laptop with Leica Cyclone SCAN software provides added scanner control and valuable field QA.
  - Wireless LAN (WLAN) is also fully integrated.
- CHIROPTERA II.
  - Targeting market demand for high-accuracy, environmental data when surveying shallow water regions.
  - Multispectral.

Phoenix Aerial Systems – http://www.phoenix-aerial.com/

- Ranger LiDAR Series.
  - Survey grade LiDAR mapping system, featuring the Riegl VUX-1 and Fiber Optic Gyro (FOG) IMU.
- Aerial LiDAR AL3-16, AL3-32, AL2.
  - Multi-platform high-definition LiDAR mapping systems.

TopCon – http://www.topcon.co.jp/en/positioning/products/product/3dscanner/IP-S2_Lite_E.html

- Mobile Mapping System IP-S2 Lite.
  - Integrates 3-D video image with GIS database.
  - Captures 360° video with positional information while driving.
  - Camera vector technology assigns 3-D.
  - Coordinates to video images.
  - Measurements can be taken on video screen.
  - Generates 3-D CG of roadside features.
  - Overlays 3-D CG on video image.
  - Active linkage with GIS software.

LiDAR USA – http://lidarusa.com/

- ScanLook 2.0 (~Snoopy).
  - Super small.
  - Extremely configurable.
  - Easily transported.
  - Flexible mounting.
  - RTK and post process.
  - Static and mobile.
  - GIS and survey grade.

Routescene® – http://www.routescene.com/

- Routescene LidarPod® – Can be used in mobile or UAV. Uses Velodyne scanners.
  - Weight: 2.5 kg (including GPS antennas and cables).
  - Dimensions [mm]: 320 length × 100 diameter.
  - 65 × 120 m footprint at 80 m altitude.
  - Absolute position accuracy of 0.03 m at 20 m range.
  - Absolute position accuracy of 0.06 m at 40 m range.
  - External power.
  - Switchable power from UAV to ground supply.
  - Supply voltage: 12–55 VDC, 28 watts.
  - Operating temperature: −10° to +40° C.

Velodyne High Definition LiDAR – http://velodynelidar.com/lidar/hdlproducts/hdl32e.aspx

- HDL-64E LiDAR Sensor.
  - Designed for obstacle detection and navigation of autonomous ground vehicles and marine vessels. Its durability, 360° field of view, and very high data rate makes this sensor ideal for the most demanding perception applications, as well as 3-D mobile data collection and mapping applications.
  - Full 360° horizontal FOV by 26.8° vertical FOV, 5–15 Hz user-selectable frame rate, and over 1.3 million points/sec output rate.
  - Patented one-piece design uses 64 fixed-mounted lasers to measure the surrounding environment, each mechanically mounted to a specific vertical angle, with the entire unit spinning. This approach dramatically increases reliability, FOV, and point cloud density.
- HDL-32E LiDAR Sensor.
  - Small, lightweight, ruggedly built and features up to 32 lasers across a 40° vertical FOV.
  - Measures only 5.7″ high × 3.4″ diameter, weighs less than 2 kg and was designed to exceed the demands of the most challenging real-world autonomous navigation, 3-D mobile mapping, and other LiDAR applications.
  - Lasers are aligned from +10° to −30° to provide a vertical FOV, and its patent-pending rotating head design delivers a 360° horizontal FOV natively.
  - Generates a point cloud of 700,000 points/sec with a range of 70 m and typical accuracy of ±2 cm.
- VLP-16 Sensor – LiDAR Puck.
  - Smaller, vastly more cost-effective and developed with mass production in mind. At the same time, it retains the key features of Velodyne's breakthroughs in LiDAR: "Real-time, 360°, 3-D distance and calibrated reflectivity measurements."
  - Preliminary specifications call for a range of more than 100 m, with a target range of 150–200 m.
  - The unit's low power consumption (<10W), lightweight (about 600 grams), compact footprint (Ø100mm × 65 mm), and dual return option make it ideal for UAVs.
  - Velodyne's LiDAR Puck supports 16 channels, ~300,000 points/sec, a 360° horizontal FOV, and a 30° vertical FOV, with ±15° up and down.

- The Velodyne LiDAR Puck does not have visible rotating parts, making it highly resilient in challenging environments.

RIEGL Laser Measurement Systems – http://www.riegl.com/

- Terrestrial Laser Scanners.
  - RIEGL LMS-Z620 high-performance, long-range 3-D scanner using operating and processing software RiSCAN PRO, and a mounted high-resolution digital camera.
  - **Used by Kansas DOT.**
- Mobile Laser Scanners.
  - RIEGL VQ-450 – Extremely high speed, echo digitization and online waveform processing, multiple target capability, "full circle" FOV 360°.
  - RIEGL VQ-250 – High speed, echo digitization, and online waveform processing, multiple target capability, "full circle" FOV 360°.
  - RIEGL VQ-180 – Online Waveform Analysis, multiple target capability, vertical FOV 100°.
- Mobile Laser Scan Systems.
  - RIEGL VMQ-450 – Compact Single Scanner Mobile Mapping System.
  - RIEGL VMZ – Hybrid Mobile Laser Mapping System for 3-D static and kinematic data acquisition.
  - RIEGL VMX-450-RAIL – Optimized for the demanding field of mobile railway mapping.
  - RIEGL VMX-250 – Mobile Laser Scanning System for 3-D data acquisition from moving platforms, two RIEGL VQ-250 laser scanners integrated.
  - RIEGL VMX-450 – High-speed Mobile Laser Scanning System for 3-D data acquisition from moving platforms, two RIEGL VQ-450 laser scanners integrated.
- Aerial Scanning Systems.
  - RIEGL VP-1 – Helipod for Airborne Laser Scanning with RIEGL VUX-SYS for ALS fully integrated.
  - RIEGL VQ-880-G – Topo-hydrographic ALS system with online waveform processing and full waveform recording.
  - RIEGL LMS-Q1560 – Fully integrated ALS system for ultra-wide area mapping.
  - Complete Platform Systems – All-purpose system for ALS and photogrammetry.

ENSCO, Inc. – www.enscorail.com

PHOTO/VIDEO IMAGERY

Earthmine – http://www.earthmine.com/html/products_mobile.html

- High-resolution stereo panoramic imagery collected automatically on a distance-based interval at regular driving speeds.
- Mobile mapping for 3-D street level imagery.

Newport Sensors, Inc. – http://www.newportsensors.com/technology.html

- Sensors and nondestructive evaluation technologies including continuous monitoring on-structure sensors and NDE inspection.
- Fiber optic dynamic sensors.
    - Total immunity to electromagnetic interference and lightning strikes due to the non-existence of electric signals or electric cables.
    - Unique safety in dangerous environments where electric sparks cause explosion concerns, such as gas and oil tanks and pipes.
    - High sensitivity and resolution in a wide dynamic range, particularly at very low frequencies.
    - Measure both strong motion and ambient vibration with the same high sensitivity.
    - Small sensor heads and lightweight optical fiber cables, and the resulting ease of installation.
    - Robustness against environmental (e.g., temperature and moisture) changes.
    - Lower cost than conventional optical fiber sensors due to their simple signal processing.
- Vision-Based Displacement Monitoring.
    - Low-cost, non-contact, real-time displacement monitoring system composed of a digital camcorder that streams captured images into the computer and uses proprietary image-processing software to compute the structural displacement in real time.

PAVEMENT INSPECTION

Pathway Services – http://www.pathwayservices.com/

- PathRunner Data Collection Vehicle is a state-of-the-art service tool equipped with the latest computer, sensor, and video equipment designed to efficiently collect data and video images of the roadway and pavement surface.
- The system's software was designed to take advantage of the latest real-time graphical data collection technology, allowing the vehicle's operator to verify the proper operation of the sensor equipment in real time. The results are quality data on schedule at minimum cost.
- Close to 20 separate subsystems have been developed and integrated to ensure that our clients can collect, reduce, and deploy as many data types as possible with a single pass of the roadway.

Fugro Roadware Infrastructure Asset Management Solutions – http://www.roadware.com/products/

- Automated Road Analyzer (ARAN) – Specially modified vehicle with an extensive set of sensors (including laser reflectometers, ultrasonic sensors, accelerometers, GPS, gyroscopes, video and machine vision systems), computers and advanced technology subsystems.
- Traffic speed data collection.
- Assesses – Ride quality of the roadway, wearing of the roadway, grade and cross-slope of the roadway, real-time video imagery of the roadway pavement and right of way

imagery, precise location information of specific features on or near the roadway, and faulting of concrete pavements are able to be calculated by this system.
- **Michigan DOT, City of Tucson, AZ DOT usage – http://www.transview.org/aran/.**

RavelDetect – http://brunopop.com/raveldetect/
- Automated detection and classification of raveling for interstate inventory using laser data.
- Relies on laser data acquired by two devices pointing to the surface of the road and mounted on a data collection vehicle that collects an intensity image (grayscale photo) and a depth image for every 5 m of travel. Each image is slightly wider than a lane and has size 1000 × 4160 pixels, each pixel having for value the distance from the device to the surface of the road.

Surface Systems & Instruments, Inc. – http://www.smoothroad.com/products/pavementmanagement/
- Mobile imaging and asset inventory system for pavement.
- eRoadInfo system modules allow varying degrees of automated pavement management tasks, including road inventory, data collection, data analysis, decision support, budgeting, and reporting.
- Fully automated option uses a high-speed line-scan imaging device to collect images, detect crack conditions, and produce road condition data in AASHTO or PMIS standard formats.
- eRoadInfo pavement surface profiling system module is an ASTM E950-98 Class I Profiler that exceeds all DOT specifications and certification requirements, including compliance with AASHTO PP50-02, PP51-02, and Texas 1001-S standards. The profile data are reported under several specified profile indices, including International Roughness Index (IRI), Profilograph Index (PI), Ride Quality Index (RQI), Ride Number (RN), etc.

Resource International – http://www.resourceinternational.com/services/groundpenetratingradar.aspx
- Ground penetrating radar for assessing roadway infrastructure health.
- **Caltrans, Missouri, NYSDOT, ODOT.**

Pavemetrics – http://www.pavemetrics.com/

INO – http://www.ino.ca/en/industries/transportation/
- Automated inspection technology for both daytime and nighttime operation.
- Sensors produce high-resolution 2-D images and 3-D profiles of road/runway/tunnel surfaces at speeds up to 100 km/h.
- Wide variety of infrastructure management applications including: road pavement condition evaluation, detection of foreign object debris (FOD) at airports, and high-speed-train-tunnel vault lining inspection.
- Laser Crack Measurement System (LCMS) – Allows the automatic detection of cracks and the evaluation of rutting, macro-texture, and other road surface features.

- Laser Tunnel Scanning System (LTSS) – Uses multiple high-speed laser scanners to acquire both 2-D images and high-resolution 3-D profiles of tunnel linings. The LTSS is 100 times faster and 10 times more accurate than typical LIDAR technology; it can scan a full tunnel vault (24 m) at 1 mm image resolution and 3-D data at acquisition speeds of up to 20 km/h.
- Laser Rail Inspection System (LRAIL) – Automatically detects railway features such as rails, ties, and fasteners as well as defects such as cracking on concrete ties. Track geometry, gauge width, alignment, cant/cross-level, twist, longitudinal level, and railhead 3-D profile and wear are also measured. The LRAIL allows an accurate inspection of the railway network at high speed.
- Laser FOD Detection System (LFOD) – Uses high-speed cameras, custom optics, and laser line projectors to acquire both 2-D images and high-resolution 3-D profiles of airport runways, taxiways, and aprons in order to automatically detect even the smallest objects at highway speeds. The LFOD system can be operated both during daytime and nighttime, as well as under all types of lighting conditions; surfaces lit by the sun or covered by shadows as well as various pavement types ranging from dark asphalt to concrete can be scanned at inspection speeds from 0 to 100 km/h.
- Laser Digital Terrain Mapping System (LDTM) – Allows for the mapping of road surfaces in 3-D acquiring 45 million points/sec that are seamlessly merged together into a high accuracy digital terrain map.
- Laser Road Imaging System (LRIS) – Designed to increase the contrast and visibility of both small longitudinal and transverse road cracks.
- Laser Rut Measurement System (LRMS) – Is a transverse profiling device that detects and characterizes pavement rutting. The LRMS can acquire full 4 m width profiles of a highway lane at normal traffic speeds, with two options of maximum sampling rate: 30 or 250 Hz.

Waylink Systems Corporation – http://www.waylink.com/dhdv.htm

- Digital Highway Data Vehicle (DHDV) – Real-time multi-functional system for roadway data acquisition and analysis, particularly for pavement surface distress survey and roadside asset management.
- Full-lane width distress survey of pavements at speeds of up to 60 mph (100 km/h) and processes cracking data in real time with ADA with laser-based imaging subsystem for shadow-free image collection. ADA can also be used offline in office environment.
- Full-lane width rutting measurement, using accurate lasers that can detect ruts down to 1 mm depths.
- Longitudinal profiling system to present longitudinal roughness, and calculate IRI, RN, and macrotexture (MT) values, in accordance with the ASTM standards.
- Pavement Right-of-Way imaging system, with multiple high-resolution, digital color cameras to capture imagery of roadway and roadside structure. Varying camera options are available, including 1080-p high-definition (HD) cameras.
- Positioning System Array consisting of a differential GPS receiver, DMI, and a multi-axis solid-state Gyroscope. User also can select high-precision IMU.
- Multimedia Highway Information System (MHIS) – A user-friendly application designed to dynamically display the DHDV-produced data sets in a descriptive, visual, and flexible

user interface. The deluxe version of MHIS allows user to manually edit and add various distresses defined through LTPP, MicroPaver, and others.

International Cybernetics – http://www.intlcybernetics.com/index.html

- CrackScope.
  - Utilizes customized image-processing algorithms to perform both online and offline pavement crack inspection.
  - The algorithms permit the detection of cracks in one image to be done in the same time when the frame grabber accumulates line images from the linescan camera to form a new image frame.
  - Able to perform pavement survey in real-time, full-lane, and 100 percent coverage, and highway speed.
  - Differentiates flexible and rigid pavements, and classifies the distresses into two distinct rating summary formats.
  - Flexible pavements reports the data in both the PMIS and AASHTO ACP formats. The PMIS data include transverse and longitudinal cracks, as well as alligator and block cracking, while the AASHTO data include crack densities in four separate paths.
  - Rigid pavements reports the AASHTO data as well as the counts of spalled cracks and punch-outs. The system can output snapshot images and crack maps, a graphical file showing the locations of various cracks. The system records the distress data and the crack map at an interval of 0.1 mile pavement. The survey data are time-independent and weather-invariant.
- ICC Lightweight Profilers and High-Speed Road Profilers.
  - MDR408x road profilers are precision, non-contact ASTM E950 Class 1 pavement profilers.
  - Primarily consist of infrared laser height sensor(s), precision accelerometer(s), a distance measuring unit, and an industrial hardened IBM-compatible PC.
  - Mounts into a vehicle according to the customer's data collection needs.
  - The profilers can be configured with multiple height sensors, single or dual accelerometers, and any subsystem the client wishes.
  - Primarily used to rate pavement ride (IRI, PI, RN, Rolling Straightedge), rutting, texture, and faulting. In addition, the system will produce a profilograph simulation with bump/dip locations and must grind lines. The system collects accurate, repeatable data between 5 and 70 mph.
  - Non-vehicle dependent and measurements will not be affected by vehicle speed or suspension, temperature, sunlight, pavement color or texture, and wind.
- All data are collected in real time, displayed on a Flat Panel for the operator viewing, recorded to the hard drive for future analysis, and sent to a printer for a graphical report.
- Subsystems and Optional Equipment.
  - Longitudinal profile/Inertial profilometer.
  - Rutting.
  - Transverse profile.
  - Distress measurement.
  - Roughness/Ride.
  - 3-D Imaging.

- Faulting.
- Ground penetrating radar.
- Texture.
- Mirolux reflectometer.
- Falling weight deflectometer.
- Cross slope.
- LiDAR.
- Automated cracking.
- Digital imaging (right of way [ROW], forward and 360°).
- Pavement imaging.
- Pavement management software.
- Friction HFST and specialty testing.
- Retroreflectivity.
- Geometrics.

Dynatest – http://www.dynatest.com/equipment.aspx

- Dynatest 5051 Mk III Road Surface Profilometer (RSP).
  - Measures a number of indices and characteristics including the longitudinal profile, IRI, RN, transverse profile, rutting, macrotexture, and geometrics (crossfall, gradient, and radius of curvature).
  - It can also provide data for the Boeing Bump Index calculation.
  - The RSP has a unique "Stop & Go" functionality enabling the equipment to operate in an efficient manner in urban areas, at traffic lights, stop signs, junctions, and roundabouts.
  - The equipment meets the highest ASTM, AASHTO, and State road standards for accuracy, ensuring that the data can be used for project and network evaluation and in pavement management systems.
  - The RSP-III is a fully upgradable system offering up to 21 lasers.
  - The RSP-IV is the portable version easily attached to any vehicle with the capability to attach one or two lasers. Options include texture capable lasers, DGPS, and ROW cameras.
- Dynatest Multi-Functional Vehicle (MFV).
  - Combines the functionality of the RSP with the LRMS and/or the laser road imaging system (LRIS), or the LCMS from Pavemetrics.
  - The MFV measures the IRI/RN, longitudinal and transverse profile, macrotexture, geometrics (crossfall, gradient, and radius of curvature) plus 2-D or 3-D pavement imagery, and provides photologging by up to five ROW cameras.
  - Allows surveys of roads and airports to be performed from a vehicle at normal traffic speeds, day or night.
- 6875 Highway Slip Friction Tester (HFT).
  - Self-contained Continuous Friction Measurement Equipment mounted in various sizes of trucks.
  - The truck platform allows a wide variety of water tanks for continuous friction evaluation of the highway network.
  - The HFT closely matches the braking action of ABS-equipped vehicles by testing at traffic speed with a test wheel simulating ABS braking.

- 1295 Pavement Friction Tester (PFT).
  - Locked wheel friction tester.
  - Meets the requirements of ASTM E274 providing the majority of state department of transportations in the United States with locked wheel, skid number (SN) friction data.
- 995 Tire Traction Tester (TTT).
  - The trailers perform traction measurements in full compliance with ASTM E274 and F408, ISO 15222, ISO 23671, and ECE (R117) standards.
  - The trailers are available for both C1 and C2 tire loading ranges with ECE R228, ISO 15222, and ISO 23671 reporting capabilities.

Geophysical Survey Systems, Inc. – http://www.geophysical.com/products.htm

- RoadScan™ 30.
  - Data acquired at highway speeds.
  - No coring required for calibration.
  - Data quality not affected by rough road conditions.
  - Quick determination of pavement layer thickness.
  - 1.0 or 2.0 GHz antennas provide superior data resolution.
  - Multi-channel data collection capability allows one to four antennas to be used simultaneously.
  - ASCII output files for simple data transfer to other software programs.
  - Results output as Google Earth™ .kml file.

DBi Services –www.dbiservices.com/road-marking-assessment

- Mobile road marking assessment system.
  - High-speed service for the survey and evaluation of day and night performance of road markings.
  - Surveys can be completed in heavy traffic and identify road markings that are noncompliant with specifications.
  - Up to 185 miles of road markings can be tested per day.
  - Results can be presented in the form of graphs or computer files containing the mean values for contrast and reflectivity over zones up to over 60 miles.

Terrasolid – http://www.terrasolid.com/products.php

- Provide software for processing airborne and mobile LiDAR data and images.
- Most of the Terrasolid applications are built on top of Bentley software.

Quick Terrain Modeler – http://appliedimagery.com/

- 3-D point cloud and terrain visualization software package.
- Designed for use with LiDAR, but flexible enough to accommodate other 3-D data sources.

ACOUSTIC

Mistras Group, Inc. – 4-CHANNEL AE WIRELESS NODE (1284)
http://www.mistrasgroup.com/products/company/Publications/2$Acoustic_Emission/USB_AE_Node.pdf

- USB AE Node is a full-featured, low-cost acoustic emission (AE) system that plugs conveniently into the USB port of a user's PC or laptop.
- The system can be expanded to 4 channels (synchronized).
- AE technology can be used to monitor initiation of cracks or internal defects.
- Single-channel AE system is just palm size and can be plugged into a USB port of a laptop or a desktop PC to perform AE test without using external power and preamplifier.
- A load sensor or cycle counter can also be connected to a parametric channel of the USB AE node to make a historical trending record in conjunction with the AE so that the load magnitude, the testing time or fatigue cycle of crack initiation can be recorded in the same time and displayed in the same graph.
- Free LabView/C++ driver is available for customers to develop their own application programs.

Germann Instruments – http://germann.org/all-products

MIRA Tomographer –
http://www.germann.org/TestSystems/MIRA%20Tomographer/MIRA%20Tomographer.pdf

- Instrument for creating a 3-D representation (tomogram) of internal defects that may be present in a concrete element using ultrasonic pitch-catch method and an antenna composed of an array of dry point contact (DPC) transducers, which emit shear waves into the concrete.
- The transducer array is under computer control and the recorded data are transferred wirelessly to a host computer in real time.
- The computer takes the raw data and creates a 3-D image of the reflecting interfaces within the element:
    - Thickness measurement.
    - Detection of voids in grouted tendon ducts.
    - Detection of poor quality bond in overlays and repairs.
    - Detection of delaminations.
    - Detection of voids and honeycombing in concrete members.
- MIRA Tomographer Specifications.
    - DPC shear-wave transducers with ceramic wearing tip.
    - 50-kHz center frequency with 15- to 150-kHz operating frequency.
    - Transducers are spring-loaded to conform to rough surfaces.
    - Phased array antenna containing 40 transducers in a 4 × 10 configuration; dimensions 435 × 235 × 146 mm; weight 4.5 kg.
    - Wireless communication (WLAN).
    - Testing depth: 50 to 2500 mm.
    - Rechargeable batteries.
    - Time to process data at test location: Not more than 3 seconds.

- 3-D tomographic display.
- Operating temperature: 0 °C to 45 °C.

UAV/UAS

ArchAerial – http://archaerial.com/
OCTO-Octocopter – http://archaerial.com/octocopter-2/

- Hardware.
  - Woven carbon fiber frame.
  - Built for tough conditions.
  - Collapses to fit into a Pelican Case.
  - Water-resistant in light rain conditions.
  - Payload capacity: 15 lbs.
  - Total flight time: 12–15 min.
- Software.
  - Program GPS Waypoint Flightpaths.
  - Flight modes: Loiter, Altitude Hold, Autoland.
  - "Follow Me Mode."
  - Return to Home.
  - Geofence Capable.
- Sensor Options.
  - Camera (up to 7 lbs – requires a gimbal).
  - Near-infrared sensor.
  - Thermal sensor.
  - LiDAR sensor.

Atlas-1 Quad – Quadcopter – http://archaerial.com/atlas-1-quadcopter-uas/

- Hardware.
  - Woven carbon fiber frame.
  - Built for tough conditions.
  - Collapses to fit into a backpack.
  - Water-resistant in light rain conditions.
  - Payload capacity: 2 lbs.
  - Total flight time: 12–15 min.
- Software.
  - Program GPS Waypoint Flightpaths.
  - Flight modes: Loiter, Altitude Hold, Autoland.
  - "Follow Me Mode."
  - Return to home.
  - Geofence capable.
- Sensor Options.
  - Camera (up to 2 lbs).
  - Near-infrared sensor.
  - Thermal sensor.

Cyphy Works – http://cyphyworks.com/robots/eapf/

- PocketFlyer.
  - Vehicle-mounted spooler eliminates tangling and tension in the Microfilament Tether.
  - Drone's capabilities include: Automatic launch, tele-operation through culverts and tunnels, hovering over areas of interest, perch and stare, and automatic landing.
  - Able to fly through doors and windows, and down corridors.
  - Direct connection with controller can't be intercepted, jammed, or spoofed.
  - High quality, full frame rate, unbroken video: Continuous, unbroken, 720 p, 30 FPS, HD video.
  - 1000-ft range: Maintain a safe standoff distance.
  - Operating range: 250 ft.
  - Vehicle weight: 80 grams.
  - Case size: Fits into cargo pants pocket.
  - Mission duration per battery: 2 hours of flight time; several days in perch mode.
  - OCU: Tablet or smart phone.

AeroVironment – http://www.avinc.com/uas/

- Puma AE (All Environment).
  - All environment: Fully waterproof.
  - 3.5+ hour flight endurance.
  - Smart bBattery options to support diverse missions.
  - Gimbaled EO and IR payload.
  - Increased payload capacity with optional under wing Transit Bay.
  - Powerful and efficient propulsion system.
  - Precision navigation system with secondary GPS.
  - Plug-and-play secondary power adapter.
  - Reinforced fuselage for improved durability.
  - Payloads: Gimbaled payload, 360° continuous pan, +10° to −90° tilt, stabilized EO, IR camera, and IR Illuminator all in one modular payload.
  - Range: 15 km.
  - Endurance: 3.5+ hours.
  - Speed: 37–83 km/h, 20–45 knots.
  - Operating altitude (typ.): 500 ft (152 m) AGL.
  - Wing span: 9.2 ft (2.8 m).
  - Length: 4.6 ft (1.4 m).
  - Weight: 13.5 lbs (6.1 kg).
  - GCS: Common GCS with Raven, Wasp, and Shrike.
  - Launch method: Hand-launched, rail launch (optional).
  - Recovery method: Autonomous or manual deep-stall landing.
- Qube.
  - GCS: Rugged touchscreen tablet with digital.
  - Payloads: Dual high-resolution color and thermal cameras.
  - Range: 0.62 mile (1 km) line-of-sight.*
  - Endurance: 40 min (with payload).

    - Operational altitude: 100–500 ft (30–152 m) AGL.*
    - Length: 3 ft (90 cm).
    - Weight: 3 ft (90 cm).
      *Flight restriction imposed by FAA
- Raven®.
    - B DDL® System – An enhanced version of the battle-proven Raven B system, is a lightweight solution designed for rapid deployment and high mobility for military applications, requiring low-altitude surveillance and reconnaissance intelligence.
    - Can be operated manually or programmed for autonomous operation, utilizing the system's advanced avionics and precise GPS navigation.
    - With a wingspan of 4.5 ft and a weight of 4.8 lbs, the hand-launched Raven provides aerial observation, day or night, at line-of-sight ranges up to 10 km.
    - The Raven – Now available with an optional stabilized gimbaled payload, delivers real-time color or infrared imagery to the ground control and remote viewing stations.
- Wasp AE.
    - Micro Air Vehicle (MAV) – Is the all-environment version of AeroVironment's (AV).
    - Payloads: Gimbaled payload with pan and tilt stabilized high-resolution EO and IR camera in a compact aerodynamic modular payload.
    - Range: 5 km line-of-sight, 5+ km with DDL relay.
    - Endurance: 50 min.
    - Speed: 20 knots cruise, 45+ knots dash.
    - Operating altitude (typ.): 500 ft AGL, 150 m AGL; max.
    - Wing span: 3.3 ft (102 cm).
    - Length: 2.5 ft (76 cm).
    - Weight: 2.85 lbs; 1.3 kg.
    - GCS: Compatible with FoS (Raven DDL, Puma DDL).
    - Launch method: Hand-launched in a confined area with remote launch capability.
    - Recovery method: Deep-stall landing in a confined area.
    - **Used by U.S. Air Force and U.S. Marine Corps.**

FLōT Systems – http://www.flotsystems.com/

- FLōT Systems Prophex 50.
    - Vertical takeoff and landing UAS.
    - Flight time: 10 hrs.
    - Payload: 50+ lbs.
    - FAA approved: Yes.
- FLōT Systems Arc 65 Fixed Wing UAS.
    - Short takeoff and landing.
    - Flight time: 16 hrs.
    - Payload: 65+ lbs.
    - FAA approved: Yes.

Micro Aerial Projects LLC – www.microaerialprojects.com

- 20-Hz V-Map System for precise UAV-camera exposure positioning.
  - L1/L2 GPS phase measurements recorded onboard at 20 Hz.
  - Power input ranging from 5V to 36V.
  - LED indicator to monitor satellite reception.
  - LED indicator to monitor proper data storage.
  - Event marker port.
  - One PPS outputs.
  - Removable microSD card for data retrieval.
  - Dual frequency helix antenna.

Yamaha RMAX – http://rmax.yamaha-motor.com.au/industrial-use

- RMAX can be flown at 164 ft (50 m) in height from ground level, 500 ft (150 m) distance away from the pilot and a maximum speed of 25 mph (40 km/h).
- Flight duration approximately 45 minutes to 1 hour depending on weather conditions and the payload.
- **Utah DOT.**

Aerosonde – http://www.aerosonde.com/

- Florida DOT considering using this vendor.

MartinUAV – http://martinuav.com/uav-products/

- Super Bat DA-50.
- Super Bat.
- Bat 4.
- V Bat.
- Tracker.
- **Washington DOT.**

Microdrones – http://www.microdrones.com/en/products/microdrones/

Draganfly Innovations Inc. – http://www.draganfly.com/industrial/products.php

- Draganflyer Guardian.
  - 420 gram payload capacity.
  - Carbon Fiber airframe.
  - GPS, Alt hold and Return Home.
  - Digital video and quick release.
  - Compact and backpackable.
- Draganflyer X6.
  - 335 gram payload capacity.
  - Folding Carbon Fiber frame.
  - GPS, Alt hold and Return Home.
  - Digital video and quick release.
  - Tool-less removable CF props.

- Draganflyer X4-P.
    - X4-P Features at a Glance.
    - 800 gram payload capacity.
    - Folding Carbon Fiber frame.
    - GPS, Alt hold and Return Home.
    - Digital video downlink.
    - Tool-less removable CF props.
- Draganflyer X4-ES Ultra-Portable.
    - 800 gram payload capacity.
    - Ultra-portable folding CF frame.
    - GPS, Alt hold and Return Home.
    - Digital video and quick release.
    - Tool-less removable CF props.

Parrot AR Drone – http://ardrone2.parrot.com/

- Can be controlled using iPhone/iPodTouch/iPad device through its onboard Wi-Fi system.
- Initially designed for the Apple iOS platform, but now it can also be controlled with any Android device or even a computer and a joystick.

AIBOTIX – https://www.aibotix.com/en/overview-aibot-uav.html

- Aibot X6 – Used at the Hamburg Port Authority Köhlbrand Bridge, Hamburg, Germany.
- "The Aibot could be a great help for improving inspection quality, particularly for inspections in accordance with DIN 1076. The copter is small and can easily fly around areas that are otherwise difficult to access, like zones located high above water or areas inside pylons," says Martin Boldt, who is responsible for port infrastructure and building inspection at Hamburg Port Authority.

Phoenix Aerial Systems – http://www.phoenix-aerial.com/products/

- Penguin LiDAR System.
    - UAVFactory Penguin B UAV with integrated Phoenix Ranger LiDAR and Photogrammetry payload.
- TerraHawk.
    - UAV with integrated Phoenix AL3 LiDAR and Photogrammetry payload.
- Vapor 55™ UAV.
    - Single-rotor UAV for RANGER Series LiDAR System.
- AL3 S1000 UAV.
    - Ready-to-fly multi-rotor for the AL3.

XactSense – http://www.xactsense.com/

- XactSense MAX-8 Utility UAV.
    - Wingspan: 48″ motor center to motor center.
    - Prop Size: 17″.
    - Max Payload: 20 lbs.
    - Max Flight Time: 25 min.

    - AUW: 5 lbs without battery.
    - Battery: Up to 32,000 mah 6s.
- XactSense SSP-360 Stable Sensor Platform.
    - Version: Currently on V2.
    - Gimbal Drive: High Quality Brushless Gimbal Motors.
    - Onboard CPU: 2.0 GHz quad core and Cortex™-A7 quad core CPUs.
    - Connectivity: 5.8 GHz Wi-Fi TCP.
- Sensor options:
    - Velodyne HDL-32e.
    - Velodyne VLP-16.
    - FLIR Tao2 Thermal.
    - SONY Alpha A7s / A7r.
    - SONY Alpha A6000.
    - SONY Cmos 36× Optical Zoom.
    - NDVI.
    - Headwall Multispectral.

RIEGL Laser Measurement Systems – http://www.riegl.com/

- UAS/UAV Laser Scanner.
    - RIEGL VUX-1UAV – Very lightweight, survey-grade laser scanner for UAS/UAV application.
    - RIEGL VQ-480-U – Lightweight airborne laser scanner with online waveform procession.
- UAV/UAS Laser Scanning System.
    - RIEGL RiCOPTER – Remotely piloted aircraft system.
    - RIEGL RiCOPTER with VUX-SYS – Ready-to-fly remotely piloted airborne laser scanning system.

Bergan R/C Helicopters – http://www.bergenrc.com/

- Quad, Hexa, and Octocopter.
- Prebuilt and test flown.
- Include Brushless Motors, 14 × 5.5 APC props, 60 amp Opto-isolated ESC's, and the Wookong M A2 autopilot from DJI Innovations.
- Include as standard, a 2-axis camera mount (pitch and roll) that can be stabilized by the Wookong M A2.
- This camera mount is sized to accept most full-size DSLR cameras, such as the Canon 5D or Nikon D7000. The RED Scarlet and Epic can also ride under the Octocopter.
- Folding Hexacopter, making transportation much easier in a standard vehicle. The folding option requires no tools to fold or deploy, and is easy to get ready to fly in a short amount of time.
- **Michigan DOT.**

DJI Phantom 2 Vision – http://www.dji.com/product/phantom-2-vision

- Small quadcopter, available on Amazon for $799 (as of Oct. 21, 2014) that comes with an integrated 14-mp camera, onboard GPS, rechargeable battery capable of 25 minutes

of flight time, and real-time video capabilities via a Wi-Fi range extender and smart phone app.
- The 14-mp camera sensor is capable of taking both JPEG and RAW image formats, can record 1080 p HD video, and its wide-angle lens photos can be corrected to a more "normal" look using an Adobe lens profile. The camera sensor and lens quality and type are not designed for making measurements or other uses needed high-resolution, high-quality imagery, but are meant for rapid, easy-to-collect aerial photography (*56*).
- **Michigan DOT.**

Blackout Mini H Quadcopter – http://www.minihquad.com/

- The small quadcopter frame, available in kit from the Blackout Mini H Quadcopter website for $382 almost ready to fly (ARF).
- This aerial vehicle is designed to be highly agile and customizable, making it an ideal base platform on which to develop a system for deployment in confined spaces.
- An Ardupilot Mega open source flight controller ($50) was paired with a 3-D Robotics uBlox GPS/Compass module for control of the system. This Arduino-based flight controller provides the option to add application-specific sensors to the platform in the future for flight control, e.g. a rangefinder(s) for automatic positioning in a confined space.
- The MTRI Blackout is also equipped with a FatShark FPV 720 p system that enables the user to see what the Blackout "sees" and permits flying without being able to see the aircraft, which is useful in confined spaces.
- The camera module of this system also records the video stream to a standard microSD memory card. This system is available from Amazon for $430 (as of Oct. 24, 2014). This system can be used with any four-channel (or greater) radio system (*56*).
- **Michigan DOT.**

FPV Factory Mariner Waterproof Quadcopter – http://www.fpvfactory.com/products/mariner-accessory/mariner-rtf/fpvfactory-waterproof-quadcopter-mariner-rtf-kit-fly-with-gopro-waterproof-camera-625.html

- Available on Amazon as a ready-to-fly (RTF) package for $918.
- This includes the same flight control system found in a DJI Phantom, a Naza Lite controller, for flight stabilization and GPS positioning.
- This platform has then been paired with a GoPro Hero 3 camera ($330) and its suction cup mount ($40).
- This permits the gathering of 1080 p HD video at 48 FPS, or 12 mp images at 2 FPS.
- The camera can be mounted on either the bottom or the top of the aircraft and can be pointed to any angle.
- It is also possible to carry two cameras, both top and bottom mounted, at the same time.
- Flight time with a single camera is estimated at 15 minutes (*56*).
- **Michigan DOT.**

Walkera QR 100S

- Camera can transmit the video live to a smart phone or tablet. Video and stills are saved to the external device (smart phone) as there is no onboard storage capacity.

- Size: 5.7 inches × 5.7 inches with a weight of 0.20 pounds (89 grams).
- **Michigan DOT.**

Heli-Max 1 Si – http://www.helimaxrc.com/helicopters/hmxe0830-1si/
- Flight time of 10 minutes.
- Small camera that is able to capture 720 p video or 1 mp stills.
- MicroSD memory card of up to 32 GB can be used to save video from the camera.
- Size: 5.44 inches × 5.44 inches and is 1.77 inches tall with a weight of 0.10 pounds (46 grams).
- **Michigan DOT.**

UAV Global – http://www.uavglobal.com/list-of-manufacturers/
- 425 UAS/UAV manufacturers.
- All UAV manufacturers (civilian and military) from around the world are shown below, along with their country and region and a link to their company website.

RETROREFLECTIVITY

Advanced Mobile Asset Collection (AMAC) – http://www.amacglobal.com/
- Advanced, mobile, and highly accurate automated system that measures traffic sign and pavement marking retroreflectivity while creating a comprehensive asset inventory and condition assessment.
- Integrating state of the art advanced lighting and artificial vision techniques in an instrumented vehicle operating at night at highway speeds, AMAC safely, quickly, and cost-effectively assesses the actual performance of traffic signs and pavement markings.
- AMAC objectively measures traffic sign and pavement marking retroreflectivity levels, luminance, position, dimensions, and color. The collected data are analyzed, geo-positioned, and can then be integrated into existing GIS or maintenance management systems.

ECODYN mlpc® – http://vectrafrance.com/materiels-et-solutions/auscultation-des-chaussees/ecodyn-mlpcR-visibilite-des-marquages
- Continuous monitoring device of daytime and nighttime visibility of road marking that measures retroreflected luminance coefficient of road markings as well as their contrast to the day and night relative to the floor.
- Ecodyn emits white light, frequency modulated and catches the retroreflected light flux, which is superimposed the flow from the ambient illumination. An appropriate signal processing is used to separate two types of light and calculate the coefficients RL and contrasts day and night marking with respect to the floor.
- Equipment installed on a specially equipped minivan-type vehicle. It comprises a measuring box, outside the vehicle, an electronic unit for transmitting and receiving signals and a microcomputer for data acquisition and data processing. The acquisition (not ≈ 40 cm) is independent of the vehicle speed. The position of the camera relative to the road marking is controlled by the driver using a bar graph on the dashboard of the vehicle.

GNSS/GIS/GPS

DTSGIS – http://www.dtsgis.com/our-services/products/

TIPvue – http://www.tipvue.com/

- Reduced compilation time by up to 60 percent.
- Manage, edit, and track projects.
- Supports multiple modes and TIP sections.
- Automatically formats reports required by FHWA/FTA.
- Templates and ability to customize multiple reports.
- Maintains data across multiple years.
- Amendments tracking.
- Integrates GIS Maps with project report.
- Funding comparison tools.
- Searchable by project, name, number, type, or area.
- Provides public transparency.
- Simplifies database management.
- Web-based multi-user support – A single authoritative database.
- Responsive design for smart phones and tablets.
- Secure administration.
- Public comment support.
- Supporting performance measures.

VUEWorks® – http://vueworks.com/

- Web-enabled Integrated GIS, Enterprise Asset Management.
- Designed for use by state and local governments, utilities, corporations, schools, theme parks, and other organizations that need to track the condition, minimize failure risk, and optimize expenditures and service delivery of their physical assets.

TransVUE

- Provides tools that support long-range planning, transportation improvement programs (MPO, district/region, and state levels), communication/coordination tools, document management, approval tracking, straight line diagramming, videologs, asset & work order management, traffic information, and environmental management.

NovAtel Inc. – http://www.novatel.com/industries/mobile-mapping/#products

- Receivers: OEM board level and board + enclosure GNSS receiver options.
- SPAN GNSS Inertial Systems – Combining GNSS receiver technology with INS provides a superior positioning solution with 3-D position, attitude (roll, pitch, and yaw) and velocity.
- Antennas: GNSS receiver performance is dependent on your choice of antenna. We offer high performance, compact, low cost and ground reference station antennas. Our anti-jam antenna is available for military or homeland security applications.
- SMART antennas: NovAtel SMART antennas are high-precision products that include a board level GNSS receiver and GNSS antenna integrated into one compact enclosure.

- Firmware Options & PC Software: Proprietary card level programs and PC software.
- Waypoint Software: NovAtel's Waypoint Products Group develops powerful GNSS and GNSS-INS post-processing software as well as real-time trajectory determination software.
- Scintillation &Total Electron Content (TEC) Monitor: GNSS Ionospheric Scintillation and TEC Monitor (GISTM) receiver for measuring changes in the ionosphere due to solar flare activity.
- Accessories: Optional accessories for NovAtel products.

Virtual Geomatics SmartLiDAR™ – http://www.virtualgeomatics.com/

- VG4D Virtual Navigator
    - Three products, consisting of the Virtual Navigator Server, Virtual Navigator Pro, and the Virtual Navigator, designed to host, edit, view, and digitize point and line features from 360-degree panoramic Images and LiDAR.

SERVICE PROVIDERS

Infrasense, Inc. – http://www.infrasense.com/ Service Vendor

- **Bridge Deck Scanning** – Infrasense uses GPR, infrared thermography (IR), and high-resolution video to scan bridge decks at normal driving speeds and detect:
    - Rebar-level delaminations.
    - Overlay debonding.
    - Corrosion-induced concrete deterioration.
    - Thickness of asphalt overlays.
    - Rebar concrete cover.
    - Patching and spalling.
    - The NDE data is collected according to ASTM 6087-08 and ASTM 4788-03, using state-of-the-art technology, and triggered with a high-resolution distance encoder.
- Deliverables.
    - Plan-view condition maps showing subsurface and surface defects.
    - Plan-view concrete cover and asphalt overlay contour maps.
    - CADD-compatible versions of maps.
    - Quantities provided by span, lane, or both.
    - Quantities provided by repair class.
- **Pavement Structure Evaluation** – High-speed vehicle-based ground penetrating radar system in combination with other NDT methods to detect:
    - Pavement layer thicknesses.
    - Changes in pavement structure, defining base material type.
    - Subsurface voids and moisture.
    - Relative density of new HMA pavements.
    - The GPR data are collected according to ASTM 4748-10, and synchronized with both linear distance and GPS coordinates for location referencing.
    - Cross-section plots of the pavement structure showing depth of all layers.
- Deliverables.

- Tabular results showing layer thicknesses at defined FWD test locations (synched with GPS).
- Quantities and maps of areas with subsurface voiding or relatively high moisture levels.
- Geospatial plots or geodatabase layers (i.e., ArcGIS).
- Plan-view contour plots of pavement thickness or relative density.

Sanborn – http://www.sanborn.com/products/mobilemapping

- Fleet of nine aircraft, six digital aerial mapping cameras, three airborne LiDAR systems, 600 TB of storage, 300 CPUs for geospatial data processing, a technical staff of over 150 (including engineers, surveyors, photogrammetrists, GIS specialists, and PMP project managers), Sanborn can effectively manage, control, and produce the required information and value-added products required from the Lynx mobile mapping System.

NEW PATENTS

Chen, S., Hauser, E., Boyle, C., Natarajan, M. 2013. *Method and System for Remotely Inspecting Bridges and Other Structures*. Patent Application US 20130216089 A1. https://www.google.com/patents/US20130216089?dq=US+20130216089+A1&hl=en&sa=X&ei=eFxvVY-SJI_YoATksIKIDg&ved=0CB4Q6AEwAA

Spatially Integrated Small-Format Aerial Photography (SFAP) is one aspect of the present invention. It is a low-cost solution for bridge surface imaging and is proposed as a remote bridge inspection technique to supplement current bridge visual inspection. Providing top down views, the airplanes flying at about 1000 feet can allow visualization of sub inch (large) cracks and joint openings on bridge decks or highway pavements. Onboard GPS is used to help georeferenced images collected and facilitate damage detection. Image analysis is performed to identify structural defects such as cracking. A deck condition rating technique based on large crack detection is used to quantify the condition of the existing bridge decks.

APPENDIX B: OVERVIEW OF SMALL UAS NOTICE OF PROPOSED RULEMAKING

Overview of Small UAS Notice of Proposed Rulemaking

Summary of Major Provisions of
Proposed Part 107

The following provisions are being proposed in the FAA's Small UAS NPRM.

Summary of Major Provisions of Proposed Part 107 The following provisions are being proposed in the FAA's Small UAS NPRM.	
Operational Limitations	• Unmanned aircraft must weigh less than 55 lbs (25 kg). • Visual line of sight (VLOS) only; the unmanned aircraft must remain within VLOS of the operator or visual observer. • At all times the small unmanned aircraft must remain close enough to the operator for the operator to be capable of seeing the aircraft with vision unaided by any device other than corrective lenses. • Small unmanned aircraft may not operate over any persons not directly involved in the operation. • Daylight-only operations (official sunrise to official sunset, local time). • Must yield right-of-way to other aircraft, manned or unmanned. • May use visual observer (VO) but not required. • First-person view camera cannot satisfy "see-and-avoid" requirement but can be used as long as requirement is satisfied in other ways. • Maximum airspeed of 100 mph (87 knots). • Maximum altitude of 500 feet above ground level. • Minimum weather visibility of 3 miles from control station. • No operations are allowed in Class A (18,000 feet and above) airspace. • Operations in Class B, C, D and E airspace are allowed with the required ATC permission. • Operations in Class G airspace are allowed without ATC permission • No person may act as an operator or VO for more than one unmanned aircraft operation at one time. • No careless or reckless operations. • Requires preflight inspection by the operator. • A person may not operate a small unmanned aircraft if he or she knows or has reason to know of any physical or mental condition that would interfere with the safe operation of a small UAS. • Proposes a microUAS option that would allow operations in Class G airspace, over people not involved in the operation, provided the operator certifies he or she has the requisite aeronautical knowledge to perform the operation.

Summary of Major Provisions of Proposed Part 107 The following provisions are being proposed in the FAA's Small UAS NPRM.	
Operator Certification and Responsibilities	• Pilots of a small UAS would be considered "operators". • Operators would be required to: o Pass an initial aeronautical knowledge test at an FAA-approved knowledge testing center. o Be vetted by the Transportation Security Administration. Obtain an unmanned aircraft operator certificate with a small UAS rating (like existing pilot airman certificates, never expires). o Pass a recurrent aeronautical knowledge test every 24 months. o Be at least 17 years old. o Make available to the FAA, upon request, the small UAS for o Inspection or testing, and any associated documents/records required to be kept under the proposed rule. o Report an accident to the FAA within 10 days of any operation that results in injury or property damage. o Conduct a preflight inspection, to include specific aircraft and control station systems checks, to ensure the small UAS is safe for operation.
Aircraft Requirements	• FAA airworthiness certification not required. However, operator must maintain a small UAS in condition for safe operation and prior to flight must inspect the UAS to ensure that it is in a condition for safe operation. Aircraft Registration required (same requirements that apply to all other aircraft). • Aircraft markings required (same requirements that apply to all other aircraft). If aircraft is too small to display markings in standard size, then the aircraft simply needs to display markings in the largest practicable manner.
Model Aircraft	• Proposed rule would not apply to model aircraft that satisfy all of the criteria specified in Section 336 of Public Law 112-95. • The proposed rule would codify the FAA's enforcement authority in part 101 by prohibiting model aircraft operators from endangering the safety of the NAS.

CHAPTER 2. EVALUATION OF MOBILE TECHNOLOGIES FOR SAFETY AND OPERATION INFRASTRUCTURE ASSESSMENT

INTRODUCTION

Asset management is a strategic approach to the optimal allocation of resources for the management, operation, maintenance, and preservation of transportation infrastructure. Asset management combines engineering and economic principles with sound business practices to support decision making at strategic, network, and project levels.

One of the key aspects of the development of asset management is data collection. The way in which transportation agencies collect, store, and analyze data has evolved along with advances in technology, such as mobile computing (e.g., laptops, tablets), sensing (e.g., laser and digital cameras), spatial technologies (e.g., global positioning systems [GPS], geographic information systems [GIS], and spatially enabled database management systems). These technologies have enhanced the data collection and integration procedures necessary to support the comprehensive analyses and evaluation processes needed for asset management.

Data collection is costly. In determining what data to collect, agencies must weigh these costs against the potential benefits of better data. Traditional pavement and bridge management approaches are data intensive, requiring extensive data collection activities of most or all pavement and bridge assets on an annual or biannual basis. These efforts can be justified given the cost of agencies' pavement and bridge programs. However, depending on the level of technology needed and the associated costs, it may be difficult to justify similarly extensive data collection efforts for safety and operation assets.

While many of the technology innovations and improved data collection processes have been in the bridge and pavement areas, there are emerging technologies in the safety and operation infrastructure areas that have yet to be applied to the transportation space. These technologies are driving the costs and efficiencies to the point that makes good sense in terms of the tradeoffs between fiscal responsibilities and advantages of having the data. Therefore, while this research covers all highway infrastructure areas, it includes an emphasis on technologies to assess safety and operation infrastructures. Ultimately, through the three-phased approach, the research strives to bundle the best technologies that maximize sensors and computing power in an effort to achieve the vision of one day having an all-in-one data collection system for infrastructure assessment.

Phase 1: Identify, Develop, and Demonstrate Advanced Technologies

Currently under contract with the Texas Department of Transportation (TxDOT) for Phase I of the project, the research team will identify existing and emerging technologies that have the potential to remotely sense and inspect the highway infrastructure from data collection vehicles traveling at normal operating speeds. The research team will also develop and demonstrate new technologies that have the potential to either significantly improve the data being collected or leverage new technologies with existing data collection efforts. The overall goal of this effort is to identify, develop, and demonstrate technologies that can be used to inspect highway infrastructure from mobile platforms. The outcomes will be to improve traveler and worker

safety by reducing and possibly eliminating the need for workers to be on the roadway or roadside manually collecting and inspecting the highway infrastructure. Another outcome will be realized cost efficiencies from bundling infrastructure inspection technologies so that fewer data collection vehicles are needed. To complete Phase I research the following 5 Tasks are proposed:

- **Task 1:** Identify Existing and Emerging Technologies.
- Task 2: Evaluate of Mobile Technologies for Safety and Operation Infrastructure Assessment.
- Task 3: Develop and Testing Prototype Technologies for Safety and Operation Infrastructure Inspections.
- Task 4: Develop and Testing Prototype Technologies for Bridge Inspections.
- Task 5: Develop and Testing Prototype Technologies for Pavement Infrastructure Inspection.

For the purposes of this Interim Tech Memorandum, ITM-2, the remainder of the report will focus on "Task 2. Evaluation of Mobile Technologies for Safety and Operation Infrastructure Assessment."

Task 2: Evaluation of Mobile Technologies for Safety and Operation Infrastructure Assessment

The objective of this task (Task 2) is to evaluate the existing technologies and systems available to assess safety and operation infrastructure. Because this area is not as developed as bridges and pavements, there is a wide array of claimed benefits of various technologies that have yet to be evaluated in a systematic way. In addition, TxDOT has recently started an evaluation of automated pavement distress technologies using camera-based systems. Understanding the capabilities and limitations of the recently developed technologies and systems used to assess safety and operation infrastructure will provide the research team a mechanism to understand the gaps in capabilities, which will help steer subsequent tasks. A list of the subtasks undertaken to achieve the above include:

- **Subtask 2.1:** Development of Testing Protocol.
- **Subtask 2.2:** Identification and Selection of Contractors.
- **Subtask 2.3:** Data Collection.
- **Subtask 2.4:** Evaluation of Results.

SUBTASK 2.1: DEVELOPMENT OF TESTING PROTOCOL

The primary objective of this subtask is to develop a testing protocol for evaluation of the mobile technologies for Safety and Operations Infrastructure Assessment (SOIA). The testing protocol will include several key elements such as a list of SOIA assets of interest to TxDOT, routes and testing conditions that will be assigned, and the performance metrics that will be used to compare and assess the technologies tested.

Previous Documented Efforts

Before developing a testing protocol specific to TxDOT roadways, researchers investigated a selection of previous mobile technology evaluation efforts carried out for the (1) Illinois, (2) Michigan, (3) North Carolina, and (4) Virginia Departments of Transportation (DOTs). The primary goal of this investigation was to assess and compare protocols developed for similar studies assessing high speed technologies and their performance in roadside asset management.

As established, the future protocol is divided into three key elements including SOIA Assets, Testing Routes and Conditions, and Performance Metrics. In addition to looking into each study (included in Task 1) they are further broken down below by the specific elements that will be found in the TxDOT protocol.

SOIA Asset Review

In reviewing these documents, it is obvious that there is no standard SOIA framework or architecture. Often some assets are considered roadside elements by one DOT while other DOTs further divide roadside elements into categories such as vegetation and right-of-way (ROW) assets.

No single asset was studied in all four efforts (see Table 14). Three of the studies collected data on signing, guardrails, and drainage features.

Table 14. Assets Collected in Similar Mobile Technology Studies.

General Category	Asset	Illinois	Michigan	North Carolina	Virginia
Roadway	Lane		X	X	
	Shoulder		X	X	
	Slope	X			
	Curb miles		X	X	
	Horizontal Curves			X	
	Vertical Curves			X	
	Centerline			X	
	Intersections			X	
	Medians			X	
	Median Openings			X	
	Driveway	X		X	
Traffic Control Devices	Signs		X	X	X
	Sign Support	X			
	Object Markers				X
	Markings			X	
	Raised Pavement Markers			X	
	Signals		X		X
	Illumination		X		
Roadside	Trails		X		
	Edge Treatment (Rumble)			X	
	Barriers			X	
	Guardrail	X	X		X
	Guardrail End Treatments		X		
	Attenuators		X	X	
	Fence	X	X		
	Sound Wall		X		
Maintenance	Sweepable Approaches		X		
	Mowable Acres		X		
	Trees	X			
Other	Bridges		X		
	Pavement		X		
	Drainage Features		X	X	X

Testing Routes and Conditions Review

The four selected studies also provided details on study sites where data collection was performed. Researchers developed Table 15 to better understand how similar research considered

functional class, length, and control condition (open/closed course). In addition to these three test route conditions the studies also considered traffic volume, parking, and speed limits.

Table 15. Testing Routes Summaries of Similar Studies.

State	Route Details	Control Condition
Illinois	1. Site 1- Rural multi-lane highway: South University Drive from University Park Drive to IH 270, 8 miles 2. Site 2 - Freeway segment: IH 270 from IL-157 to IL-159, 4 miles 3. Site 3 - Rural two-lane highway: IL-140 from IL-159 to IL-157, 12 miles 4. Site 4 - Urban and suburban arterials: Governor's Parkway from Esic Road to District Drive, 4 miles *Total: 28 miles | Average: 7 miles*	Open course, uncontrolled
Michigan	1. Principal Arterials (NFC 1): 11 miles 2. Minor arterials (NFC 2): 13 miles 3. Collectors (NFC 3): 22 miles 4. Local roads (NFC 4): 130 miles *Total: 176 miles*	Open course, uncontrolled
North Carolina	1. IH 440: Inner freeway beltline around Raleigh, NC 2. IH 40: Major interstate across NC 3. Wade Avenue: Freeway extension between IH 40 and IH 440 4. US-70/Glenwood Avenue: Primary arterial in Raleigh, NC 5. IH 540: Outer freeway bypass around Raleigh, NC 6. US-1/Capital Boulevard: Primary arterial heading north from Raleigh, NC 7. NC-98: Rural two-lane highway 8. NC 39: Rural two-lane highway 9. US-64/US-264: Important freeway heading to Eastern NC *Total: 90 miles | Average: 10 miles*	Open course, uncontrolled
Virginia	1. VTTI Smart Road: contains eighteen tenth-mile long segments that are marked by mile markers *Total: 1.8 miles*	Open, controlled

Performance Metrics Review

In addition to assets and testing routes, it was necessary to understand which performance metrics were considered important and then used to evaluate mobile technologies. Researchers discovered from the selected studies that the following were considered for evaluation:

- Equipment Cost.
- Labor Cost.
- Data Collection Time.
- Safety.
- Data Completeness.
- Data Quality.
- Disruption of Traffic.
- Software Cost.
- Data Reduction Cost.
- Data Storage Cost.
- Processing Time.
- QA/QC Provisions.

Proposed TxDOT Testing Protocol Framework

As discussed earlier, the testing protocol will include three key elements: a list of SOIA assets of interest to TxDOT, routes and testing conditions, and the performance metrics that will be used to compare and assess the technologies tested (see Figure 25).

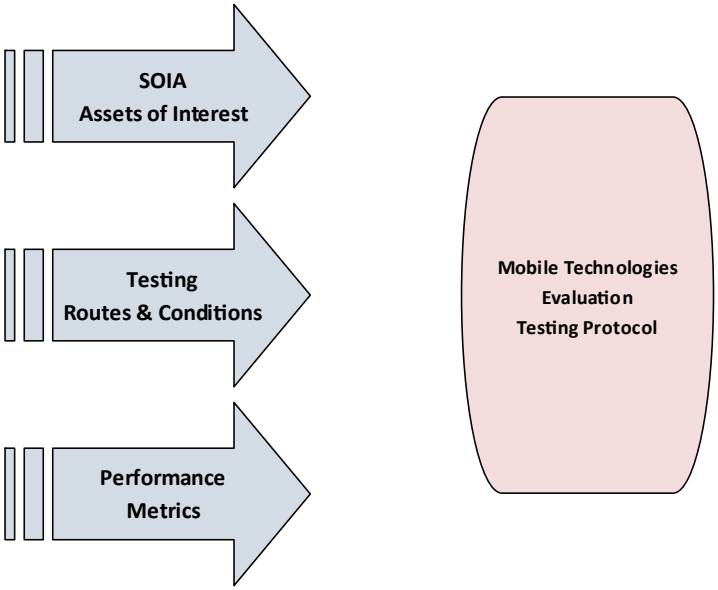

Figure 25. Mobile Technologies Evaluation Testing Protocol Framework.

SOIA Assets of Interest

The list should be thought of as a comprehensive list; however, vendors might not be able to include all of them in their testing. This is acceptable as the ultimate goal will be to bundle technologies to meet the core needs of data collection and condition assessment. Based on our findings in the literature, the following architecture for SOIA Assets will be used for the project: categories, types, and attributes. Figure 26 shows an example of the asset architecture.

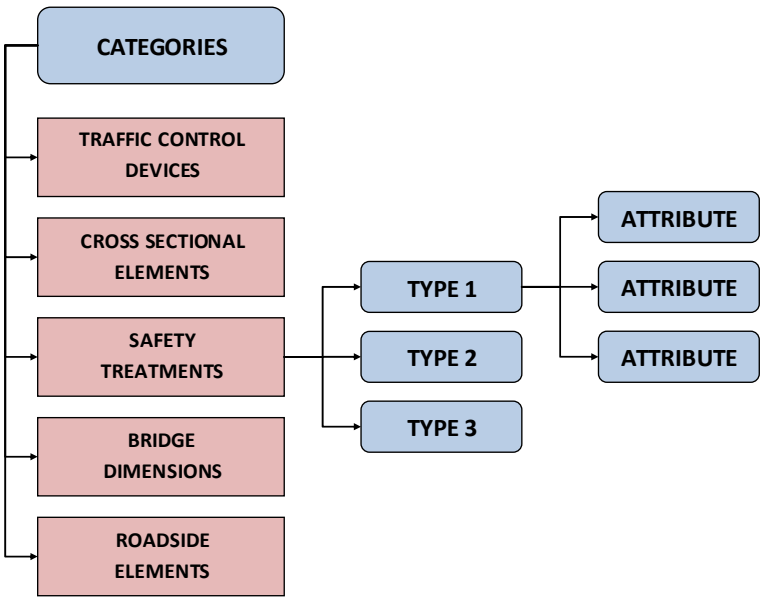

Figure 26. Example SOIA Asset Architecture with Project Categories.

Assets for Evaluation

After reviewing the selected literature and several white board sessions, a preliminary list of assets was developed. Researchers then traveled to the field to confirm the presence of assets and further refined the list. From this list and the asset architecture, a draft data dictionary was prepared.

Data Dictionary Structure

The data dictionary for this project includes 5 Asset Categories and 20 Asset Types and their corresponding attributes. The Asset Categories include: Traffic Control Devices, Cross Sectional Elements, Safety Treatments, Bridges (Dimensions), and Roadside Elements. For a uniform approach to organization, Asset Codes were developed and applied to individual asset attributes for ease in identification. These Uniform Asset Codes can be found in Table 16.

Table 16. Asset Type and Uniform Codes.

Category	Type	Code	Attributes
Traffic Control Devices	Sign	SGN	Table 5
	Sign Support	SGNSUP	Table 6
	Pavement Marking Linear	PVML	Table 7
	Pavement Marking Point	PVMP	Table 8
	Signal Heads	SIG	Table 9
	Signal Pole	SIGPL	Table 10
	Delineators	DEL	Table 11
	Object Markers	OBM	Table 12
Cross Sectional Elements	Lane	LAN	Table 13
	Shoulder	SHLD	Table 14
	Median	MED	Table 15
	Median Opening	MEDOP	Table 16
	Drive Way	DRWY	Table 17
Safety Treatments	Rumble Strip	RMBL	Table 18
	Barrier	BARR	Table 19
Bridge	Bridge	BRDG	Table 20
Roadside Elements	Drainage	DRAIN	Table 21
	Illumination	ILLUM	Table 22
	Mail Box	MLBOX	Table 23
	Vegetation	VEG	Table 24

Data Dictionary Asset Attributes

Asset Attributes are detailed for each asset type and prepared in tables with five columns including:

- Field.
  - Names the attribute.
- Data Type.
  - Identifies the output type for each attribute measurement (like text and number).
- Unit/Format.
  - Demonstrates the unit of measure for the attribute and the format required in the report, for example mile/0.000 means that measurement should be recorded in mile with three decimal digits precision.
- List.
  - A list of attributes to be chosen from. If not within the list "other" should be used.
- Description.
  - Defines each attribute, its measuring method, and the federal and state references that could be used for more information.

Data Dictionary Attribute Tables

For each Asset Type, attribute details can be found in Appendix A (Tables A1 through A19).

Point Assets versus Linear Assets

The assets in the data dictionary are divided into two general data types: Linear Assets and Point Assets.

Linear Assets are those assets that run the length of the roadway like pavement markings, lanes, shoulders, etc. To collect the attributes of linear assets, uniform sections will be used. A uniform section is where the specific linear asset attributes do not change significantly for some distance. For example, a uniform pavement marking section is the section of the marking or markings that its type, width, color, and material are uniform along the section. As soon as one or more of these attributes change, the current section ends and a new uniform section starts. To measure the linear asset, one should measure the uniform attributes along that section.

Point Assets includes assets like signs, sign supports, illuminations, etc. Since the assets of this kind are singular at their respective locations, only the desired attributes for that specific asset will be collected at that point location.

Asset Summary Inventories

In addition to the Asset Data Assessment Spreadsheet built from the data dictionary, an inventory for some assets will be conducted/developed from the data collection (see Table 17). Single assets and asset attribute combinations should be summarized in an Asset Inventory Table (see Table 18). For example, the total length of 4-inch, white, solid, Type I pavement markings should be included in this summary table along with other attribute combinations.

Table 17. Asset to Be Included in the Summary Inventory.

Asset Type	By Attribute Combination (if applicable)
Sign	MUTCD Designation
Sign Support	
Pavement Marking(L)	PVML_MAT, PVML_WIDTH, PVML_TYPE, PVML_COLOR
Pavement Marking (P)	PVMP_MAT, PVMP_WIDTH, PVMP_TYPE, PVMP_COLOR
Lane	LAN_TYP
Shoulder	SHLD_TYP
Rumble Strip	RMBL_TYP
Barrier	BARR_TYP, BARR_END_TRT
Drainage	DRAIN_TYP
Illumination	ILLUM_TYP
Bridge	
Signal Heads	SIG_TYP
Signal Pole	
Mail Box	
Median	
Median Opening	
Delineators	
Vegetation	
Drive Way	

Table 18. Inventory Table.

Field	Data Type	Description
ASSET_NAME	Text	Name of the asset.
ASSET_ATRB	Text	Asset attributes combinations for which that inventory should be reported.
TOT_COUNT	Number	Total number of asset with specific type.

References Used in Data Dictionary Extraction

To prepare the data dictionary a wide range of references including federal and state guidelines, standards, and specification manuals were used including:

- Standards: *Manual on Uniform Traffic Control Devices (MUTCD), Texas version for MUTCD (TMUTCD).*
- TxDOT Manuals: *Texas Roadway Design Manual, TxDOT Maintenance Operation Manual.*

- Specifications: *TxDOT 2004 Standard Specifications for Construction and Maintenance of Highways, Streets, and Bridges.*
- TxDOT Standard Details.

Testing Routes and Conditions

The second key element of the testing protocol was the selection of the testing route and conditions. Researchers heavily considered roadway characteristics, open versus closed course, and other factors such as safety, repeatability, and technology limits. Past experience/use was also heavily considered.

Selecting Test Routes

A preliminary list of potential sites was developed and included both open road sections and the possibility of a closed course at the Texas A&M Transportation Institute's (TTI's) Riverside Facility. The initial list of candidate sites was reviewed to determine if they met the needs of the projects. The candidate sites that were considered for the project included:

- IH 45 near Madisonville.
- FM 3090 in Navasota.
- IH 45 North of IH 610 in Houston.
- IH 10 West of IH 610 in Houston.
- A closed course at TTI's Riverside Campus.

The candidate sites were compared for characteristics and other factors. The aim of the site selection was to select roadways sections that provided a diverse set of SOIA assets, diverse roadway conditions, consistent sections of highway speeds, and that also provided a safe environment for manual data collection.

Roadway Characteristics

A matrix of site roadway conditions was prepared for comparison purposes and included functional classification, land use, AADT, ROW width, alignment, speed, vegetation, and line of sight (see Table 19).

Table 19. Roadway Characteristics of Candidate Sites.

HWY	FM 3090	IH 10	IH 45	IH 45	Riverside
Location	Navasota	Houston	Madisonville	Houston	Bryan/College Station
Functional Class	Two-Lane Highway	Interstate	Interstate	Interstate	Customizable
Land Use	Rural	Urban	Rural	Urban	
AADT	Low	High	High	High	
ROW	<100'	>100'	>100'	>100'	
Alignment	Winding/Hilly	Interstate	Interstate	Interstate	
Speed	Varies	High	High	High	
Vegetation	Tree and Shrubs	None	Grass	None	
Line of Sight	Restricted	High	High	High	

Other Factors

Other factors were also considered in an analysis of potential repeatability, safety (for manual data collection), technology (testing limits), cross-talk potential, asset inventory, past experience (with the site), and proximity to TTI (see Table 20).

Table 20. Other Factors of Candidate Sites Considered.

HWY	FM 3090	IH 10	IH 45	IH 45	Riverside
Repeatability					++
Safety	+		+		++
Technology	+				++
Cross-Talk		++	+	++	Customizable
Inventory	+	+	++	+	Customizable
Past Experience	++		++		+++
Proximity	++		++		++

Sites Eliminated

Three sites were eliminated from consideration including the closed course site at Riverside and the two interstate locations in Houston. The researchers felt that a closed course site was not needed to evaluate the mobile technologies. The success of open road data collection has been well documented in literature. However, if repeatability (for certification purposes) ever becomes a high priority, the closed course site at TTI's Riverside Facility should be reconsidered. The researchers also determined that the safety of staff performing manual data collection was questionable on the urban freeway sections in Houston, and these sites were eliminated from consideration.

The Selected Test Routes

Based on the comparison of candidate sites, TTI identified two study locations for data collection including one interstate highway cross section and one rural cross section. Two segments and limits have been identified:

- IH 45 [CS 0675-05] from TX-OSR Interchange to CR 200 (~10 miles south of TX-OSR) (see Figure 27).
  - Characteristics: Divided Interstate highway with frontage roads with open ditch drainage.
- FM 3090 [CS 0643-05] from CR 404 to CR 186 (~10 miles) (see Figure 28)
  - Characteristics: A winding rural two-lane roadway with open ditch drainage.

Figure 27 and Figure 28 display the location of each of these segments on a Google© map, and Table 21 demonstrates the more details for each segment including control section number and start-end GPS coordinated.

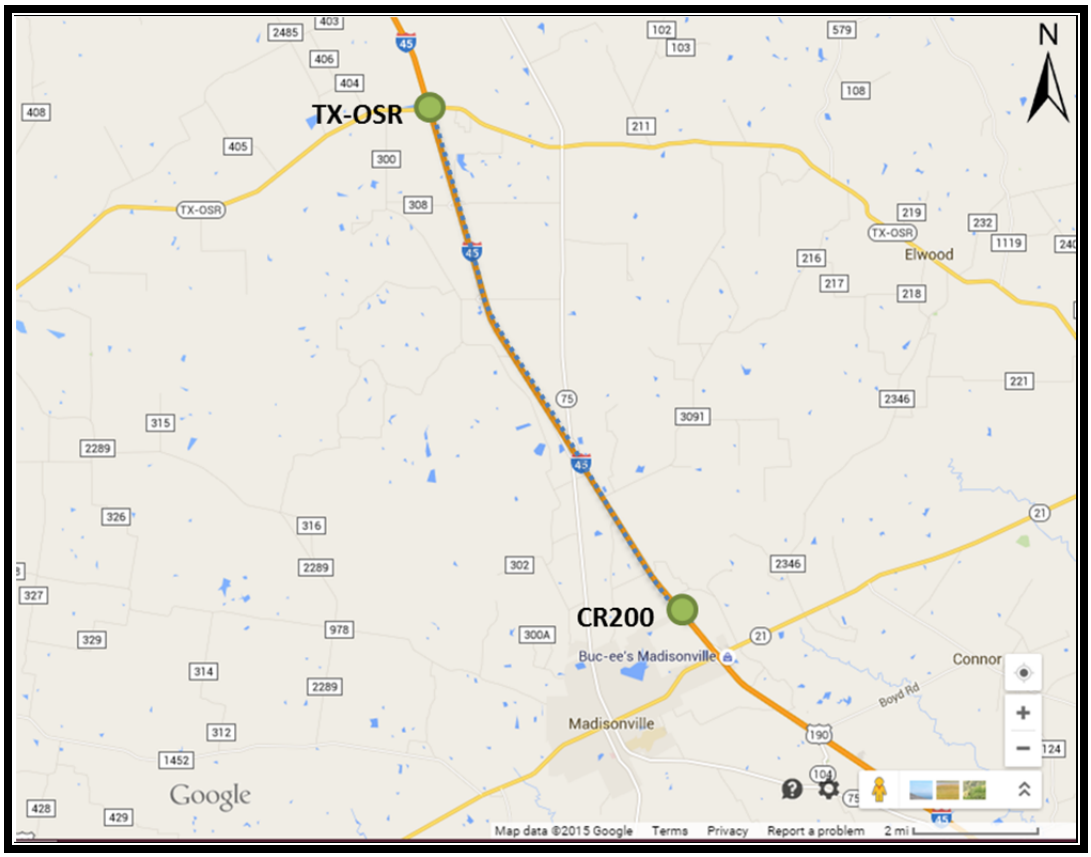

Figure 27. IH 45 [CS 0675-05] from TX-OSR Interchange to CR 200.

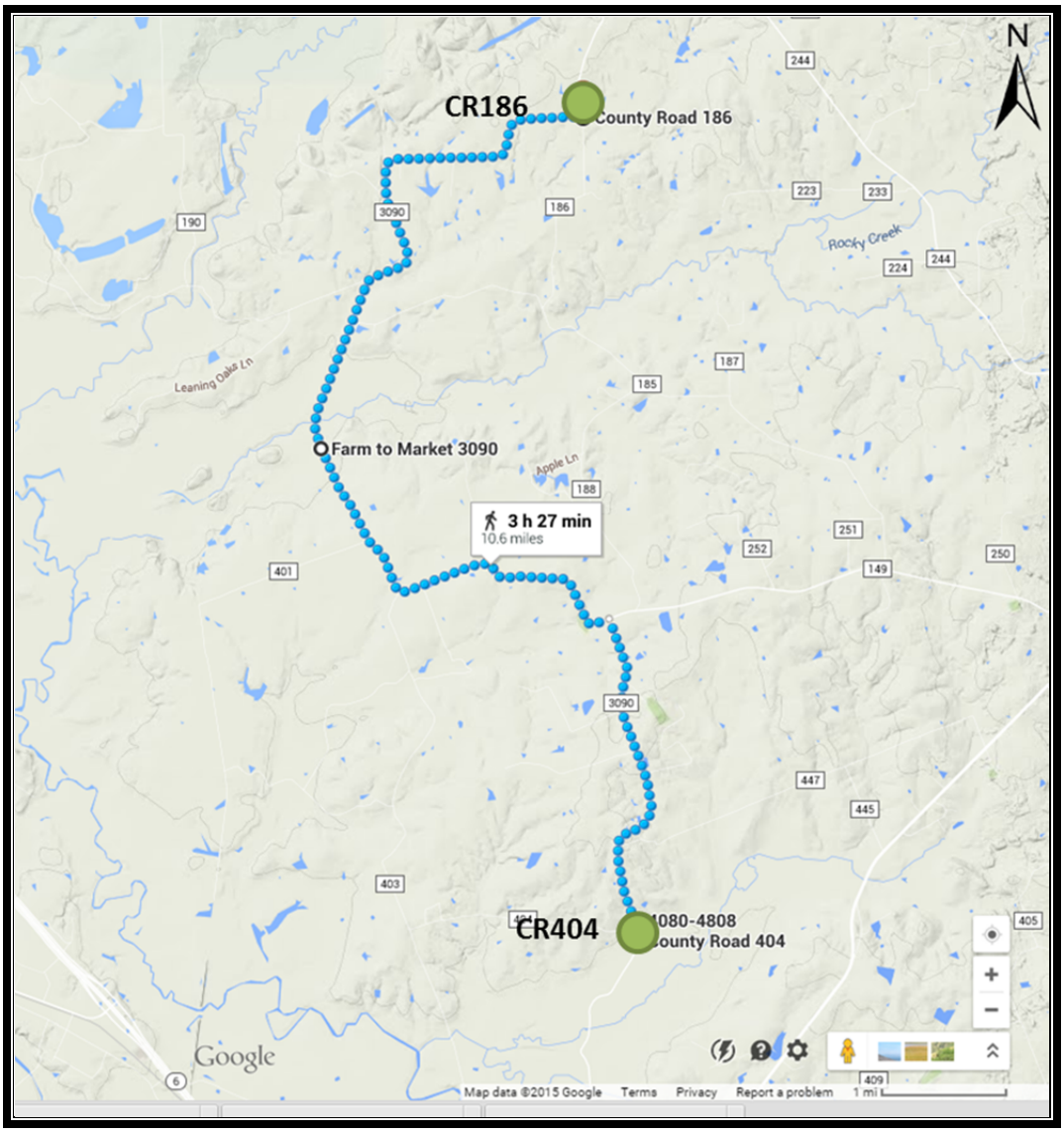

Figure 28. FM 3090 [CS 0643-05] from CR 404 to CR 186.

Table 21. GPS Coordinates for Selected Study Sites.

Study Site	Control Section No.	Starting Latitude	Starting Longitude	Ending Latitude	Ending Longitude
FM 3090	0643- 05	30.449798	-96.056144	30.544930	-96.063570
IH 45	0675-05	30.975531	-95.892594	31.092526	-95.961037

Performance Metrics

Another key element of the testing protocol was the selection of performance metrics that will be used to determine the effectiveness of the technologies. The initial proposal presented a preliminary list of metrics that included:

- Data extraction capabilities (ability capture the desired infrastructure).
- Turnaround time (how long did it take to provide the usable data after the data were collected).
- Quantities of infrastructure elements.
- Accuracy of GPS data.
- Cost.
- Proprietary restrictions that would prevent bundling of technologies.

However, after completing the data dictionary, discussing capabilities with contractors, and conducting test manual data collection efforts, it was determined that the metrics should be divided into four categories: service, identification, quantification, and accuracy.

Service Metrics

Comparable service metrics include mobilization time, data collection time, processing time, approximate cost, data storage, and proprietary restrictions.

Identification Metrics

Identification metrics include asset identification (e.g., MUTCD sign designations), asset material (e.g., sign sheeting, pavement markings), and general sizes.

Quantification Metrics

This performance metric category would include asset quantities in both count and linear totals.

Accuracy Metrics

Generally, accuracy metrics would be limited to horizontal, linear, and elevation measurements (GPS accuracy). However, it was determined that there are other accuracies that can be evaluated such as sign text, retroreflectivity measurement of signs and pavement markings, and area measurements such as mowable acres.

SUBTASK 2.2: IDENTIFICATION AND SELECTION OF CONTRACTORS

In this subtask, the research team identified and selected the technology owners/operators that have been asked to participate in the evaluation. The initial list of vendors was identified in Task 1 of this project. The final list was based on several factors including technology diversity, past experience, availability, working relationships, and mobile platforms. A portion of the budget was set aside in two phases to compensate technology owners/operators for participating in the study. Phase 1 (completed) of the study included an aggressive data collection schedule (30 days from contract execution), and Phase 2 (on-going) included data processing and reporting.

Technology Owners from Task 1

The research team investigated potential technology owners in Task 1: Literature Review. Seven vendors from the literature were contacted to garner interest level in participating and also asked to complete a brief capabilities survey. The contractors were also asked to provide an

approximate cost per mile to perform data collection, processing, and reporting for the two selected sites.

Selection Process

At the time of the initial survey, the research team was not certain that all contractors could be compensated for their participation. The capabilities survey was intended to be used to select roughly 5 vendors. However after receiving approximate costs, it was quickly realized that all vendors could be contracted to participate. For the purposes of completeness the evaluation matrix can be found as Table 22. Due to the aggressive data collection schedule no re-evaluation of other vendors from Task 1 was feasible.

Table 22. Technology Owner Evaluation Matrix.

	Technology	Platform	Past Experience	Availability	Working Relationship (w/TTI)
DTSGIS	L, P	Ground	Yes	Yes	No
DBi	L, P, R	Ground	Yes	Yes	Yes
ArchAerial	P	Air	Yes	Yes	Yes
Mandli	L, P	Ground	Yes	Yes	Yes
Pathway	L, P	Ground	Yes	Yes	Yes
Fugro	L, P	Ground	Yes	Yes	Yes
Facet-Tech	L, P, R	Ground	Yes	Yes	Yes

L – Lidar | P – Photogrammetry | R - Retroreflectivity

Selected Technology Owners

The seven technology owners for this project include:

- Data Transfer Solutions (DTS).
- DBi Services.
- Arch Aerial LLC (AALLC).
- Mandli Communications.
- Pathway Services Inc.
- Fugro Roadware.
- Facet Technology Corp. (“Facet”).

The following, in no particular order, are company details provided by each technology owner. Additional details on technology owner equipment and data collection process will be provided by the contractors in the Phase 1 deliverable and added to the final technical memorandum for this project.

> **Contractor A: Data Transfer Solutions (DTS)** “is a transportation asset management, planning, engineering, and GIS solutions company focused on asset management and performance-based analysis of infrastructure. DTS brings a variety of capabilities including roadway image collection; condition-based analysis of asset infrastructure; integrated web-based roadway asset image viewers; geodatabase design, software integration and implementation; roadway data analysis software (EarthShaper™), asset

management software (VUEWorks®) and business process analysis. DTS's expert asset management staff understands how to maximize an agency's ability to make confident asset condition decisions."

Contractor B: DBi Services "provides highway, industrial and commercial service solutions for clients including federal, state, and local governments, railroads, utilities and large industries throughout the United States and worldwide. DBi will be using their AMAC mobile data collection system for this project."

Contractor C: Arch Aerial LLC (AALLC) "is a commercial unmanned aerial systems (UAS) operator and hardware manufacturer authorized by the FAA for aerial services in the United States. Through the provision of nationwide rapid response mapping and 3D modeling solutions for businesses in the agricultural, insurance, and energy sectors, Arch Aerial puts easy-to-use data solutions in the hands of operations managers for quick and deliberate decision making."

Contractor D: Mandli Communications "is based in Madison, Wisconsin. Mandli is an industry leader in the design and development of highly specialized digital imaging, data collection equipment, and operational methodologies for various Departments of Transportation throughout the United States.

Since 1983, Mandli has made available to the transportation industry a complete range of imaging, pavement, and positioning equipment. Together with a suite of supporting GIS software and services, Mandli has enabled their clients to design, manage and maintain safe and efficient transportation infrastructure networks.

Mandli has worked with over 30 states across the country, and has brought technology solutions to several nations outside of the U.S. Mandli currently functions exclusively form the Madison office. The corporation has employees with various skill levels in engineering, business, sales, production, programming, human resources, data collection, data processing and management."

Contractor E: Pathway Services Inc. "was established in 1996 and has been providing equipment sales and contract services for automated road and pavement condition surveys to transportation agencies around the globe. Our PathRunner Data Collection vehicles are fully developed and manufactured by our team of experts with decades combined of industry experience. With offices in both North and Central America, we have the pleasure of providing equipment and services to much of the Western Hemisphere, utilizing the largest fleet of full-service data collection vehicles of its kind in the United States. The goal of Pathway Services Inc. is to be the company of choice when an agency wants to collect quality road and pavement condition data. In order to accomplish this goal, we have made our customers the number one priority, placing top importance on quality of data to best serve them. We realize that after the images and data are collected, processed, and delivered, a transportation agency must have the best information to make the best roadway maintenance decisions."

Contractor F: Fugro Roadware "has over 45 years of experience with pavement and roadway asset data collection and offers a strong record of successfully providing services that are described in this solicitation. Fugro offers a wealth of experience with new technologies and methods used by Departments of Transportation to monitor existing roadway conditions and prioritizing maintenance and capital improvements.

Fugro Roadware's Pavement Engineering and Asset Management teams offer state-of-the-practice services and equipment.

Fugro Roadware's pavement and asset management experience is unrivalled. We researched, developed and manufactured the first automated road survey ARAN (Automatic Road Analyzer) vehicle. Our roadway asset data collection vehicles are the leading mobile data collection platform, able to collect the full spectrum of infrastructure information in a single pass at highway speeds. We continue to improve the ARAN and to invest in innovative solutions for data processing, analysis and viewing."

Contractor G: Facet Technology Corp. ("Facet") "has been collecting and processing asset management data for city, county and state DOTs for 15 years. Early efforts focused on signs, signals and pavement markings. Since 2009 the types of information gathered and processed has expanded to all items viewable in the imagery and indexed by LiDAR. With the advent of intellectual property for automated retroreflectivity measurement and sheeting type determination Facet established a market leadership position in sign assessment."

SUBTASK 2.3: DATA COLLECTION (PROCESSING AND REPORTING)

During this subtask, the data were collected for setting the ground truth base level. Data were collected manually by the research team, with the exception of pavement marking retroreflectivity, which was collected with TTI's mobile retroreflectivity vehicle. The timing was coordinated such that the manually collected data and the mobile collected data provided for technology owners to collect data within two weeks of TTI's ground truth effort. This subtask also includes data collection from the technology owners/operators identified in the previous subtask.

Subtask Organization

Due to state fiscal year limitations, this subtask was divided into two phases:

- Phase 1: Data Collection.
- Phase 2: Processing and Reporting.

Phase 1: Data Collection (Completed)

Contractors were required to collect safety and operational asset infrastructure data using any available (proven or unproven) technologies, so long as the data collector is mobile and of high speed. TTI researchers collected data using current manual and electronic technologies with the exception of the pavement marking profiler. The following sub-sections provide details regarding the requirement of contractor deliverables.

Phase 1 Technical Memorandum Template [for Contractors]

The primary contractor deliverable for Phase 1 was a technical memorandum. TTI developed a Phase 1 technical memorandum template outlining what information was important to the success of the project. The outline of the requested information included details about the

contractor or technology owner and the equipment used to collect asset data. Additional details including mobilization time, staff requirements, average speed, and data collection costs were also requested and are later summarized in the evaluation section of this report. The following is the Phase 1 technical memorandum template:

1. Data Collection Equipment
    a. Mobile Platform (Van/Truck) Description
    b. On-Board Sensors and Technology
        i. Capabilities of Technology
        ii. Accuracies of Technology
2. Data Collection Log
    a. Mobilization Time
    b. Staff Requirements
    c. Start and Stop Details and Times
    d. Average Speed During Collection
    e. Approximate Data Collection Costs
        i. Travel
        ii. Manpower
        iii. Administration
3. Amount and Type of Data Collected (if available)
    a. Data Storage Details
4. QA/QC Process (if any)
5. Other notes

Required Equipment and Data Collection Methods

Researchers did not require that contractors utilize any specific equipment or technology for this phase. Rather, the research team requested that contractors utilize the most recent developments in mobile data collection technologies and that data collection must be mobile and of high speed. As long as the data can be extracted, processed and reported, the testing of new technologies was not considered out of scope for this project. The research team required contractors to provide detail regarding the equipment that was used for data collection as well as detail any proprietary restrictions that could possibly prevent technology bundling in a technical memorandum deliverable.

Phase 2: Data Processing and Reporting

Contractors were required to process the data collected in Phase 1 and provide an asset data assessment spreadsheet as well as a technical memorandum detailing their data processing methodology. In addition to the asset data assessment spreadsheet, contractors were provided the option to submit data in their own desired format. The research team also reduced the ground truth data and completed the asset data assessment spreadsheet.

Phase 2 Technical Memorandum Template [for Contractors]

The research team developed the following Phase 2 technical memorandum template for contractors:

1. Post Collection/Pre-Processing Activities
    a. Describe essentially getting the data from the vehicle to the start of processing.
2. Data Processing Equipment
    a. Essentially what is your data processing operation from start to finish just prior to reporting?
        i. What equipment is used to process the data?
        ii. How are the data processed?
        iii. Who processes the data?
        iv. Provide details and photos (if available)
    b. Data Storage Details
3. Data Processing Performance Measures
    a. Time to Process the data
        i. Business Days
        ii. Full Time Equivalent Man-hours
    b. Staff Requirements
        i. Number of staff
        ii. Experience
        iii. Supervision
    c. Approximate Data Processing Costs
        i. Equipment
        ii. Software
        iii. Labor
4. Reporting
    a. How does your firm report the findings?
        i. To clients (apart from the requested spreadsheet)
        ii. Does your firm deploy a software package?
        iii. Does your firm use GPS/GIS?
        iv. Does your firm utilize a specific database
    b. Provide details and photos (if available)
5. QA/QC Process (if any)
    a. Details
6. Other notes
    a. Did you come across any issues in processing and reporting based on the provided data dictionary that should be addressed in a future project?
    b. Suggestions on how to integrate the data with existing TxDOT databases available.

Required Equipment and Processing Methods

Researchers did not require contractors to utilize any specific equipment for data processing. In addition, researchers did not provide any restrictions regarding required methodology for data processing. However, contractors were required to detail the methodology used for data processing and record the duration, in days, from the start of data processing to completion (including reporting time). TTI requested that, if possible, contractors report the data processing duration in full time equivalent man hours. Researchers believed this approach would be beneficial to the project, but did not require it. The research team also recorded the time spent reducing the collected data.

Assets Information Required for Reporting

Researchers only required contractors provide the same asset information that was collected for the ground truth data set (if capable). However, contractors were encouraged to provide all asset information collected. At a minimum, contractors were required to complete (full or partial) the asset data assessment spreadsheet provided by TTI. The spreadsheet was populated with categories from the data dictionary.

The research team encouraged contractors to provide 3D models of the study segments if possible, though this was not required. Researchers noted the potential benefit of integration of 3D models into current TxDOT systems such as the Texas Reference Marker System and or Automated Roadway Inventory Diagrams.

Ground Truth Data Collection [TTI]

As part of Phase 1 Data Collection, the research team carried out data collection efforts on FM 3090 and IH 45 in August 2015. During data collection, the team further refined data collection technique, the data dictionary, and data needs.

Determining How Much Data to Collect

After identifying the desired assets and their features, the team manually collected asset data. Researchers categorized the basic types of asset data collected by the research team (ground truth data) and contractors. In the expected data's most basic form, it is expected that the performances of contractor technologies will be evaluated by calculating the accuracies of measure for each of the following categories:

- Horizontal measure.
- Vertical measure (linear).
- Location (GPS).
- Elevation.
- Length.
- Area.
- Quality: color, size, shape.
- Presence (inventory).
- Condition: functional, non-functional.

The above list represents all the basic measurements that each technology owner has been asked to collect. Despite there being different types of SOIA assets with multiple features to measure, all the collected data will fall in to one of the nine basic categories listed above.

This fact decreases the required sample sizes necessary for evaluation, since multiple assets shares several similar features like length or location. Therefore, regardless of asset type, the ground truth data should include unique features/measurements that include these basic measurements. As a result the research team was able to transition from collecting detailed attributes for every asset on FM 3090 and IH 45 to collecting only a sample of assets that included attributes containing the basic measurements. To insure that researchers could establish statistical significance for the evaluation, sample size calculations were required for these basic measurements.

Sample Size Calculation

To calculate the sample size, it is assumed that the performance of the high speed technologies is comparable with manual collection through their percentage of errors against the manually collected data. For this purpose the following formula was used:

$$n = \frac{z^2 p(1-p)}{e^2 + \frac{z^2 p(1-p)}{N}} \quad (1)$$

Where:

z: is the standard normal variable or standard score.
p: is the rate of the technologies accuracy.
e: is the error, or confidence interval that we want our final estimation falls in.
N: is the population size.
n: sample size.

Equation 1 calculates the number of samples needed to estimate the mean value of errors between the high speed technologies and manual data collection with 95 percent confidence that the estimated error lies in E($\hat{p}$)±e, where E($\hat{p}$) is the estimated mean error and e is the range of researcher's confidence interval. Table 23 displays the sample size calculations for several set ups of parameter. As shown in this table, the sample size for an extreme condition where both the population and technologies error are assumed to be very high (2000, 0.2) is only 43 samples.

Table 23. Sample Size Calculations for Various Parameters.

Parameter	z(95%)	p	e	N	n
Selected Values	1.65	0.9	10%	200	22
	1.65	0.9	10%	400	24
	1.65	0.85	10%	600	33
	1.65	0.8	10%	2000	43

According to the calculated sample sizes in Table 23, the minimum number of samples determined for a worst case scenario is 43 samples for each basic measurement.

For measurements where there are not enough assets, like illumination or traffic signals, the entire sample of existing assets were included in the data collection.

Manual Data Collection Process

After preparing all of the preliminary requirements, including determination of study sites, identification of the desired assets and features, and calculating the sample sizes, researchers carried out the ground truth data collection effort.

Mobilization

Prior to beginning data collection, TTI researchers prepared a list of required equipment needed for the effort. The team also performed several preliminary test collections near College Station and at the test routes to explore the accuracy of equipment and identify any concerns and/or challenges. After determining the equipment needs and possible issues and/or challenges, the research team made several trips to the study sites to familiarize themselves with the equipment and prepare for the final data collection effort.

Data Collection Equipment

The research team used the following list of equipment to carry out the ground truth data collection effort:

- Laser distance measurement unit.
- Measuring tape.
- Retroreflectometer.
- Rolling distance measuring wheel.
- Video camera.
- Laptop (to be connected to GPS unit).
- GPS device.
- GPS enabled camera.
- Ladder.
- Measured rod.
- Odometer.

Preliminary Data Collection Efforts

In order to evaluate the functionality of the equipment, identify the possible challenges of manual collection as well as evaluate the accuracy of the research team's measurements, researchers conducted several preliminary data collection efforts. The team selected four sites in College Station and considered several sample assets including signs, guardrails, and drainage structures. The team measured the assets and recorded the desired measurements of each asset according to the data dictionary that had been prepared. During this effort, researchers identified several areas in the data dictionary that needed improvement. These areas were addressed and the data dictionary updated for future use.

Testing Route Site Visits

Prior to final data collection, the TTI team planned and executed trips to both study sites. Start and end points were established using GPS, and researchers drove the routes to check the general condition of the facility and the facility's assets. Several irregularities were found during the trip, specifically with linear assets like the lane and shoulder widths or markings. The research team decided to ignore the local irregularities and look for the nominal measures (e.g., any shoulder less than 1 ft was lumped into a less than 1 ft measurement). This approach was adopted for other irregularities as well and has been addressed in a revision of the data dictionary.

Manual Data Collection

Manual data collection took place during August 2015. Several visits to the study control sections were made during July 2015 to determine the site specific issues. A pilot study was completed at four sites in College Station to confirm planned data collection procedures. These pilot studies ensured that procedure included all safety and accuracy measures necessary for manual data collection and that researchers had all required data collection tools.

Manual data collection started on Friday, August 7, 2015. Researchers utilized a GPS unit connected to a laptop. Signs and other assets were selected randomly until the calculated sample size was reached. A GPS-equipped retroreflectometer was also used to collect retroreflectivity of signs.

Assets were divided into two primary categories: Sampled Assets and Inventoried Assets. Sampled Assets include those assets detailed to obtain the number of samples needed for statistical significance. An example of this type of asset would be a sign, where all attributes including offset, mounting height, sign mount, retroreflectivity, etc. are measured. An Inventoried Asset is one where the asset information was collected for inventorying purposes only. For example, an inventoried sign would only include the MUTCD designation and GPS coordinate but not include horizontal offset and mounting height measurements.

The following summarizes detailed activities during the data collection period.

August 7, 2015

Data collection started at FM 3090 at the intersection of CR 404. Sampled Assets such as signs, driveways, delineators, mail boxes, culverts and lane and shoulder properties related to the northbound segment of the roadway were collected first. Because collecting the data manually required pulling over or backing up, the GPS points for sample assets and Inventoried Assets were not collected at the same time. Researchers then collected Inventoried Assets while traveling southbound (returning). Assets were collected in their primary direction. Drainage features and signs to the right of the vehicle were collected while those on the left were collected in another pass going in the opposite travel direction.

August 12, 2015

The team began the day at the intersection of FM 3090 and CR 404. Northbound travel was dedicated to Inventoried Assets and southbound travel to Sampled Assets.

August 17, 2015

Researchers began data collection for IH 45 and its frontage roads. The team collected roadway data on the east side and west side frontage roads. The research team had been experimenting with combining video data, and it was tested.

August 18, 2015

This date was scheduled for video recording along FM 3090. To add a control measure to our GPS data, researchers marked every 0.1 mile with a specific ASCII tag in a GPS software to assess its accuracy. The video taken along this road was also voice tagged for inventory and control purposes.

August 19, 2015

Video data for IH 45 frontage roads was collected as well as the pavement marking data for both frontage roads. The team used ASCII tagging in GPS software to mark pavement marking start and end points.

August 20, 2015

The rest of the inventory and asset data on the related to IH 45 main lanes collected on this day. The team started on the west side frontage road, and for Sampled Assets, the truck was parked at the shoulder of the frontage road and the team walked to each asset.

August 24, 2015

Sampled Asset information was collected on the west side frontage road. Video recording for the main lanes of IH 45 was also performed. The team again used voice tagging on the recorded video. The team maintained a speed of 50 mph during the video recordings. The video camera was attached to the passenger side front window during most of data collection period. To record median data, the video camera was attached to the driver side back window.

Technology Owner Data Collection [Contractors]

Technology owners completed all data collection by August 31, 2015. The primary deliverable for this effort was a technical memorandum due to the TTI team by August 31, 2015. The technology owners were not required to submit data in its raw form though this data was available if needed by the research team or TxDOT.

Technical memorandums from each contractor were received by TTI on August 31, 2015. TTI researchers reviewed deliverables and provided comments as well as requests for additional details and clarifications. Many of the contractors responded to requests, but some failed to provide additional information after multiple requests. The majority of the received technical memorandums are very thorough and provide great detail. These memorandums have been summarized below for brevity. Additionally, the most up-to-date versions of contractor Phase 1 Technical memorandums can be found in Appendix B. Data collection equipment and quality control procedures are summarized below. The results of the Data Collection Log along with TTI's metrics are compared and then discussed in the evaluation section of this report.

Data Collection Equipment

In this research seven contractors were selected in total to test their proposed technologies. These contractors are listed as follows:

- Contractor A: Data Transfer Solutions (DTS).
- Contractor B: DBi Services.
- Contractor C: Arch Aerial LLC (AALLC).
- Contractor D: Mandli Communications.
- Contractor E: Pathway Services Inc.
- Contractor F: Fugro Roadware.
- Contractor G: Facet Technology Corp. ("Facet").

Data collection equipment including on-board equipment is discussed in detail below. It should also be clarified that the information detailed below was primarily provided by the contractors. In some instances, TTI has reached out to a contractor for clarification and received input and sometimes not been provided any additional information. Table 24 provides a quick overview of technologies by contractor.

Table 24. Overview of Contractor Technologies.

Contractor	Navigation/GPS	DMI	Cameras	Lidar
A	X	X	X	X
B	X		X	
C	X		X	
D	X	X	X	X
E	X	X	X	X
F	X	X	X	X
G	X		X	X

Contractor A: Data Transfer Solutions (DTS)

DTS used one of its five Mobile Asset Collection (MAC) vehicles to collect ROW imagery data and light detection and ranging (LiDAR) data for this project. This vehicle made up of a Ford E-350 passenger van, which was chosen specifically for the internal space, shortened hood (which allows to not have the vehicle showing in imagery), and enhancements in the suspension/chassis Ford introduced in these models resulting in better handling and more payload. Figure 29 displays a photo of this vehicle.

Figure 29. DTS MAC Vehicle.

Each MAC vehicle consists of the same technology components/sensors, which allows for redundancy across all vehicles in the event a vehicle has equipment failure or accident. Below is a breakdown of the technology utilized on each vehicle along with accuracy information:

Applanix POS LV 420e V5 Navigation System:

- The POS LV system generates precise, robust positioning and orientation information for mobile data acquisition systems. The system combines all the advantages of GPS with those of inertial technology, to provide continuous and accurate data. By utilizing the POS LV system, data capture can be undertaken quickly and efficiently.
- IMU: Inertial Measurement Unit generates a true representation of vehicle motion in all three axes, producing continuous, accurate position and orientation information. The onboard sensors and technologies on DTS vehicle that was used in this project are listed as follows:
- PCS: POS (Position and Orientation System) Computer System enables raw GPS data from as few as one satellite to be processed directly into the system, to compute accurate positional information in areas of intermittent, or no GPS reception.
- GPS Receivers: Embedded GPS receivers provide heading aiding to supplement the inertial data.
- GPS Antennas: Two GPS antennas generate raw observables data.
- Sub-meter accuracy: The system is rated to get 0.3 m accuracy in the X,Y position and 0.5 m in the Z position.

Distance Measuring Indicator (DMI):

- BEI 5000 Pulse Incremental Encoder.
- Provides 5,000 measurements per rotation of the wheel, with accuracy translating to readings at interval of 0.0048 inches per reading.

- Allows for collection of high resolution imagery at posted speeds.
- Aids in computing of vehicle trajectory.

Cameras:

- Allied Vision Prosilica GX1920C.
- Schneider Compact Lenses.
- Frame rate 15 images per second, 1936×1456 color resolution.
- High-definition cameras with precision lenses calibrated to remove radial distortion, allowing for highly accurate asset extraction.

Pavement Imaging System:

- INO Laser Road Imaging System (LRIS).
- Two linescan cameras and lasers configured to image 4m transverse road sections with 1 mm resolution (4000 pixel) at speeds that can reach 100 km/h.
- Allows fully illuminated pavement image collection even in heavy shadow/canopy areas.

Surface Road Profiler:

- ICC 5-laser System (Two Selcom SLS5200/300, Three Selcom SLS6375/750).
- Angle Lasers (SLS5200/300) have a typical accuracy of 0.0002 inches.
- Point Lasers (SLS6375/750) have a typical accuracy of 0.00037 inches.
- Used to collect accurate and precise Rutting and Roughness (IRI) values while traveling posted speed limits.

Acquisition Server/Software:

- Dell Image Acquisition Server running Windows 7 Ultimate with Qcorei7, 8gb RAM, (8) 2Tb disk drives.
- Allows for RAID data capture to prevent loss of data.
- Utilizes Norpix's Streampix Acquisition software, capable of handling up to 6 cameras triggering simultaneously, with precise timestamps encoded into image EXIF.
- Streampix allows for on-the-fly image enhancements for dark or bright lighting conditions.

Mobile LiDAR Unit (transferable unit able to mount on each MAC vehicle):

- Leica Pegasus: Two – compact high-speed phase-based laser scanner with great precision, 119 m range and 360° field of view.
- Scan rate of more than 1 million points per second and maximum scan speed of 200 profiles/sec.
- GNSS/IMU/Span Sensor capable of 200 Hz frequency.
- Typical Accuracy (without control points, open sky condition) of 0.020 m RMS Horizontal, 0.015 m RMS Vertical.

Contractor B: DBi Services (DBi)

DBi' s mobile asset collections system captures detailed sign information through the combination of black and white cameras, high resolution color cameras and an infrared system (see Figure 30). DBi's mobile system is designed to perform sign inventory and assessment as well as capture the retroreflectivity of both the background and legend of signs and pavement markings and pavement messages within the prescribed MUTCD specifications. Raised pavement markers are simultaneously inventory inventoried and assessed during the retroreflectivity runs. In addition to the sign and pavement marking data collection system, the mobile asset collection system also includes a system for collecting ROW data. The system consists of six high sensitivity cameras, of which five provide a horizontal 360°perspective and one vertically mounted, pointing upward.

Figure 30. DBi Mobile Platform.

The incorporated technologies include sets of cameras and sensors that their accuracies are described as follows:

- Two panchromatic cameras with sensor arrays, 4008×2672, lenses of 85 mm and 25 mm, 12 bit depth with a range of sensitivity to capture the luminance from the sheeting material in the visible range of the EM spectrum.
- Two near infrared sensors (cameras), 2352×1728 14 mm lens, 8 bit depth producing a stereo pair of coordinated imagery mounted at a distance apart to provide imagery in this range of the spectrum.
- Set of cameras mounted at the rear of the vehicle to capture rear facing signs retroreflectivity with 2048×2048, 25 mm lens, and 8 bit depth.
- A camera system that captures the retroreflectivity of line marking with 2048×2048 resolutions and a 17mm lens. A simultaneously captured pair of images is taken at 1 m intervals along the roadway allowing a data resolution of 1 m.

- The daytime high-resolution camera system automatically processes images to produce 360° digital video with no less than 30 megapixels (MP) of total resolution and transmits full bit-depth (12-bit) images. All imagery is correlated with high precision differential GPS through a cellular based VRS (virtual reference station) system supplemented and integrated with a highly accurate 3 axis IMU (inertial measurement unit) that incorporates three angular rate sensors (gyros) and three servo-grade accelerometers that blends with GPS information to maintain high accuracy measurements in challenging environments.

Using a photogrammetric approach to obtaining the retroreflectivity measurements the system shall captures pavement line markings of white, yellow, and red color:

- Following ASTM Standard E1710-11, the system measures retroreflectivity of all pavement markings (lines and pavement graphics) at the ASTM prescribe 30 m geometry according to the pitch and roll data from the vehicle's inertial system. A simultaneously captured pairs of images are taken at 1 m intervals along the roadway allowing a data resolution of 1 m.
- Camera System has 2048×2048 resolutions with a 17 mm lens.

360°Video System

The daytime high-resolution camera system automatically processes images to produce 360° digital video with no less than 30 megapixels (MP) of total resolution and transmits full bit-depth (12-bit) images. The 360° video system consists of consists of six high sensitivity cameras, of which five provide a horizontal 360° perspective and one vertically mounted, pointing upward. The system creates a panoramic scene of the surroundings that enables a full 360° field of view allowing the user to infinitely choose the field of view of interest. All imagery is correlated with high precision differential GPS through a cellular based VRS (virtual reference station) system supplemented and integrated with a highly accurate 3 axis IMU (inertial measurement unit) that incorporates three angular rate sensors (gyros) and three servo-grade accelerometers that blends with GPS information to maintain high accuracy measurements in challenging environments.

Contractor C: Arch Aerial LLC (AALLC)

Arch Aerial LLC is a commercial unmanned aerial systems (UAS) operator and hardware manufacturer authorized by the FAA for aerial services in the United States. Arch Aerial uses small UAS under the protocols associated with the Section 333 Exemption granted to AALLC in April 2015. For TxDOT Project 0-6869, AALLC deployed one AALLC survey vehicle with two OCTO multi-rotor aircraft (see Figure 31), an AALLC mobile ground station, and associated survey equipment. The Arch Aerial OCTO has an 8 kg payload capacity, and a 22-minute flight time at minimum payload, and 14-minute flight time with a full payload. The OCTO was accompanied by a 4×4 Dodge Ram 1500 outfitted with a laptop stand and equipped with spare parts and survey equipment.

UAS Payload: The main payload for this project was a Sony A600. Crop sensor, 24.3 megapixel, 10.1 ounce, mirrorless. It is unclear how the camera and the UAS' GPS were linked for post processing.

Figure 31. Arch Aerial OCTO UAS Platform.

Contractor D: Mandli Communications (Mandli)

Mandli uses a combination of multiple technologies to collect the required highway asset data. The vehicle utilized for this data collection effort was an E53. The vehicle featured high-resolution cameras, the Laser Crack Measurement System (LCMS), the Applanix POS with DMI and IMU. This vehicle is depicted in Figure 32. For the purpose of this project they added dual LiDAR heads to the vehicle.

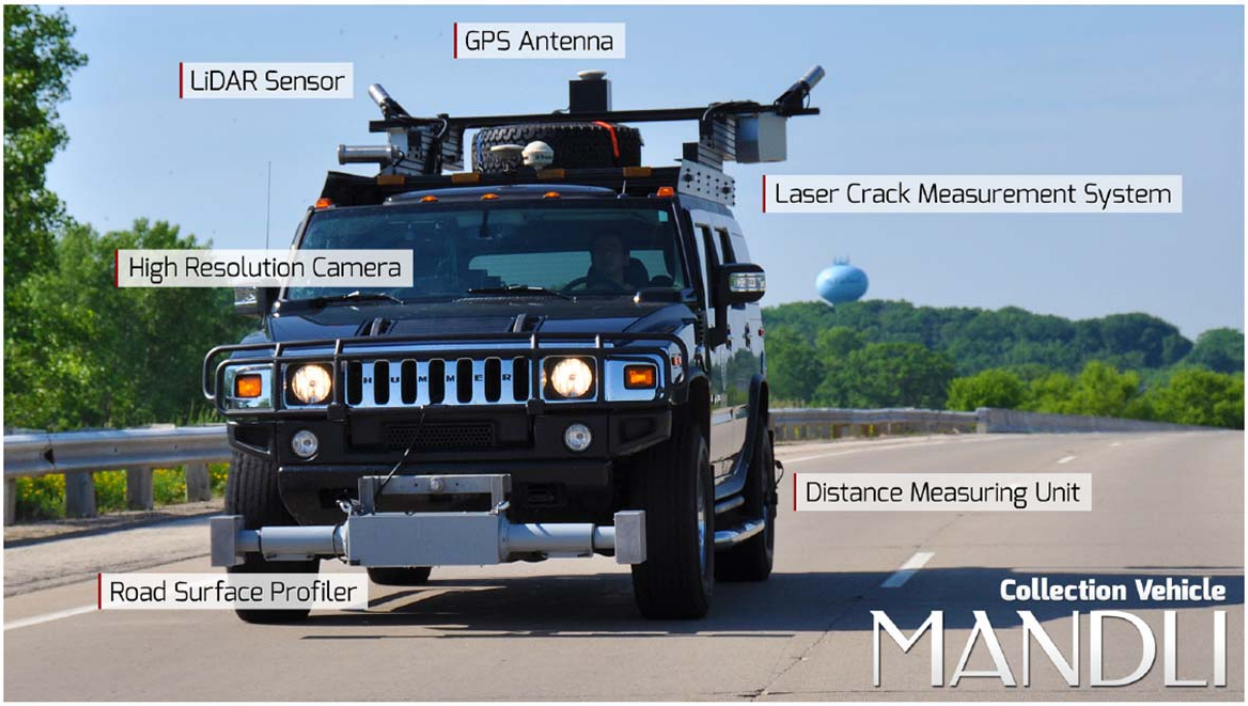

Figure 32. Mandli Communications' Collection Vehicle.

- **ROW Imaging System:** Mandli used high-resolution cameras that produce 2448×2050 pixel images and can be utilized for advanced asset identification and management. The

imaging software controls data collection with real-time image viewing, camera controls, GPS data, route setup and management features, and DMI calibration and operation. The imaging system is triggered by the DMI and Triggered with DMI and GPS accurate ±1 m.

- LiDAR: The system features frame rates of 5–15 Hz and collects over 1.4 million data points per second, creating a 3D data set with a greater level of accuracy than can be obtained through 2D and photo technology. The system features a relative accuracy (point-to-point) of ±2.54 cm @ 2 sigma within appropriate operating conditions.
- DMI: The DMI they use The DMI is capable of measuring distance accurate to within ±one thousandth (0.001) per mile, and can display the distance in miles or kilometers to four decimal places.
- GPS: The GPS Mandli use incorporates the Applanix POS LV unit, and Inertial Measurement Unit (IMU) with real-time differential incorporated with a wheel encoder. Its accuracy is within ±1 m.

Contractor E: Pathway Service Inc. (PSI)

Pathway Services' PathRunner Data Collection Vehicle (see Figure 33) is a state-of-the-art service tool equipped with the latest computer, sensor, and digital imaging equipment designed to efficiently collect pavement condition data and imagery of the roadway and pavement surface. Pathway's newest generation of PathRunner data collection vehicles, utilize innovative computer technologies to collect high-resolution data and images at highway speeds. A user-friendly and real-time Windows application is at the heart of our collection system and seamlessly integrates all of the following:

- 3D laser-based pavement surface images.
- High-resolution video log roadway imaging.
- 3D-based rutting and faulting measurements.
- Longitudinal and transverse profile.
- MacroTexture.
- Road geometrics.
- GPS location data.
- Automated Crack Detection.
- LiDAR Mobile Mapping.

Pathway Services' research and development team has developed and integrated nearly 20 separate subsystems into the data collection system so it can collect, deploy, and maintain as many data types as possible with a single pass of the roadway. Additionally, the system's software incorporates live graphical feedback of all its subsystems which allows the vehicle's operator to verify the proper operation of the sensor equipment in real-time. Voice animated GPS mapping and diagnostics allows the vehicle to efficiently and accurately collect all sensor data and images over long distances and periods of time. This results in quality data on a tight schedule at minimum cost.

Data Type	Pathway Subsystem used to Collect per spec.	Precision / Accuracy
Cracking	Pathway 3D with AutoCrack software	1 mm or better, 90%+ repeatability
IRI	PathRunner XP	Class 1, TTI certified
Rutting	Pathway 3D	1 mm or better
Faulting/Texture	Pathway 3D	1 mm or better
GPS	Onboard DGPS with IMU	Submeter up to .02 m
Geometric Data	Onboard DGPS with IMU	+/- .015 degrees
Pavement Imaging	Pathway 3D	Up to 1mm cracking
MacroTexture (MPD)	Pathway Macro	64 KHz
Roadway Imagery	3 cameras, Super HD, 120 Degree FOV, rear option	2750 X 2200 pixels / camera
Roadway GPS	Onboard DGPS with IMU	Submeter up to .02 m
360 Degree Imaging	Pathway 360	Up to 30 megapixels using six 2048x2448 CCDs
Viewing software	PathView II and PathWeb option (hosted)	NA
Roadway Asset Data (image)	PathView II Asset Module (IDOT license too)	inches (based on imaging)
Roadway Asset Data (LiDAR)	1M points per second, project-level LiDAR	Hor 0.020 m, Vert 0.015m

Figure 33. Pathway Services PathRunner Data Collection Vehicle.

Capabilities of Technology: With so many data types available completely synchronized and tied to GPS/linear referencing systems, numerous departments within the transportation industry benefit from the data and results produced by our advanced and versatile data collection system. Pavement management systems are supported by the pavement condition data such as IRI roughness, transverse profile, rutting, faulting, texture, cracking and patching. Pathway's 3D pavement surface images allow for fully-automated distress detection and evaluation. Asset maintenance groups utilize the digital images and LiDAR point clouds of the roadway to inventory asset characteristics, such as signs, guardrails, barriers, etc. Traffic safety programs use high-resolution digital images and curvature data for reporting and legal issues.

Accuracies of Technology: In regard to location accuracies, the stated accuracy without post processing of the GPS will be submeter. Additionally, most asset locations will have accuracies as low as inches and as high as a few feet when compared to real-world static collection.

Contractor F: Fugro Roadware (Fugro)

Fugro uses the ARAN data collection vehicles including ARAN 9000 and ARAN 7000 RoadProfiler (see Figure 34). The ARAN is a network of tightly integrated subsystems used to synchronously collect data and geo-referenced imagery for video log and roadway infrastructure management applications.

Figure 34. Fugro's Automatic Road Analyzer.

The list of equipment and instruments and their specification installed on ARAN for in this project is as follows:

- **Mobile Laser Mapping System:** This laser has 355° field of view (FOV) and comes with accuracy of 5 mm and precision of 3 mm.
- **On-Board GPS and Inertial Navigation System:** It provides accuracies of latitude, longitude, within ±0.3 m (1 ft) and elevation within: ±0.50 (1.6 ft).
- **Real Time Kinematic Global Positioning System (RTK- GPS) with a Global Navigation Satellite System:** It includes Trimble Differential Global Positioning System with 12 channel mobile receiver and real-time DPGS services such as OmniStar and Coast Guard Beacon.
- **DMI:** It has accuracy of Accurate to ±0.02 percent and its rugged duty heavy shaft encoder capable of recording 2,000 revolutions per minute.
- **Pave3D Subsystem:** It incorporates two lasers with sampling rate of 5,600 profiles/s or 11,200 profiles/s. It has the capability of identification of fine cracks of widths 0.08 inches or greater.
- **Laser SDP (South Dakota Profiler) with GoCater Sensors:** It includes contactless sensors (GoCater) in the left and right wheel paths spaced at 66 inches apart. It collects

longitudinal profile at user defined intervals as low as 0.5 inches (12.5 mm). Its travel distance accuracy is 0.02 percent.

- **Sony High Definition (HD) Camera (3CCD broadcast quality):** It comes with a 90° field of view and 1920 × 1080 pixels with true 24-color pixels.
- **Smart Texture:** It is Selcom 64KHz. laser with accuracy of 0.005 inches (0.13 mm) and precision of 0.00126 inches (0.03 mm).
- **Roadway Geometry:** Longitudinal grade accuracy of ±10 percent against rod and level measurements, horizontal cross slope/super elevation (slope) accuracy of ±10 percent, and export intervals of < 16 ft.

Contractor G: Facet Technology Corp. (FACET)

Facet uses Chevrolet Tahoe vehicles for all data collection. The vehicles are customized to supply sufficient AC power to the sensors and on-board computing systems. Touch-screen control of all systems is available to the vehicle operator, and real-time mapping information is provided during data collection activities (see Figure 35).

Figure 35. Facet Data Collection Vehicle.

Facet uses following sensors and technology to collect data:

- **Quantity 2 Velodyne HDL-32 LiDAR Units:** This unit produces a 360° horizontal field of view and a 41° vertical field of view with usable returns up to 70 m. The device produces 700,000 points per second and the stated accuracy is <2 cm (one sigma at 25 m).
- **Point Grey Labybug 5 Spherical Camera:** The Ladybug 5 camera has a horizontal field of view of 360°, a vertical field of view of 270°, and captures up to eight frames per second in its highest resolution (30 megapixel) mode.

- **Quantity 3 Point Grey 5 MP Grasshopper Cameras:** Point Grey 5 MP Grasshopper cameras are capable of producing 15 full-resolution images per second.
- **SICK LiDAR Unit:** The SICK LiDAR unit produces 80,000 points per second.
- **Applanix POS/LV220 v4:** The Applanix POS/LV220 can produce 1.2 m positioning and 0.7° accuracy on heading for the real-time navigation solution. Utilizing post-processing software the guidance solution accuracy is 20 cm with angular heading accuracy of 0.6°.

Contractor Equipment Summary

Researcher using the information gathered from the Phase 1 Technical Memorandum and follow-up communication developed a matrix of on-board technologies (see Table 25) and a matrix of equipment accuracies (see Table 26).

Table 25. Contractor On-Board Equipment Matrix.

	Navigation/GPS	DMI	Cameras	LiDAR
DTS	Applanix POS LV	BEI 5000	Allied Vision Prosilica GX1920C	Leica Pegasus (2)
DBi	Virtual Reference Station (Cellular)		Panchromatic (2), Infared (2), Other (set)	
AALLC	Unknown		Sony A6000	
Mandli	Applanix POS LV	Unknown	Unknown	Unknown
PSI	PSI Proprietary	PSI Proprietary	PSI Proprietary	PSI Proprietary
Fugro	Applanix POS LV Trimble Differential	BEI HS35	Sony HD	Riegl VMQ-450
FACET	Applanix POS LV		Point Grey Ladybug Point Grey Grasshopper	Velodyne HDL-32 SICK

Table 26. Contractor On-Board Equipment Accuracies Matrix.

	Navigation/GPS	DMI	Cameras	LiDAR
DTS	0.3 m (x,y) 0.5m (z)	0.0048 in/read	1936x1456	1,000,000 pts/sec 0.02 m H 0.015 m V
DBi			4008×2673 (Panchromatic) 2352×1728 (Infrared) 2048×2048 (Other)	
AALLC			24.3 megapixel	
Mandli	"±1m"	"±0.001/mi"	2448×2050	1,400,000 pts/sec ±2.54 cm
PSI	Submeter	±0.001/mi	2750×2200	1M+ pts/sec 0.02 m H 0.015 m V
Fugro	0.3 m (x,y) 0.5 m (z)	"±0.02%"	1920×1080	1,000,000 pts/sec 0.05 m H 0.05 m V
FACET	1.2 m		30 megapixels	700,000 pts/sec <2 cm

Quality Assurance

TTI also requested information regarding each contractors their QA/QC process and not only received information regarding data collection but data processing as well. Contractor responses ranged from highly general comments regarding data checks to details flow charts and discussions of 9001 compliance.

Contractor A: DTS

DTS data collection operators continually monitor GPS/IMU signals and image quality in real-time and note anomalies for adjustment (i.e., image brightening in canopied areas) as needed. DTS also reviews and verifies and visually looks at collected imagery again once in the office (10 percent of beginning, mid-day and end of day collection) to ensure imagery is not blown out, too dark, free of obstructions (i.e., bugs on camera lens). DTS marks anything not passing QA for recollection.

Contractor B: DBi Services

DBi provided a single figure of their QA/AC Process (see Figure 36).

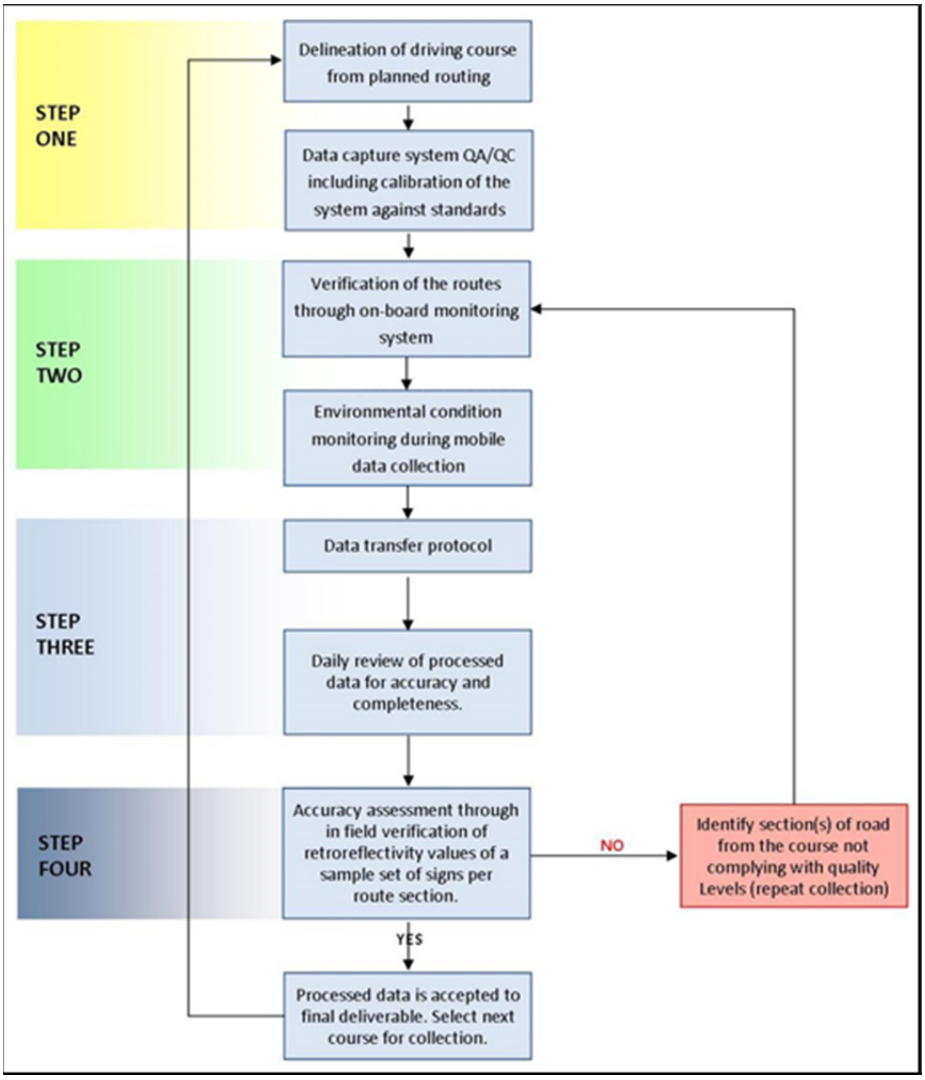

Figure 36. DBi Services QA/QC Process.

Contractor C: Arch Aerial

ArchAerial's process involved real-time checks. An ArchAerial UAS technician and pilot would review imagery on a 15-inch monitor after each flight to give a "Go" or "No-Go" for the next leg of the survey. ArchAerial reported that the QC/QA process triggered two additional flights to ensure accurate data.

Contractor D: Mandli

For the Mandli team, collected data are checked against system thresholds specific to each data set. Mandli then automatically flags any data that does not pass these checks. Sections of the GIS data are exported to shape files and compared to existing maps and other photos for accuracy. Exported shapefiles are also utilized to check for any overlapping features. ROW images are analyzed for over-exposure, focus, and readable item issues.

Mandli also provided a set of hardware and data checks:

Hardware Checks

DMI System

- Check tire pressure with a tire gauge and adjust accordingly to match manufacturer's recommendation when tires are cold, which should also match what the tire pressure was during calibration.
- During collection, monitor recorded distance against expected distance provided in feature files; any large (0.1 miles or greater) discrepancies are flagged and office personnel notified.
- Use internal verification program to verify that complete data set has been collected.

GPS

- Check GPS accuracies. Accuracies should be sub-meter to begin collection.
- During collection, monitor accuracies to ensure that accurate data are being collected.
- Use internal verification program to verify that complete data set has been collected and that it was collected with desirable accuracies.
- In office, day after collection, compare traces to shape files and other photos for proper accuracy.

ROW Imaging

- Clean windshield to ensure surface is free of insects, dirt, watermarks, etc.
  - Monitor windshield throughout the day and clean as needed.
- Ensure proper camera functionality prior to collection - Check focus.
  - Check color balance.
- During collection, monitor image quality and adjust the following as necessary:
  - Camera alignment, focus, and color balance.
  - Appropriate settings for given lighting conditions.
- Use internal verification program to verify that complete data set has been collected.
- In office, day after collection, review sample of images to ensure desirable quality has been collected.

Data Checks

Global Position System (GPS) Daily Checks:

- Compare collection traces to customer provided KML to ensure complete coverage of roadway and accuracy of trace.
- Check to ensure positive and negative route traces do not overlap each other.

ROW Imaging System Daily Checks:

- Review focus check images.
- Review random image samples.
- Confirm that images are free of debris/smudges.

- Confirm that images are properly focused.
- Confirm that images are properly color balanced.
- Confirm that images are properly aligned.
- Confirm that roadway signage can be clearly seen.
- Confirm that roadway details are distinguishable!
- Confirm that guardrails, intersection geometry, and traffic control devices are distinguishable.
- Confirm pavement characteristics are distinguishable.
- Confirm roadway signage can be read from a distance of 1 frame.
- Confirm images are void of van shadows.
- Use internal verification program to verify completeness of data set.

Contractor E: Pathway Services

Pathway services did not go into great details regarding their QA/QC process but offered a list of general data check including spatial data checks and completeness checks.

Contractor F: Fugro

Fugro utilizes a Data Quality Management Plan. This plan employed the use of Fugro's ISO 9001:2008 registered Quality Management System (QMS) for every data collection project. This QMS includes a comprehensive set of Standard Operating Procedures (SOPs) for defining work processes and methods, and for controlling quality; both in the field collection and in-office processing of automated pavement condition data. These SOPs are available through a business management system so that both Fugro employees and client's staff can access in real-time and ensure each task is performed with consistency and discipline ensuring data accuracy, repeatability, and delivery in a timely manner. Note: TTI did not access this system.

Fugro's system relies on two cloud based applications, Force.com and Atlassian (Confluence).

Opportunities for Improvement (Force.com)

Within Fugro Roadware's business system they maintain a database of opportunities for improvement. These come from employee, supplier and client suggestions. Fugro focuses on reviewing and implementing every one of these and measure themselves on the Mean Time to Resolve.

Non-Conformities Report (NCR) - Internal Identification (Force.com)

When a client staff member identifies an issue with data or a system, a NCR is completed in Force.com and tracked. This can lead to either a software improvement recorded and linked in Atlassian or a Corrective Action in Force.com.

Software, Hardware or System Feature Request and Bug Report (Atlassian)

All new features and bug reports are recorded in Altassian. They may be linked to a support case in Force.com. The software source code repository is stored in Altassian so that when a feature or bug is fixed it is recorded automatically in the software release notes.

Business Process and Project Console (Atlassian)

Each core client has a "space" in their Atlassain collaboration tool. Fugro publishes the entire project plan and scope of work including the exact process we will follow and records any changes we may make as a team.

Corrective and Preventative Actions (Force.com)

A key element of Fugro's QMS is ensuring lessons are learned and applied from all mistakes and near misses. The genesis of every issue is tracked and the implementation of any changes required is managed through a Corrective Action and Preventative Action (CAPA) system. Fugro measures themselves on the mean time to resolve CAPAs. All CAPAs require a root cause analysis to determine the effective action and triggers are employed to identify high priority items that are escalated to their Senior Management Team for immediate attention. Independent verification is required to determine the effectiveness of the action(s) in preventing such issues from reoccurring.

Red Flags (Force.com)

Fugro Roadware has built a system that automatically raises issues using RED FLAG emails to all senior management.

Equipment Calibration

Automatic Road Analyzer (ARAN) Certification – The ARAN Certification process ensures that data collection vehicle settings and data collected are within project guidelines. This process will enable subsequent data collection by Fugro to meet the requirements of the project, and ensures all ARANs are comparable.

Daily Quality Assurance Cycle – At the beginning and end of each collection day, a quality assurance cycle is performed on all subsystems to ensure each is operating properly. The data collected at the end of the day is also checked for completeness against log sheets and routing schedules. Samples from each system are then uploaded to be evaluated by Data Services personnel to ensure settings and results are within project guidelines.

Daily Verification - The ARAN Collection Software (ACS) interface controls all ARAN subsystems independently to ensure maximum flexibility and robustness during testing/collection. The ACS software provides step-through wizards for easy calibration, diagnostics to monitor system health and a collection screen with built-in mission management.

These systems allow Fugro operators to perform daily verification that ensures every vehicle delivers optimum data accuracy and repeatability, using features such as user-specified data ranges to establish out of range or non-functioning subsystems. Each day, a data subset is uploaded and examined by trained data analysis staff in the office.

Real-time Quality Monitoring on the ARAN – Quality control subsystems are built into each ARAN vehicle. Each ARAN is equipped with a front-mounted computer and video monitors that enable the operator to selectively monitor all images and data in real time. Onboard software monitors the individual data collection subsystems in real-time and alerts the operator when data are either out of range or there is equipment malfunction. If a sensor is recording out-of-range (International Roughness Index [IRI], rutting, GPS), or does not register

a change for a predetermined length of time, the system alerts the operator to the potential malfunction and the need to take action. Newly-enhanced real-time health monitoring ensures that only good quality data is collected, and live remote access into any ARAN by Fugro's technical support team is now standard.

ARAN Project Verification

Prior to commencement of data collection for any project, the ARAN is configured to the specific project requirements. We have developed comprehensive SOPs to verify configuration and the validity and accuracy of data collected by the ARANs.

Pre-Mobilization Calibration and Verification – Prior to mobilization, all data elements to be produced by the ARAN for the TTI project was tested and verified.

Data Collection Start-up Process and Calibration – Once on-site, Fugro surveyed (8) control sites (4 asphalt and 4 concrete sites) of 1,500 ft each. They completed collection in three repeat runs for each control site. Through this exercise, precision and bias tests were conducted for all data items. Calibration procedures, camera angles and coverage, data calculation methods and standard operating procedures were verified. Some project specific control and calibration procedural examples used to ensure project accuracy were:

Pre-collection

- Perform a static alignment while maintaining a minimum 5 minute static period at the beginning of the collection to align the IMU and initialize the GPS signal.
- Immediately following the static alignment, drive the ARAN in a figure eight pattern for 3–5 minutes in order to refine the heading or yaw IMU measurement.
- Once the figures eights are complete, the system is ready for data collection.

During Collection

- Verify point cloud coverage and density.
- Inspect for roll/pitch or elevation change errors.

Post Collection

- After data collection is completed, drive the system in a figures eight pattern for 2–3 minutes.
- Immediately following the end of collection of the figures eights, the ARAN must complete a static session for a minimum of 5 minutes.
- Verify calibration values by sampling areas outside the calibration data set.
- Sample lines to produce an accuracy report.
- Generate a ground truth report to ensure RMS results meet or exceed project specifications.
- Generate point data in its final form.

Contractor G: Facet Technologies

Facet provided no information regarding their QA/QC procedures despite multiple requests.

Ground Truth Data Processing [TTI]

Documenting the ground truth data processing was important to truly establish a way to compare efforts between the ground truth data processing and contractor processing. The ground truth data reduction process started with extracting GPS locations of different assets. Assets were recorded in GPS software using a specific ASCII tag. ArcMap© (10.2) software was used to input GPS points. The control sections maps were also extracted from TxDOT's "Roadway Inventory" data (2013) available from the TxDOT's website. All collected data aligned well with the TxDOT roadway inventory data. The team also took geotagged pictures of every Sampled Asset that was collected and input them into ArcMap software using a built it tool called "GeoTagged Photos To Points (Data Management)." The next steps was to use recorded video to develop roadway inventory and condition data for FM 3090 and IH 45.

Post Collection/Pre-Processing Activities

TTI research team data are divided into two types of data: Sampled Data and Inventory Data. For Sample Data, the team filled out paper forms in the field and used the written forms to fill out spread sheets once back in the office. For Inventory Data, video files were downloaded from the memory card and renamed based on date and location of data collection. The research team used sound tracks on video files to record location, date and time, as name video types based on location and time for easier late reference.

Data Processing Equipment

After data collection, two desktop computers were used to process the data.

Data Processing

For inventory data, the research team started by playing the videos. Figure 37 provides a screenshot of the recorded video next to a picture from the sign. For each section of the selected study site, a separate spread sheet was designed to record data inventory only.

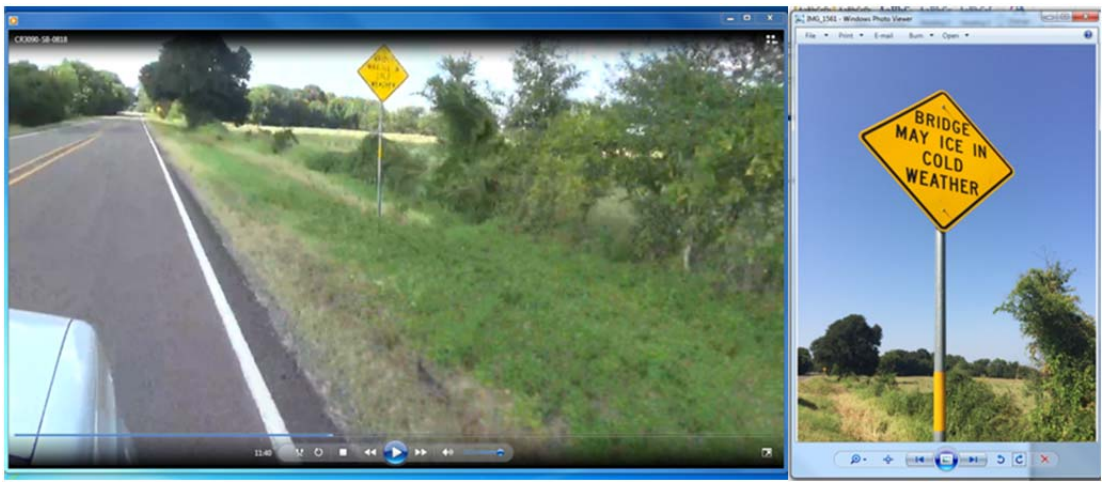

Figure 37. Example of Video Processing of Ground Truth Data.

For inventory purpose only basic information regarding each asset was collected. Table 27 shows look of inventory tables during processing.

Table 27. Example of Inventory Table from Ground Truth Processing.

ID	MP	ASSET	DIR	POS	TYPE	W	L	NOTES
77	3.35	DRAIN	+	RIGHT	CROSS			
78	3.85	SGN	+	RIGHT	W8-13aT			
79	3.85	SGNSUP	+	RIGHT	SCHEDULED80			
80	3.95	SGN	+	RIGHT	W8-15			
81	3.95	SGNSUP	+	RIGHT	SCHEDULED80			
82	4.00	SGN	+	RIGHT	W1-2L			
83	4.00	SGN	+	RIGHT	W13-1P			45 MPH
84	4.00	SGNSUP	+	RIGHT	SCHEDULED80			

For Sampled Data, after identifying minimum sample size and different attributes, the team traveled on site to collect data. For each asset type, samples were chosen completely at random and the team tried to choose different parts of the selected study sites to collect data. A GPS enable computer application was used to geo-tag points while driving on the road. These ASCII tagged points were used to identify different assets for data reduction purposes. Table 28 shows the ASCII tags that were used in data collection:

Table 28. ASCII Tags Used in Ground Truth Data Processing.

M	Sign Mount	S	Shoulder	V	Driveway
L	Lane	D	Delineator	X	Mailbox
T	Culvert	G	Guardrail	N	Pavement Marking
B	First face of the bridge in the driving direction	R	Middle on in/out ramp section		

In addition to having ASCII tags for each asset, the team collected other information in predesigned forms (see Figure 38).

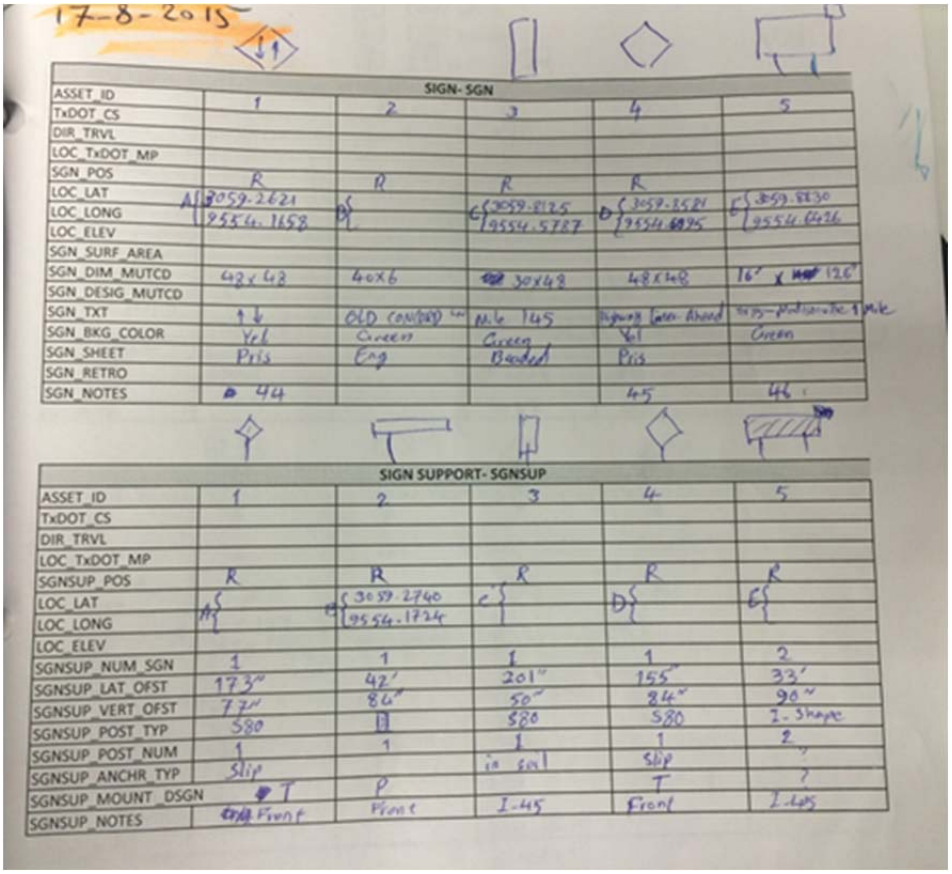

Figure 38. Ground Truth Data Processing Form.

The information on the ASCII coded GPS enabled files were matched with manually collected data and then were compiled into in one spreadsheet. Mile points also were added later by mapping the data into ArcMap® and calculating mile points based on defined routes and its pertinent procedure (see Figure 39).

Whenever possible, the research team cross matched all collected data to ensure data were collected and reported properly.

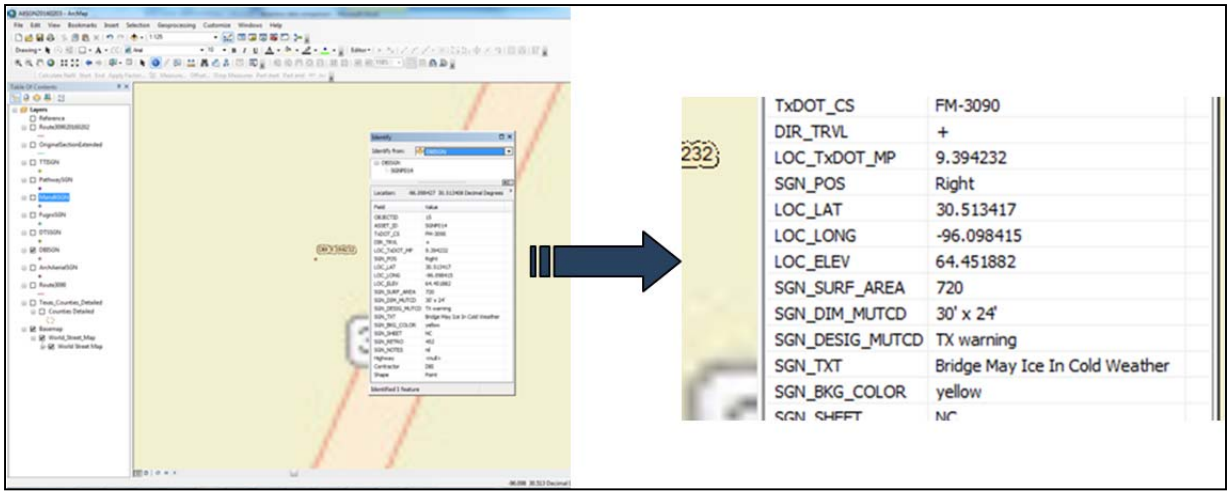

Figure 39. ArcGIS Point Attributes for Ground Truth Data Processing.

Staffing

Two researchers carried out most of the data processing effort.

Data Storage Details

GPS data and spreadsheets were stored on a server that was accessible to different offices working on the project. The video files were too large to store on a shared server and were stored on local desktop computers.

Miscellaneous Data Processing Methodologies

There were several data collection methodologies that lay outside basic "see, measure and record," including: mowable acres and sign retroreflectivity.

Calculating Mowable Acres [Ground Truth]

ROW boundaries were not always obvious in the field and it was thought impossible by the research team to field measure mowable acres. However, the city of Navasota, Texas, maintains current GIS maps (http://navasotamaps.com/mobile/) that provides private parcel information for all of Grimes County (see Figure 40). To determine mowable acres using the Navasota GIS maps, researchers adhered to the following calculations:

- Calculate the **Total ROW** between parcels with private ownership adjacent to FM 3090 (A).
- Calculate approximate **Road Surface Area** along the study section (B).
- Calculate **Mowable Acres** by determining the difference between Total ROW and Road Surface Area.

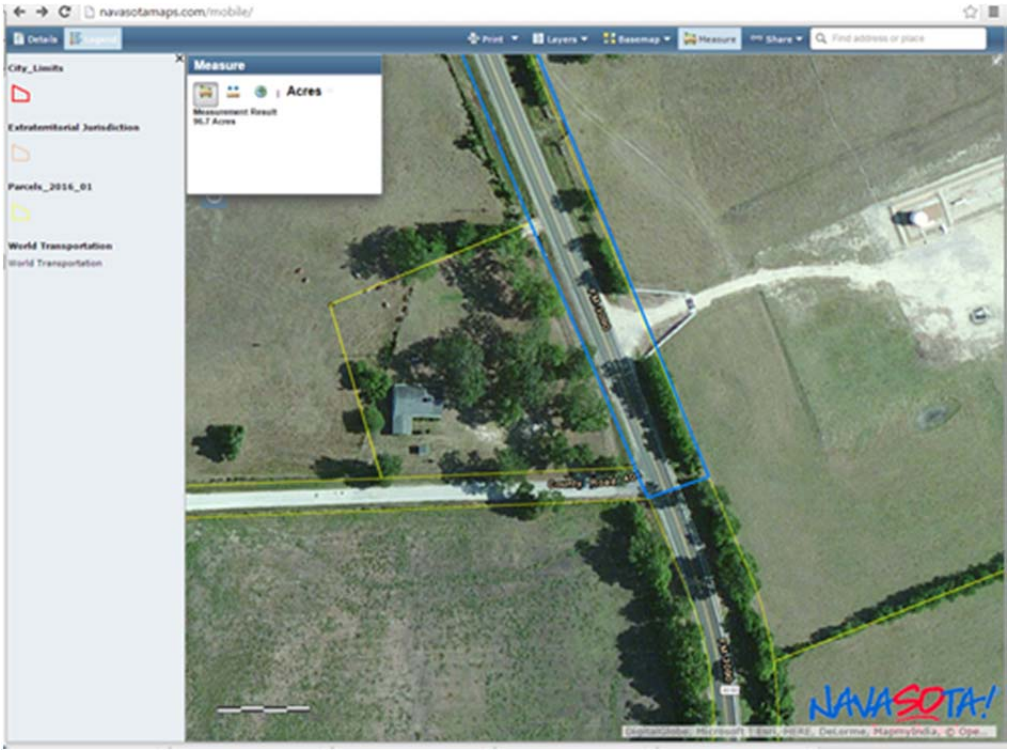

Figure 40. City of Navasota Parcel GIS Tool.

Technology Owners Data Processing [Contractors]

Phase 2 Technical Memorandums for processing and reporting were turned in December 31st along with the Asset Data Spreadsheet. Each contractor provided details on their data processing efforts. For brevity the technical memorandums have been summarized below but complete details can be found in full copies of the delivered Phase 2 Technical Memorandums in Appendix C.

In general, the collected data were taken from the data collection vehicles, placed on a mobile hard drive and sent back to contractor offices for post processing and asset attribute extraction. Post processing aligns the positional data with the imagery and LiDAR point cloud data (if used) for asset attribute extraction purposes.

Contractor A: Data Transfer Solutions (DTS)

DTS uses POSPAC MMS by Applanix to reduce GPS, IMU, and DMI data and verifies data with ARCGIS. DTS also uses Corpscon software to better triangulate a more accurate image position to the State Plane coordinate system. They extract asset attribute data and location information using EarthShaper a proprietary stereo imagery/LiDAR/Aerial photogrammetric production software.

Contractor B: DBi Services

DBi has two options for post processing including AMAC proprietary software and Tridetn Trimble Spatial Analysis software. DBi also extracts sign retroreflectivity, which takes multiple passes through the data set.

Contractor C: ArchAerial LLC

After extracting images from the payload camera, data are organized by flight. A photogrammetry program is used to determine asset location and attributes along with Google Earth Pro.

Contractor D: Mandli Communications

Mandli uses proprietary Roadview Workstation viewing software to determine asset position and attributes post processing (see Figure 41).

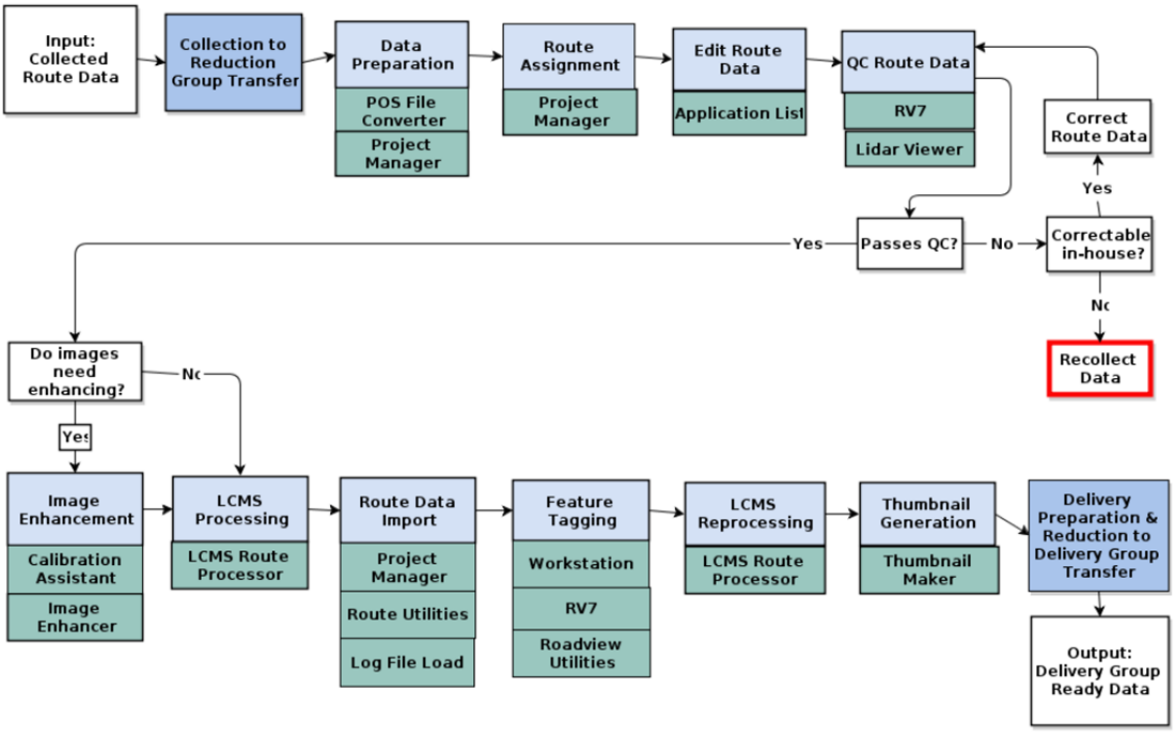

Figure 41. Mandli's Route Processing Project Flow.

Contractor E: Pathway Services

Pathway uses automated and semi-automated proprietary software that is customized to a specific data dictionary. For LiDAR data Pathway also uses Lieca ArcMap.

Contractor F: Fugro Roadware

Fugro uses a 10-Stage process as well as their own propriety software for data extraction for asset location and attribution (see Figure 42).

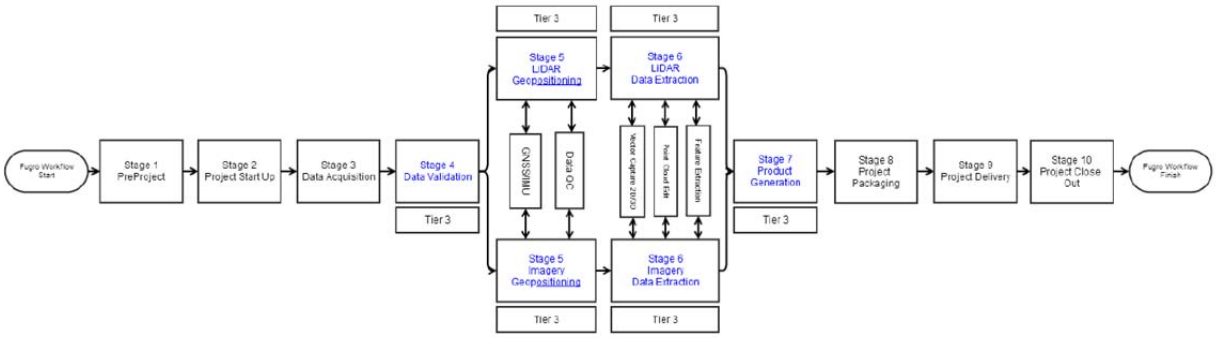

Figure 42. Fugro's Geospatial Project Workflow.

Software utilized during this process include Microstation, Terra Solid Terra Scan, ArcGIS, Global Mapper, and Fugro proprietary softwares.

Ground Truth Data Reporting

The TTI research team delivered data in the asset data spreadsheet in the same format as the contractors. TTI used ArcMap® to conduct a proximity analysis and data comparison and analysis. The main deliverable for this project is the Asset Data Spreadsheet and this technical memorandum to TxDOT.

Technology Owners Data Reporting [contractors]

Researchers at TTI conducted a high-level evaluation of the viewing software provided by the six contractors who conducted an asset inventory. Researcher's conducted phone interviews with all contractors in order to get a demonstration of the viewing software. The demonstrations covered the installation, cost and basic functionality of the software. Some contractors provided demonstrations for multiple software platforms. The following software platforms were evaluated:

- Pathway Services Incorporated: PathView II, PathWeb and LiDAR data.
- DBi Services: 360 Viewer, Sign Viewer, and Pavement Viewer.
- Fugro Consultants: FugroViewer and iPath.
- Mandli Communications: Roadview Workstation and Roadview Explorer.
- DTS VUEWorks.

Note that ArchAerial has not developed an asset viewing software, so are not included in this evaluation.

Pathway Services: PathView II and PathWeb

Pathway Services has two software platforms available to clients, PathView II and PathWeb. In addition, Pathway collects data using LiDAR technology. The following is a review of the functionality of PathView II and PathWeb and the LiDAR data extracted.

PathView II

PathView II is an in-depth software platform that is designed for power users who have the ability to not only view collected assets, but edit asset databases and rate assets. The PathView II software platform requires users to install the software directly onto their computer. In addition to the PathView II software, users are required to install ArcGIS Explorer Desktop in order to view GPS imagery. The program has six windows that open independently of one another. To optimize the viewing experience, Pathway staff suggested using two screen to view the program. Figure 43 provides a screenshot of Screen 1 of the user interface and Figure 44 provides a screenshot of Screen 2 of the PathView II user interface.

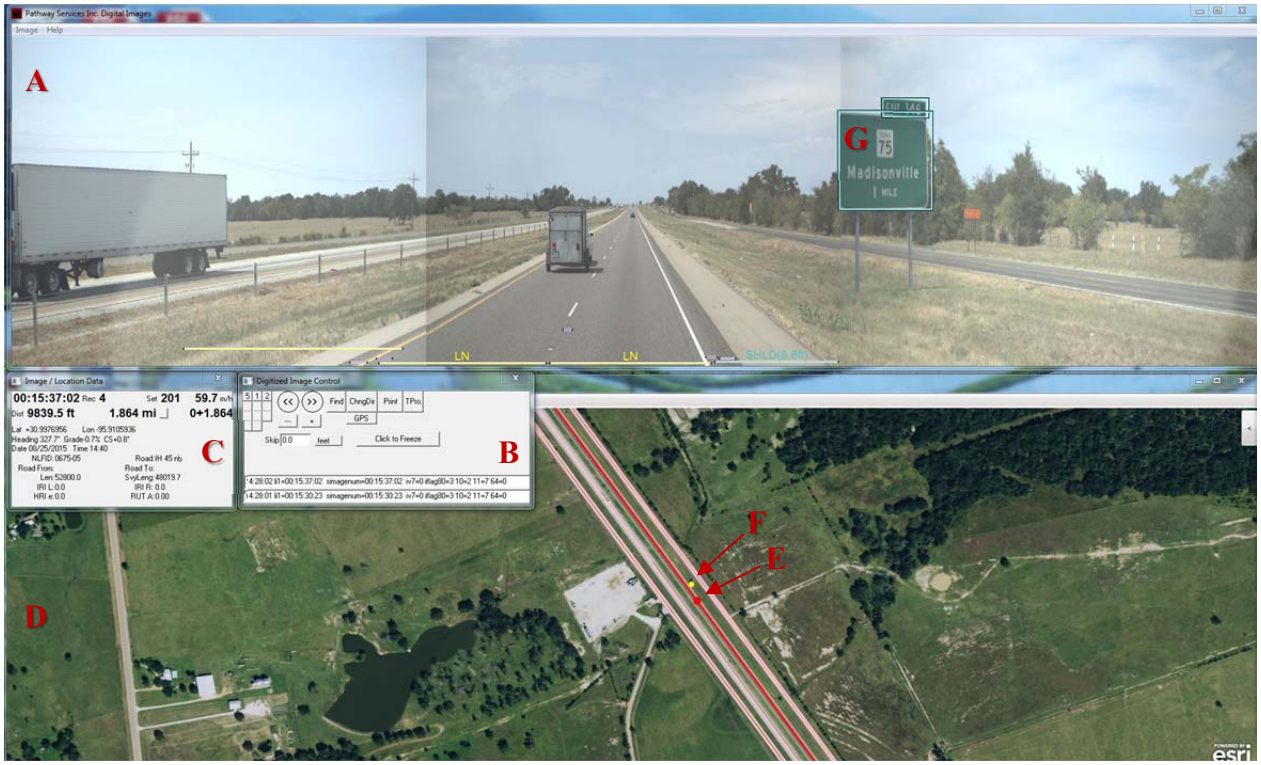

Figure 43. Screen 1 of PathView II User Interface.

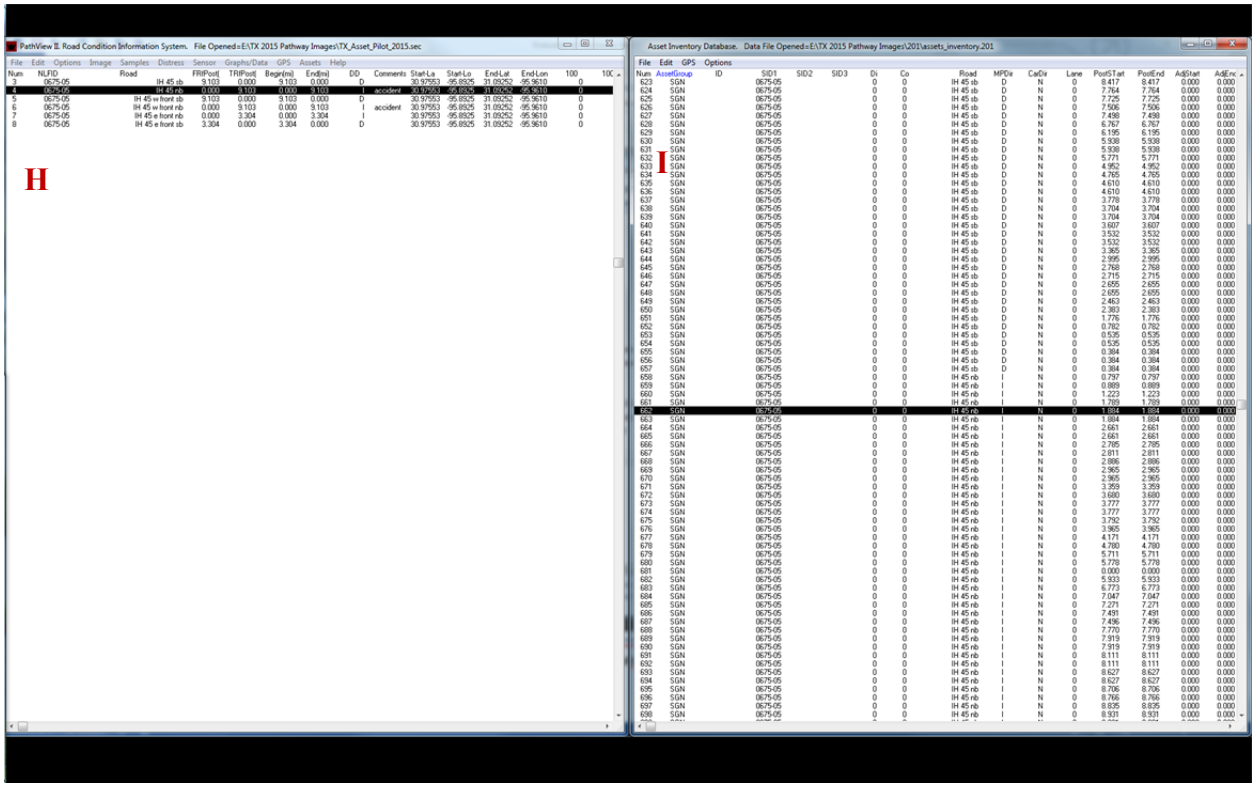

Figure 44. Screen 1 of PathView II User Interface.

The PathView II software has four primary windows (note the letters in Figure 43 and Figure 44 above):

- The digital image screen (shown as A in Figure 43).
- The GPS map (shown as D in Figure 43).
- The main control panel (shown as H in Figure 44).
- The asset inventory (shown as I in Figure 44).

These four windows constitute the main user interface for the PathWeb II asset viewing software. The digital image screen shows the high-resolution digital imagery captured by the Pathway vehicle (Pathrunner). The digital image screen is comprised of imagery from three cameras (left, middle, and right) on the front of the Pathrunner vehicle. The images are calibrated to provide a seamless panoramic view of the roadway (users can adjust the brightness, contrast, etc. to ensure continuity amongst camera views). Pathway staff indicated that additional cameras are also used for other projects (such as bottom cameras to capture pavement imagery) but those cameras were not utilized for this project. The digital image screen is controlled by the digital image control (shown as B in Figure 43). The digital image control allows users to move along the roadway (note arrow buttons) by either pressing once on the forward or backward arrow button (this jogs the image forward/backward 20 ft at a time) or in a continuous feed if the space bar is pressed (giving the user the experience of travelling along the roadway). Users can also change the number of feet that the viewer skips in the box below the arrows. The digitized image control provides the user with the ability to change direction (if asset data were captured in the opposite lane). The image/location data window (shown as C in Figure 43) provides a range of

information about the location of the imagery shown in the digital image screen, including speed travelled, distance travelled and latitude and longitude. Users can measure distance on the digital image screen by dragging the mouse along the digital image screen (example of measurement of shoulder shown in Figure 45). In addition you can zoom in to great detail on the digital image screen.

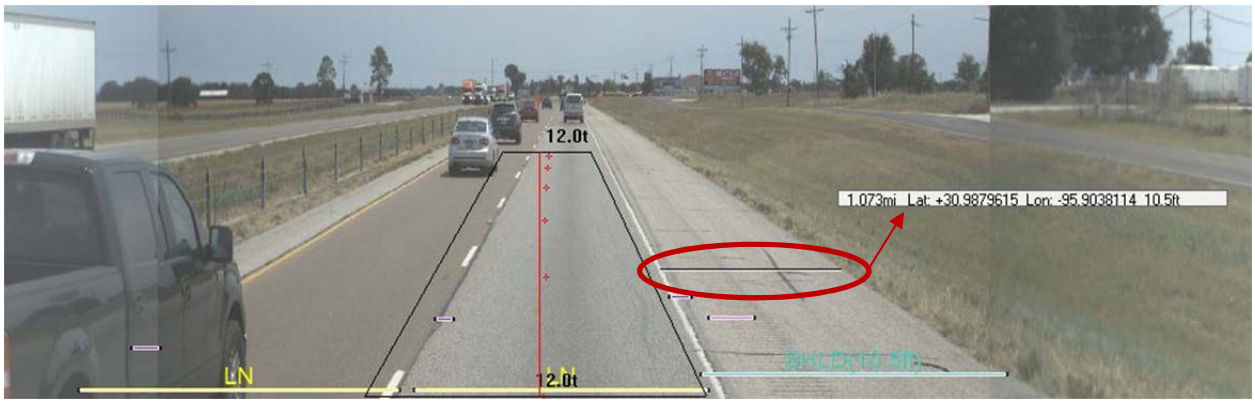

Figure 45. Example of Measurement Tool in PathView II.

The GPS map shown as D in Figure 43 shows aerial imagery of the area that the asset collection occurred. Note that the red dot, shown as E in Figure 43, is the location where the imagery was captured and is being shown in the digital image screen (i.e., the GPS map and digital image screen are synchronized). Users can zoom in and out of the GPS map and double click on the roadway and the digital image screen will move to that location. Note that the red line on the GPS map shows the roadway that is currently being viewed (travelled along) in the digital image viewer and the pink lines show additional roadways where data were collected. The user can double click on any of these line segments and the digital image viewer will move to that location. The yellow dot, shown as F in Figure 43 is the location of a collected asset, in this case a sign. Note that the sign is also highlighted in the digital image screen (G in Figure 43).

The main control panel, shown as H in Figure 44, provides all user controls, and lists all of the roads that data collection was performed on (note that the TTI project only collected data on two roadways so the data sample was far smaller than most projects loaded in PathView II). Finally, the asset inventory, shown as I in Figure 44, is the database with information on all of the collected assets. Note that in the example shown in the asset inventory in Figure 44, the highlighted row of data is the sign that is shown in the GPS viewer and digital image viewer (all three screens are synchronized). The asset inventory provides all of the information that has been collected for this particular sign (e.g., height, offset, condition).

Users can access a vast range of functionality to edit and rate assets through the main control panel, though it is not extremely intuitive and training is required for users to achieve a level of ease with the software. Pathway does provide training for the PathView II software.

PathWeb

PathWeb is a web-based tool designed for a full range of end-users, as it is far more user-friendly, but lacks much of the advanced functionality offered by PathView II. PathWeb is a web-based tool that Pathway provides clients in order to easily view full resolution images,

without having to incur a great deal of training or even possess a high level of technological acumen. The tool only requires an internet browser with the Silverlight add-on installed in order to access and use PathWeb. Figure 46 provides a screenshot of the PathWeb user interface.

Figure 46. Screenshot of PathWeb User Interface.

Pathweb has the following components, as shown in Figure 46:

- The digital image screen (shown as A in Figure 46).
- The image control, which controls the digital image screen (shown as B in Figure 46).
- The GPS Map (shown as C in Figure 46).
- Configure GPS Map window (shown as D in Figure 46).

The digital image screen (A) provides the same full resolution images shown in PathView II and allows users to zoom and pan the images (useful for zooming into roadway assets). The digital image screen is controlled by the image control screen (B), which allows users to turn off cameras in the digital image screen (middle, left and right camera). Users can move forward and backward either frame by frame or on a continuous loop. The GPS map provides an aerial view of the data collection area. The configure GPS map window (D) allows users the ability to toggle layers on and off. In the example in Figure 46, users can turn the following layers on and off:

- Roadways that the Pathrunner vehicle collected data on.
- Point assets.
- Linear assets.

Note that users can add individual layers of assets into PathWeb, which would create the ability to toggle individual asset layers on and off individually. In Figure 46 point assets are turned on. In the GPS map the blue dot (E) is the location of the digital image screen and the small red dot,

marked as F, is the location of an asset (sign). Users can click on the point data and all of the collected data about that asset is shown in the window (G) in the upper right corner of the GPS map.

The menu options at the top of the screen (H) provide users with the ability to find specific road locations by mile marker, access a help menu, change direction as well as save the images that are in the current screen.

The PathWeb tool is highly accessible and easy to navigate. Users can display rated assets on the GPS map as well as the image viewer, but there is no functionality to rate or edit assets within PathWeb. In addition there is no functionality to measure within PathWeb. Users have the ability to create reports and raw images and create graphs and charts of data. Finally, users can add additional geo-located data (e.g., .kml or .shp files) to PathWeb, so there is additional versatility of the tool to accommodate numerous data sets.

LiDAR Data

In addition to the high resolution imagery that is displayed in PathView II and PathWeb, Pathway also collects LiDAR data. The LiDAR data are viewable in GIS programs, such as ArcGIS. Figure 47 shows an example of the LiDAR data.

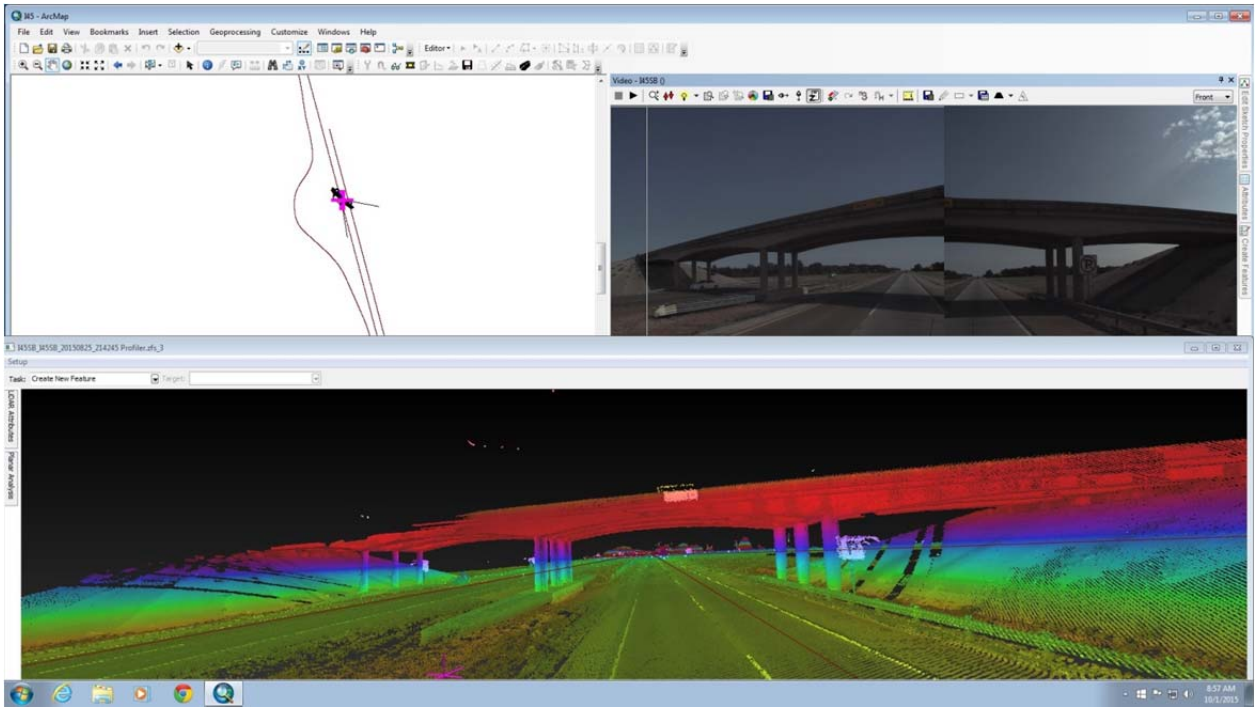

Figure 47. Pathway LiDAR Data.

The LiDAR data shown in Figure 47 are primarily used to measure vertical assets (e.g., bridge clearances, sign heights), and Pathway Inc. has not developed software specifically to view LiDAR data.

Pathway Software Takeaways

The PathView II software is extremely complex and provides the user with advanced functionality to edit (e.g., edit asset information), analyze (e.g., conduct stress or cracking tests) and rate roadway assets but is not user-friendly or intuitive whatsoever. In addition, since the user interface contains numerous windows the user-experience suffers. It takes the user time to set the windows up to fit their computer screen in order to utilize the entire functionality of the program. Because not all windows are synchronized with each other, the separate windows occasionally move or disappear, which can be confusing to new users. Pathway offers training on the software, and stressed that the software was designed with power users in mind, so very few individuals within an agency would use it. In addition, there is a thorough instruction manual provided, but overall there is a fairly steep learning curve in order to become proficient in the use of PathView II.

PathWeb on the other hand is much more intuitive as almost any user can figure out how to view data on assets without much instruction. PathWeb does a good job incorporating attribute data about assets into the user interface so users can select assets and look at size, condition, location, etc. The tool would benefit from some additional basic functionality, such as a measurement tool.

DBi Services: 360 Viewer, Sign Viewer and Pavement Viewer

DBi services provide end users with three separate platforms to view their data. The Pavement Viewer and Sign Viewer require users to install software provided by DBi, whereas the 360 Viewer is a web-based data viewing tool developed by DBi. All three platforms have limited functionality and were developed primarily to provide the end-user with the ability to view captured imagery. DBi staff emphasized that the vast majority of their clients ask for geo-databases and that is what they provide their customers with every contract.

360 Viewer

The 360 Viewer is a web-based asset viewing tool that provides users with the ability to view 360° of ROW imagery. The tool only requires access to the internet and a web browser. DBi Staff explained that the software is proprietary, but the client's imagery can be uploaded to the 360 Viewer server at the request of the client (indicating that the use of the software does not result in an additional cost to the client). Figure 48 provides a screenshot of the 360 Viewer user interface.

Figure 48. DBi Services 360 Viewer User Interface.

The 360 Viewer user interface provides an aerial view (A) of the location where assets have been extracted. The aerial view shows the location of the 360 imagery window (B) as a yellow dot (C) and shows assets (in this case signs) as red dots (D). 360 Viewer users can toggle layers (in this case the layers are different assets) on and off by using the "Toggle Layers" button in the upper left corner of the screen. Note that for the TTI project, DBi only loaded the sign layer into the 360 Viewer demo. The 360 imagery window (B) allows users a full 360° view of high resolution imagery. The 360 imagery window is extremely user friendly, as there are arrows on the outside of the image to advance the location forward or backward, as well as controls to move the camera within the image at the bottom of the image itself. In addition, users can use the mouse to move the camera 360°, as well as use the mouse's scrolling wheel to zoom in and out. The 360 imagery window can also be expanded to full screen. The example in Figure 48 shows an image where a sign has been zoomed in. There is no way to view data that were collected about an asset manually (for example by clicking on the asset in the aerial view), but the Nearby Road Features window (E) automatically provides data about the asset nearest to the current location of the 360 imagery window. In addition the window marked F provides data about the location of the ROW in the (longitude, latitude, etc.) and the window marked G provides users with the ability to add and edit existing features (this feature was not made available for the TTI demo). DBi staff explained that users can also export data in the 360 Viewer into a GIS format. There is no additional functionality beyond viewing the assets and data attributed to them, as well as editing asset data.

Sign Viewer

The Sign Viewer software provides users with the ability to view data extracted for signs. Sign Viewer requires users to download and install the software on their computer. This program is proprietary, though similar to 360 Viewer, DBi indicated that they provide this software at no

additional cost to their clients. The primary purpose of Sign Viewer is to measure the retroreflectivity levels of signs. Figure 49 provides a screenshot of the sign viewer user interface.

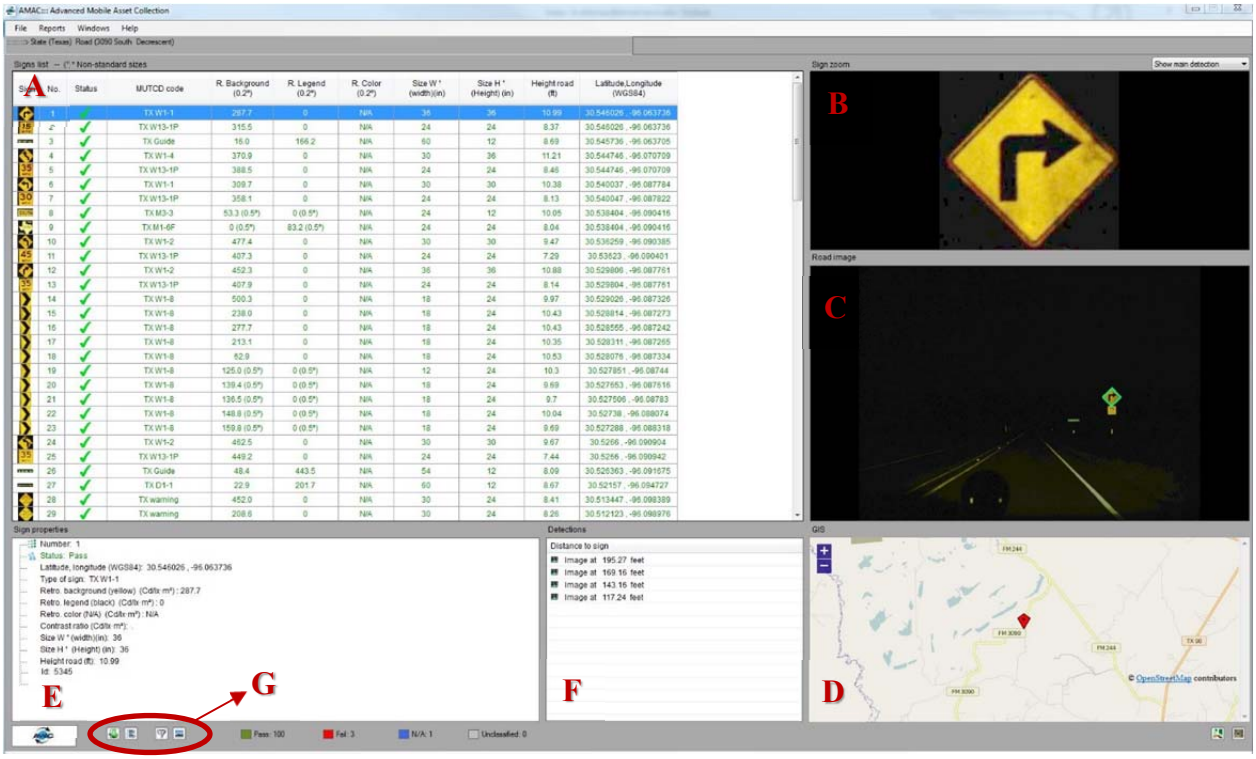

Figure 49. DBi Services Sign Viewer User Interface.

The user interface provides users with the ability to view all signs extracted along a right-of way where data collection has occurred. The signs list (shown as A in Figure 49) provides a picture of the sign as a thumbnail along with all of the collected data associated with that sign (including whether the retroreflectivity passes federal requirements, noted as a checkmark in the status column). Users can click on each row and it will bring up a photograph of the road image where the sign is located (C), a zoomed in version of the photograph (B) (always taken at night to test retroreflectivity) and a GPS map, which shows an aerial view of where the sign is located (D). In addition, the user interface features a window that provides the sign properties (E), which is much of the same information shown in the signs list window (A). The distance to sign window (F) provides the option for users to view the sign at four separate distances. Users can click on each distance and view the sign from that distance. Finally, the Sign Viewer provides users with the ability to export the data, add new data, and filter existing data (shown as G in Figure 49).

Pavement Viewer

The Pavement Viewer software provides users with the ability to view data extracted for pavement markings. Pavement Viewer requires users to download and install the software on their computer. As with the 360 Viewer and Sign Viewer, DBi indicated that they provide this software at no additional cost to their clients. Similar to Sign Viewer, the primary purpose of the Pavement Viewer is to show the retroreflectivity levels of pavement markings. Figure 50 provides a screenshot of the Pavement Viewer user interface.

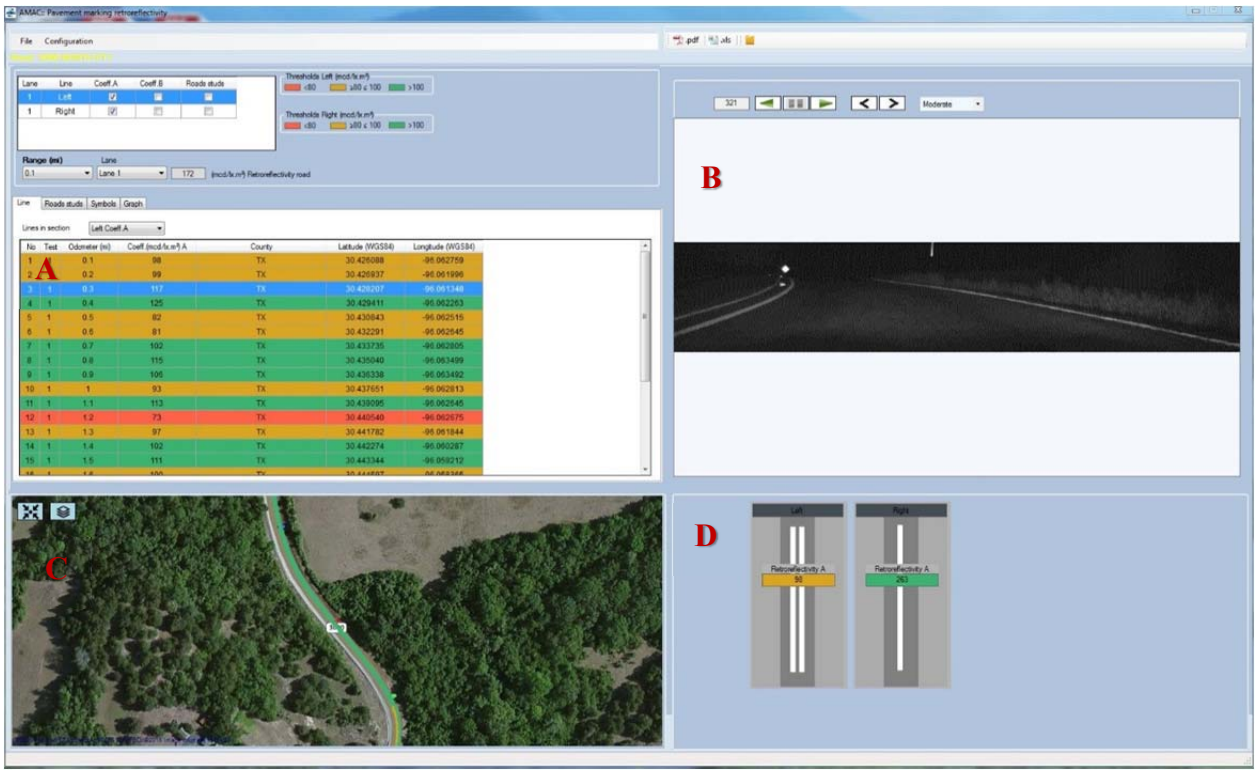

Figure 50. DBi Services Pavement Viewer User Interface.

The Pavement Viewer tool provides users with the ability to view retroreflectivity levels of extracted pavement markings. DTS explained that they capture and rate the retroreflectivity levels every tenth of a mile. Each location where reflectivity is photographed and measured is detailed in the window shown as A in Figure 50. The retroreflectivity rating is shown as passing (green), near failure (orange) or failing (red). The window shown as B in Figure 50 shows the photography (always taken at night) where the pavement marking's retroreflectivity was measured. Window C provides an aerial view of the location where pavement marking data were captured. Users can click on the roadway and move along the roadway and the retroreflectivity levels are shown along the aerial photography. Finally, the retroreflectivity scores are shown in window D for both north and south bound lanes.

DBi Software Takeaways

DBi staff acknowledged that they don't aim to develop and provide a software platform for their end-users and emphasized that providing a geo-database for use with a powerful GIS program is more than sufficient. The 360 Viewer is a reasonably effective web-based platform for users who do not have then technical acumen to run ArcGIS for example, but are still interested in viewing extracted roadway asset data. The tool would benefit from some additional functionality (e.g., measurement tool) and the way that roadway asset data are shown (only appearing when the image viewer is close to an asset with no specific indication of which asset the data are linked to) could be problematic in an area with multiple assets right next to each other. That being said, the 360 Viewer is extremely user friendly, and provides a very easy method for viewing captured ROW imagery in high-resolution. The ability to move the camera in the 360 Viewer a full 360° (at all angles) is extremely useful.

The Sign and Pavement Viewers are easy to use, but provide zero additional functionality outside of the ability to view the retroreflectivity levels of the extracted assets (signs and pavement markings). The limited functionality should not overshadow how effective the programs are at accomplishing what they are designed to achieve: look at the pictures of signs and pavement markings and understand where retroreflectivity levels are at risk.

Fugro Consultants: iVision and FugroViewer

Fugro provides clients with two software platforms to view captured asset data: iViewer and FugroViewer.

iVision

iVision is a web-based tool that allow users the ability to view and analyze high resolution imagery and extracted roadway asset data. Users only need access to a web browser and internet connection to use the software. A range of ROW and pavement imagery as well as associated data can be viewed in a user-customizable workspace and all views remain synchronized with each other. iVision is a proprietary platform developed by Fugro, and Fugro will build the use of iVision into the scope of a project if clients are interested in using this tool (i.e., not included in the base cost of data collection and delivery). Figure 51 provides a screenshot of the iVision application user interface.

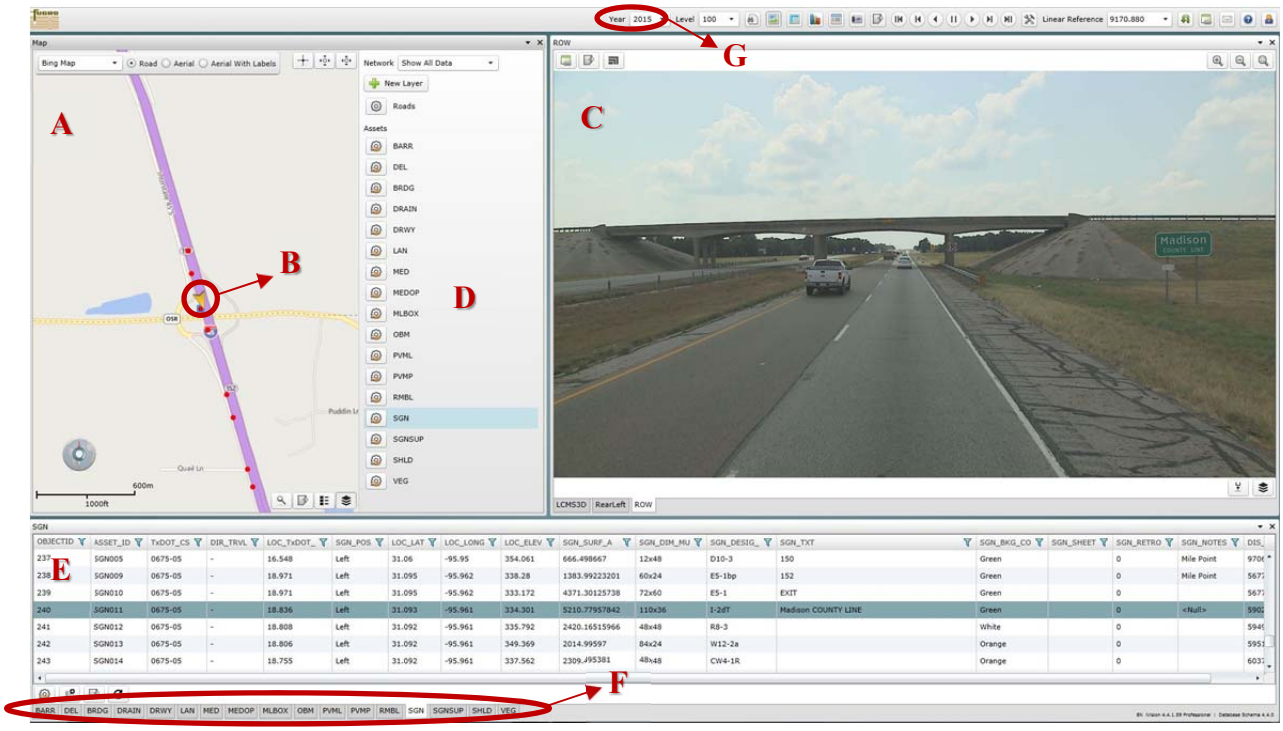

Figure 51. Fugro iVision User Interface.

The iVision user interface is extremely intuitive and allows the user numerous options to view high-resolution imagery of extracted assets as well as the associated data collected for roadway assets. The user interface provides an aerial view of the roadway (A). The yellow arrow (B)

shows where the imagery in the digital image window (C) is located. Users have the ability to toggle a wide range of layers on and off of the aerial map using the layer tool (D). In the example in Figure 51, all of the collected assets are set up as individual layers and users can toggle the layers on individually or at the same time. In addition, users can easily customize the size, color and symbology used for each layer. In the example in Figure 51, only the SGN (signs) layer is turned on. In the aerial view, users can click on any asset in the aerial view (shown as red dots) and the digital image viewer will move to that location. In addition, the user interface will also highlight the data captured for that asset in the sortable database at the bottom of the screen (E) (i.e., the entire program is synchronized). In addition, when users click on an asset in the aerial view, a small pop-up box will provide the same data that are provided in the sortable database at the bottom of the screen. The aerial map also includes a search by address tool and optional legend tool (useful when numerous layers have been added). The digital image viewer provides full resolution imagery that can be zoomed in and navigated using the mouse scroll wheel or the controls at the top of the screen. Note that that the bottom of the digital image screen there are tabs for each of the three cameras. iVision can store up to six camera views, though Fugro only captured three images for this project (ROW, rear left of the vehicle and pavement). The sortable database is neatly organized by asset as well, and users can click on each of the asset tabs on the bottom of the screen (F) and it will bring up the database for each asset. Users can click on each asset and the aerial view will move the location of the digital image viewer to that location as well. Additional iViewer functionality includes the ability for users to add additional shapefiles, export databases, export images from the digital image viewer (both as jpeg and image link) and quickly create reports on data such as pavement conditions. Figure 52 provides an example of rutting level analysis on the right and left side of the pictured ROW.

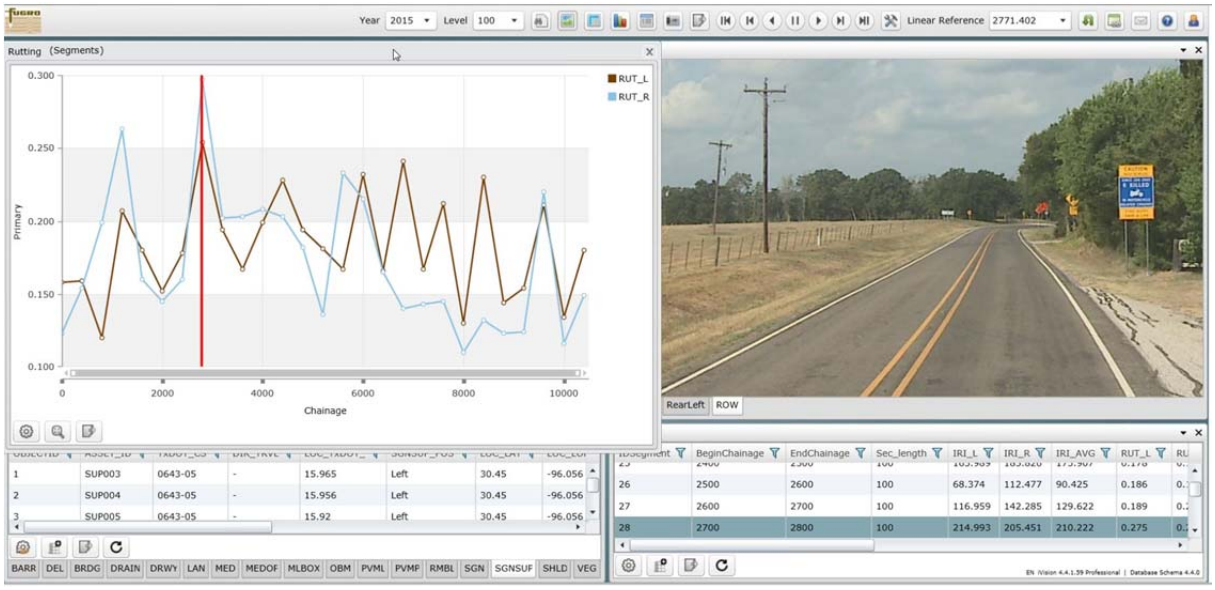

Figure 52. iViewer Rutting Report.

Fugro staff produced the report shown in Figure 52 very quickly and explained that users need very little training in order to learn how to use all of iViewer's functionality. Fugro staff also noted that a measurement tool has been added to the next update of iViewer and will be a standard function of iViewer moving forward. Fugro staff also emphasized that this software was designed to allow their clients the ability to easily compare roadway assets from one year to the

next. The top of the user interface includes a year pull down option (G). Fugro staff explained that the tool works very well in building an easily accessible, longitudinal database so that staff can quickly review the conditions of particular assets over time.

FugroViewer

FugroViewer allows users to view geospatial data, and specializes in showing LiDAR data. The software was developed by Fugro but is classified as "freeware" as Fugro allows free downloads of the software to any user, as opposed to just clients, on their website. Figure 53 provides a screenshot of the FugroViewer user interface showing a LiDAR data set of a highway and bridge overpass.

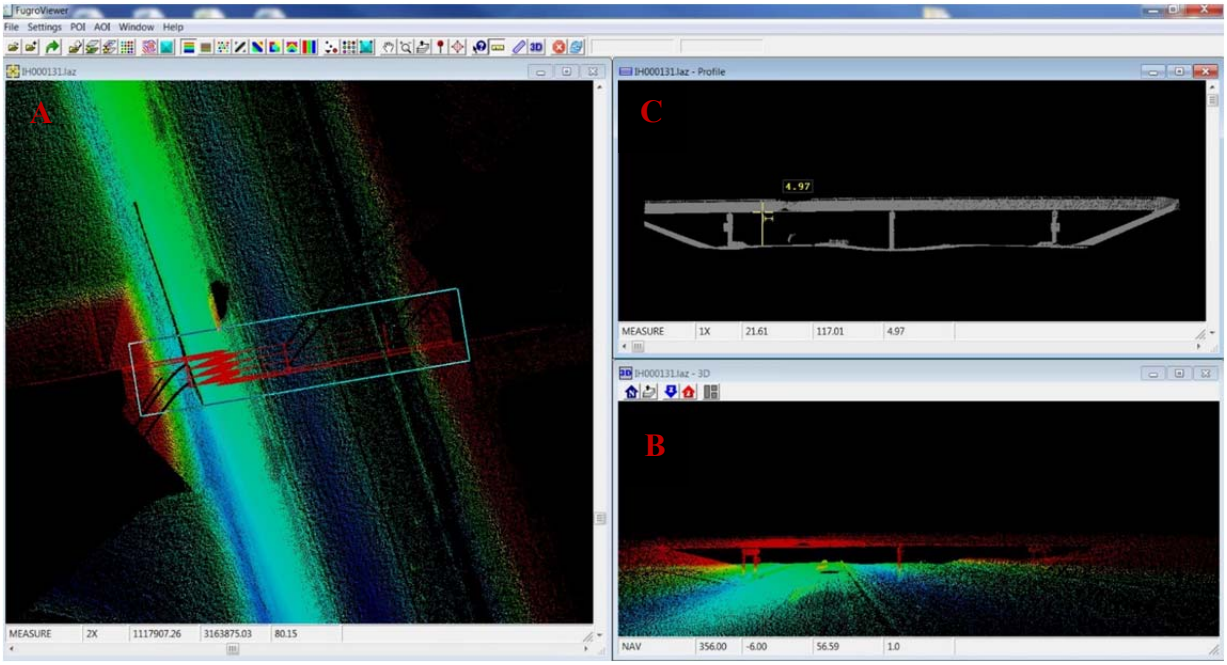

Figure 53. FugroViewer User Interface

FugroViewer is a tool for aerial viewing of LiDAR data. FugroViewer provides the user with a range of color customization options for contour lines (e.g., earth tones, elevation) and users can overlay asset data over the LiDAR data (such as .shp files). Users are able to view multiple angles of the LiDAR data, including aerial (A) and from ground level (B). Users are not able to edit files, though users can add markers to flag a point of interest which can be saved within the data, which can then can be exported and edited outside of FugroViewer. Users can use FugroViewer to export LiDAR data to GIS formats such as .shp or .tin files. FugroViewer is primarily used as a viewing software so while users can overlay asset data, there is no additional information about the asset data within Fugro Viewer. Note that users can use FugroViewer to measure distances. An example of this is shown in the window marked C, where the vertical bridge clearance is measured within FugroViewer.

Fugro Software Takeaways

iViewer is an extremely well designed, intuitive and easy to use program that provides a reasonable range of functionality for users who need the ability to view asset locations, high-

resolution imagery and a range of data associated with specific assets. The tool is especially effective for users who want to have access to a large variety of asset and asset data, as the tool does a phenomenal job at seamlessly organizing numerous assets in one easy to use user interface. The only drawback to this software is the lack of the ability to edit and rate assets.

FugroViewer is a fairly easy to use program to view LiDAR data. There is very limited functionality, and no synchronization of GIS based asset data so the usefulness of this program beyond viewing, exporting and measuring distances for LiDAR data is limited. It would be far more useful if users could view more detailed data about assets along with LiDAR data.

Mandli Communications: Roadview Workstation and Roadview Explorer

Mandli Communications provides end users with two data viewing and asset inventory software platforms: Roadview Workstation and Roadview Explorer.

Roadview Workstation

Roadview Workstation provides users with the ability to view and analyze route information, high-resolution imagery, GPS, pavement, and LiDAR data in a fully synchronized viewing environment. Users must install Roadview Workstation on their computer as it is a proprietary software that Mandli charges customers for. Figure 54 provides a screen-shot of the Roadview Workstation's user interface.

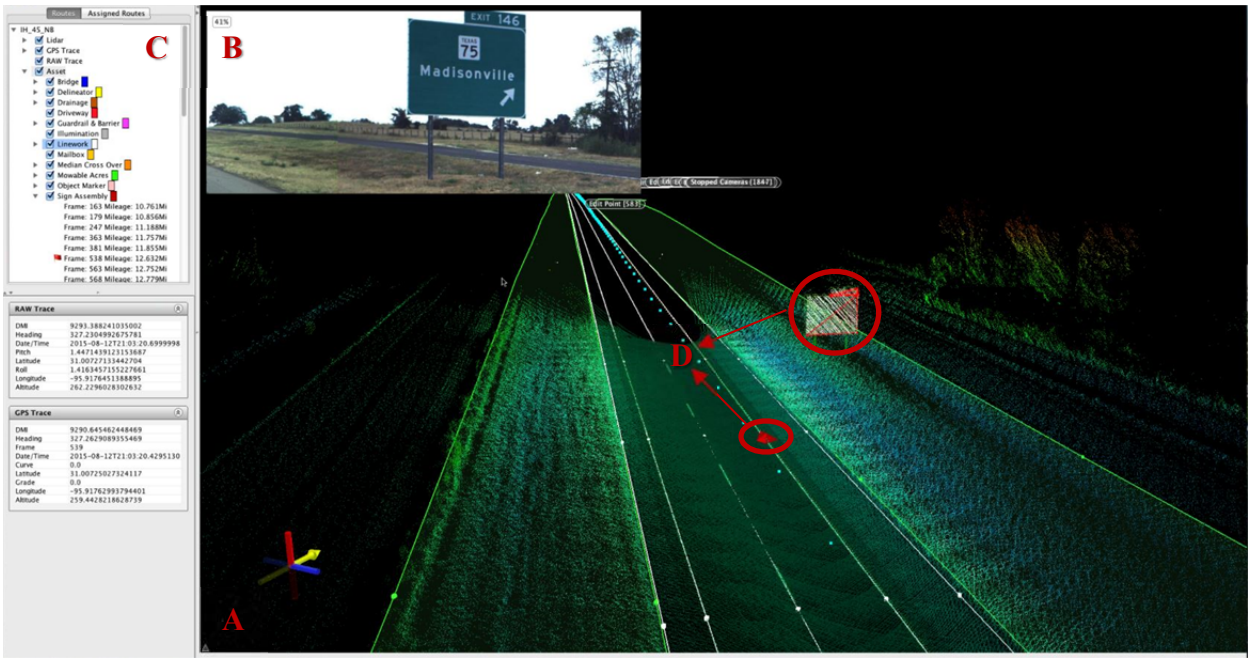

Figure 54. Mandli Roadview Workstation User Interface.

Roadview Workstation provides users with the unique ability to view LiDAR data that are synchronized with other extracted roadway assets. The user interface presents the LiDAR data in a fully interactive 3D environment (A). Users can view and interact with the roadways by moving along the roadway with a 360° view shed by using the mouse to grab and move the screen and mouse-wheel to zoom in and out. In addition to the 3D environment, users can view

the digital imagery of the correlating location in the digital image window (B). Note that asset data is not shown in the digital image window, but the window synchronizes with the location the user is viewing in the 3D environment. In addition, users can zoom in on digital imagery. Users can also add assets to the 3D environment within Roadview Workstation (GIS data). These data are shown as a pyramid in the 3D environment, but is synchronized with the actual asset (note the sign and pyramid marked D in Figure 54). The asset data layers can be toggled on and off using the layer window (C). Users can customize assets as different colors so they can be distinguished from other assets in the 3D environment. There is a wide range of functionality and reporting in this robust tool from the ability to calculate distance and vertical clearances to calculating the mowable acreage of grass in medians. The software is developed for advanced users to provide the ability to view, edit, analyze and rate roadway assets. The advanced functionality of Roadview Workstation means the software is far less intuitive, but Mandli provides extensive training.

Roadview Explorer

Roadview Explorer is web-based tool that provides users with the ability to view high-resolution imagery using a web browser. Figure 55 provides a screenshot of Roadview Explorer's user interface.

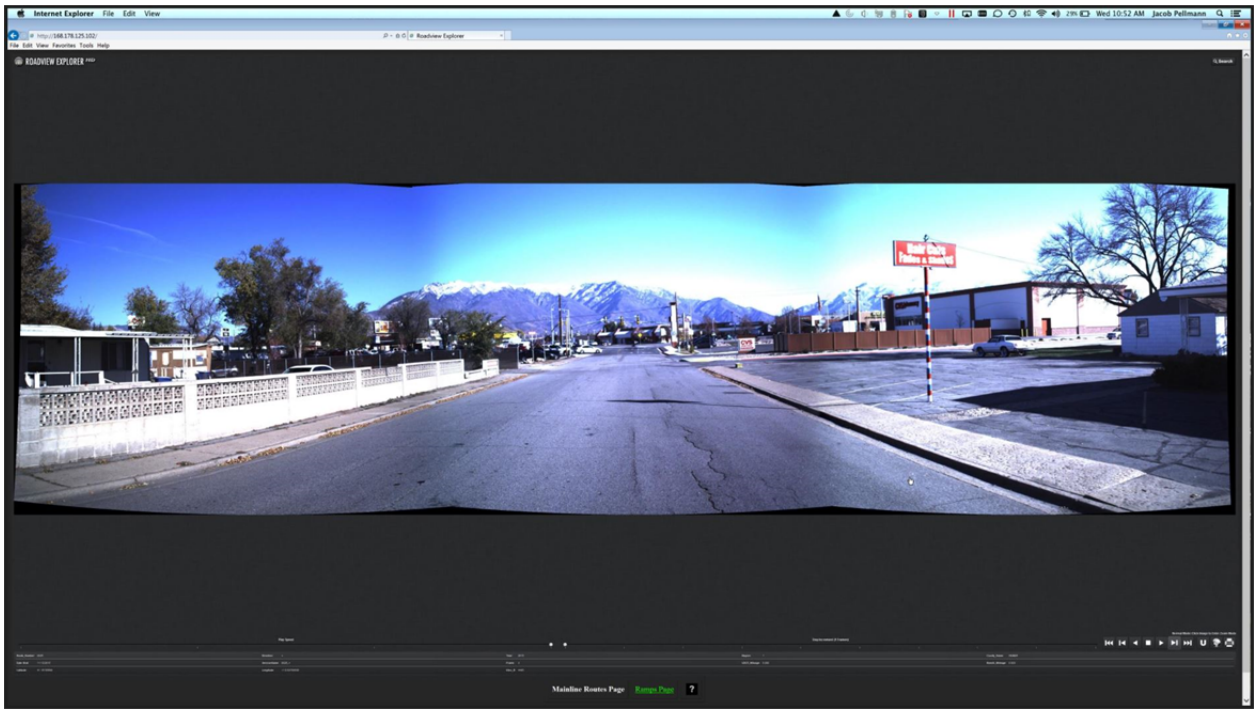

Figure 55. Roadview Explorer User Interface.

As shown in Figure 55, Roadview Explorer provides users with the ability to view high-resolution imagery of ROW imagery. The layout and controls allow for easy location referencing and navigation. The user is able to designate whether forward and side view images are viewed individually or simultaneously. The software does not have any asset data incorporated into the viewer and there is no additional functionality outside of the ability to view the imagery.

Mandli Software Takeaways

Roadview Workstation is an extremely robust tool that integrates GIS data with LiDAR data to provide an extremely rich 3D environment. Of all software platforms evaluated for this project, Mandli's seamless integration of LiDAR data into their software platform is unmatched. The software provides a wide array of functionality from using LiDAR data to analyze roadway rutting to measuring vertical clearances of highway overpasses. The ability to navigate within the user interface is intuitive and the synchronization between LiDAR data and high-resolution imagery make it fairly easy for users who are interested in simply viewing asset and LiDAR data to navigate the environment. The advanced functionality requires a much steeper learning curve though, and as noted, Mandli provides extensive training for Roadview Workstation.

Roadview Explorer is a very user-friendly tool to view high-resolution ROW imagery, but the functionality begins and ends there. Mandli staff explained that they were in the process of looking at Roadview Explorer to consider adding additional functionality, but currently the tool provides only the ability to view imagery and does not have the ability to contain any asset information whatsoever.

Data Transfer Solutions (DTS): VUEWorks

DTS provides one software to view and analyze extracted assets called VUEWorks.

VUEWorks

VUEWorks is a web-based software that users only need access to a web browser with an internet connection in order to use. While VUEWorks is perfectly sufficient in viewing extracted roadway assets and associated asset data, VUEWorks is designed provides users with a fully integrated suite asset management functionality that is unique from the other products featured in this project. The product is GIS-integrated so users have much of the same functionality that many GIS tools such as ArcMAP provide (VUEWorks was developed using ArcMAP software). VUEWorks is a proprietary software that DTS charges for in addition to their data collection efforts. Figure 56 provides a screenshot of the VUEWorks user interface (note that DTS did not provide VUEWorks for the TTI pilot project so the example is from a project conducted in Fort Worth).

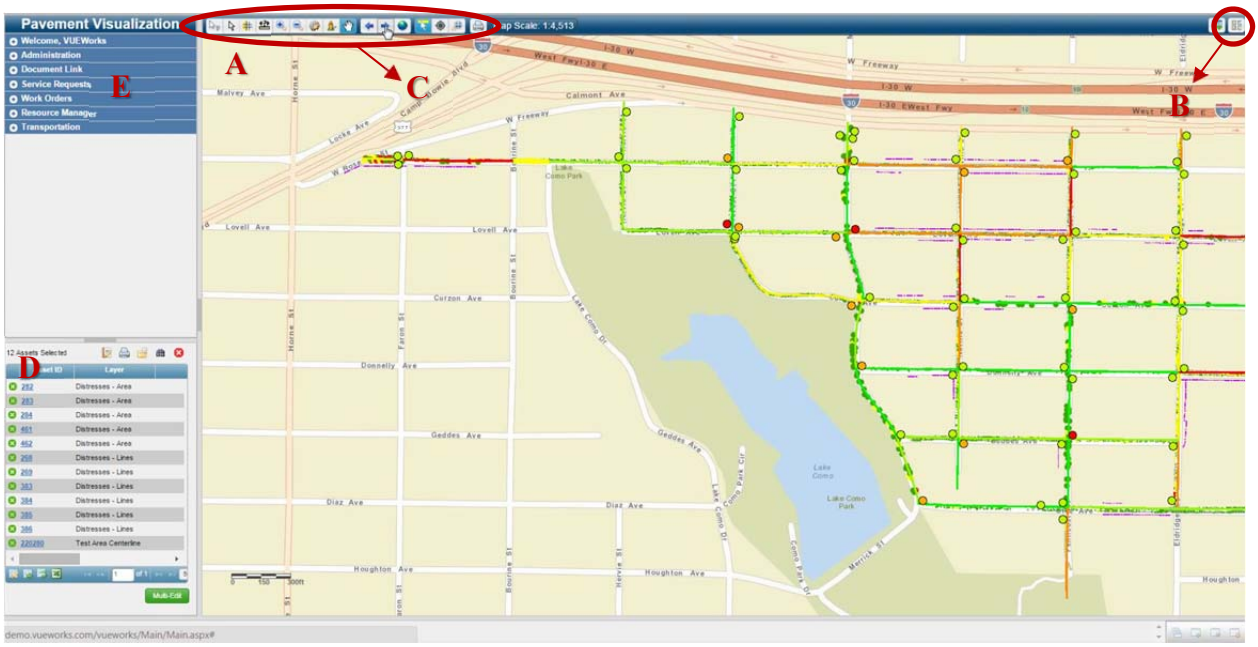

Figure 56. DTS VUEWorks User Interface.

As shown in Figure 56, the user interface of VUEWorks home-screen primarilly features the aerial view (A) of extracted assets in a GIS environment. The points and lines represent a variety of assets in the main screen. Users can toggle numerous layers (assets) on and off using the layer tab in the upper right side of the screen (B). When this tab is open users can customize the symbology of all assets shown in the aerial view. Users can zoom in and out, pan, measure and select individual assets (similar controls to ArcMap) using the tool bar at the top of the screen (C). Once a user selects an individual asset, details about that asset are provided via a pop-up window (not shown) as well as in the asset data viewing screen in the lower left of the user interface (D). This area provides users with the ability to view a wide range of data associated with each asset. In addition to the previous functionality, VUEWorks provides a range of functionality for users to edit data, rate assets, and create work-orders and service requests. Figure 57 shows the screen to view, edit, and rate assets.

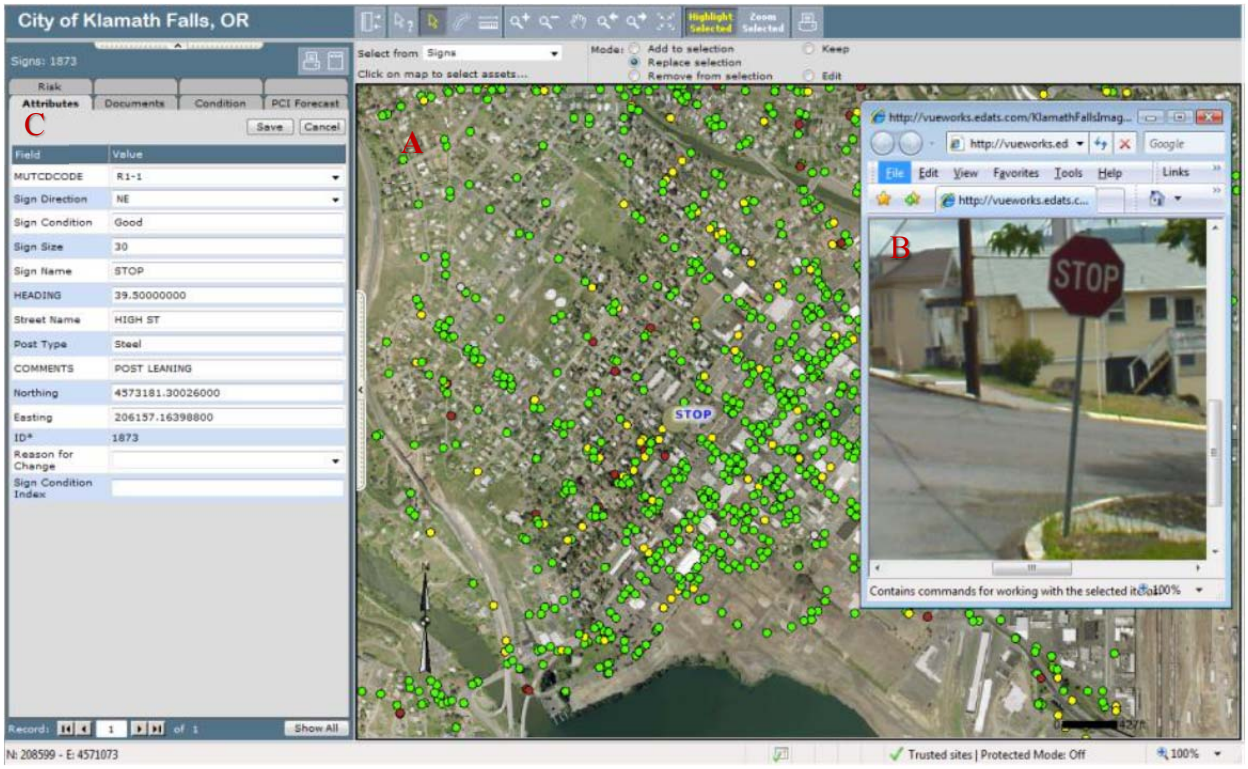

Figure 57. DTS VUEWorks Asset Data and Imagery.

As shown in Figure 57, users can select assets (example from Klamath Falls, OR, shows stop sign locations) and once a specific asset is selected in the aerial view (A), a high-resolution image of the asset pops up for users to view. In addition, a wide range of data for the selected asset such as direction, condition, size, etc. are shown in the attribute window on the left of the screen (C). Users can use the attribute screen to view, edit and rate assets.

DTS staff explained that VUEWorks is designed to be a fully integrated asset-management software platform that incorporates all aspects of the asset management process. This includes not only the ability to view, edit and rate assets (as shown in Figure 57), but to conduct risk analyses of assets and ultimately create work orders and service requests for repair or replacement of assets. Figure 58 provides a screenshot of the user interface for creating a service request.

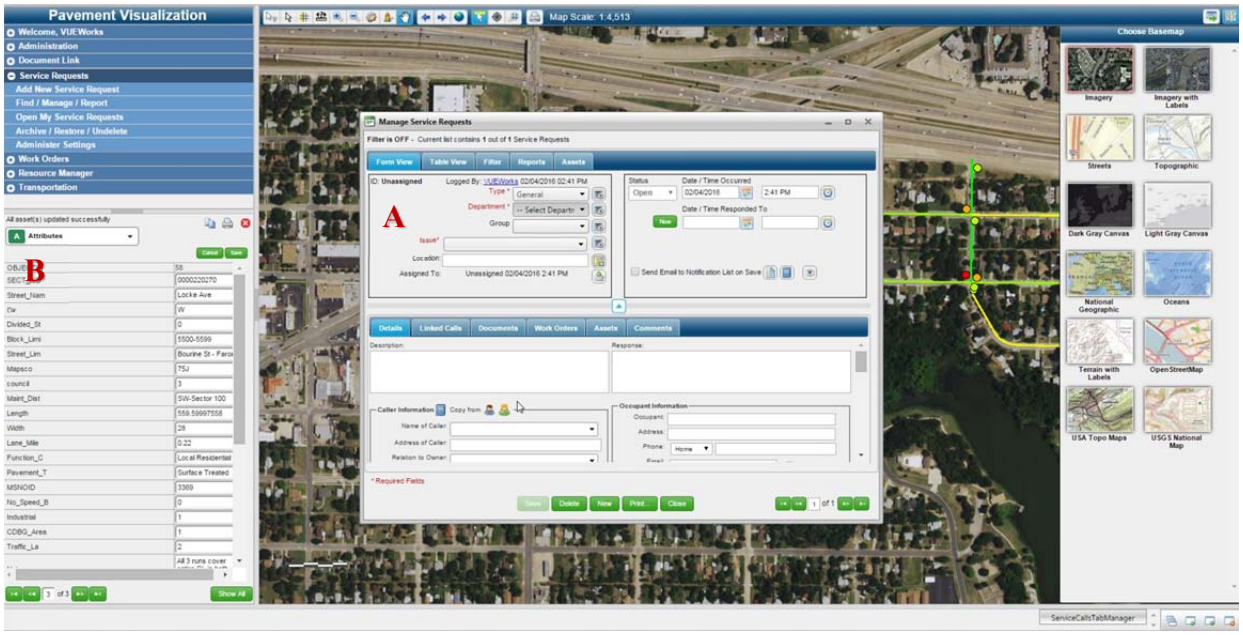

Figure 58. DTS VUEWorks Service Request.

Users can easily select an asset (or series of assets) and create a service request. In the example shown in Figure 58, the service request window (A) provides a range of options for users to provide specific instructions regarding the asset and can assign the work to a specific department. The attribute window (B) on the left of the screen provides all of the data about the asset that users need to create the service requests. DTS staff also explained that users can use VUEWorks to manage service requests for an entire city/state within the program. Finally, DTS staff explained that the entire tool is mobile-optimized so users can access the platform on their smartphone or tablet while in the field.

DTS Software Takeaways

VUEWorks is an extremely comprehensive program that focuses on the entire asset management process, as opposed to only viewing and rating assets. The program was developed with the ESRI ArcGIS platform, so much of the user interface and functionality are similar. So users with familiarity with ArcGIS will feel immediately comfortable with the layout and basic functionality of VUEWorks. The user interface is much more centrally focused on an aerial view, as opposed to featuring high resolution ROW imagery, which is a staple of many of the software platforms evaluated for this report. High resolution imagery of assets is a component of VUEWorks though, as each asset has imagery stored in the asset database. For users who are reliant on the flexibility of viewing high-resolution imagery of the entire ROW, as opposed to simply seeing the asset, this platform does not perform as well. That however, is the only area where VUEWorks falls short. The focus on creating a one-stop-shop for asset management and integration of functions such as asset risk assessments and service request creation and management provide a highly powerful tool with an extremely wide range of functionality for asset management. In addition, the mobile-optimization of the software provides a tool that can be used in the field, which should be highly useful for users who want to QC the collected data by doing field visits. The extensive functionality of the software means that the learning curve is steeper than other web-based tools evaluated here. That being said the software is far from being

the most unintuitive of the software platforms evaluated here, and the extensive amount of functionality makes the tool one of the most impressive offerings available.

Conclusion Regarding Contractor Data Reporting

The primary takeaway from this evaluation is that the level of intuitiveness of each software platform fluctuates from user-friendly to extremely complicated as additional functionality is added. Some of the web-based products that simply allow users to view high-resolution imagery are generally free to the end-user, and can be learned with a quick tutorial or by exploring the software for less than an hour. On the other hand, some of the software platforms are powerful enough for users to monitor and rate the condition of assets and even create work orders for asset management. However those tools require extensive training by the developer that can last weeks and significantly increase the cost to the end user. Clients of data collection companies must consider the tradeoff between ease of use and functionality when deciding whether to invest in a software platform. In addition, the decision as to whether some of the more complicated software platforms are worth investing agency resources in (both man hours and money) depends on how the asset management process is currently conducted within the agency. For example, if the existing processes to rate the condition of assets or create service requests is efficient and effective, integrating a full service tool such as VUEWorks may not be worth the investment, and one of the more basic software platforms may meet the needs of the agency.

SUBTASK 2.4: EVALUATION OF RESULTS

Using the performance metrics identified in Subtask 2.1, the research team evaluated the results of each of the contractor technologies tested. All of the technologies will be compared individually to the ground truth data. This is not to say that the ground truth data are perfect. However for the purposes of this report the ground truth data are the value by which all error will be established. The contactor technologies have also been compared to each other. The evaluation helped identify opportunities moving forward in subsequent tasks and phases.

The four evaluation metrics include: Service, Identification, Quantification, and Accuracy. For the purposes of evaluation contractors will be referred to by their letter designation:

- Contractor A: Data Transfer Solutions (DTS).
- Contractor B: DBi Services.
- Contractor C: Arch Aerial LLC (AALLC).
- Contractor D: Mandli Communications.
- Contractor E: Pathway Services Inc.
- Contractor F: Fugro Roadware.
- Contractor G: Facet Technology Corp. (“Facet”).

Service Metrics Evaluation

Comparable service metrics include many of the components of data collection, data processing, and data reporting. The ground truth data effort was compared to the technology owner data effort and includes: mobilization/calibration times, data collection time, data storage amounts, staffing, processing time, data reporting approximate costs, and proprietary restrictions.

Data Collection Comparisons (TTI vs. Contractors)

Contractors were issued contracts for execution on August 3, 2015, with a contract deadline of August 31, 2015. Researchers are limited to the information provided in the technical memorandums submitted by the contractors. Despite the contracts specification of frontage roads, not all contractors collected the adjacent two-way frontage roads at the IH 45 study site. It may have been that photogrammetry and/or LiDAR data were collected but not processed. The project schedule did not allow for additional time to inquire and request additional data collection. Contractor C, the UAS vendor, did not collect IH 45 after discussions with the Federal Aviation Administration (FAA). Contractor G failed to submit both a Phase 1 and Phase 2 technical memorandums or meet the agreed upon deadlines (see Table 29).

Table 29. Locations of Data Collection Summary.

	FM 3090	IH 45 ML	IH 45 FR (W)	IH 45 FR (E)	IH 45 RAMPS
TTI	X	X	X	X	X
A	X	X			
B	X	X	X	X	X
C	X				
D	X	X			
E	X	X	X	X	
F	X	X			
G	No Data				

TTI was sensitive to the proprietary nature of the information requested and gave complete freedom to the contractors to provide only that information that they were comfortable with concerning the operation of their technology.

Data Collection Speed

Reported data collection travel speed was reported by the contractors and can be found in Table 30.

Table 30. Data Collection Speed of Selected Contractors.

	Avg. Speed (mph)	
	IH 45 ML	FM 3090
A	54.01	43.10
B	60.00	38.75
C	NA	15.65
D	62.23	46.06
E	Posted	Posted
F	45.30	42.50
G	Did Not Provide	

Data Collection Times

Data collection dates (no travel to site), calibration, setup times, and the total time spent collecting asset data can be found in Table 31.

Table 31. Data Collection Dates and Times.

	Collection Dates	Calibration (min)	Site Setup (min)	Collection Time (min)
TTI	8/7-8/24	NA	NA	2,070 (34.5 hrs)
A	8/8/2015	120	50	74
B	Unknown	120	60	292
C	8/29/2015	Unknown	240	475
D	8/12/2015	120	45	66
E	Unknown	48 hrs		480
F	8/15/2015	240	180	17
G	Non-Performing			

It should be clarified that the above collection times should not be compared to each other to establish trends but rather to make the point that compared to manual data collection, the use of contractor technologies are much quicker. For example Contractor B needed 292 minutes to collect data, which is roughly 5 hours. However it is not mentioned above that Contractor B completed double passes for both study sites including the IH 45 frontage roads and ramps. Similarly Contractor C, the UAS contractor, only collected data on FM 3090 but was required to stop approximately every mile due to FAA line of site restrictions. TTI recorded a total effort of 34.4 hours (2,070 minutes) in the field. Researchers were also able to limit field exposure by using video and a GPS program. Although there are some overlapping processing efforts, since most of the contractors mobile mapped the facility and then processed the information, the mobile mapping technology alone reduced staff field exposure 10 fold or better.

Amount of Data Collected

The amount of data and storage details were also provided by the contractors (see Table 32). It can be concluded that there is a higher need for data storage for mobile mapping technologies compared to manual data collection.

Table 32. Data Amounts from Contractor Data Collection.

	Image Data (gb)	Lidar Data (gb)	Other Data (gb)
TTI	4.558		.007 (Spreadsheets)
A	36	104	
B	303	NA	871 (Sign Retro)
C	55	NA	
D	.29296/mi	.31948/mi	
E	~70		
F	1.4	9.0	
G	Non-Performing		

Staff Requirements

Another interesting comparison is the total man-hours required to complete the field data collection. At time the ground truth data collection required four persons, while all contractor technologies, with the exception of the UAS vendor, required only two staff members, a driver and operator (see Table 33).

Table 33. Staffing and Data Collection Man-Hours.

	Staff	Collection Time (Man-hours)
TTI	2-4 (varies)	139.5
A	2	2
B	2	10
C	5 (Includes Law Enforcement)	40
D	2	2
E	2	8
F	2	1
G	Non-Performing	

Data Processing and Reporting Comparisons (TTI vs. Contractors)

Contractors were issued contracts for execution in September, the 2016 fiscal year, with a contract deadline of December 31, 2015. All but one contractor delivered the Asset Data Spreadsheet deliverable and Phase 2 Technical Memorandum prior to or near the December 31 deadline. Facet Technologies failed to deliver any Phase 2 deliverable despite multiple opportunities including a last minute request in early February 2016.

Data Processing and Reporting Times

Technology owners were asked to provide data processing and reporting man-hours as wells as overall business days. It was found that all performing contractors were able to process and develop reporting materials within a calendar month (see Table 34).

Table 34. Data Processing and Reporting Time Metrics.

	Total Man-Hours	Business Days
TTI	600*	54**
A	170	12
B	150	20
C	97.5	25
D	100	13
E	130	Unknown
F	425	12
G	Non-Performing	

* Estimated does not include man-hours required to write this memorandum.
**Estimated. Due to the use of part time staff this measure may not be appropriate for direct comparison.

All contractors indicated that the number of hours required for processing would reduce on larger scale projects (greater than 20 miles of roadway). It is also important when comparing these values to consider the variation in data collection efforts. For example Contractor C only collected data on FM 3090 whereas the other contractors collected data on both FM 3090 and IH 45. Although staffing data were requested it was found in contractor responses that it varies greatly ranging from 1 to 13 persons when added up over the various stages of processing and reporting efforts. TTI used 7 different researchers and students to accomplish the task of processing and reporting. However not all TTI staff were full time researchers (students) or dedicated 100 percent of their time to the project.

Data Reporting

TTI conducted a review of the reporting mechanism provided by the contractors and developed an evaluation matrix. Table 35 provides an overview of the ease of use and functionality of each tool. Ease of use and functionality are rated in the following manner:

- + = Fair.
- + + = Good.
- + + + = Great.
- + + + + = Exceptional.

In addition a range of features is provided at the bottom of the table with a check mark denoting whether the software platform includes that functionality.

Table 35. Summary of Findings from Software Platform Evaluation.

	Pathway Services		DBI Services			Fugro Consultants		Mandli Communications		DTS
	PathView II	PathWeb	360 Viewer	SignViewer	Pavement Viewer	iVision	FugroViewer	Roadview Workstation	Roadview Explorer	VUEWorks
Ease of use	++	+++	+++	+++	+++	++++	++	+	++++	+++
Functionality	+++	++	++	+	+	++	++	++++	+	++++
FEATURES										
Asset attribute data	✓	✓	✓			✓		✓		✓
High-res imagery	✓	✓	✓	✓	✓	✓		✓	✓	✓
Edit asset data	✓							✓		✓
Rate asset conditions	✓							✓		✓
LiDAR data							✓	✓		
Measurement tool	✓					✓	✓	✓		✓
Toggle asset layers on/off		✓	✓			✓		✓		✓
Ability to add GIS data		✓				✓	✓	✓		✓
Can export to GIS/excel file	✓		✓	✓	✓	✓	✓	✓		✓
Can export high-res imagery		✓				✓				
Create asset condition reports						✓		✓		✓
Create work orders										✓
Mobile optimization										✓

Total Costs of Technology Owner Data Collection, Processing and Reporting

TTI requested approximate costs from the technology owners involved with data collection, processing and reporting. It is unclear if the technology owners provided actual costs incurred as the majority of the reported costs provided added up to the original fee that TTI paid contractors for completing the work. Therefore, the cost analysis will only consist of an evaluation of contracted costs.

Contractor Fees

TTI entered into contracts with seven technology owners (see Table 36). The agreed upon fees do not necessarily reflect direct costs and/or for profit fees but an agreed upon amount to complete the project. However based on the delivered Phase 2 technical memorandum these agreed upon fees most likely include some multiplier of profit. For example in a detailed breakdown of hours, Contractor A reported a GIS technician at a rate of $85 per hour and a Senior Engineer at a rate of $160 per hour. These rates are, in the experience of the author, typical profit loaded rates for transportation related consultants. Researchers had been in contact with Contractor D to confirm the negotiated fee was representative of a typical fee TxDOT might see under normal contracting conditions. The Contractor D representative could not confirm the negotiated fee was a loaded fee but was to investigate further with staff. Contractor D failed to follow-up before the submission of this memorandum.

Table 36. Negotiated Contractor Fees for Data Collection, Processing and Reporting

	Collection	Processing/Reporting	Total
A	$ 15,020.12	$ 9,979.88	$ 25,000.00
B	$ 16,436.62	$ 11,396.38	$ 27,833.00
C	$ 13,873.97	$ 8,833.73	$ 22,707.69
D	$ 6,770.12	$ 1,729.88	$ 8,500.00
E	$ 13,320.12	$ 8,279.88	$ 21,600.00
F	$ 19,760.12	$ 14,719.88	$ 34,480.00

Table 37 shows a per mile fee by segment length which is approximately 20 miles (10 for FM 3090 and 10 for IH 45). Contractor C only collected FM 3090 resulting in 10 segment miles. Contractor G was removed from the cost analysis as they were non-performing. Table 38 shows the per mile fee by total miles delivered. Since some contractors submitted both IH 45 mainlanes and frontage roads it was important to determine if this was built into their fee. Table 39 shows the per mile fee breakdown of surface oriented technology owners. Contractor C, the UAS vendor, was removed to better understand fees by surface based contractors only.

Table 37. Negotiated Contractor Fees per Segment Miles.

	Segment Miles	Collection	Processing/Reporting	Total
A	20	$ 751.01	$ 498.99	$ 1,250.00
B	20	$ 821.83	$ 569.82	$ 1,391.65
C	10	$ 1,387.40	$ 883.37	$ 2,270.77
D	20	$ 338.51	$ 86.49	$ 425.00
E	20	$ 666.01	$ 413.99	$ 1,080.00
F	20	$ 988.01	$ 735.99	$ 1,724.00
Per Mile Average		$ 825.46	$ 531.44	$ 1,356.90

Table 38. Negotiated Contractor Fees per Total Miles Delivered.

	Delivered Miles	Collection	Processing/Reporting	Total
A	20	$ 751.01	$ 498.99	$ 1,250.00
B	42	$ 391.35	$ 271.34	$ 662.69
C	10	$ 1,387.40	$ 883.37	$ 2,270.77
D	20	$ 338.51	$ 86.49	$ 425.00
E	40	$ 333.00	$ 207.00	$ 540.00
F	20	$ 988.01	$ 735.99	$ 1,724.00
Per Mile Average		$ 698.21	$ 447.20	$ 1,145.41

Table 39. Negotiated Contractor Fees per Total Miles Delivered (Surface Based).

	Delivered Miles	Collection	Processing/Reporting	Total
A	20	$ 751.01	$ 498.99	$ 1,250.00
B	42	$ 391.35	$ 271.34	$ 662.69
D	20	$ 338.51	$ 86.49	$ 425.00
E	40	$ 333.00	$ 207.00	$ 540.00
F	20	$ 988.01	$ 735.99	$ 1,724.00
Per Mile Average		$ 560.37	$ 359.96	$ 920.34

Since Contactor D's total negotiated fees were atypical compared to the others, an additional analysis was completed. By removing Contractor D from the analysis, the negotiated fees for surface based contractors equaled $1,044.17 per delivered mile.

Identification Metrics

Identification metrics include asset identification (e.g., MUTCD sign designations), asset material (e.g., sign sheeting, pavement markings), and general sizes of assets. It was concluded that many of these attributes could be analyzed using the sampled data attributes of signs.

Determining Samples for Analysis

After comparing sign data side by side, researchers determined that the following attributes would be evaluated for identification performance:

- Loc_TxDOT_MP.
- Sign surface area.
- MUTCD sign dimensions.
- Sign designation.
- Sign color.
- Sign text.

Ground Truth Sample Sign Data

Based on the earlier statistical analysis it was concluded that approximately 43 fully sampled assets were required in the worst case scenario to establish statistical significance during analysis. TTI collected the following sign and sign support data for the two study sites (see Table 40).

Table 40. Sampled Sign and Sign Support Data for Ground Truth.

Roadway	Control Section	SGN	SGNUP
FM 3090	0643-05	41	30
IH 45 Main Lanes	0675-05	9	8
IH 45 Frontage East		15	14
IH 45 Frontage West		10	9
	Total	75	61

Ultimately it was decided that the analysis would compare 22 sampled signs from each study site. Taking 22 signs from both FM 3090 and IH 45 would exceeding the worst case statistical scenario of 43 sampled assets.

Matching Data Points

Not all contractors provided the same type of data. For example Contractor C supplied only sign (SGN) data instead of Sign Support (SGNSUP) data. TTI researchers initially began work using the Contractor C google earth file to match signs in the ground truth database and the Contractor C database. Researchers later found that using ArcGIS to match signs was far superior that Google Earth matching. Matching was completed manually by reviewing a GIS map containing both ground truth and technology owner data points for signs. Research essentially picked the technology owner points closest to the TTI data point. It was initially thought that matching could be completed by using reported milepoints but the following table shows discrepancies between ground truth milepoints and the reported milepoints from technology owners. Table 41 shows a small sample of signs that were matched through GIS. For FM 3090 (064-05). Only Contractors A, B, C, and F reported similar milepost markings to the ones recorded in the ground truth data. After matching all of the points individually, researchers placed them in an excel spreadsheet for further analysis.

Table 41. Sample of Reported Milepost Location of Signs.

Sign ID	Cont. Sec	TTI MP	E	D	F	A	B	C
SGN10	0643-05	13.43	7.875	8.058	13.335206	14	13.437389	13.26
SGN11	0643-05	13.32	7.758	8.175	13.217909	14	13.324899	10.96
SGN12	0643-05	10.91	5.804	10.134	11.260618	12	11.270027	10.96
SGN15	0643-05	10.76	5.31	10.63	10.764291	11	10.778508	8.86
SGN16	0643-05	8.88	3.376	12.563	8.8301559	9	8.909386	7.436
SGN17	0643-05	7.41	1.888	14.056	7.3364481	8	7.446322	7.436
SGN19	0643-05	5.84	0.068	15.878	5.512628	6	5.521764	5.576
SGN20	0643-05	5.84	0.068	15.878	5.5126285	6	5.521713	5.576
SGN21	0643-05	5.45	0.043	15.904	5.4866959	6	5.493545	5.546
SGN61	0675-05	16.21	2.715	12.693	15.257831	146	12.389844	#N/A
SGN63	0675-05	13.28	8.485	18.475	13.645133	152	18.383099	#N/A
SGN64	0675-05	13.26	7.725	17.714	13.613671	151	17.647061	#N/A
SGN65	0675-05	13.27	2.463	12.441	15.2093	146	12.137822	#N/A
SGN66	0675-05	10.56	2.383	12.362	15.204536	146	12.058409	#N/A
SGN67	0675-05	11.30	2.715	12.693	15.257831	146	12.389844	#N/A

Prior to statistical comparisons, asset IDs were used to match the data entries of each contractor to the ground truth samples. Table 42 shows how many of the TTI samples match up with the data provided with each contractor.

Table 42. Total Matching Signs and Sign Support.

	Sign Matches		Sign Support Matches	
	FM 3090	**IH 45**	**FM 3090**	**IH 45**
A	39	12	29	7
B*	41	31	29	20
C	43	0	0	0
D	40	15	29	9
E*	41	31	26	22
F	47	24	29	8
G	No Data			

*Collected both IH 45 main lanes and frontage roads.

Table 42 shows that each contractor collected more than 22 samples of signs and sign support data for FM 3090. However, Contractor C did not provide any sign and sign support data for IH 45 and Contractors A, D, and F did not provide any sign and sign support data for the IH 45 frontage roads.

Ideally, for direct comparison and analysis, a significant number of samples where all contractors have data should be used for each site and then together. This was possible for FM 3090, but was not possible for IH 45 due to multiple contractor not delivering frontage road information. For FM 3090 there were 29 sign entries and 26 sign support entries that had data from all contractors. For IH 45 there were 10 sign data matches (not enough for statistical significance) where all contractors provided data and 5 matches for sign supports.

Because of the lack of matches on IH 45, researchers used the set of 29 signs, and 26 sign support matches (from all contractors) from FM 3090 for most of the statistical analysis. However, where appropriate, a combined statistical analysis was completed including both sign matches from FM 3090 and IH 45. The remaining data for IH 45 were still used but commonalities were not investigated and each contractor was analyzed individually.

A Z-test statistical analysis was used according to the same procedure used by Findley et al. (5). The following sections will show the analysis for each attribute.

Sign Color

The TTI team identified 6 categories for color. Table 43 shows the color comparison between the TTI sample and the contractor data.

Table 43. FM 3090 Sign Color Comparison.

	Green	Red	Yellow	White	Black & White	Fluorescent Yellow-Green	Total
Ground Truth [TTI]	8	1	13	3	3	1	29
A	8	1	13	3	3	1	29
B	8	1	14	4	2	0	29
C	4	2	17	0	5	0	28
D	8	1	13	4	2	1	29
E	8	1	14	4	2	0	29
F	8	1	14	3	3	0	29
G	No Data						

All contractors categorized fluorescent signs as either green or yellow, with the exception of Contractor A and D. Also, all contractors categorized black and white signs as either black or white. For this analysis if a contractor categorized a fluorescent green/yellow sign as a green or yellow sign then they were marked as identified. Table 44 shows the number of signs identified when contractor data were matched up with ground truth sign data on highway FM 3090.

Table 44. FM 3090 Correct Matches of Sign Color.

Contractor	FM 3090	Total Samples	Percent Correct
A	29	29	100%
B	29	29	100%
C	14	29	48%
D	29	29	100%
E	29	29	100%
F	29	29	100%
G	No Data		

Table 45. FM 3090 and IH 45 Correct Matches of Sign Color.

Contractor	Combined	Total Samples	Percent Correct
A	39	39	100%
B	39	39	100%
C	14	29	48%
D	39	39	100%
E	39	39	100%
F	31	39	79%
G	No Data		

Table 46 shows that determining the sign background color was not difficult for most contractors. The only difficulty may be in defining when a sign has either white background and black lettering or a black background and white lettering.

For IH 45 the maximum sample size was 25 signs. Not all contractors provided data for the same 25 signs; therefore, there were more data for some contractors than others.

Table 46. IH 45 Correct Matches of Sign Color (Varying Sample).

Contractor	IH 45	Total Samples	Percent Correct
A	12	12	100%
B	23	25	92%
C	No Data		
D	13	13	100%
E	25	25	100%
F	2	10	20%
G	No Data		

Sign MUTCD Designation

The TTI research team discerned the following MUTCD classification for the signs sampled on highway FM 3090:

- D21-2T.
- R1-1.
- D1-1.
- D20-1TR (L).
- W1-1R (L).
- W13-1P.
- W1-3R (L).
- M3-3.
- M1-6F.
- W8-13aT.
- W1-2R (L).
- R2-1.
- S3-1T.
- W2-6D.
- M2-1.
- W3-1.

Table 47 shows the total correct classifications from each contractor for FM 3090 and Table 48 shows total correct matches for both FM 3090 and IH 45.

Table 47. FM 3090 Correct Matches of MUTCD Designation.

Contractor	FM 3090	Total Samples	Percent Correct
A	23	29	79%
B	8	29	28%
C	9	29	31%
D	16	29	55%
E	19	29	66%
F	20	29	69%
G	No Data		

Table 48. FM 3090 and IH 45 Correct Matches of MUTCD Designation.

Contractor	Combined	Total Samples	Percent Correct
A	29	39	74%
B	14	39	36%
C	No Data		
D	20	39	51%
E	23	39	59%
F	20	39	51%
G	No Data		

Leniency was applied when analyzing the data. For example, for sign designation "W8-13aT," some contractors noted the designation as W8-13. When such was the case, the answer was marked as identified. Signs that almost all contractors had difficulty identifying were sign designations: M1-6F, W2-6D, D21-2T, D20-1TR (L), W1-3R (L), and W1-2R (L). Examples where credit was not awarded included when a broad statement was given, such as warning sign or regulatory sign. There were also 13 signs in the ground truth data that did not have a clear MUTCD designation. As a result, these entries were omitted from the analysis. Table 49 shows the results of the analysis of sign designation identification from IH 45.

Table 49. IH 45 Correct Matches of MUTCD Designation (Varying Sample).

Contractor	IH 45	Total Samples	Percent Correct
A	7	8	88%
B	15	18	83%
C	No Data		
D	7	9	78%
E	12	18	67%
F	0	6	0%
G	No Data		

MUTCD Sign Dimension

For sign dimension only exact dimensions were marked as identified. Table 50 shows the total of correct matches and the total percentage of correct matches given by each contractor.

Table 50. FM 3090 Correct Matches of MUTCD Sign Dimension.

Contractor	FM 3090	Total Samples	Percent Correct
A	11	29	38%
B	6	29	21%
C	3	29	10%
D	21	29	72%
E	NA	29	NA
F	17	29	59%
G	No Data		

Table 51. IH 45 and FM 3090 Correct Matches of MUTCD Sign Dimension.

Contractor	Combined	Total Samples	Percent Correct
A	16	39	41%
B	13	39	33%
C	3	29	10%
D	29	39	74%
E	No Data		
F	17	39	44%
G	No Data		

Contractor E did not provide dimensions for the signs they observed. Some entries by Contractor A include the word "varies" (i.e., varies X 18). A sign that was 36×36 was the one mostly misclassified by contractors. All contractors determined that sign to be 48×48, 24×24, or 30×30. For IH 45, there were 7 signs where the sign dimensions given by the TTI research team were not clear. Therefore these signs were removed from the sampling. Table 52 shows the results from the IH 45 analysis.

Table 52. IH 45 Correct Matches of MUTCD Sign Dimension (Varying Sample).

Contractor	Identified	Total Signs	Percent Identified
A	6	12	50%
B	14	24	58%
C	No Data		
D	9	13	69%
E	No Data		
F	0	10	0%
G	No Data		

Sign Surface Area

The total surface area was given by the contractors and the research team. For this analysis, the hypothesis that mean difference in surface area measurement is 0, Equation 2 was used (5):

$$Z = \frac{(Xt - Xi) - (\mu t - \mu i)}{\sqrt{\frac{s_t^2}{nt} + \frac{s_i^2}{ni}}} \quad (2)$$

Where;

Z = Z-statistic.

Xi = the mean surface area measured by the contractor.

Xt = the mean surface area measured by the TTI research team.

s_i = standard deviation of the samples given by the contractor.

s_t = standard deviation of the samples given by the TTI research team.

ni = the number of samples of the contractor measurements.

nt = the number of samples of the TTI measurements.

$(\mu t - \mu i)$ = difference between μt and μi under the null hypothesis.

And the hypothesis being tested are:

$$H_0: \mu t - \mu i = 0$$

$$H_1: \mu t - \mu i \neq 0 \quad (3)$$

Table 53. FM 3090 Sign Surface Area Z-Statistic Calculations.

	Total Area	Average Sign Area	Standard Deviation	Z-statistic
Ground Truth [TTI]	27711	955.55	522.66	
A	34217	1179.9	815.7	-1.24706
B	24588	847.86	464.68	0.82922
C	No Data			
D	28467	981.62	526.5	-0.18923
E	No Data			
F	29725.84	1025.03	473.34	-0.5306
G	No Data			

When testing for the 5 percent level of significance (Z=±1.96), there is not enough evidence to reject the null hypothesis for any of the contractors that provided data. This means that the

differences in measurements are not statistically significant. Contractor C, E, and G did not provide any measurements.

Table 54. IH 45 and FM 3090 Sign Surface Area Z-Statistic Calculations.

	Total Area	Average Sign Area	Standard Deviation	Total Samples	Z-statistic
Ground Truth [TTI]	58239	1493.31	1126.74	39	
A	65351	1675.67	1203.12	39	-0.60
B	51660	1324.62	937.46	39	0.62
C	No Data				
D	55539	1424.08	892.96	39	0.26
E	No Data				
F	39026	1000.66	524.95	39	2.13
G	No Data				

When testing for the 5 percent level of significance (Z=±1.96), there is enough evidence to reject the null hypothesis for Contractor F. This means that the differences in measurements are statistically significant for the set of sign dimension for Contractor F. Contractor C, E, and G did not provide any measurements. As shown below, when all sign matches are considered (many above 39) Contractor F's data are not statistically different than other contractors and the ground truth data.

The same methodology was used for IH 45 when testing the statistical significance between the averages of the surface area measurements. The same equation was applied, but assuming that both populations are normally distributed, the test statistic will have t-distribution because the number of samples is equal or less than 25 (6). The degrees of freedom are calculated using the following equation:

$$df = \frac{(\frac{st^2}{nt}+\frac{si^2}{ni})^2}{\frac{(\frac{st^2}{nt})^2}{nt-1}+\frac{(\frac{si^2}{ni})^2}{ni-1}} \quad (4)$$

Table 55. Statistical Analysis of IH 45 Sign Surface Area Measurements.

	Total	Average	Standard Deviation	Samples	Degrees of Freedom	t-Statistic	Two-Tailed p-Value
Ground Truth [TTI]	82071.3	3282.85	4408.33	25			
A	61504	5125.33	7598.32	12	14.67	8.70018	5.09E-07
B	74052	2962.08	4269.26	25	47.95	6.533813	4.17E-08
C	No Data						
D	54288	4176	5813.47	13	19.38	15.11869	4.79E-12
E	No Data						
F	9299.981	930	663.84	10	26.57	80.29385	1.10E-32
G	No Data						

The small p-values means that the null hypothesis cannot be rejected. If we were to combine both FM 3090 and IH 45, samples than a Z distribution can be used.

Table 56. Z-Statistic Analysis Sign Surface Area for All Sites.

	Total Area	Average Sign Area	Standard Deviation	Total Samples	Z-statistic
Ground Truth [TTI]	109782.3	2033.01	3238.09	54	
A	95721	2334.66	4535.95	41	-0.29
B	98640	1826.67	3108.3	54	0.25
C	No Data				
D	82755	1970.36	3581.4	42	0.07
E	No Data				
F	39025.82	1000.66	524.95	39	1.69
G	No Data				

As seen in Table 56 the difference between TTI measurements and the contractor measurements is not statistically significant when considering all signs collected.

Sign Text

For this analysis, only data entries with all words as recorded during the ground truth data collection were marked as correct. Contractor C did not provide any data for text found in the signs. Contractor F did provide data; however, they only provided the numbers written on the sign. For example if the sign said “CO RD 186,” then Contractor F only wrote “186” in the data field. In addition to the text, Contractor D provided the location of the text. For example, “CO RD 186” was written as “CO RD 186 (TO THE RIGHT).” Since all text in the sign was transcribed they were considered to have given the right answer. Contractor B was more

descriptive in their explanation of the text in the sign. For example, the sign in Figure 59 was described in the ground truth data set as saying "Carlos Anderson" and Contractor B described it as "Left Arrow Carlos Anderson Right Arrow."

Figure 59. Photo of Sign on FM 3090.

In the ground truth data set, there were graphic signs that were annotated by TTI in the data set. However none of these signs were explained by the technology owners. For example, Contractor E just described them as "graphic" and did not explain the meaning of the graphic. In such occasion the entry was marked as not being identified.

Table 57. FM 3090 Correct Matches of Sign Text.

Contractor	FM 3090	Samples	Percent Correct
A	22	29	76%
B	26	29	90%
C	No Data		
D	16	29	55%
E	21	29	72%
F	0	29	0%
G	No Data		

Table 58. FM 3090 and IH 45 Correct Matches of Sign Text.

Contractor	Combined	Samples	Percent Correct
A	35	42	83%
B	49	54	91%
C	No Data		
D	24	42	57%
E	43	54	80%
F	0	39	0%
G	No Data		

Table 59. IH 45 Correct Matches of Sign Text (Varying Sample).

Contractor	IH 45	Samples	Percent Correct
A	13	13	100%
B	23	25	92%
C	No Data		
D	8	13	62%
E	22	25	88%
F	0	10	0%
G	No Data		

Quantification Metrics

This performance metric category would include asset quantities in both count and linear totals. As discussed earlier in the Data Collection portion of the evaluation (Table 29) not all contractors delivered data for all lane miles of the selected study sites. All contractors collected FM 3090. However, only two contractors collected the adjacent frontage roads on IH 45 despite the executed agreements including language about frontage roads. Due to the project schedule and time needed for analysis and evaluation, there simply was not enough time to request those technology owners that did not deliver frontage road data, to resubmit their deliverable. This created a situation where appropriate data comparison was then limited to the selected study site where all contractors delivered data – FM 3090. All quantification metrics were determined using FM 3090 data only. The following subsections will compare inventory data collection by asset type.

Sign Inventory

The sign inventory comparison evaluated the total number of signs collected that were not chevrons, which has been detached and evaluated immediately following this comparison. Although Chevrons are considered signs, they are unique typically being two sided sign and as a result, can be assigned to both sides of the roadway on a two way highway. To avoid the confusion of double counting or single counting these signs they were removed from this analysis. A comparison of the total number of signs located on FM 3090 can be found in Table 60.

Table 60. Comparison of Total Number of Signs for FM 3090 (Minus Chevrons).

	Number Reported	Number not Including Chevrons	Difference from Ground Truth	Percent Error
Ground Truth [TTI]	135	135		
A	227	143	8	5.93%
B	220	136	1	0.74%
C	126	84	-51	-37.78%
D	220	136	1	0.74%
E	214	140	5	3.70%
F	232	148	13	9.63%
G	No Data			

With the exception of Contractor C all contractors were within 10 percent of the ground truth inventory numbers.

Chevron Sign Inventory

As discussed earlier, the research team evaluated chevron signs separately as shown in Table 61. All contractors have reported chevrons with high accuracy, which potential indicates chevrons are easier to detect.

Table 61. Comparison of Chevrons for FM 3090.

	Number Reported	Difference from Ground Truth	Percent Error
Ground Truth [TTI]	84		
A	84	0	0.00%
B	84	0	0.00%
C	82	-2	-2.44%
D	84	2	0.00%
E	81	-3	-3.70%
F	84	3	0.00%
G	No Data		

Sign Support Inventory

Table 62 summarizes reported sign support inventory. With the exception of Contractor E, other contractors were within an accuracy range of 10 percent in reporting sign supports.

Table 62. Comparison of Sign Supports for FM 3090.

	Number Reported	Difference from Ground Truth	Percent Error
Ground Truth [TTI]	125		
A	129	4	3.20%
B	124	-1	-0.80%
C	No Data		
D	124	-1	-0.80%
E	111	-14	-11.20%
F	136	11	8.80%
G	No Data		

Point Pavement Markings Inventory

Point pavement markings include pavement marking that are located at a single point, versus linear markings that would run the length of the roadway. A comparison of ground truth and technology owner inventory can be found in Table 63. Point pavements markings include:

- Bike.
- Box.
- Cross Walks.
- Hatchlines.
- Lane Merge Arrows.
- Lane Reduction Arrow.
- Lane Use Arrow.
- Railroad Crossing.
- Stop Bar.
- Symbols.
- Text.

Table 63. Comparison Point Pavement Markings for FM 3090.

	Number Reported	Difference from Ground truth	Percent Error
Ground Truth [TTI]	1		
A	1	0	0%
B	1	0	0%
C	7	6	600%
D	1	0	0%
E	No Data		
F	7	6	600%
G	No Data		

The research team investigated why two of the technology owners deviated greatly from the ground truth inventory value. It was found that these contractors reported point pavement markings (Stop Bars) from intersecting roadways and driveways (see Figure 60).

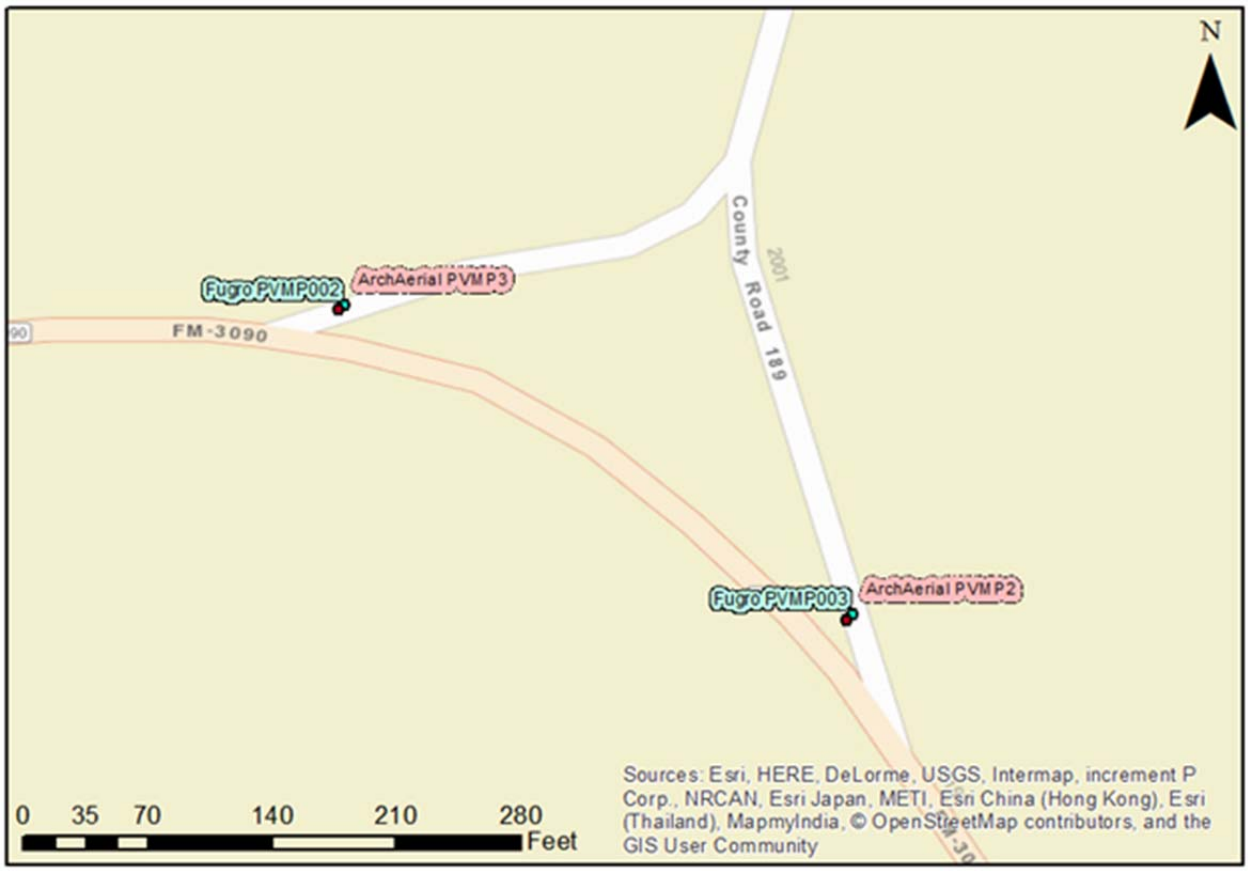

Figure 60. GIS Screenshot Illustrating Technology Owners Reporting Stop Bars.

Linear Pavement Marking Inventory

Linear pavement marking inventory (lengths) was collected for both the ground truth and by technology owners. It was discovered that yellow pavement markings were collected differently between the ground truth data collection and even between the technology owner data sets. Therefore the only measure that could be compared with some accuracy is the amount of solid white pavement markings (see Table 64).

Table 64. Comparison of White Linear Pavement Markings for FM 3090.

	Linear Feet	Difference from Ground Truth	Percent Error
Ground Truth [TTI]	111,586		
A	111,880	294	0%
B	109,580	-2,006	-2%
C	90,816	-20,770	-19%
D	111,586	0	0%
E	109,913	-1,673	-1%
F	111,778	192	0%
G	No Data		

Yellow Pavement Markings

Although the data dictionary called for both broken and double it appears that some contractors measured doubles as two singles; for example, multiple contractor listed quantities of double solid yellow close to 95,000 ft (see Table 65). The length of FM 3090 is approximately 53,000 ft (10 miles). This leads the research team to believe the double yellows were counted multiple times (in both directions). In comparison, the single solid white markings average across both the ground truth and contractors summed to a total of 20.48 miles, which is very close to the length of the study site in both directions.

Table 65. Yellow Pavement Marking Inventory Summary for FM 3090.

	Yellow Double Broken	Yellow Double Solid	Yellow Single Broken	Yellow Double Solid/Broken	Total Yellow
Ground Truth [TTI]	9,723	42,744	3,626	9,423	65,517
A	86,551	94,433	12,650		193,634
B	-	104,098	5,538		109,636
C	8,606	48,523	3,960		61,090
D	9,435	42,303	3,569		55,308
E	43,308	9,403	12,853		65,565
F	44,191	9,475	13,025		66,691
G	No Data				

Lane Lengths and Surface Type

Along FM 3090 there are two sections on the bridges that have a concrete surface type. Four out of 6 contractors did not detect these concrete sections and reported the whole study section lanes as Asphalt only. Contractor C reported the concrete section length by +0.38 percent, which shows they detected the surface type precisely. Due to some contractors not being able to identify the concrete surface, the research team used the total length of the study section to establish error values (see Table 66).

Table 66. Comparison of Linear Pavement for FM 3090.

	Asphalt (ft)	Concrete (ft)	Total (ft)	Difference from Ground Truth	Percent Error
Ground Truth [TTI]	110600	520	111120		
A	112586	0	112586	1466	1.32%
B	111256	0	111256	-1330	0.12%
C	104355	522	104877	-6379	-5.62%
D	111123	0	111123	6246	0.00%
E	109897	802	110700	-423	-0.38%
F	114697	0	114697	3997	3.22%
G	No Data				

Barrier Inventory

The ground truth data collection discovered four W-beam barriers with mixed wooden and I-beam supports on the FM 3060. All contractors reported the correct number of barriers and stayed reasonably close to the actual length of the barriers (see Table 67).

Table 67. Comparison of Barrier Count and Length for FM 3090.

	Number Reported	Length Reported	Percent Error
Ground Truth [TTI]	4	1353	0
A	4	1320.37	-2.41
B	4	1343.47	-0.7
C	4	1397.41	3.28
D	4	1351.1	-0.14
E	4	1340.7	-0.91
F	4	1333.11	-1.47
G	No Data		

Drainage Inventory

Drainage includes both driveway drainage structure and cross drainage structure (perpendicular to roadway). Findings from an evaluation of drainage structures can be found in Table 68.

Table 68. Comparison of Drainage Structures for FM 3090.

	Number Reported	Percent Error
Ground Truth [TTI]	60	
A	60	0%
B	96	60%
C	51	-15%
D	45	-25%
E	10	-83%
F	73	22%
G	No Data	

It is not clear why there are significant differences other than the possibility of double counting drainage structures, for example, counting both sides of a driveway structure or cross drainage structure.

Mailbox Inventory

Contractors were asked to report total number of mail box supports with the understanding that TxDOT is responsible for the safe installation of supports regardless of number of mail boxes attached. Table 69 summarizes the reported mail box support inventory for FM 3090. It is evident that some contractors may have simply counted the number of mailboxes.

Table 69. Comparison of Mailbox Assemblies for FM 3090.

	Number Reported	Percent Error
Ground Truth [TTI]	83	
A	70	-16%
B	87	5%
C	95	14%
D	66	-20%
E	65	-22%
F	68	-18%
G	No Data	

Delineator Inventory

Table 70 summarizes delineator inventory for FM 3090.

Table 70. Comparison of Delineators for FM 3090.

	Number Reported	Percent Error
Ground Truth [TTI]	75	
A	99	32%
B	78	4%
C	78	4%
D	47	-37%
E	77	3%
F	83	11%
G	No Data	

Object Marker

As per MUTCD standards, TTI researchers only reported object markers mounted on the mailbox supports. There were 59 object markers and only DTS GIS reported a similar number of object markers. Other contractor reported different numbers. Table 71 summarizes reported Object markers but does not compare their accuracy because of high deviation in reported inventory.

Table 71. Comparison of Object Marker Inventories for FM 3090.

	Number Reported	Percent Error
Ground Truth [TTI]	59	
A	57	-3%
B	2	-97%
C	No Data	
D	135	129%
E	No Data	
F	187	217%
G	No Data	

Driveways

Driveways are roads that separate from the study section and provide access to local areas and properties. Since TxDOT maintains driveways, it is important to be able to collect their data and monitor changes based on driveway permits issued by TxDOT. Table 72 summarizes reported driveway data by contractors.

Table 72. Comparison of Driveway Inventories for FM 3090.

	Number Reported	Percent Error
Ground Truth [TTI]	99	
A	97	-2%
B	109	10%
C	110	11%
D	113	14%
E	No Data	
F	110	11%
G	No Data	

It appears that collecting the number of driveways is a bigger challenge than instinct would lead the researchers to believe. Although the percent difference is potentially acceptable the variation among all data may simply lie in what defines an official driveway.

Accuracy Metrics

Generally, accuracy metrics would be limited to horizontal, linear and elevation measurements (GPS accuracy). However, it was determined that there are other accuracies that can be evaluated such as sign text, retroreflectivity measurement of signs and pavement markings, and area measurements such as mowable acres.

Review of GPS Accuracies

Researchers evaluated the accuracy of a sample of GPS coordinates for sign locations provided by contractors using ArcGIS. Researchers mapped the GPS coordinates for signs provided by contractors as well as the GPS coordinates for signs collected by the TTI research team. Researchers created buffers around each contractor's data points in order to take into account the margin of error for the GPS unit used by and provided to TTI researchers by each contractor. The following are the accuracies of the GPS units used to collect sign locations:

- TTI: 3 m.
- Mandli: 1 m.
- Fugro: 0.3 m.
- DTS: 0.3 m.
- Pathway: No accuracy provided; 1 m was assumed for this evaluation.
- ArchAerial: No accuracy provided; 1 m was assumed for this evaluation.
- DBi: No accuracy provided; 1 m was assumed for this evaluation.
- FACET: Contractor provided no deliverable.

The following figures provide a visualization of the spatial analysis researchers conducted to evaluate the accuracy of each contractor's GPS readings. Figure 61 provides the spatial analysis for the sign identified by researchers as SGN10. Note that in the upper left corner of all of the

following figures a photograph of the captured asset is shown. As seen in Figure 61, the sign reads: Carlos (left) and Anderson (right).

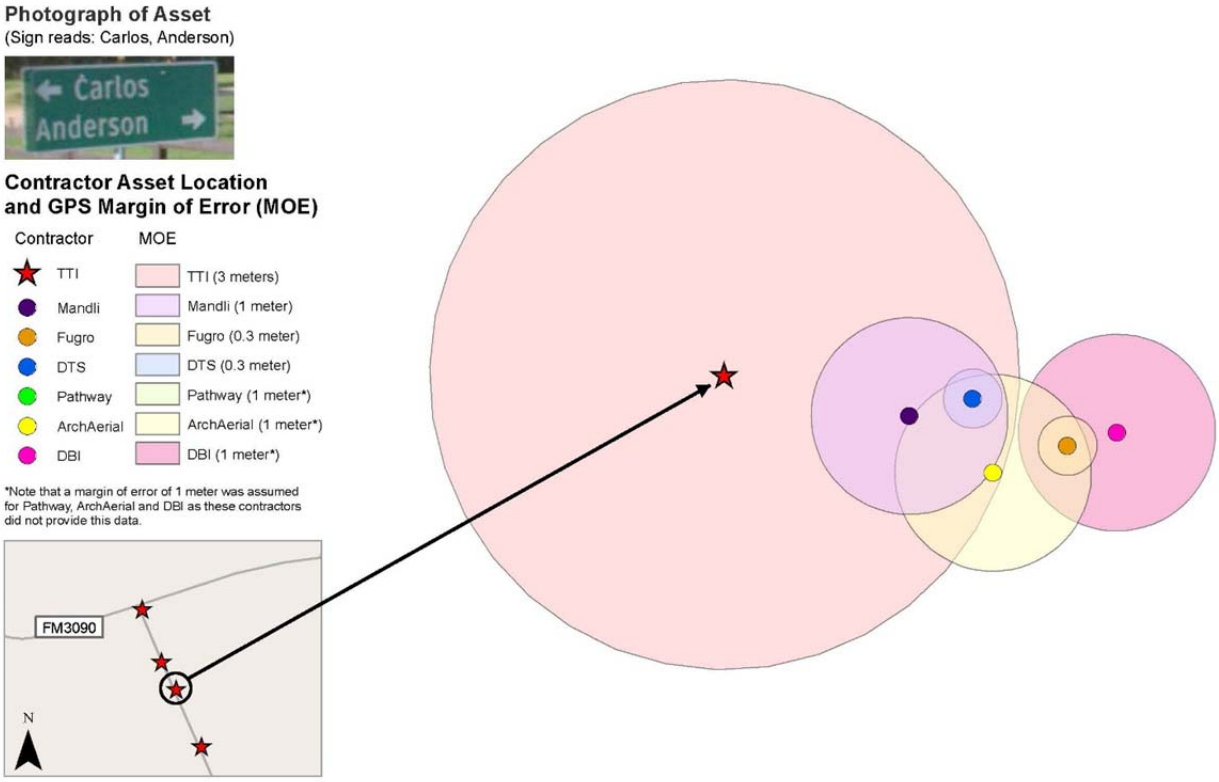

Figure 61. Contractor and TTI Asset Location with Margin of Error for SGN10.

As shown in Figure 61, all contractor's accuracies are within the margin of error based on the TTI asset location, with the exception of Fugro and DBi. Note that Pathway is not shown in Figure 61 as they did not capture this asset. Figure 62 provides a visualization for the spatial analysis for the sign identified by researchers as SGN15, which reads: County Road 401 (left).

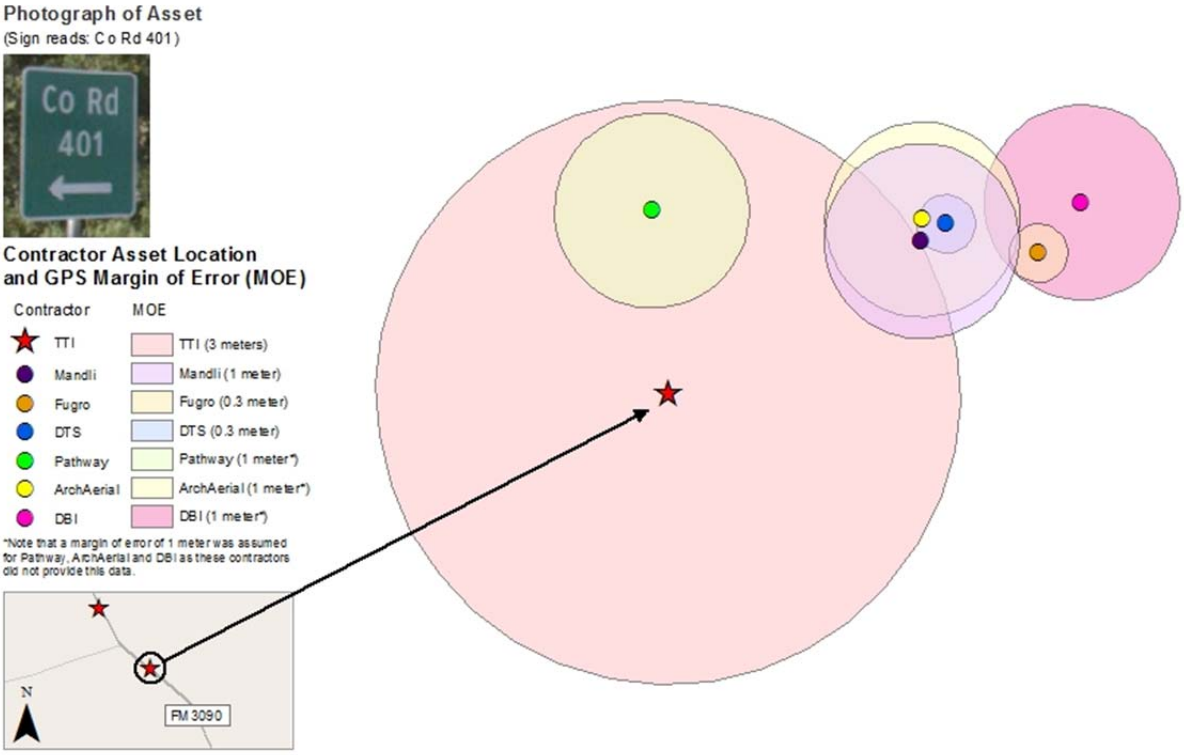

Figure 62. Contractor and TTI Asset Location with Margin of Error for SGN15.

As shown in Figure 62, the asset locations captured by Fugro, DTS, and DBi fall outside the margin of error for the TTI research teams manually captured GPS coordinates. Figure 63 provides the visualization for the spatial analysis conducted for the sign identified by researchers as asset SGN16, which reads County Road 185 (right).

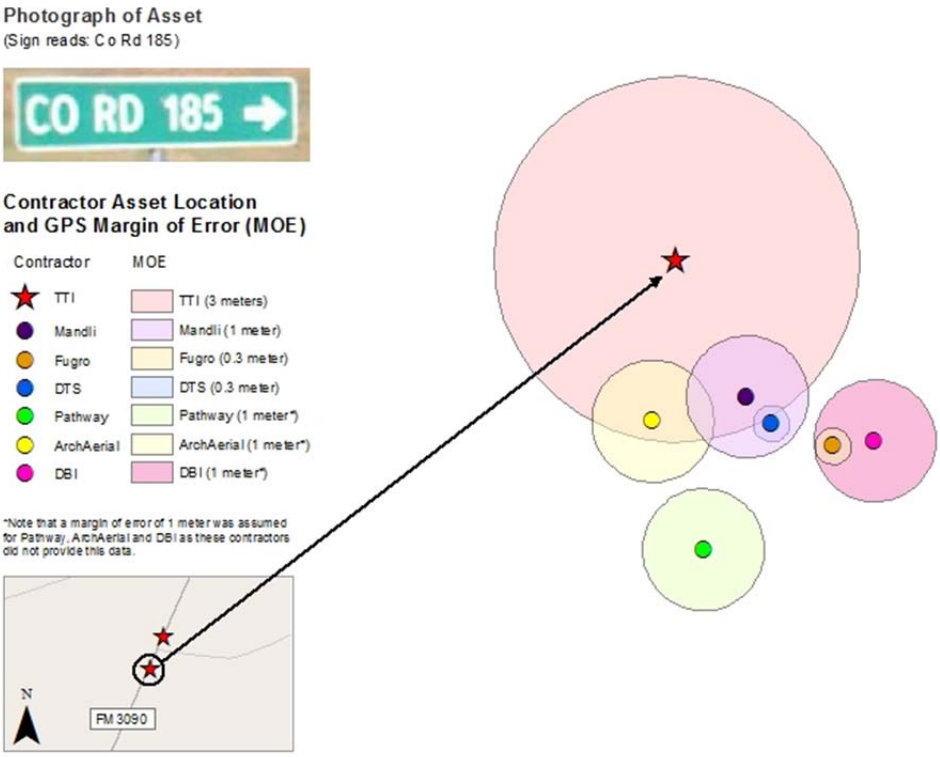

Figure 63. Contractor and TTI Asset Location with Margin of Error for SGN16.

Figure 63 shows that for asset SGN16, Pathway, Fugro and DBi's GPS coordinates fell outside of the 3 m margin of error for the manually collected GPS coordinates retrieved by the TTI research team. Figure 64 provides the visualization for the spatial analysis conducted for the sign identified by researchers as asset SGN21, which reads County Road 186 (right).

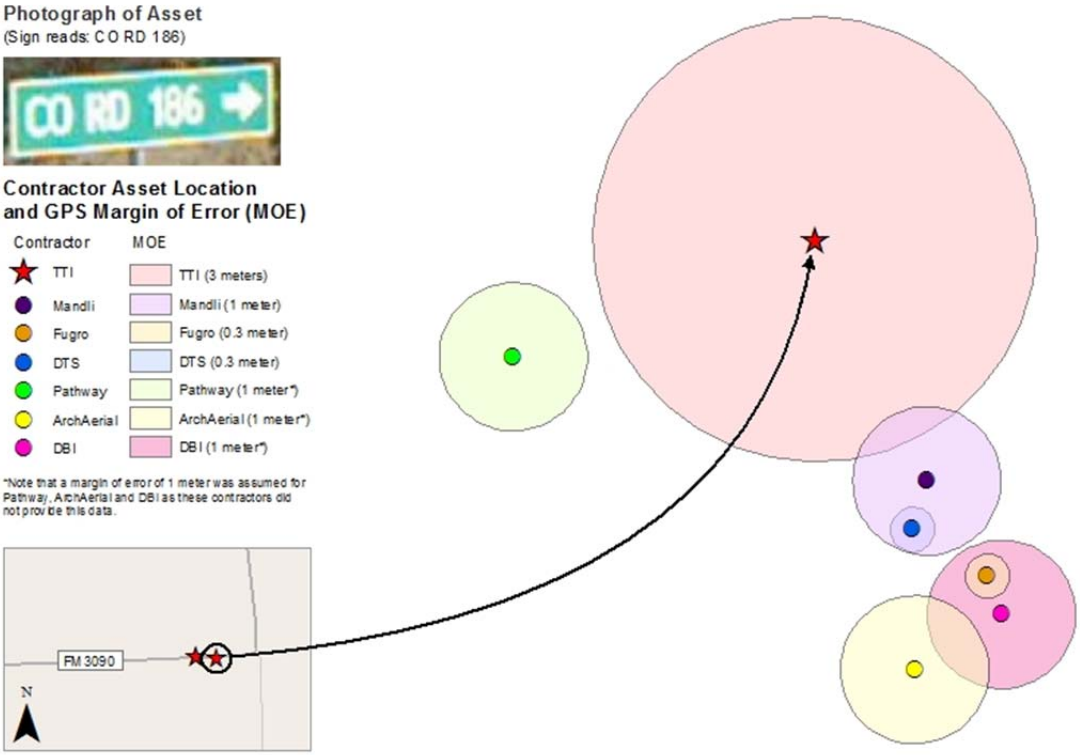

Figure 64. Contractor and TTI Asset Location with Margin of Error for SGN21.

As shown in Figure 64, only the GPS coordinates provided by Mandli fall within the 3 m margin of error for the manually collected GPS coordinated retrieved by the TTI research team. Figure 65 provides the visualization for the spatial analysis conducted for the sign identified by researchers as asset SGN41, which reads School Bus Stop Ahead.

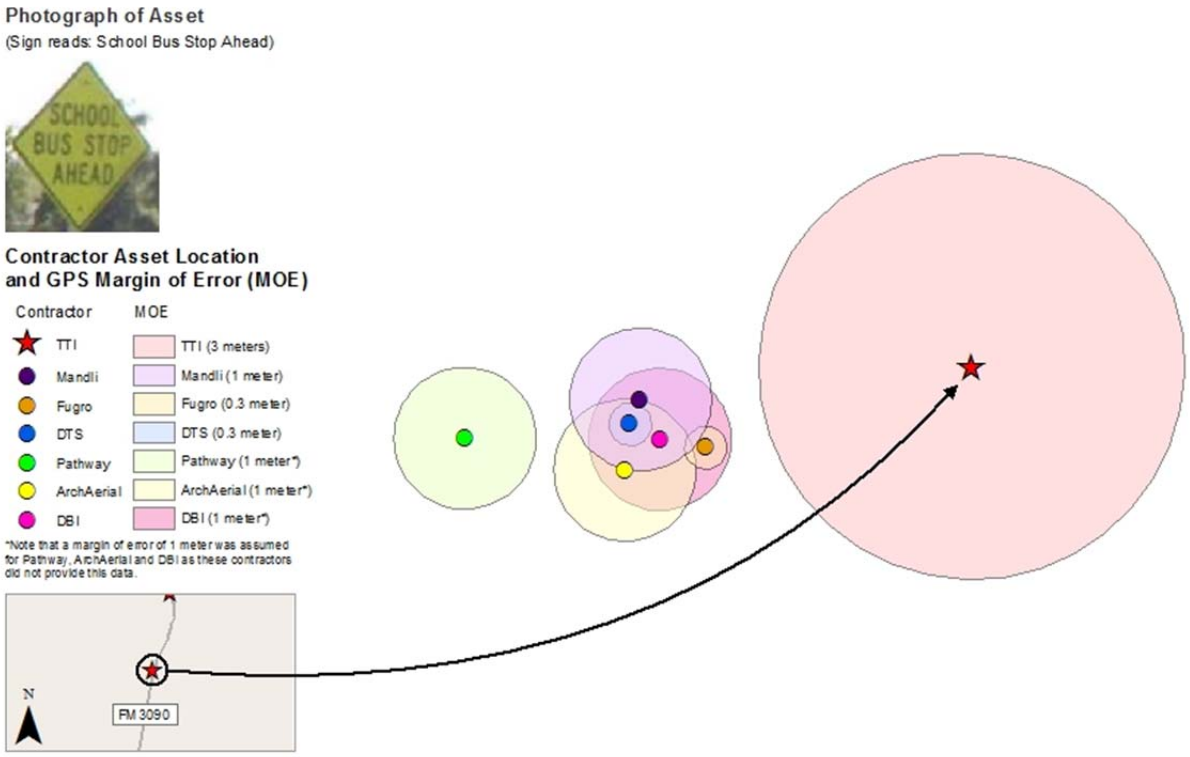

Figure 65. Contractor and TTI Asset Location with Margin of Error for SGN41.

As shown in Figure 65, all of the GPS coordinates provided by contractors for the sign identified by researchers as SGN41 fall outside of the 3 m margin of error for the manually collected GPS coordinated retrieved by the TTI research team.

Lane and Shoulder Widths

Researchers reviewed lane and shoulder widths for FM 3090—the study site where all contractors delivered data with the exception of Contractor G. As shown in Table 73, all contractors were with 10 percent of the ground truth data lane width measurements.

Table 73. Lane Width Statistics for FM 3090.

	Min	Max	Average	Percent Error
Ground Truth [TTI]	11	11	11	
A	10	10	10	-9%
B	12	12	12	9%
C	9.33	10.55	10.03	-9%
D	10.6	11.1	10.84	-1%
E	9.3	10.3	10.54	-4%
F	9.85	10.03	9.87	-10%
G	No Data			

Shoulder widths were also reviewed (see Table 74). However due to the variation in widths it was difficult to establish percent error. Maximum and minimum values do indicate that with the exception of Contractor B, contractors determined accurate shoulder widths (the majority of FM 3090 having 1-ft shoulder widths.

Table 74. Shoulder Width Statistics for FM 3090.

	Min	Max	Average
Ground Truth [TTI]	1	7.5	2.65
A	1	5	3.1816
B	3	3	3
C	1	5.5	2.09
D	0	4.89	2.4573
E	1.1	8	3.6131
F	0.633	8.1561	2.4332
G	No Data		

Sign Supports

For sign support there were a total of 25 samples for FM 3090, and a maximum of 17 for IH 45. Some entries were omitted from the analysis due to lack of measurement, and because there were repeated entries in the TTI database. Contractor C did not provide any sign support data.

Number of Signs Supports

For the number of sign supports all contractors performed very well, as shown in Table 75 and Table 76.

Table 75. Comparison of Sign Support Inventories for FM 3090.

	Identified	FM 3090 Samples	Percent Identified
A	24	25	96%
B	23	25	92%
C	No Data		
D	24	25	96%
E	24	25	96%
F	24	25	96%
G	No Data		

Table 76. Comparison of Sign Support Inventories for IH 45.

	Identified	IH 45 Samples	Percent Identified
A	3	4	75%
B	14	14	100%
C	No Data		
D	6	6	100%
E	16	16	100%
F	6	6	100%
G	No Data		

Sign Support Lateral Offset (Horizontal Measurements)

For the lateral offset, a z-statistic was used for FM 3090 to measure is the difference between mean lateral offset was significant. For IH 45, a t-statistic was used because there were less than 25 samples. Table 77 shows the results of the analysis.

Table 77. FM 3090 Lateral Offset Statistical Analysis.

	Max	Min	Average	Standard Deviation	Total Samples	Z-statistic
Ground Truth [TTI]	15.67	8.75	14.06	1.35	25	
A	14	7	10.84	1.57	25	7.783453
B	17.62	10.33	14.82	1.34	25	-2.01099
C	No Data					
D	15.9	8.7	14.18	1.38	25	-0.30937
E	No Data					
F	15.71	8.78	14.09	1.35	25	-0.09785
G	No Data					

For Contractor D and F, there is enough evidence that suggest the mean difference between the TTI measurements and the contractor measurements for FM 3090 is close to 0. For Contractor A and B, this hypothesis is rejected. Table 78 shows the analysis for IH 45.

Table 78. IH 45 Lateral Offset Statistical Analysis.

	Max	Min	Average	Standard Deviation	Number of Samples	Degrees of Freedom	t-Statistic	Two-Tailed p-Value
Ground Truth [TTI]	33	6.5	16.47	5.51	17			
A	21	7	11	5.79	4	4.377434	0.087837	0.93
B	26.98	5.71	14.1	6.56	16	29.38588	0.496514	0.62
C	No Data							
D	116.1	17.7	34.45	37.77	5	4.050157	1.904033	0.13
E	No Data							
F	19.78	13.38	16.73	2.11	5	18.00733	2.076719	0.05
G	No Data							

From the t-distribution analysis it can be inferred that the null hypothesis ($\mu t-\mu i=0$) cannot be accepted, with the possible exception of Contractor F.

Table 79. IH 45 and FM 3090 Lateral Offset Statistical Analysis.

	Max	**Min**	**Average**	**Standard Deviation**	**Total Samples**	**Z-statistic**
Ground Truth [TTI]	33	6.50	15.03	3.84	42	
A	21	7.00	10.86	2.60	29	5.46
B	26.98	5.71	14.54	4.24	41	0.55
C	No Data					
D	116.1	8.70	18.70	18.49	30	-1.07
E	No Data					
F	19.78	8.78	14.53	1.79	30	0.74
G	No Data					

For Contractor B, D and F, there is enough evidence that suggest the mean difference between the TTI measurements and the contractor measurements for FM 3090 is close to 0 at the 0.05 confidence level.

Sign Support Vertical Offset of Sign

Table 80 shows the analysis for FM 3090.

Table 80. FM 3090 Statistical Analysis for Vertical Offset.

	Max	Min	Average	Standard Deviation	Total Samples	Z-statistic
Ground Truth [TTI]	8	6.67	7.25	0.43	25	
A	10	7	8.32	0.61	25	-7.1264
B	10.93	7.15	8.54	0.78	25	-7.2366
C	No Data					
D	8.3	6.3	7.04	0.46	25	1.723364
E	No Data					
F	8.25	6.42	7.2	0.41	25	0.475513
G	No Data					

For Contractor D and F, the vertical offset is close to the measurements taken on the field by the TTI team. Table 81 shows the statistical analysis for IH 45.

Table 81. IH 45 Statistical Analysis for Vertical Offset.

	Max	Min	Average	Standard Deviation	Number of Samples	Degrees of Freedom	t-Statistic	Two-Tailed p-Value
Ground Truth [TTI]	7.5	6.42	7.04	0.34	16			
A	9	7	8	0.71	4	3	0.99544	0.39
B	12.17	5.71	8.39	1.78	14	14	2.97054	0.01
C	No Data							
D	6.8	6.3	6.65	0.19	6	17	1.343552	0.2
E	No Data							
F	9.22	6.3	7.09	0.98	6	5	1.553438	0.18
G	No Data							

From the t-distribution analysis it can be inferred that the null hypothesis ($\mu t - \mu i = 0$) cannot be accepted, with the possible exception of Contractor B.

Table 82. IH 45 and FM 3090 Vertical Offset Z-Test.

	Maximum Vertical offset	Minimum Vertical offset	Average	Standard Deviation	Number of Samples	Z-statistic
TTI	8	6.42	7.17	0.410297	41	
DTS	10	7.00	8.28	0.637698	29	-8.20787
DBi	12.17177	5.71	8.49	1.251405	39	-6.25207
AALLC	No Data					
Mandli	8.3	6.30	6.96	0.45129	31	2.027048
PSI	No Data					
Fugro	9.215861	6.30	7.18	0.569435	31	-0.05354
FACET	No Data					

Contractor F passes this statistical test at the 0.05 significant level.

Mowable Acres

One of the biggest challenges during the ground truth data collection effort was determining the approximate quantity of mowable acres for the selected study sites. It is of course important for TxDOT to control vegetation to maintain safe sight distances along its facilities. For FM 3090, the research team was able to utilize the City of Navasota's parcel GIS file to determine ROW areas and subtract road surface areas to calculate mowable acres. A comparison with three technology owners whom calculated mowable acres can be found in Table 83.

Table 83. FM 3090 Mowable Acres Comparison.

	Mowable Acres	Percent Difference from Ground Truth
Ground Truth [TTI]	59.29	0.00%
A	No Data	
B	No Data	
C	55.42	-6.53%
D	57.2	-3.53%
E	No Data	
F	55.88	-5.75%
G	No Data	

Three contractors were not able to report vegetation data (Contractor G was non-performing). Three of contractors reported results within 10 percent of the ground truth calculations.

Bridge Clearance Measurements

There are three overhead bridges on IH 45 and ground truth clearance measurements were recorded. Out of the seven contractor two reported minimum bridge clearance: Contractor A and Contractor F (see Table 84). The errors were within 12 inches of the ground truth measurement.

Table 84. IH 45 Overhead Bridge Clearance Measurements.

	Number Reported	Min	Max	Average	% Error (from Min)
Ground Truth [TTI]	3	17	17	17	
DTS	2	18	19	18.5	6%
DBI	3	No Data			
AALLC	No Data				
MANDLI	No Data				
PSI	No Data				
FUGRO	3	16.54	17.54	16.89	-3%
FACET	No Data				

Sign Retroreflectivity

As part of this project, the research team gathered retroreflective data for pavement markings and signs on FM 3090 and IH 45. Ground truth retroreflectivity measurements were recorded with a 922 Handheld Retroreflectometer manufactured by RoadVista. Only one contractor provided retroreflectivity readings for signs along both roads. Table 85 shows the sign samples and the retroreflective values.

Table 85. Retroreflectivity Measurements.

Asset ID	Sign Background Color	Sign Sheeting	Retroreflectivity Values		Difference (TTI-DBi)
			TTI	DBi	
SGN10	Green	Beaded High Intensity	24.5	26.8	-2.3
SGN11	Red	Prismatic	104.05	68.6	35.45
SGN14	Yellow	Prismatic	405.5	444.7	-39.2
SGN15	Green	Beaded High Intensity	49.45	69.4	-19.95
SGN16	Green	Beaded High Intensity	18.3	39	-20.7
SGN17	Yellow	Prismatic	356.5	314.3	42.2
SGN18	Yellow	Prismatic	360.5	349.5	11
SGN19	Yellow	Prismatic	213.5	308.1	-94.6
SGN20	Yellow	Prismatic	196	246.5	-50.5
SGN21	Green	Beaded High Intensity	25.3	27.6	-2.3
SGN24	Yellow	Prismatic	387.5	309.7	77.8
SGN25	Yellow	Prismatic	414	358.1	55.9
SGN28	Green	Beaded High Intensity	20.85	22.9	-2.05
SGN29	Yellow	Prismatic	420	452	-32
SGN30	Green	Beaded High Intensity	43.45	49.1	-5.65
SGN31	Yellow	Prismatic	372.5	270.4	102.1
SGN32	Yellow	Prismatic	392.5	419.9	-27.4
SGN33	White	Beaded High Intensity	187.5	217.2	-29.7

Asset ID	Sign Background Color	Sign Sheeting	Retroreflectivity Values		Difference (TTI-DBi)
			TTI	DBi	
SGN37	Green	Beaded High Intensity	22.75	11.8	10.95
SGN39	White	Beaded High Intensity	138.6	223.7	-85.1
SGN41	Fluorescent Yellow-Green	Prismatic	323.5	405.9	-82.4
SGN42	Yellow	Prismatic	83.3	75.4	7.9
SGN45	Yellow	Prismatic	404.5	344.8	59.7
SGN46	Green	Beaded High Intensity	23.2	21	2.2
SGN49	Black & White	Beaded High Intensity	167.6	221.6	-54
SGN50	Yellow	Prismatic	282	376.8	-94.8
SGN53	Yellow	Prismatic	312.5	231.3	81.2
SGN54	Green	Beaded High Intensity	39.85	35.9	3.95
SGN61	White	Beaded High Intensity	204	244.9	-40.9
SGN63	White	Prismatic	414	474.1	-60.1
SGN64	Yellow	Prismatic	222	233.9	-11.9
SGN65	White	Prismatic	368.5	439	-70.5
SGN67	White	Beaded High Intensity	204	244.9	-40.9
SGN7	White	Beaded High Intensity	164.8	199.5	-34.7
SGN70	Yellow	Prismatic	403	405.7	-2.7
SGN71	Yellow	Prismatic	403	443.7	-40.7
SGN72	White	Prismatic	414	474.1	-60.1
SGN74	Green	Beaded High Intensity	22.6	27.1	-4.5
SGN75	White	Prismatic	368.5	439	-70.5

A total of 39 signs had retroreflective measurements. To use a paired t-test for this analysis the differences between values has to be normally distributed. The histogram in Figure 66 shows that the data are not normally distributed. Therefore, the Wilcoxon Signed-Rank Test was used to evaluate the statistical significance of the difference between measurements. The analysis yielded that the difference between measurements is significant (p-value = 0.0192), which indicates that the mean differences between measurements is negative. This means that the retroreflective measurements given by the contractor were higher than the measurements taken by the TTI research team.

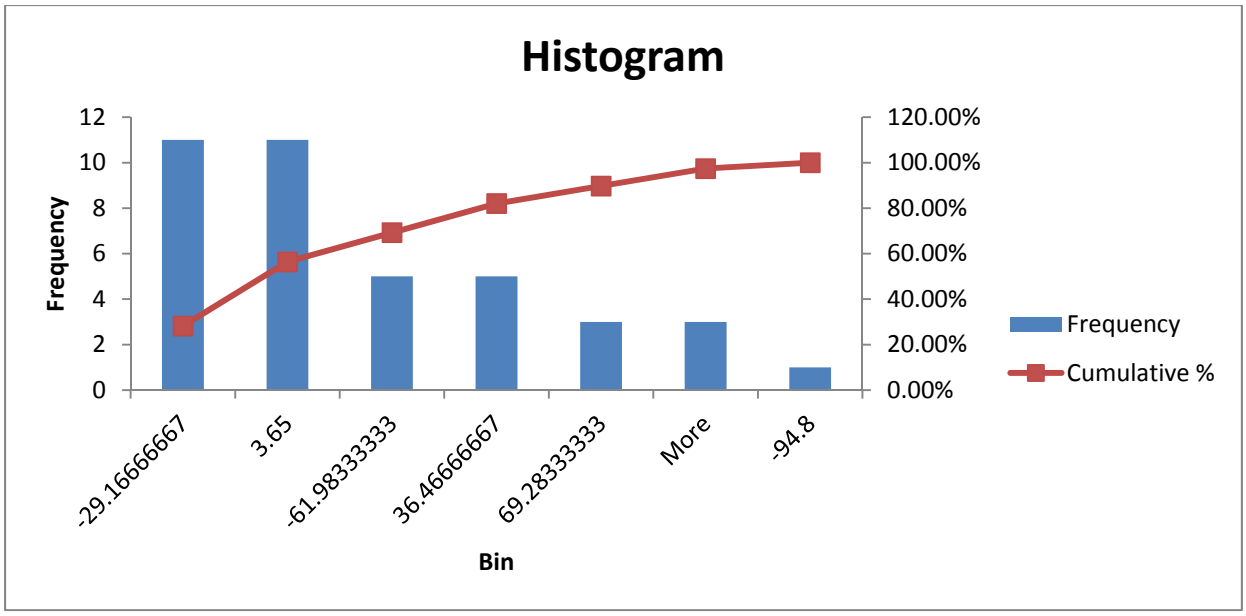

Figure 66. Histogram of the Difference between TTI and DBi Measurements.

Researchers attempted to determine if there were any trends in the mobile retroreflectivty data as ground truth values approach minimum MUTCD requirements (see Figure 67). Findings suggest that mobile retroreflectivity measurements are typically lower than handheld readings which is understood to be due to the fact that measurement geometries will never be exactly the same as a handheld device.

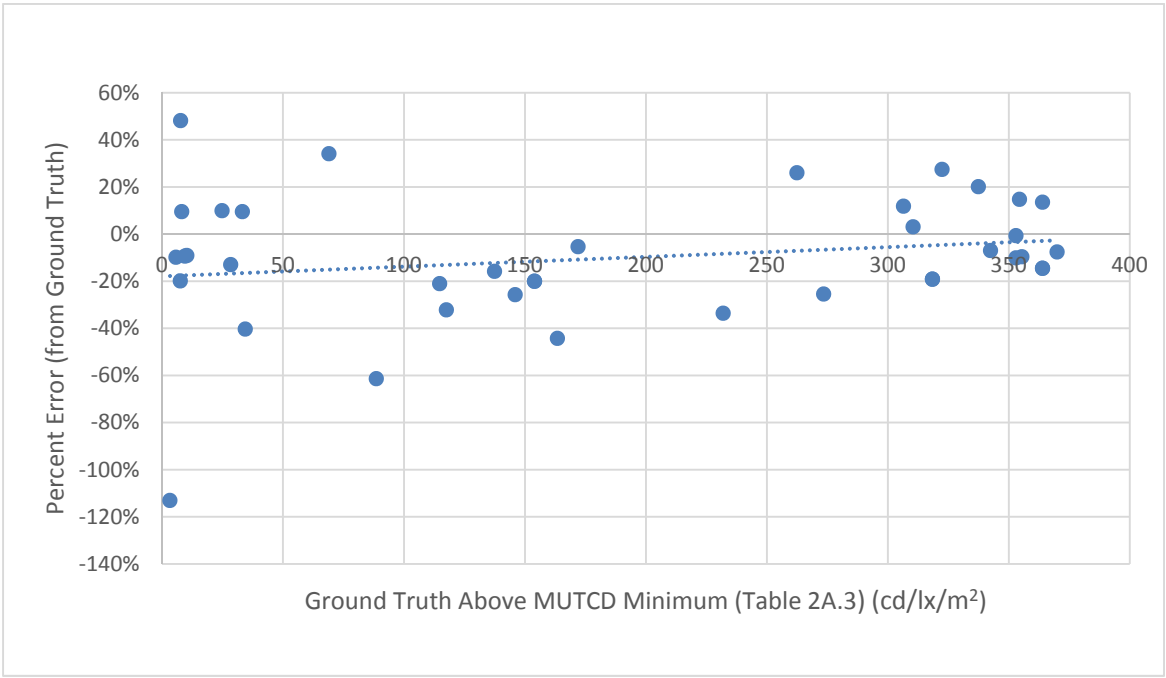

Figure 67. Retroreflectivity Error when Approaching MUTCD Minimums.

Pavement Marking Retroreflectivity

Contractor B was the only contractor that provided linear marking retroreflectivity measurements. The Wilcoxon Signed Rank-Test was again used for this analysis (see Table 86).

Table 86. FM 3090 Pavement Marking Retroreflectivity Statistical Analysis.

FM-3090	NB White edge line	SB White edge line	SB Yellow Right	SB Yellow Left	NB Yellow Right	NB Yellow Left
Sign	-	+	+	+	-	+
T	2522	0	0	0	1725	86
E(T)	2525	2575.5	2575.5	2328	2626.5	2328
St. dev.	290.839	295.191	295.191	273.649	299.564	273.649
Z	-0.0103	-8.725	-8.725	-8.507	-3.009	-8.193
p-value	0.496	>.0000001	>.0000001	>.0000001	0.0013	>.0000001
n	100	101	101	96	102	96

Key

Sign = sign of the minimum summation of ranks
T = total sum of the ranks
E(T) = mean of the T distribution
St. dev. = standard deviation of the T distribution
Z = Z value looked up from table
n = number of samples

For the measurements given for the white edge line in the NB direction there is not sufficient evidence to reject the null hypothesis that the median difference is 0 between the TTI and DBI measurements. For all other measurements the analysis shows that the values reported by DBI were higher than the measured values by TTI, with the exception of the right yellow pavement markings in the NB direction. This could largely be due to measurements being taken at different times. TTI attempted to capture pavement marking retroreflectivity measurement near the same time the contractors were at the study sites. However there could have been weeks between measurements as the dates DBi visited the sites are unknown, while TTI made measurements on September 7, 2015.

CONCLUSIONS AND RECOMMENDATIONS

Ideally, this project would identify only opportunities for improvements in technology. However, the greatest opportunity to ensure accurate high speed mobile asset management comes down to developing a common language and ensuring TxDOT agents and contractors are trained to collect and report the appropriate data.

Brief Summary of the Evaluation

Before discussing the opportunity to improve guidance for contractors it is important to summarize the positives and the areas in need of improvement based on the evaluation results. It should be stated that no clear level of accuracy has been established for this project outside of typical statistical confidence intervals. For this reason it has been stated in the recommendations section to better establish TxDOT priority assets and acceptable accuracy thresholds.

Results Indicating Accurate Collection of SOAI

Of the assets evaluated, there were several that the majority of the contractors delivered accurate results including:

- Sign Color.
- Sign Surface Area.
- Sign Inventory.
- Chevrons Inventory.
- Linear Pavement Markings Inventory.
- Mowable Acres.
- Guardrail.
- Driveway Inventory.
- Lane Widths.

Results Indicating Areas in Need of Improvement

- MUTCD Sign Designation.
- MUTCD Sign Dimensions.
- Sign Text Recognition.
- Sign Support Identification.
- GPS Accuracy.
- Sign Retroreflectivity.
- Lateral Offset Measurements.
- Bridge Height.
- Mailbox Inventory.
- Delineator.
- Object Marker.

Opportunities for Technology Advancement

There are multiple opportunities for technology advancement including location accuracies, asset data, sign retroreflectivity and sheeting type, illuminance.

GPS Accuracies

It was observed during the evaluation (primarily due to the convenience of having multiple GPS coordinates from varying technology owners) that GPS accuracies were often overstated as can be seen in Figure 61 through Figure 65. There is an opportunity to improve this through

establishing either additional procedure (benchmark/control point) or through the development of additional technologies

Asset Data Communication Technology

There also are opportunities to communicate information from assets to the data collection vehicles. This can be done through RFID technologies or emerging connected vehicle technologies, including sign asset attributes that need improvement including MUTCD designation and size, sign text, sign sheeting, etc. This technology could also be used to communicate life cycle information from all important assets such as installation date.

Sign Retroreflectivity

Although Contractor B attempted to establish sign retroreflectivity, it was found to be inaccurate compared to the ground truth manual measurement. This could be due to the difference in measurement geometries. The handheld equipment that TTI used for ground truth data provides retroreflectivity with exact geometries, regardless of sign twist or lean. Mobile data collection equipment provides retroreflectivity with relative geometries as experienced the road users. There is an opportunity to re-engage this contractor to develop more accurate technologies.

Illuminance Data Capture

No contractor provided illuminance data for the two signal mounted luminaires on IH 45. Although in discussions with several contractors capturing these data seemed possible. Further study on developing this technology is needed.

Opportunities for Improving Communications

It was quite evident during the evaluation of data from seven different sources that the main reason for many differences in results or errors was due to the lack of understanding the data dictionary, TxDOT standards details and TxDOT Specifications. Despite the development of the data dictionary, several contractor simply processed and reported data based on their own data dictionary. Some even added their version of the data dictionary to the submitted deliverable. It is vital to the success of any future SOAI mobile data collection efforts that these miscommunications be cleared up through standardization of the language used in the data dictionary. These issues not only lie with the assumption that contractor staff know and understand TxDOT assets but with breaking a cycle of contractor experiences collecting for other agencies.

There were several examples of assets described in detail within the data dictionary that, when collected by a third party, were not collected correctly. The first example is that of double yellow pavement markings. Some contractors collected this in a single direction, while others collected in both direction and doubled the inventory totals. Another concern with double yellow pavement markings involved some contractor counting them both as single markings and double markings. Another example of a communication issue was with mailboxes. It was assumed that contractors understood to count mailbox support assemblies vs. the number of actual mailboxes. A third and final example are the number of driveways along the study sites. TTI researchers thought this value would be very accurate. However the error was close to 10 in 100 driveways

above or below the ground truth measurement. A clear definition of a driveway and required condition may help improve this quantification measurement. Recommendations to resolve some of these issues have been provided in the following section.

Recommendations

Based on the results of the evaluation and the completion of Task 2 there are several recommendations that can move forward into Task 3 and even further into potential Phase 2 tasks.

Recommendations for Task 3 Study

- Investigate GPS/Photogrametry/LiDAR positioning systems to determine the potential reasons for errors beyond stated accuracies.
- Investigate technologies to communicate with assets to improve identification metrics.
- Develop technologies or improve the accuracy of using LiDAR for sign retroreflectivity and or sign sheeting identification.
- Develop technologies to measure illuminance using a mobile platform.

Recommendations for Phase 2 (TTI Tasks)

1. Conduct a series of workshops to develop robust accurate statewide data dictionary for mobile asset data collection:
    a. Determine TxDOT asset priorities.
    b. Determine TxDOT thresholds for asset data accuracies.
    c. Develop a set of data collection, processing and reporting standards for mobile asset data collection.
    d. Utilize high performing technology owners and TxDOT input refine current protocol/data dictionary based on Task 2 findings.
    e. Develop Change Management Process for continuing protocol/data dictionary improvement.
    f. Develop asset data collection guidance for post processing (asset images and annotation).
2. Develop a series of training modules for data collection, processing, and reporting:
    a. Training modules would be used to educate contractors that desire to collect asset data using mobile technology for TxDOT.
    b. Develop certification program for state contractors that desire to contract mobile data collection services with TxDOT.

REFERENCES

1. Zhou, H., Jalayer, M., Gong, J., Hu, S., and Grinter, M. 2013. *Investigation of Methods and Approaches for Collecting and Recording Highway Inventory Data*. Illinois Center for Transportation. Accessed at https://apps.ict.illinois.edu/projects/getfile.asp?id=3166.
2. Dye Management Group, Inc. (DMG). 2014. Monitoring Highway Assets with Remote Technology. Michigan Department of Transportation, RC-1607. http://www.michigan.gov/documents/mdot/RC-1607_466453_7.pdf
3. Findley, D, Cunningham, C., Hummer, J., Comparison of mobile and manual data collection for roadway components, Transportation Research Part C 19 (2011) 521–540.
4. Howerton, C. and Sideris, D. 2010. A Study of Implementation of IP-S2 Mobile Mapping Technology for Highway Asset Condition Assessment. Virginia Polytechnic Institute and State University Virginia Department of Transportation. http://www.champs.eng.vt.edu/docs/research/HowertonSideris%20P&R%20Final%20Report.pdf.
5. Findley, Daniel J., Cunningham Christopher M., Hummer, Joseph E. "Comparison of mobile and manual data collection for roadway components." Transportation Research Part C volume 19 pp. 521-540. Elsevier, August 2010.
6. Washington, Simon P., Karlaftis Matther G., Mannering, Fred L. "Statistical and Econometric Methods for Transportation Data Analysis." CRC press, second Edition, 2011.

CHAPTER 3. MULTISPECTRAL LIDAR

MULTISPECTRAL LIDAR

Introduction

Most LIDAR units currently operate at 905 nm. This sinlge band LIDAR has limitations in assess retroreflective infrastructure. Researchers tested the feasibility of using multispectral LIDAR to obtain more information about the retroreflective infrastructure that would be beneficial for asset management purposes.

SINGLE BAND LIDAR TESTING

The initial testing was conducted in the TTI Visibility Research Laboratory (VRL) with a Velodyne LiDAR, specifically the HDL-32E. This LiDAR unit is relatively small and lightweight. It is a popular LiDAR for mobile application because of its ruggedly built construction. The HDL-32E has 32 infrared lasers (operating at 905 nm) providing a 40° vertical field of view and producing up to 700,000 points per second. A close-up image of the HDL-32E is shown in the left image of Figure 68 along with one of Ford's autonomous research vehicles equipped with four of the same LiDAR units (many vehicle companies are developing autonomous vehicles using LiDAR to sense the environment around the vehicle).

Figure 68. Velodyne HDL-32E and Ford's Test Vehicle.

The initial testing has been with various types and colors of retroreflective sign sheeting materials to assess whether the returned intensity of the infrared lasers could be used to assess sign retroreflectivity (and/or color). Samples of retroreflective sign sheeting materials were acquired and mounted to aluminum substrate. The samples measured 12-in by 36-in. The materials included in this study are:

- New 3M Diamond Grade 4000 series (white, red, green, blue).
- New 3M High Intensity Prismatic (HIP) 3600 series (white, red, green, blue).
- New Nippon Carbide High Intensity Beaded N500 series (white, red, green, blue).
- New Avery Dennison engineer grade and super engineer grade (white).
- Weathered samples of engineering grade (white and blue).

The testing was conducted at three distances: 5, 10, and 15 meters. Each sample was tested at the three distances. Figure 69 shows the set-up in the VRL.

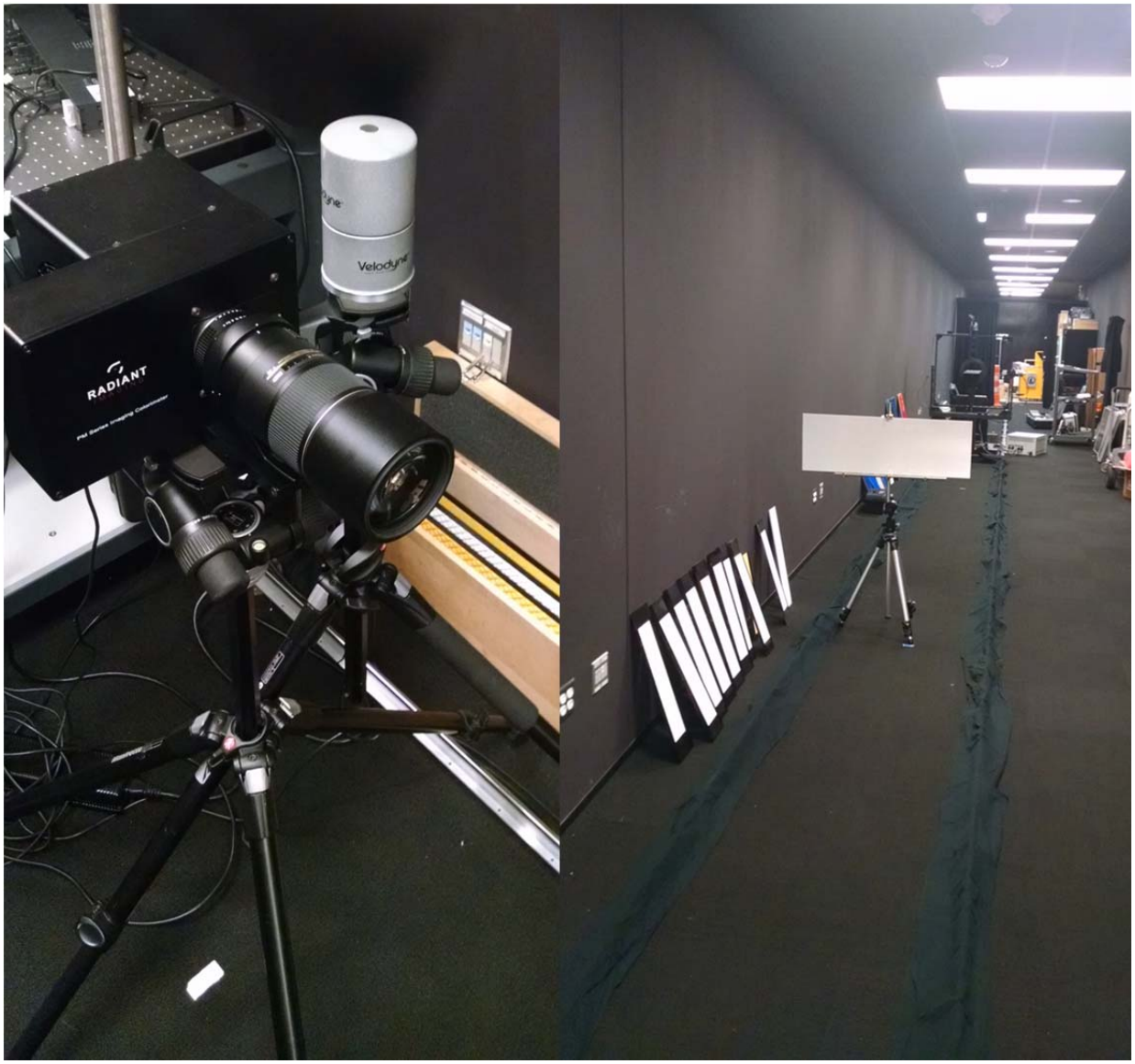

Figure 69. Velodyne HDL-32E and Ford's Test Vehicle.

The left image of Figure 69 shows the LiDAR unit next to a digital photometer that was used in conjunction with the LiDAR software to determine the signal from the LiDAR unit. The right image of Figure 69 shows a white sample of retroreflective sign sheeting material supported on a

tripod. This image was the 10 meter distance. The testing at each distance also included rotation of the panels so that they were all tested at angles of 0, 5, 10, 15, and 20 degrees.

The first look at the data shows how the measured retroreflectivity of the panels compares to the LiDAR signal obtained using the Velodyne software (Figure 70). This initial look at the data does not account for color of the sheeting materials or the construction type of the sheeting materials. The results are not promising but much more analyses are needed.

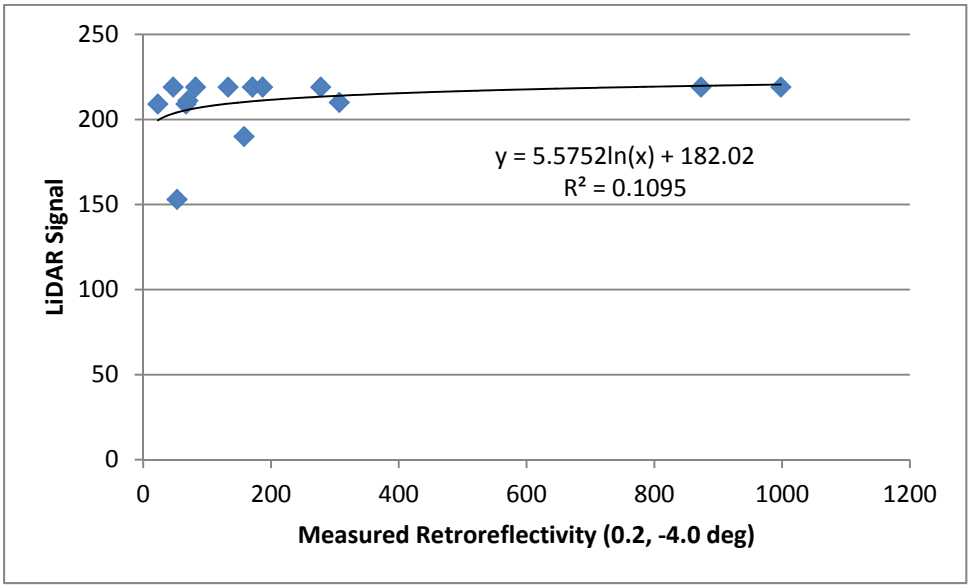

Figure 70. Retroreflectivity and LiDAR Signal.

Figure 71 shows the relationship between different types of retroreflective sheeting materials and the LiDAR signal. In this testing, all of the retroreflective sheeting materials were white. From left to right, the sheeting materials can be classified as ASTM D4956 Type I, II, III, IV, and XI. The potential of LiDAR is evident here in that the optical design of the sheeting materials can mostly be identified (except the prismatic materials, Type IV and Type XI, which provide similar LiDAR signals).

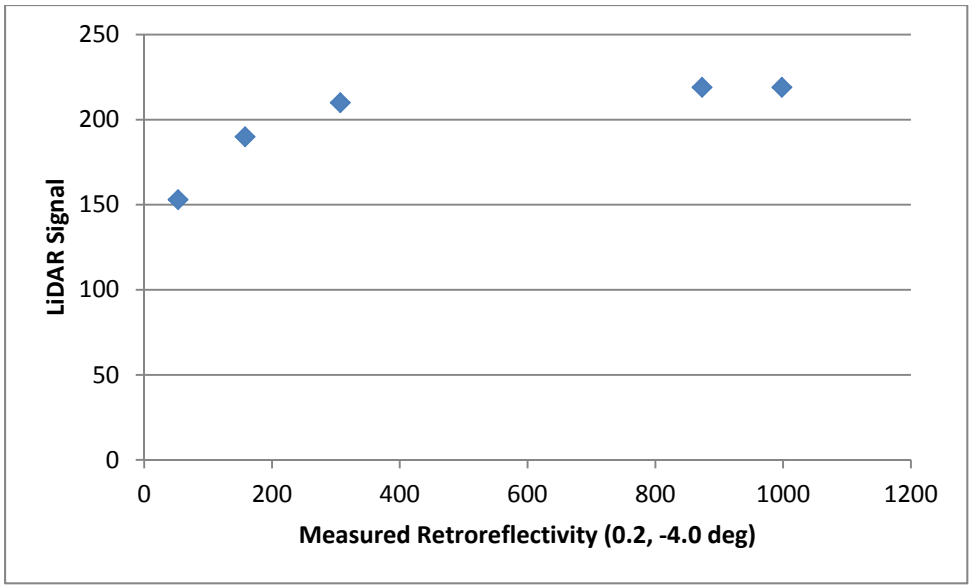

Figure 71. Retroreflective Sheeting Material and LiDAR Signal.

Table 87 shows a summary of the initial data that has been measured so far. The data in Table 87 are sorted by measured retroreflectivity, from lowest to highest.

Table 87. Measurements from the VRL.

ASTM D4956 Sheeting Type	Color	Measured Retroreflectivity (0.2, −4.0°)	LiDAR Signal		
			5m	10m	15m
III	blue	23	209	221	222
IV	blue	47	219	235	251
I	white	53	153	156	145
III	green	67	209	223	221
III	red	70	211	221	225
XI	blue	82	219	235	251
IV	green	133	219	235	251
II	white	158	190	200	184
XI	green	171	219	235	251
IV	red	187	219	235	251
XI	red	278	219	235	251
III	white	307	210	223	225
IV	white	873	219	235	251
XI	white	998	219	235	251

Initial Conclusions

The initial conclusion from the LiDAR testing is that the single band laser is not sensitive to the color of sheeting materials but is somewhat sensitive to the optical design of the materials (there

are repeatable differences in sheeting Types I, II, III, and the prismatic materials IV and XI but no differences between IV and XI).

MULTISPECTRAL LIDAR TESTING

The research team traveled to the University of Houston to conduct the multispectral LIDAR testing. The University of Houston has equipment that is capable of a large range of testing wavelengths and the cost to purchase or even rent the equipment was outside the scope of the project resources. The same panels were tested but throughout a range of wavelengths starting about 400 nm and continuing out beyond 2000 nm. The test results are shown in Figure 72.

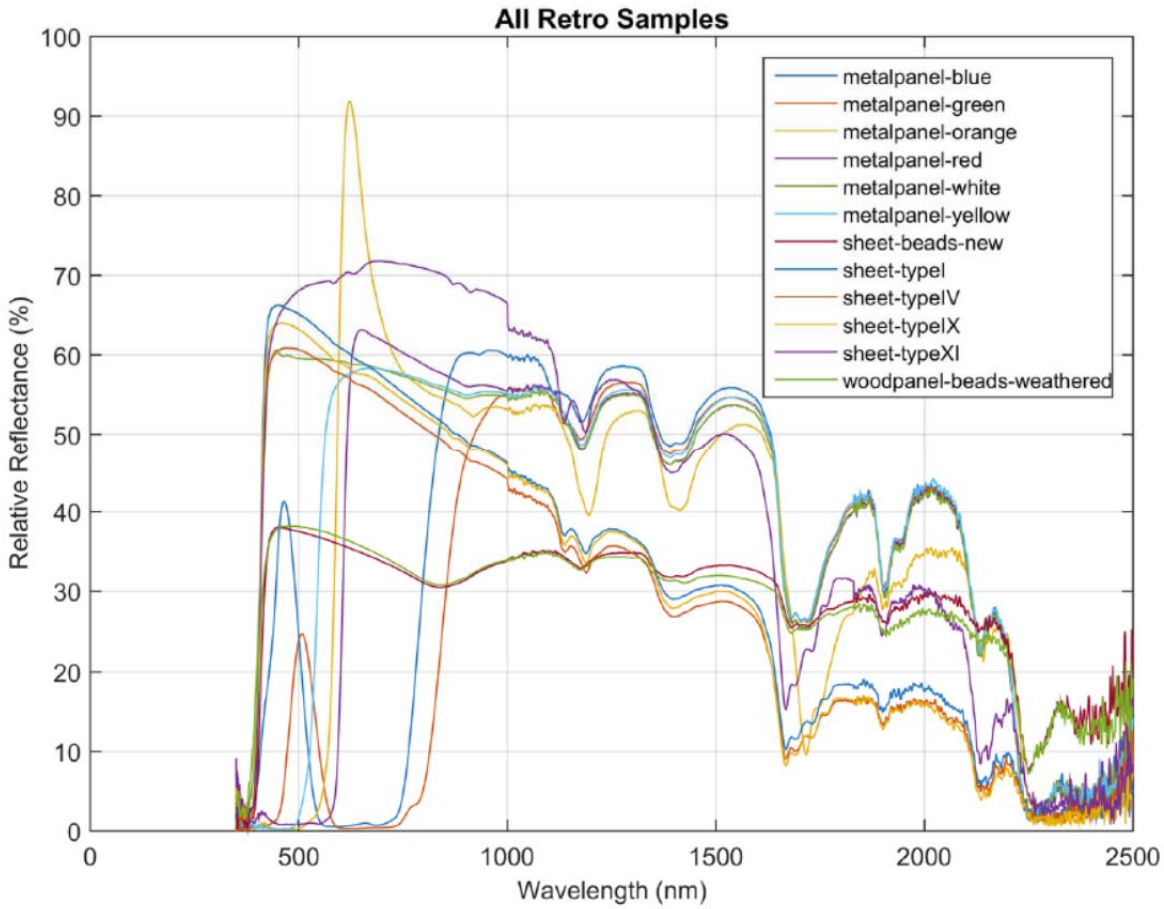

Figure 72. Results from Multispectral Testing.

Conclusions

The results of the testing show that multispectral LIDAR has significant advantages in terms of being able to identify various types and condition of retroreflective infrastructure. However, there are currently no multispectral technologies that can be used on a mobile platform, even at low speeds. In addition, the costs of the currently available systems are in excessive of $100,000. For these reasons, further testing of the multispectral LIDAR concept was tabled and the resources were redirected toward the machine vision technologies.

MOBILE LUMINANCE SYSTEM

Introduction

The objective of this task was to develop and demonstrate emerging technologies and systems with strong potential to significantly improve the efficiencies of safety and operation infrastructure assessment. This report includes the progress and conclusions regarding the development of a prototype mobile stereoscopic vision and luminance system for assessing traffic control device condition.

Background

TTI previously developed a prototype mobile luminance system as a proof-of-concept for TxDOT Project 0-6647: Developing Luminance-Based Mobile Highway Delineation Equipment and Level of Service Guidelines for Safe Nighttime High-Speed Travel. This system provided a semi-automated method to assess luminance of TCDs at highway speeds that could be correlated to both minimum retroreflectivity and driver preference. However, the interface required a power-user, and it was not as automated as TxDOT wanted for statewide use. Subsequently, Task 3.2 was included on TxDOT Project 0-6869.

TTI researchers took what they learned on Project 0-6647 and other research experience and developed a specification that they submitted for bid to industry to develop the next generation mobile luminance system. The primary focus of the revision was on improving the automation, and a secondary improvement was adding stereoscopic vision. The winning bid was provided by Graftek Imaging out of Austin, Texas, which is a National Instruments Alliance Member. Once, the work was authorized, TTI setup a plan to carry out the work in three primary phases:

- Develop the initial prototype of field data collection equipment and laboratory demonstration.
- Revise the prototype, develop the post-processing software, and complete a field demonstration.
- Take possession of the prototype, evaluate the revised data collection software, evaluate the post-processing software, and develop a list of recommended changes.

Prototype Development and Laboratory Testing

The research team designed a prototype consisting of two Basler ACE 1920 cameras with 35 mm Kowa megapixel lenses and an 850 nm infrared radiation (IR) light source. One of the cameras was color and one was monochromatic with an 850 nm IR filter. The cameras and the IR light source were synchronized, whereby the IR light source flashed once when the monochromatic camera took an image while the color camera did not take a picture, then the light source turned off and a simultaneous pair of images was taken with both the monochromatic and the color camera. The first image would help isolate retroreflective TCDs from the other background objects in the image. The pair of images taken immediately following would allow for distance measurement two the TCDs and applying color.

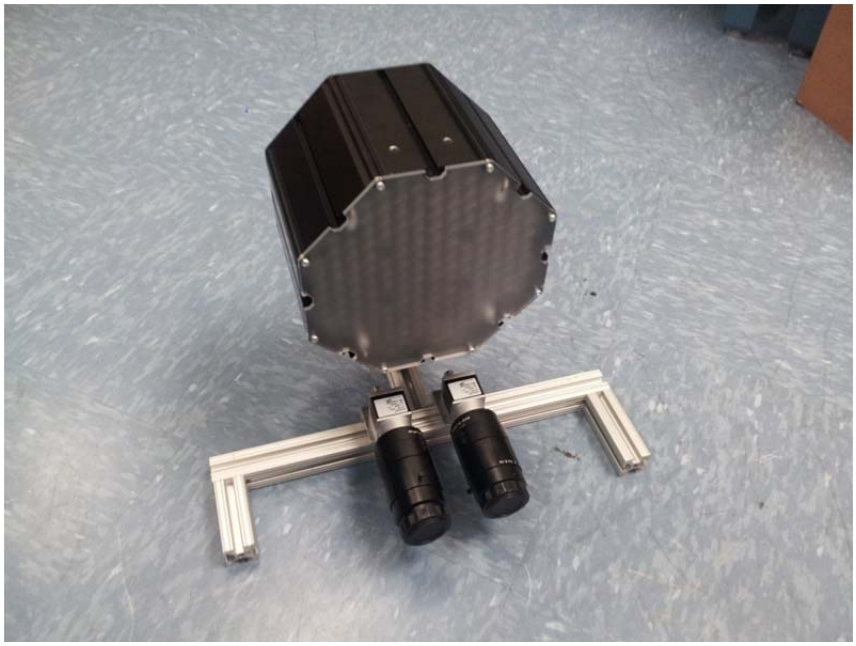

Figure 73. Mobile Stereoscopic Vision and Luminance Prototype 1.0.

The recommendations focused on the GUI for field data collection, and the required output from either the field data collection software or from a separate post-processing software package. For the GUI, researchers recommended that the incoming GPS data should visible to ensure good incoming geo-tagging. The GUI should allow for other descriptors such as the roadway name and a method to tag the incoming data. In the least, the incoming data could be tagged as non-TCD (i.e., a false positive), or as a missed TCD, which probably resulted from being below minimum retroreflectivity levels either from age and wearing or misalignment. Researchers recommended having this as a touchscreen option, but Graftek Imaging was not sure whether that feature would be in the first version or a later version. The post-processing output was to be a text-based file that included GPS, the number of objects in the image accessed as TCDs, their shape, color, distance, luminance, and any user inputs, such as missed TCD.

Researchers also decided that TTI would supply several TCD samples for use during the initial testing by Graftek Imaging. Two sets of samples were provided. The first set was sent with them that included sample minimum retroreflectivity calibration panels developed by TTI. The second set was a group of panels specifically designed to test the dynamic range of the cameras with respect to not only luminance range but background versus legend resolution. **Error! Reference source not found.** shows four separate test samples. Each panel consists of two different colors and retroreflective sheetings. One sheeting is ASTM Type I and one is ASTM type IV. These retroreflectivity sheeting types were selected because ASTM Type I is very near the minimum retroreflectivity values detailed in the *Manual on Uniform Traffic Control Devices*, and ASTM Type IV is as bright as it was believed the system would need to report in terms of performance, because anything higher would be far above minimum retroreflectivity requirements. The simulated "T" and diagonal lines represented the smallest letters that might need to be measured from TCDs. The two larger rectangular pieces near the middle of each sample were meant to provide a reference to the values that would be measured within the smaller segments. These samples were scaled for a 50-ft viewing distance based on the maximum distance available

within the Graftek Imaging laboratory. Researchers decided that joint field testing would be completed by the TTI and Graftek Imaging team in the middle of July out at the Texas A&M Riverside Facility to evaluate the version 1.1.

Figure 74. Laboratory Retroreflectivity Test Samples.

FIELD TESTING

For field testing, one member from TTI and one member from Graftek Imaging conducted a limited set of tests out at Riverside on August 8. Figure 75 shows the setup prior to data collection. A 2015 Ford F150 quad-cab was outfitted with the mobile stereoscopic vision and luminance system. The equipment consisted of a two Basler ACE cameras, IR light source, power source, GPS receiver, and computer. Everything except the computer was mounted to 1-inch aluminum tubing, and an optically clear plexiglass was placed in front of the cameras to protect the system. The frame was secured to the roof with three heavy-duty suction cup clamps. The resulting system made considerable wind noise, and there was a concern over potential vibrational noise being added to the imaging from the wind, as well as a concern of dislodging the suction cup mounts from the roof at high speeds. Subsequently, the team decided to move the light source to the front of the vehicle and lower, and move the cameras inside the vehicle. The revisions will be discussed later as Task 3.2.3 continues.

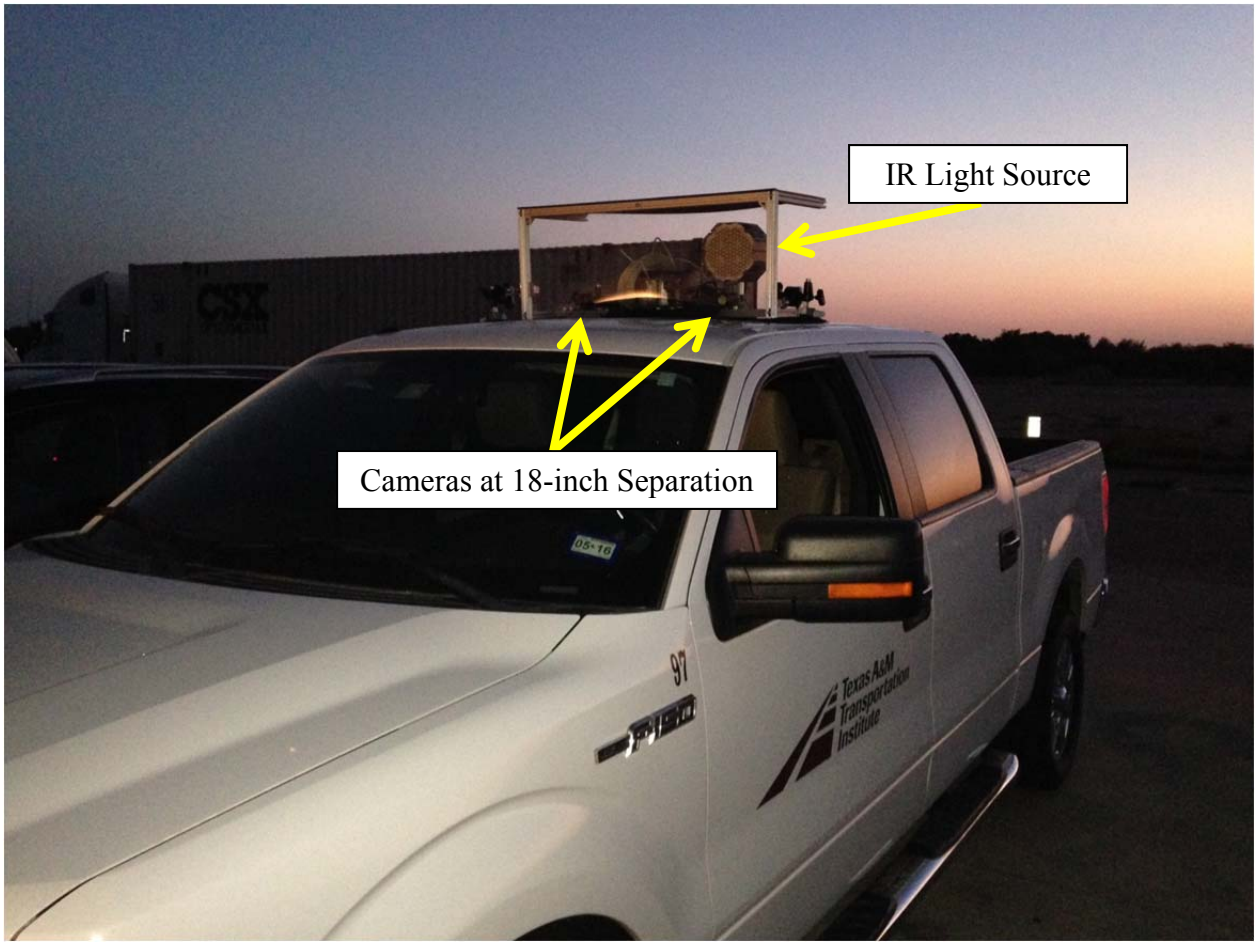

Figure 75. Field Testing.

SUMMARY

Testing was conducted in late 2015 and early 2016. The existing system was capable of automatically detecting retroreflective objects in real-time, but it does not store the information and it required manual (extensive) post-processing efforts. Efforts to move this concept forward stalled when the estimated equipment and software development were north of $100,000. In the spring of 2016, this effort was tabled to focus more resources on the machine vision idea for road markings.

CHAPTER 4. SLAM TECHNIQUES WITH GPR FOR IN-TRAFFIC BRIDGE DECK INSPECTION

Bridges are critical components of modern transportation infrastructure. However, bridges deteriorate over time due to natural and human factors. In order to evaluate the condition of bridge deck beforehand, the objective of this project is to combine state-of-the-art simultaneous localization and mapping (SLAM) techniques with a ground-penetrating radar (GPR) for in-traffic bridge deck inspection. As shown in Figure 76(a), a lidar and a camera are used to detect and segment deck surface for reconstruction of the bridge above ground surface; the GPR is employed to obtain the subsurface structure of the bridge. The surface and subsurface are then fused to reconstruct bridge deck in 3D structure, and the concept is displayed in Figure 76(b).

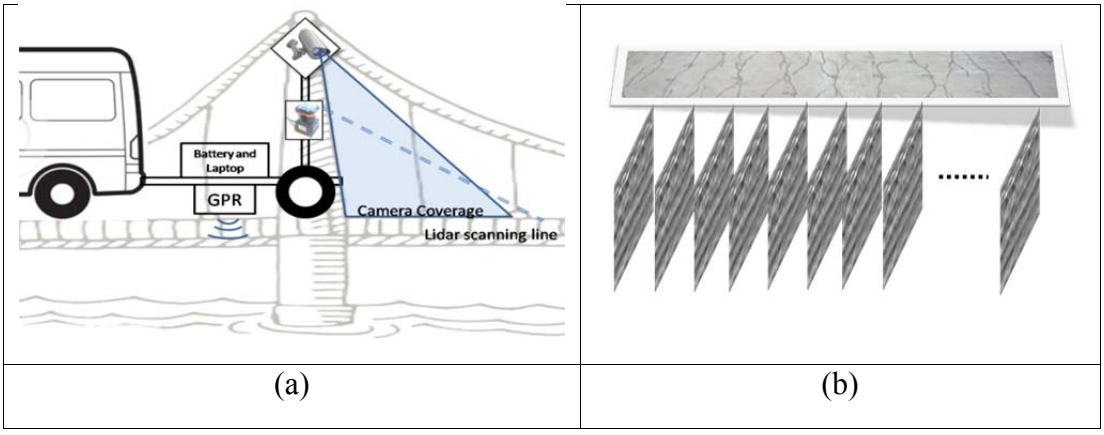

(a) (b)

Figure 76. (a) System Design (b) Fusion of Surface and Subsurface Images.

In the following sections, we will report the progress done so far and arrange the sections as follows. In the first section, we will first show the mechanical design and fabrication of the sensing suite for this project. Firstly, we will discuss how we design and build the sensing suite, and how we develop supporting technical knowledge. We will also explain our design of the calibration platform and the selection of calibration objects. Secondly, we will explain the technical development for the calibration of each sensors. In this section we show the information of each sensor and the calibration procedure for each sensors. We will mainly address the GPR calibration in detail. After the calibration part, we will step into our new calibration problem, the joint camera and GPR calibration. We will show how we are going to define and solve this problem.

SENSING SUIT MECHANICAL DESIGN AND FABRICATION

In this section, we will show the configuration of our sensing suit and the design for our artificial bridge in this current stage. The design for our sensing suit and the artificial bridge follows the progress of our calibration experiment. The detail will be addressed in the following section. The Figure 77(a) is our latest design.

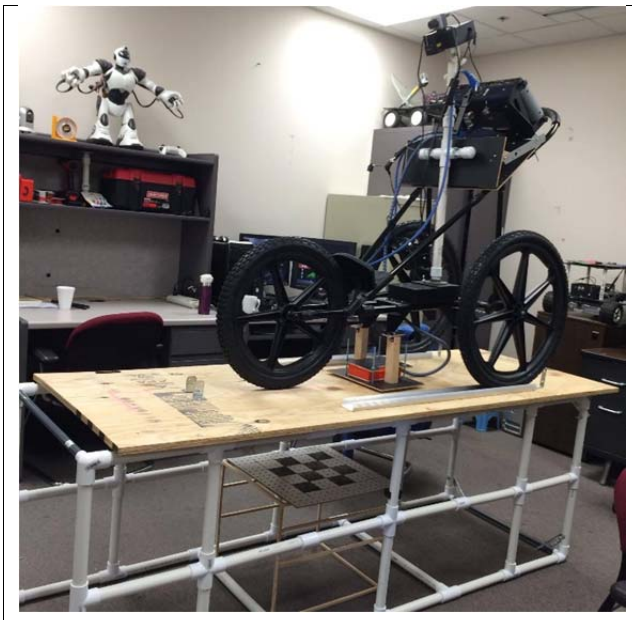

(a)

(b)

Figure 77. (a) Sensing Suit on an Artificial Bridge Platform with the Checkerboard (b) Metal Ball (Diameter: 1.00 inch).

The sensing suit is built on a cart equipped with the GPR, a camera and a lidar (also known as laser range finder). We treat our sensing suit as a rigid body when considering relative poses among sensors in our calibration work. To ensure the rigid body relationship, we would like to make sure every mounted sensor is fixed on the sensing suit. We fix a vertical PVC pipe in the middle as the new support among the sensing suit. This PVC pipe connects the GPR, the camera and the lidar together. We use the camera and the lidar to observe and sense the information above the ground plane; we use the GPR to detect the information below the ground plane. Therefore, we separate the sensors into two parts, the top and the bottom parts, because of the different functionality. The camera and the lidar are mounted on the top of the PVC pipe with a black box containing synchronization circuitry, and the GPR retains in the same position as the original design from the manufacturer (i.e., GSSI. The black box on the top of the PVC pipe is also a platform for the camera and the lidar). It not only provides the base for both sensors but also contains the circuits and power supply for them. The adjustable flag pole fixed between the black box and the PVC pipe is our mechanism to make the black box able to face down with adjustable angle. This adjustable flag pole had different angle settings. We can use this to adjust the perspectives of both the camera and the lidar. We want to ensure the camera and the lidar can sufficiently cover the ground plane. At the same time, we also want to avoid the front tire from blocking their fields of view. The bottom part of our sensing suit is the GPR. The GPR was fixed in a small box and connected to the cart originally. However, this box would vibrate during the cart movement. To solve this problem, we replace the box holder with one wooden plane. We stick the GPR to the wood plane. We also change the fixture between the GPR with the cart to ensure a rigid body relationship. Moreover, we still follow the setting of the GPR. We retain the distance between the GPR and the ground plane to make sure the GPR able to perform well.

Figure 78 shows the image from the camera view. This image can tell our new calibration setting swith three mirrors.

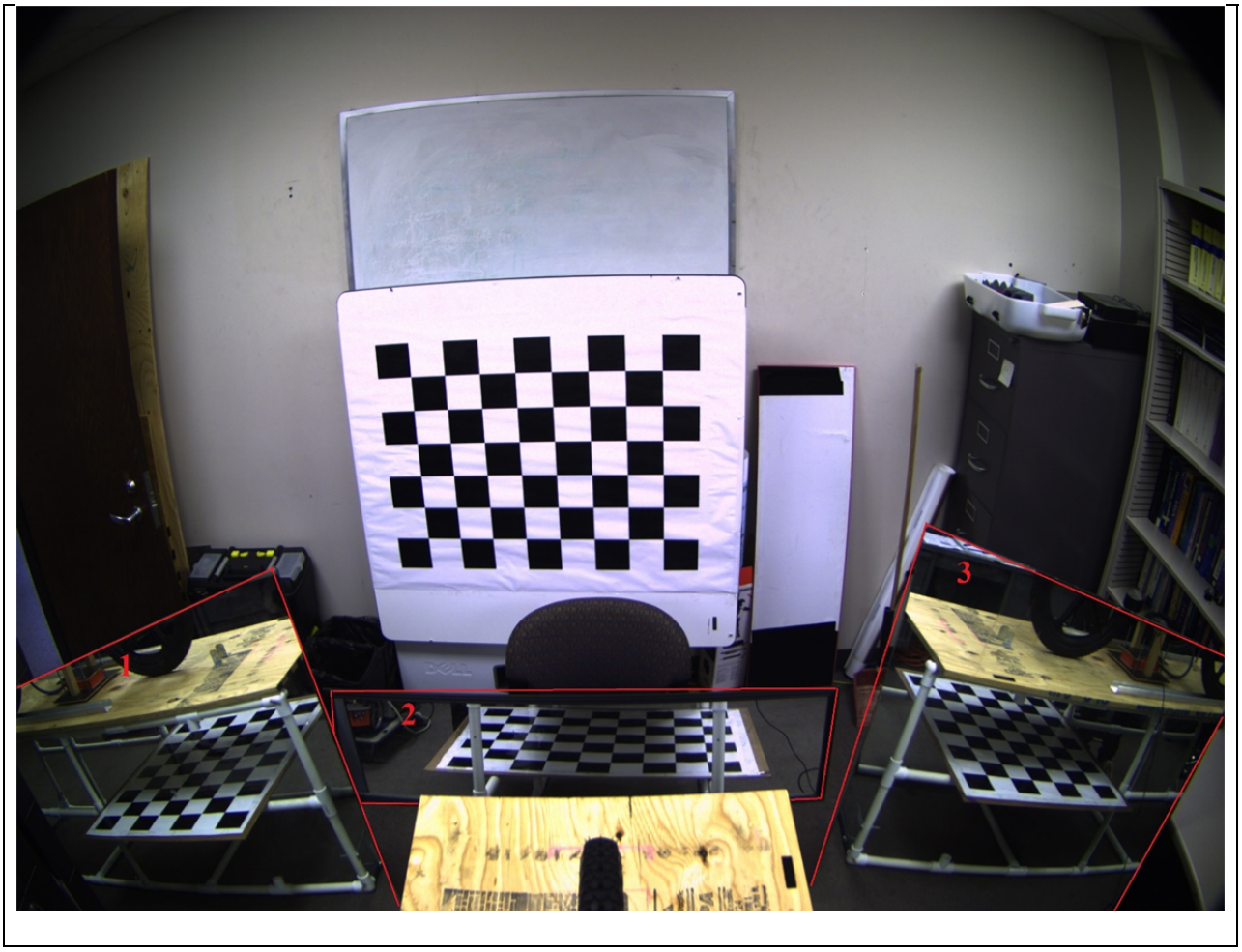

Figure 78. Experiment Setting for Calibration from the Camera View.

The artificial bridge is also part of our fabrication for this work. To calibrate the GPR with or without other sensors, we have to know what component is under the bridge. Therefore, we compose one hallow artificial bridge for our calibration experiment. We use the PVC pipes as the body of the artificial bridge. We place one wooden board on it as the ground plane. The length of the bridge is 82.0 inches which gives sufficient distance for the cart to sense and gain information underneath the bridge deck. The width of the bridge is 27.0 inches based on the width of the cart in order to make sure that the cart can travel along the plane. The height in 29.0 inches which can allow us to have more space to put different pattern inside the bridge. Moreover, we add two tracks, the starting line and the finishing line to make sure every trajectory is the same. At current stage, we try to do the calibration between the camera and the GPR. To attain this goal, we have to make the camera and the GPR sense the same calibration objects every time. Here our approach adapt the concept of the camera calibration by using the mirror and the checkerboard for the camera calibration. Here our calibration object are the metal balls (Figure 2(b)) and the checkerboard. We put the metal balls on the grid of the checkerboard. Moreover, we place the three mirrors in front of the bridge. These three mirrors can reflect the

calibration objects below the ground plane to make the camera able to view the calibration object simultaneously. The detail of the calibration will be addressed in the calibration model section.

CALIBRATION PROCEDURE

The calibration procedure is the most critical stage in this work. It allows us to obtain geometric relationship between sensors and the relationship is the basis for fusion the data from different sensing modalities in the bridge deck inspection. In this section, we will introduce the specifications of each sensor that we use here firstly. Then we will introduce the calibration for each sensor.

CAMERA CALIBRATION

The camera we use is the CMOS camera with external trigger and its model is DS-CFMT1000-H. In order to get the coordinates information hidden inside each captured image, we need to do the calibration for our camera first. Via the calibration, we can get some internal information for our camera such as focal length, scaling factor, or lens distortion. Based on this information and images, we can not only reconstruct the world model but also interact with the world coordinate from our camera coordinate and our image coordinate. In our case the relation and interaction with the world coordinate is our final purpose.

In the camera calibration, the checkerboard is our calibration pattern. On the checkerboard, it is composed of high contrast black and white squares which connect together alternately and in sequence. This pattern makes the vertices of each square clearly detected. Therefore, it is easy and clear for our program to collect information on each image. After gaining sufficient points, the program can calculate the internal parameters for our camera. However, it doesn't mean every set of images can complete the calibration. It depends not only on the amount of images taken but also on whether the images have captured enough information for the calculation such as distortion effect. Based on those input set of images, the program would generate corresponding internal parameters. Figure 79 are our result before and after the camera calibration.

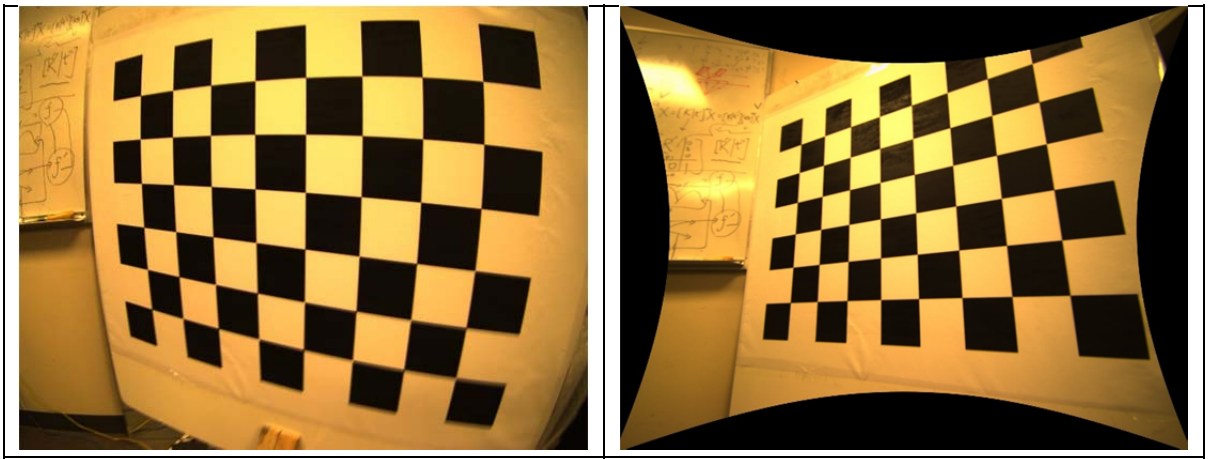

(a) (b)

Figure 79. (a) Before Camera Calibration (b) After camera Calibration.

LIDAR CALIBRATION

The lidar we use here is Hokuyo UST-20LX. This lidar is a laser range finder with the range between 0.2 to 20 meters. The scanning range is 270°, and the scanning rate is 25 milliseconds. The interface for this lidar is Ethernet.

The purpose for the lidar in this sensing suit is to provide the current sensing distance information from the obstacles within the sensing range rather than build up the map after sensing. Moreover, the lidar has been considered as a high accuracy sensor. Based on above the reasons, we would like skip the calibration for lidar and get into the GPR calibration.

GPR CALIBRATION

Unlike the camera calibration or the lidar calibration, the GPR calibration is not a well-studied problem. Here we will present our GPR model, the GPR calibration problem and how we solve the problem. Details of this work are documented in our recent publication [2].

When GPR moves along a straight line to register data, it will record: 1) the traveled length collected by survey wheel encoder, and 2) the microwave traveling time between GPR position and calibration object position. We assume that the dielectric material is a uniform dielectric and the velocity of microwave is constant, so the microwave traveling time between GPR and calibration point can be converted into physical distance. These two information will be assembled in the GPR image (see Figure 80). Yk indicates the GPR position at frame k and Xk indicates the i-th calibration point position. dk represents the distance between Yk and Xk , and lk represents the GPR's traveled length from frame 1 to frame k. Figure 80 indicates the coordinate frame relationship.

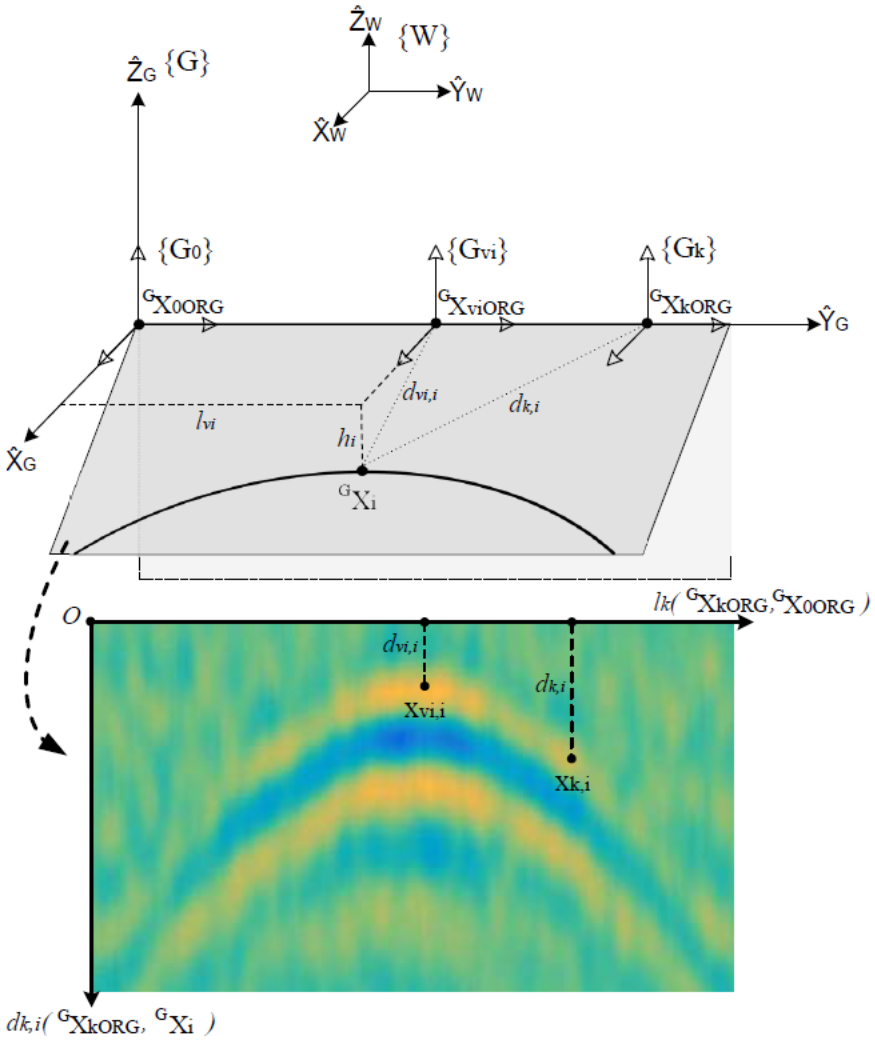

Figure 80. **Coordinate Frame Relationship and a GPR Image.**

According to the GPR model, we define the hyperbola as Hi = [pi; qi], where [pi; qi] is the vertex of that hyperbola. It means that only two degree of freedom is enough to represent a hyperbola. This definition is reasonable because the general conic sections equation is of the form ax2+bxy+cy2+dx+ey+f=0 and the degree of freedom is five (since we can set one of the coefficients to 1 and scale the others accordingly). In our case, the degree of freedom becomes to two since b = 0, e = 0, and a = c.

Next, based on the GPR model, our problem is defined as: given at least 3 calibration objects coordinates Xi with respect to world coordinate system, and its correspondence hyperbolas Hi in GPR image, i = 1,2...n, we hope to determine the GPR position and orientation with respect to world coordinate system. To solve this problem, there are three stages: 1) hyperbola estimation, 2) calibration objects coordinates estimation, and 3) rotation and translation estimation.

In the first stage, we estimate Hi = [pi; qi] by choosing m points in the hyperbola from GPR image. Let xij = [uij; vij] be the chosen points, where j=1,2...m. The measurement error function is given by

$$C(\mathbf{H}_i) = \begin{bmatrix} v_{i1} - \sqrt{(u_{i1} - p_i)^2 + q_i^2} \\ v_{i2} - \sqrt{(u_{i2} - p_i)^2 + q_i^2} \\ \vdots \\ v_{im} - \sqrt{(u_{im} - p_i)^2 + q_i^2} \end{bmatrix}$$

Then the MLE of Hi can be obtained by minimizing the following equation:

$$\mathbf{H}_i^* = \underset{\mathbf{H}_i}{\operatorname{argmin}}\ C(\mathbf{H}_i)^{\mathsf{T}} \Sigma_i^{-1} C(\mathbf{H}_i)$$

where i is the covariance matrix of Hi.

In the second stage, we compute the calibration objects coordinates Xi'=(xi, yi, zi)' with respect to GPR coordinate system through [pi; qi] and hi, where hi is the vertical distance from the calibration object to the ground surface where GPR is located. We assume hi is known from measurement since it is part of our calibration object. Hence, the calibration object coordinate is computed as follows

$$\begin{bmatrix} x_i \\ y_i \\ z_i \end{bmatrix} = \begin{bmatrix} \sqrt{q_i^2 - h_i^2} \\ p_i \\ h_i \end{bmatrix}$$

Finally, the third stage, we will compute the rotation matrix R and translation vector t through Xi' and Xi since we know that Xi'=RXi'+ t. We assume that this is a rigid body transformation, so R and t totally contains six degree of freedom. In order to solve R and t, at least three correspondence points are needed since each correspondence provides two equations. That is why we need at least 3 calibration objects to solve this problem. Therefore, we use Horn's method [1] to solve R and t.

CAMERA AND GPR CALIBRATION

After we finish the calibration for each sensor, we can start to work on the calibration for all sensors. Here we will start from the calibration between the camera and the GPR. The calibration between the camera and the lidar has been well-studied. Therefore, we would like to use the camera as an intermediate reference in the whole calibration among three sensors. We want to separate the whole calibration into two part: 1) the camera and the lidar and 2) the camera and the GPR. After we finish these two part, we can combine the information together since the camera exists in both parts. Hence, our problem currently will be how to do the calibration between the camera and the GPR, and we will address it in the following.

As mentioned before, we adapt the mirror in our new calibration experiment since the camera is also needed to observe the same calibration objects which are below the artificial bridge. We now place three mirrors in front of our artificial bridge to provide sufficient observation to solve the calibration problem. Moreover, with this setting, we can take this calibration problem as a hand-eye calibration problem. We will have to find three transformation: 1) the transformation between the camera and the mirror, 2) the transformation between the mirror and the calibration object and 3) the transformation between the calibration object and the GPR. With these transformation, we are able to get the transformation between the camera and the GPR. To be specific, we are going to process the reflection problem, the camera projection problem and the GPR calibration problem. The experiment for this part is still on the progress. Figure 81 is the relation between each coordinate frame during camera and GPR calibration.

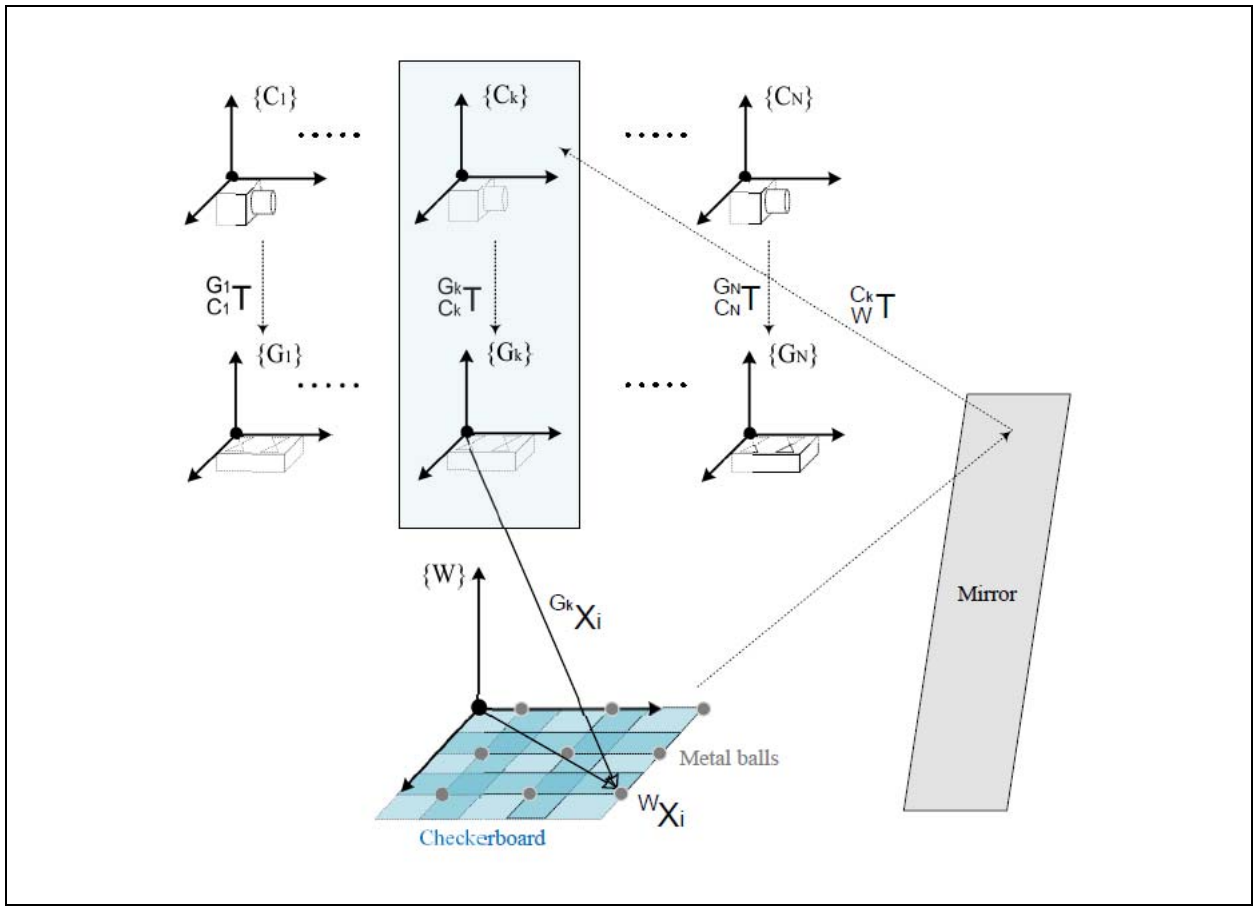

Figure 81. **Coordinate Frame Relationship in Camera and GPR Calibration.**

FUTURE AND CURRENT WORK

With calibration work done, we will perform tests and develop SLAM algorithms for bridge deck inspection. This will be built on our recent work [3]. We will bring our motion-vector based background separation into the system to enable in-traffic inspection [4].

REFERENCES

[1] B. K. Horn, “Closed-form solution of absolute orientation using unit quaternions,” JOSA A, vol. 4, no. 4, pp. 629–642, 1987.

[2] Chieh Chou, Shu-Hao Yeh, Jingang Yi, Dezhen Song, Extrinsic Calibration of a Ground Penetrating Radar, IEEE Conference on Automation Science and Engineering (CASE), Fort Worth, TX, USA, August 21-24, 2016

[3] Yan Lu and Dezhen Song, Visual Navigation Using Heterogeneous Landmarks and Unsupervised Geometric Constraints, IEEE Transactions on Robotics (T-RO), vol. 31, no. 3, June 2015, pp. 736 – 749.

[4] Wen Li and Dezhen Song, Featureless Motion Vector-based Simultaneous Localization, Planar Surface Extraction, and Moving Obstacle Tracking, The Eleventh International Workshop on the Algorithmic Foundations of Robotics (WAFR), August 2014, İstanbul, Turkey

CHAPTER 5. DEVELOPING AND TESTING PROTOTYPE TECHNOLOGIES FOR PAVEMENT INFRASTRUCTURE INSPECTION

BACKGROUND

Existing Equipment and Capabilities, Cost, and limitations

For determining a deflection profile of the pavement and material properties of the pavement layers, several current technologies are used. These include the falling weight deflectometer (FWD), rolling dynamic deflectometer (RDD), the Applied Research associates' rolling wheel deflectometer (RWD), airfield rolling wheel deflectometer (ARWD), road deflection tester (RDT), and high speed deflectograph (HSD) are applied in the field or on the process of research and development. Figure 82 shows a typical FWD. Pavement engineers must stop the test vehicle to perform the FWD deflection measurements at a randomly selected location which will require traffic control. The deflections obtained from the FWD are non-continuous.

Figure 82. Typical Falling Weight Deflectometer (TxDOT 2015).

The RDD consists of a vibroseis truck and a servo-hydraulic vibrator to generate dynamic load as shown in Figure 83. The dynamic forces are transferred to the pavement and the vertical deformations are measured by four rolling deflection sensors. RDD can provide a continuous moving deflection basin profile of pavements with sufficient accuracy, but it can only run at a very low speed of 1 to 2 mph, which also interrupts the traffic.

Figure 83. Rolling Dynamic Deflectometer (Arora et al. 2006).

The RWD is constructed using a specially designed 53-ft long tractor-trailer to apply a load of 18,000 lb to the pavement and measures the single moving deflection responses using high precision laser distance measuring devices. Deflection is the difference between deflected and un-deflected profiles. RWD can run at a highway speed (e.g., 55 mph), but it produces relatively high variance and limited accuracy of deflection, which may not be used to quantify the pavement structural capacity qualitatively but not quantitatively. Figure 84 shows an RWD.

Figure 84. Rolling Wheel Deflectometer (Hall et al. 2004).

The ARWD measures pavement deflections at a moving speed of 20 mph. There are four sensors mounted to the device to estimate the deflection. ARWD is instrumented based on a sound principle that is proven to be effective at slow speeds. It may not be successful at or near highway speeds. Moreover, it has the limitations that the trailer is too long and its vibratory motion results in the observed loss of accuracy. Figure 85 shows the ARWD prototype developed by Quest Integrated.

Figure 85. Airfield Rolling Wheel Deflectometer (Briggs et al. 1999).

The RDT was developed by the Swedish National Road Administration and Swedish National Road and Transport Research Institute. It consists of two arrays of laser range finders, which is composed of 20 sensors in a line transverse to the direction of travel. RDT can travel up to 60 mph. Figure 86 presents a typical RDT. The theory of operation and analysis employs an assumption of which the validity still needs to be investigated.

Figure 86. Road Deflection Tester (Andr´en and Lenngren 2000).

The HSD was developed by the Danish Road Institute and Greenwood Engineering. It has wheel loads up to 11 kips and can travel 50 mph. The device uses Doppler laser sensors to measure the velocity, and then the velocity is converted to the deflection. The Doppler technique is simple and well known. The undeflected and deflected profiles of the pavement are measured by the HSD. The difference between these two values is the deflection of the pavement. Figure 87 shows the instrument of the HSD.

Figure 87. High Speed Deflectograph (Hildebrand 2002).

Measurements of deflection vary by 20 to 50 percent between FWD, RDD, RWD, and HSD depending on pavement temperature, texture, stiffness, composition, and deflection magnitude. Except for the FWD, all the other devices are in different developmental stages. Comparisons of these devices have been conducted and are summarized in Table 88.

Table 88. Summary of Dynamic Deflection Devices (Arora et al. 2006).

Device	Texas Rolling Dynamic Deflectomoter (RDD)	Airfield Rolling Weight Deflectormeter (ARWD)	Rolling Wheel Deflectometer (RWD)	Rolling Deflection Tester (RDT)	High Speed Deflectograph (HSD)
Manufacturer	UT Austin	Dynatest Consulting and Quest Integrated	Applied Research Associates	Swedish National Road Administration and VTI	Greenwood Engineering
Operational Speed	1 mph	20 mph	45 to 65 mph	60 mph	50 mph
Distance Between Readings	2 to 3 ft	9 ft	0.5 in	0.001 s	0.8 in (20 mm)
Applied Load	10 kips static + 5 kips dynamic	9 kips	18 kips fixed	8 to 14 kips (40 to 70 KN)	11 kips (49 KN)
Deflection Sensor Accuracy	0.05 mils	N/A	±2.75 mils (±0.070 mm)	±10 mils (±0.256 mm)	±4 mils/s (±0.1 mm/s)
System Accuracy	N/A	1 mil at 6 mph	N/A	N/A	0.2 mils (5μm)
Other Features	GPS Equipped	N/A	GPS Equipped	N/A	GPS Equipped
Number of Operators	2	N/A	2	2	2
Calibration Process	Yes	N/A	Yes	Yes	Yes
Comments	Too slow for Network level	No Release Date Available	No Release Date Available	No Release Date Available	Sold two devices so far.

The FWD, as the most commonly used nondestructive device, can effectively measure the deflection data of the pavement under the loading plates in order to obtain the stiffness and other characteristics of the pavement. However, it has several obvious weaknesses such as needing to stop to make its measurements and the requirement for traffic control.

Objectives of Pavement Data Collection Equipment

The objective of this task is to develop a system with strong potentials to significantly improve the efficiencies of pavement inspection especially in the aspects of moving speed and deflection measurement. The potential benefits of the technology advancement are:

- The highway-speed deflection measuring system will produce a continuous deflection profile for a pavement to replace the existing deflection test at random locations such as the falling weight deflectometer (FWD).
- The highway-speed deflection measuring system will eliminate the potential user time delay costs and avoid safety problems resulting from the traffic control required by the

traditional deflection test. The moving deflection measuring system can be operated at normal highway speed, e.g., 60 mph, thus it will cause no disruptions to the traffic.

- The pavement manager can employ this system to obtain real-time conditions of the pavement and make the best decisions on the timing of pavement maintenance so as to expect the longest service life, the least maintenance costs and the least delay costs.
- The pavement construction engineers can use this system to locate, fix, and eliminate the weak spots of pavement structures at the time of construction, and eventually to assure quality construction to reduce life cycle costs and expect a longer service life.
- Linking these deflection measurements that can be made in real time with GPS to the GIS database will generate map-based information on the locations of the weak spots in the pavement structure and low load transfer efficiency of concrete pavements and locations where overlays are vulnerable to reflection cracking.
- Advance warning of two to three years of developing pavement distress to permit rational pavement maintenance and rehabilitation managements.

Due to the aspects of moving speed increase and the deflection data measurement technology improved in the task, the primary work finished are:

- Develop methodology for fitting the deflection basins under loads of highway speed and back calculating pavement layer properties with the deflection data measured by the equipment.
- Develop numerical models with finite element software to explore characteristics of deflection basins under various moving speed and layer properties.
- Explore feasibilities of various deflection measurement techniques such as cameras and lasers at highway speed.
- Develop programming for backcalculation of material properties of the pavement and laser control system.
- Construct laboratory testing apparatus for laser control and data collection.

NEW CONCEPT OF HIGH-SPEED PAVEMENT DEFLECTION MEASUREMENT

Current Nondestructive Structural Evaluation of Pavement

Measurement of the deflection of the surface is an increasingly important part of the structural evaluation of pavements. Especially, nondestructive testing is generally used in pavements under or after construction for evaluating and predicting behavior of pavements in order to save costs for maintenance.

The Falling Weight Deflectometer (FWD) is a typical nondestructive pavement evaluation device. It can produce transit impulse loading by the loading plate. The resulting deflections of points at given distances from the plate can be collected by geophones and the deflection basin of the pavement can be determined.

As a device applying dynamic static loads on the pavement, the FWD sets each load with two peaks to simulate a vehicle with two axies passing a given point as illustrated in Figure 8.

Because of this, the deflection basin measured by the FWD can be treated as the actual deflection basin of the pavement under moving loads.

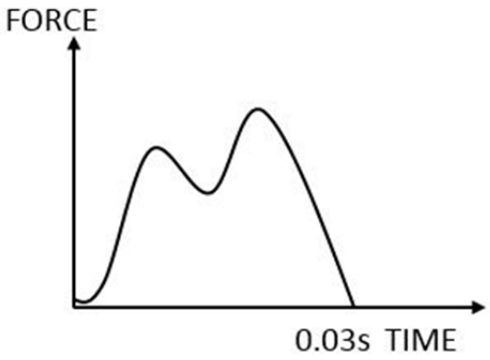

Figure 88. Force-Time Relationship of FWD Load.

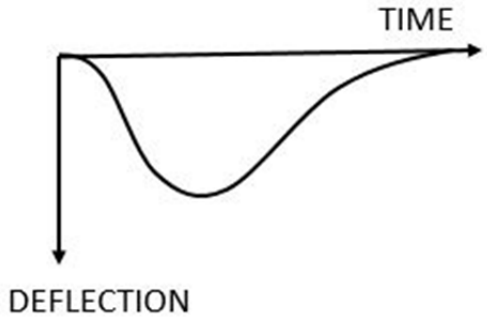

Figure 89. Deflection-Time Relationship of the Pavement.

However, considering the size, complexity and time-consuming loading procedures of FWD, traffic control is required during an insitu test. Accordingly, costs for traffic delay and technician security need to be taken into account. Therefore, researches on testing devices with high speed are not only for more precise loading simulation but also for a decrease in funding spent for tests. Below is a list including several devices which are likely to be applied in the future.

Lytton pointed out there are two types of waves named body wave and surface wave are created and move in the pavement when the load is acted on the surface of the pavement, just as the falling weight drops to the pavement surface (Lytton 1989). For most backcalculation cases, the peak load and deflection are extracted from graphs of load versus time impulses and deflection versus time response created by FWD to evaluate elastic material properties. However, there is much more information in these signals. If fast Fourier transform is performed on the impulse and response, signals will be transformed into forms of frequency-dependent components which is a complex number for each frequency. The modulus of different materials of layers can be represented as this kind of complex modulus (Lytton 1989).

$$E^*(f) = E'(f) + iE''(f) \quad (1)$$

where,

$E^*(f)$ – the complex modulus.

$E'(f)$ – the real part of the complex modulus, which is the in-phase component of stress divided by the strain.
$E''(f)$ – the imaginary part of the complex modulus which is made up of the lagging component of the stress divided by the strain.
There is a relationship between the lag angle ϕ and material damping ratio β.

$$2\beta = \tan\phi(f) = \frac{E''(f)}{E'(f)} \tag{2}$$

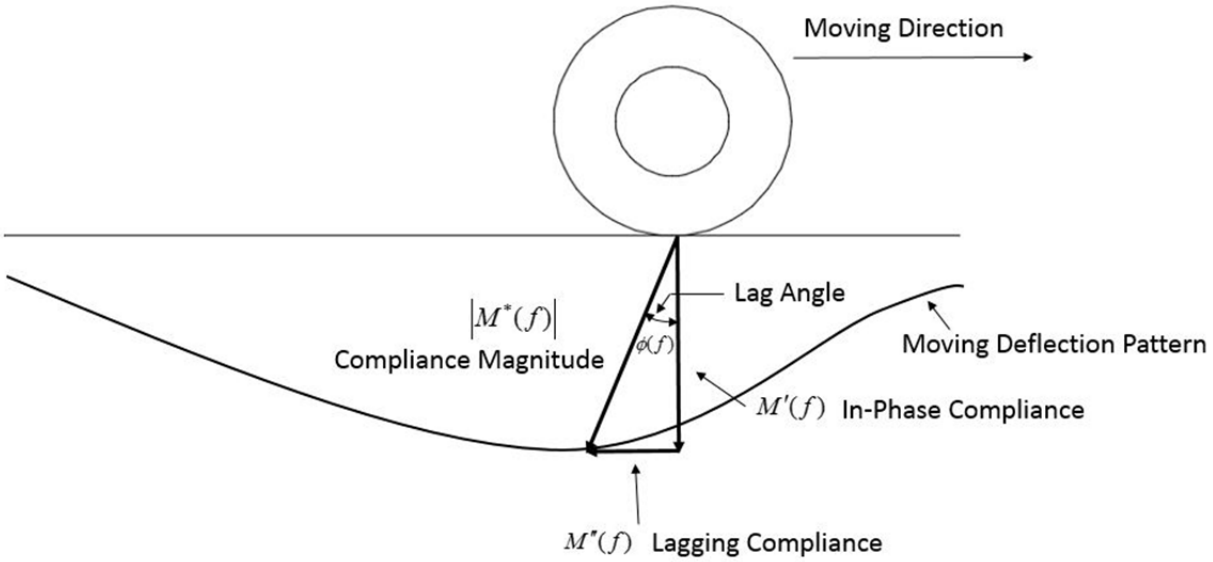

Figure 90. A Moving FWD, Deflection Basin and Complex Modulus.

From the left part of Equation (2), it can be observed that the value of the lag angle relies merely on the damping ratio of the material which is independent of the properties of external loads. However, from the other part, there is an obvious relationship between the lag angle and the ratio of the real part and the imaginary part of the complex modulus, both of which are frequency-dependent.

This task is to study characteristics of the actual deflection basin, figure out factors affecting it and then backcalculate those important material property coefficients. For example, the deflection-time graph Figure 9 shows is made by the data collected from the geophone. It is clear that it takes more time for resilience than achievement of the peak deflection and the whole deflection basin shows obvious asymmetry. It is likely that the inelasticity of the pavement and foundation cause such phenomenon. Hence, in this task, detailed and complex characteristics of the supporting layer of the pavement will be discussed. Improved expressions and parameters will be applied and studied to describe properties which can reflect the real situation better. The detailed material properties of the supporting layers will be described in subsequent sections.

Theory of Highway Speed Deflection Basin-Pavement Material Property Measuring System

This apparatus will measure the moving deflection basin at highway speeds under pavement design loads, and determine analytically the viscoelastic material properties of the surface layer and the supporting layers of both concrete and asphalt pavements. Previous measurements made on Texas pavements have indicated that the characteristic length of such pavements is approximately 20–30 ft. The characteristic length is defined as the decorrelation distance of a pavement in which the surface roughness pattern at one point is decorrelated from the roughness pattern at a second point one decorrelation distance away. Figure 91 shows typical Texas pavement decorrelation distances. Over this distance, this apparatus will make at least 50 such deflection basin measurements. The mean and standard deviation of these measurements will be used to determine the characteristic viscoelastic properties of the surface layer and the supporting layers and their variances.

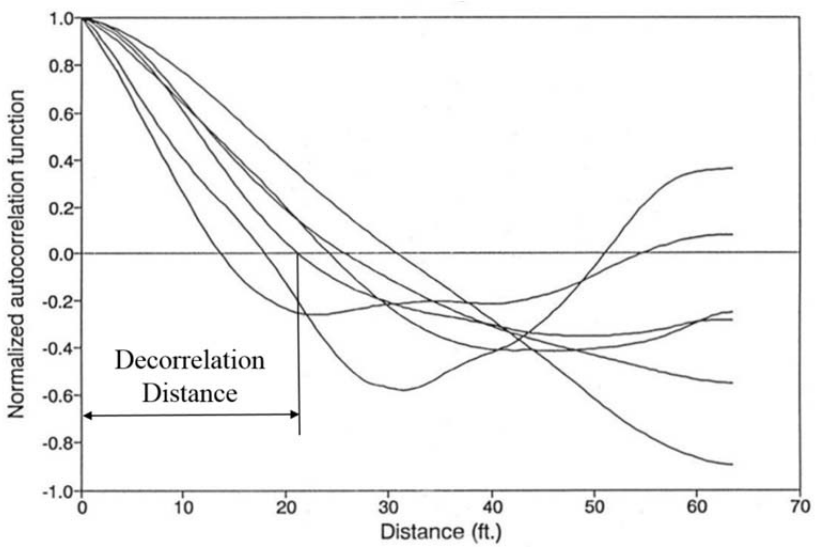

Figure 91. Concept of Characteristic Length of Pavement.

Concrete pavements are expected to respond to the moving loads as an elastic surface layer with a viscoelastic supporting layer, the softness of which is indicative of expected rapid deterioration of the concrete pavement distress. Asphalt pavements are expected to respond to the moving loads as viscoelastic layers in both the surface and supporting layers. Aged and brittle asphalt will respond as being more elastic until cracks begin to appear, either growing from the bottom up or from the top down. As such, these measurements will be an advanced indicator of future pavement cracking. The softer supporting layers will, as with the concrete pavements, indicate a more rapid deterioration rate of cracking and of rutting. Stabilized supporting layers will respond as being more elastic until cracks begin to appear, reducing the effective support they provide to the surface layer. Water entering these supporting layers will soften them, making them respond in a more viscoelastic way. Table 89 shows these four pavement responses.

Table 89. Type of Pavement Responses under a Moving Load.

Pavement Type	Type of Pavement Responses	
	Surface Layer	Supporting Layers
Asphalt	Viscoelastic	Viscoelastic
Concrete	Elastic	Viscoelastic
Asphalt over stiff support	Viscoelastic	Elastic
Concrete over stiff support	Elastic	Elastic

Viscoelastic responses will produce an asymmetric deflection basin with a steep leading edge and a shallow trailing edge, as shown in Figure 92. The greater the maximum deflection and steeper the leading edge indicate pavements that are more susceptible to load-related distress.

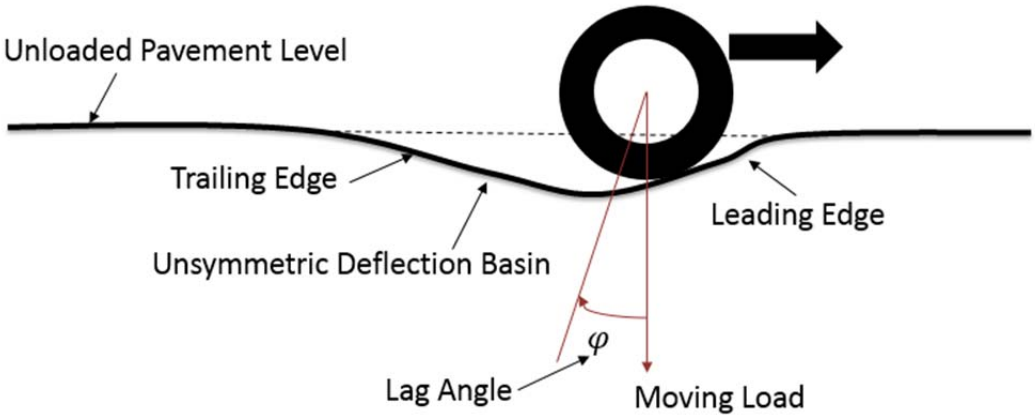

Figure 92. Illustration of Asymmetric Deflection Basin under a Moving Load.

Having such information acquired at highway speeds for every characteristic length of the pavement along its entire length will pinpoint trouble spots long before serious distress begins to develop. This makes possible an effective planning program for maintenance and rehabilitation of entire pavement networks.

Conceptual Field Testing Equipment

The project team designed the field testing equipment as shown in Figure 93. The main beam is mounted to the towing vehicle. The dual tires support the main beam and are smooth tires. The project team has explored the possibility of borrowing or renting a United States Air Force Fighter Aircraft Bogey, on which our measurement equipment can be mounted and then tried out

on selected pavements. If this full scale trial run performs satisfactorily, we will then proceed to design and construct the high speed deflection measuring apparatuses shown schematically in Figure 93. To ensure adequate deflection that can be detected by the laser measuring system, loads are added in front of and behind the dual tires. The sum of the loads will be at or above the dual tire loads of a standard design axle load. The high-speed high resolution laser sensors are mounted to the laser support beam, and then it is hung to the main beam. To account for the effects of temperature gradients and vibrations of longer beams, a hinge is used to connect the laser support beam, which makes the beam deform freely under the thermal stress. For the issue of vibration due to high speed of the tow vehicle, Figure 94 shows a conceptual picture of a trailer equipped with magnetic adaptive dampers to eliminate vibrations from the trailer. The slope indicators are fixed to the laser support beam to measure the deformation caused by the temperature gradients and instantaneous motion of the laser support beam segments.

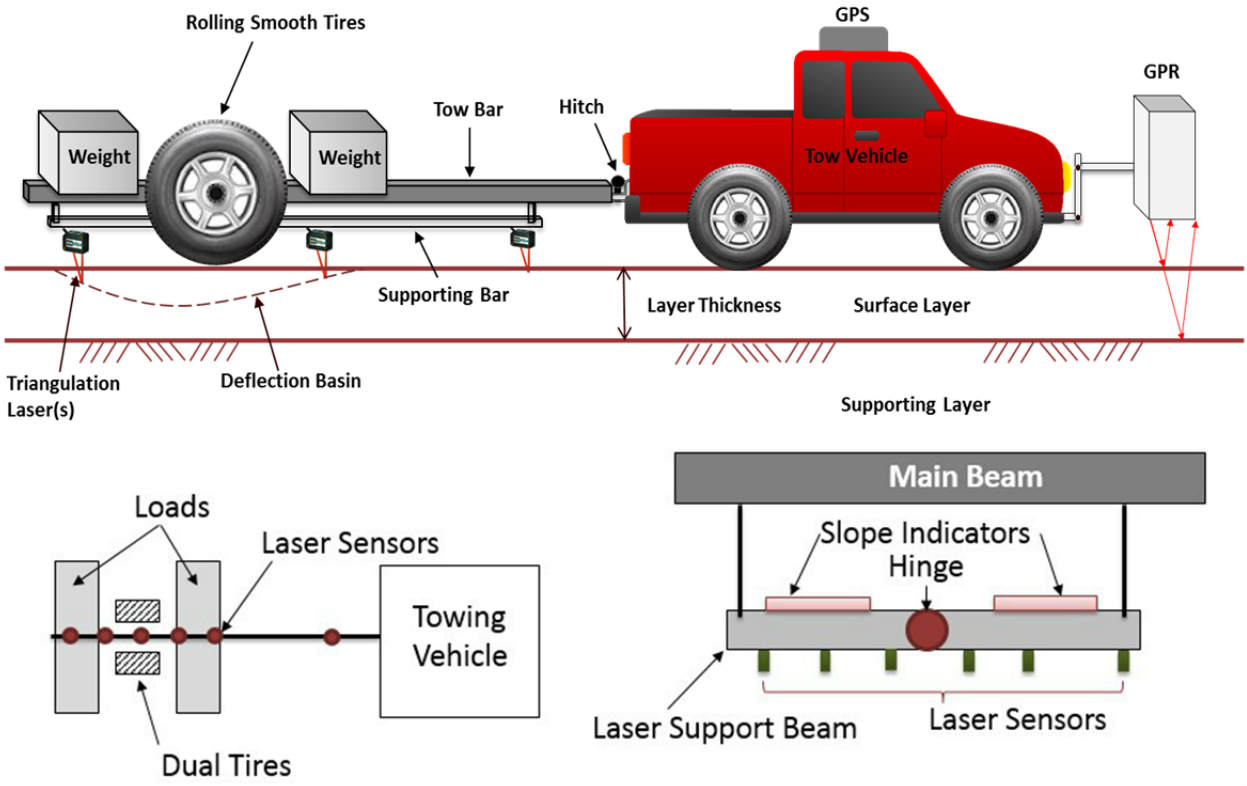

Figure 93. Illustration of Design of Field Testing Equipment.

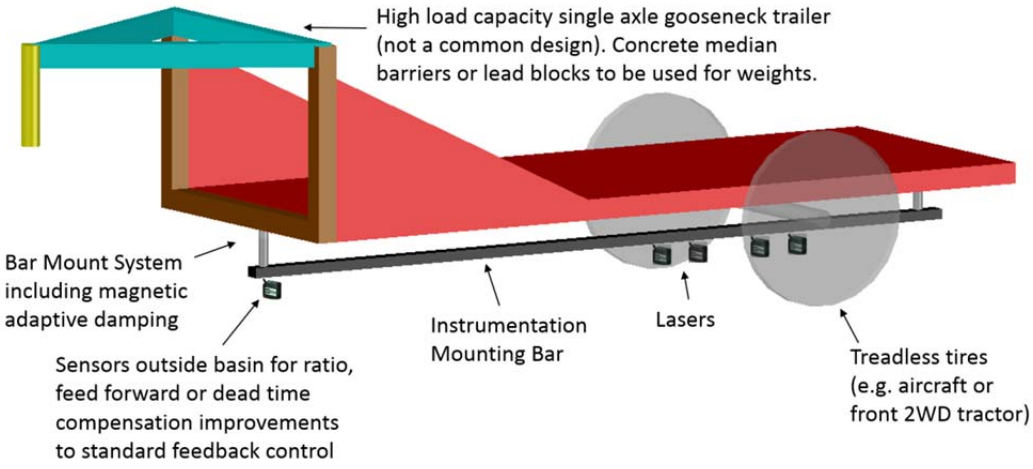

Figure 94. Concept of High-Speed Deflection Basin Measuring Trailer.

Full-Scale Field Equipment Calibration Facility

In order to evaluate the accuracy of the field testing equipment as described above, the project team proposed a full-scale calibration program as shown in Figure 95. This calibration facility will be built at the Texas A&M University Riverside campus, where there are many testing facilities to accommodate a variety of transportation research and implementation projects. A pavement test section will be selected and a trench will be constructed in the test section. A metal plate supported by a series of springs is placed on the top of the trench. When the field testing system travels along the metal plate, the measuring system is able to record the deflection of the metal plate. Then the stiffness of the spring can be back-calculated from the measured deflection. This back-calculated spring stiffness is compared to the known spring stiffness for the purpose of calibration.

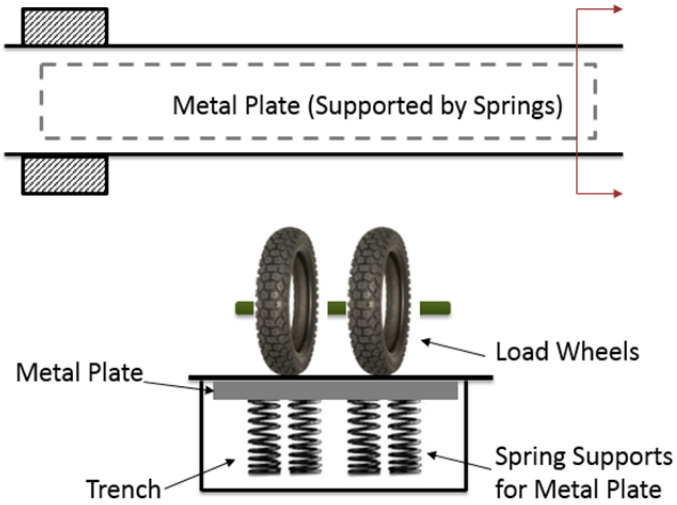

Figure 95. Illustration of Design of Full-Scale Field Equipment Calibration Facility.

Architecture of Highway Speed Deflection Basin Measuring System

To achieve the continuous measurement of the deflection basin, several different kinds of sensors are integrated into a measuring system, as shown in Figure 96. The system consists of five levels. The multi-sensors level contains all the sensors involved in the system. The system integration level is responsible for the synchronization of the whole system. The data collection level connects the hardware and software for real-time data collection. Once the data are collected, the data processing level performs analysis of the raw data and produces readable and meaningful results.

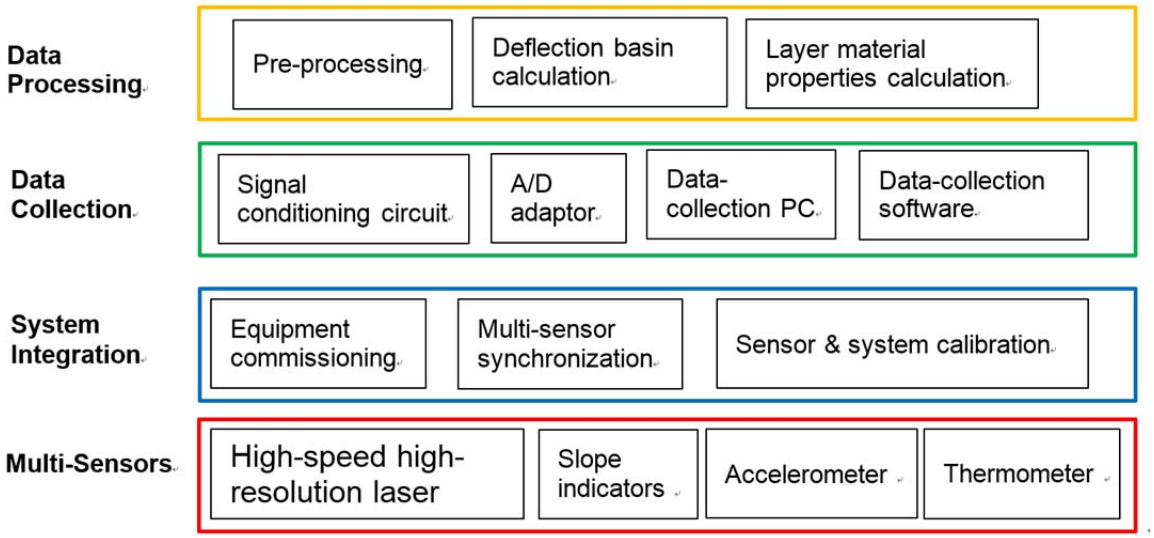

Figure 96. Architecture of Highway Speed Deflection Basin-Pavement Material Property Measuring System.

High-Speed High-Resolution Laser Sensor

In order to capture the profiles of the pavement deflection basin at high speeds, the project team reviewed various types of laser sensors and finally identified the candidate: Gocator displacement sensor. It is a non-contact laser distance measurement device ideal for determining 3D thickness, height, and surface roughness. The scan rate of this sensor is up to 32 kHz and the resolution is micron. It has a built-in web server and interface, so the real-time data can be viewed on a connected computer, as shown in Figure 97.

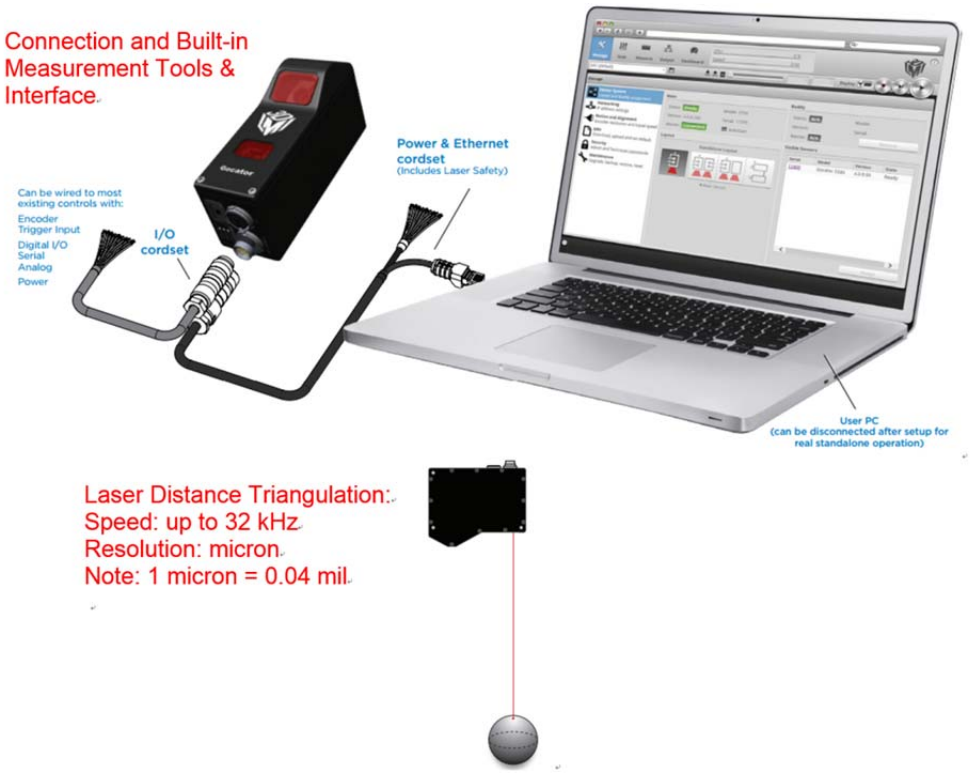

Figure 97. Gocator Displacement Sensor.

The deflection basin measuring system consists of five lasers hanging on the support bar, as shown in Figure 17. Five sensors are set along the whole distance which is approximately 15 feet to determine deflections at four locations of the basin as well as the spot where the deflection value is zero. All sensors are connected and controlled by a computer system which makes sensors measure the distances to the pavement surface simultaneously, then takes the mean value of the deflection data at each spot and draws the shape of the deflection basin.

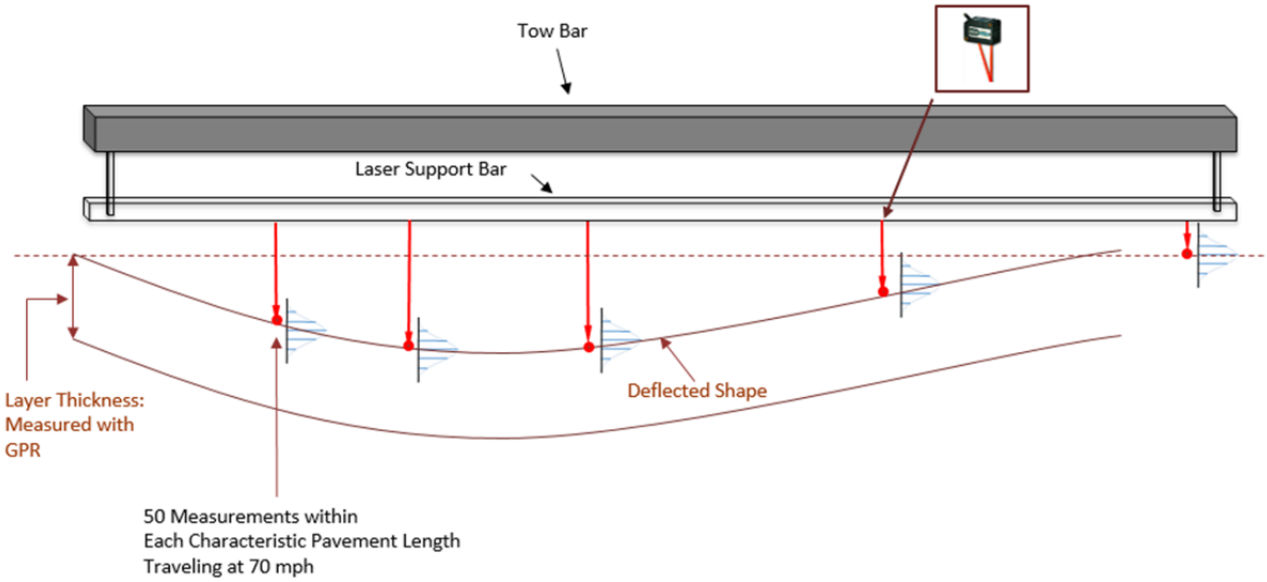

Figure 98. Deflection Basin Measured by Sensors.

Laboratory Test and Field Equipment Design

The purpose of the laboratory test is to examine the accuracy, resolution and sensitivity of the laser sensors purchased from the LMI Technologies. The project team purchased four Gocator laser sensors and power/Ethernet wires. Figure 99 shows the design of the laboratory test facility. The four Gocator laser sensors are mounted to the laser support beam. The beam underneath the laser support beam is fixed to the ground. Then a solenoid-actuated loading apparatus is connected to this beam to exert cyclic loading. The four laser sensors will measure the deformation of the beam that is driven by the actuator.

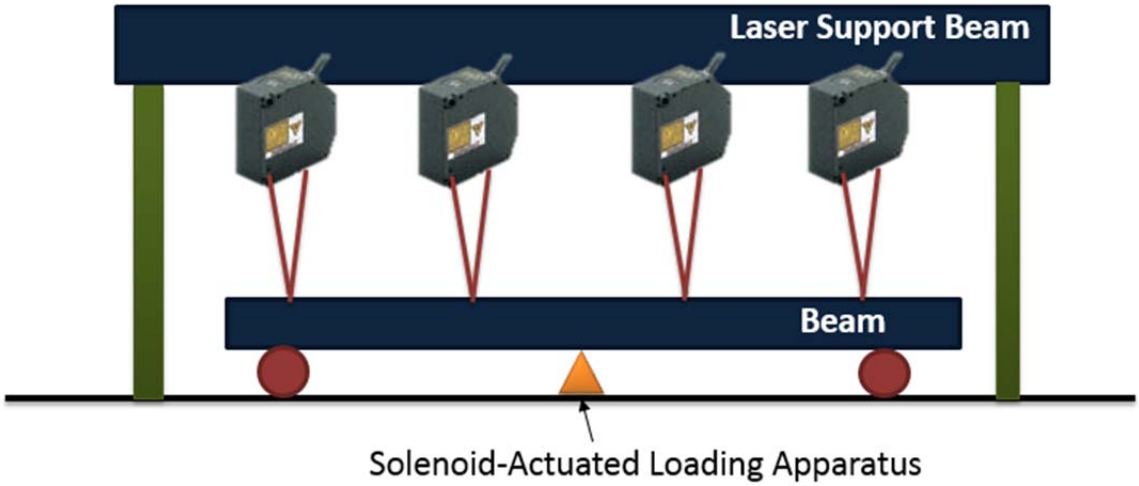

Figure 99. Illustration of Design of Laboratory Calibration Facility.

Elastic Solution of Pavement Deflection

The solution of beams on elastic foundation (Hetenyi 1946) calculates the deflection of an arbitrary point along a pavement under various types of loading. Due to the parameters of surface and supporting layer the solution includes, beam-on-elastic foundation solution can be applied in the back calculation of material properties of each layer with measured deflection data. The assumption made in the beam-on-elastic foundation solution is that the beam is supported on the elastic foundation. A unit deflection of the beam will cause relevant reaction of the foundation in Figure 19. The assumption and calculation method for the reaction of the foundation was introduced by Winkler in 1867.

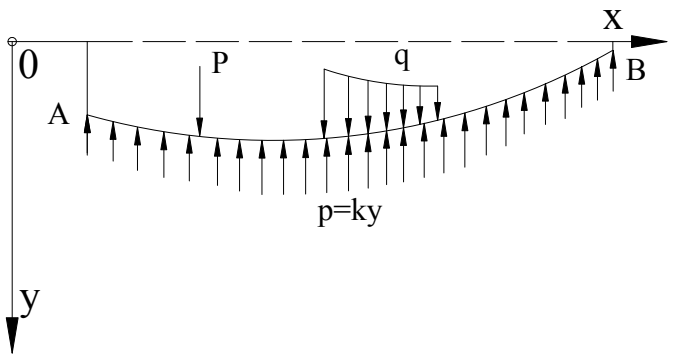

Figure 100. Beam on Elastic Foundation.

Assume that a beam is supported on the foundation and acted upon a concentrated load, the equation of external force acted on the beam can be expressed as:

$$p = bk_0 y = ky \tag{3}$$

p – reaction load of the foundation per unit length

b – width of the beam

y – deflection of the beam

k_0 – modulus of the foundation

The form of the reaction follows Hooke's law and the value is proportional to all three dimensions. Having defined the reaction of the foundation, based on the equilibrium state of the beam (Figure 101), the summation in the vertical direction can be expressed as:

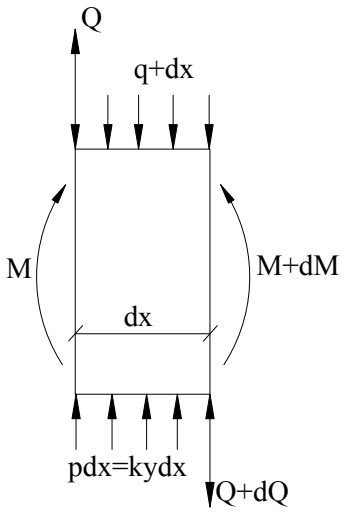

Figure 101. Vertical Equilibrium State of an Element of the Beam.

$$Q - (Q + dQ) + kydx - qdx = 0 \tag{4}$$

It can be simplified that,

$$\frac{dQ}{dx} = ky - q \tag{5}$$

Based on the known conditions that the shear force is the first derivative of the moment,

$$Q = \frac{dM}{dx} \tag{6}$$

and the differential equation of a beam in bending,

$$EI\frac{d^2y}{dx^2} = -M \tag{7}$$

E – elastic modulus of the beam
I – moment of inertia of the cross section of the beam
by using Equation (4)~(7), it can be derived that,

$$EI\frac{d^4y}{dx^4} = -ky + q \tag{8}$$

The solution of the differential Equation (8) can be obtained from the homogeneous part and a particular part corresponding to q. Especially when the beam is loaded by an individual concentrated load, the solution will consist of the homogenous part only.

For the homogeneous part, assume that

$$y = e^{mx} \tag{9}$$

Then, substitute Equation (9) into (8), four roots of two different values can be obtained.

$$m_{1,2,3,4} = \sqrt[4]{\frac{k}{4EI}}(\pm 1 + i) \tag{10}$$

in which the factor $\sqrt[4]{\frac{k}{4EI}}$ is called the characteristic of the system, denoted as λ, the dimension is length^{-1}.

So, the solution of the homogeneous part is

$$y = A_1e^{\lambda(1+i)x} + A_2e^{-\lambda(1+i)x} + A_3e^{\lambda(-1+i)x} + A_4e^{-\lambda(-1+i)x} \tag{11}$$

Replace the complex index with the trigonometric functions,

$$\begin{cases} e^{i\lambda x} = \cos\lambda x + i\sin\lambda x \\ e^{-i\lambda x} = \cos\lambda x - i\sin\lambda x \end{cases} \tag{12}$$

Equation (11) can be expressed as:

$$\begin{aligned} y = e^{\lambda x}\left[\cos\lambda x(A_1 + A_4) + \sin\lambda x(A_1 i - A_4 i)\right] \\ + e^{-\lambda x}\left[\cos\lambda x(A_2 + A_3) + \sin\lambda x(A_2 i - A_3 i)\right] \end{aligned} \tag{13}$$

Assume that,

$$\begin{cases} A_1 + A_4 = C_1 \\ i\left(A_1 - A_4\right) = C_2 \\ A_2 + A_3 = C_3 \\ i\left(A_3 - A_2\right) = C_4 \end{cases} \tag{14}$$

The solution can be rewritten as follows,

$$y = e^{\lambda x}\left(C_1\cos\lambda x + C_2\sin\lambda x\right) + e^{-\lambda x}\left(C_3\cos\lambda x + C_4\sin\lambda x\right) \tag{15}$$

In order to obtain the four parameters $C_1 \sim C_4$ of the Equation (14), actual boundary conditions should be taken into consideration. First, compared to the length of the pavement, no matter what the loading form is, the wheel of vehicles or loading plates, the scale of the loading along the pavement is fairly small. Hence, it is reasonably assumed that, at the spot long enough from the loading area, the deflection approaches zero. The terms including $e^{\lambda x}$ vanish in the Equation (15), which becomes

$$y = e^{-\lambda x}\left(C_3\cos\lambda x + C_4\sin\lambda x\right) \tag{16}$$

Second, when the beam is acted on by a concentrated load, the deflection would show a characteristic of symmetry from two sides of the loading point, which means that the first derivative of Equation (16) would be zero at the point $x = 0$.

$$y'\big|_{x=0} = e^{-\lambda x}\left[\left(C_4 - C_3\right)\lambda\cos\lambda x - \left(C_4 + C_3\right)\lambda\sin\lambda x\right] = 0 \tag{17}$$

So, it can be derived that,

$$C_4 = C_3 = C \tag{18}$$

Then, back to the equilibrium state of the beam, the beam is acted on by the concentrate force and reaction from the foundation, which should counteract in the equilibrium state of the beam.

$$P = 2\int_0^\infty kydx = 2kC\int_0^\infty e^{-\lambda x}\left(\cos\lambda x + \sin\lambda x\right)dx \tag{19}$$

Eventually,

$$C = \frac{P\lambda}{2k} \tag{20}$$

Therefore, the deflection of a beam of unlimited length acted by a concentrated load can be expressed as:

$$y = \frac{P\lambda}{2k} e^{-\lambda x} \left(\cos \lambda x + \sin \lambda x \right) \tag{21}$$

When the beam is under uniform loads, the analysis procedures are similar. The uniform load can be treated as a combination of multiple concentrated loads, therefore, the deflection can be calculated by the integral of multiple deflections under concentrated loads. As the location of the calculated point varies, the deflection can be divided into three types when the beam is under uniform load.

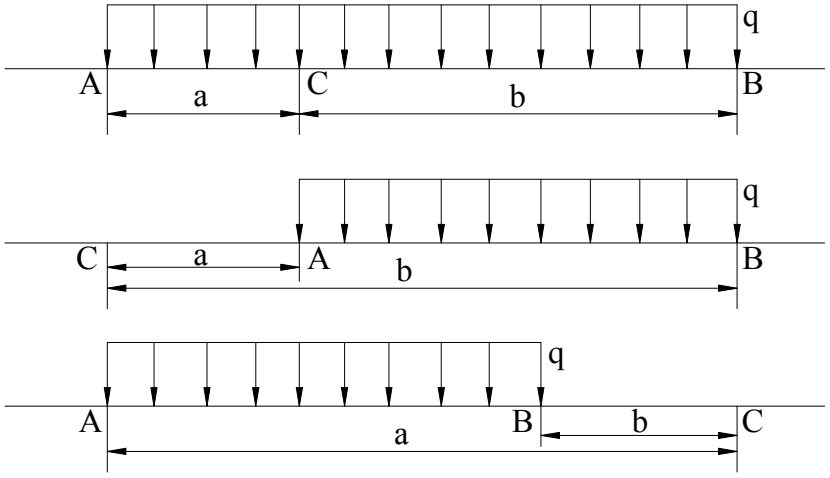

Figure 102. Three Cases of the Beam under Uniform Loads.

Figure 102 shows that the point needs calculating is located under and at two sides of the loading, the deflection of point C can be expressed separately as

$$\begin{cases} y_1 = \dfrac{q}{2k}\left(2 - e^{-\lambda a}\cos\lambda a - e^{-\lambda b}\cos\lambda b\right) \\ y_2 = -\dfrac{q}{2k}\left(e^{-\lambda a}\cos\lambda a - e^{-\lambda b}\cos\lambda b\right) \\ y_3 = \dfrac{q}{2k}\left(e^{-\lambda a}\cos\lambda a - e^{-\lambda b}\cos\lambda b\right) \end{cases} \tag{22}$$

Though Hetenyi's solution expresses sensible assumptions, analysis and calculation method for deflection of the beam under various types of loading, the parameters applied in this method are not time-dependent thus none of them are representative when the loading in this task is at highway speed. The form of the deflection equation, the parameters of the beam and foundation should be modified to represent their dynamic characteristics.

Modification of Modulus of the Foundation

As for soil-structure interaction problems, Winkler's assumption is applied broadly which denote k_0 as the modulus of foundation and the reactive pressure the foundation acts on the beam is proportional to the vertical deflection of the foundation like an elastic spring (see Equation(1)). Beam-on-elastic foundation solution does not contain any description for the determinant of the modulus k_0. Actually in early research, the modulus k_0 is taken as a known constant for a given

type of foundation. The reaction at a given point is related only to the modulus at that point and the whole foundation system is like an individual spring laying at intervals under the beam.

In 1955, Terzaghi pointed out that the reaction of subgrade is correlated to the elastic properties as well as the dimensions of the area acted upon. (Terzaghi 1955). In 1937, Biot published a paper determining the relationship of the modulus k_0 and properties of the soil and the beam (Biot 1937). He pointed out when a concentrated load acted on a three-dimensional subgrade, by evaluating the maximum bending moment the correlation with the Winkler's model for the maximum moment could be expressed as:

$$k = \frac{0.95E_s}{(1-\nu_s{}^2)}\left[\frac{E_s B^4}{(1-\nu_s{}^2)EI}\right]^{0.108} \tag{23}$$

where

E_s – elastic modulus of the soil

I – moment of inertia of the beam

ν_s – Poisson's ratio of the soil

E – elastic modulus of the beam

B – width of the beam

Also, in 1961, Vesic extended such situation by considering deflection, shear and moment distribution along the beam (Vesic 1961).

$$k = \frac{0.65E_s}{(1-\nu_s{}^2)}\sqrt[12]{\frac{E_s B^4}{EI}} \tag{24}$$

Above are two examples of relations researchers found about the modulus of the soil and properties of the beam and soil. Later researchers figured out that the modulus of the soil is a complex parameter affected by the distribution of loading, thickness of the surface and many other factors which represent the characteristics of the whole system.

The modulus k_0 will be expressed in a new form in this task. In *Design and Construction of Post-Tensioned Slabs-on-Ground (2nd edition)*, when it comes to differential deflection distance, for slabs over 50 feet, the effective distance for determining the allowable differential deflection is 6β (β is the characteristic length) rather than the entire length of slabs. Similarly, transform the modulus of the soil from k_0 to E_2 and λ .

$$k = \frac{E_2}{6/\lambda} \tag{25}$$

where

E_2 – elastic modulus of the soil

λ – characteristic of the system (length^{-1})

For convenience, denote $1/\beta$ as the characteristic length.

$$\beta = \lambda = \sqrt[4]{\frac{k}{4EI}} = \sqrt[4]{\frac{E_2}{4E_1 I \bullet 6/\beta}} \tag{26}$$

where,
E_1 – elastic modulus of the beam
E_2 – elastic modulus of the soil
I – moment of inertia of the beam, $I = \frac{bh^3}{12}$, b, h are the width and height of the cross section of the beam respectively
β – characteristic of the system (length^{-1})
In the Equation (26),

$$\beta = \frac{1}{h}\left(\frac{E_2}{2E_1}\right)^{1/3} \tag{27}$$

$$k_0 = \frac{1}{6h}\frac{\left(E_2\right)^{4/3}}{\left(2E_1\right)^{1/3}} \tag{28}$$

In the task, the surface of the pavement can be seen as the 'beam' on the foundation and h is the thickness respectively.

Viscoelastic Solution of Pavement Deflection

Viscoelastic Properties of Asphalt Mixtures

For elastic solids, the stress is proportional to the strain. The strain of the object will not change when the stress is fixed at a constant value. The ratio of the stress and strain is the Young's modulus E. For a viscous fluid, the force applied is proportional to the rate of elongation. The ratio is denoted as the viscosity. For a linear viscous material, assume that the strain is held constant from the beginning, the stress will increase to the required value then decrease to zero immediately. Different from these materials of which strain (force) is ideally proportional to strain or its derivative, viscoelastic materials are those for which the relationship between stress and strain depends on time. The properties of viscoelastic materials can be described by creep and relaxation.

Creep is a progressive deformation of a material under constant stress.

$$J(t) = \frac{\varepsilon(t)}{\sigma_0} \tag{29}$$

where,
J – creep compliance
ε – strain of the material
σ – stress of the material
For a viscoelastic material, it is typically that the strain increases with fixed stress and decreases toward zero when the stress vanishes. The creep compliance of a viscoelastic solid will eventually increase to a boundary value, while for viscoelastic fluid, it will increase to infinity.

Relaxation is a progressive decrease of stress when the strain remains constant.

$$E(t) = \frac{\sigma(t)}{\varepsilon_0} \tag{30}$$

where,
E – relaxation modulus
ε – strain of the material
σ – stress of the material
E represents the stiffness of the material which is the Young's modulus in elastic materials. For viscoelastic materials, the relaxation modulus is a function of time and decreases with a fixed strain. The relaxation modulus of a viscoelastic solid has a limit value greater than zero when time approaches infinity.

Asphalt is a typical material for the surface of pavements and shows characteristics of viscoelastic solids. For convenience of prediction and analysis of material properties, series of exponentials, power laws, and logarithmic functions are used to represent creep compliance and relaxation modulus varying with time.

In this task, the Power Law and Prony-series models are applied to represent the creep and relaxation function.

$$E(t) = E_1 t^{-m} \tag{31}$$

The Power Law equation is mainly used in the backcalculation of material property coefficients for its simplicity but including key variables which sufficiently introducing the characteristics of viscoelastic solids. In the programming of backcalculation, small number of coefficients contributes to relatively simpler calculation and better precision. Besides, in latter sections, physical meaning of m will be introduced and deflection basins will be compared with different values of m to describe the importance to backcalculate it.

The coefficients of Prony-series can be defined directly by users in the commercial finite element software (ABAQUS 2010). By defining instantaneous elastic modulus E_0 and certain sets of shear modulus ratio g_i, bulk modulus ratio k_i and relaxation time τ_i, based on the relationship between shear, bulk and elastic modulus, time-dependent shear, bulk and elastic modulus can be determined.

$$G(t) = G_0\left[1 - \sum_{i=1}^{n} G_i\left(1 - e^{-t/\tau_i}\right)\right] \tag{32}$$

$$K(t) = K_0\left[1 - \sum_{i=1}^{n} K_i\left(1 - e^{-t/\tau_i}\right)\right] \tag{33}$$

where $G(t)$ and $K(t)$ are relaxation shear and bulk modulus, G_0 and K_0 are instantaneous shear and bulk modulus which can be transferred from user-defined instantaneous elastic modulus E_0.
Based on the relationship between shear, bulk and elastic modulus as well as other input coefficients, the relaxation modulus of a linearly viscoelastic material can be expressed as

$$E(t) = E_{\infty}^{a} + \sum_{i=1}^{n} \left(E_i^a e^{-\frac{t}{\tau_i}} \right) \tag{34}$$

where E_{∞}^{a}, E_i^a and τ_i are regression coefficients in the model and satisfy equations below.

$$E_i^a = E_i E_0 \tag{35}$$

$$E_{\infty}^{a} = E_0 - \sum_{i=1}^{n} E_i^a \tag{36}$$

$$E_i = g_i = k_i \tag{37}$$

The dynamic modulus is given by

$$E'(\omega) = E_{\infty}^{a} + \sum_{i=1}^{n} \frac{\omega^2 \tau_i^{\,2} E_{\infty}^{a}}{1 + \omega^2 \tau_i^{\,2}} \tag{38}$$

$$E''(\omega) = \sum_{i=1}^{n} \frac{\omega \tau_i E_{\infty}^{a}}{1 + \omega^2 \tau_i^{\,2}} \tag{39}$$

$$\left| E^* \right| = \sqrt{E'^2 + E''^2} \tag{40}$$

$$\tan \phi = \frac{E''}{E'} \tag{41}$$

where $E'(\omega)$ and $E''(\omega)$ are the storage and loss modulus respectively, ω is the angular velocity, $\left| E^* \right|$ is the magnitude of the dynamic modulus, ϕ is the phase angle. From Equation (38) ~ (41), it can be seen that the magnitude and phase angle of modulus depend upon frequencies of loads. Hence, the shape of the deflection basin ought to vary with loading speeds. For a certain deflection basin, relative dynamic modulus and phase angle can be obtained as follows.

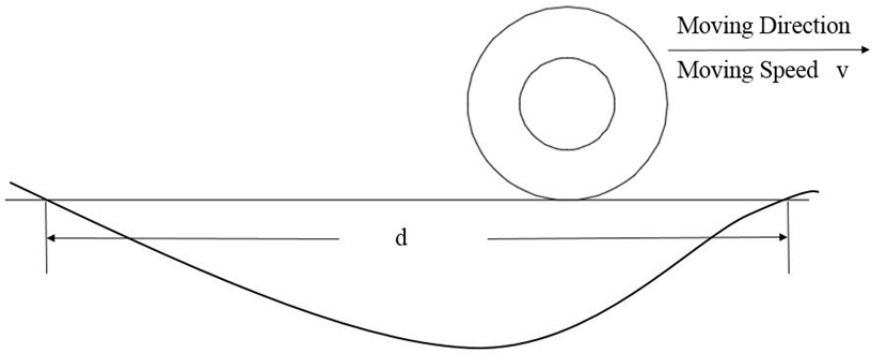

Figure 103. A Deflection Basin under Moving Load.

where d, v are length of the deflection basin and moving speed respectively. From Figure 103, the loading time is

$$t = \frac{d}{v} \tag{42}$$

which is half of the period,

$$T = 2t \tag{43}$$

The frequency of the load, which is denoted as ω,

$$\omega = \frac{2\pi}{T} \tag{44}$$

In previous parts, concepts of the lag angle and characteristic length of the deflection basin have been introduced. It is convenient to calculate the dynamic modulus and phase angle of one material if its Prony series or other transformed expressions are known. In current FWD tests, impulse loads are applied and the transient deflection of the pavement is measured. The peak load and peak deflection are assumed to be static measurements and elastic parameters are back-calculated. Actually, parameters representing viscoelasticity of materials can play the similar or better role. For example, Figure 104 shows that as an asphalt mixture cracks under repeated loading, the dynamic modulus decreases slowly as the phase angle increases almost linearly.

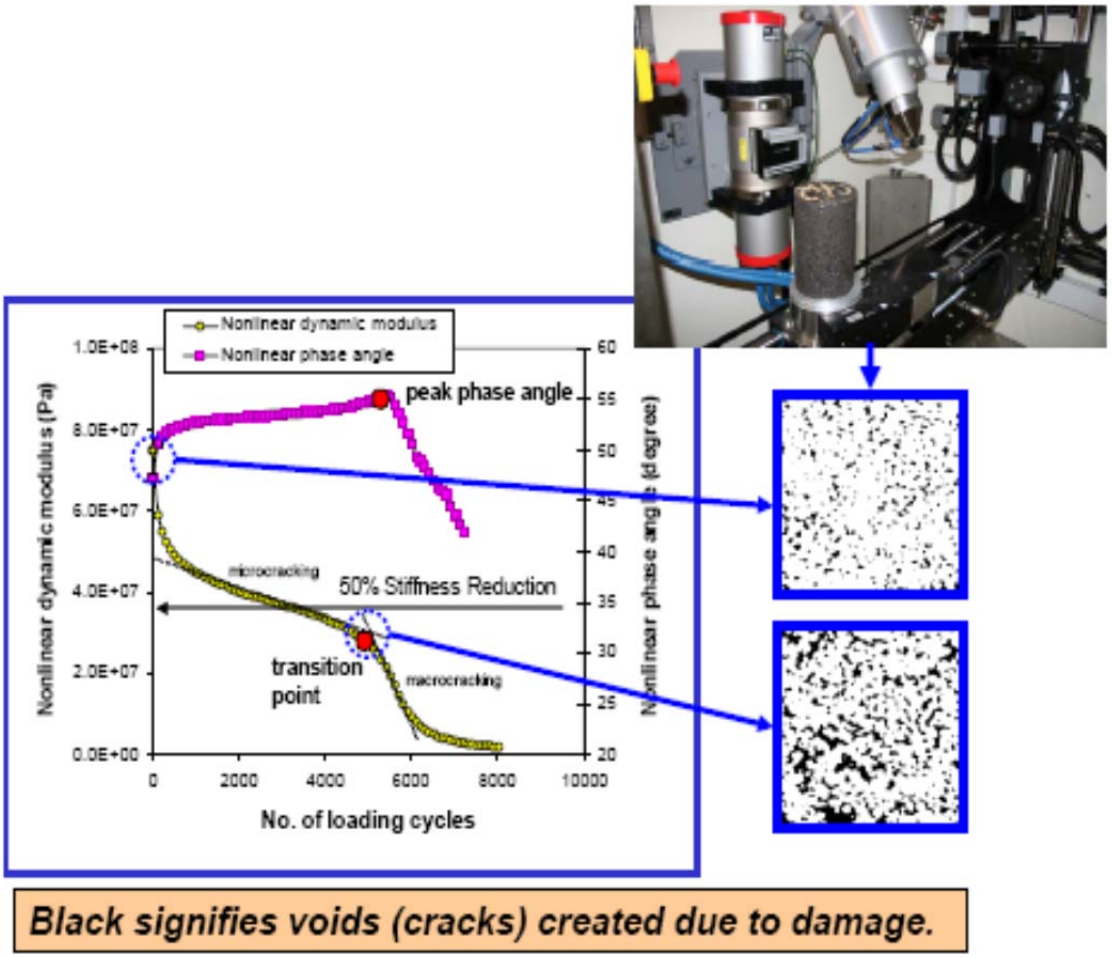

Figure 104. Characteristic Phase Angle and Modulus of Asphalt Pavement Surface in Service Life

After construction, an asphalt surface layer has the maximal value of modulus and low phase angle. With repeated loading, the modulus decreases due to fatigue and fractures while the phase angle is increasingly greater. An approximate relationship between phase angle and the value of m as in Equation (31) is

$$\phi = \frac{\pi}{2} m \tag{45}$$

The phase angle approaches its maximal value when the pavement is about to fail. After that, the pavement develops large cracks completely through the surface layer. Hence, if modulus and phase angle (or m) can be measured during service of a pavement, the current and impending conditions of the pavement can be effectively evaluated and predicted.

Laplace Transform of Material Coefficients

Beam-on-elastic foundation solution is based on the assumption that both pavement and foundation materials are linear elastic which are independent of time. Such assumption cannot explain the asymmetry of deflection basins. Moreover, viscoelastic properties of surface and damped elastic properties of supporting layers are of vital importance to evaluating and predicting the current and impending conditions of the pavement. Therefore, in this task, material property coefficients are required to be expressed as time or frequency dependent functions and certain coefficients will be back calculated.

In previous sections, a power-law function and a Prony-series express the modulus of viscoelastic materials as time-dependent functions. Equation (31) and (34) express the relationship between relaxation modulus and time which effectively represent the characteristic of viscoelastic solids. As time approaches infinity, the relaxation modulus decreases to a value greater than zero. For the time dependent modulus and frequency dependent modulus, Laplace transform is applied. For Equation (31),

$$E(s) = \mathrm{L}\left[E(t)\right] = \int_0^\infty E_0 t^{-m} e^{-st} dt = E_0 s^{m-1} \Gamma(1-m) \tag{46}$$

where the gamma function Γ is defined as follows

$$\Gamma(m) = \int_0^\infty t^{m-1} e^{-t} dt = (m-1)! \tag{47}$$

The reason why Laplace transform is applied to obtain time-dependent viscoelastic response is that Laplace transformed equations of viscoelastic responses are identical with the responses of an elastic material. Laplace Transformed solutions can be calculated by standard elastic analysis, and then inverted to obtain the time-dependent response (Cost 1964). For the relationship between the time-dependent response of one viscoelastic material and its transformed response, an approximate inverse Laplace transform was developed by Cost (1964).

$$E(t) \cong \left[sE(s)\right]_{s=\frac{1}{2t}} \tag{48}$$

s is a real and non-negative parameter in Laplace transform. In approximation method, the value evaluated for s is $\frac{1}{2t}$.

No matter what expression (Equation (31) or Equation (34)) is applied to express the time-dependent modulus of viscoelastic surface of the pavement, Laplace transform can provide efficient approximation of time dependent modulus of viscoelastic materials.

Equation (1) expresses the complex modulus of supporting layers of the pavement. Similarly, the modulus of the base can also be written in a Power law form,

$$E(t) = E_0 + E_2 t^{-m} \tag{49}$$

where E_0 , E_2 and m are all coefficients, and E_0 is generally taken as zero.
Hence, coefficients k and β can be transformed into time-dependent terms.

$$k(t) = \frac{1}{6h} \frac{\left[E_2(t)\right]^{4/3}}{\left[2E_1(t)\right]^{1/3}} \tag{50}$$

$$k(t) \cong \left[sk(s)\right]_{s=1/2t}$$

$$\beta(t) = \frac{1}{h}\left[\frac{E_2(t)}{2E_1(t)}\right]^{1/3} \tag{51}$$

$$\beta(t) \cong \left[s\beta(s)\right]_{s=1/2t}$$

where $E_1(t), E_2(t)$ are the time-dependent modulus of surface and base respectively.
In the life cycle of the pavement, conditions of the pavement varying with the number of load applications, the degrees of damage cause changes in the material damping ratio of the material and are also reflected significantly in the terms ϕ and m . Therefore, in order to make accurate and timely evaluation and prediction of conditions of the pavement, insitu tests with high-speed loading are necessary.

ANALYTICAL RESULTS

Three Dimensional Finite Element (FE) Simulation

Construction of Numerical Models

The objectives of building numerical models using a finite element software (ABAQUS 2010) are:

- Due to the complexity of the problem and lack of insitu testing data, a finite element software is essential for obtaining deflection data of the surface of the pavement to backcalculate properties of materials.
- The shape of a deflection basin is affected by various factors such as the speed of loading, material properties and so on. A finite element software can effectively control input variables for researchers to figure out how those variables influence the shape individually.
- Based on previous assumptions and analysis, loading with highway-speed is of necessity to replace current static FWD loads from two aspects: getting rid of traffic control and providing more information for evaluation and prediction of the pavement. A finite element software can provide cases with different loading speeds, which give a straightforward comparison of deflection basins of different loading speeds.

For convenience of modeling and calculation, the numerical models and simulation of a moving vehicle are simplified in terms of following aspects:

- The whole system is divided into two parts, of which the top is the surface of the pavement and the bottom is the base course. The thickness of the top layer can be adjusted in order to simulate different thicknesses of flexible or rigid pavement surface layers. The thickness of the base course is fixed and set to be much greater than the surface. For typical asphalt surface over unstabilized base, thickness of surface and base courses are taken 4 and 70 inches, respectively.
- The contact area of tires and pavement surface is assumed to be a rectangular, of which the size is 8.4×7.2 in. The tire pressure is assumed to be the uniform pressure, of which the value is 100 psi.
- The movement of vehicles can be represented by consecutive loading steps in which the location of the loading areas are changed with time. For precision of the modelling, one contact area is divided into three parts in the moving direction. The length of each step equals the time vehicles travel at the distance of one part at a given speed.

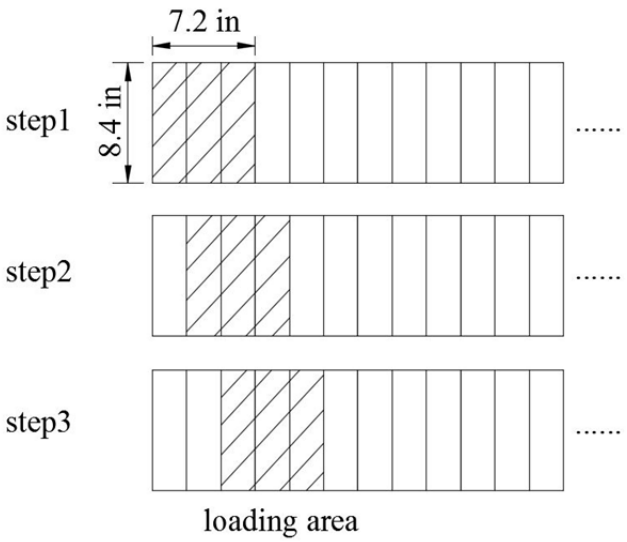

Figure 105. Simulation of Moving Load.

- The mesh size of the system is determined by dimensions of different sections. For loading sections, the mesh size coincides with width and length of the contact area. For other sections, mesh sizes are adjusted based on dimensions of sections to maintain a reasonable ratio for each element.

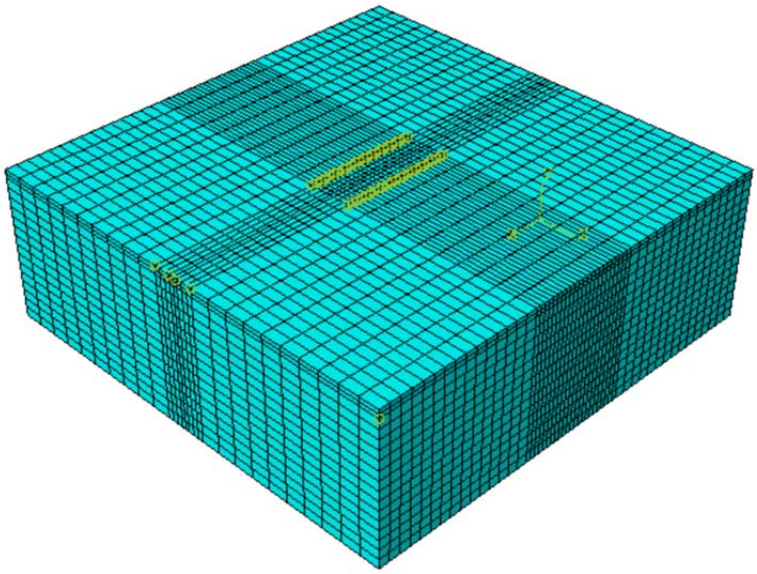

Figure 106. Numerical Model after Meshing.

Material Properties of Different Cases

Figure 106 shows four sets of different phase angles and modulus representing material properties in four stages in the life cycle of an asphalt surface. Such trends can be also applied in representing changes in properties of the base. Besides viscoelasticity of materials, basic information defining the surface and base inertial damping are input into ABAQUS.

Table 90. Basic Properties of Surface.

Basic Properties of Surface	Density (lbf s^2/in^4)	0.0002098
	Rayleigh Inertial Damping Ratio (Alpha)	0.93
	Rayleigh Inertial Damping Ratio (Beta)	0.0027

Table 91. Basic Properties of Base.

Basic Properties of Base	Density (lbf s^2/in^4)	0.0001798
	Rayleigh Inertial Damping Ratio (Alpha)	0.41
	Rayleigh Inertial Damping Ratio (Beta)	0.0061

Table 90 and Table 91 show basic inertial damping of asphalt surface and base for all four stages. The material properties of the asphalt surfaces in four stages reflect on their changing viscoelasticity as in Figure 106. Equation (31) expresses the modulus as time-dependent and Equation (38) ~ (41) describe frequency-related properties. By adjusting values in Prony series, different modulus and m can be obtained. For example, input instantaneous modulus and Prony series in ABAQUS as Table 92.

Table 92. Prony Series and Instantaneous Modulus.

i	tau	Gi,Ki,Ei	E_instantaneous(ksi)
1	4.09E-06	0.3620	4000
2	2.56E-04	0.3630	
3	7.71E-03	0.1765	
4	2.10E-01	0.0740	
5	3.88E+00	0.0165	
6	6.53E+01	0.0057	

Equation (34) provides time-dependent modulus using Prony series coefficients, which can be transformed into a Power function. Input different Prony series coefficients which can obtain different time-dependent functions, then compare relevant deflection basins. Appendix B shows three different types of surface.

Results of 3D FE Simulation

Six examples of the results of the computer simulations are listed below in Figure 107 to 32. More results are presented in Appendix.

1. Moving deflection basins for pavement with different surface layer material characteristics and constant base course material properties: the differences between surface materials reflect mainly on their values of modulus and m (E_1, m_1 are properties of surface, E_2, m_2 are properties of base). It can be seen from Figure 26 that the maximal deflection data within each basin does not change much even though the modulus varies, which can be explained by the fact that not only the modulus but also the value of m (or phase angle) determined the shape of the deflection basin (the value of maximal deflection and location where it is).

Hence, it is not enough to focus on the maximal deflection caused by static or slowly moving loads. The value of the static modulus cannot evaluate the current damaged conditions of pavements effectively.

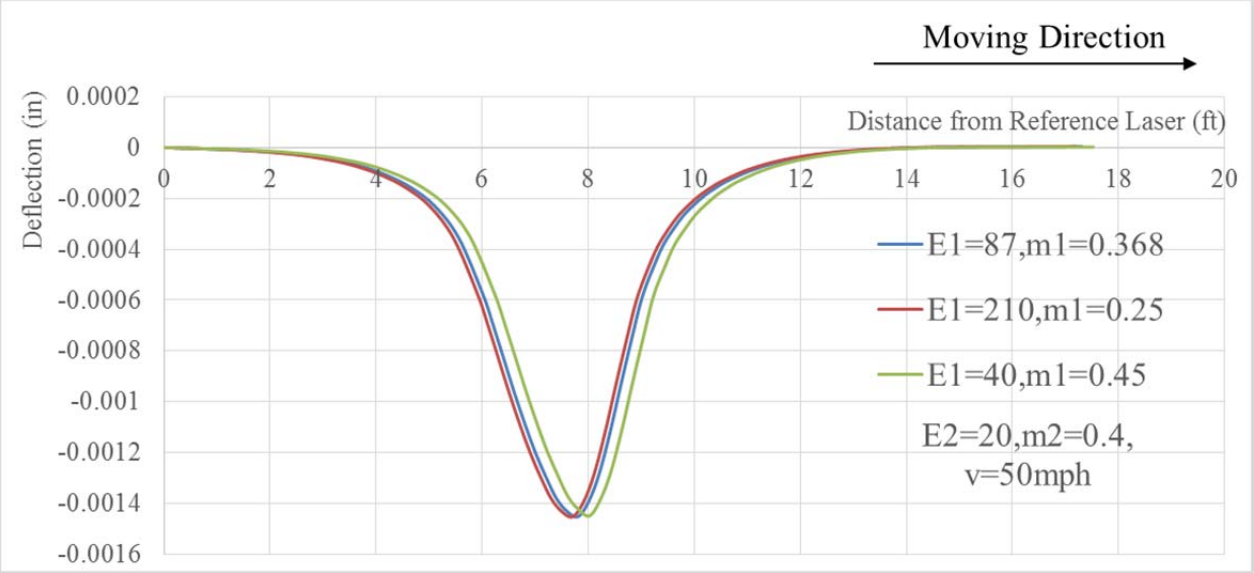

Figure 107. Deflection Basins of Different Surface Properties

2. Moving deflection basins for pavement with different supporting layer material characteristics and constant surface course material properties: the differences between surface materials reflect mainly on their values of modulus and m (E_1, m_1 are properties of surface, E_2, m_2 are properties of base). It can be seen from Figure 108 that the maximal deflection data within each basin does not happen in the case with the minimal modulus value, which also can be explained by the fact that not only the modulus but also the value of m (or phase angle) determined the shape of the deflection basin (the value of maximal deflection and location where it is).

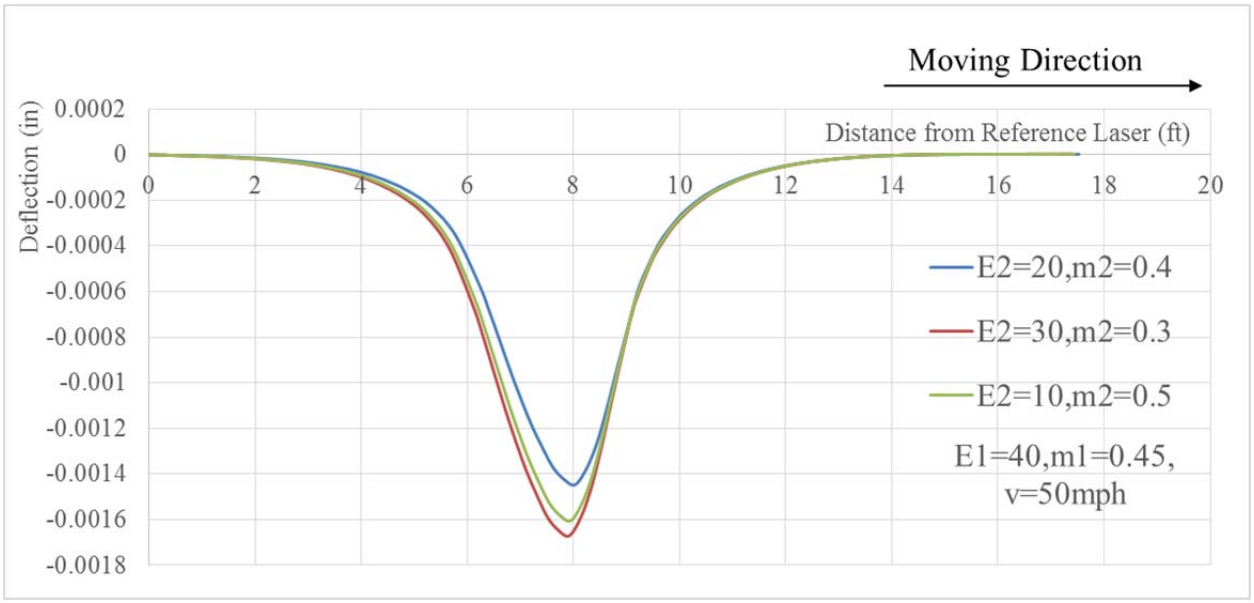

Figure 108. Deflection Basins of Different Base Properties.

3. By comparing deflection basins caused by loads of different velocities in Figure 109, velocities of moving loads affect not only the values of the deflection but also distance of the location where maximal deflection is relative to the reference laser.

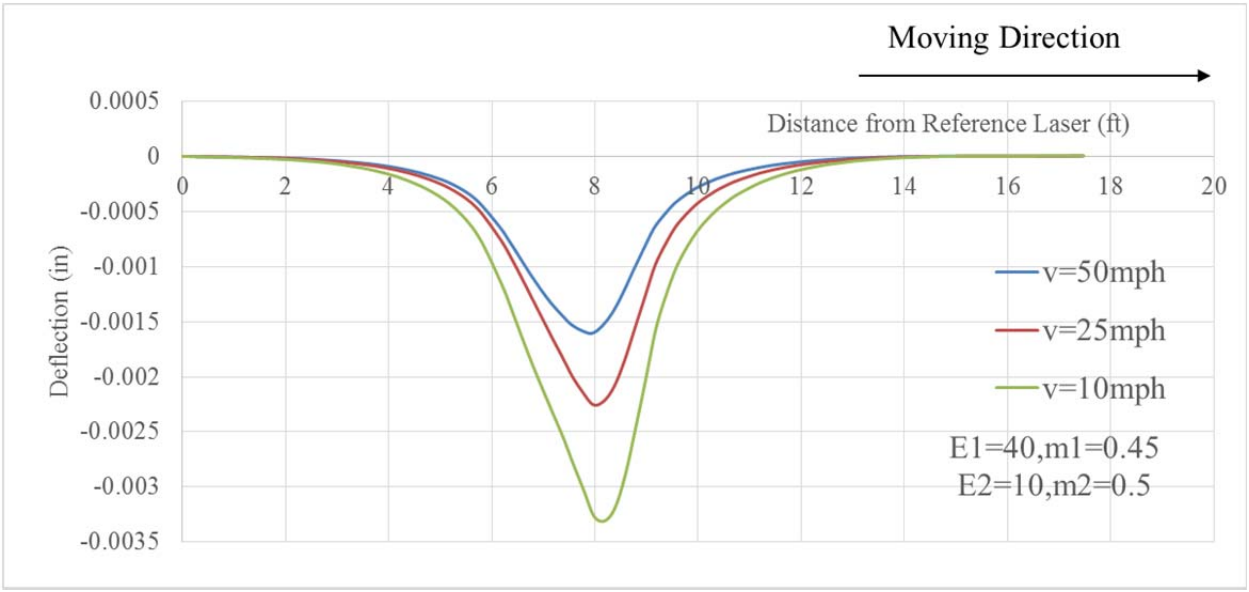

Figure 109. Deflection Basins of Different Moving Velocities.

Back-Calculation Analysis

Shape of Deflection Basin-Deflection and Slope

Figure 107–Figure 109 show deflection basins of pavement under moving load. From those graphs, distances between the locations where maximal deflection and zero deflection happen are

not equal. In order to obtain such asymmetric deflection shape using data measured by lasers set on the tow vehicle, Gumbel probability density curve is applied in this task.

$$W(x) = W_0 e^{-(\rho/x)^{\beta}} \tag{52}$$

where,

$W(x)$ – the cumulative probability curve of the Gumbel distribution.

x – the measuring distance.

$W_0,\ \rho,\ \beta$ – the model coefficients.

The shape of slope of Gumbel probability density curve is similar to the asymmetric deflection basin. Five measured data by lasers are enough to calculate coefficients $W_0,\ \rho,\ \beta$ which can be applied to obtain approximation function of the whole deflection basin. In Figure 107–Figure 109, the location of reference laser lags behind the moving vehicle. For curve fitting, it is set to be advanced to the vehicle.

Take four set of data from ABAQUS results and use 'nlinfit' commander in a mathematics software (MATLAB 2015), the model coefficients can be obtained. The fitting results are shown in Figure 110.

Table 93. Data from ABAQUS.

Distance from Reference Laser(ft)	Deflection(in)
6.038	-1.119120E-03
7.038	-1.373800E-03
8.038	-8.229610E-04
8.885	-3.530610E-04

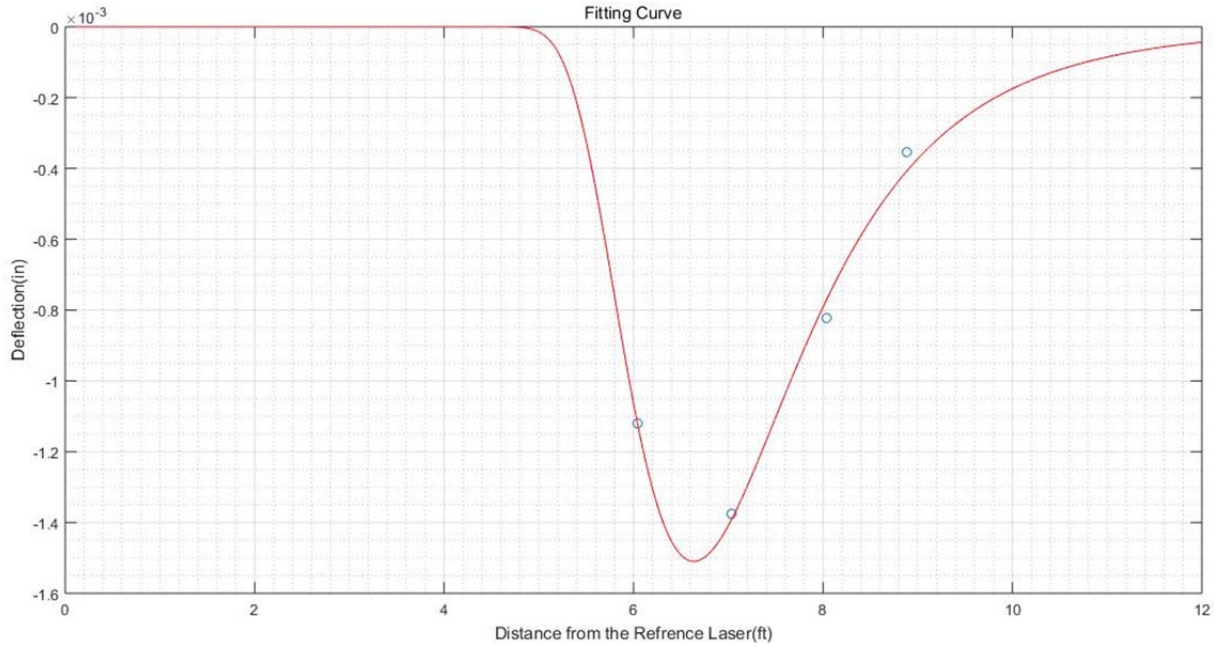

Figure 110. Fitting Curve Using MATLAB.

Table 94. Data Comparison.

Laser Number	Data from ABAQUS(in)	Data from Fitting Curve(in)	Relative Error(%)
1	-1.119120E-03	-1.115980E-03	0.281
2	-1.373800E-03	-1.389511E-03	1.144
3	-8.229610E-04	-7.703797E-04	6.389
4	-3.530610E-04	-4.074925E-04	15.417

After calculating coefficients W_0, ρ, β, the Gumbel probability density curve and the slope of the curve at any point can be determined.

Beam-on-Elastic Foundation Formulation Using Correspondence Principle

Beam-on-elastic foundation solution is introduced in previous sections, by transforming coefficients of the solution from elastic to viscoelastic, applying the approximate inverse Laplace Transform, the deflection of the points where lasers are set can be expressed as in Figure 111.

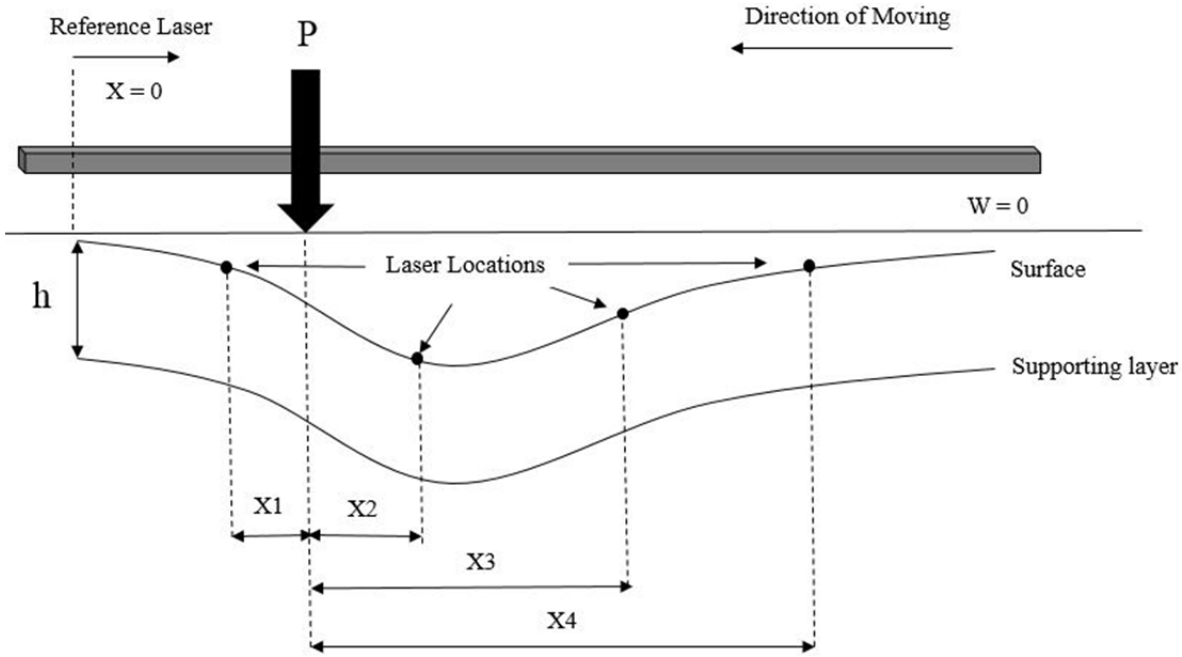

Figure 111. Locations of Lasers and Loads

h is the thickness of the surface, $x_1 \sim x_4$ are distances of lasers and the location where the load acts. Denote v as the velocity of the vehicle. Based on Hetenyi's solution (Hetenyi 1946), express the deflection values and the slope of the deflection basin under static loads as

$$w(x) = Ae^{-\beta x}\cos\beta x + Be^{-\beta x}\sin\beta x + q/k \tag{53}$$

$$w'(x) = \beta(B-A)e^{-\beta x}\cos\beta x - \beta(B+A)e^{-\beta x}\sin\beta x \tag{54}$$

then change terms β, k into ones in Equation (50) and (51) to obtain $w(x,t), w'(x,t)$,

$$w(x_i,t) \cong \left[s_i w(s_i,t) \right]_{s_i=1/2t_i} \tag{55}$$

$$w'(x_i,t) \cong \left[s_i w'(s_i,t) \right]_{s_i=1/2t_i} \tag{56}$$

$$t_i = \frac{x_i}{v} \tag{57}$$

Four lasers can provide data $w(x_1,t) \sim w(x_4,t)$, and the fitted Gumbel probability density curve can provide $w'(x_1,t) \sim w'(x_4,t)$. Eight data are enough for solving the unknown coefficients A, B, E_1, E_2, m_1, m_2.

The analysis described above also requires the thickness h of the pavement surface layer that can be determined with sufficient accuracy by an accompanying Ground Penetrating Radar (GPR) survey. Both the moving deflection basin and the GPR surface layer thickness will be coordinated with the on-board sub-meter accuracy of GPS equipment.

EQUIPMENT DEPLOYMENT

Figure 112 through Figure 114 show the current status of the laboratory testing facility. For the purpose of laboratory testing, the wood beam is steady enough to serve as the laser support beam. The project team made a movable steel carrier to hold each laser sensor, so it can move horizontally and vertically along the support beam. Figure 113 shows the data collection system including the laser sensor, power/Ethernet connection, and real-time data recording. The purchased laser sensor is found to be very sensitive and can measure the deformation at micron levels. In order to integrate all of the four laser sensors, a breakout board is needed. The project team has ordered the LMI Gocator Master 800 breakout board that is especially designed for Gocator laser sensors. After receiving it, the project team is able to finish the circuit of the data collection system, which is shown in Figure 113. Figure 114 shows the actuator that the project team purchased to exert cyclic loading.

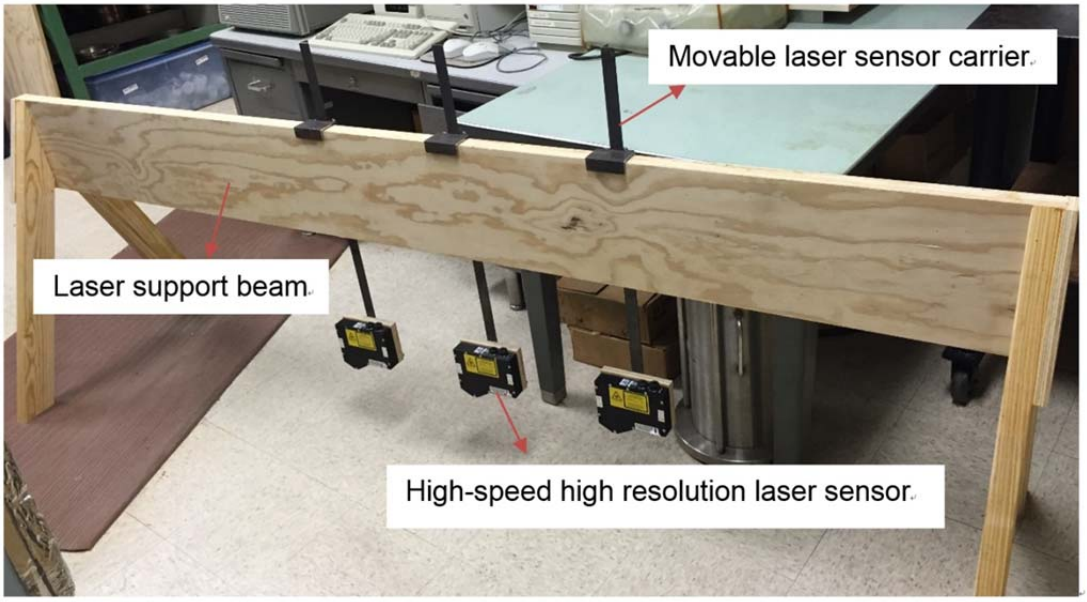

Figure 112. Laser Support Beam and Movable Carriers Constructed in the Laboratory.

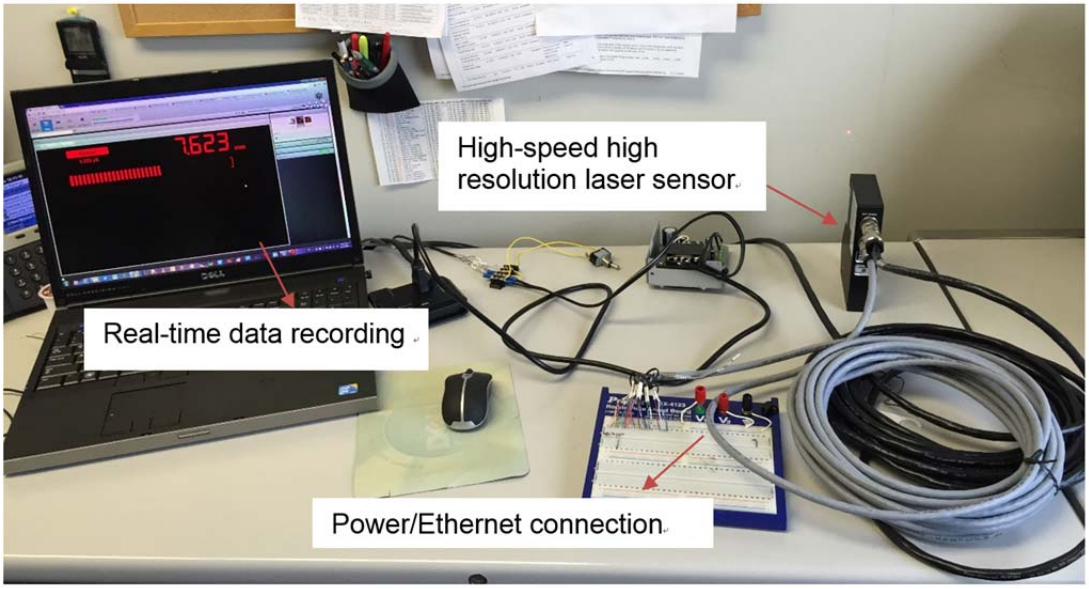

Figure 113. Laser Sensor Measurement Data Collection.

Figure 114. Solenoid-Actuated Loading Apparatus.

SUMMARY

Capabilities of New Concept

Based on the work that has been accomplished to this point, the project team made the following findings:

- The literature review reveals that the current deflection measurement systems generally consist of two types: static (like FWD) or quasi-static (like RDD traveling very slowly) and dynamic (like RWD, RDT and HSD that travel at 20 to 50 mph). Measurements of deflection vary by 20 to 50 percent between FWD, RDD, and RWD depending on pavement temperature, texture, stiffness, composition, and deflection magnitude. Only FWD (static) and RDD (quasit-static) measure deflection basins in the moving direction and are able to determine material properties. AWRD apparently measures a moving lateral basin transverse to the direction of travel which does not reveal the asymmetric shape of the moving longitudinal deflection basin from which layer material properties can be determined. Except for FWD, all the other devices are in different developmental stages.
- The project team proposed a highway speed deflection basin-pavement material property measuring system. It uses a new concept of measuring the shape of the deflection basin instead of just the values of a single deflection, based on which the viscoelastic properties of the pavement layers can be calculated in addition to the elastic properties in the existing back-calculation approaches that are used with the FWD.
- The analytical process for analyzing the results of the field moving deflection basin measurements has been completed and only needs to be programmed.
- It appears in our preliminary testing that all of the equipment has proven to be more than adequate to capture the field data at the expected rate of data collection. Furthermore, the resolution and sensitivity of the high speed high resolution lasers has proven to meet all of our requirements.

After delays in receiving the laser equipment, the project team has assembled the laboratory calibration equipment and is in position to make calibration measurements.

Financial Justifications

The annual cost of maintaining a serviceable State pavement network is the largest single cost item in the 10-year budget estimate by the Texas Department of Transportation, amounting to 35 percent of the total budget. The 10 year estimate for Preventative Maintenance and Rehabilitation is $12.6 Billion out of a State-wide ten year estimate of $35.5 Billion as shown in Table 95 and Figure 115.

Table 95. 2016–2025 UTP Funding Availability by Category.

Funding Category	2016-2025 UTP Funding (in Dollars)
1. Preventative Maintenance and Rehabilitation	$12,576,703,400
2. Metro and Urban Area Corridor Projects	$2,364,770,150
3. Non-traditionally Funded Transportation Projects	$5,443,480,000
4. Statewide Connectivity Corridor Projects	$603,416,750
5. Congestion Mitigation and Air Quality Improvement	$1,603,430,000
6. Structures Replacement and Rehabilitation	$3,000,000,000
7. Metropolitan Mobility and Rehabilitation	$2,955,680,000
8. Safety	$1,858,400,000
9. Transportation Enhancements	$485,960,000
10. Supplemental Transportation Projects	$660,120,000
11. District Discretionary	$872,866,700
12. Strategic Priority	$3,085,083,000
Total	$35,509,910,000

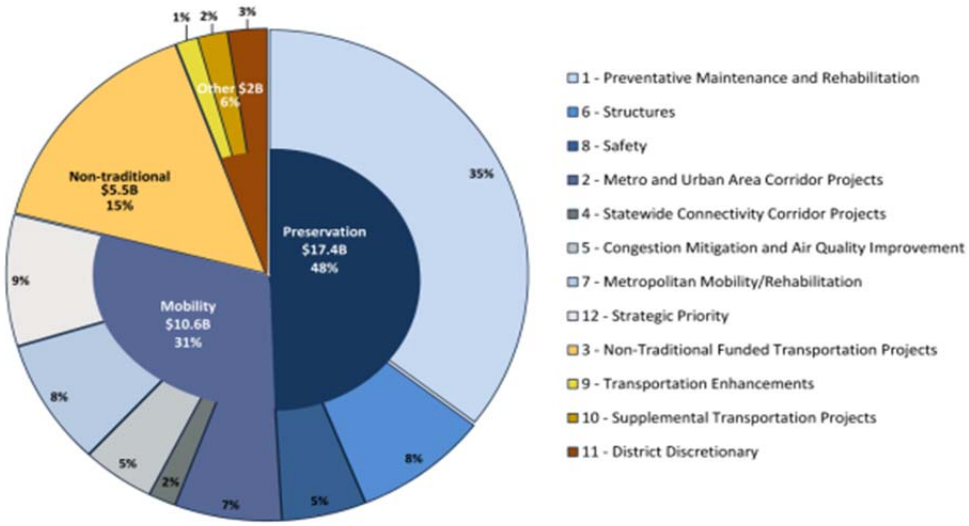

Figure 115. UTP Funding Overview by Category.

Estimating the annual cost of such a large program requires the knowledge of the cost patterns that occur to maintenance and rehabilitation processes. A simple example of this kind of process is the replacement of light bulbs. If you started out with 100 light bulbs and replaced each one as it burned out, you would find that the collection of light bulbs would have a distribution of the life of a light bulb like the picture that is shown in Figure 116. Some would burnout quickly and others would last longer with the bulk of the light bulbs wearing out somewhere in between the extremes.

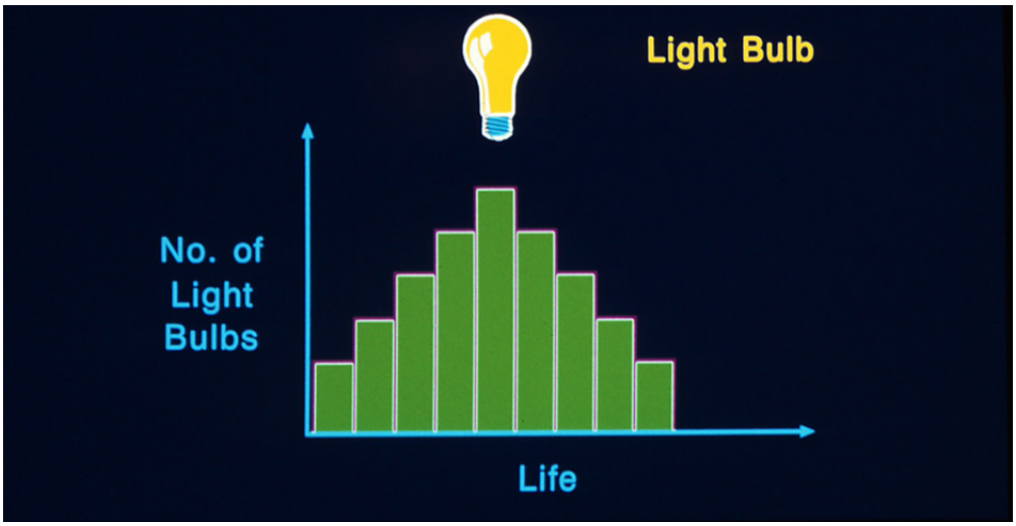

Figure 116. Life Distribution of One Light Bulb.

If you kept up with the number of bulbs that you replaced over a long period of time, you could use the life-time distribution to predict how many light bulbs that you could expect to replace in any given time interval. You would find that the number of such light bulbs will oscillate around a stable mean as shown in Figure 117.

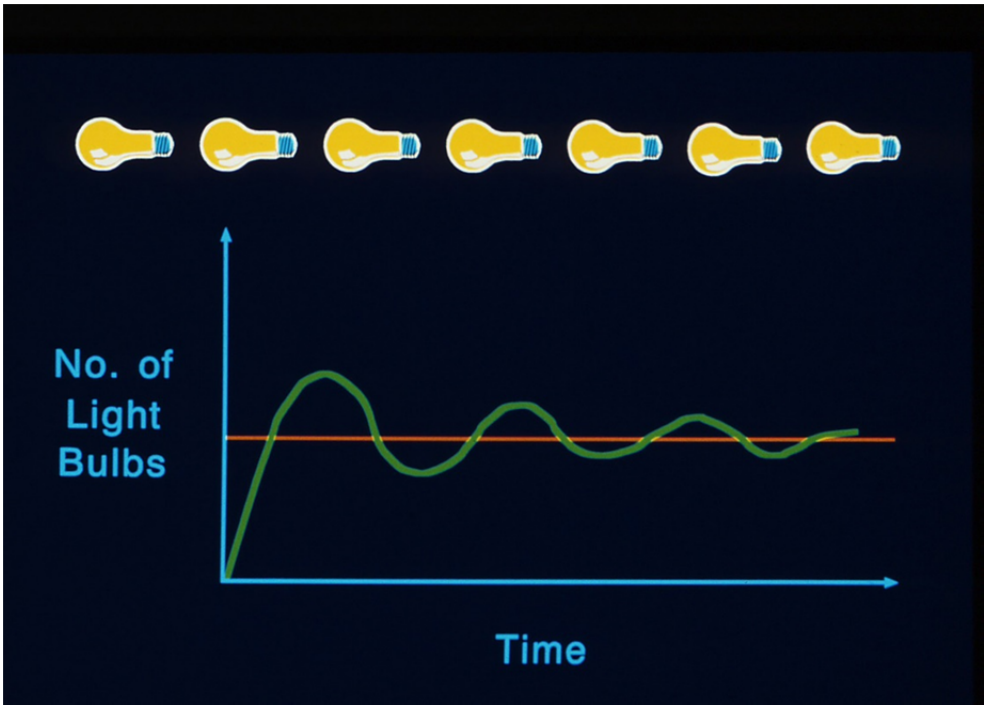

Figure 117. Number of Light Bulbs Replaced over Time.

The annual cost patterns for maintenance and rehabilitation are more complicated than the case of light bulbs because you have to take into account the decreasing annual cost of the initial construction cost as well as the increasing annual cost of maintenance or rehabilitation. The sum of the two is the annual cost of keeping the pavement in service and it forms a U-shaped curve, as shown in the following figure. The bottom of the U marks the best time and the best thing to do to have the most cost effective maintenance and rehabilitation management strategy. Delaying any action beyond the bottom of the U-shaped curve is deferred maintenance. The longer it is delayed, the more the annual costs mount up.

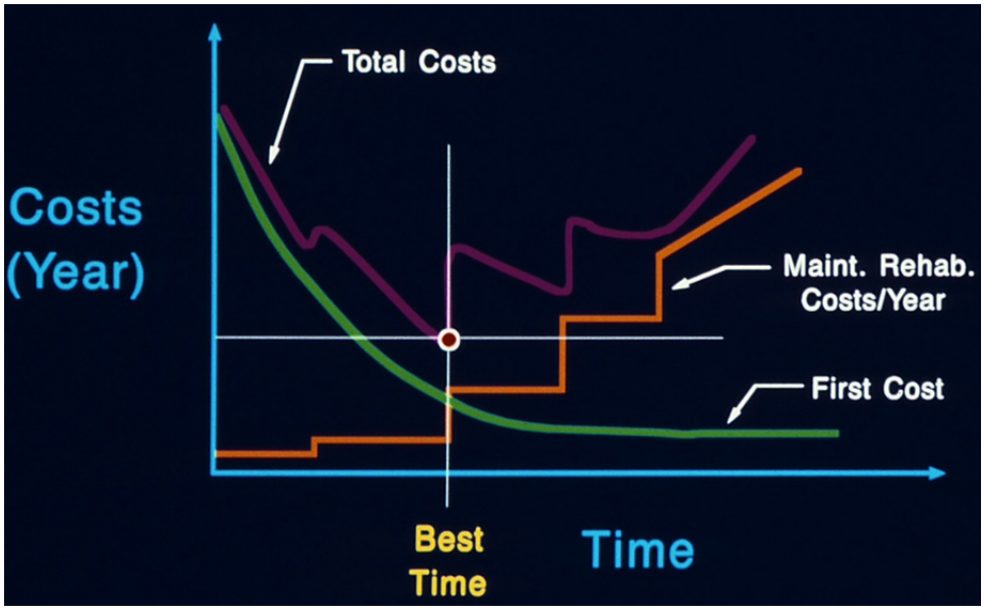

Figure 118. Infrastructure Cost Patterns.

The long-term cost patterns of the two management strategies of using deferred maintenance and using the minimum cost strategy are illustrated in the following figure. Both annual cost patterns will oscillate. However, the annual cost of the deferred maintenance strategy will continue to increase with time while the minimum cost strategy remains stable. It is estimated that at the present age of the Texas state pavement network, the annual cost of the deferred maintenance strategy is roughly 40 percent greater than the minimum cost strategy. At the current rate of annual expenditure in Texas, the savings that could be realized with a minimum cost strategy is approximately $503,000,000 per year. The problem with the minimum cost strategy is that it requires advance warning before a pavement reaches the minimum of the annual cost curve so that plans could be made and funds allocated prior to reaching the optimum annual cost point. As explained in the text above the ability to pick up the phase angle in both the surface and the supporting layers while traveling at highway speeds is the key to being able to give a reliable advance warning. Based on our current knowledge of the rate of change of the phase angle of asphalt mixtures in the field, it is estimated that this method will provide an advance warning of around three years.

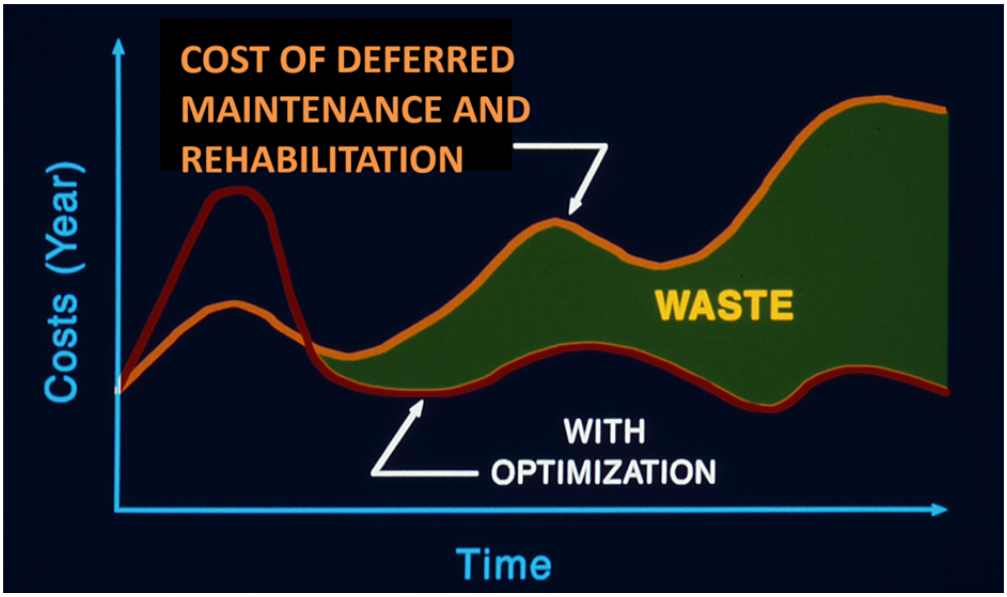

Figure 119. Infrastructure System Costs.

It will take a number of years to develop this Advance Warning System into a practical operating mode. Phase II will build and thoroughly evaluate a prototype vehicle complete with Ground Penetrating Radar (GPR) and Global Positioning System (GPS). The evaluation will also include the analytical software, the laser measuring system and the data acquisition system. Phase II will try out this Advance Warning System on a variety of pavements in different conditions. With all of the bugs worked out, Phase III will implement the developed system. After it enters the implementation mode, this Advance Warning System will begin to realize some of the cost savings in the Preventive Maintenance and Rehabilitation process. With complete coverage of the State network lane-miles in a single year with two crews and the widespread use of advance warning in the planning, fund programming and construction processes, more of the expected savings from the use of the minimum cost strategy will be realized.

Recommendations for Future Work

1. Install Laser-Based Deflection Measuring Devices

The Performing Agency shall design and install a laser-based system to accurately and efficiently measure the deflections. In this task, the Performing Agency shall:

- Install all of triangular lasers and solenoid loading apparatus on the lab loading setup.
- Examine the ability of the devices to measure deflections rapidly and simultaneously.
- Demonstrate the feasibility of the laser-based devices to measure the highway-speed pavement deflections.

2. Build a Highway-Speed Deflection Measuring System

The Performing Agency shall build a highway-speed measuring system that will produce continuous deflection profile for a pavement. In this subtask, the Performing Agency shall:

- Design a highway-speed measuring system (See Figure 1), which includes a tow vehicle equipped with a ground-penetrating radar and a global positioning system, and a trailer equipped with a weight adjustment system and five laser-based deflection measuring devices. Note that the magnetic suspension devices will be used to stabilize the vibrations on the laser support bar in the trailer.
- Acquire equipment for the trailer.
- Build the trailer and install the laser-based deflection measuring devices.

3. Develop a New Modulus Backcalculation System

The Performing Agency shall develop a software product to backcalculate the moduli of pavement layers using the measured highway-speed pavement deflections. In this subtask, the Performing Agency shall:

- Finalize the backcalculation analytical process.
- Make ABAQUS runs using pavement layer properties for intact and deteriorated pavements to verify the accuracy of the backcalculation process.
- Decide whether we need to convert the analytical backcalculation process into artificial neural network models.
- Develop a final version of new modulus backcalculation software.

4. Run Trials on Full-Scale Flexible and Rigid Pavements

The Performing Agency shall run trials on the full-scale flexible and rigid pavements to examine the efficiency and accuracy of the highway-speed deflection measuring system. In this subtask, the Performing Agency shall:

- Run trials on full-scale flexible and rigid pavements using the highway-speed deflection measuring system to generate the continuous deflection profiles.
- Backcalculate the moduli of pavement layers from the obtained deflection profiles using the new modulus backcalculation software.
- Conduct the laboratory modulus tests on at least 10 drilled cores from the full-scale pavements.
- Calibrate the new modulus backcalculation system to minimize the prediction error from the laboratory-measured modulus data.

5. Implement the Highway-Speed Deflection Measuring System to the In-Service Pavement Sections in Texas

The Performing Agency shall implement the highway-speed deflection measuring system to the in-service pavement sections in Texas. In this subtask, the Performing Agency shall:

- Conduct the highway-speed deflection measurements on at least 5 in-service pavement sections (e.g., farm to market roads) in Texas. The Performing Agency shall evaluate at least 1,000 ft in length for each in-service pavement section.
- Backcalculate the moduli of pavement layers from the obtained deflection profiles using the calibrated new modulus backcalculation software.

- Conduct the laboratory modulus tests on at least 5 drilled cores from each in-service pavement section.
- Evaluate the prediction error from the laboratory-measured modulus data.

REFERENCES

ABAQUS. *ABAQUS, Finite Element Computer Program*, Hilbert, Karlsson and Soreson, Inc, 2010.

Andr´en, P. and C. A. Lenngren. Evaluating pavement layer properties with a high-speed rolling deflectometer. In A. K. Mal (Ed.), *Nondestructive Evaluation of Aging Aircraft, Airports and Aerospace Hardware IV Proceedings*, Volume 3994, Newport Beach, CA, USA, pp. 192–200. SPIE—The International Society for Optical Engineering, 2000.

Arora, J., Nazarian, S., and Tandon, V. *Continuous Deflection Testing of Highways at Traffic Speeds*. Research Report 0-4380-1, Center for Transportation Infrastructure Systems, The University of Texas at EI Paso, EI Paso, 2006.

Biot MA. *Bending of An Infinite Beam on An Elastic Foundation*. Zeitschrift fiir Angewandte Maihematik und Mechanik. 1922 Jun;2(3):165-84.

Briggs, R. C., Johnson, R. F., Stubstad, R. N., and Pierce, L. *A Comparison of the Rolling Weight Deflectometer with the Falling Weight Deflectometer*. Nondestructive Testing of Pavements and Backcalculation of Moduli: Third Volume, ASTM STP 1375, S. D. Tayabji and E. O. Lukanen, Eds., American Society for Testing and Materials, West, Conshohocken, PA, 1999.

Cost, Thomas L. *Approximate Laplace Transform Inversions in Viscoelastic Stress Analysis*. AIAA Journal 2, no. 12 (1964): 2157-2166.

Gay, Derek A. *Development of a Predictive Model for Pavement Roughness on Expansive Clay*. Ph.D. dissertation, Texas A&M University, 1994.

Hall, Jim W., and Steele, Douglas A. *Rolling Wheel Deflectometer (RWD) Demonstration and Comparison to Other Devices in Texas.* ERES Consultants, 2004.

Herr W, Halla JW. Jr, White TD, Johnson W. *Continuous Deflection Basin Measurement and Backcalculation under a Rolling Wheel Load Using Scanning Laser Technology.* Proc. of The Transportation Congress, Vol. 1, pp. 600-611.

Hetenyi, M. *Beams on Elastic Foundation*. The University of Michigan Press, Ann Arbor, 1946.

Hildebrand, Gregers, and Rasmussen, Søren. *Development of a High Speed Deflectograph*, Road Directorate, Denmark, 2002.

Lakes, Roderic S. *Viscoelastic Materials*. Cambridge University Press, 2009.

LMI Technologies. *Gocator All-in-One 3D Smart Sensor*. http://lmi3d.com/sites/default/files/BROCHURE_Gocator_3D-Smart-Sensors2.4_WEB.pdf. Accessed December 10, 2015.

Lytton, R., *Backcalculation of Pavement Layer Properties*, Nondestructive Testing of Pavements and Backcalculation of Moduli, STP19797S, G. Baladi and A. Bush, Ed., ASTM International, West Conshohocken, PA, 1989, pp. 7-38.

MATLAB. R2015a, The MathWorks Inc., Natick, MA, 2015.

Schapery, R. A. A theory of crack initiation and growth in viscoelastic media. *International Journal of Fracture* 11.1, 1975, pp. 141-159.
Schapery, R.A. *Correspondence Principles and a Generalized J Integral for Large Deformation and Fracture Analysis of Viscoelastic Media*. International Journal of Fracture, Vol. 25, No. 3, 1984, pp. 195–223.
Terzaghi K. *Evaluation of Coefficients of Subgrade Reaction*. Geotechnique. 1955 Dec;5(4):297 326.
TxDOT, *Technical Advisory: Frequently Asked Questions about the Falling Weight Deflectometer (FWD).* ftp://ftp.dot.state.tx.us/pub/txdot-info/cst/tips/falling_weight_deflectometer.pdf. Accessed December 10, 2015.
Vesic AB. *Bending of Beams Resting on Isotropic Elastic Solid*. Journal of the Engineering Mechanics Division. 1961 Apr;87(2):35-54.
Wineman, Alan S., and Kumbakonam Ramamani Rajagopal. *Mechanical Response of Polymers: An Introduction*. Cambridge University Press, 2000.

APPENDIX A. COMPARISON OF DEFLECTION BASINS OF DIFFERENT SURFACES, BASES AND VELOCITIES OF LOADS

Three graphs below are deflection basins comparison of constant base properties and different surface properties under a high-speed moving load.

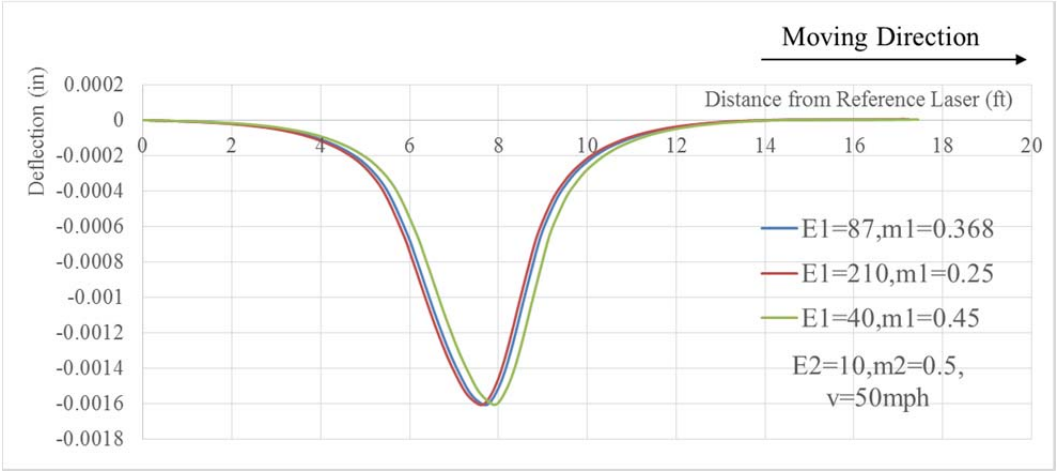

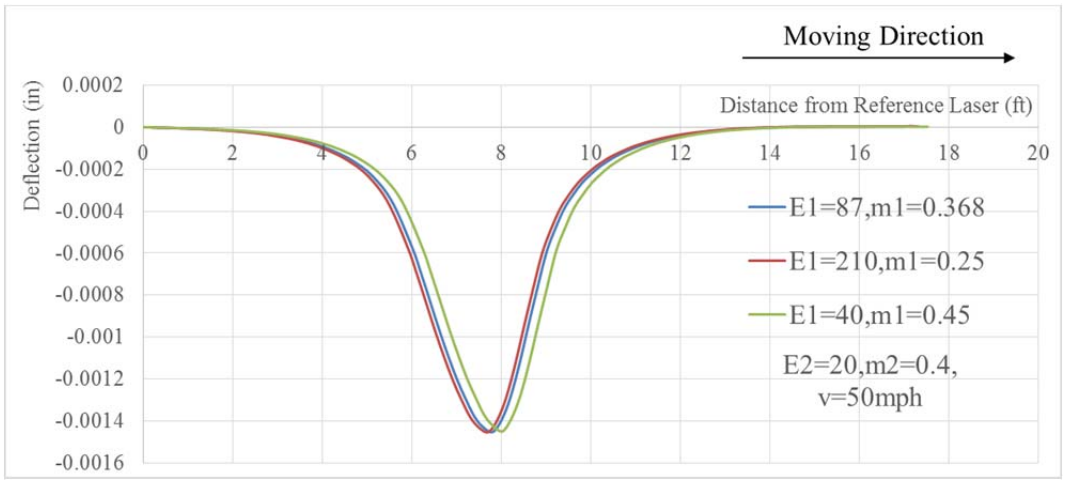

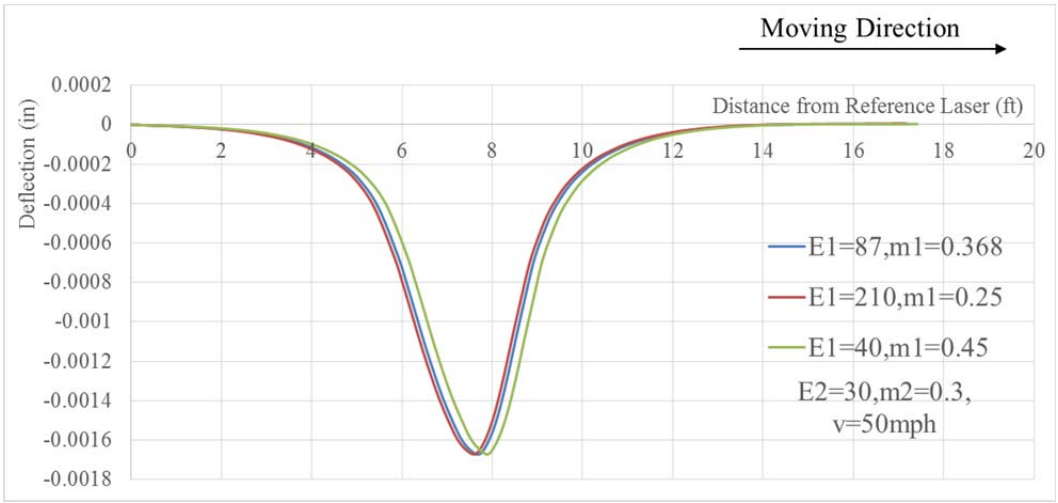

Three graphs below are deflection basins comparison of constant surface properties and different base properties under a high-speed moving load.

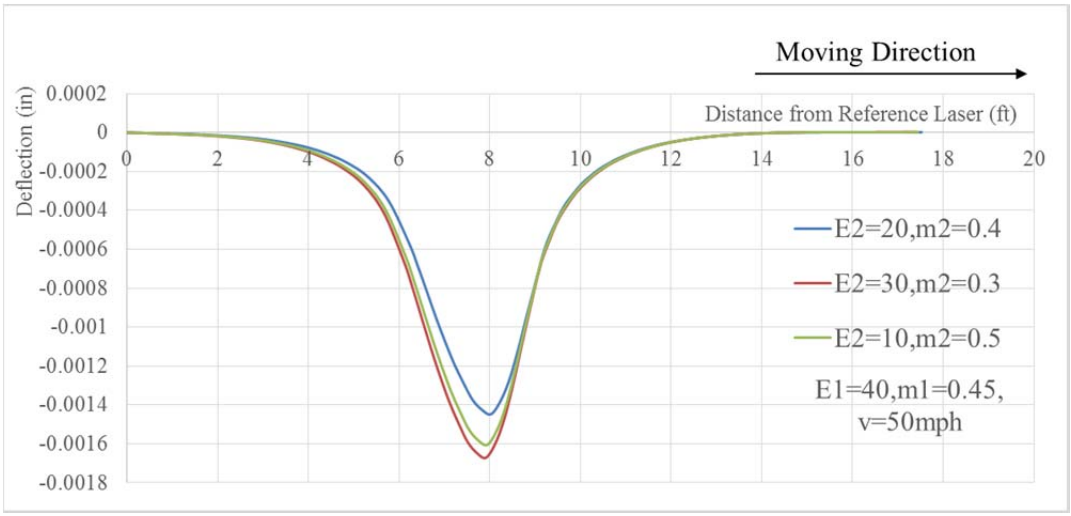

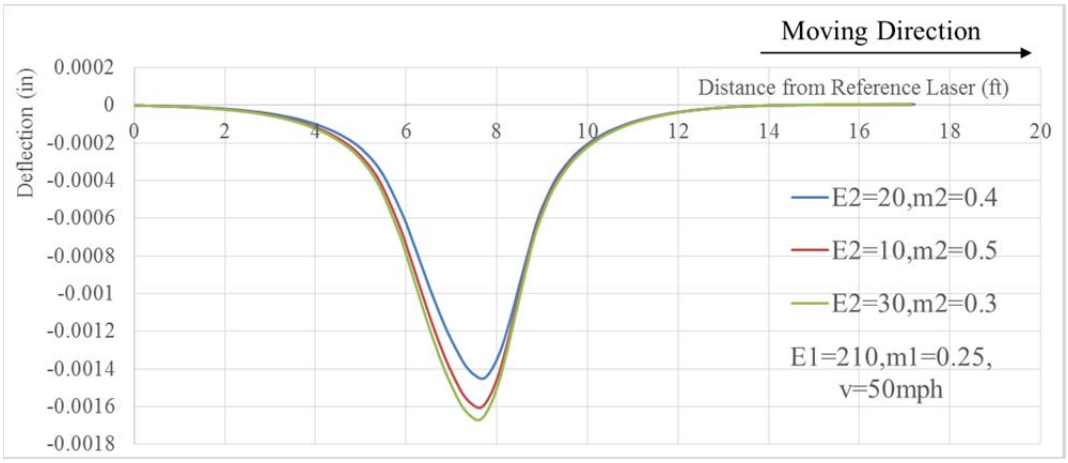

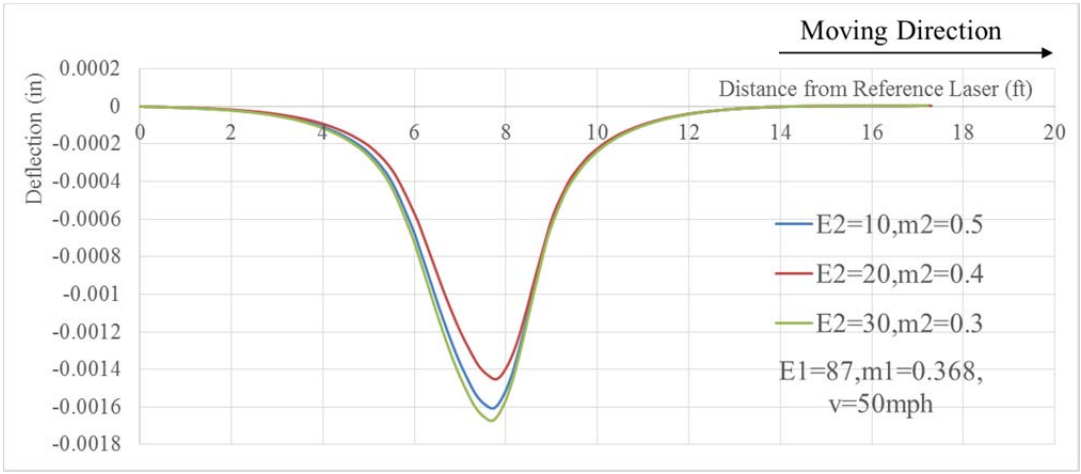

Nine graphs below are deflection basins comparison of constant surface and base properties under moving loads with different speeds.

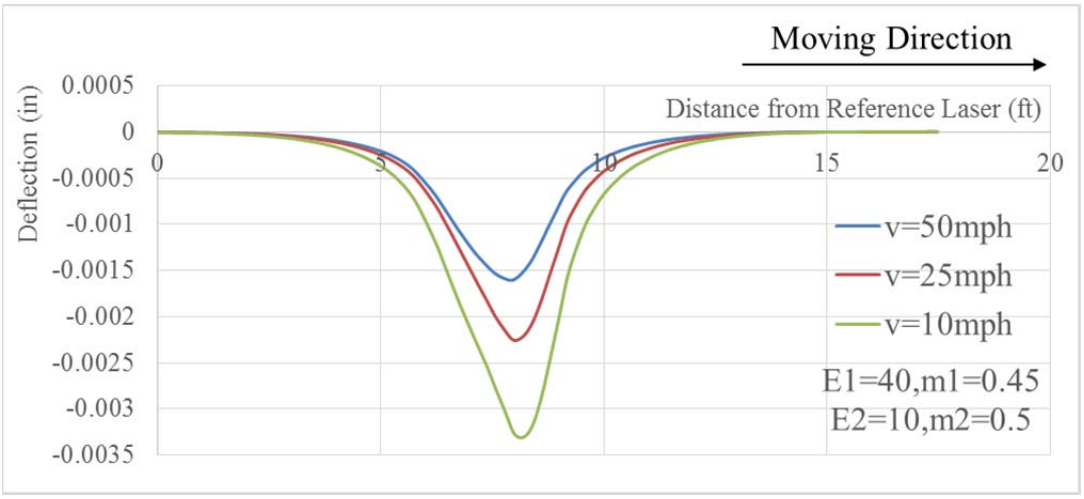
Moving Direction
Distance from Reference Laser (ft)
Deflection (in)
0.0005
0
-0.0005
-0.001
-0.0015
-0.002
-0.0025
-0.003
-0.0035
0
5
10
15
20
v=50mph
v=25mph
v=10mph
E1=40,m1=0.45
E2=10,m2=0.5

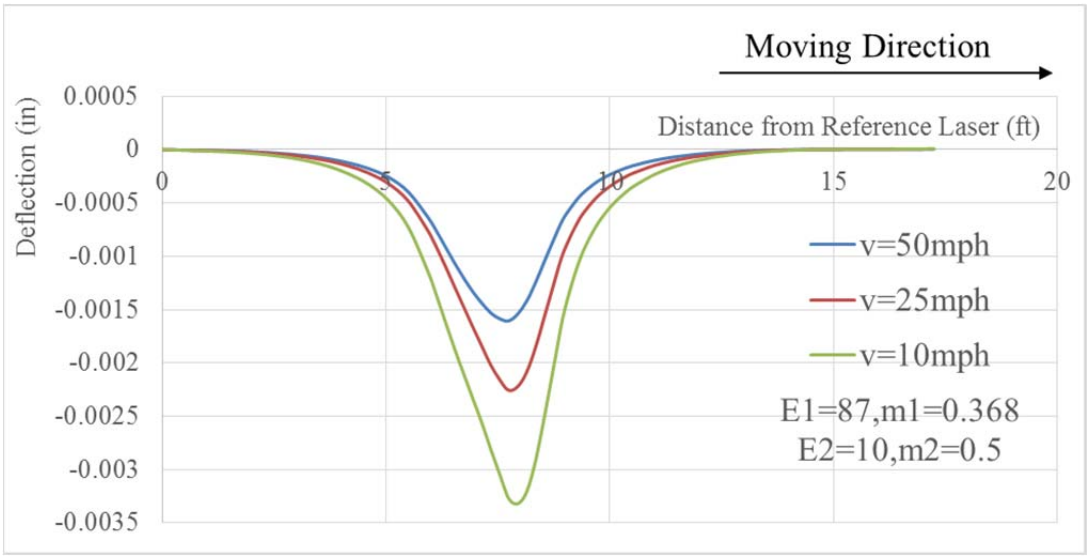
Moving Direction
Distance from Reference Laser (ft)
Deflection (in)
0.0005
0
-0.0005
-0.001
-0.0015
-0.002
-0.0025
-0.003
-0.0035
0
5
10
15
20
v=50mph
v=25mph
v=10mph
E1=87,m1=0.368
E2=10,m2=0.5

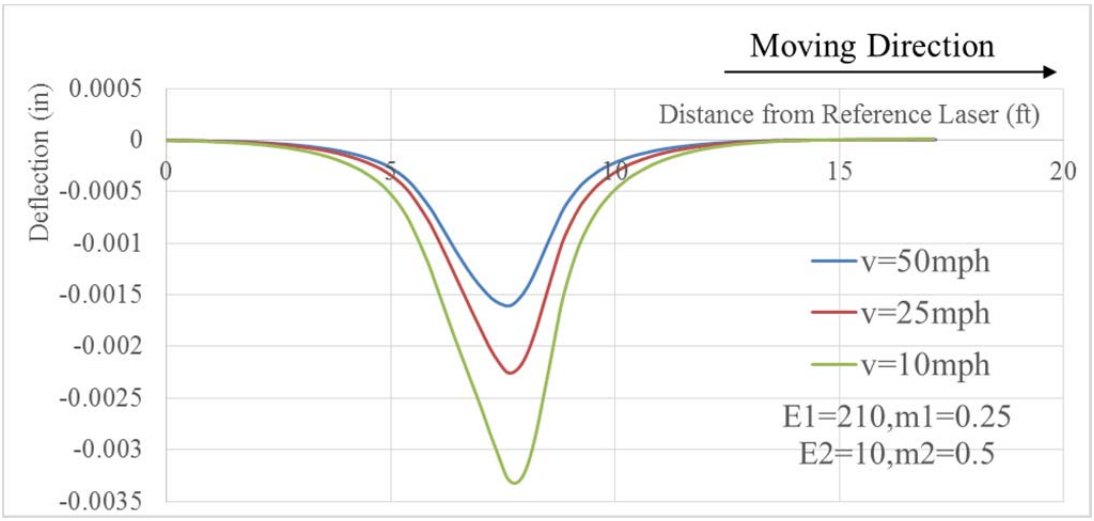
Moving Direction
Distance from Reference Laser (ft)
Deflection (in)
0.0005
0
-0.0005
-0.001
-0.0015
-0.002
-0.0025
-0.003
-0.0035
0
5
10
15
20
v=50mph
v=25mph
v=10mph
E1=210,m1=0.25
E2=10,m2=0.5

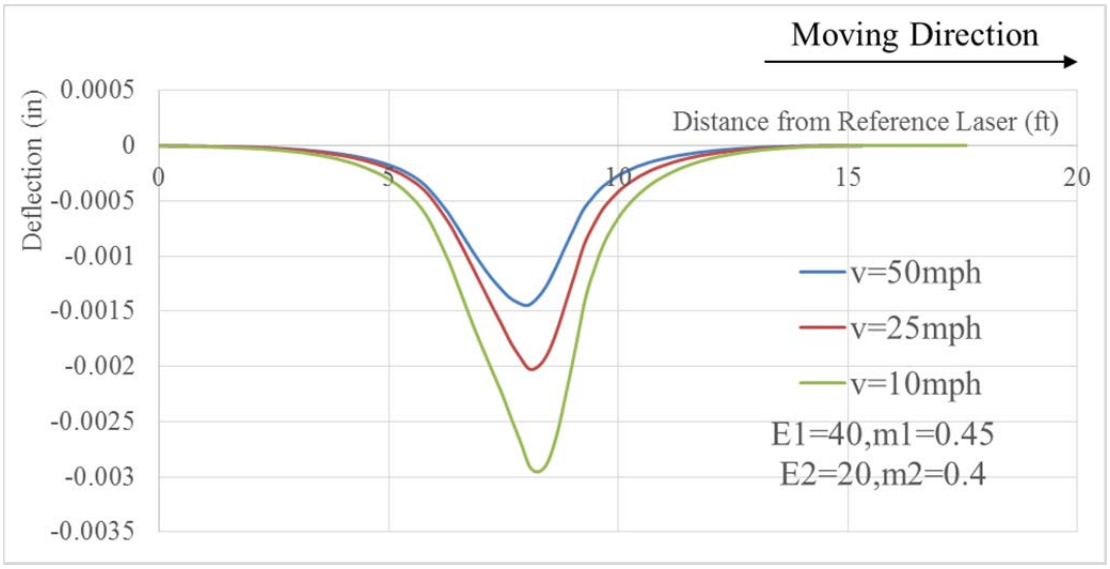
Moving Direction
Deflection (in)
0.0005
0
-0.0005
-0.001
-0.0015
-0.002
-0.0025
-0.003
-0.0035
Distance from Reference Laser (ft)
0
5
10
15
20
v=50mph
v=25mph
v=10mph
E1=40,m1=0.45
E2=20,m2=0.4

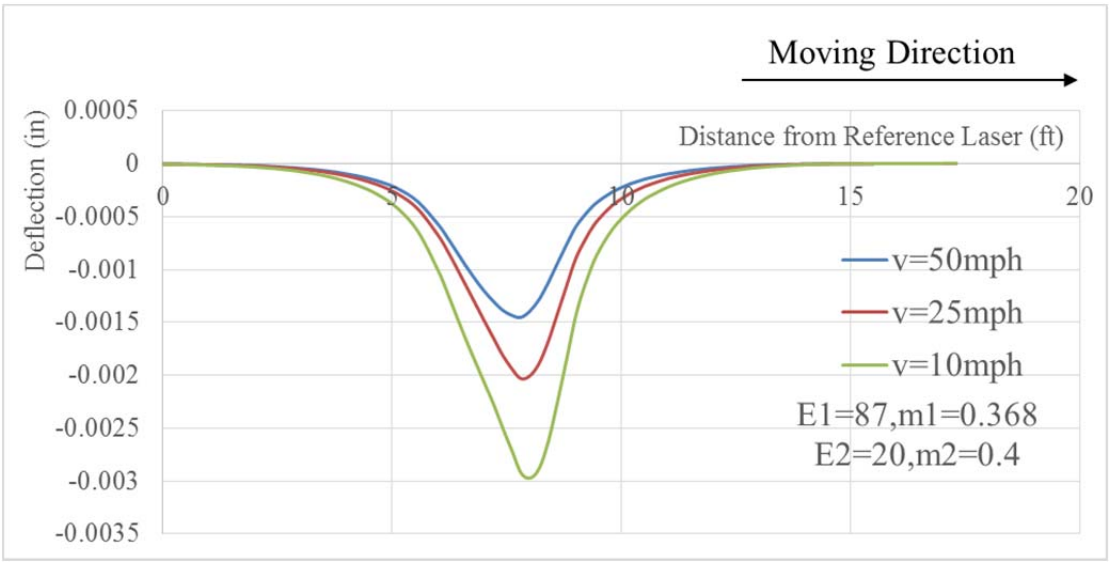
Moving Direction
Deflection (in)
0.0005
0
-0.0005
-0.001
-0.0015
-0.002
-0.0025
-0.003
-0.0035
Distance from Reference Laser (ft)
0
5
10
15
20
v=50mph
v=25mph
v=10mph
E1=87,m1=0.368
E2=20,m2=0.4

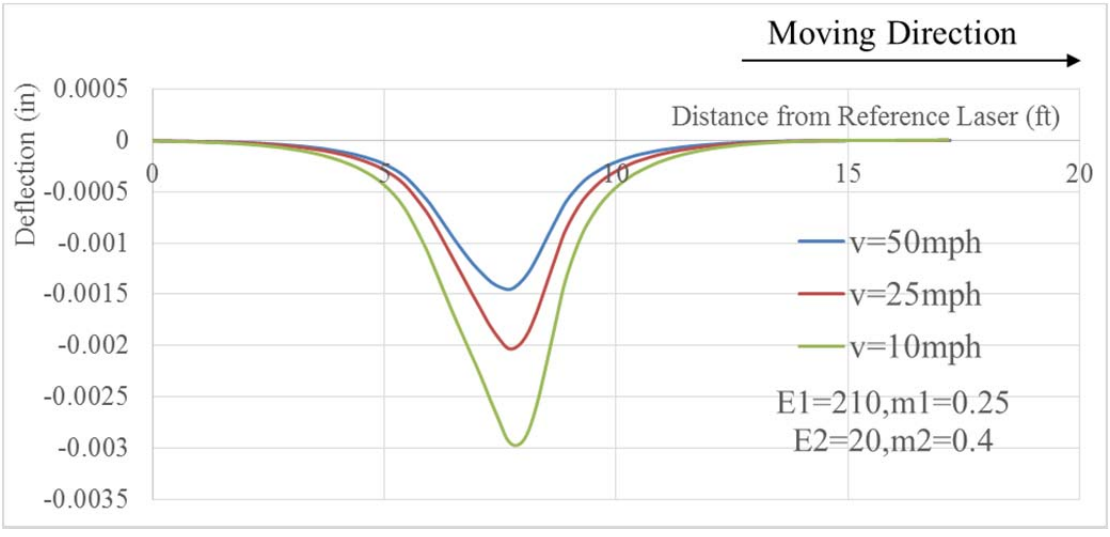
Moving Direction
Deflection (in)
0.0005
0
-0.0005
-0.001
-0.0015
-0.002
-0.0025
-0.003
-0.0035
Distance from Reference Laser (ft)
0
5
10
15
20
v=50mph
v=25mph
v=10mph
E1=210,m1=0.25
E2=20,m2=0.4

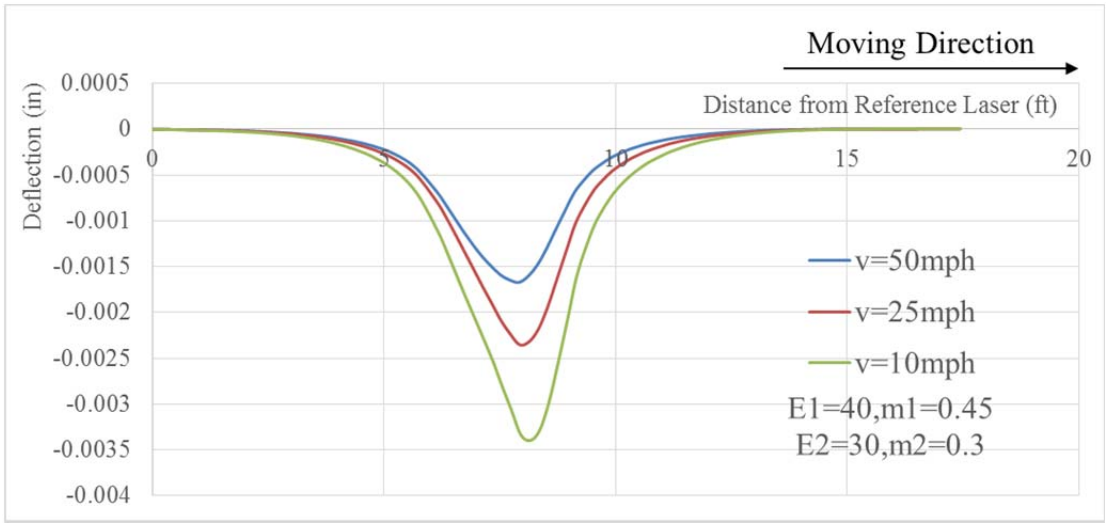
Moving Direction
Distance from Reference Laser (ft)
Deflection (in)
0.0005
0
-0.0005
-0.001
-0.0015
-0.002
-0.0025
-0.003
-0.0035
-0.004
0
5
10
15
20
v=50mph
v=25mph
v=10mph
E1=40,m1=0.45
E2=30,m2=0.3

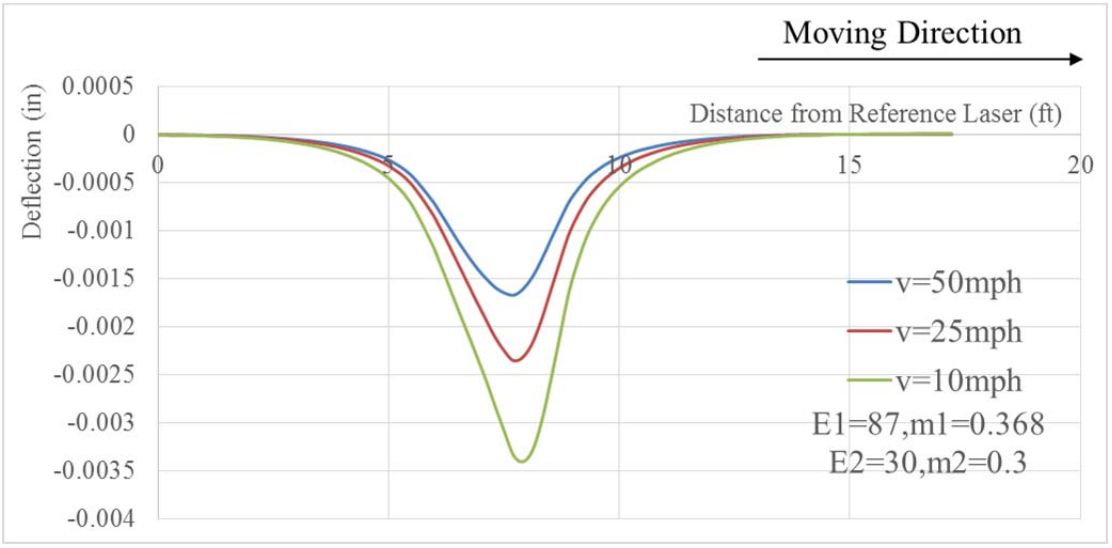
Moving Direction
Distance from Reference Laser (ft)
Deflection (in)
0.0005
0
-0.0005
-0.001
-0.0015
-0.002
-0.0025
-0.003
-0.0035
-0.004
0
5
10
15
20
v=50mph
v=25mph
v=10mph
E1=87,m1=0.368
E2=30,m2=0.3

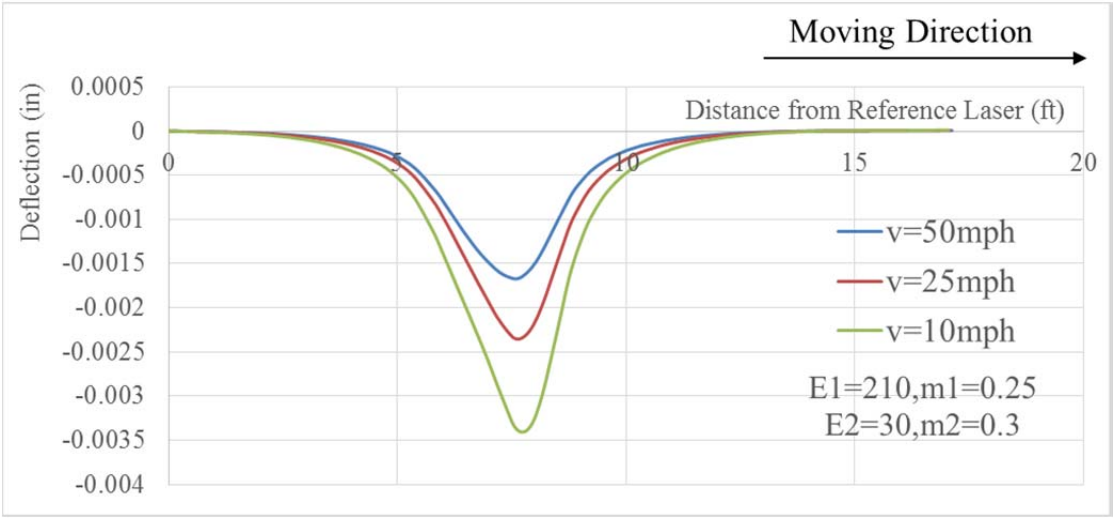
Moving Direction
Distance from Reference Laser (ft)
Deflection (in)
0.0005
0
-0.0005
-0.001
-0.0015
-0.002
-0.0025
-0.003
-0.0035
-0.004
0
5
10
15
20
v=50mph
v=25mph
v=10mph
E1=210,m1=0.25
E2=30,m2=0.3

APPENDIX B. TABLES OF PRONY SERIES COEFFICIENTS AND FITTED POWER FUNCTIONS OF SURFACE LAYERS

Three types of surface properties are given below. Based on the information lasted in tables, the fitting equations of time-dependent modulus in the Power law form are shown in the graphs.

i	tau	Gi,Ki,Ei	E_instantaneous(ksi)
1	4.09E-06	0.3649	3000
2	2.56E-04	0.3631	
3	8.00E-03	0.1765	
4	2.10E-01	0.0750	
5	3.88E+00	0.0164	
6	6.53E+01	0.0040	

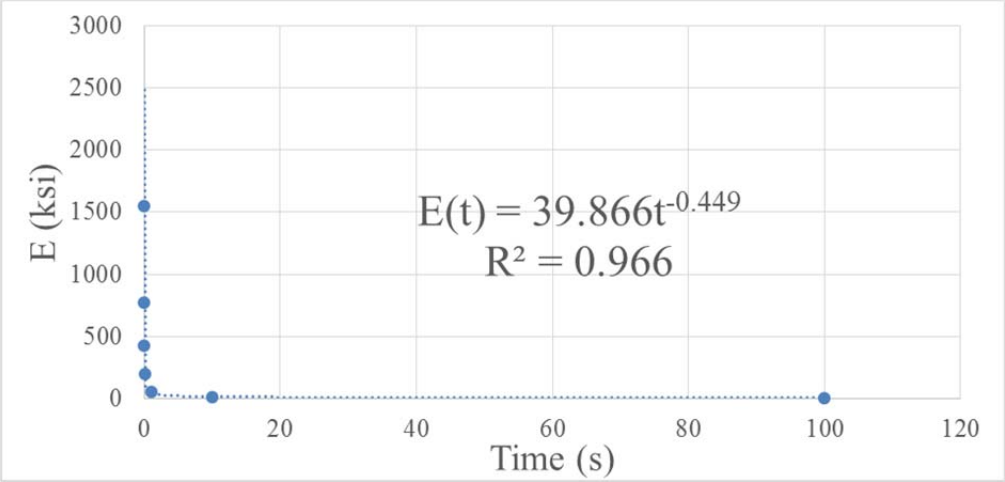

i	tau	Gi,Ki,Ei	E_instantaneous(ksi)
1	4.09E-06	0.3620	4000
2	2.56E-04	0.3630	
3	7.71E-03	0.1765	
4	2.10E-01	0.0740	
5	3.88E+00	0.0165	
6	6.53E+01	0.0057	

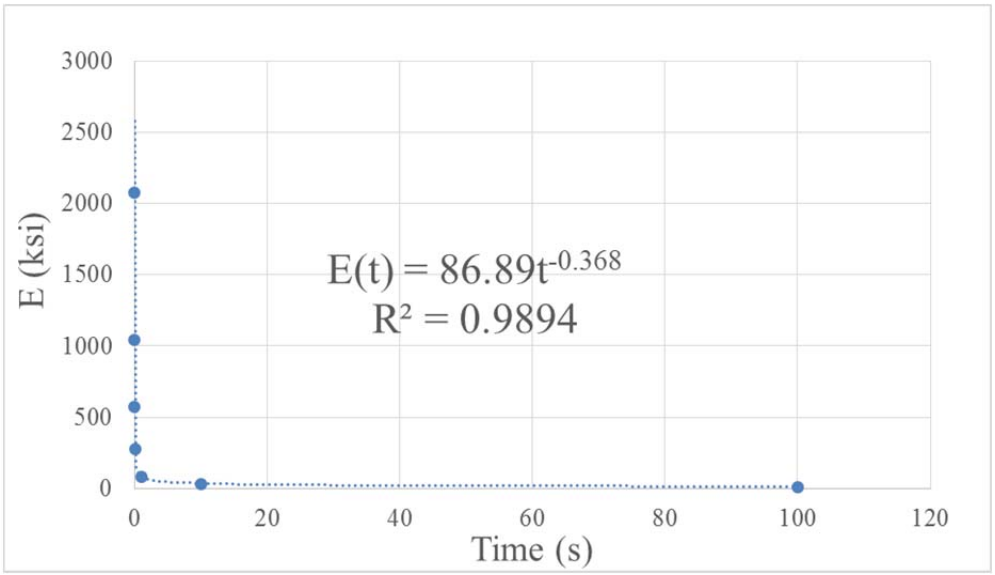

i	tau	Gi,Ki,Ei	E_instantaneous(ksi)
1	4.09E-06	0.3620	4500
2	2.56E-04	0.3590	
3	7.71E-03	0.1710	
4	2.10E-01	0.0690	
5	3.88E+00	0.0155	
6	6.53E+01	0.0055	

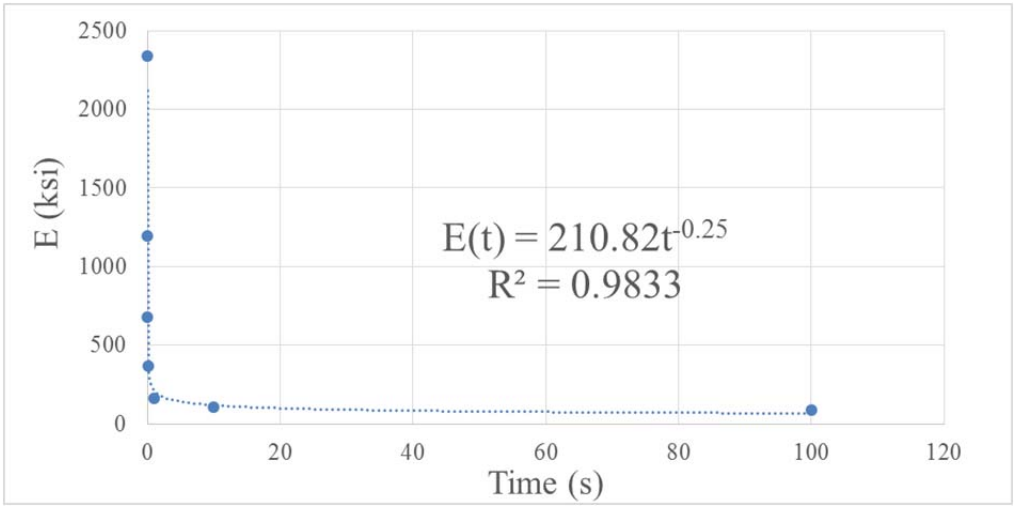

CHAPTER 6. ZERO-INTRUSIVE TRANSPORTATION INFRASTRUCTURE MAINTENANCE USING HIGH-SPEED ULTRASONIC TOMOGRAPHY

SECTION 1: INTRODUCTION

Context of Research

Bridges and roadways are critical to the nation's infrastructure. Improper monitoring and maintenance of this critical infrastructure could have significant economic and social impacts. It is expensive to sustain and upgrade structures in order to meet continuously growing demands and changing standards, therefore, it is necessary for engineers to develop high-speed nondestructive evaluation methods for the inspection of roadways and concrete bridge decks. Current nondestructive testing (NDT) technologies are not adequate for rapid monitoring and evaluation of deteriorated bridge decks. Since a majority of defects begin below the surface, visual inspection of civil structures is not adequate to determine their health and sustainability.

Objective

The purpose of this study is to investigate the feasibility of creating a zero-intrusive, ultrasonic tomography device that can rapidly collect and analyze data, thereby providing a real-time image of the deteriorated bridge deck. The three major tasks that are investigated in Phase I of this project are:

- Design a prototype ultrasonic tomography device which features a compact and lightweight system that can be operated by a single investigator.
- Develop and validate Synthetic Aperture Focusing Technique (SAFT) algorithm to ensure its reliability and applicability.
- Validate the capabilities of ultrasonic tomography in detecting rebar, delamination, air voids, and water voids in concrete slabs with known conditions.

Scope

Upon conclusion of the introduction, Section 2 investigates the concrete degradation process, current nondestructive methods, and emerging technologies. These technologies are evaluated for high speed application. Section 3 is comprised of a brief introduction and mathematical background to the SAFT algorithm. Additionally, an in-house SAFT algorithm is compared to the existing program for validation of the abilities of this algorithm in detecting flaws in concrete. Section 4 presents the experimental program, where a handheld ultrasonic tomography device is used to inspect concrete slabs with known conditions. A total of 11 concrete slab specimens are inspected using the ultrasonic tomography device. The results from the inspection are compared with the reinforcement layout, and defect keys. This experimental program provides the necessary validation for the use of ultrasonic tomography for detecting rebar, delamination, air voids, and water voids in concrete decks. In addition to testing the method's abilities to detect various details in concrete slabs, overlapping measurements, which are critical to the success of the SAFT algorithm, are also investigated. The outcome of this experimental program will help determine the capacity of ultrasonic tomography to be integrated to an

automated device. Finally, Section 5 provides a summary of the findings from Phase I of TxDOT 0-6869.

SECTION 2: LITERATURE REVIEW

Bridge Deterioration Background

Concrete bridge decks can deteriorate at an alarming rate from consistent use, which in turn could contribute to catastrophic failure and result in injury or cost human lives. Heavy traffic, constant cyclic loading, poor quality of construction, overloading, freeze-thaw cycles, and deicing salts may lead to rebar corrosion, delamination, cracking, and concrete degradation. In concrete, multiple deterioration mechanisms may integrate, making the deterioration process of concrete structures complex. It is well known that concrete is weak in tension. To improve the performance of concrete structures under tension, reinforcing steel bars are typically embedded in concrete. ACI 318 (2014) specifies minimum concrete cover thickness for various reinforced concrete structures to ensure that the reinforcing steel is protected from the elements. The use of deicing salts, which contain chloride, can corrode the reinforcing steel, ultimately affecting the bridge deck capacity. Gucunski (2013) notes that the two most common corrosion processes are chlorine-induced pitting and carbonation. The two types of corrosion can usually be visually determined. Chlorine pitted corrosion leaves black marks along the steel, whereas carbonation will leave a gold-brown or red colored rust. Corrosion is a time dependent deterioration mechanism which usually depends on the type of steel used, temperature, moisture content, and exposure levels. Freeze-thaw cycles also greatly contribute to the process of rebar corrosion. Reinforcement corrosion may lead to delamination in the concrete deck. When reinforcing steel corrodes, it expands, which induces stress on the concrete surrounding the bar. The concrete cracks and these cracks propagate, leading to the deterioration of the structure. In addition to stresses caused by the corrosion of steel, other factors may accelerate concrete cracking including the curing process of concrete, air temperature, traffic loads, and the geometry of the bridge. Deterioration of concrete can lead to a reduction in the load carrying capacity of the structure, which is a major cause for concern.

Other situations that may cause concrete deterioration include micro cracking, Alkali-Silica Reaction (ASR), Delayed Ettringite Formation (DEF), and plastic shrinkage. ASR is fueled by the reactive silica in aggregates and the alkalis in cement, which in turn produces a gel that increases in volume in the presence of water. Similar to delamination, this volume increase causes stress, which produces cracking internally and at the surface of the structure. Unlike corrosion, which happens at the rebar location, ASR can cause cracking anywhere in concrete. DEF is the formation of ettringite and associated expansion when concrete is subjected to high temperature during its curing period. At elevated curing temperatures (>70°C) the formation of calcium silicate hydrate (C-S-H) gel is accelerated when compared to ettringite. The accelerated formation rate of C-S-H gel physically traps some of the sulphates and aluminates in its layered structure before they can react to form ettringite. At high curing temperatures, the trapping continues until the C-S-H gel becomes fully saturated with sulphates. After the concrete has gone through the entire heat curing cycle, and when stored in a moist environment at ambient temperatures, the sulphates diffuse out of the C-S-H gel into the pore solution. This provides an internal source of sulphate and triggers the reformation of ettringite in hardened concrete. This reformation of ettringite causes expansion and eventually cracking of concrete. This delayed or

secondary formation of ettringite in hardened concrete is widely known as DEF. However, the DEF mechanism can be prevented by limiting the curing temperature of concrete to a below 70°C. It has also been established that Type III cement is more likely to contribute to this phenomena. A possible defect mechanism, especially in aged concrete bridges, is the de-bonding of asphalt concrete from the underlying Portland cement concrete. This exposes the Portland cement concrete deck to a variety of foreign materials such as water and chlorides, which contribute to the defects discussed previously.

It is critical to detect the deterioration caused in concrete by the various deterioration mechanisms. Proper and timely identification of defects in concrete can help the various transportation agencies to take remedial actions to prevent failure of the transportation system/structures and avoid expensive repairs and replacements. Various non-destructive testing (NDT) techniques may be used for detecting defects in concrete structures. Non-destructive testing allows engineers to use various analysis techniques without compromising the integrity of the structure. The following section briefly discusses the various NDT techniques that have been used in the past for the evaluation of bridge decks.

Nondestructive Testing Methods

Brief History of Nondestructive Testing

While visual inspection can be considered as one of the earliest techniques of evaluation, this technique is only useful when the concrete cracks are visible on the surface. It does not give any indication on the condition of the concrete below the top surface. In past years, several nondestructive techniques have been used in the transportation industry for the evaluation of concrete bridge decks. All nondestructive testing techniques involve a sent signal (wave) and a received response. One early nondestructive testing technique included researchers exciting a specimen with sound, like dropping a coin, and listening for the reflected sounds wave to detect abnormalities (White 2012). Sergei Sokolov, a famous Soviet scientist, who is known as the father of ultrasonic testing, indicated in the 1920s that he could detect flaws in metal through a transmission technique. He proposed the idea of the first ultrasonic camera which used sound waves at a frequency of 3000 MHz and received the reflected waves with a large piezoelectric transducer. After the signal is received, the face of the transducer is scanned with a metal contact beam to produce an “image”, even though advanced for the time period, it did not produce an image of enough quality, and therefore it could not practically be used. During the same time period, extensive research on flaw detection of metals was taking place in Germany.

In 1933, Muhlhauser received a patent for a system that transmitted ultrasonic energy and detected the response with secondary transducers. Following in 1936, Raimar Pohlman developed the “Pohlamn Cell,” which was an image converting device. By 1942, Donald Sproule essentially used echo-sounding techniques to detect various defects in steel. Development progressed over the next decades with various researchers from around the world taking multiple approaches to refine nondestructive testing. (NDT.net) Modern nondestructive testing techniques include, but are not limited to, impact echo, chain dragging and hammer sounding, impulse response, electrical resistivity, ground penetrating radar, infrared thermography, and ultrasonic pulse echo. Each one of these methods is briefly discussed in what follows.

Impact Echo

The impact echo testing technique is useful in detecting delamination in concrete. In this technique stress waves are generated by striking the bridge deck surface. The response waves are recorded with contact or air-coupled sensors near the site of impact. From this test, the frequency and the depth of reflection can be determined. This depth could be the possible location of a change in material, which can be the source of delamination in a bridge deck. Delamination causes the steel and concrete to separate, causing air voids. Once the location of the delamination is determined, there are various ways to determine the severity of the delamination and how it will affect the overall health of the structure. One way to analyze the condition of the delamination is by observing the frequency pattern. A delaminated point will shift the frequency to higher amplitudes because the reflections occur at more shallow depths (Cheng and Sansalone, 1995). Figure 120 shows a simple schematic of the impact echo procedure.

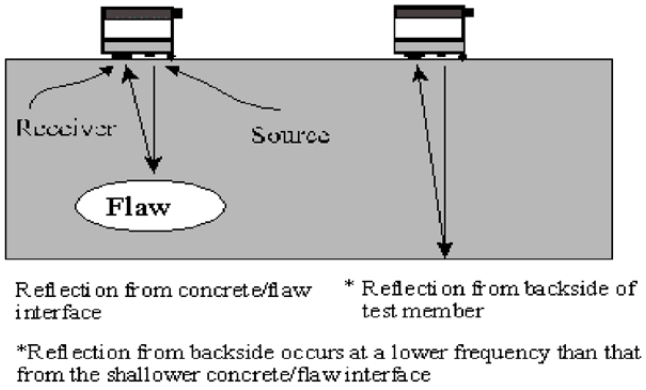

Figure 120. Schematic of Impact Echo Method (Tinkey et al., 2003).

Guncunski et al. (2013) explains that the initial delamination between the layers of concrete and steel can be detected by relating the reflected waves and frequencies from the delamination site and the bottom of the bridge deck. These are most difficult to detect in comparison to progressed delamination which can be clearly seen with a single peak frequency, which corresponds directly to the depth of the delamination. For shallow delamination, usually low frequency waves are reflected due to flexural-mode oscillations from the top portion of delamination.

Impact echo is useful because it only requires one side access to a structure, and can detect the depth of various defects. Although it fits basic criteria for testing, an experienced operator is needed, because the same specimen can give various results depending on the engineer and it is also only applicable to a certain depth. In addition, the measurements have to be performed in a dense test grid, which makes impact echo a slow process.

Chain Dragging and Hammer Sounding

This is a common inspection method that is utilized to inspect concrete bridge decks. This technique relies on changes in sound between quality concrete and concrete with voids when chains are dragged across the bridge deck, or when the deck is lightly tapped using a hammer.

Chain dragging is limited to horizontal surfaces, but the hammer sounding technique can be used for a wide range of structure.

This can detect late stage delamination. However, the detection in sound differences is subjective. This method is also ineffective on bridge decks with overlays.

Impulse Response

In the impulse response technique stress waves are generated using a hammer and the dynamic response is measured using geophone or an accelerometer. This method detects honeycombing, voids under joints, and delamination. It is also effective in detecting cracking in concrete elements and debonding of asphalt and concrete overlays on concrete decks. However, smaller defects may go undetected and the interpretation is dependent on the selection of the test points.

Electrical Resistivity

Electrical resistivity is a commonly used technique to detect anomalies in concrete, since it easily detects moisture which can be directly related to the presence of cracks. The presence of water insinuates the presence of chlorides, which can be linked directly to corrosion and delamination of steel from concrete. The damages and cracked areas of concrete are the paths of least resistance, the preferred path of electric current. The most common set-up of electrical resistivity is the Wenner set-up (Gowers and Millard, 1999). It calculates resistivity due to the difference in potential between electrodes. It is highly valuable in detecting potentially corrosive areas that could affect bridge health in the long term.

Although the data collection is simple, interpretation can be difficult since the resistance can depend on moisture and salt content, and therefore poor evaluation can lead to false conclusions. In addition, the device needs the surface to be wetted prior to gathering data. Resistivity measurements can also be used to determine permeability, but in general they need to be coupled with other NDT test methods in order to verify results. Carbonation may also seriously impacts resistance so it is generally recommended to avoid using the electrical resistivity method for defect detection in concrete (Wimsatt et al, 2009).

Air Coupled Ground Penetrating Radar

Ground penetrating radar (GPR) has already been used on roadways at high speeds, up to 70 mph, for pavement profiling, object detection, and construction quality. For the evaluation of bridge decks, GPR is commonly used to determine the thickness of concrete layers, the reinforcement configuration, detection of air voids, and estimate concrete electrical properties.

Figure 121 shows a picture of the air coupled GPR system. The setup consists of a radar antenna attached with a fiberglass arm to the front of a moving vehicle. The antenna, which is directed to the ground, emits a high frequency electromagnetic wave and then captures the reflection in real-time.

Figure 121. Air Coupled GPR System (Wimsatt et al., 2009).

The variation in electrical properties of the constituent materials results in a change in response of the reflected energy. Using the relation of dielectric permittivity values, engineers can determine a change in material since a portion of the wave will be reflected back to the antenna. In relation to the condition of a bridge deck, an engineer will evaluate the attenuation of the reflected waves at the top of the steel reinforcement. Advantages of the GPR system include the fast-paced nature, the use of electromagnetic waves that can penetrate concrete and other non-ferrous materials, ability to detect embedded materials, and 10% accuracy for location and depth of reinforcement to true location.

However, there are certain limitations for air coupled GPR (Wimsatt et al, 2009). For instance, if the concrete contains excessive amounts of water and/or many free chloride ions from deicing chemicals, the signal and recorded attenuation can be greatly affected. This results in inaccuracy, making it difficult for engineers to draw any conclusions. Temperature can also cause skewed results. In addition, it is not possible to directly image the delamination in the bridge deck, determine the mechanical properties of concrete, or conclusively detect corrosion. An additional obstacle for the implementation of GPR is that the Federal Communications Commission regulates transmitting power output and pulse rates, which makes it difficult to design and build new and improved systems (Barnes and Trottier, 2000). In addition, the test equipment, if available, is expensive and an engineer needs extensive training to accurately interpret results (Wimsatt et al, 2009).

Infrared Thermography

Infrared thermography has been used for a few decades to detect flaws in bridge structures. This technology looks at electromagnetic radiation in relation to temperature and infrared wavelength to determine the location of cracks and delamination. The infrared camera looks at the rates of heating and cooling, comparing their infrared radiation. This energy is converted to an electrical signal and processed to create a temperature map for the user to see, making misinterpretation minimal. The infrared camera functions on the principal that different materials emit different

amounts of thermal radiation: the infrared camera detects differences in material, allowing the user to identify air voids that result from cracking and delamination.

For infrared thermography to work, the structure must be heated either by solar radiation or a heater. The infrared camera then displays how the structure emits heat since heat flows from a hot region to a cold region. Cracks or delaminated areas are usually filled with air or water, and these areas usually change temperature faster than surrounding materials.

Though the infrared camera can detect where a delamination or void is present in reference to the surface, it cannot detect the depth location of the flaw (Gucunski et al., 2013). This technique is also affected by surface anomalies and boundary conditions. Figure 122 shows a typical mobile infrared thermography setup as well as a thermal map.

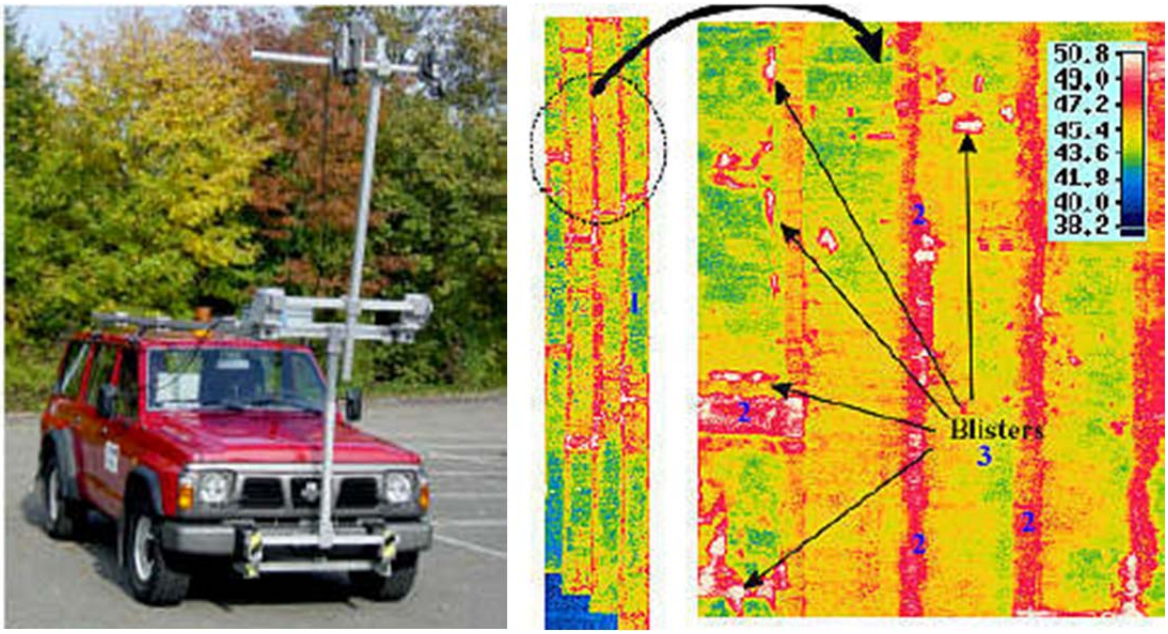

Figure 122. Mobile IR Measuring Equipment (Left) and Typical Thermal Map (Right) (Stimolo, 2003).

Ultrasonic Pulse Echo

Ultrasonic pulse echo is similar to impact echo, but uses an acoustic stress instead of producing one by impact. These acoustic waves are produced by exciting a piezoelectric material.

Ultrasonic testing was not used regularly in analyzing reinforced concrete structures until recently due to high scatter and attenuation, both of which had made it difficult to determine any defects. In addition, probes had to be coupled to the ground with grease or wax, making the process slow and messy. Low-frequency, dry-coupled tip transducers have been developed to combat these issues in analysis of reinforced concrete.

Ultrasonic Tomography

Ultrasonic tomography is an extension of the ultrasonic pulse echo method in which the transducers are usually set up in an array. In each row, one transducer fires the ultrasonic signal while the others act as receivers of the reflected signal. All transducers can both emit and receive signals. The basic principal behind ultrasonic nondestructive testing is that the waves travel through the medium and when they interface with an anomaly, a portion of the wave energy is reflected and captured by the receiving transducers. The velocity of the reflected wave helps identify acoustical impedance, which is then analyzed to determine defects. A clear decrease in velocity of the reflected waves is usually indicative of substantial deterioration.

After the reflected waves are received, a Synthetic Aperture Focusing Technique (SAFT) algorithm is used to construct an almost real time image to identify cracking, debonding, delamination, or other defects. This method is extremely useful for structures that only have one-sided access, such as reinforced concrete bridge decks. In order for the device to accurately reflect the condition of the structure, a closely spaced test grid is essential. It also takes time for the SAFT algorithm to create the display of the concrete. In addition, the resolution of the scan depends on how well the transducers are in contact with the structure, meaning that on rough surfaces it may be difficult to accurately detect flaws (Bishko et al., 2008).

In concrete, ultrasonic tomography can detect voids within 13 mm (0.5 in.) and delamination within 19 mm (0.75 in.). Since there are a few drawbacks, especially the difficulty in detecting defects close to the surface, the nature of ultrasonic testing makes it a prime candidate for the evaluation of concrete bridge decks. The most recognizable and popular device utilizing this technology is the 1040A MIRA device.

Previous work has been conducted by using the ultrasonic tomography system, shown in Figure 123(b), to verify the technique's ability to detect a wide variety of common defects at critical locations in structures. Ultrasonic tomography is a relatively new technology in the field of nondestructive testing, and incorporates advanced pulse-echo ultrasonics with tomographic representation of a test field.

Typical systems employ an array of low-frequency shear wave transducers with a center frequency of 50 kHz. The ultrasonic tomography system incorporates a 4-by-12 grid of mechanically isolated and dampened dry-point-contact (DPC) transducers that do not require the use of a coupling agent. The device can fit the profile of a rough concrete testing surface with a variance of up to 10 mm (0.4 in.). The system is then manually applied at every desired testing point for data collection shown in Figure 123(a).

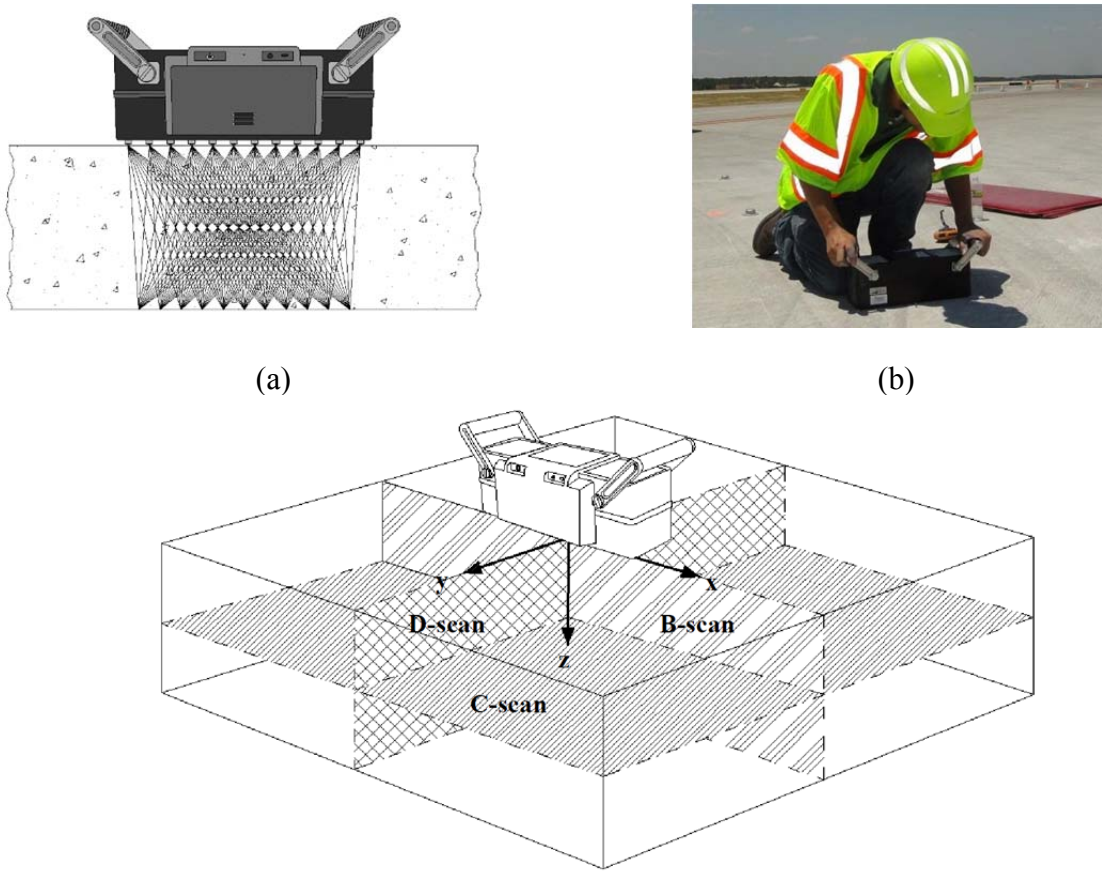

Figure 123. (a) Operational Sketch, (b) Mode of Physical Data Collection, (c) B-, C-, and D-Scans Relative to Tomograph.

Using this linear array of elements, there is a wide coverage of shear wave pulses that reflect at internal interfaces where the material impedance changes. With the help of a digitally focused algorithm (an alteration of the SAFT algorithm), a 3D volume is presented with each point of possible reflection in half-space represented by a color scheme, scaled according to reflecting power. This 3D image can also be dissected into each of the three planes, shown in Figure 123(c) representing its volume: the B-scan, C-scan, and D-scan.

On each scan, the various intensities reported by the returned waves are color-coded from dark blue to deep red, representing low reflectivity (typically sound concrete) and high reflectivity (any type of impedance), respectively. With this intensity scaling, it is easy to see any discontinuities with distinctly different wave speeds, such as voids, delamination, cracks, and other abnormalities.

Various engineers have used the ultrasonic tomography technique extensively for applications ranging from bridge decks, highway pavements, airport runways, and tunnel linings. It has been successful at accurately and precisely locating delamination (both widespread and localized), air- and water-filled voids, slab thickness, reinforcement mesh layout and depth, and deleterious materials such as clay lumps (Im et al., 2010; Shokouhi et al., 2011; White et al., 2014; Wimsatt

et al., 2014). The UST method by itself is classified as a very low-speed NDE system that can collect data at approximately 1-2.5 min/ft^2 (White et al., 2014; Wimsatt et al., 2014).

NDT Summary

Previous research shows that various NDT techniques can be used for the detection of flaws in reinforced concrete decks. This is essential in the maintenance and repairs of the current transportation infrastructure. Specifically, technology is needed to characterize bridge deck deterioration in real time in order to determine early concrete deterioration and other potentially catastrophic defects. Fast, easy, and accurate detection would increase employee safety and save money and time while quickly identifying bridge deck damage for repair.

From the review of various NDT techniques above, the ultrasonic tomography technique shows the most promise in detecting anomalies in concrete. However, its sluggish pace majorly hampers widespread application with bridge decks. For developing a zero-intrusive, high-speed, and high resolution system, a dry coupled, spring loaded, ultrasonic transducer, system may be the most viable solution, and needs a detailed investigation.

Current Bridge Deck Evaluation Technology

A1040 MIRA

A1040 MIRA (MIRA) is an ultrasonic tomographic device developed by Acoustic Control Systems used to image the internal configuration of a concrete structure with access to only one side. It is desirable to detect defects such as honeycombing, cracks, holes, and delamination. This is possible because MIRA produces high quality, informative images for engineers to assess quality of construction and detect critical flaws in structures. It uses dry contact 50 kHz transducers, which eliminate the need for contact gels to maintain a clean surface. MIRA consists of a linear array of 48 transducers in a configuration of 4 by 12. MIRA emits shear waves and receives the reflected signal by various transducer pairs which allow for various incident angles. This is critical to analysis of nonhomogeneous materials (Hoegh 2013). The transducers are equipped with wear resistant tips that minimize damage and allow MIRA to be used on rough surfaces. (Acoustic Control Systems) MIRA can be seen below in Figure 124, from the Acoustic Control Systems website.

Figure 124. A1040 MIRA Ultrasonic Tomographic Device (Acoustic Control Systems 2015).

Monostatic vs Bi-static Transducers

A monostatic transducer both emits and receives signals while a bi-static system's transducers are for only one purpose, either emitting or receiving. In a bi-static system, a single or number of other transducers are near the one emitting the signal to receive the signal. MIRA A1040 is a bi-static system since a signal is sent from a single transducer to and received by the remaining transducers in the matrix. Each transducer in the matrix will send a signal while the others receive the reflected waves, meaning MIRA emits 48 signals simultaneously at its rate of 50 Hz. Each image is processed and layered to produce the final image, which displays the defects within the concrete. The process of the emitting process is shown in Figure 125.

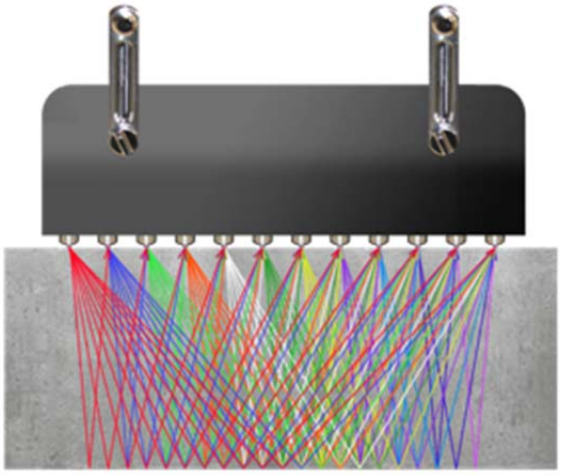

Figure 125. MIRA Emitting and Receiving Signals for One Scan (ACSYS, 2015).

DATA Files from MIRA

When extracting the data from MIRA, the user will observe that there are four different files for each scan. There will be an image file, which contain the final post processed images of the

concrete. Also present is a .bin file that contains the saved tomogram, which is all the data associated with the image file. The size of the .bin files is related directly to the number of pixels. The .lvb file contains the raw data (initial data array) received by the transducers prior to any post processing. This will be useful because the processed images from MIRA can be compared with the final images created by the Texas A&M produced SAFT algorithm to verify the program. The last file is a .cfg file, which encompasses a description of the configuration of the saved post-processed image. IdealViewer is the available commercial product to transform raw data files to a three dimensional model of the area scanned. This allows an engineer to quickly and easily assess the location and magnitude of defects.

The University of Illinois Impact-Echo Device

The University of Illinois at Urbana-Champaign developed a multi-sensor air-coupled impact echo device that could be manually moved over a bridge deck surface of about 1000 square feet in approximately 90 minutes. The device consists of a linear microphone array which is manually moved over the surface while automatically producing impacts. This technology allows for the engineer to identify and characterize defects close to the surface. The technology includes automated data and image processing, so the engineer can receive real time visual representation of the scan.

Pros of this system include the automated data collection and processing systems in addition to the ease of use. The drawbacks include time for collection. This is a significant improvement in comparison to commercial products, but would still require construction to be halted or an already completed structure to be closed (Schickert, 2015). Figure 126 shows the configuration of the device.

Figure 126. Impact Echo Device University of Illinois Urbana-Champaign (Wimsatt et al., 2009).

Lund University Non-Contact Wave Testing

Lund University developed a device similar to the University of Illinois at Urbana-Champaign. However, instead of impact echo, it sends surface waves through an automated impact source

while an array of microphones receive the signal. The data is then processed to compile a dynamic elastic modulus and yield map of pavement (Schickert, 2015).

This is very applicable for pavement testing and integrity but may not be the best application for concrete bridge decks, since it doesn't directly acquire data for the desired characteristics. Another significant drawback is that the machine needs to be manually pushed as a slow rate to receive data properly, which is not applicable to the current project. Figure 127 from Ryden, Lowe, and Cawley (2008), depicts how the microphones receive the surface waves.

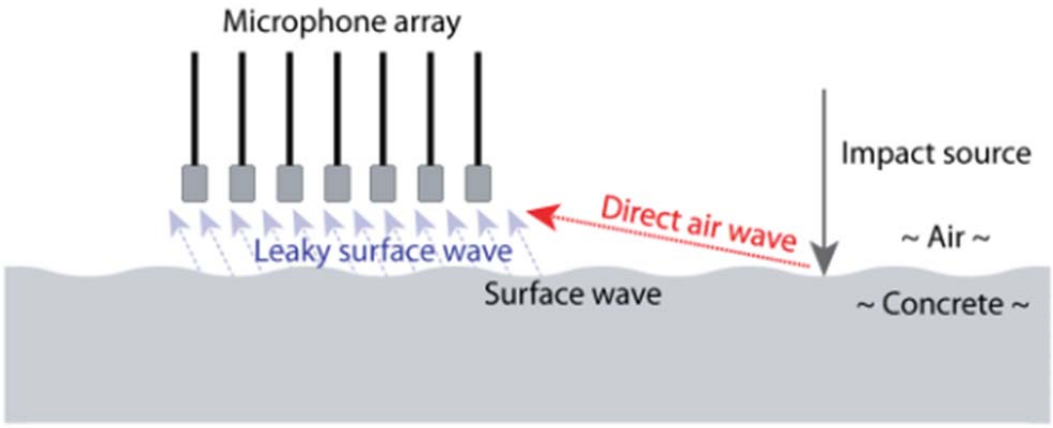

Figure 127. Description of Non-Contact Wave Testing (Ryden, Lowe, and Crawley, 2008).

FLEXUS

Another ultrasonic measurement and imaging system, FLEXUS, consists of a 3-axis scanner with low frequency transducers in an area of approximately of 9 square feet. It uses a total of 48 transducers, arranged in 3 axial groups of 16 with a traditional or combination SAFT to produce images. An interesting feature allows the user to choose to either produce high quality images or reduce scanning time to approximately 1 minute per a square foot (Schickert, 2015). This is still substantial amount of time to scan an entire concrete bridge deck. Additionally, FLEXUS is primarily for walls and other vertical structures; a horizontal scanning system is desired for this project. Figure 128 displays the FLEXUS configuration.

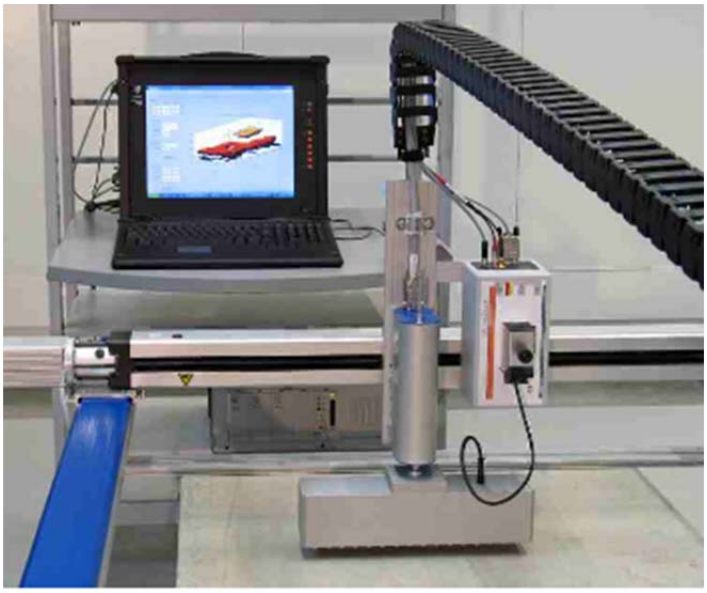

Figure 128. FLEXUS Multipoint Scanner (Hillger, 2014).

RABIT

Rutgers University designed an autonomous robot, named RABIT, to detect rebar corrosion, concrete degradation, delamination, and other common defects. It contains a variety of nondestructive testing equipment including GPR, ultrasonic surface wave sensors, impact-echo, and electrical resistivity in addition to high resolution digital camera for a clear depiction of the surface and GPS for exact location of the device. The data must be extracted to use online data analysis tools, which produce multiple maps to represent the concrete's condition (Schickert, 2015). It is a fully automated device, but with the large variety of NDT technology it requires a complex understanding to determine the best approach for various structures. Figure 129 depicts the RABIT configuration and shows all non-destructive technologies.

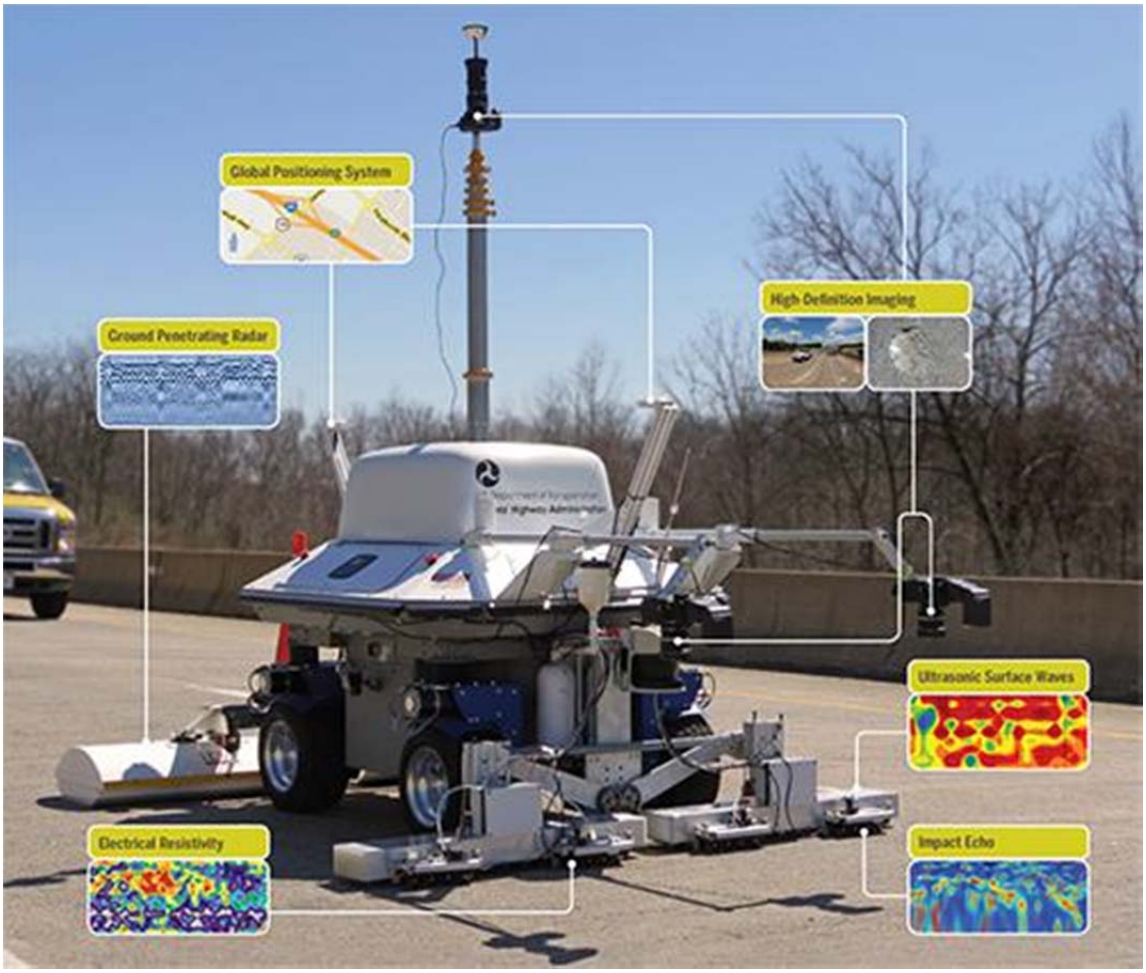

Figure 129. Image of RABIT (Center for Advanced Infrastructure and Transportation, 2014).

BetoScan

Another measurement system, the BetoScan, is a self-navigating robot consisting of both contact and noncontact sensors and has the potential for mapping, radar, and ultrasonic techniques. It includes optical analysis, microwaves, ultrasonics, eddy current methods, and radar. It is specifically designed to investigate the impact of deicing salts on concrete integrity since chloride is directly related to high corrosion (Schickert, 2015).

BetoScan uses multiple characteristics to assess the condition of concrete decks including bridges and parking structures. These include electrochemical potential, chloride profiles, carbonation depth, cover adequacy, delamination, cracks, and corrosion. According to Reichling et al. (2009), the BetoScan can simultaneously measure the desired characteristics and cover "thousands of square meters per a day" on horizontal surfaces, due to its multisensory set up. The BetoScan also uses the ultrasonic system, A1220 Monolith, also known as EYECON, to determine structure thickness and map defects. Figure 130 and Figure 131 from Reichling et al. (2009), depict the physical BetoScan and show the capabilities of the device and their specific use for determining characteristics, respectively.

This indicates that the A1220 Monolith is a flexible device that can be utilized in a larger, automated or mobile NDT device.

Figure 130. BetoScan Automated Robot (Reichling et al., 2009).

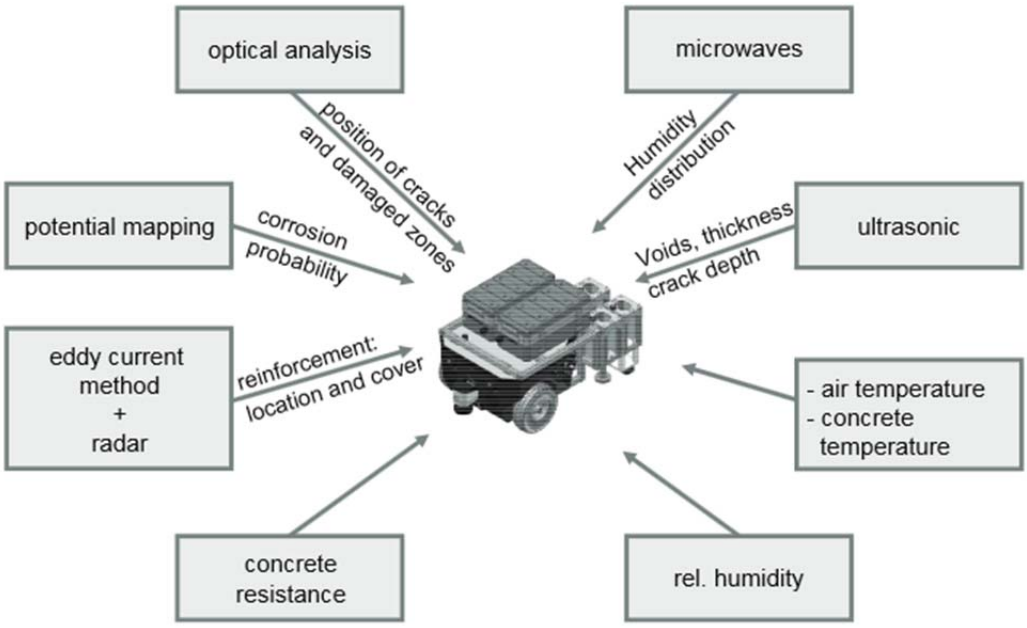

Figure 131. BetoScan Capabilities (Reichling et al., 2009).

EYECON A1120 Monolith

EyeCon, also known as the A1120 Monolith, is a handheld ultrasonic tomography device. Like MIRA, EyeCon is a portable device that can successfully determine concrete thickness, delamination, voids, honeycombing, and bond quality using the ultrasonic pitch-catch method in the time domain. Figure 132 shows the EyeCon device and its included transducer array.

Figure 132. Transducer Array (Foreground) with EyeCon Handheld Computer (Background).

Also, similar to MIRA, it uses dry-contact transducers, which eliminate the need for messy contact gels. The device usually displays results as individual A-scans, which shows the reflected amplitude versus depth, or C-scans, which display the bird's-eye cross section of the concrete being scanned. The pitch-catch method is an ultrasonic pulse-echo method where transmitting and receiving transducers are separate (bi-static). The packaged transducers are bi-static and arranged in a 4 by 6 array. The first three columns in Figure 133, 12 transducers, transmit the shear wave at 50 kHz, while the remaining 12 receive the reflected waves. A more detailed image can be seen in Figure 133, taken from the Germann Instruments (2015).

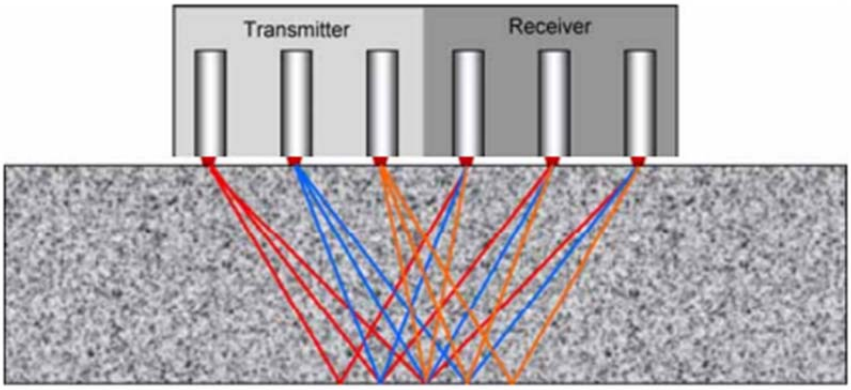

Figure 133. Transmitting and Receiving Configuration of EyeCon (Germann Instruments, 2015).

Each transducer is spring-loaded to account for surface irregularities. Noise is reduced by using multiple transmitting and receiving transducers. Another image of the transducer array can be seen in Figure 134, where the dry-contact tips can be seen clearly. This piezoceramic tip is sturdy and long-wearing.

Figure 134. Transducer Array for EYECON.

EYECON is of particular importance, since the ultimate goal is to integrate multiple transducer arrays into a zero-intrusive ultrasonic tomography device that can easily and efficiently characterize the condition below bridge deck surfaces.

Existing Technology Conclusions

From the literature review, it is evident that current nondestructive testing devices do not meet the needs to produce the needs for high speed application. They may be suited to determine defects below the concrete surface, but are unable determine defects at high speeds. In addition, several machines are bulky. A lightweight, portable machine is desired to quickly and effectively produce high resolution images depicting the interior condition of a concrete structure. EyeCon, a portable handheld ultrasonic device, has several desirable qualities; spring loaded transducers for proper contact, dry-coupled wear-resistant piezoceramic tips for quick measurements, and quick data collection. For these reasons, the transducer array is desirable and needs to be integrated into a fast-paced device.

SECTION 3: SAFT ALGORITHM

Introduction

The Synthetic Aperture Focusing Technique (SAFT) algorithm is a post-processing algorithm that converts the reflected ultrasonic data into a high resolution image. The first one-dimensional implementation of the SAFT algorithm was in the late 1970s, following the wide use of radar technology. For smaller transducers at lower frequencies, the SAFT algorithm performs with higher accuracy when compared to other imaging techniques (Dengzhi, 2007). In 1982, Pacific Northwest Laboratory conducted studies to incorporate the SAFT algorithm in field equipment, following extensive research conducted by Hall et al. (1986). It is important to note that the basic theory for the SAFT algorithm is only applicable to homogeneous materials, but it can be modified in order to accurately work for non-homogenous materials like reinforced concrete.

The SAFT algorithm creates high-resolution images by superimposing several pulse echo signals that have been measured at various positions (Kotoky and Shekhar, 2013). The linear SAFT algorithm aides in the clarity of the images by numerically superimposing the data transmitted and received by the array of dry contact transducers. SAFT creates images based on results from either B- or C-scans, series of received signal that are perpendicular and parallel to the surface, while filtering out scattering. This leads to a clear and more precise image that can accurately depict the defects (Burr et al., 1998).

To minimize attenuation, transducers using low frequencies between 30 and 80 kHz are typically used for the inspection of concrete (Kotoky and Shekhar, 2013). For reinforced concrete which has nonhomogeneous property causing lots of noise, minimizing the structural noise is critical because it can disguise some defects and inaccurately display others.

Most commercial SAFT algorithms in nondestructive testing are inaccessible and designed for specific geometries of devices. Therefore, in-house SAFT algorithm based on time-domain for the prototype device was developed.

Geometry of SAFT Algorithm

As measurements are required at various positions, it is necessary to have the device send pulse echoes in an array. Using the post-processing algorithm, engineers can translate ultrasonic data

into images that can accurately identify the vast majority of defects, such as; delamination, water filled void, air voids, and honeycombing.

It is critical to know the path traveled by the ultrasonic wave from the emitting transducer to the defect and back to the receiving transducer, for SAFT to create images from the ultrasonic transmission data. Therefore, an A-scan is necessary to provide geometric guidance and restore the image. Once the receiving transducers have received all emitted signals, the algorithm superimposes this computed data, resulting in a high resolution image. A time-frequency template of the signals is used over a Fourier transform. The time-frequency analysis is based on Wigner-Ville distribution.

Kotoky and Shekhar (2013) explain that the basics of the SAFT algorithm rely on geometrical reflection of wave. For this, the focus of the ultrasonic transducers can be assumed to be in constant phase (so, the amplitude is consistent) before diverging at various angles in a cone shape. The angle of deflection is determined by transducer properties, primarily focal length and diameter. Because of this, it is necessary for the system to use a single type of transducer, because waves propagating at various angles would make the algorithm difficult, if not impossible. The properties of the transducer can be calculated easily knowing the path length and travel time for a signal moving along that path. The aperture of the transducer, and the diameter of wave perpendicular to wave propagation, are critical because it assists in the layering of the A and B scan. The aperture width of the transducer corresponds to the width of the cone, and at what range it can be applied. The path length that the signal must travel corresponds to the phase shift seen in the signal. From these geometric properties, an engineer can construct images that simplify the detection of defects below the concrete surface (Kotoky and Shekhar, 2013). This geometric interpretation can be seen in Figure 135 through Figure 137.

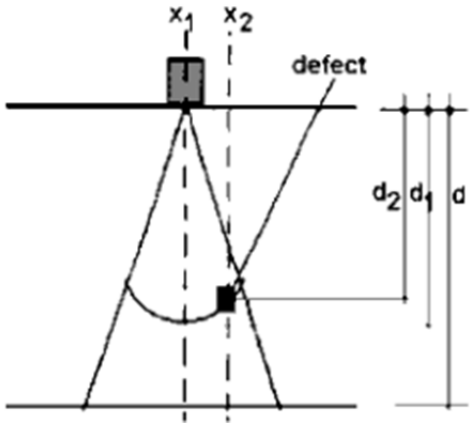

Figure 135. Display of the Waves Passing through the Defect Zone (Kotoky and Shekhar, 2013).

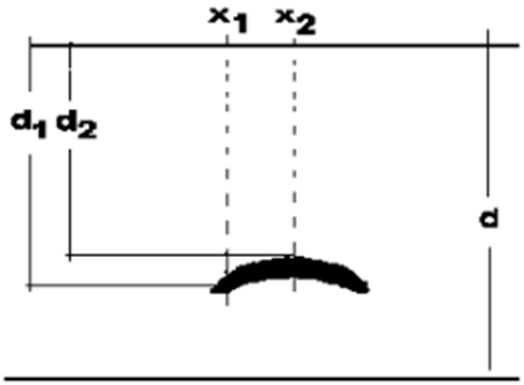

Figure 17. B-Scan of the Iron Defect (Kotoky and Shekhar, 2013).

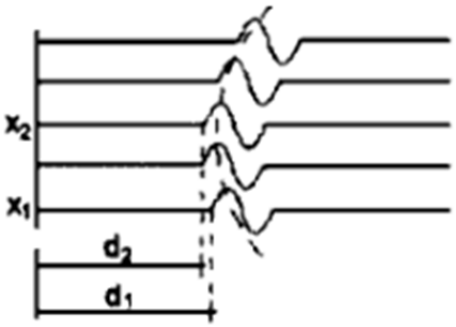

Figure 137. Resulting Image Produced from the Wave Passing Through the Defect (Kotoky and Shekhar, 2013).

As shown in Figure 135, the wave is sent from the transducer at a distance x_1 in a conical shape, interacting with the defects at x_2. When the wave interacts with the defect, which is at a depth d_2, the same wave is at a depth d_1 from the surface directly below the transducer. From this, Figure 17 can be obtained showing the shape of the waves and the various distances. This image displays the detection of a single round hole in an iron block. The final broad image is then produced using the transducer aperture width. With this technique, the A-scan is focused below the transducer as shown in Figure 135, which corresponds to the B-scan in Figure 17. These images are ultimately used to produce the final image in Figure 137.

With SAFT, the intention is to determine a parabola at each data point where a significant amount of energy is dispersed. If the summation of energy values over this parabola at a point is high, it is marked as a scattering point. For the scattering of signal in non-homogeneous materials, it is important to know properties of this parabola, or conical shape, to reduce noise. In order to successfully reduce scattering, the parabola must be short in comparison with the whole array of transducers because of its larger size. In addition, by producing a smaller parabola, the algorithm is more efficient. Apart from relative shortness, it is important that the parabola be thick in order to average out noise due to small changes in the material. By using a thicker line, the amplitude indicating flaws is not as large, and it evens out noise for non-homogeneous

material. Only a flaw with the same length or larger than the thickness of the parabola can be detected, removing all the noise present in a non-homogeneous material (Burr et al., 1998).

Nonlinear SAFT

In the mid-1990s, it was difficult to interpret the results using the original SAFT algorithm, and it usually required a trained engineer to decipher recorded data (Burr et al., 1998). The algorithm as later modified to overcome these shortcoming. The modifications to the SAFT algorithm, previously known as a non-linear SAFT algorithm, are necessary for concrete structures which are non-homogeneous. Non-linear modification requires that the A-or B-scan of the surface be known from the linear system.

Noise Reduction

Noise reduction is relatively simple in homogeneous materials when compared to non-homogeneous materials. The spectrum of displacement may be calculated from the spectrum of the signal (at a specific location and frequency) multiplied by the signal's impulse response (from passage through the structure). From deconvolution, the incident wave scattering is easy to handle in a homogeneous material, but not with a non-homogeneous material like reinforced concrete. In non-homogeneous materials, the calculated scatter does not match with the actual scattering of the signal. The SAFT algorithm can be further modified to account for flaw lengths that are much larger than the length of the non-homogeneous particles. The correlation between two reflected signals at two different points in the transducer array may be used to differentiate between the signals from the defects and those that are related to structural noise.

Basic Theory of SAFT Algorithm in Time Domain

One of the main goals in developing an in-house SAFT algorithm was to develop an algorithm that shall be easy to develop and implement. A time-domain SAFT algorithm was developed for this investigation. The two major assumptions that were made in this study in order to develop a SAFT algorithm were: (1) isotropic material, which means that wave in material medium propagates at a constant speed, and (2) material homogeneity, because the prototype device has lower frequency range, which means that it has longer wave length than the size of aggregate and non-homogeneous property of reinforced concrete rarely affect the result of SAFT. So, an area under inspection that has different stiffness or density is considered to indicate an anomaly, such as a damaged region, or rebar location.

Mathematically, sectional material properties can be described using the reflectivity. The relationship between the reflectivity function, $f(x,z)$, and the A-scan data, $s(x_e,x_r,t)$, is given by

$$s(x_e,x_r,t)=\int_x\int_z f(x,z)\delta\big(t^*(t,x_e,x_r,x,z)\big)\mathrm{d}z\,\mathrm{d}x, \tag{3.1}$$

where δ is the transmitted impulse, x_e and x_r are the horizontal location of emitting and receiving transducers respectively, x and z are the horizontal and vertical position in the region of interest (ROI) respectively, t is the time, and t^* is defined as

$$t^* = t - \frac{1}{c}\left(\sqrt{z^2 + (x - x_e)^2} + \sqrt{z^2 + (x - x_r)^2}\right), \tag{3.2}$$

where c denotes the wave velocity and is a constant.

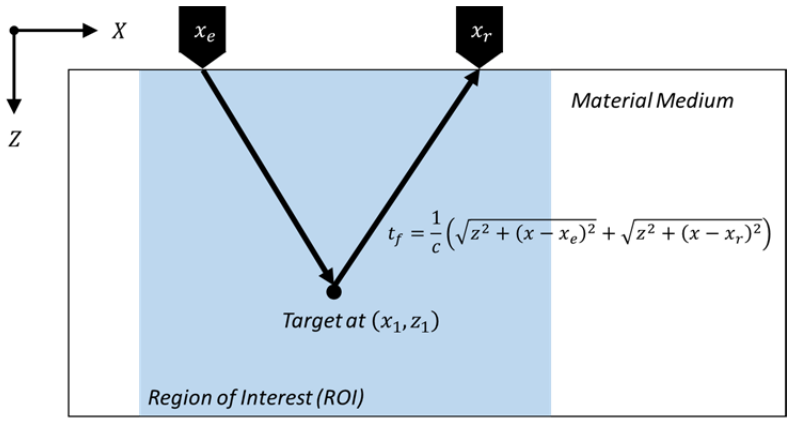

Figure 19. Geometry of Measuring Wave Propagation.

Predicting the exact behavior of transmitted impulse and calculating the reflectivity function using (3.1) is rarely possible since measured data has noise. To overcome this difficulty sectional image is reconstructed from the received A-scan data. The equation for the reconstructed image, $O(x, z)$ for a continuous system is described as

$$O(x, z) = \int_{x_{emin}}^{x_{emax}} \int_{x_{rmin}}^{x_{rmax}} \alpha(x_e, x_r, x, z) s\left(x_e, x_r, t_f\right) \mathrm{d}x_r \, \mathrm{d}x_e, \tag{3.3}$$

where $[x_{emin}, x_{emax}]$ and $[x_{rmin}, x_{rmax}]$ is the range of emitting and receiving transducers respectively, α is the apodization factor, and t_f is the time of flight that is given by

$$t_f = \frac{1}{c}\left(\sqrt{z^2 + (x - x_e)^2} + \sqrt{z^2 + (x - x_r)^2}\right). \tag{3.4}$$

Apodization factor is a weighing function that reduces the effect of side lobe artifacts in the focused image. The Hann function as shown in Figure 20 was used as an apodization function, in this study.

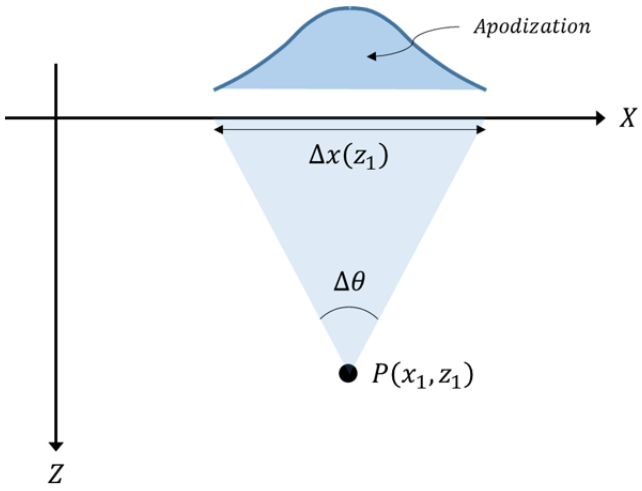

Figure 20. Illustration of Hann Function.

However, the transducers used in this research generate finite number of A-scan pairs. The discrete form of (3.3) is given as:

$$O(x,z) = \sum_{e=1}^{T-1} \sum_{r=e+1}^{T} \alpha(x_e, x_r, x, z) s\left(x_e, x_r, t_f\right), \tag{3.5}$$

where T is the number of sensor locations, and e and r are the indexes for the emitting and receiving transducers. Datasets with more A-scans generally have higher resolution.

Validation

In order to verify the feasibility of the developed SAFT algorithm, B-scan image from the MIRA A1040 device was used. The MIRA device has 4 by 12 array of transducers and provides reconstructed B-scan images using its own embedded SAFT algorithm. The device generates a series of A-scans from the single scan. In a single scan, 1st column of transducers transmits wave impulse and 2nd to the last of arrays record wave reflections. And then 2nd column of transducers array transmits wave impulse and 3rd to last arrays record wave reflections. Like this way, 66 pairs of A-scans were generated. Figure 21 shows an example of the B-scan results from the MIRA device, and the corresponding A-scan data extracted from the device. The B-scan image identities two groups of defects located at a depth of 120 mm and 300 mm (4.7 and 11.8 in.) from the surface.

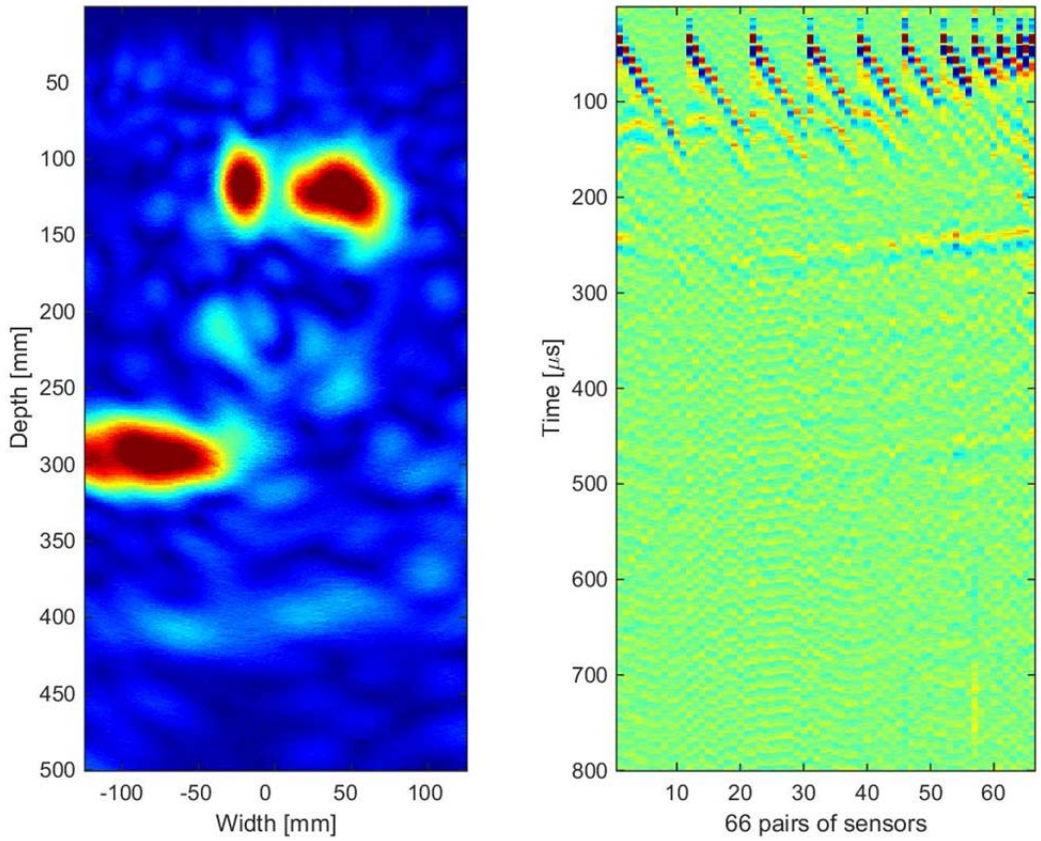

Figure 21. B-scan Image (Left), and Extracted A-Scan Data (Right) from the MIRA Device.

The A-scan data were extracted from the MIRA device and, used as input data to the developed SAFT algorithm. Figure 22 shows a comparison of the B-scan images obtained from the MIRA device and the developed SAFT algorithm. Similar defect shapes were reconstructed in both cases. The developed algorithm generated slightly rougher image compared to the MIRA device. Both, however, are equally effective in detecting areas of high reflectivity. Additionally, the B-scan from the developed SAFT algorithm detects the defects approximately 30 mm below the defects detected in the B-scan from the MIRA device.

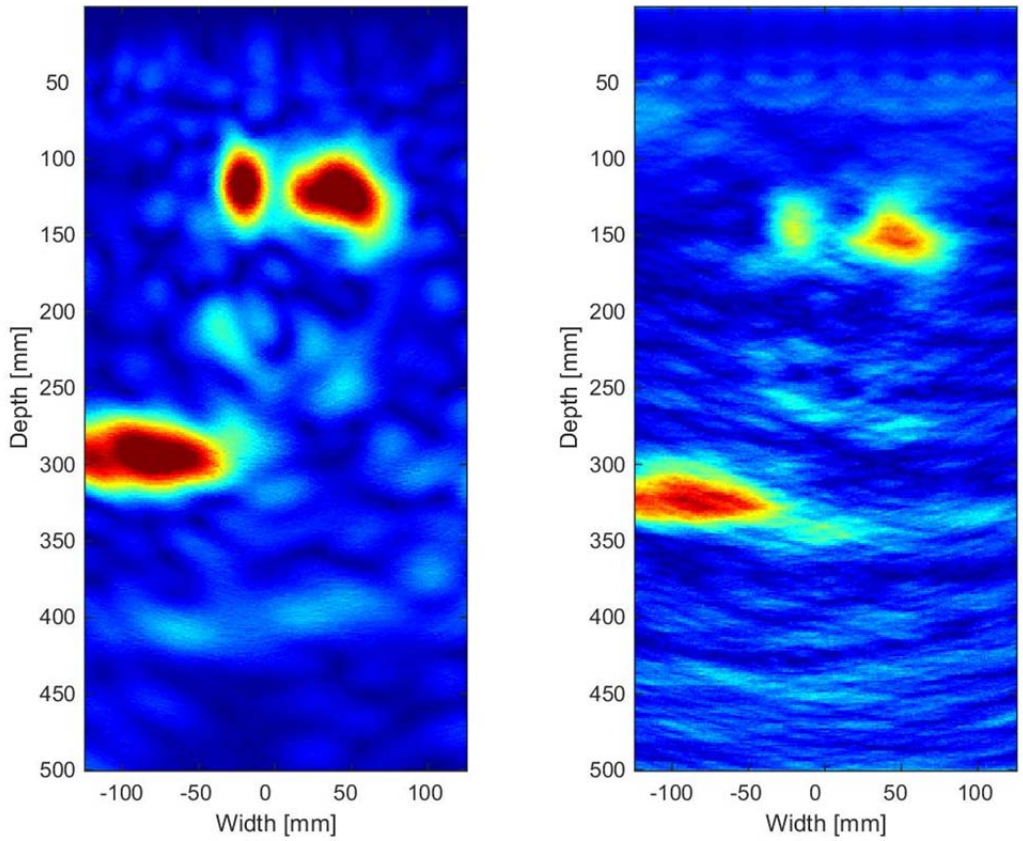

Figure 22. Comparison of B-Scan Images from the MIRA Device (Left) and the Developed SAFT Algorithm (Right).

3D Visualization and Other Sectional Views

The B-scans provide only sectional information, and the users may have difficulty understanding the three-dimensional distribution of defects from the two-dimensional B-scans. On the other hand, three-dimensional view of SAFT images help users to intuitively understand the location of defects relative to each other.

A three-dimensional visualization tool was developed using MATLAB. Once multiple layers of B-scan images are obtained, the reflectivity values between the layers are calculated by linear interpolation. As shown in Figure 23 points that have reflectivity above a certain value are represented in three dimensional perspective.

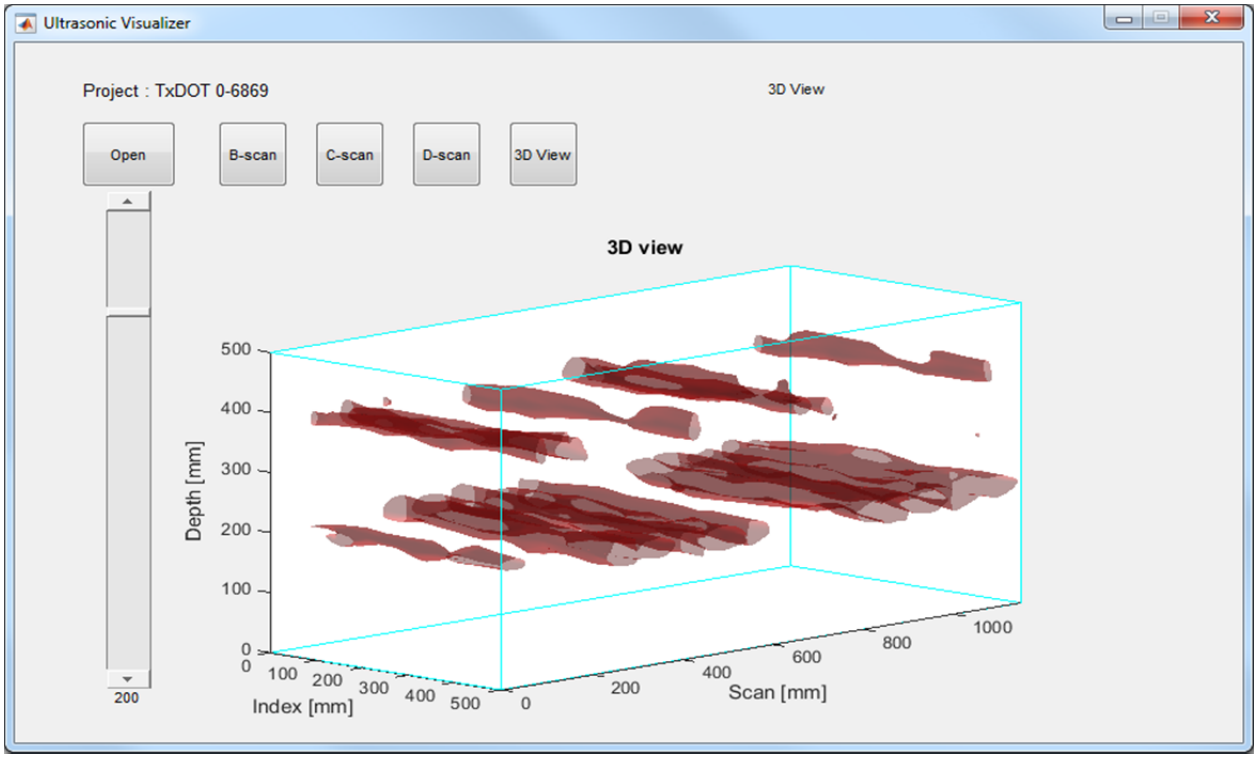

Figure 23. 3D View of Reflectivity.

The three-dimensional visualization tool allows the users to change reflectivity displayed using a slide bar. Additionally, users can also rotate the three-dimensional view.

A complete section view provides the information of the entire section, so users can easily detect high reflective areas in a particular section. This visualization tool also provides sectional view functions like B-scan, C-scan, and D-scan. The B-scan of the entire section in Figure 24 is generated by combining B-scan images on the same plane. C and D-scans of the entire section shown in the Figure 25 and Figure 26, respectively, are extracted from three dimensional reflectivity.

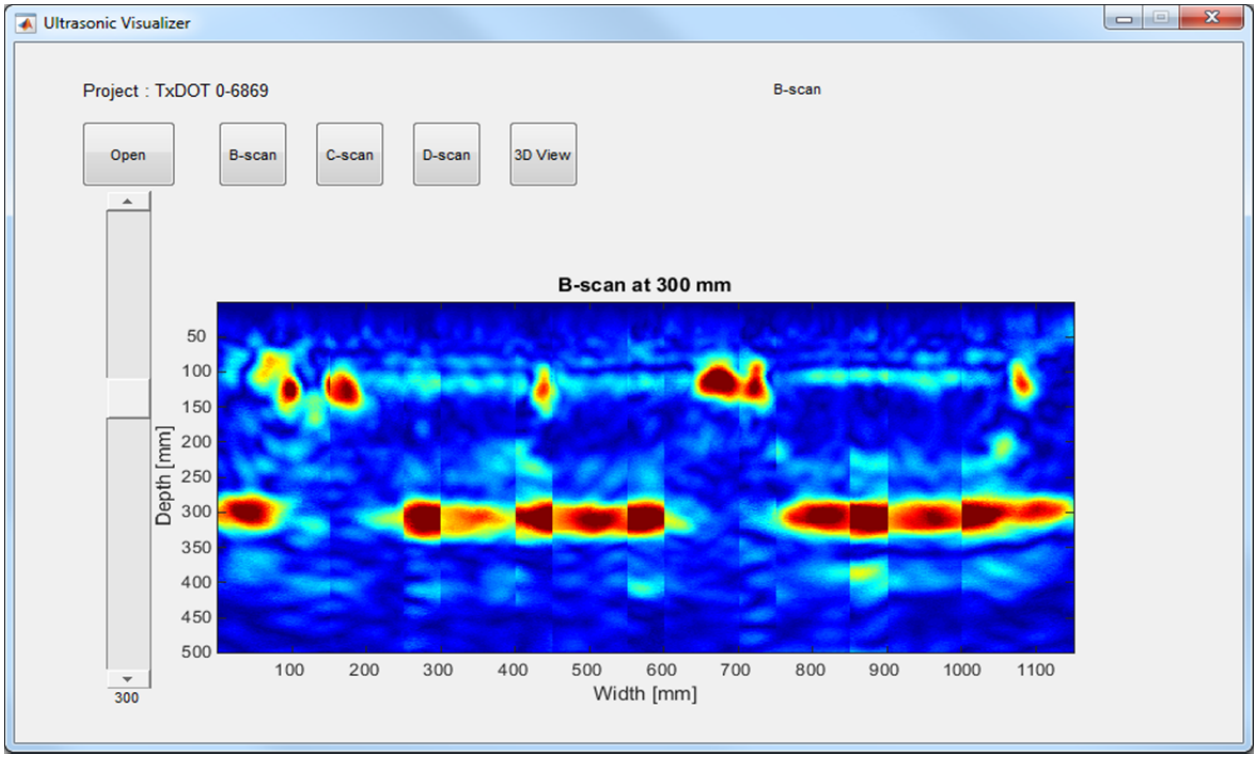

Figure 24. B-Scan of Complete Section.

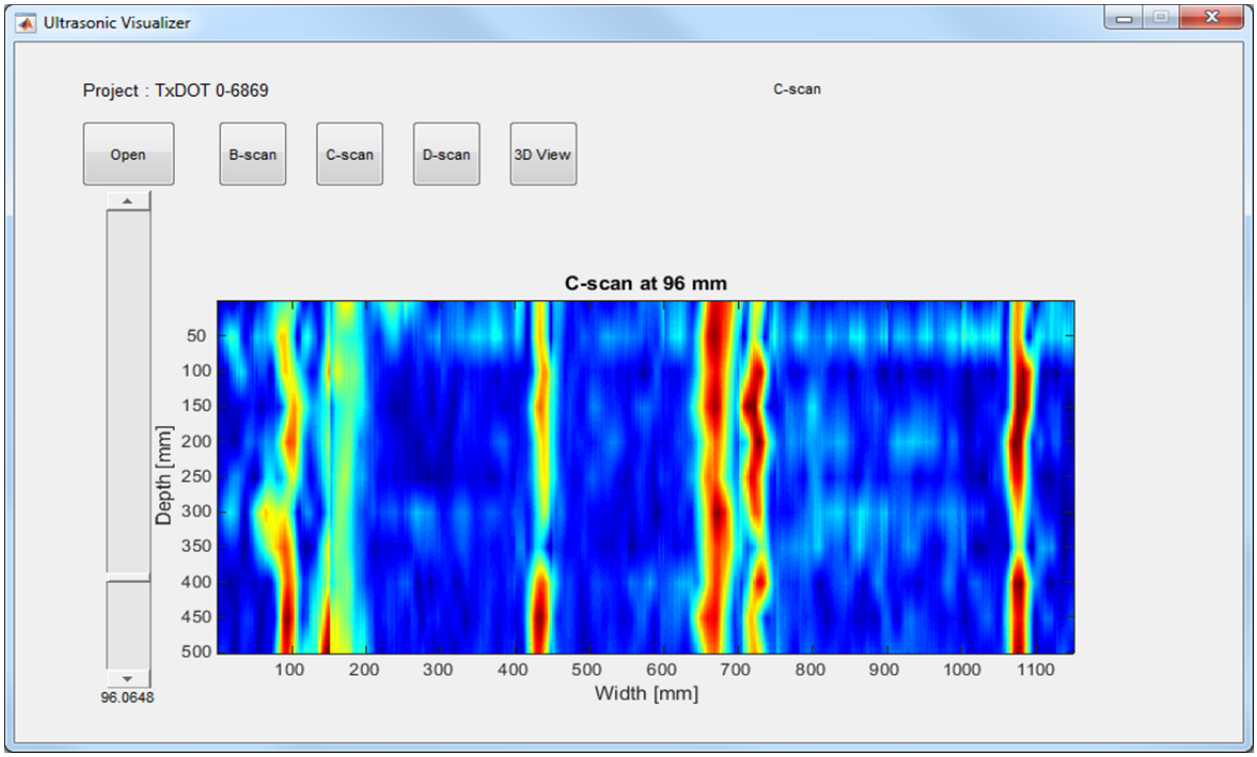

Figure 25. C-Scan of Complete Section.

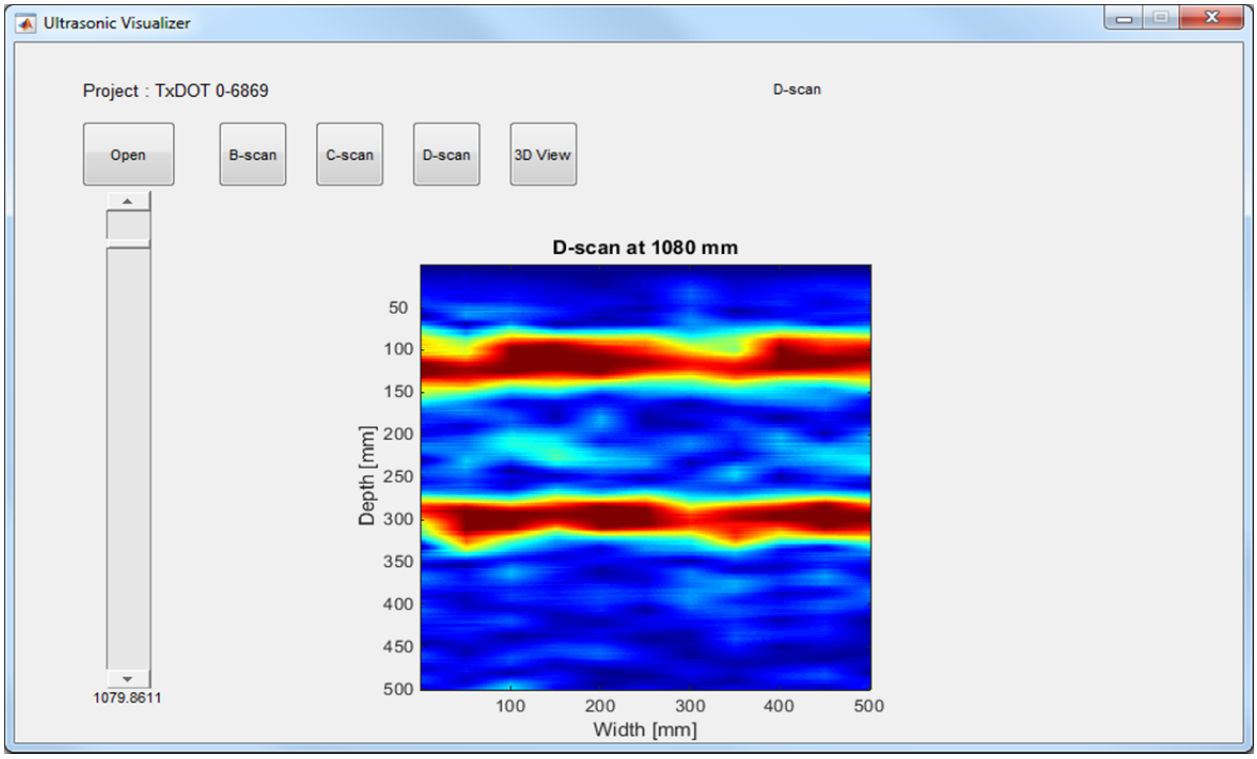

Figure 26. D-Scan of Complete Section.

Conclusion

A SAFT algorithm based on time-domain was developed for this study, and it shows reliable results compared to the embedded SAFT algorithm in the MIRA device. Ultrasonic visualizer for three-dimensional and other complete sectional views (B-, C-, and D-scans) was also developed by linearly interpolating B-scans resulted from the developed algorithm. It provides a lot of intuition about defects to users.

SECTION 4: VERIFICATION OF ULTRASONIC TOMOGRAPHY

Introduction

Wimsatt et al. (2008) identified the need for the implementation of NDT methods into the transportation industry in order safely and efficiently identify potential hazards. It was suggested that researchers conduct demonstrations with techniques that exist, but not widely used, such as ultrasonic tomography. In the years that followed, researchers were able to successfully apply ultrasonic tomography for the classification of defects within tunnel linings that include identifying debonding, delaminations, and moisture undetectable to the naked eye (Wimsatt et al., 2013). This chapter aims to determine the applicability of ultrasonic tomography to the transportation industry in order to maintain and improve the infrastructure.

EyeCon is a portable handheld device that uses ultrasonic waves to detect flaws in concrete. It uses an array of 4 by 6 dry point contact transducers to emit and receive shear waves into concrete. This handheld ultrasonic tomography device is capable of determining the concrete thickness and detecting flaws in concrete such as, delaminations, voids, honeycombing, and

other defects using the ultrasonic pitch-catch methods in the time domain. The device can determine concrete thickness up to 600 mm (26.3 in.) for normal strength concrete and the accuracy of flaw depth is within 10% of the total depth of the concrete. However, it is essential that the capabilities of this device be validated using control test specimens with known conditions, before they can be used in real-time applications. This chapter verifies the ability of this device to detect a variety of flaws that are preconstructed into eleven concrete slabs.

Experimental Setup

A total of 11 concrete slabs with varying depth, reinforcement details, and known defects were available for conducting the experimental program. During construction of the slabs, a defect key was created that documented the exact location of the simulated defects within each slab. All slabs are nominally 1.83 m by 1.83 m (6 ft by 6 ft) in length and width, but vary in depth. Table 1 summarizes the slab depth, reinforcement details, defects, and the location of the defects located within each slab. Test results were compared to this documented defect key for validation. All slabs containing rebar have two mats of No. 5 rebar at depth, *d*, from the top and bottom of the slab, and at 203 mm (8 in.) o.c. All depths of the defects are from the top of the slab. Figure 27 displays the slabs used for testing.

Table 1. Summary of Concrete Slabs with Simulated Defects (Wimsatt et al., 2013).

Slab Number	Slab Depth (mm)	Reinforcement Depth, *d* (mm)	Defect	True Depth of Defect (mm)
I	305	None	None	N/A
II	457	127	Natural Crack	N/A
III	305	127	None	N/A
IV	610	None	None	N/A
V	610	127	None	N/A
VI	381	127	None	N/A
VII	381	127	0.05 mm Thin Plastic	51
VIII	381	127	0.05 mm Thin Plastic	76
IX	381	127	0.05 mm Thin Plastic	25
X	381	127	Air Filled Void (13 mm Foam)	203
XI	381	127	Water Filled Void (Ziploc Bag)	203

Figure 27. Concrete and Shotcrete Specimens at Texas A&M University Riverside Campus, Bryan, TX.

To initiate the scans, consistent settings must be established. Table 2 depicts the settings for testing all slabs.

Table 2. Instrument Settings in Map Mode.

Setting Description	Setting Value
Horizontal Step (mm)	50
Horizontal Size (points)	Off
Vertical Step (mm)	50
Vertical Size (points)	Off
Depth (mm)	Varied by Slab
Frequency kHz	50
Probe Type	Double
Gain dB	75
Period Number	0.5
Accumulation	Off
TGV	On
Readings Discreteness	0.1
Input Signals Filter	On
Pulse Voltage (V)	200
Repetition Rate (Hz)	45
Base (mm)	Off
Scale	mm
Cursor	On
Transducer Orientation	Vertical or Horizontal

Figure 28 displays the experimental setup of the handheld ultrasonic device. The influence of the orientation of the device on the detection of flaws are also investigated for reliability purposes.

Each slab was scanned with the transducer array in the vertical and horizontal orientations. The scans in the two orientations were recorded starting from the same origin, without any changes in the device settings. Figure 29 depicts where the origin of the grid is located, as well as the orientation of all slab images.

Figure 28. Experimental Setup.

Figure 29. Origin of the Grid.

Contrast allows the user to determine if a defect is located within a specimen. The same contrast level is used for both orientations for a given slab, but the level differs between slabs. Table 3 presents a summary of the contrast levels for each slab.

Table 3. Contrast Levels for Analysis.

Slab	I	II	III	IV	V	VI	VII	VIII	IX	X	XI
Contrast Level (dB)	-10	-11	-10	-12	-14	-13	-10	-10	-10	-11	-10

The slabs were tested along a marked grid of squares. The grid comprises of 32 rows and 32 columns. The square grids were 50 mm by 50 mm (2 in. by 2 in.), of which 32 by 31 measurements were taken, comprising a total of 992 individual measurements. The origin of the slab starts 127 mm (5 in.) from the two edges, but varied slightly from slab to slab. This grid size was chosen so that there would be overlapping scanned sections that may be used to obtain images with high resolution for the SAFT algorithm to produce an overall refined image. The transducer array is approximately 120 mm (4.7 in.) long and 80 mm (3.2 in.) wide, so a 50 mm (2 in.) step size both horizontally and vertically allow for 30 mm (1.2 in.) of overlap in one direction and 70 mm (2.8 in.) of overlap in the other. The chosen step size provides a substantial amount of overlap.

In order to complete the settings for the scanning process, the velocity of sound through the slab material must be determined and entered into the settings. The A1040 MIRA to determine the average surface velocity through each slab by take five measurements at arbitrary locations. MIRA contains a fixed array that calculates the surface velocity by measuring the time it takes the wave to travel a distance of 30 mm (1.2 in.). However, this is the surface wave velocity, which has a different velocity than the shear or longitudinal waves that propagate in the medium. A more accurate way to determine the velocity through the specimen would be direct transmission, but this could not be achieved due to lack of access to both sides of the specimen. Therefore, the wave velocity obtained from MIRA is used in this investigation, and this may induce minor errors in the localization of flaws. Table 4 provides the average velocity for each slab.

Table 4. Average Sound Velocity.

Slab	I	II	III	IV	V	VI	VII	VIII	IX	X	XI
Average Velocity (m/s)	3008	2673	2893	2970	2950	2840	2635	2557	2488	2866	2498
Average Velocity (ft/s)	9869	8770	9491	9744	9678	9318	8645	8389	8163	9403	8196

Experimental Procedure

After creating a map with the settings listed in Table 2, the procedure for inspecting the slab specimens is described in what follows:

1. Configure a grid on top of the slab specimen using soapstone. For this section a grid of 32 by 32 squares is used, where each square is 50 mm (2 in.) by 50 mm (2 in.). As shown in Figure 4.3, the origin of the grid is placed approximately 127 mm (5 in.) from the corners.
2. With the transducer in the vertical orientation, take the first scan at the origin with the edges of the transducer aligned with the X and Y-axis of the grid. While on the map screen, the A-Scan will appear on the right hand side. Press the transducer down in order to ensure proper contact with the concrete and press "Enter" to take the scan.
3. Continue to hold the transducer until the measurement is recorded on the Map screen. The device will beep when the measurement has been recorded.
4. Move the transducer 50 mm (2 in.) along the positive X-axis as shown in Figure 4.3, aligning the edges of the transducer with the X-axis and the first line parallel to the Y- axis. Press "Enter" to take the measurement.
5. Continue to take measurements across the first row using the same procedure listed in Step 4.
6. After the first row is complete, move the transducer to the origin and then 50 mm (2 in.) along the positive Y-axis to the second row. Move the cursor on the Map screen to match this point. Take measurement by pressing "Enter".
7. Continue taking measurements, one at a time, in the horizontal direction until the second row is complete, then repeat the process for Rows 3 through 32, until the entire slab has been scanned.
8. Upload data into a storage device.

A visualization software was used to obtain refined C-scans of the specimens. Negative contrasts are used in order to have the defects appear bright red during the analysis. The contrast must be adjusted in order to determine if a defect is present within the concrete. Initially, without contrast, the entire slab appears red, which is the default setting. The user must adjust contrast in order to accurately locate defects. For concrete, most contrast levels are between -10 and -15 dB. After the appropriate contrast settings are applied, unaffected concrete appears as various tones of blue due to the non-homogeneous nature of concrete. The procedure is described below.

1. Open the *map.cfg* file from the folder containing the files from the scan.
2. Wait for the file to load and configure.
3. Click the settings button to ensure required settings, they can be changed at this point if necessary.
4. Press the +/- buttons in the top right corner to adjust the contrast level to clearly see defects within the slab. Most slabs were analyzed with a contrast level between -10 and -15 dB.
5. Use arrows in the left side to move through the slab is the X, Y, and Z directions to see the D, B, and C scans, respectively.

The above procedures were followed for the scans using both the vertical and horizontal transducers orientations, and the results were compiled for each slab. The scans are analyzed in depth and compared to the slab key to determine if the defects were accurately located.

Experimental Results

Plain Slabs

Slabs that contained no rebar or stimulated defects are discussed in this section. These include Slab I and IV that are 305 mm (12 in.) and 610 mm (24 in.) deep, respectively. From the results of the scan measurements, the depth of the two slabs were estimated to be 300 mm (11.8 in.) and 610 mm (24 in.), which compares well with the actual thickness of the slab. Figure 30(a) and Figure 4.3(b) show representative C-scan images from Slab I and IV. The analysis of C-scans from the two slabs predominantly revealed blue contrast, with slight variations in tone. The various tones of blue found in Figure 30 and additional images in Appendix A, are due to the nonhomogeneous nature of the concrete. The lack of any major contrast in the C-scans suggests that there no defects or reinforcement within these slabs. These findings correspond well with the defect key. However, the C-scans of Slab IV, revealed the presence of a small defect at a depth of 330 mm (13 in.), which is not documented in the defect key. This is likely due to the hollow formwork that was used to construct the slab that may have accumulated water or debris.

Scans from the vertical orientation and horizontal orientation of the device were also compared to each other. Irrespective of the orientation of the device, similar results were obtained in terms of the overall depth, and the absence of defects and reinforcement in the slab. The location of the lighter blue tones are similar, although not completely identical. There are no notable variations in contrast of the C-scans to indicate the possibility of defects within the slabs. From both transducer orientations, it is evident that the slab is clear of significant imperfections and both scans produce similar information. Additional C-scans at various depths of Slab I and IV can be found in Appendix A.

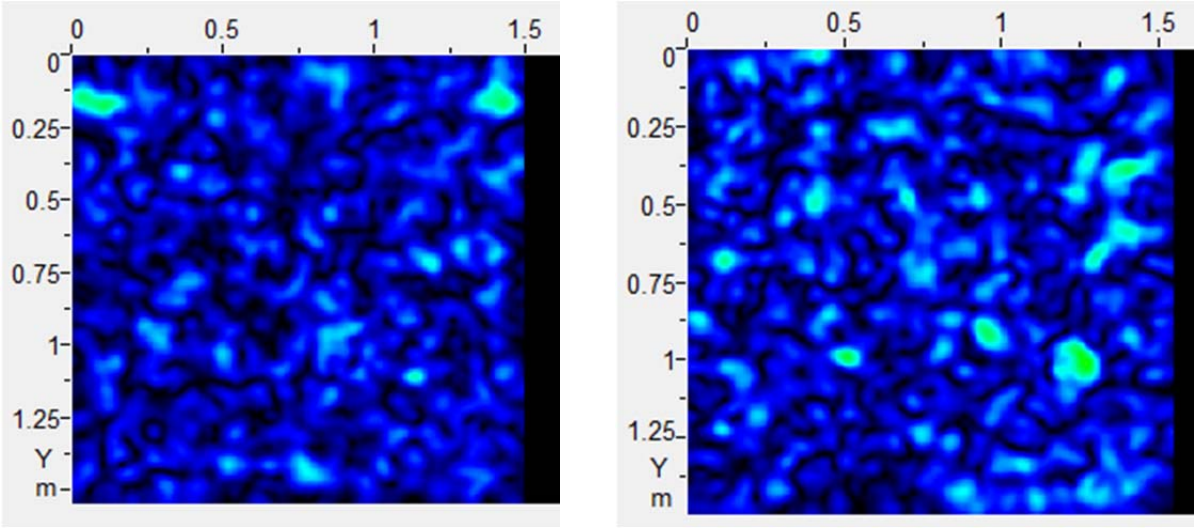

(a) Slab I at a Depth of 150 mm (5.9 in.) (b) Slab IV at a Depth 180 mm (7.1 in.)

Figure 30. C-Scans of Plain Slabs.

Reinforced Slabs without Defects

This section discusses reinforced slabs without any simulated defects. These includes Slabs II, III, V, and VI. The overall depth of Slab II and III are 457 mm (18 in.), and 305 mm (12 in.), respectively, whereas Slab V has a total depth of 610 mm (24 in.) and Slab VI has an overall depth of 381 mm (15 in.). All slabs contain two layers of No. 5 rebar at a depth of 127 mm (5 in.) from the top and bottom surface of the slab, without any simulated defects.

A review of the C-Scan images of the slabs, does not reveal any features before a depth of 100 mm (3.9 in.). A grid develops at an approximate depth of 100 mm (3.9 in.) with the contrast becoming most apparent at depths of 120 mm (4.7 in.) and 130 mm (5.1 in.). Figure 31 shows the C-scans of all the reinforced slabs at a depth of 120 mm (4.7 in.) or 130 mm (5.1 in.). From these images, it is evident that the grid shape corresponds to the first layer of reinforcement. As the image visualization program reads only to the nearest centimeter, the images shown in Figure 31 have the greatest contrast area between depths of 120 mm (4.7 in.) and 130 mm (5.1 in.). This corresponds to the actual depth of the rebar at 127 mm (5 in.) from the surface of the slab. The diameter of a No. 5 bar is 16 mm (0.6 in.), and at locations where the horizontal and vertical rebar overlap the overall diameter is 32 mm (1.3 in.). The images reflect the first indication of the rebar at a depth of 100 mm (3.9 in.), which is within 11 mm (0.4 in.) of the actual edge of the first layer of rebar at a depth of 111 mm (4.7 in.). A depth of 111 mm (4.7 in.) is where the layer should start to emerge at points where the horizontal and vertical rebar overlap. This difference accounts for a variation of 2.4 percent of the total depth of the slab, which is well within the manufacturer's tolerance of 10 percent of the total depth of the specimen.

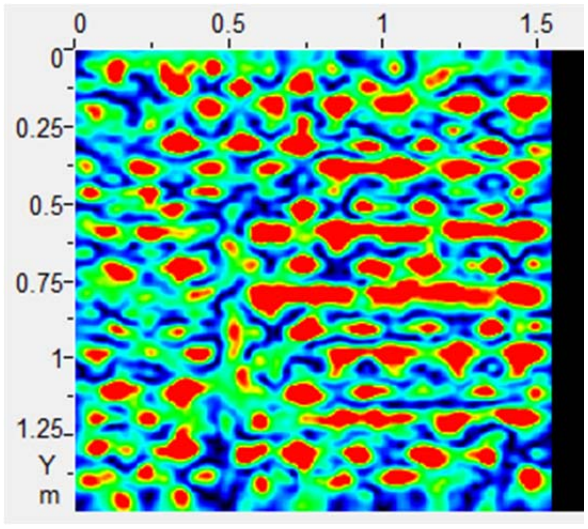

(a) Slab II at a Depth of 120 mm (4.7 in.)

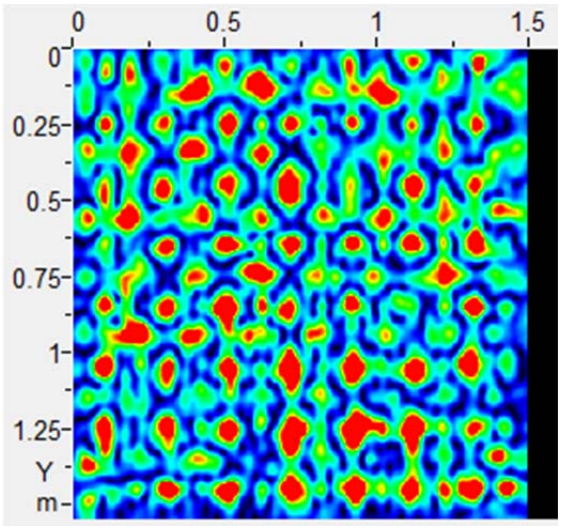

(b) Slab III at a Depth of 120 mm (4.7 in.)

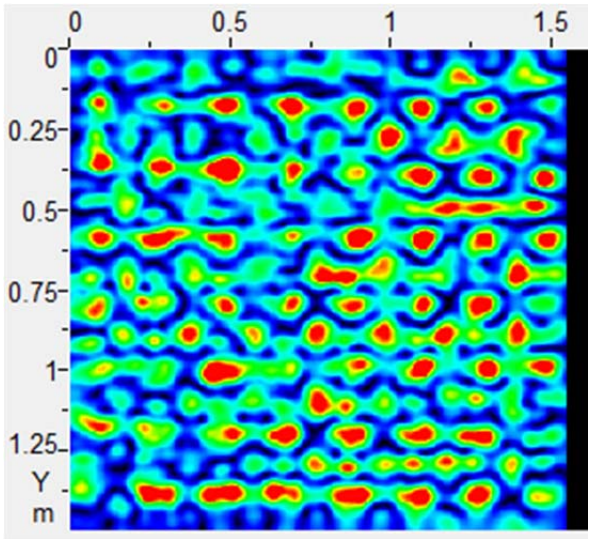

(c) Slab V at a Depth 130 mm (5.1 in.)

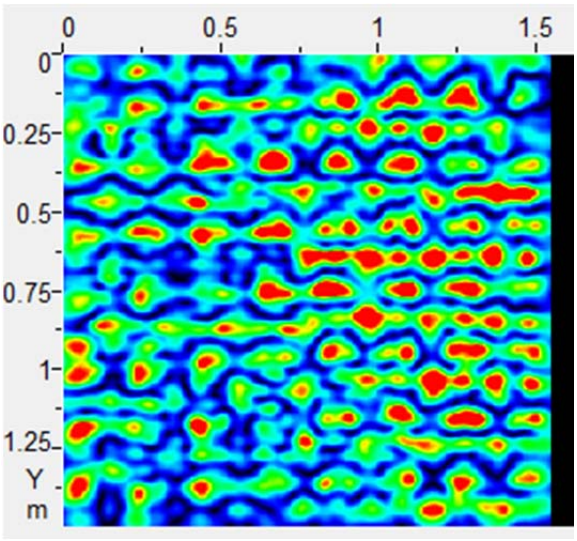

(d) Slab VI at a Depth of 120 mm (4.7 in.)

Figure 31. C-Scans of Reinforced Slabs without Defects.

Since the depth of each slab differs the location of the second layer of rebar in each slab differs as well. In Slab II, a second rough grid image emerges at a depth of 330 mm (13 in.), but become more apparent at a depth of 370 mm (14.6 in.). The center of the second layer of reinforcement is at an actual depth of 330 mm (13 in.). The scan measurements provide a good indication of the second layer of rebar. The lower accuracy may be attributed to the greater attenuation of the ultrasonic waves. The end of the concrete slab is estimated to be at 460 mm (18.1 in.), 3 mm (0.1 in.) greater than the actual depth of 457 mm (18 in.). The shallow natural crack on the surface of Slab II, which is visible to the naked eye was not detected by the scan measurements. However, these surface cracks are not deep enough to affect the internal integrity of the slab.

In the case of Slab III the second layer of grid appears at a depth of 210 mm (8.3 in.), with a more well-defined grid emerging at a depth of 220 mm (8.7 in.). The actual depth of the second

layer of No. 5 rebar is at a depth of about 180 mm (7 in.). This discrepancy in the estimated depth of the second reinforcement layer may be attributed to the close proximity of the two layers of rebar. A significant amount of the wave energy gets reflected back to the transducers after encountering the first layer of rebar, which limits the amount of wave energy hitting the second layer of rebar. Overall, the system does detect the second layer and is within 30 mm (1.2 in.) of its exact location, which is within the manufacturer's 10 percent margin of error for the 305 mm (12 in.) thick slab. The overall depth of the slab is estimated to be 300 mm, which compares well with the actual depth of the slab of 305 mm (12 in.).

C-Scan images of Slab V, do not show the presence of any defects of reinforcement between depths of 150 mm (5.9 in.) to 480 mm (18.9 in.). At 480 mm (18.9 in.) a vague grid starts to appear, with it being most clear at a depth of 530 mm (20.5 in.). However, the documented depth of the second layer of rebar is at 480 mm (18.9 in.). The error of 50 mm (2 in.) in locating the second layer of reinforcement is again attributed to the greater attenuation of the ultrasonic waves as the waves travel deeper into the reinforced concrete slab. This may alter the signal and slightly skew the depth of the second layer of reinforcement, but is still within the device's 10% accuracy.

Similar to Slab V, C-Scan images of Slab VI does not show any contrast between the depths of 150 mm (5.9 in.) to 280 mm (11 in.). At 280 mm (11.02 in.), the second layer of rebar appears as a faint grid, with it becoming more apparent at 300 mm (11.8 in.). The estimated depth of the reinforcement layer is 46 mm (1.8 in.) away from the actual location of the reinforcement at 254 mm (10 in.). This results in an accuracy of 12% of the overall depth of the slab, which is slightly above the manufacturer's 10% accuracy limit. This difference is again attributed to the attenuation of ultrasonic waves. The bottom of the slab was determined to be at 380 mm (15 in.) which corresponds closely with the actual depth of 381 mm (15 in.).

A comparison of the scans from the vertical and horizontal orientation of the transducers resulted in similar results. Both scan orientations indicate the first signs of rebar at a depth of approximately 100 mm (3.9 in.) with it being most visible between depths of 120 mm (4.7 in.) and 130 mm (5.12 in.) for all the reinforced slabs. Both orientations clearly depict the location of the first layer of rebar, though the images are slightly different. Additional C-Scan images can be found in Appendix A. The vertical orientation of the transducer shows the rebar parallel to the X-axis more clearly, while the horizontal orientation of the transducer shows the rebar parallel to the Y-axis better. This is due to the orientation of the waves emanating from the emitting transducers. Since the waves propagate in a different direction depending on the transducer orientation, they are able to locate either the horizontal or vertical rebar more clearly. Though these images are slightly different, the location and depiction of the rebar is unmistakable, meaning both orientations provide reasonable images of the interior of the slab through its depth. These results indicate that the device may have difficulty detecting defects that are parallel to the device's orientation. Overall, the system successfully locates two layers of rebar and their approximate locations for each slab, with less accuracy in locating the second layer.

Reinforced Slabs with Thin Plastic Defects

This section discusses reinforced slabs that contain simulated 0.05 mm thin plastic defects. These include Slabs VII, VIII, and IX. All slabs are 381 mm (15 in.) thick, and contain two layers of rebar at 127 mm (5 in.) and 254 mm (10 in.), with varying depths of the thin plastic defect.

Slab VII has a plastic defect at a depth of 51 mm (2 in.) from the top surface. The C-Scan images did not display any contrast between 0 mm to 60 mm (2.4 in.). At around 60 mm (2.4 in.), a faint square appears but becomes clearer at 70 mm (2.8 in.), and is most apparent at a depth of 80 mm (3.2 in.) as demonstrated in Figure 32(a). The initial indication of the plastic defect at 60 mm is relatively close to its actual depth of 51 mm (2 in.) at which the defect is located. The difference in 9 mm (0.4 in.) corresponds to 2.4% accuracy. It is also important to note that the actual defect is only 0.05 mm (0.002 in.) thick, but the C-Scan images show the presence of the defect from a depth of 60 mm (2.4 in.) to 190 mm (7.5 in.). The ultrasonic waves do not penetrate through the defect, therefore, creating a shadow effect beyond the initial location of the defect.

Similar to Slab VII, a square defect starts to emerge in Slab VIII at a depth of approximately 80 mm (3.2 in.) with it becoming more apparent at a depth of 90 mm (3.5 in.), as displayed in Figure 32(b). The first sign of the defect at a depth of 80 mm (3.2 in.), corresponds well with the actual location of the defect located at a depth of 76 mm (3 in.).

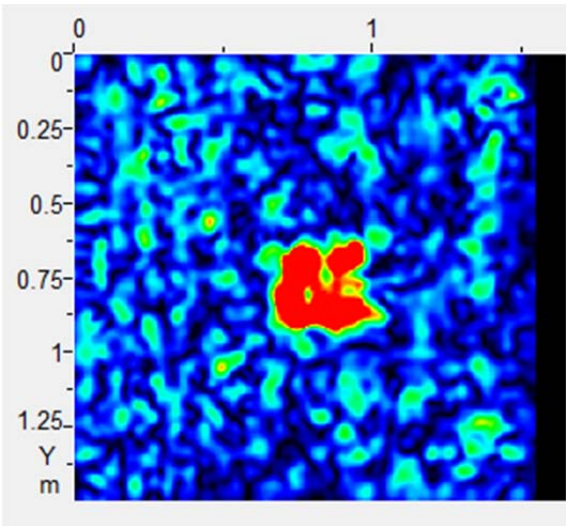

(a) C-Scan of Slab VII at a Depth of 80 mm (3.2 in.)

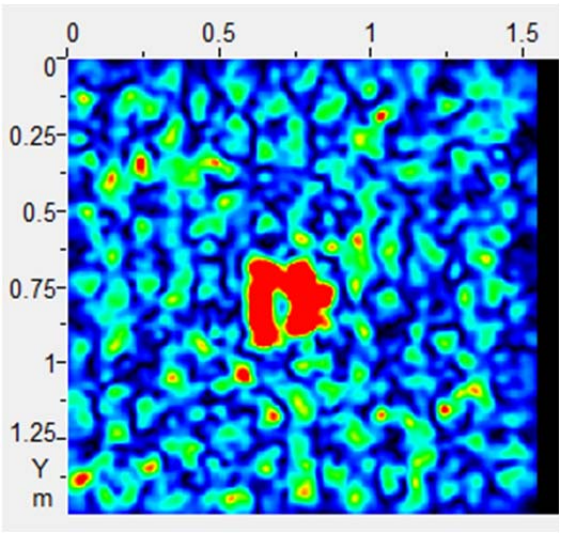

(b) C-Scan of Slab VIII at a Depth of 90 mm (3.54 in.)

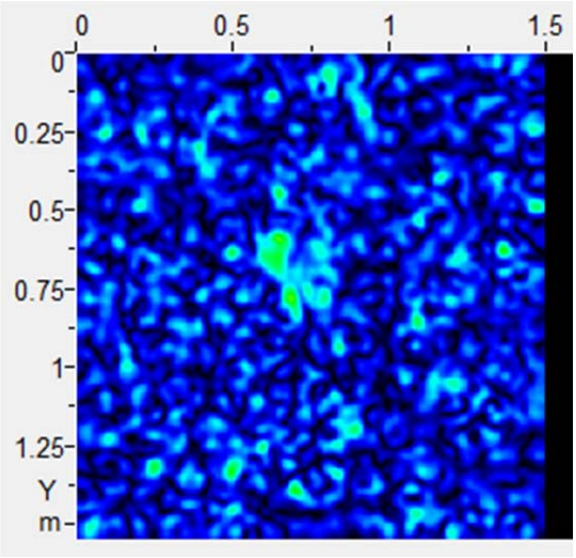

(c) C-Scan of Slab IX at a Depth of 30 mm (1.2 in.)

Figure 32. C-Scans of Reinforced Slabs with Thin Plastic Defects.

The thin plastic defect that is located at a depth of 25 mm from the top surface of the slab was not positively detected by the ultrasonic tomography device. In Figure 32(c), a small portion of the defect can be seen, but it is not as prominent as other plastic defects.

In the case of Slab VII and VIII, since ultrasonic waves are generally unable to penetrate through the plastic defect, a shadowing effect can be seen throughout the slab. Whole or partial images of the square shape can be seen at various depths further than the location of the defect. Also, at the bottom of the slab, a rough square outline can be seen in blue tones with the rest of the end of the slab being red.

Additionally, in all three slabs a layer of reinforcing steel appears at a depth of 100 mm (3.9 in.) with it most prominent at depths between 120 mm (4.7 in.) and 130 mm (5.1 in.) from the top of

the slab. This is close to the actual location of the rebar which ranges between 110 mm (4.3 in.) and 150 mm (5.9 in.). At a depth of approximate 160 mm (6.3 in.) the first layer of steel does not appear in the C-Scans. This is reasonable since at overlapping point of vertical and horizontal rebar the total diameter is 32 mm (1.3 in.). The second layer of rebar in each slab is not as clear as the first because of the attenuation of ultrasonic waves, as in previous cases. For slab VII, the lattice is most visible at 290 mm (10.6 in.), while in Slabs VIII and IX it is most prominent at 270 mm (10.6 in.) and 250 mm (9.4 in.), respectively. The second layer has a documented located of 254 mm (5 in.) in all cases. The difference ranges from 4 mm (0.16 in.) to 36 mm (1.4 in.). The differences in depth over the total depth of the slab is within 10%. Slab VII and IX are determined to be 380 mm (15 in.) thick, while Slab VIII is determined to be 370 mm (14.57 in.), which are close to the actual documented depth of 381 mm (15 in.) for each slab.

When comparing the transducer orientations, no undocumented defects were detected. The difference is that the vertical orientation shows the left and bottom edges of the plastic defect more clearly, while the horizontal orientations show the top and bottom edges. The actual depth of the plastic defect is only 0.05 mm (0.002 in.) thick in all the slabs. However, they are present in a majority of the C-Scans beyond the initial appearance of the defect, indicating that the device is unable to accurately depict the thickness of the defect. Additional images for Slabs VII, VIII, and IX can be found in Appendix A.

Reinforced Slabs with Air Filled Voids

This section discusses reinforced slabs that contain air filled voids. The overall depth of Slab X is 381 mm (15 in.), and it contains two layers of rebar at 127 mm (5 in.) and 254 mm (10 in.). The air filled void is simulated using a 13 mm (0.5 in.) thick foam and the defect is located at a depth of 203 mm (8 in.). Slab X also has a noticeable crack on the surface of the slab, but it was not detected by the ultrasonic tomography device. Similar to the other slabs, a rebar grid emerges at a depth of approximately 100 mm (3.9 in.). The grid is most clearly visible at a depth of 130 mm (5.1 in.). This corresponds to the first layer of rebar. After the first layer of rebar, a defect starts to appear approximately in the center of the slab at a depth of 210 mm (8.3 in.). As shown in Figure 33, the defect becomes most apparent at a depth of 220 mm (8.7 in.).

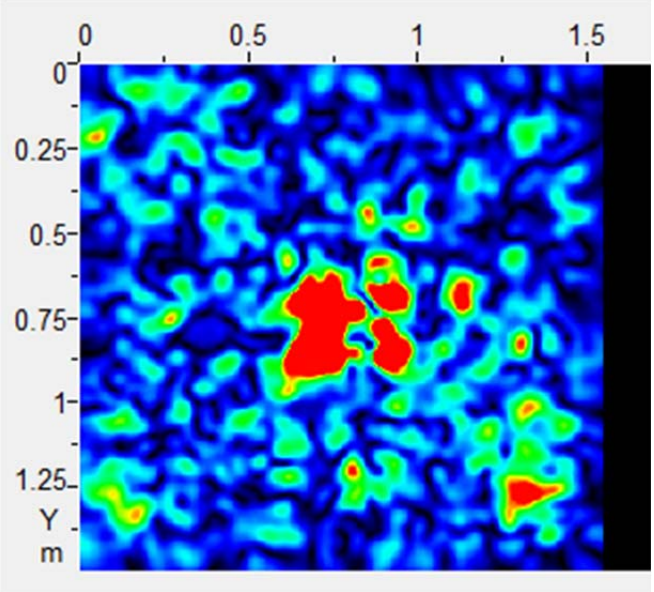

Figure 33. C-Scan of Slab X at 220 mm (8.7 in.).

The defect can also be seen at 230 mm (9.1 in.), and 250 mm (9.8 in.). The difference in contrast was evident in C-scans up to a depth of 250 mm (9.8 in.). The recorded bottom edge of the foam is located at 218 mm (8.58 in.), while the measured bottom edge is at 250 mm (9.8 in.), a difference of 32 mm (1.3 in.), which is within the acceptable 10% accuracy specified by the manufacturer. Beyond this point, small reflections may be observed. However, they are not well defined, and therefore are not considered to be part of the defect. The device was not able to clearly locate the second layer of rebar which is located at a depth of approximately 254 mm (10 in.) from the top of the slab. In Figure 33, some contrast can be seen around the air void, this may be due to the limited amount of wave energy reaching this depth. From the measurements, the slab is determined to be 380 mm (15 in.) thick, which is very close to the actual slab thickness. The bottom of the slab is not as clear as with other slabs. This may be due to the limited wave energy traveling the whole depth of the slab due to a significant amount of energy being reflected by the rebar and air void.

A comparison is also made between the scan measurements obtained from the horizontal and vertical orientation of the transducers. The crack on the surface of Slab X did not penetrate the surface and was not detected by either transducer orientation. No defects were detected in Slab X by either scan measurements, up to a depth of 100 mm (3.9 in.). At a depth of 100 mm (3.9 in.), both scans show the emerging rebar, centrally located at a depth of 127 mm (5 in.). Similar to other comparisons, the vertical transducer orientation displays a clear image of the horizontal rebar, whereas with the horizontal orientation the vertical rebar is more apparent. Though the scans are not identical, they provide similar information and clearly indicate the location and presence of the reinforcing steel. A defect starts to appear in Slab X at a depth of 210 mm (8.3 in.), and the air filled void becomes more apparent at a depth of 220 mm (8.7 in.) for both transducer orientations. The two separate scans indicate the defect is present from a depth of 210 mm (8.3 in.) to 260 mm (10.2 in.). The scans show a shadow beyond the location of the defect due to the shadowing effect that was previously described. Most importantly the scans correspond to one another at every point throughout the slab, though they are not identical. Neither scan was able to clearly identify the second layer of rebar but with some experience the

user can see suggestions that it is present within the slab. Further information regarding Slab X can be seen in Appendix A.

Reinforced Slabs with Water Filled Voids

Slab XI is a reinforced concrete slab that is 381 mm (15 in.) thick. The slab has two layers of reinforcement at a depth of 127 mm (5 in.) and 254 mm (10 in.). The water filled void is simulated by embedding a Ziploc bag filled with water. The defect is located at a depth of 203 mm (8 in.) from the surface of the concrete slab. From the C-scans, it is evident that no defects are present up to a depth of 90 mm (3.5 in.). At approximately 90 mm (3.5 in.), a grid pattern emerges and is thickest at a depth of 120 mm (4.7 in.) indicating the presence of rebar. This corresponds well with the actual location of the rebar that are located at a depth of 127 mm (5 in.). In the C-scan images, at a depth of 200 mm (7.9 in.), a change in color begins to faintly appear in the center of the slab. However, as displayed in Figure 34, the contrast is highest at a depth of 210 mm (8.3 in.).

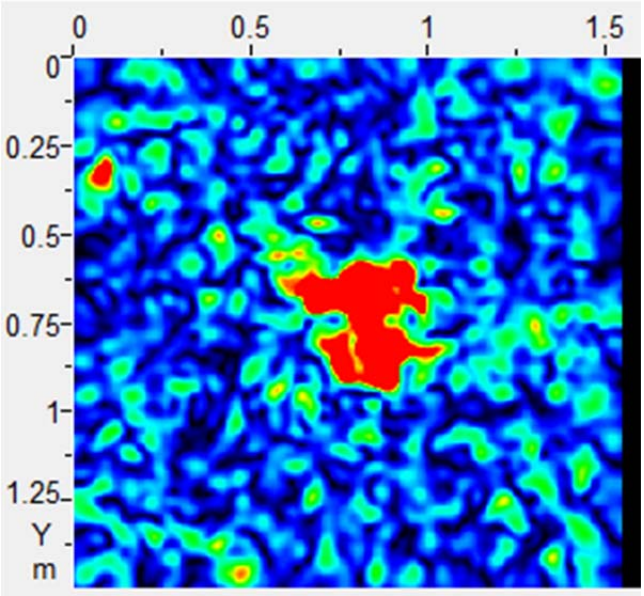

Figure 34. C-Scan of Slab XI at 210 mm (8.3 in.).

Beyond this point it begins to dissipate and disappears completely after a depth of 250 mm (9.8 in.). This compares well with the actual location of the water defect, which is located at a depth of 203 mm (8 in.) from the top of the slab. The ultrasonic tomography results also accurately determine the thickness of the defect, unlike plastic or air defects. The estimated thickness of the defect is 50 mm (2 in.), which is close to the actual defect thickness of 58.4 mm (2.3 in.). After the defect, a faint rebar grid appears thickest at a depth of 300 mm (11.8 in.). The reflection of the water void is also seen in the bottom of the slab. This was observed in all slabs with plastic, water, or air filled defects towards the center of the slab, with it being least prevalent in the case of the air void.

From the scans using the two different transducer orientations, Slab XI was determined to be roughly 380 mm (15 in.) deep. Each scan successfully identified two layers of rebar and a water void and did so at the same depths, providing identical results. C-scan images, at the same depth

compare well with each other. This indicates that transducer orientation does not significantly affect the device's abilities in identifying water filled voids in reinforced concrete slabs. Additional images of Slab XI can be seen in Appendix A.

Comparison of Image Quality with and without Overlapping Measurements

Ultrasonic tomography relies on the SAFT algorithm to construct complete 2-D or 3-D images from a compilation of individual pulse echo scans. The scans typically overlap one another in order to produce a higher resolution image. The clarity produced by using overlapping images can help when identifying defects within a concrete component. More overlapping requires a greater number of scans. This task aims to determine if defects can still be detected to a sufficient level of detail without the use of overlapping scans. Figure 35 shows the difference between the grids with overlap, and no overlap. The black rectangle represents the transducer with the vertical orientation in reference to the grid.

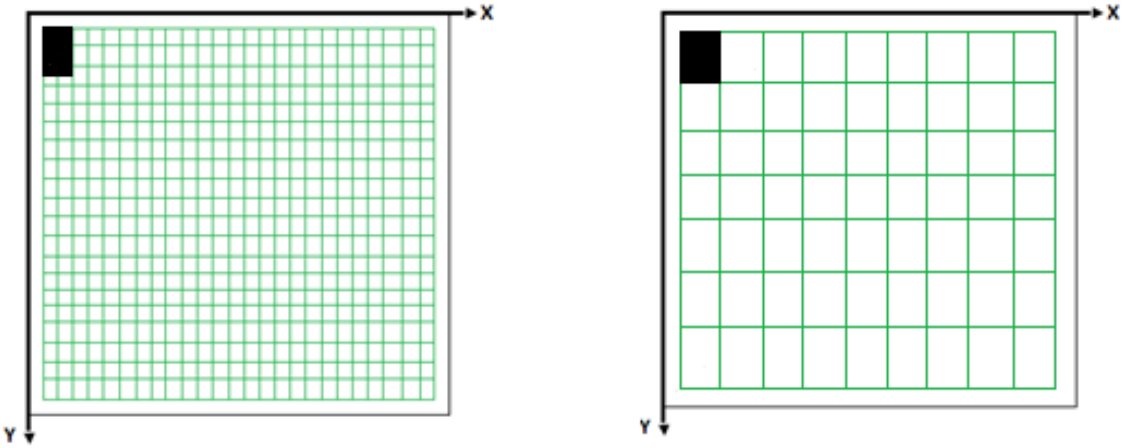

(a) For Overlapping Scans. (b) For Non-Overlapping Scans.

Figure 35. Grid for Overlapping vs Non-Overlapping Measurements.

In Figure 35(a), a grid is shown that is representative of each square being 50 mm (2 in.) along the X-axis by 50 mm (2 in.) along the Y-axis, which allows for a minimum of 30 mm (1.2 in.) overlap for the 80 mm (3.2 in.) by 120 mm (4.7 in.) transducer. Figure 35(b) displays a grid that was used for no overlap with the transducer in the vertical orientation. This means the shorter side of the transducer is parallel to the X-axis, so each rectangle is 80 mm (3.2 in.) along the X-axis and 120 mm (4.7 in.) along the Y-axis. To scan the slab with no overlap in the horizontal orientation, each rectangle in the grid would be 120 mm (4.7 in.) parallel to the X-axis and 80mm (3.2 in.) parallel to the Y-axis.

Slab VIII was chosen to investigate the effects of overlapping scans as it contains a defect as well as two layers of rebar. Comparison of overlapping and non-overlapping scans in both the vertical and horizontal transducer orientation are discussed in what follows. The two orientations with overlapping measurements were analyzed with a contrast of -10 dB, while the two orientation with non-overlapping measurements were analyzed with a contrast of -5 dB. The non-overlapping scan is not as refined and therefore requires less contrast to see defects.

Figure 36 shows a comparison of the C-scans at a depth of 30 mm (1.2 in.), obtained with and without overlapping scans with the vertical and horizontal orientation of the transducer. No defects are revealed in any of the four C-scan images presented in Figure 36, which corresponds with the actual condition of Slab VIII. Figure 36 (c) and (d) do not have the same resolution as the images in Figure 36 (a) and (b), but they are able to convey identical information to the user.

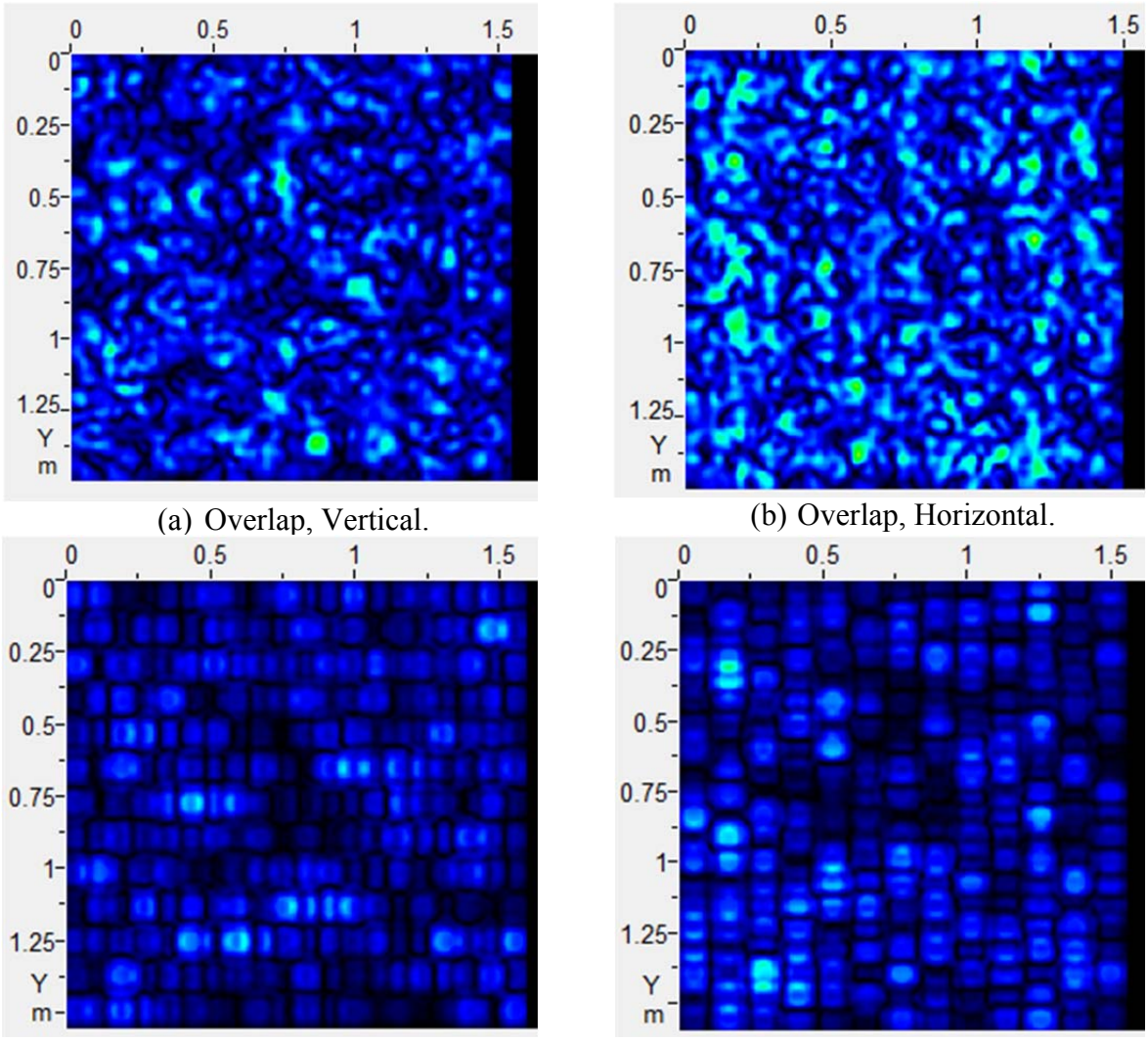

(a) Overlap, Vertical.

(b) Overlap, Horizontal.

(c) No Overlap, Vertical.

(d) No Overlap, Horizontal.

Figure 36. Comparison of C-Scans Obtained from Scan with and without Overlap – Slab VIII at a Depth of 30 mm.

Figure 37 compares the scans at a depth of 80 mm (3.2 in.). As shown in Figure 37 (a) and (b), the plastic defect at the center of the slab is clearly visible near the center of the slab with measurement overlap. Figure 37 (c) depicts a vertical transducer orientation with no overlap. In this image, red portions are indicative of the thin plastic defect, but the resolution is limited and only an experienced eye would be able to identify these red marks as a defect. Figure 37 (d), horizontal scans with no overlap, has a better clarity than Figure 37 (c), vertical no overlap, showing a more defined square defect near the center of the slab.

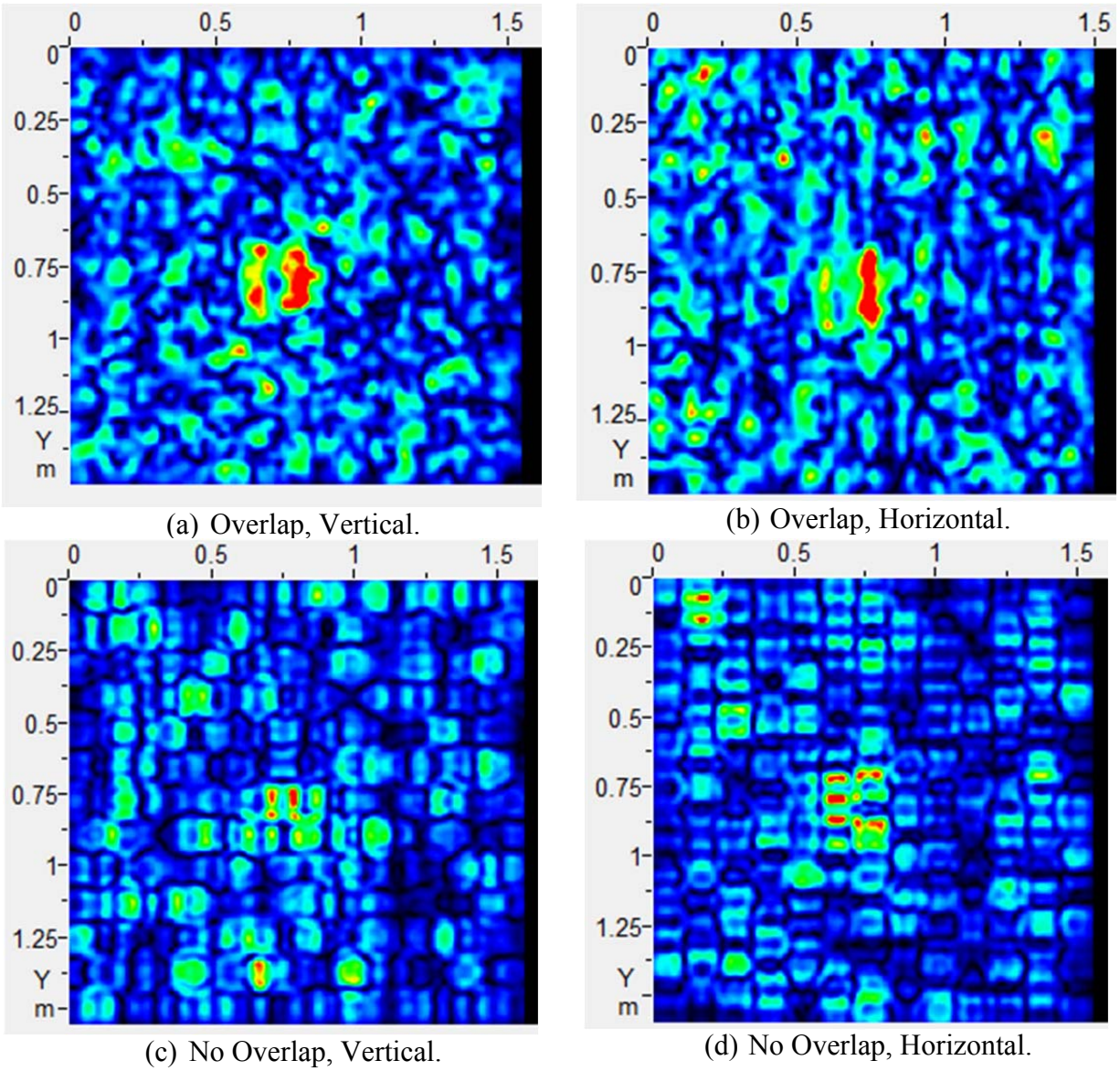

(a) Overlap, Vertical.

(b) Overlap, Horizontal.

(c) No Overlap, Vertical.

(d) No Overlap, Horizontal.

Figure 37. Comparison of C-Scans Obtained from Scan with and without Overlap – Slab VIII at a Depth of 80 mm.

Figure 38 shows a comparison of C-scan images at a depth of 100 mm (3.9 in.). Rebar emerges at a depth of 100 mm (3.9 in.). With overlapping measurements, seen in Figure 38 (a) and (b), the thin plastic defect is prominent at the center of the slab, with the shape of the reinforcing steel grid surrounding it. With no overlapping measurements, the thin plastic defect can still be identified unmistakably near the center of the slab as shown in Figure 38 (c) and (d), but the rebar is not as evident. It is more evident at 100 mm (3.9 in.) than at 80 mm (3.2 in.) for the scans taken with no overlapping measurements, indicating that the depth may not be as accurate but the device can still locate the defect with reasonable error, within 10% of the total depth.

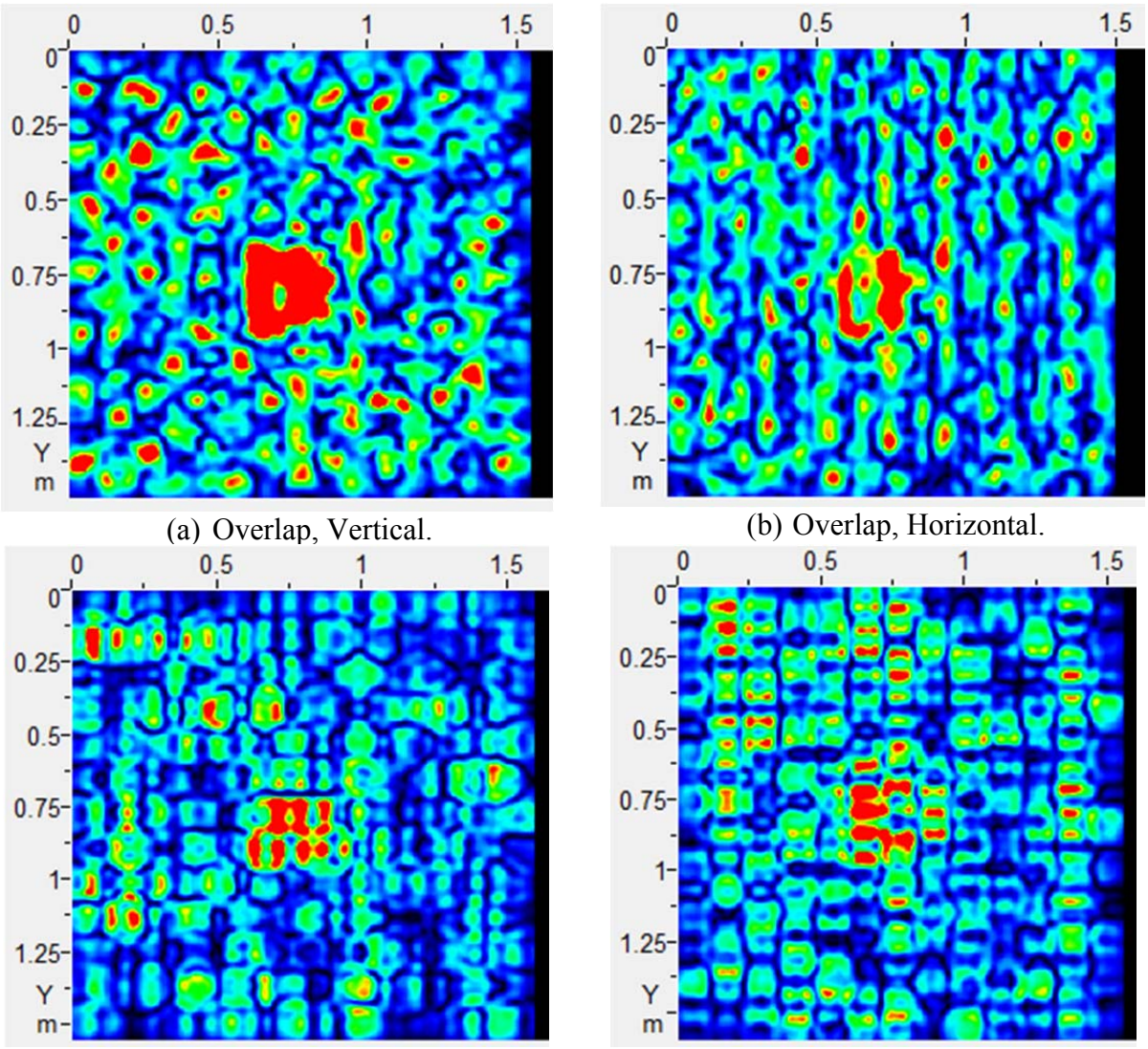

(a) Overlap, Vertical.

(b) Overlap, Horizontal.

(c) No Overlap, Horizontal.

(d) Overlap, Vertical.

Figure 38. Comparison of C-Scans Obtained from Scan with and without Overlap – Slab VIII at a Depth of 100 mm.

Conclusion

Table 5 provides a summary of the defects defected in each slab. If the slab contained reinforcing steel, the first layer is described in the table with the first layer being stated first. Slabs that contained an artificial defect are also described in the summarizing table. The error in this case is represented as the absolute value of the actual depth minus the determined depth over the total depth of the slab. The error ranges from 0.66 to 2.3 percent for the detection of reinforcement. For defects the error range is from 1 to 2.4 percent.

Table 5. Summary of Defects.

	Reinforcement			Defect		
Slab Number	**True Depth (mm)**	**Determined Depth (mm)**	**Accuracy Over Depth (%)**	**True Depth (mm)**	**Determined Depth (mm)**	**Accuracy Over Depth (%)**
I	N/A	N/A	N/A	N/A	N/A	N/A
II	127	130	0.66	N/A	N/A	N/A
III	127	120	2.3	N/A	N/A	N/A
IV	N/A	N/A	N/A	N/A	N/A	N/A
V	127	130	0.66	N/A	N/A	N/A
VI	127	130	0.66	N/A	N/A	N/A
VII	127	130	0.66	60	51	2.4
VIII	127	130	0.66	80	76	1
IX	127	130	0.66	Not Identified	25	N/A
X	127	130	0.66	210	203	1.8
XI	127	120	1.8	210	203	1.8

A comparison of results obtained from the vertical and horizontal scan orientations show some interesting trends. First, the vertical scan orientation more clearly detected the horizontal rebar while the horizontal scan orientation showed the vertical rebar more clearly. This observation was made consistently in all slabs that contained reinforcing steel. The simulated defects do not present the exact same image in each orientation but enough information is provided for the user to come to the same conclusion about the defect location. Also, in every slab with a defect, a shadow of the defect, the blue color and the shape of the defect, could be seen at the bottom of the slab. Slab IX didn't contain as clear of a shadow, but it did have a slight outline of where the defect would be located. In addition, Slab IX was the only slab to not clearly identify the defect. This is due to the lack of wave energy penetrating the full thickness of the slab. When comparing images obtained from overlapping scans with images obtained from scans with no overlap, the former provided better clarity of the defects; however, the defect could be seen with the latter case also. For the latter case, better familiarity with interpreting scan images may be required to determine the location of the defects.

Scanning the concrete slabs with overlap, as described above, takes an average of 2.5 hours per slab (6 ft by 6 ft). To scan a concrete slab without overlap takes 45 minutes. While the device can identify, localize, and size defects in concrete structures, it is labor intensive and costly. Additionally, this time does not include data processing, which could add several extra hours of work. To combat these issues, a zero-intrusive ultrasonic tomography device is necessary for the future to nondestructively test bridge decks.

SECTION 5 CONCLUSIONS

The design of the zero-intrusive ultrasonic tomography system has several key features. First, the transducers do not require any coupling agent, which decreases operating costs and time. Additionally, the transducers are spring-loaded, therefore allowing for proper contact with the test surface, irrespective of the texture of the surface. The prototype is designed to be lightweight, making it maneuverable and portable. Lastly, the design also allows for future iterations and improvements by allowing for quick and easy assembly and disassembly of the components. Overall, the research team was able to design a comprehensive and practical design for the initial prototype.

The researchers have developed and validated the SAFT algorithm. The SAFT algorithm is the cornerstone of ultrasonic imaging and flaw identification, as it compiles ultrasonic data into comprehensive two- or three-dimensional images. An in-house SAFT algorithm was created in MATLAB, and the results were compared to the images from a commercially available SAFT algorithm. The results demonstrated that the in-house algorithm was capable of producing ultrasonic B-scans analogous to the commercially generated B-scans.

The handheld ultrasonic device was able to clearly recognize a variety of artificial defects at different depths; including rebar, thin plastic, water-voids, and air-voids. The initial presence of the defects was successfully determined in all but one slab. The defect in this slab, Slab IX, was located about a 25 mm (1 in.) beneath the surface, the shallowest of any defect. In general, the ultrasonic tomography device successfully located all defects and rebar layers, proving to be capable for the intended design. Initial scans used overlapping measurements to produce a refined image using the SAFT algorithm, but non-overlapping scans also conveyed evidence of defects, demonstrating that overlapping scans provide clarity but are not absolutely necessary in locating the defects. From the experimental program, it can be concluded that ultrasonic tomography is a feasible nondestructive testing method that is capable of detecting flaws in concrete decks. However, in the current stage, scanning concrete surfaces is time-consuming and costly.

REFERENCES

"Attenuation of Sound Waves." *Nondestructive Testing Resource Center*. National Science Foundation - Advanced Technological Education, n.d. Web. 23 May 2016. <https://www.nde-ed.org/EducationResources/CommunityCollege/Ultrasonics/Physics/attenuation.htm>.

"Early History of Metal Flaw Detectors." *Early History of Metal Flaw Detectors*. NDT.net, n.d. Web. 13 Oct. 2015.

"Eyecon - GERMANN." *GERMANN RSS*. GERMANN INSTRUMENTS, n.d. Web. 12 Oct. 2015.

"File Server / ACSYS Ltd." *Index of /downloads/eng*. Acoustic Control Systems, n.d. Web. 10 July 2016

"Generating Ultrasound (Transducers)." *Olympus Corporation*. Olympus Corporation, n.d. Web. 25 May 2016. <http://www.olympus-ims.com/en/ndt-tutorials/flaw-detection/generating-ultrasound/>.

"Revolutionary RABIT™ Bridge Deck Assessment Tool." *Rutgers University*. Center for Advanced Infrastructure and Transportation, 2014. Web. 10 Oct. 2015.

(ACSYS) Acoustic Control Systems. 2015. http://www.acsys.ru/eng/production/detail/a1040-mira/

"MIRA - Ultrasonic Tomograph for Imaging of Concrete Structures." *Devices for non destructive testing of metals, plastics and concrete.* Acoustic Control Systems, 2008. Web. 24 May 2016 <http://acsys.ru/eng/>.

ACI Committee. 318 (2014). "Building Code Requirements for Structural Concrete (ACI 318-14) and Commentary." *American Concrete Institute*, Farmington Hills, Michigan, USA.

ASCE. 2013. "2013 Report Card for America's Infrastructure." *ASCE,* http://www.infrastructurereportcard.org/ (June 20, 2015).

Bamler, R. 1992 "A Comparison of Range-Doppler and Wavenumber Domain SAR Focusing Algorithms." Geoscience and Remote Sensing, IEEE Transactions. 30,706-713.

Barnes, C.L., and Trottier, J.F. 2000. "Ground Penetrating Radar for Network Level Concrete Deck Repair Management". *ASCE Journal of Transportation Engineering,* 126(3), 257–262.

Better Bridges. 2014. "Bridge Inventory." http://www.equipmentworld.com/2014-better-roads-bridge-inventory/ (July 12, 2015).

Bishko, A.V., Samokrutov, A., and Shevaldykin, V.G. 2008. "Ultrasonic Echo-Pulse Tomography of Concrete Using Shear Waves Low-Frequency Phased Antenna Arrays". *Proc. 17th World Conference on Nondestructive Testing,* Shanghai, China.

Burr, E, Große, C., and Reinhardt, H.-W. 1998 "Application of a Modified SAFT-Algorithm on Synthetic B-scans of Coarse Grained Materials." NDT.net, 3(2).

Chase, S.B., and Laman, J.A. 2000. "Dynamics and Field Testing of Bridges." *Transportation in the new millennium, Transportation Research Board.*

Cheng, C.C, and Sansalone, M. 1995. "Determining the Minimum Crack Width That Can Be Detected Using the Impact-Echo Method." *Materials and Structure,* 28(6), 74–82.

Dengzhi, W. 2007. “Non-linear synthetic aperture focusing technology ultrasonic imaging applied in non-destructive testing. ” NDT.net.

Gowers, K.R., and Millard, S.G. 1999. “Measurement of Concrete Resistivity for Assessment of Corrosion Severity of Steel Using Wenner Technique.” *ACI Materials Journal,* 96(5), 536-542.

Gucunski, N., Imani, A., Romero, F., Nazarian, S., Yuan, D., Wiggenhauser, H., Shokouhi, P., Taffe, A., and Kutrubes, D. 2013. “Nondestructive Testing to Identify Concrete Bridge Deck Deterioration.” *Report No. S2-R06A-RR-1, Strategic Highway Research Program,* Transportation Research Board, Washington, D.C.

Hall, T.E., Doctor, S.R. and Reig, L.D. 1986. “A Real-Time SAFT System Applied to the Ultrasonic Inspection of Nuclear Reactor Components.” *Pacific Northwest Laboratory*, Richland,WA < http://lib.dr.iastate.edu/cgi/viewcontent.cgi?article=1178&context=qnde>

Hillger, Wolfgang. "Flexus Concrete Automated Ultrasonic Imaging System for Concrete Elements." (2014): 1. Web.

Hoegh, K. E. 2013. "Ultrasonic Linear Array Evaluation of Concrete Pavements." Ph.D. dissertation University of Minnesota.

Hoegh, Kyle Edward. *Ultrasonic Linear Array Evaluation of Concrete Pavements*. Thesis. The University of Minnesota, 2013. N.p.: n.p., n.d. Print.

Hoegh, Kyle, and Lev Khazanovich. "Extended Synthetic Aperture Focusing Technique for Ultrasonic Imaging of Concrete." *NDT & E International* 74 (2015): 33-42. Web.

Im, S., Hurlebaus, S. and Trejo, D. 2010. “Inspection of Voids in External Tendons of Posttensioned Bridges.” *Transportation Research Record: Journal of the Transportation Research Board, TRB, National Research Council*, Washington, D.C., 2172, 115–122.

Kotoky, N., and Shekhar, S. 2014. “Damage Identification Using SAFT Algorithm.” *International Journal of Innovative Research in Science, Engineering and Technology,* 3(4), 194-199.

Reichling, Kenji, Michael Raupach, Herbert Iggenhauser, Markus Stoppel, Gerd Dobmann, and Jochen Kurz. "BETOSCAN – Robot Controlled Non-destructive Diagnosis of Reinforced Concrete Decks." *NDTCE’09, Non-Destructive Te Sting in Civil Engineering* (2009): n. pag. *Ndt.net*. Ndt.net. Web. 10 Oct. 2015.

Ryden, Nils, Michael J. S. Lowe, and Peter Cawley. "Noncontact Surface Wave Testing of Pavements Using Microphones." *The Journal of the Acoustical Society of America J. Acoust. Soc. Am.* 124.4 (2008): 2576. *Ndt.net*. Ndt.net. Web. 10 Oct. 2015.

Shokouhi, P., Wöstmann, J., Schneider, G., Milmann, B., Taffe, A., and Wiggenhauser, H. 2011. “Nondestructive Detection of Delamination in Concrete Slabs.” *Transportation Research Record: Journal of the Transportation Research Board, TRB, National Research Council,* Washington, D.C., 2252, 103.

Skjelvareid, M. H. 2012. "Synthetic aperture ultrasound imaging with application to interior pipe inspection." on for the degree of Philosophiae Doctor, University of Tromso.

Stepinski, T. 2007. “An Implementation of Synthetic Aperature Focusing Technique in the Frequency Domain.” Ultrasonics, Ferroelectrical and Frequency Control, IEEE Transactions. 54, 1399-1408.

Stimolo, M. 2003. “Passive Infrared Thermography as Inspection and Observation Tool in Bridge and Road Construction.” *Proc. International Symposium,* Berlin, Germany, 1-6.

Tinkey, Yajai, Larry D. Olson, Raul Bedon, and Christoph Lieberle. "Impact Echo Scanning Technology for Internal Grout Condition Evaluation in Post-Tensioned Bridge Ducts." *Impact Echo Scanning Technology for Internal Grout Condition Evaluation in Post-Tensioned Bridge Ducts*. Non-Destructive Testing in Civil Engineering, 2003. Web. 14 Aug. 2016.

White, J., Hurlebaus, S. Shokouhi, P. and Wimsatt, A. “Structural Impairment Detection of Tunnel Linings Using Ultrasonic Tomography: Validation Study and Field Evaluation”, *Transportation Research Record*, Vol. 2407, 2014, pp. 20-31

White, J., S. Hurlebaus, S. Nazarian, and P. Shokouhi. 2014. *SHRP 2 R06G: Tunnel Nondestructive Testing Equipment User’s Manual*. Transportation Research Board of the National Academies, Washington, D.C.

Wimsatt, A.; White, J.; Leung, C.; Scullion, T.; Hurlebaus, S.; Zollinger, D.; Grasley, Z.; Nazarian, S.; Azari, H.; Yuan, D.; Shokouhi, P. and Saarenketo., T.: Mapping Voids, Debonding, Delaminations, Moisture, and Other Defects Behind or Within Tunnel Linings" SHRP 2 Final Report S2-R06(G)-RW. Strategic Highway Research Program 2, Washington, D.C. (2013).

Wimsatt, A.J., Scullion, T., Fernando, E., Hurlebaus, S., Lytton, R., Zollinger, D., Walker, R. 2008. “A Plan for Developing High-Speed, Nondestructive Testing Procedures for Both Design Evaluation and Construction Inspection.” *Report No. S2-R06A-RW, Strategic Highway Research Program,* Transportation Research Board, Washington, D.C.

APPENDIX A: SLAB IMAGES

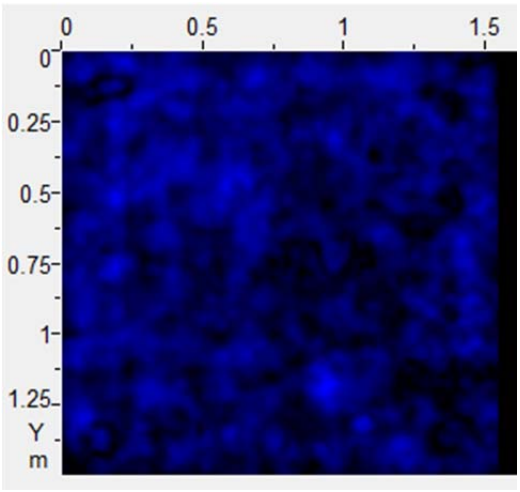

(a) Top of the Slab z =0 m.

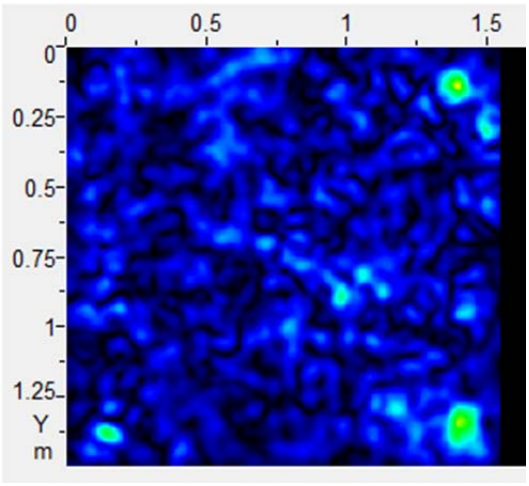

(b) Depth of 90 mm z =0.09 m.

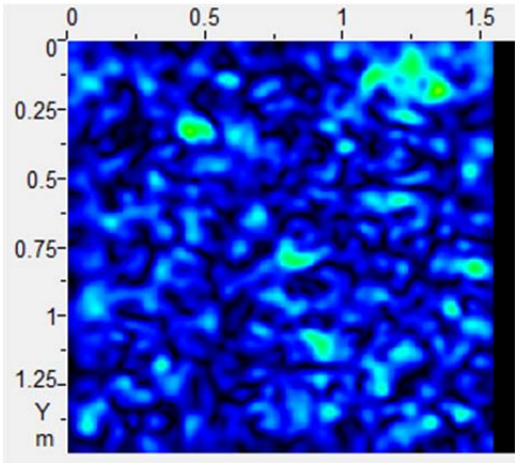

(c) Depth of 190 mm z =0.19 m.

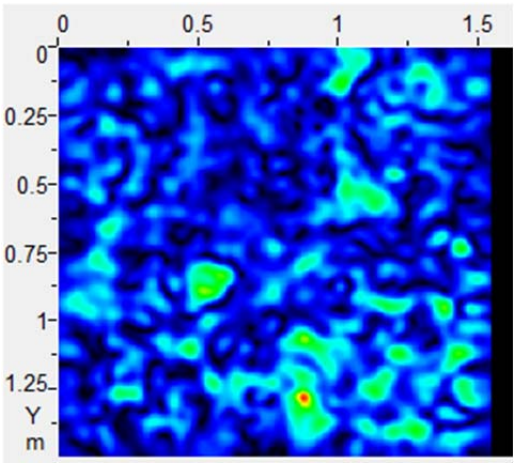

(d) Depth of 240 mm z =0.24 m.

Figure 39. C-Scans of Slab I at Various Depths using Vertical Transducer Orientation.

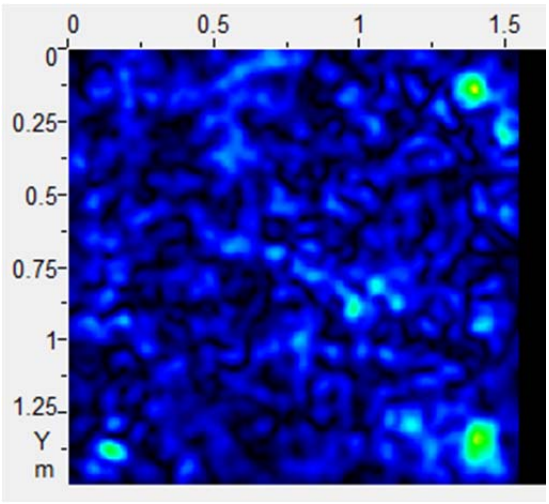

(a) Depth of 90 mm, Vertical Orientation.

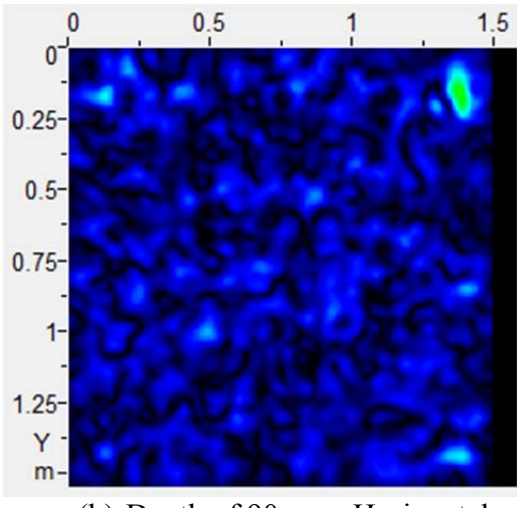

(b) Depth of 90 mm, Horizontal Orientation.

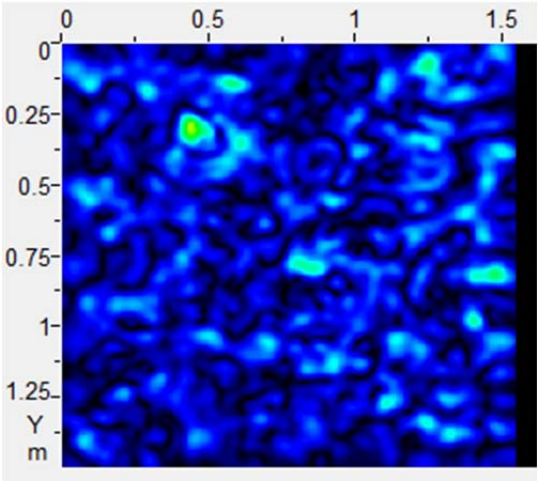

(c) Depth of 150 mm, Vertical Orientation.

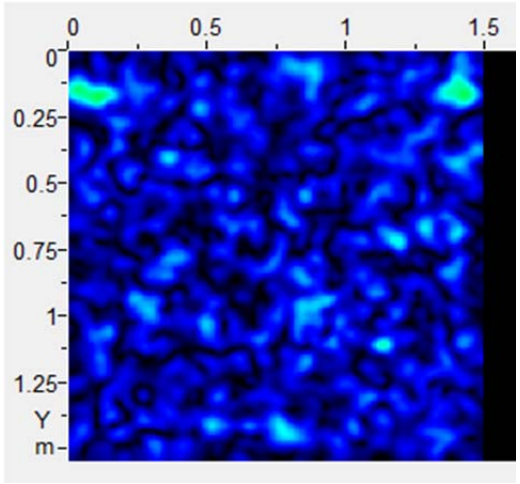

(d) Depth of 150 mm, Horizontal Orientation.

Figure 40. C-Scans of Slab I with the Vertical (Left) and Horizontal (Right) Orientations at 90 mm and 150 mm.

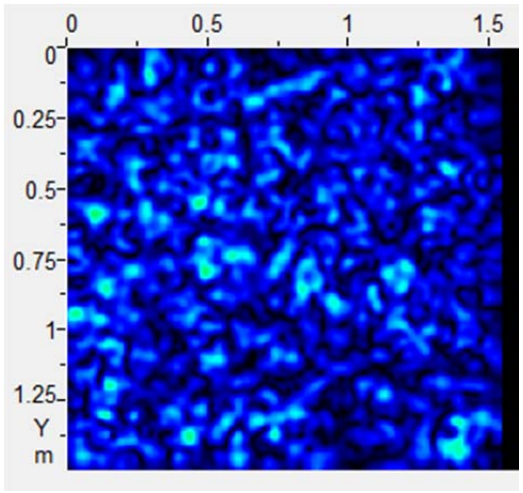

(a) Depth of 60 mm z =0.06 m.

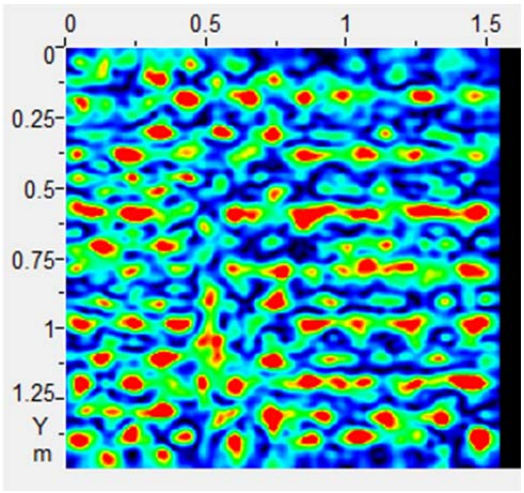

(b) Depth of 100 mm z =0.10 m.

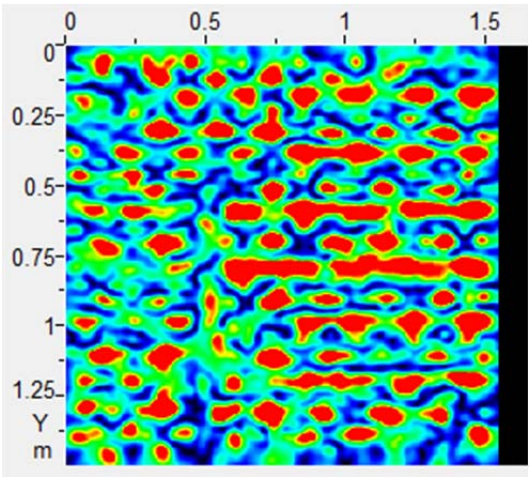

(c) Depth of 120 mm z =0.12 m.

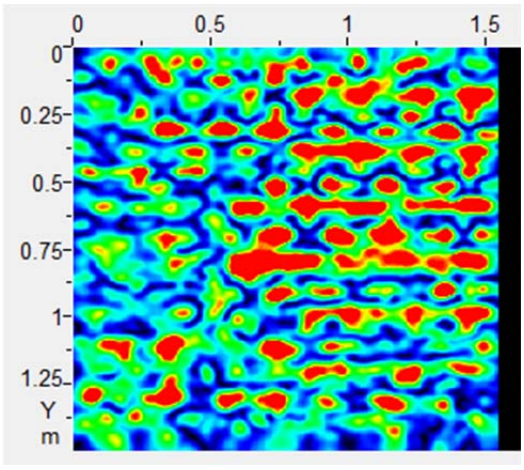

(d) Depth of 130 mm z =0.13 m.

Figure 41. C-Scans of Slab II at Various Depths from 60 mm to 130 mm.

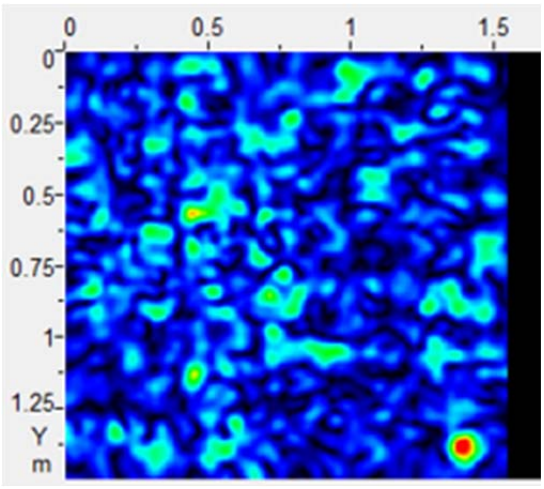

(a) Depth of 270 mm z =0.27 m.

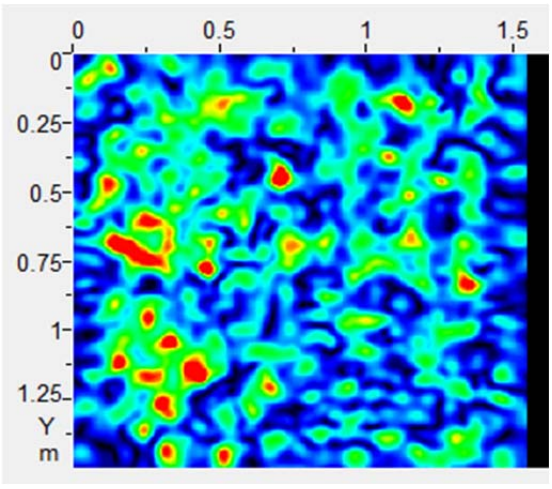

(b) Depth of 330 mm z =0.33 m.

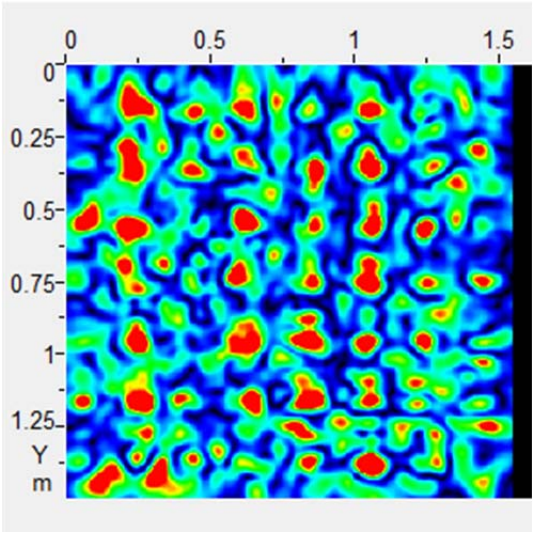

(c) Depth of 370 mm z =0.37 m.

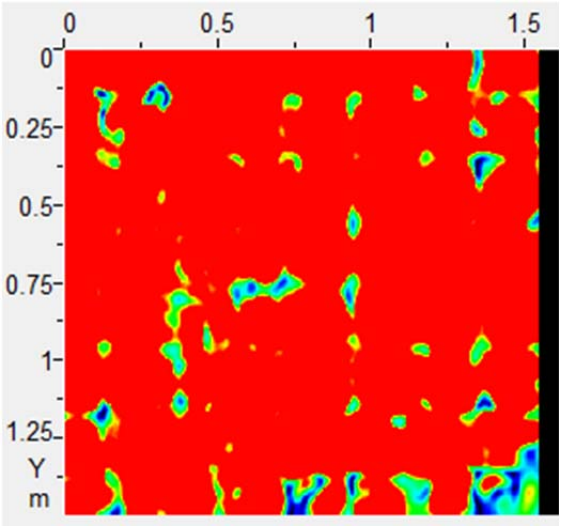

(d) Depth of 460 mm z =0.46 m.

Figure 42. C-Scans of Slab II at Various Depths from 270 mm to 460 mm.

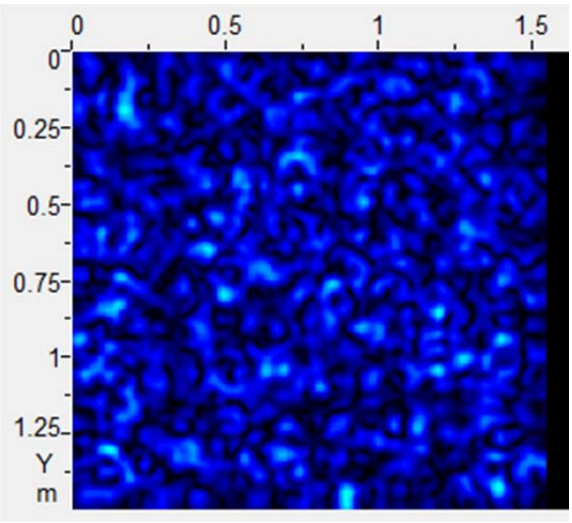

(a) Depth of 30 mm, Vertical Orientation.

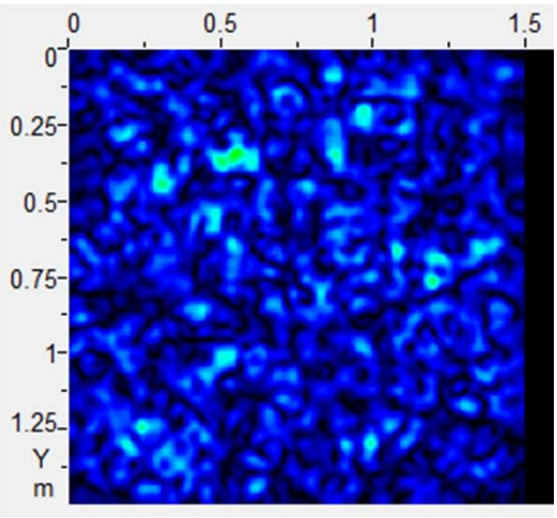

(b) Depth of 30 mm, Horizontal Orientation.

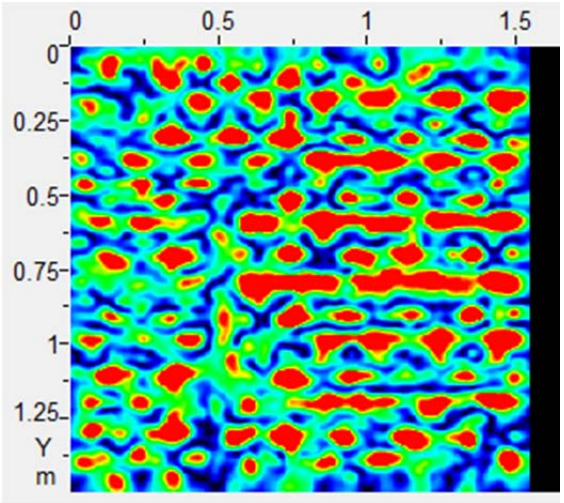

(c) Depth of 120 mm, Vertical Orientation.

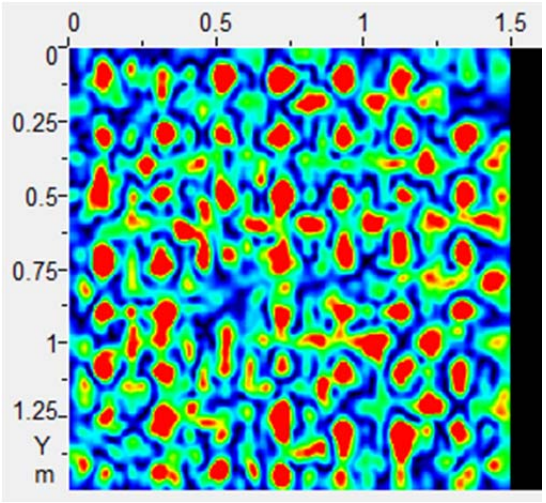

(d) Depth of 120 mm, Horizontal Orientation.

Figure 43. C-Scans of Slab II with the Vertical (Left) and Horizontal (Right) Orientations at 30 mm and 120 mm.

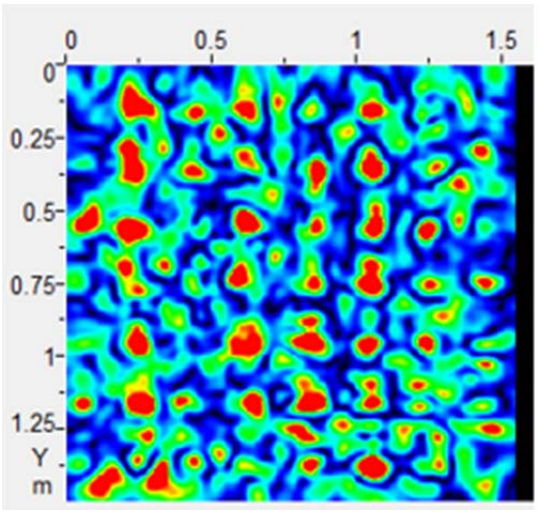

(a) Depth of 370 mm, Vertical Orientation.

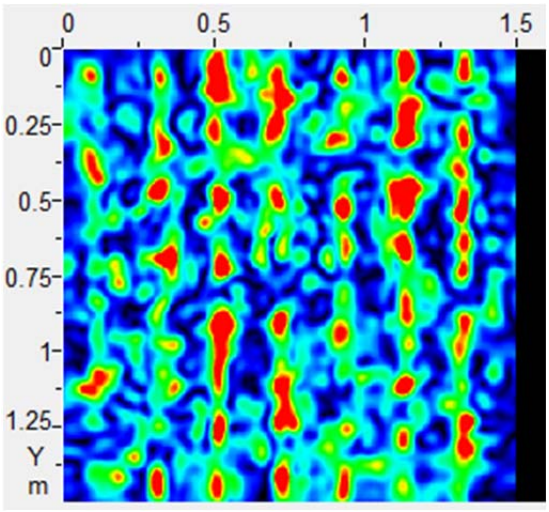

(b) Depth of 370 mm, Horizontal Orientation.

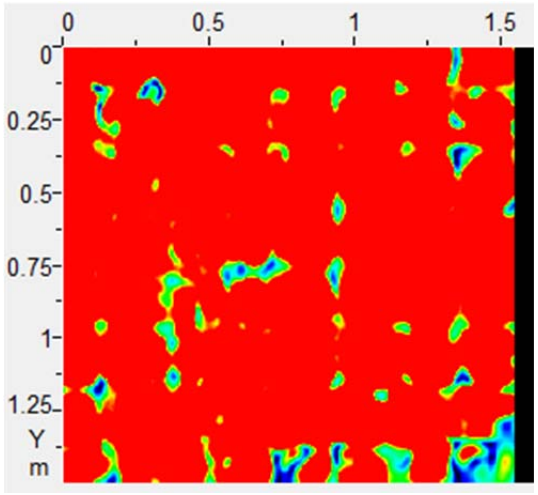

(c) Depth of 460 mm, Vertical Orientation.

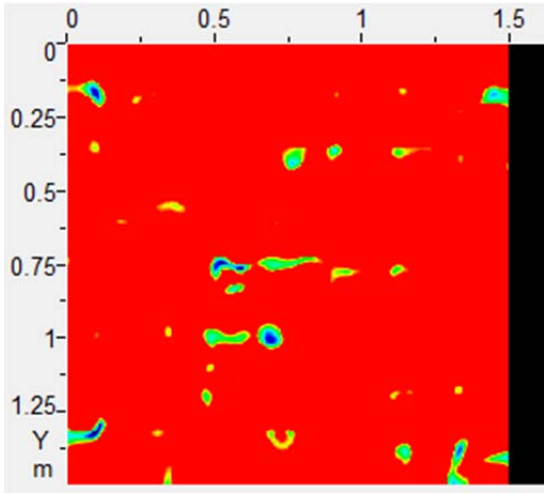

(d) Depth of 460 mm, Horizontal Orientation.

Figure 44. C-Scans of Slab II with the Vertical (Left) and Horizontal (Right) Orientations at 370 mm and 460 mm.

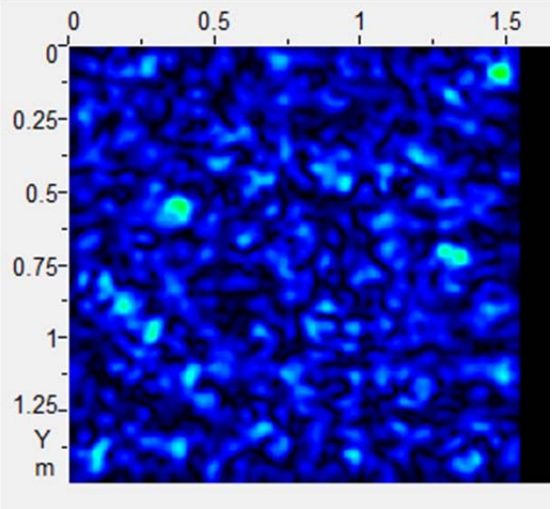

(a) Depth of 60 mm z =0.06 m.

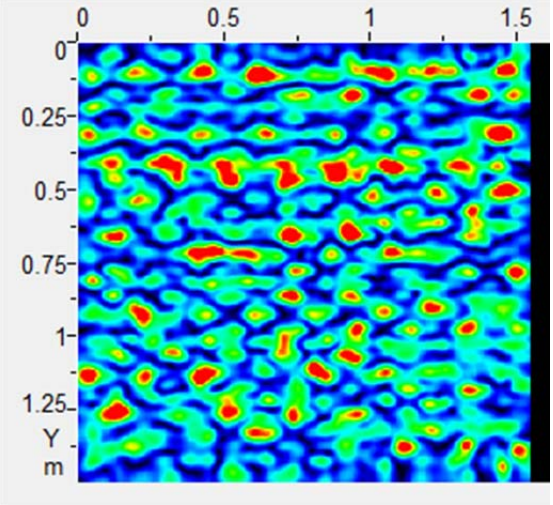

(b) Depth of 100 mm z =0.10 m.

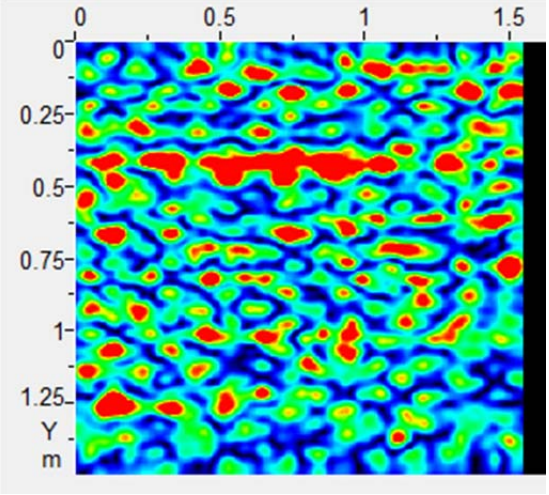

(c) Depth of 130 mm z =0.13 m.

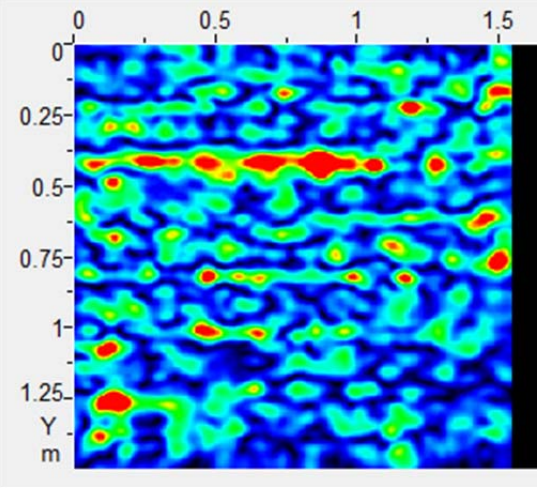

(d) Depth of 150 mm z =0.15 m.

Figure 45. C-Scans of Slab III at Various Depths from 60 mm to 150 mm.

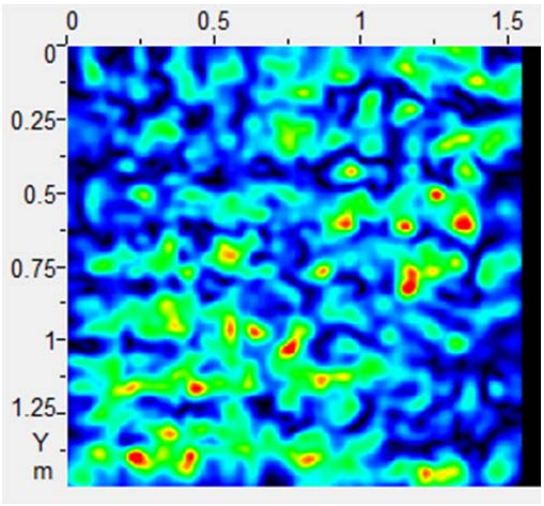

(a) Depth of 210 mm z =0.21 m.

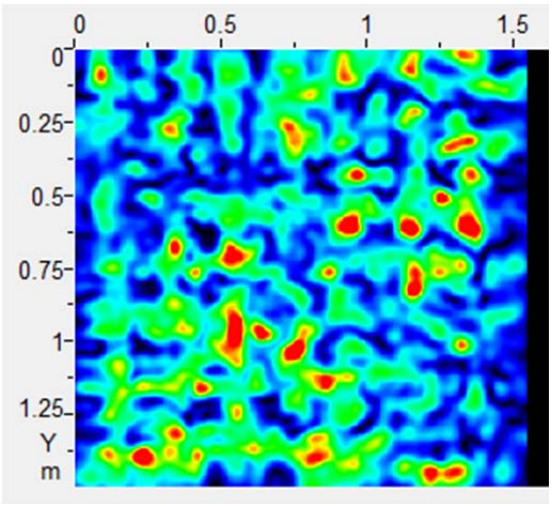

(b) Depth of 220 mm z =0.22 m.

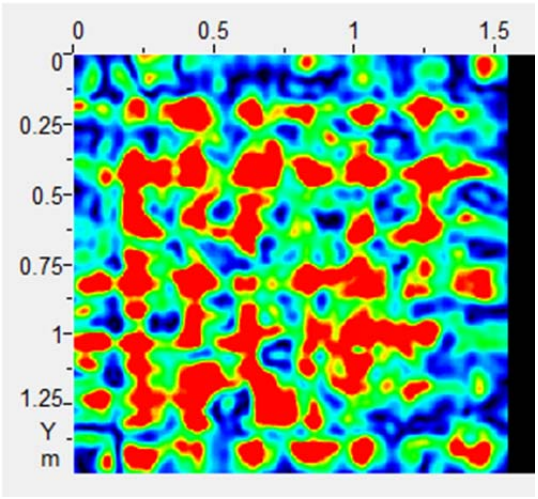

(c) Depth of 280 mm z =0.28 m.

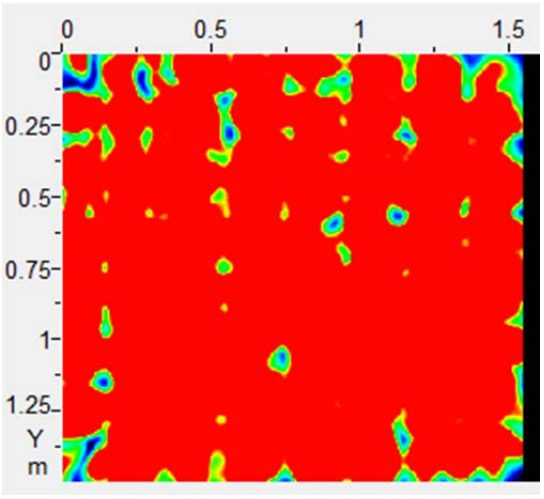

(d) Depth of 300 mm z =0.30 m.

Figure 46. C-Scans of Slab III at Various Depths from 210 mm to 300 mm.

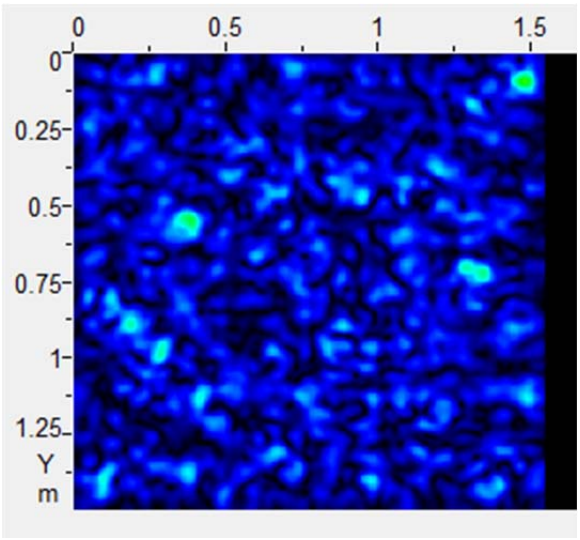

(a) Depth of 60 mm, Vertical Orientation.

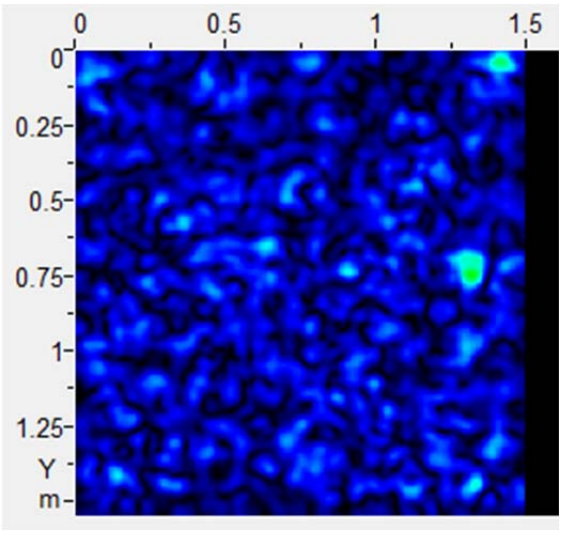

(b) Depth of 60 mm, Horizontal Orientation.

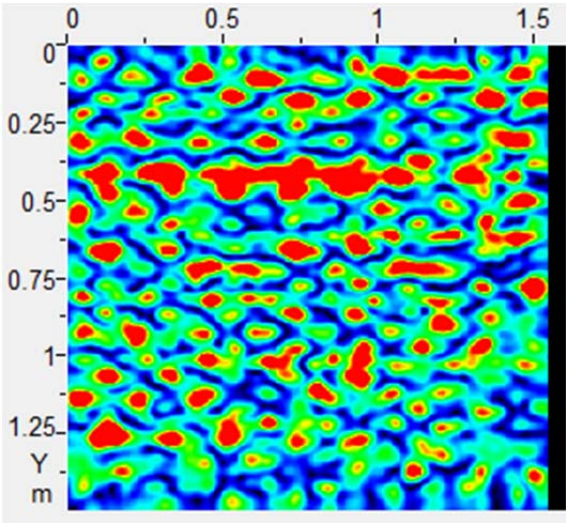

(c) Depth of 120 mm, Vertical Orientation.

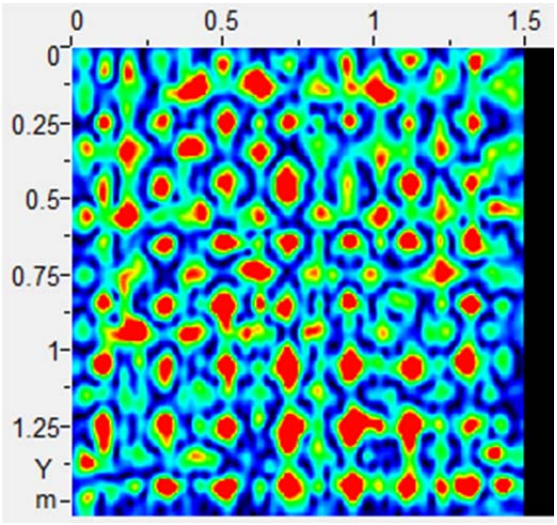

(d) Depth of 120 mm, Horizontal Orientation.

Figure 47. C-Scans of Slab III with the Vertical (Left) and Horizontal (Right) Orientations at 60 mm and 120 mm.

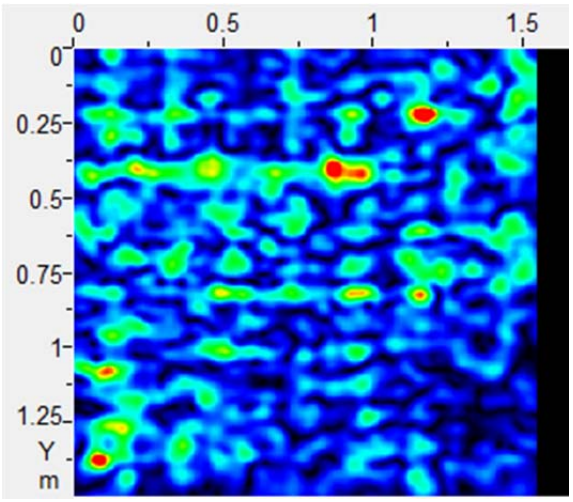

(a) Depth of 170 mm, Vertical Orientation.

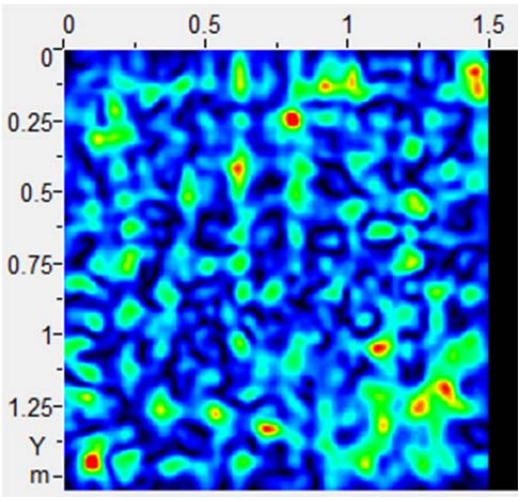

(b) Depth of 170 mm, Horizontal Orientation.

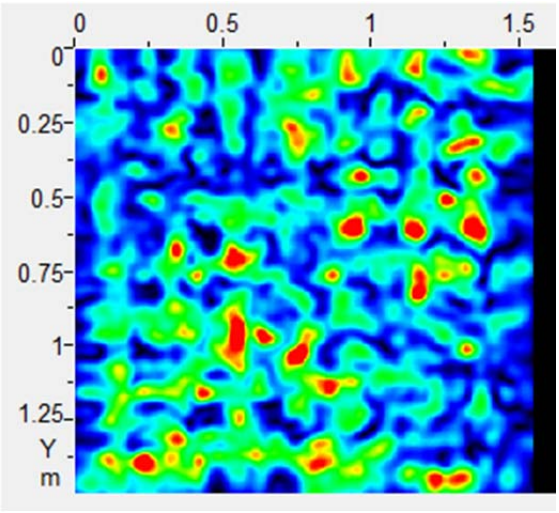

(c) Depth of 220 mm, Vertical Orientation.

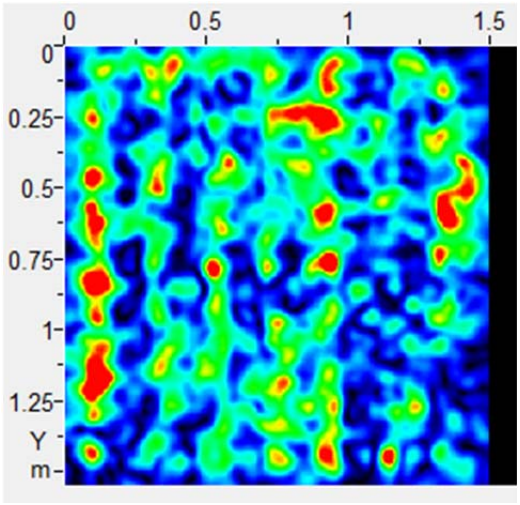

(d) Depth of 220 mm, Horizontal Orientation.

Figure 48. C-Scans of Slab III with the Vertical (Left) and Horizontal (Right) Orientations at 170 mm and 220 mm.

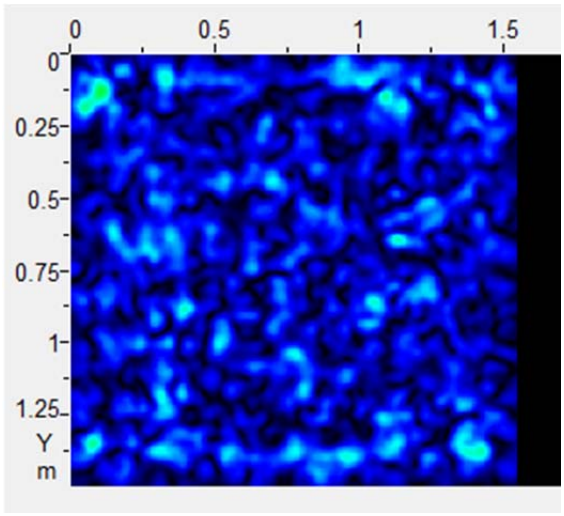

(a) Depth of 90 mm z =0.09 m.

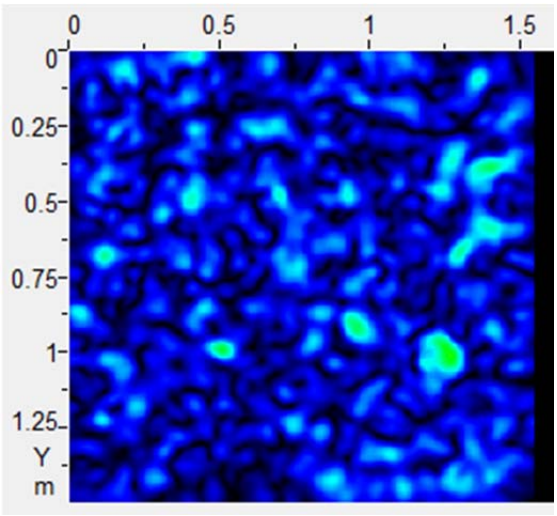

(b) Depth of 180 mm z =0.18 m.

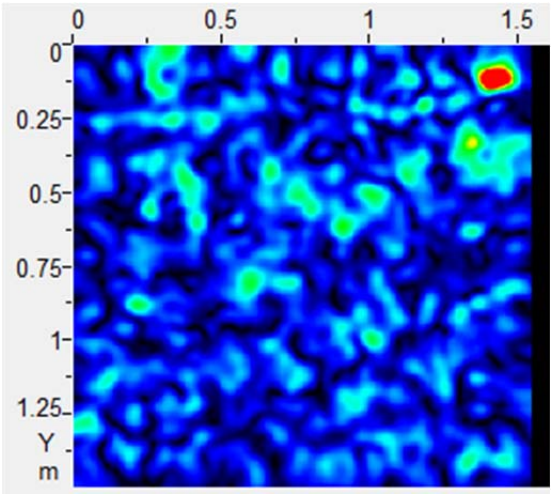

(c) Depth of 330 mm z =0.33 m.

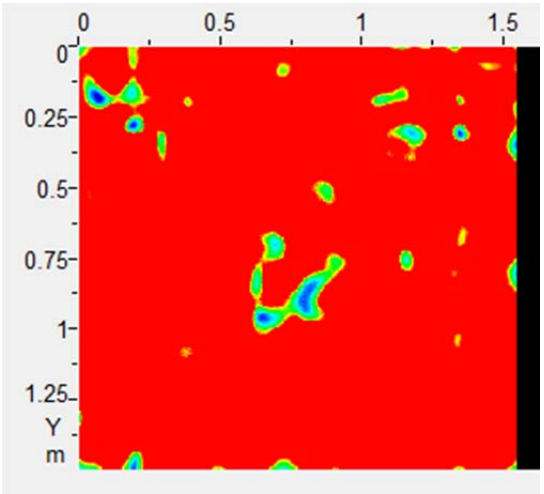

(d) Depth of 610 mm z =0.61 m.

Figure 49. C-Scans of Slab IV at Various Depths.

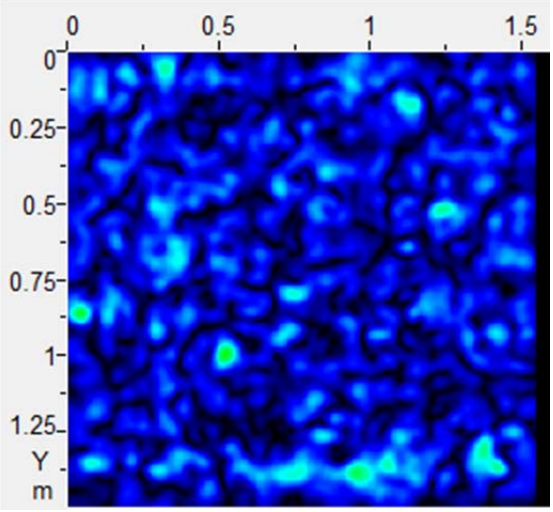

(a) Depth of 120 mm, Vertical Orientation.

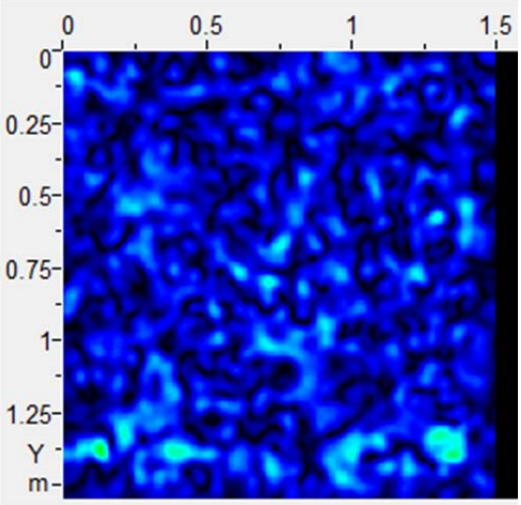

(b) Depth of 120 mm, Horizontal Orientation.

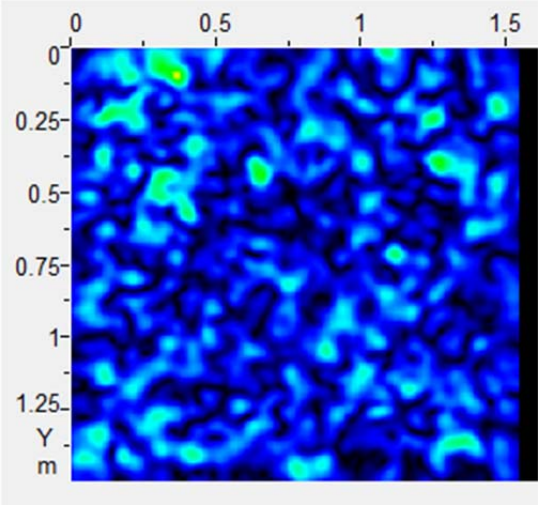

(c) Depth of 240 mm, Vertical Orientation.

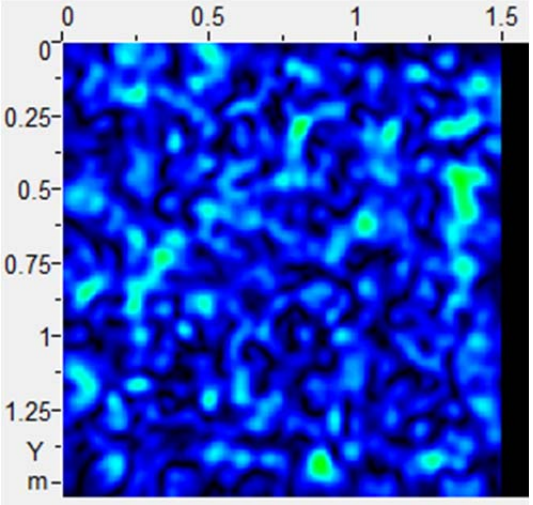

(d) Depth of 240 mm, Horizontal Orientation.

Figure 50. C-Scans of Slab IV with the Vertical (Left) and Horizontal (Right) Orientations at 120 mm and 240 mm.

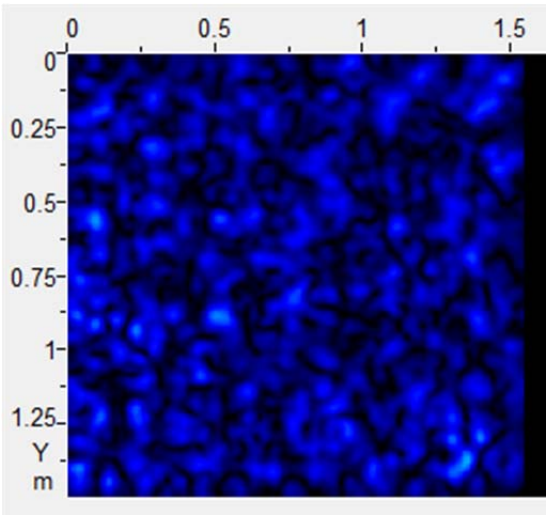

(a) Depth of 60 mm z =0.06 m.

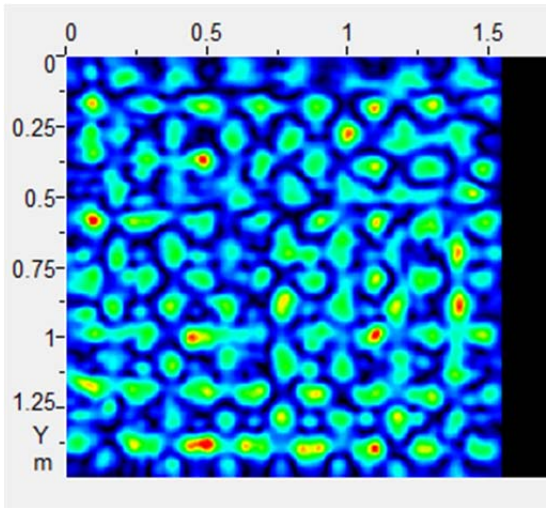

(b) Depth of 100 mm z =0.10 m.

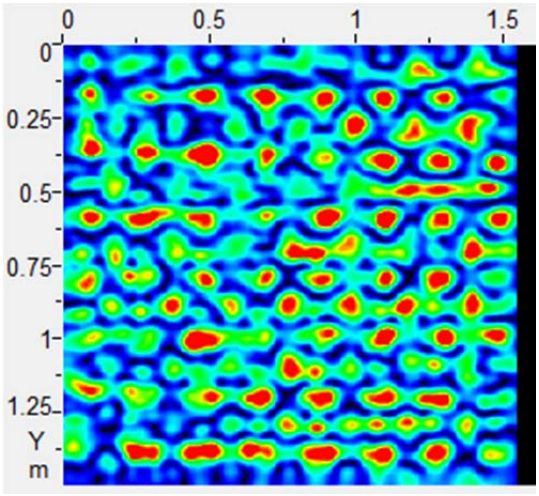

(c) Depth of 130 mm z =0.13 m.

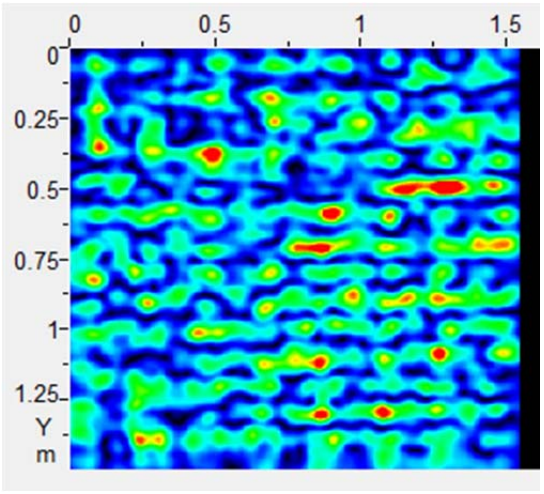

(d) Depth of 150 mm z =0.15 m.

Figure 51. C-Scans of Slab V at Various Depths from 60 mm to 150 mm.

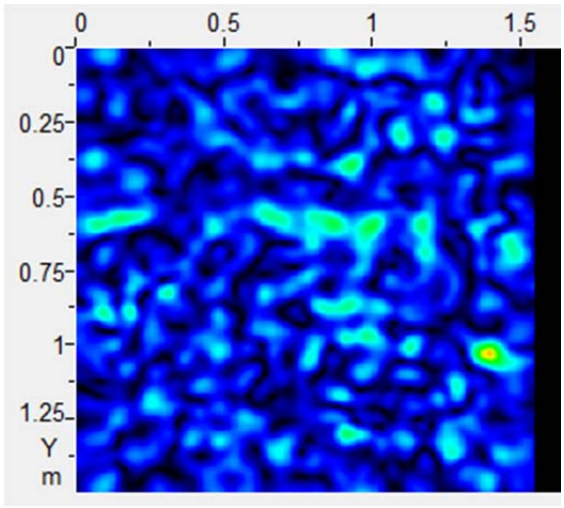

(a) Depth of 330 mm z =0.33 m.

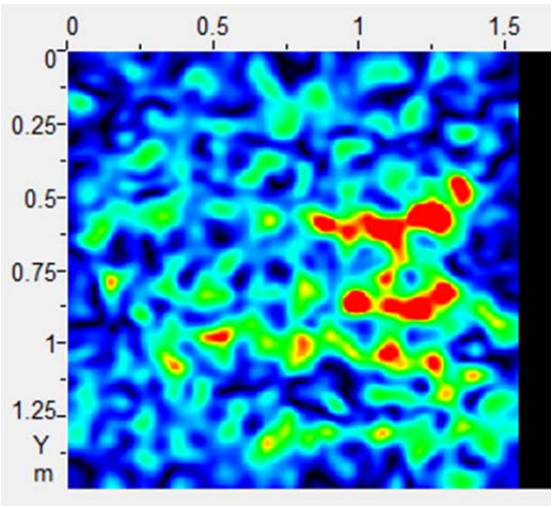

(b) Depth of 480 mm z =0.48 m.

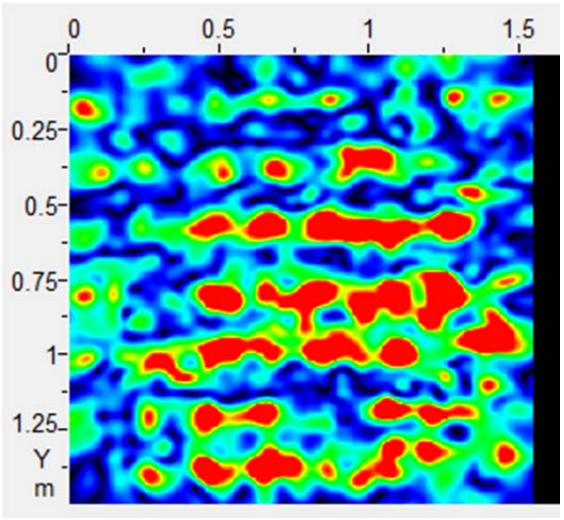

(c) Depth of 530 mm z =0.53 m.

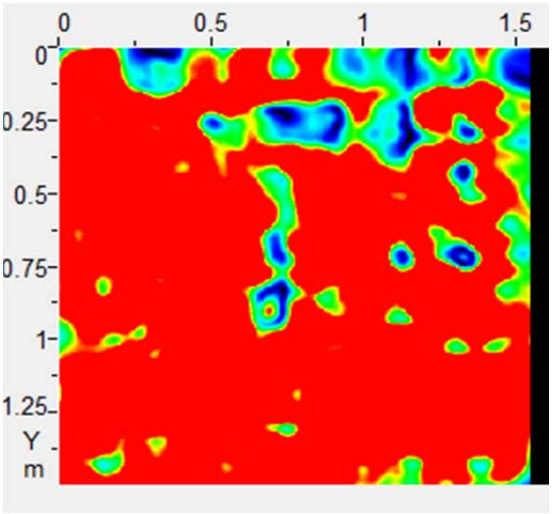

(d) Depth of 610 mm z =0.61 m.

Figure 52. C-Scans of Slab V at Various Depths from 330 mm to 610 mm.

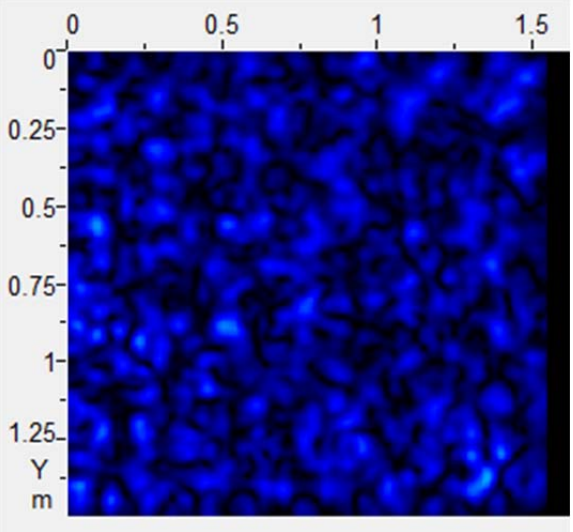

(a) Depth of 60 mm, Vertical Orientation.

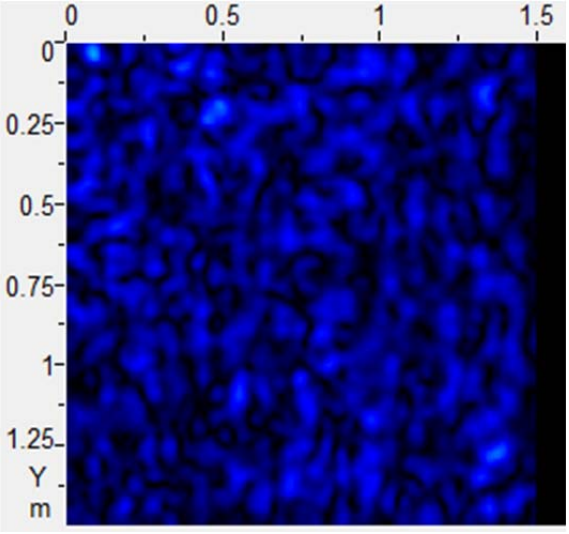

(b) Depth of 60 mm, Horizontal Orientation.

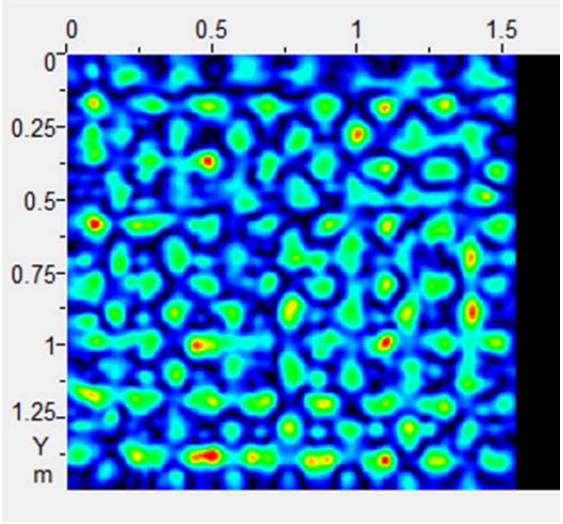

(c) Depth of 100 mm, Vertical Orientation.

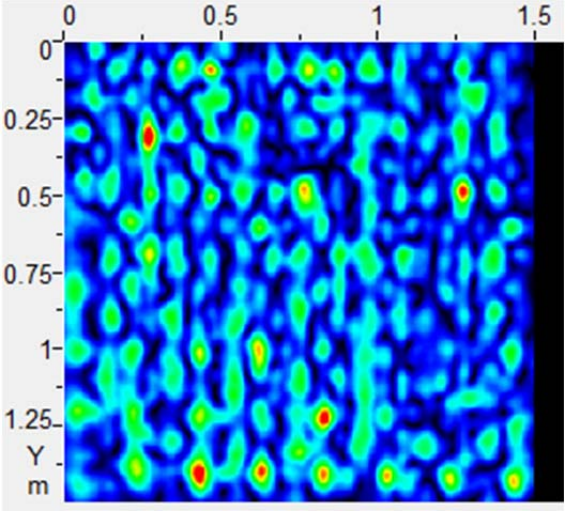

(d) Depth of 100 mm, Horizontal Orientation.

Figure 53. C-Scans of Slab V with the Vertical (Left) and Horizontal (Right) Orientations at 60 mm and 100 mm.

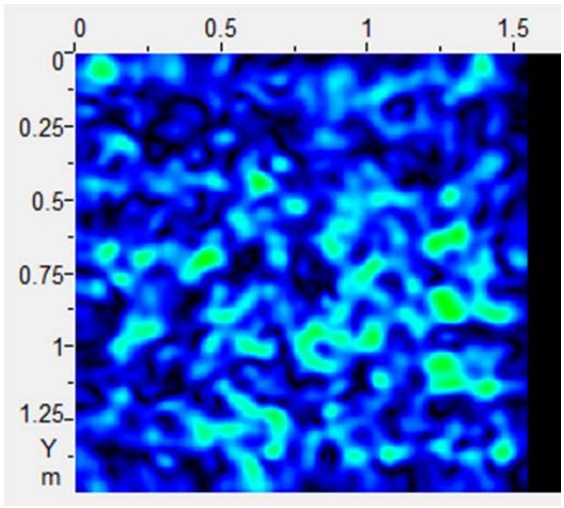

(a) Depth of 240 mm, Vertical Orientation.

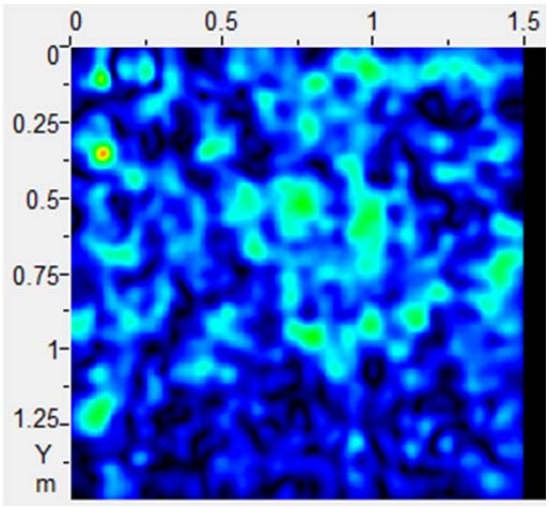

(b) Depth of 240 mm, Horizontal Orientation.

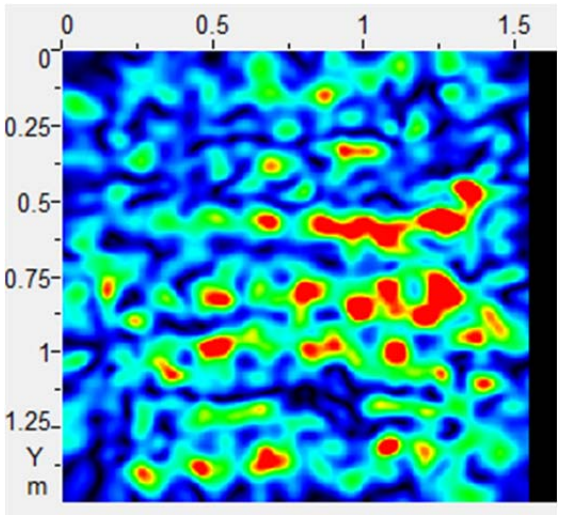

(c) Depth of 520 mm, Vertical Orientation.

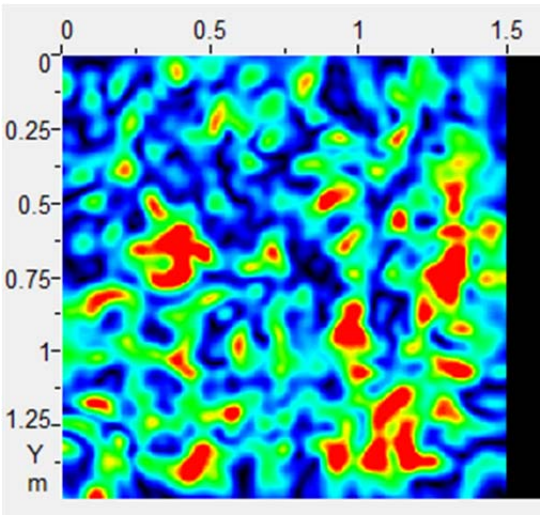

(d) Depth of 520 mm, Horizontal Orientation.

Figure 54. C-Scans of Slab V with the Vertical (Left) and Horizontal (Right) Orientations at 240 mm and 520 mm.

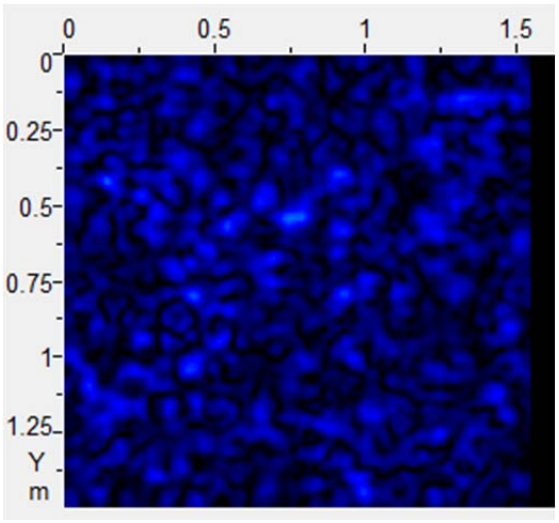

(a) Depth of 30 mm z =0.03 m.

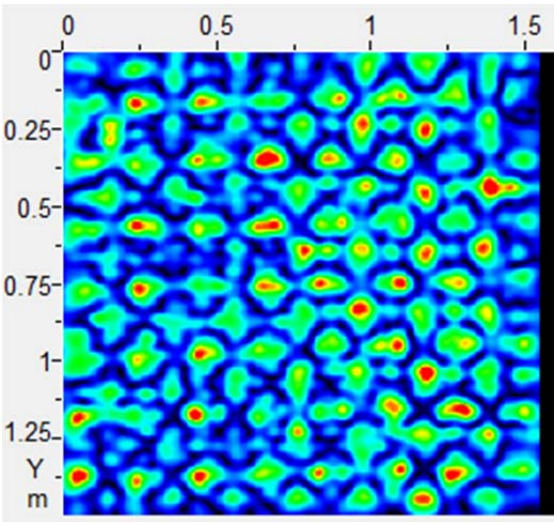

(b) Depth of 100 mm z =0.10 m.

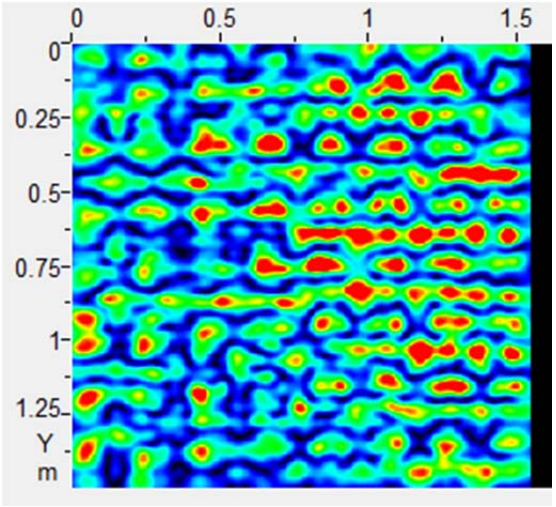

(c) Depth of 130 mm z =0.13 m.

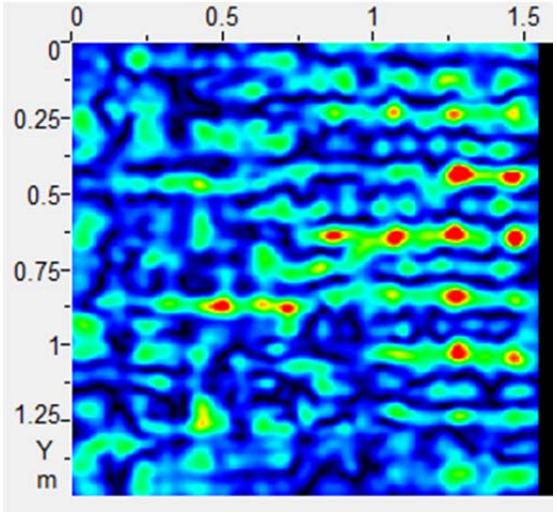

(d) Depth of 150 mm z =0.15 m.

Figure 55. C-Scans of Slab VI at Various Depths from 30 mm to 150 mm.

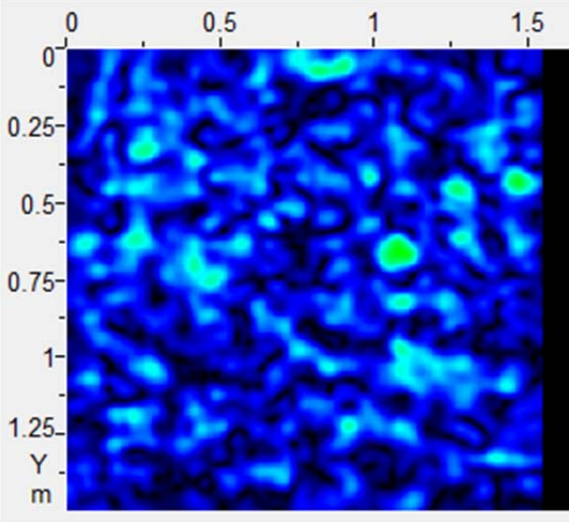

(a) Depth of 200 mm z =0.20 m.

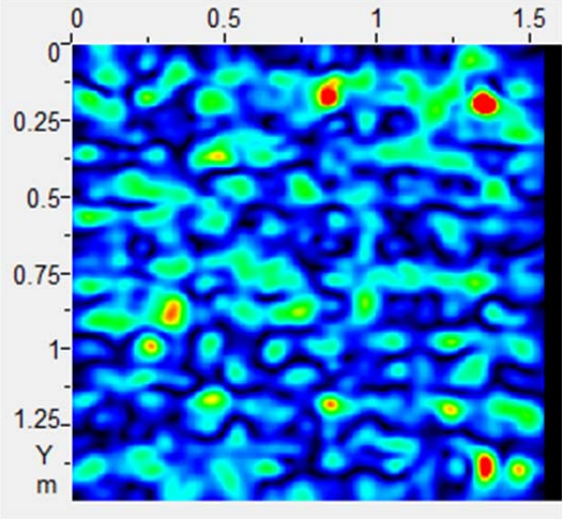

(b) Depth of 280 mm z =0.28 m.

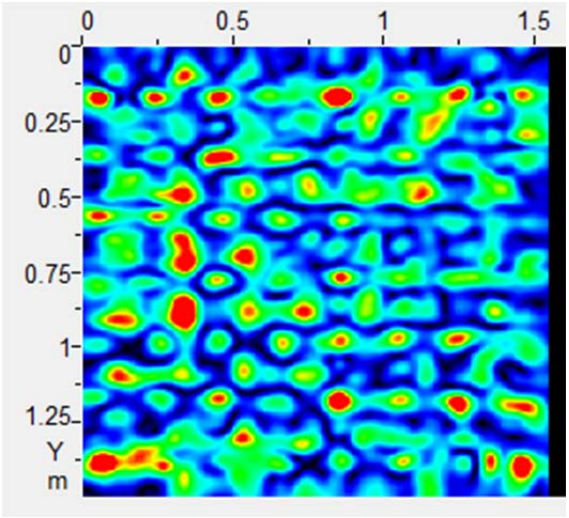

(c) Depth of 300 mm z =0.30 m.

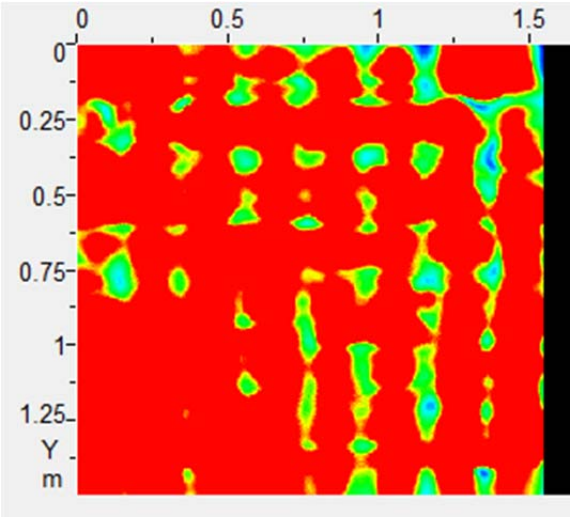

(d) Depth of 380 mm z =0.38 m.

Figure 56. C-Scans of Slab VI at Various Depths from 200 mm to 380 mm.

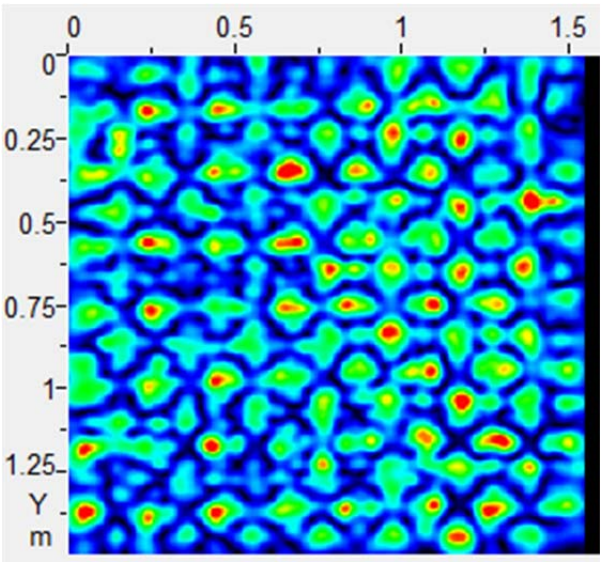

(a) Depth of 100 mm, Vertical Orientation.

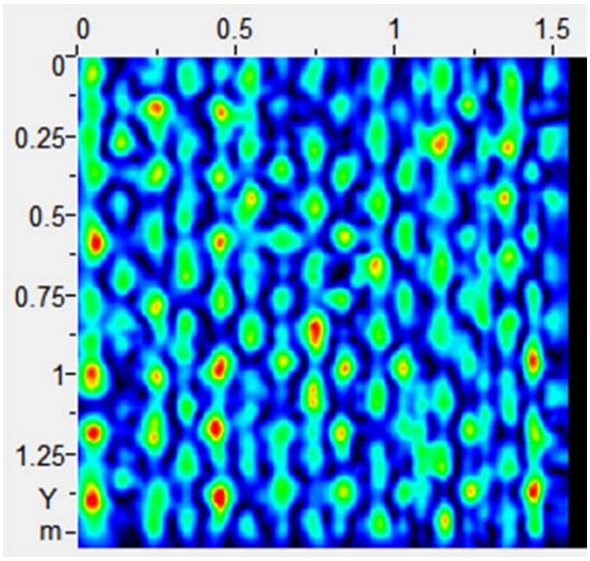

(b) Depth of 100 mm, Horizontal Orientation.

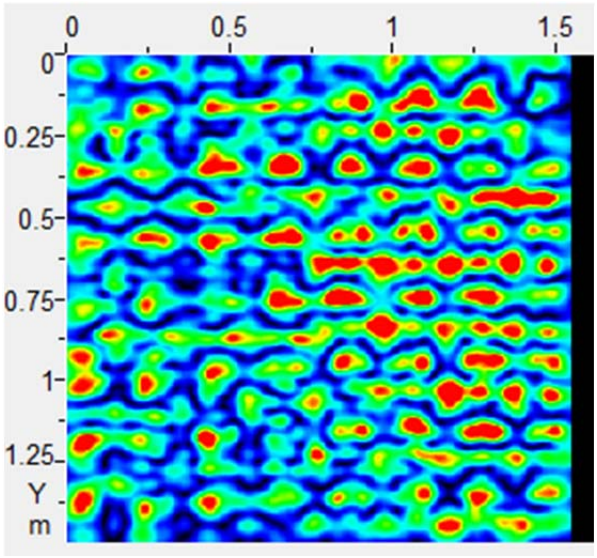

(c) Depth of 120 mm, Vertical Orientation.

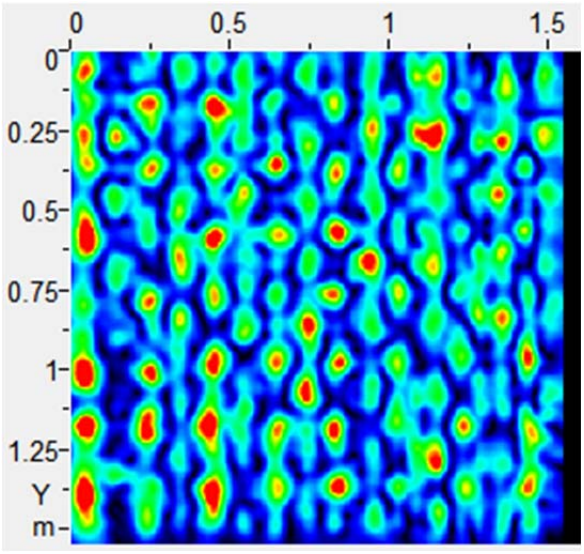

(d) Depth of 120 mm, Horizontal Orientation.

Figure 57. C-Scans of Slab VI with the Vertical (Left) and Horizontal (Right) Orientations at 100 mm and 120 mm.

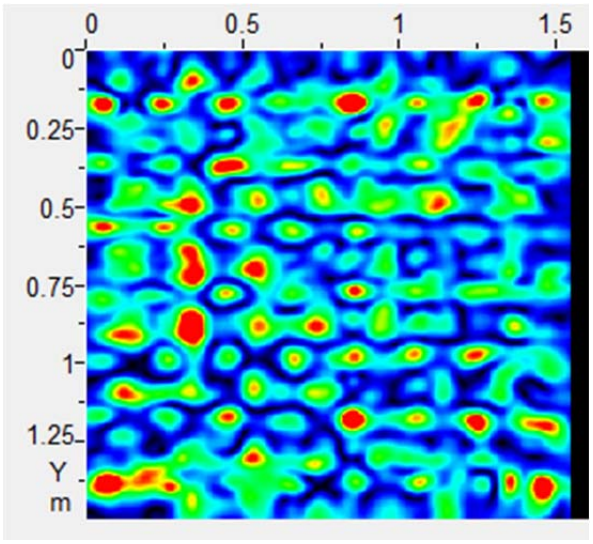

(a) Depth of 300 mm, Vertical Orientation.

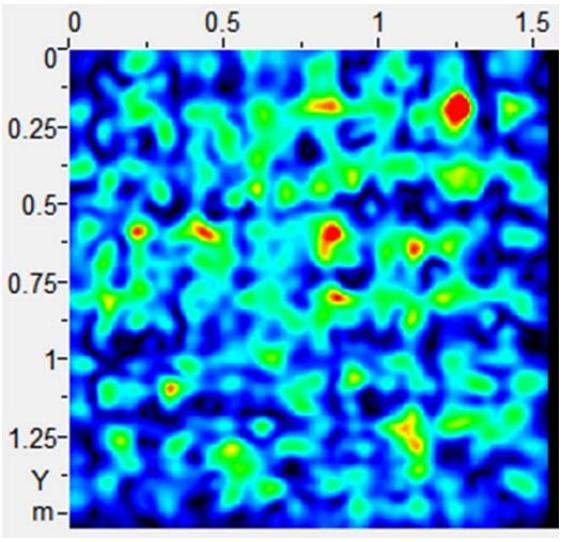

(b) Depth of 300 mm, Horizontal Orientation.

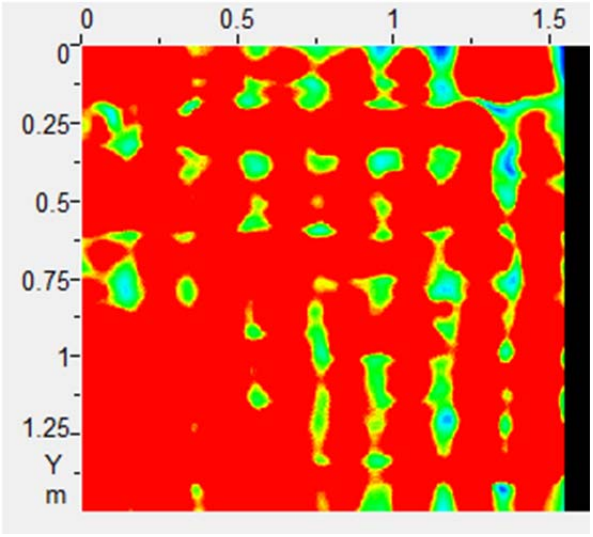

(c) Depth of 380 mm, Vertical Orientation.

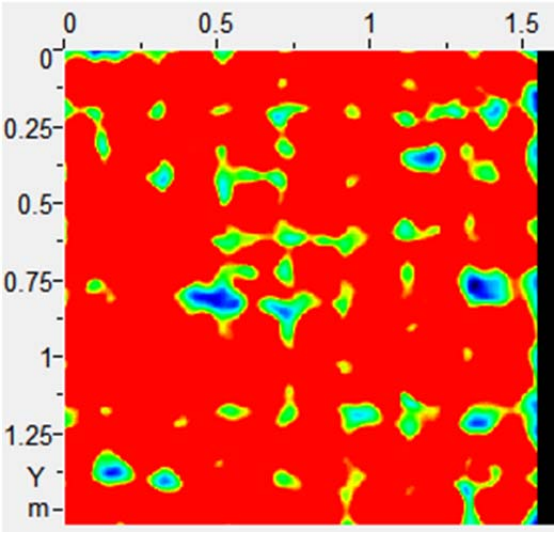

(d) Depth of 380 mm, Horizontal Orientation.

Figure 58. C-Scans of Slab VI with the Vertical (Left) and Horizontal (Right) Orientations at 300 mm and 380 mm.

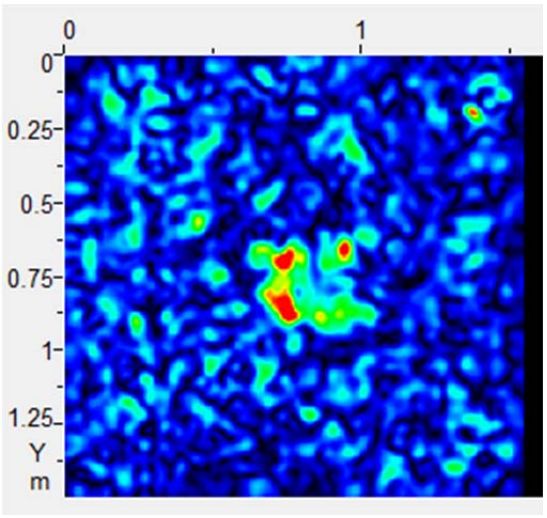

(a) Depth of 70 mm z =0.07 m.

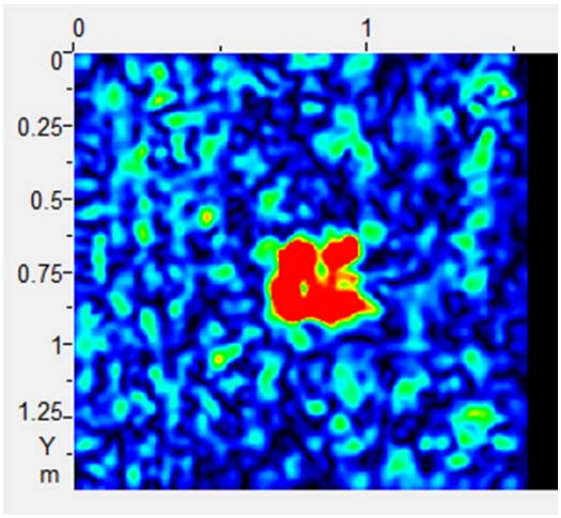

(b) Depth of 80 mm z =0.08 m.

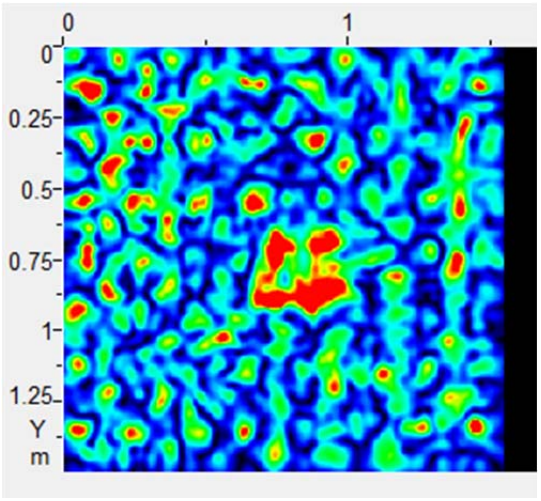

(c) Depth of 100 mm z =0.10 m.

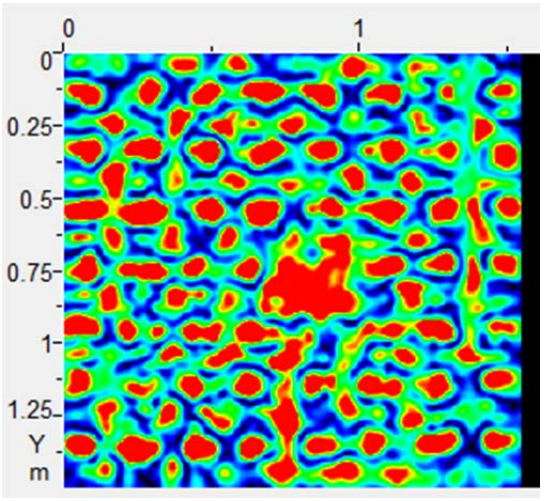

(d) Depth of 130 mm z =0.13 m.

Figure 59. C-Scans of Slab VII at Various Depths from 70 mm to 130 mm.

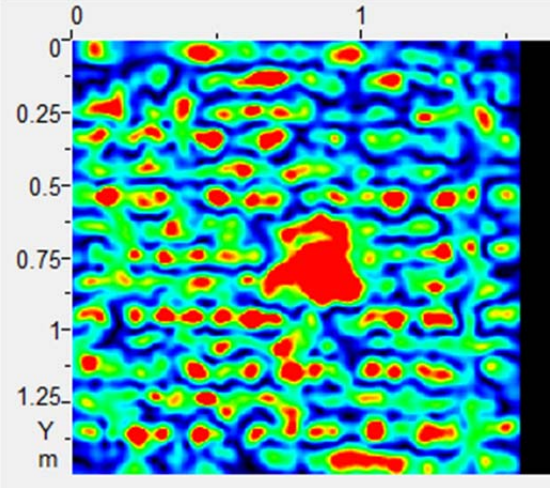

(a) Depth of 160 mm z =0.16 m.

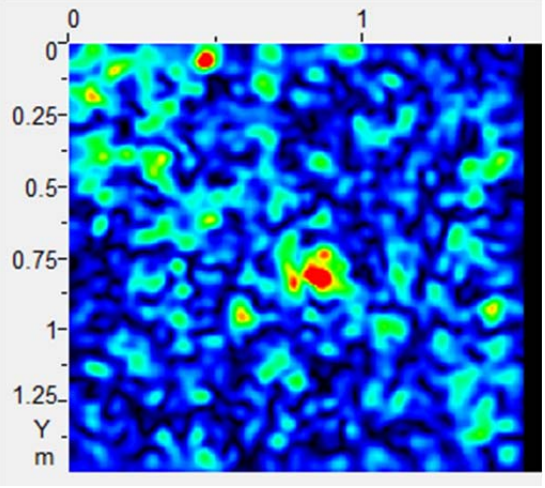

(b) Depth of 190 mm z =0.19 m.

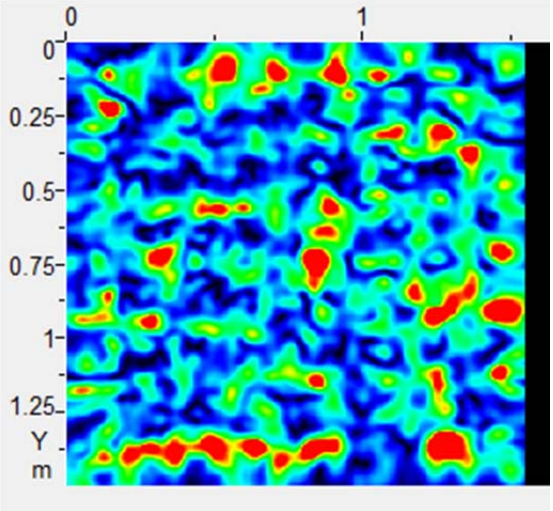

(c) Depth of 290 mm z =0.29 m.

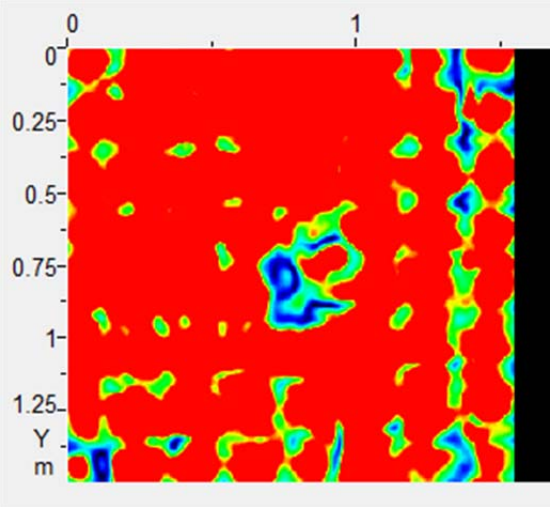

(d) Depth of 380 mm z =0.38 m.

Figure 60. C-Scans of Slab VII at Various Depths from 160 mm to 380 mm.

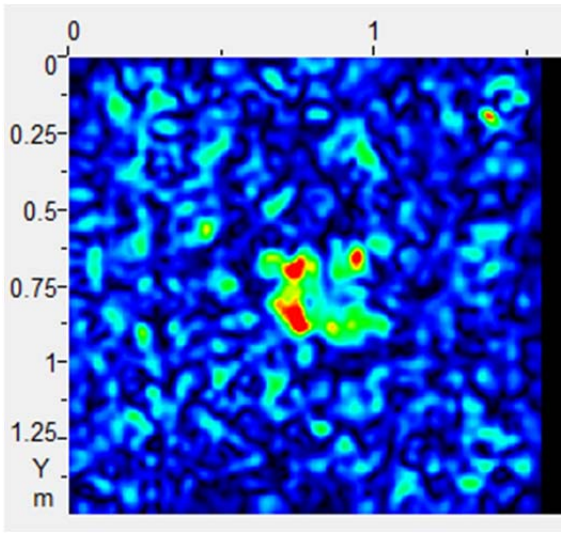

(a) Depth of 70 mm, Vertical Orientation.

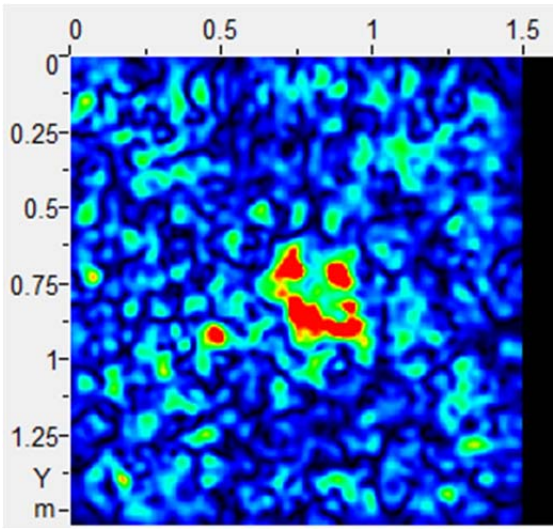

(b) Depth of 70 mm, Horizontal Orientation.

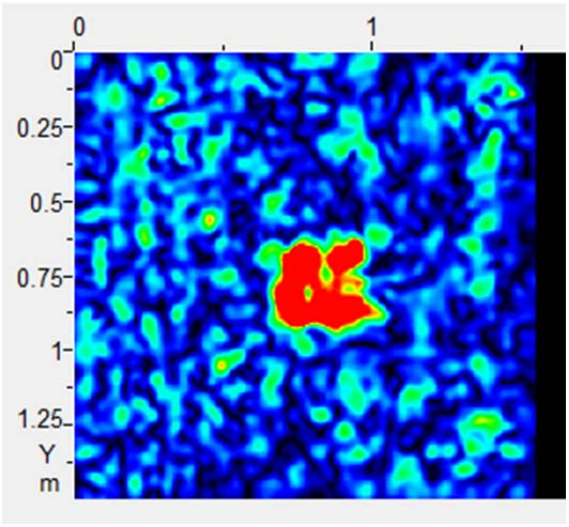

(c) Depth of 80 mm, Vertical Orientation.

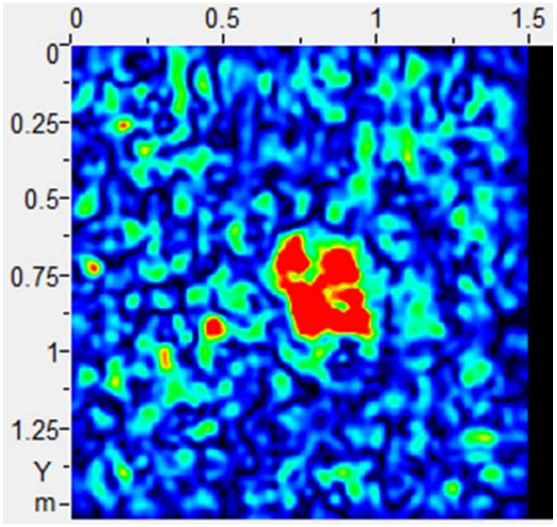

(d) Depth of 80 mm, Horizontal Orientation.

Figure 61. C-Scans of Slab VII with the Vertical (Left) and Horizontal (Right) Orientations at 70 mm and 80 mm.

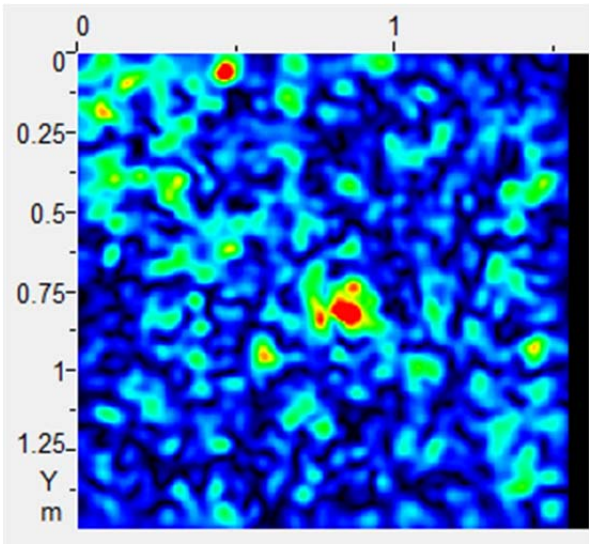

(a) Depth of 190 mm, Vertical Orientation.

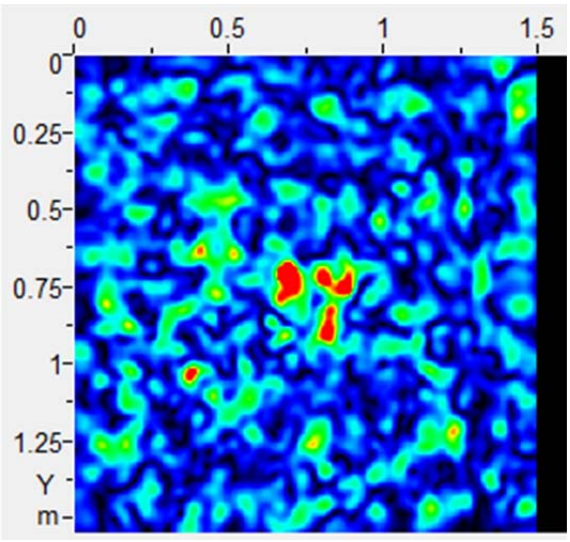

(b) Depth of 190 mm, Horizontal Orientation.

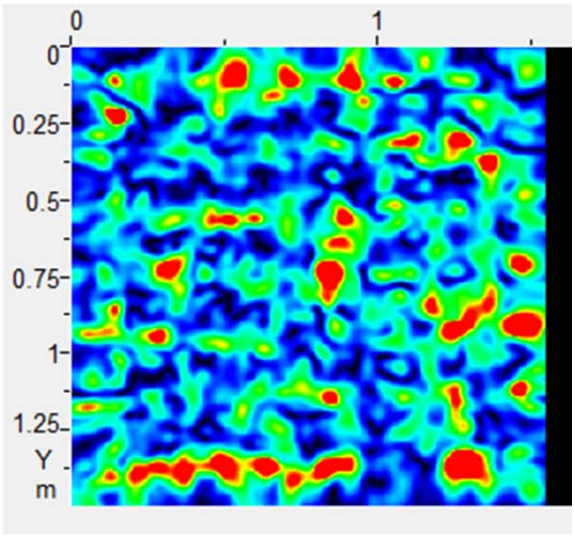

(c) Depth of 290 mm, Vertical Orientation.

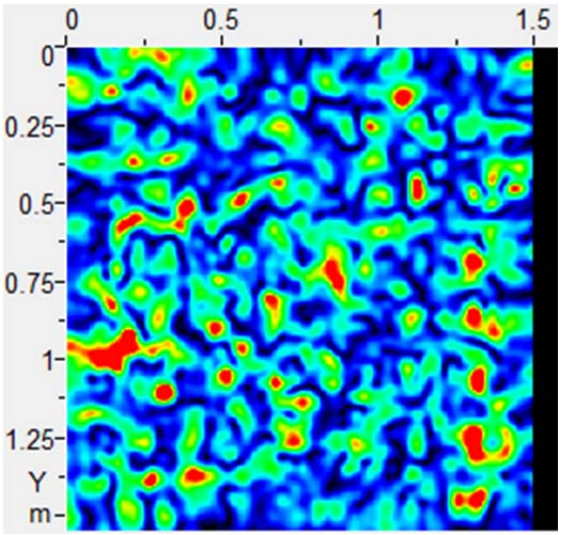

(d) Depth of 290 mm, Horizontal Orientation.

Figure 62. C-Scans of Slab VII with the Vertical (Left) and Horizontal (Right) at 190 mm and 290 mm.

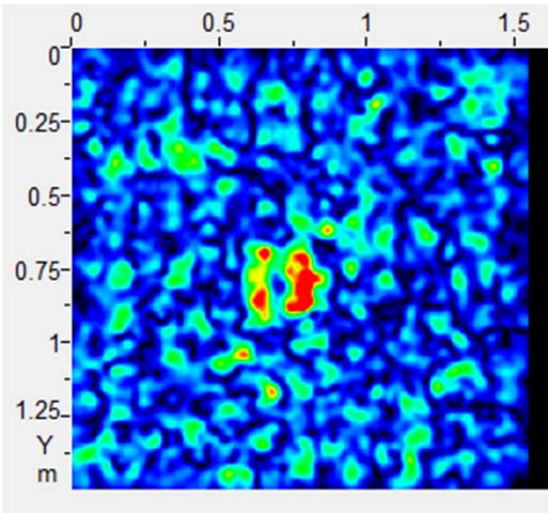

(a) Depth of 80 mm z =0.08 m.

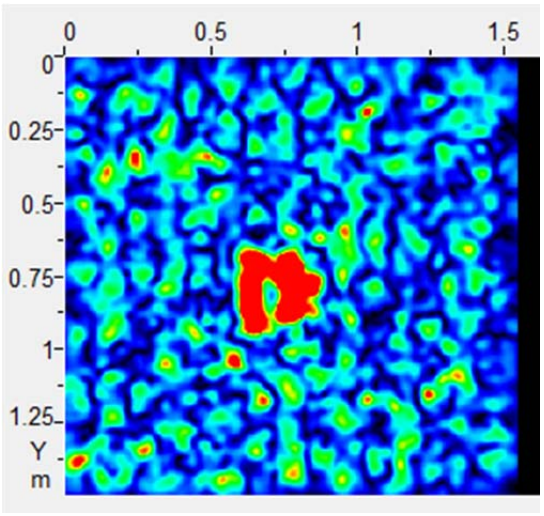

(b) Depth of 90 mm z =0.09 m.

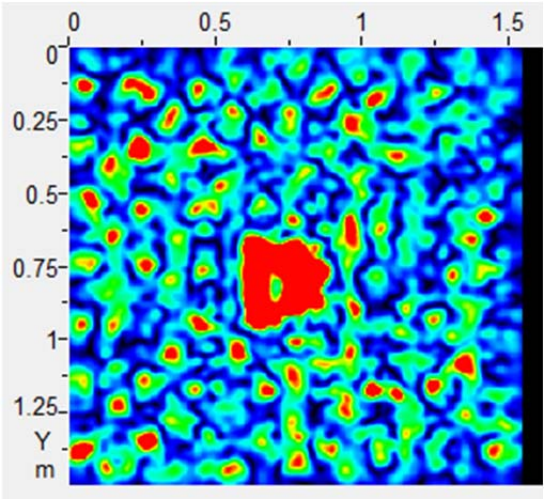

(c) Depth of 100 mm z =0.10 m.

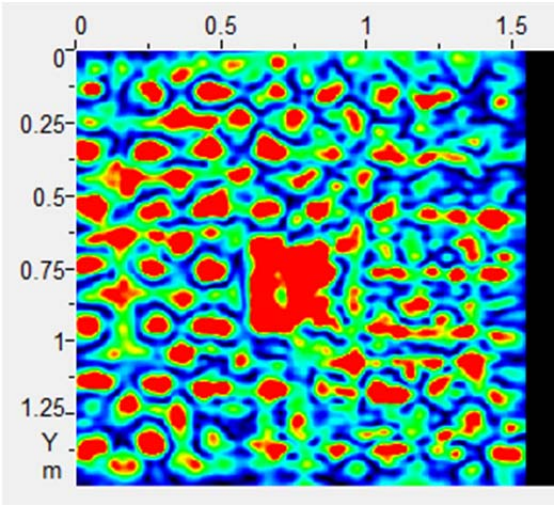

(d) Depths of 130 mm z =0.13 m.

Figure 63. C-Scans of Slab VIII at Various Depths from 80 mm to 100 mm.

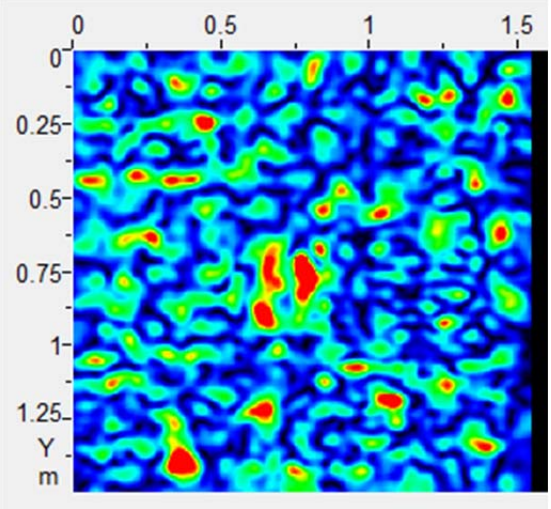

(a) Depth of 160 mm z =0.16 m.

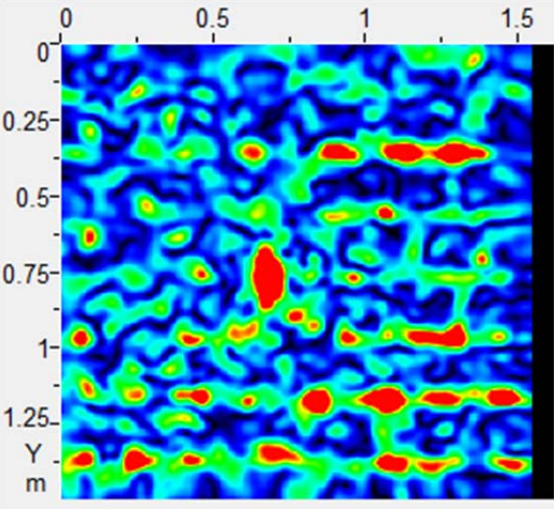

(b) Depth of 260 mm z =0.26 m.

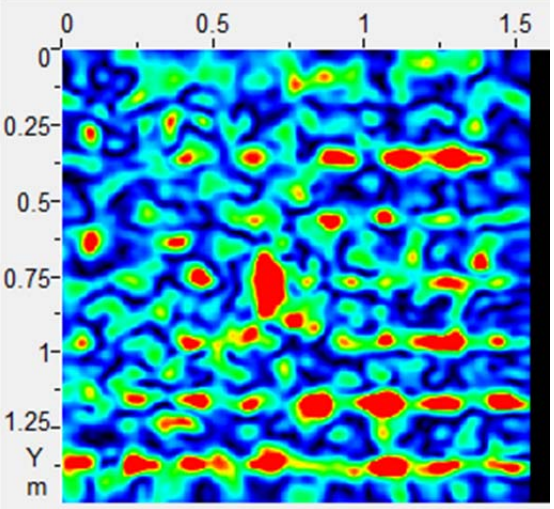

(c) Depth of 270 mm z =0.27 m.

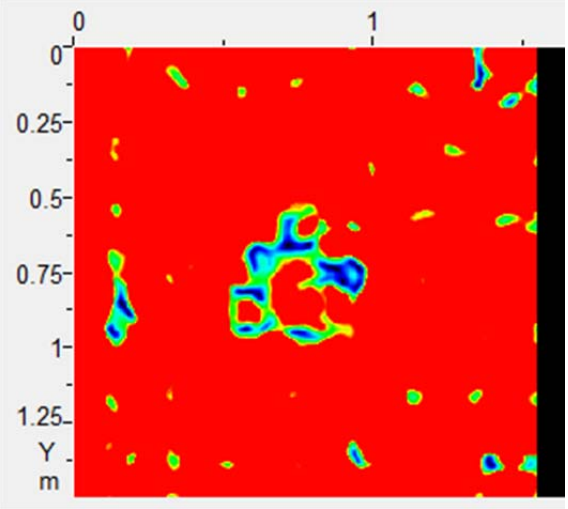

(d) Depth of 370 mm z =0.37 m.

Figure 64. C-Scans of Slab VIII at Various Depths from 160 mm to 370 mm.

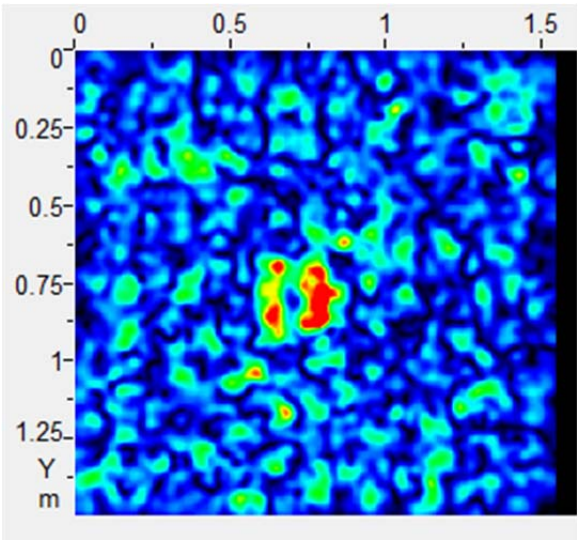

(a) Depth of 80 mm, Vertical Orientation.

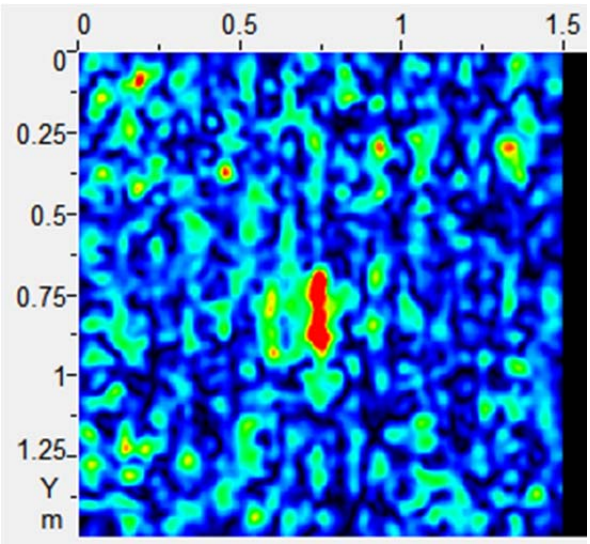

(b) Depth of 80 mm, Horizontal Orientation.

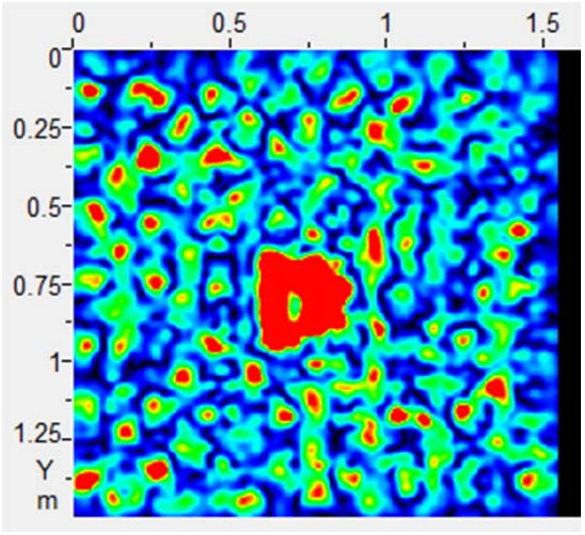

(c) Depth of 100 mm, Vertical Orientation.

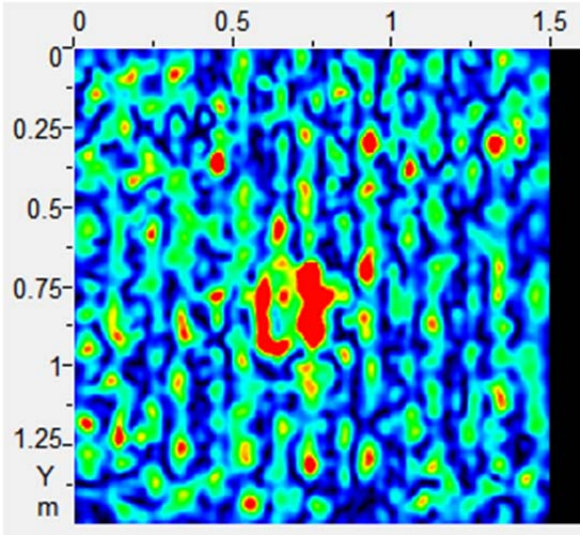

(d) Depth of 100 mm, Horizontal Orientation.

Figure 65. C-Scans of Slab VIII with the Vertical (Left) and Horizontal (Right) Orientations at 80 mm and 100 mm.

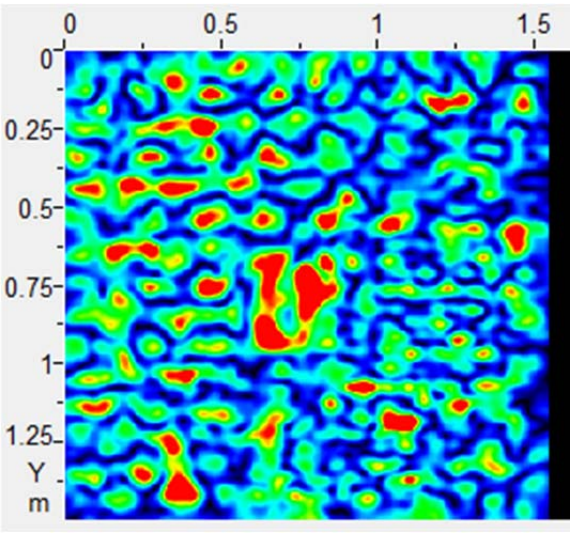

(a) Depth of 150 mm, Vertical Orientation.

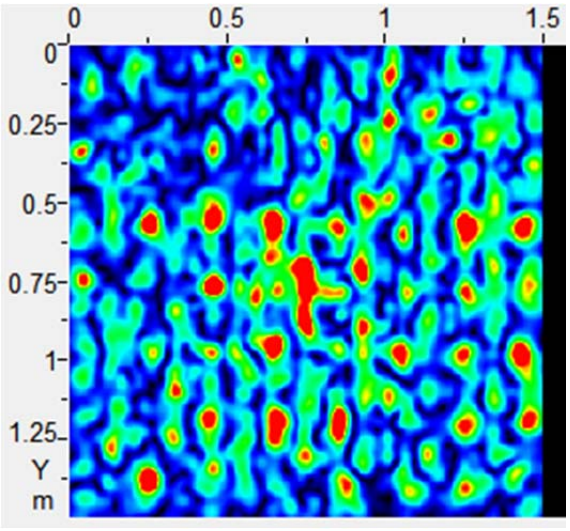

(b) Depth of 150 mm, Horizontal Orientation.

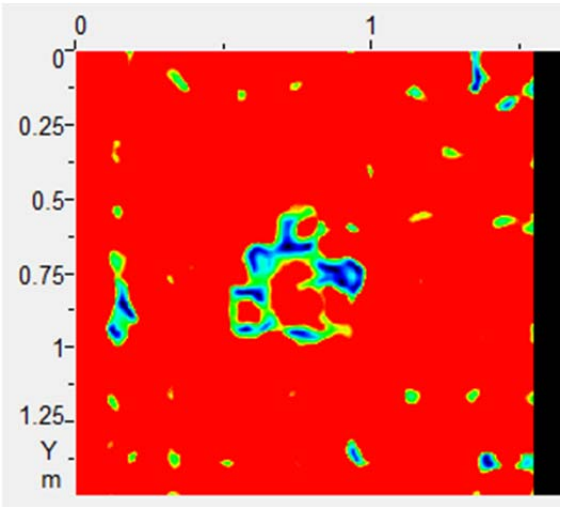

(c) Depth of 370 mm, Vertical Orientation.

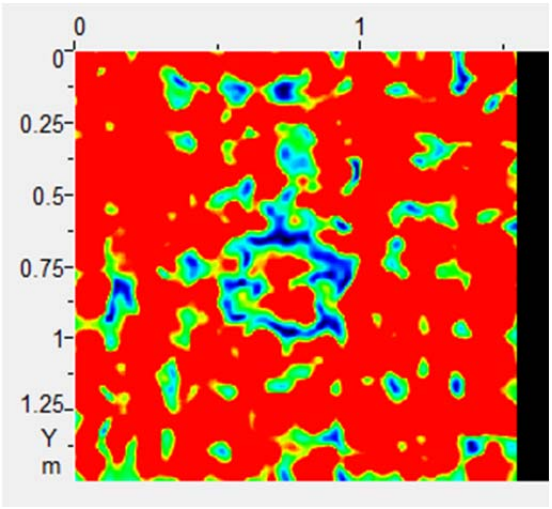

(d) Depth of 370 mm, Horizontal Orientation.

Figure 66. C-Scans of Slab VIII with the Vertical (Left) and Horizontal (Right) Orientations at 150 mm and 370 mm.

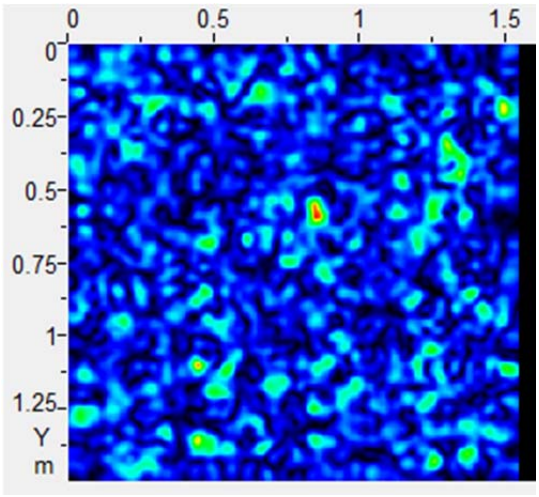

(a) Depth of 40 mm z =0.04 m.

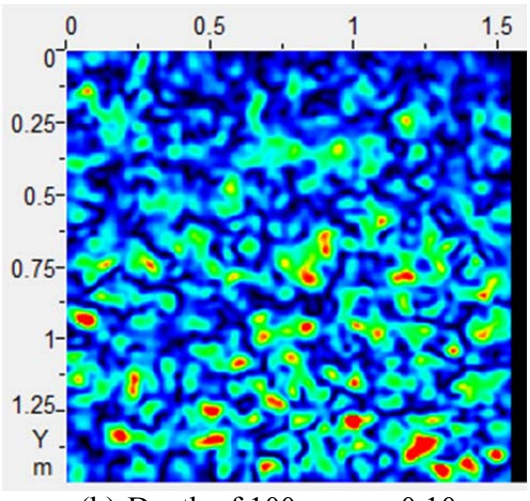

(b) Depth of 100 mm z =0.10 m.

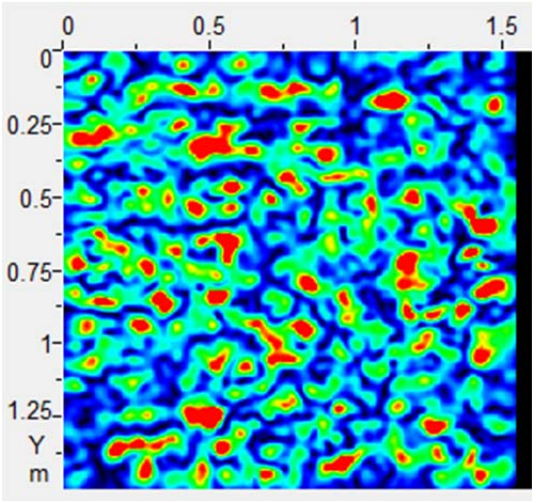

(c) Depth of 130 mm z =0.13 m.

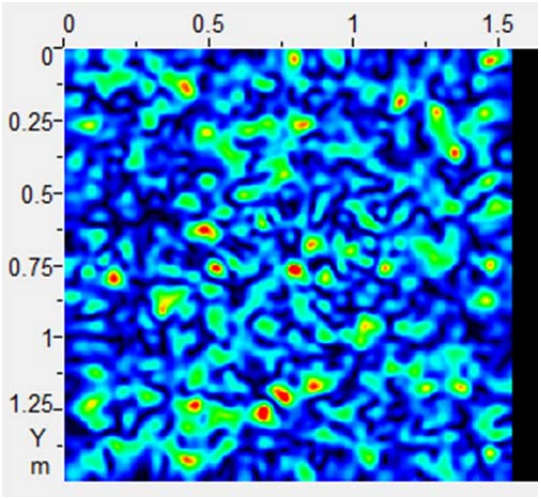

(d) Depth of 170 mm z =0.17 m.

Figure 67. C-Scans of Slab IX at Various Depths from 40 mm to 170 mm.

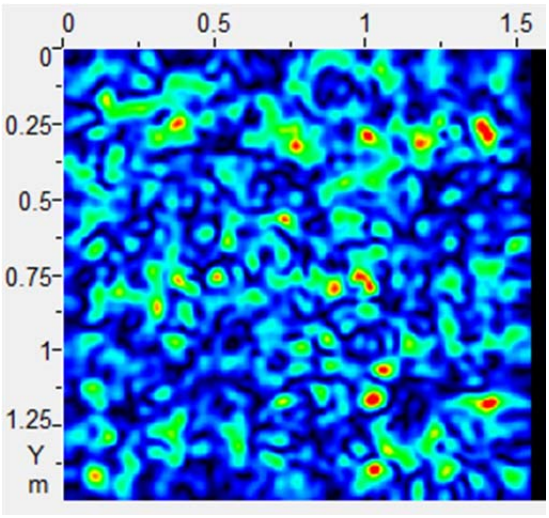

(a) Depth of 210 mm z =0.21 m.

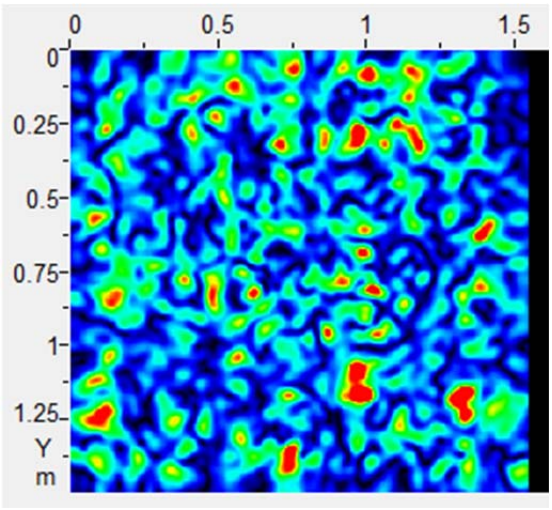

(b) Depth of 250 mm z =0.25 m.

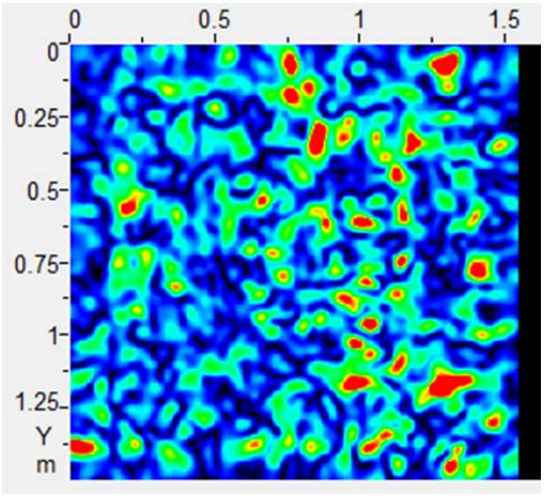

(c) Depth of 270 mm z =0.27 m.

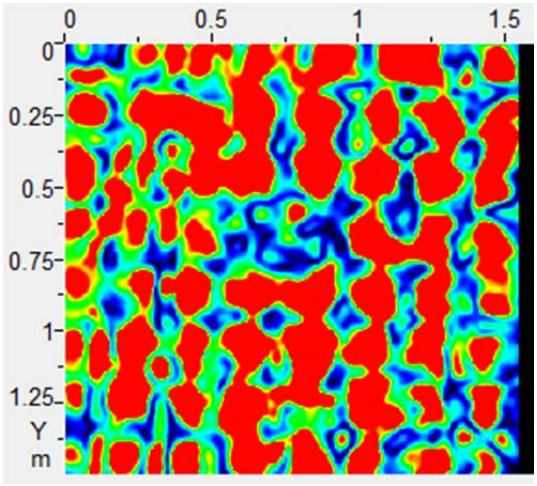

(d) Depth of 380 mm z =0.38 m.

Figure 68. C-Scans of Slab IX at Various Depths from 250 mm to 380 mm.

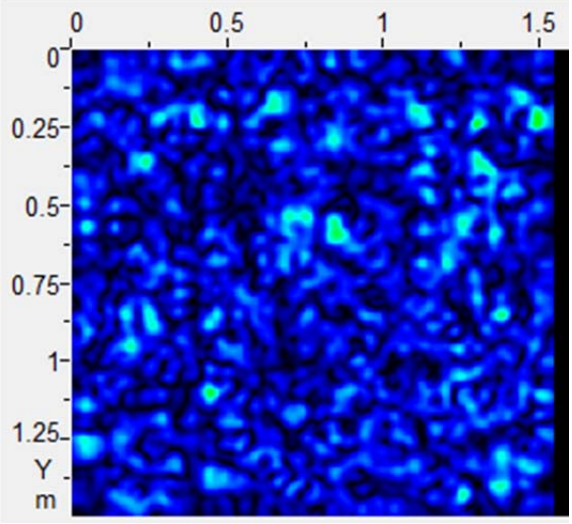

(a) Depth of 30 mm, Vertical Orientation.

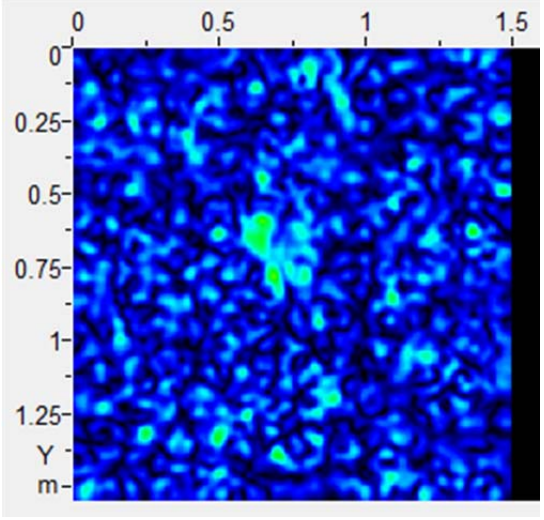

(b) Depth of 30 mm, Horizontal Orientation.

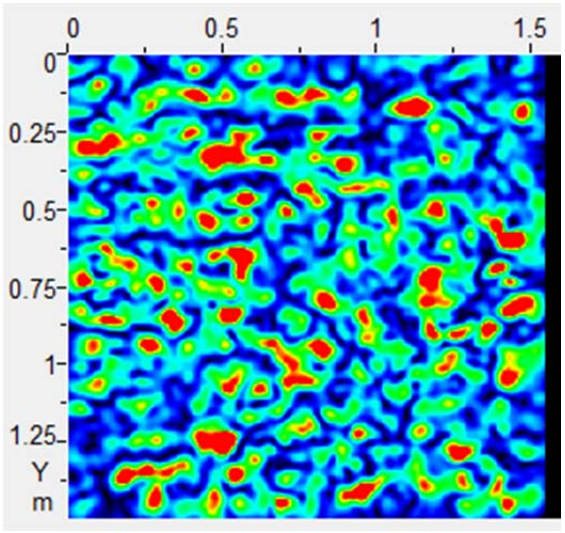

(c) Depth of 130 mm, Vertical Orientation.

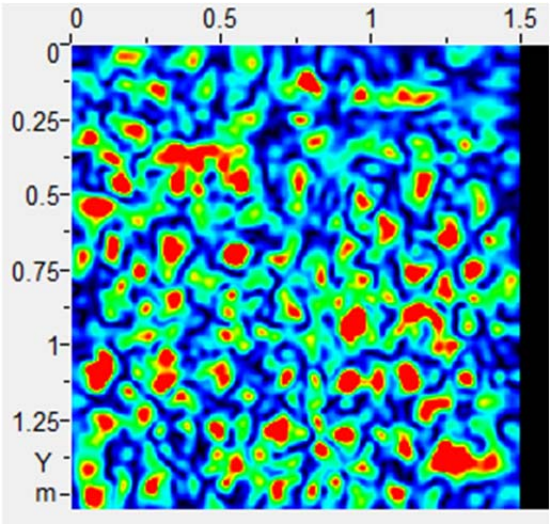

(d) Depth of 130 mm, Horizontal Orientation.

Figure 69. C-Scans of Slab IX with the Vertical (Left) and Horizontal (Right) Orientations at 30 mm and 130 mm.

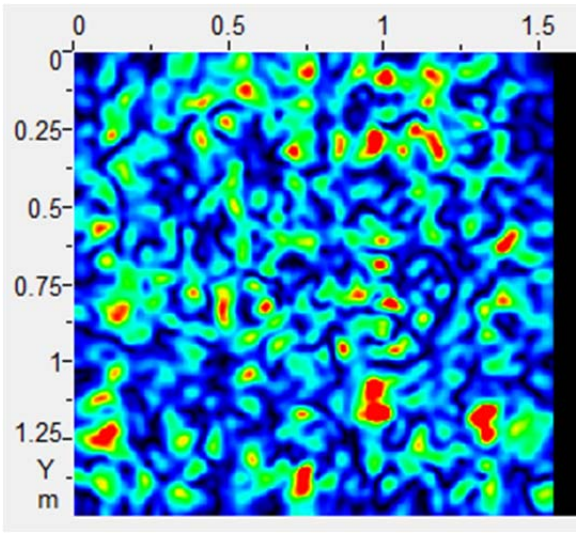

(a) Depth of 250 mm, Vertical Orientation.

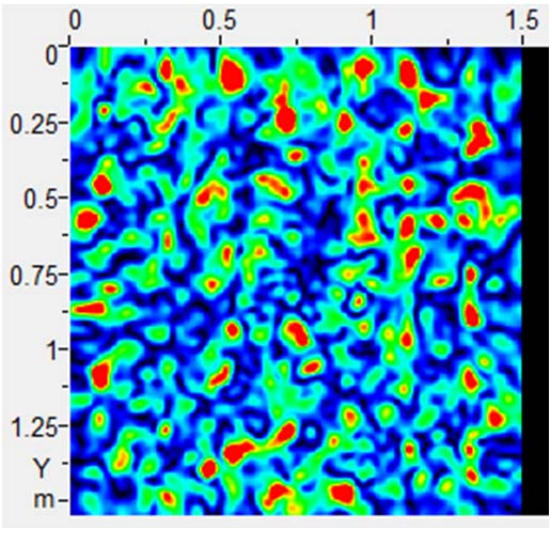

(b) Depth of 250 mm, Horizontal Orientation.

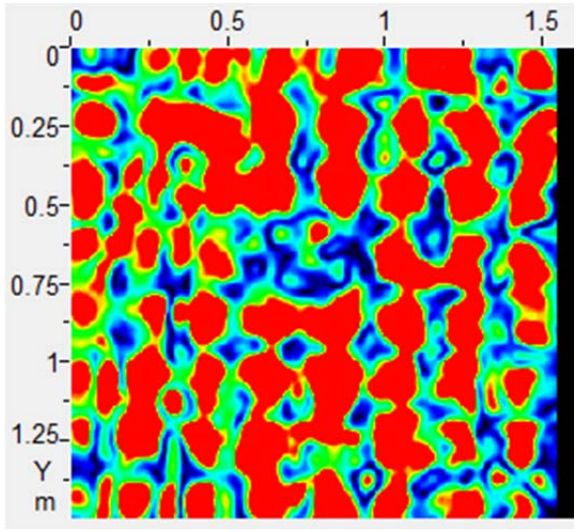

(c) Depth of 380 mm, Vertical Orientation.

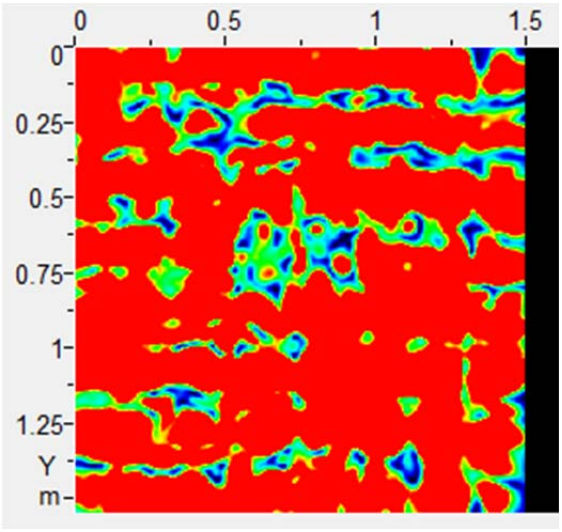

(d) Depth of 380 mm, Horizontal Orientation.

Figure 70. C-Scans of Slab IX with the Vertical (Left) and Horizontal (Right) Orientations at 250 mm to 380 mm.

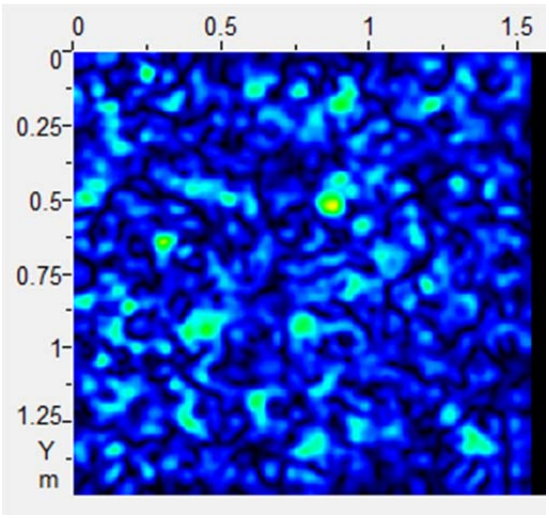

(a) Depth of 60 mm z =0.06 m.

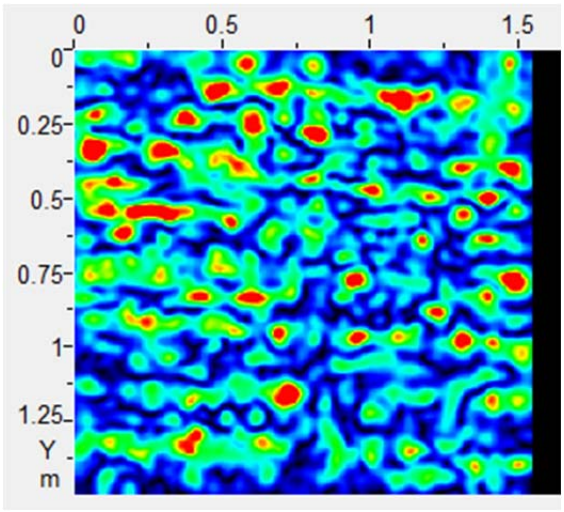

(b) Depths of 110 mm z =0.11 m.

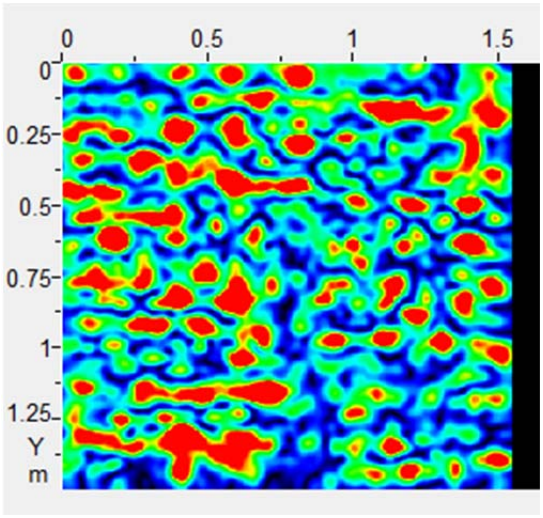

(c) Depth of 130 mm z =0.13 m.

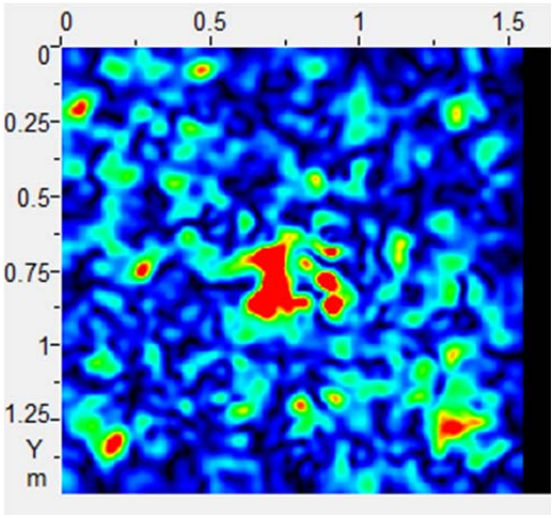

(d) Depths of 210 mm z =0.21 m.

Figure 71. C-Scans of Slab X at Various Depths from 60 mm to 210 mm.

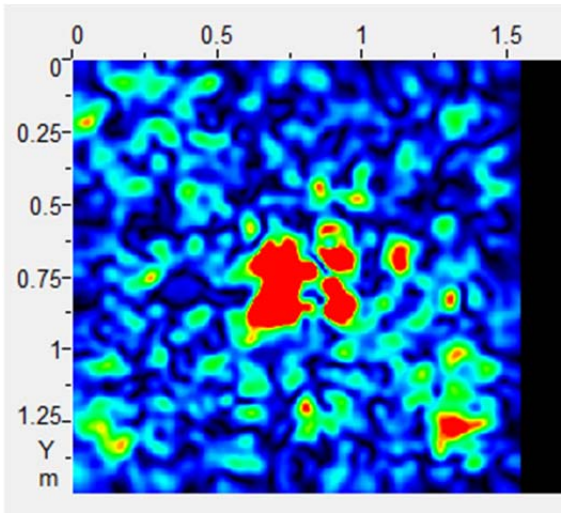

(a) Depth of 220 mm z =0.22 m.

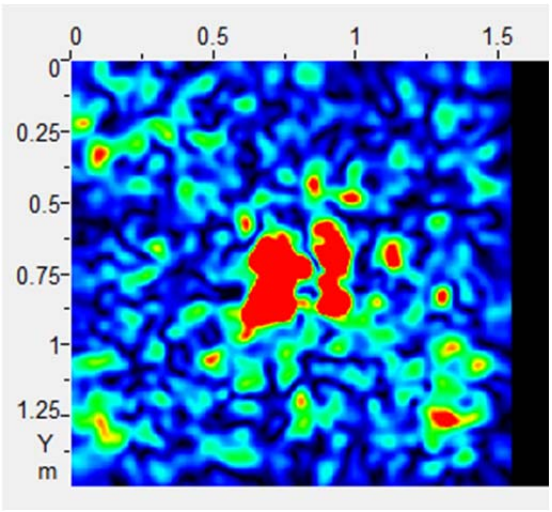

(b) Depth of 230 mm z =0.23 m.

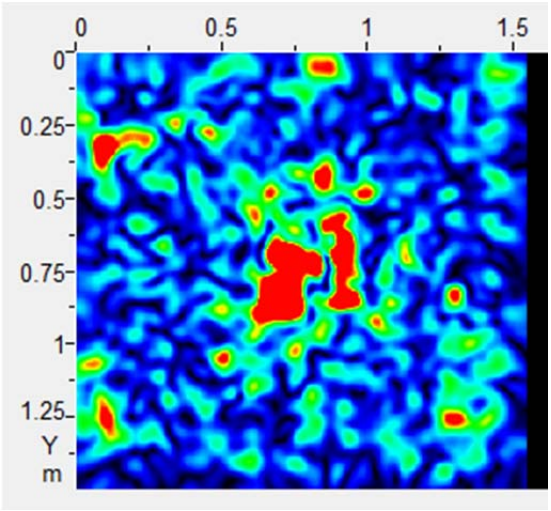

(c) Depth of 250 mm z =0.25 m.

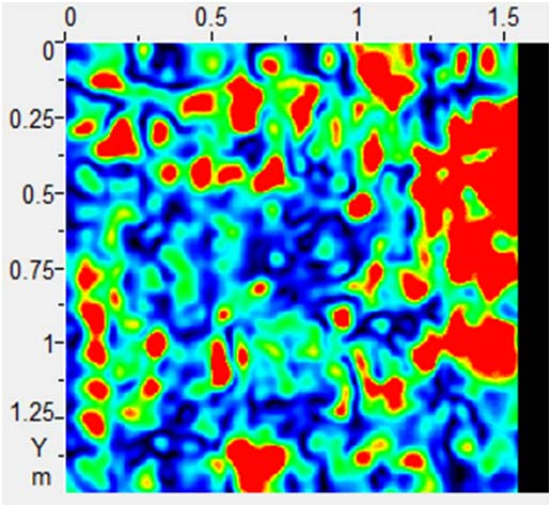

(d) Depth of 380 mm z =0.38 m.

Figure 72. C-Scans of Slab X at Various Depths from 220 mm to 380 mm.

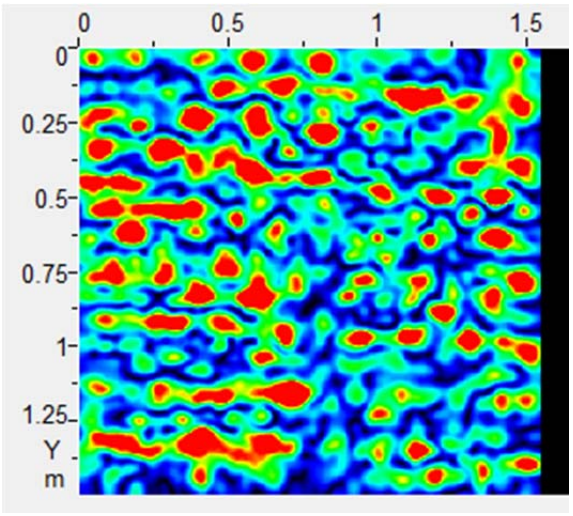

(a) Depth of 120 mm, Vertical Orientation.

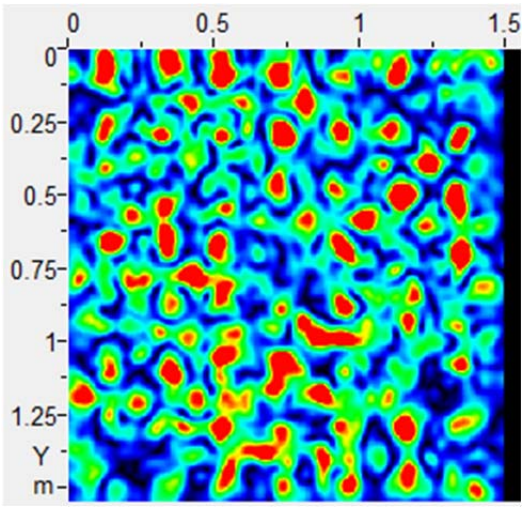

(b) Depth of 120 mm, Horizontal Orientation.

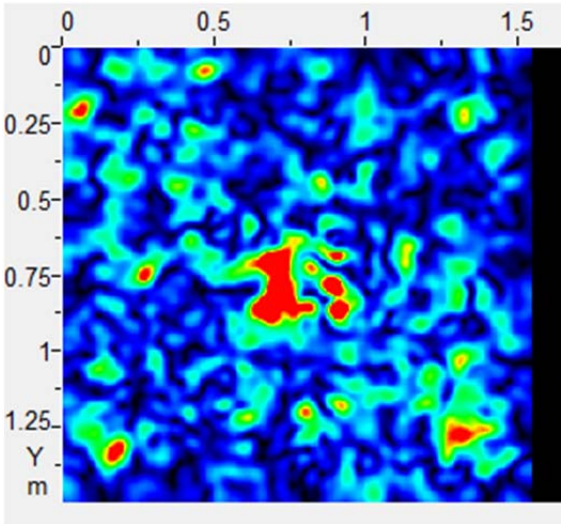

(c) Depth of 210 mm, Vertical Orientation.

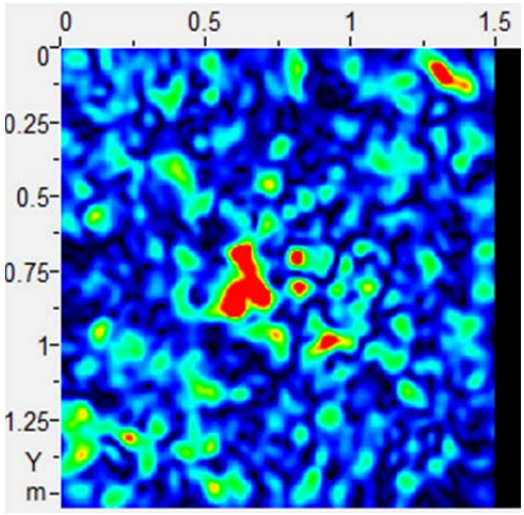

(d) Depth of 210 mm, Horizontal Orientation.

Figure 73. C-Scans of Slab X with the Vertical (Left) and Horizontal (Right) Orientations at 120 mm and 210 mm.

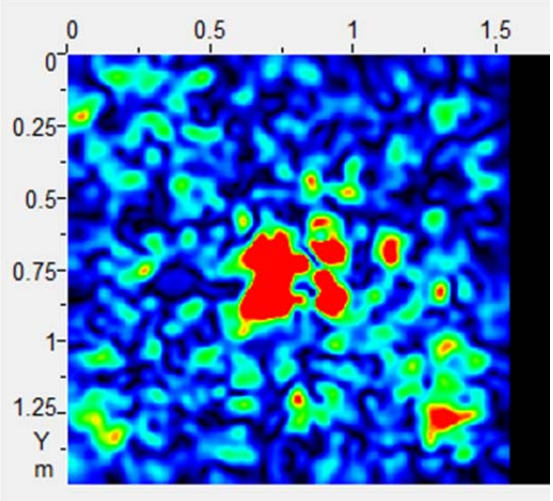

(a) Depth of 220 mm, Vertical Orientation.

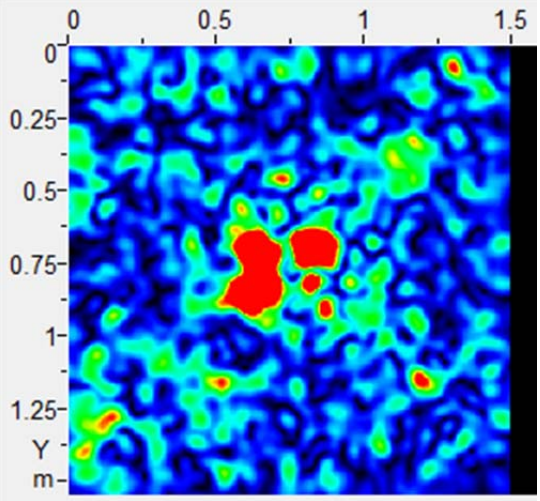

(b) Depth of 220 mm, Horizontal Orientation.

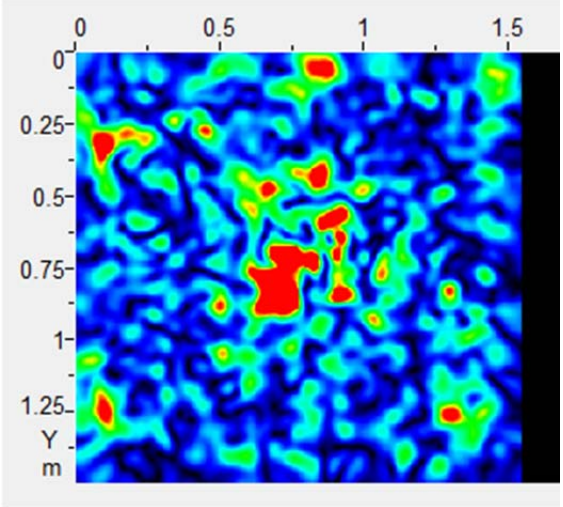

(c) Depth of 260 mm, Vertical Orientation.

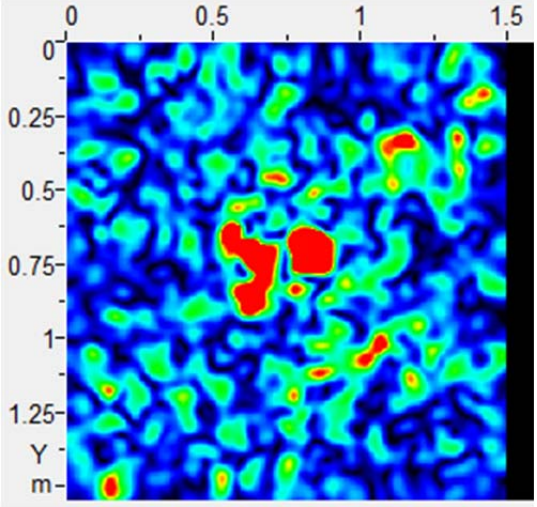

(d) Depth of 260 mm, Horizontal Orientation.

Figure 74. C-Scans of Slab X with the Vertical (Left) and Horizontal (Right) Orientations at 220 mm and 260 mm.

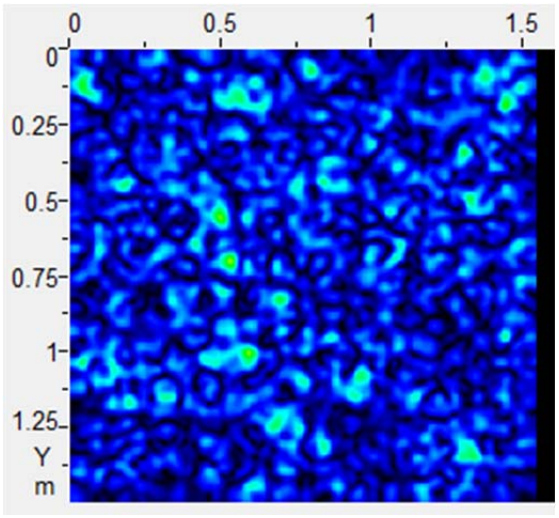

(a) Depth of 30 mm z =0.03 m.

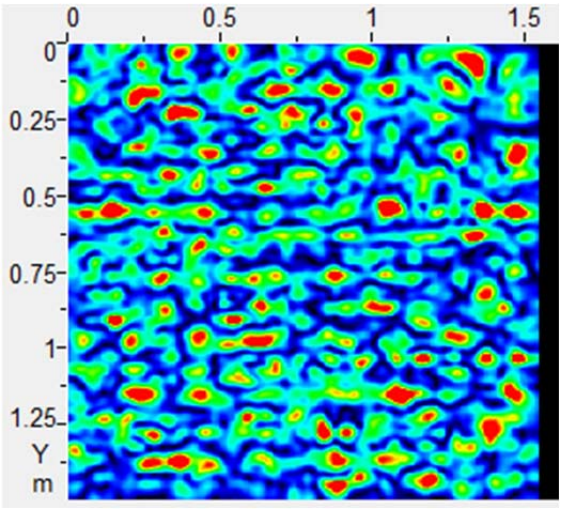

(b) Depth of 90 mm z =0.09 m.

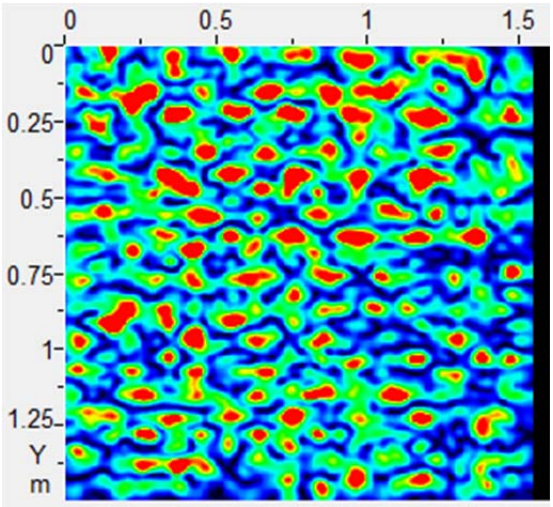

(c) Depth of 120 mm z =0.12 m.

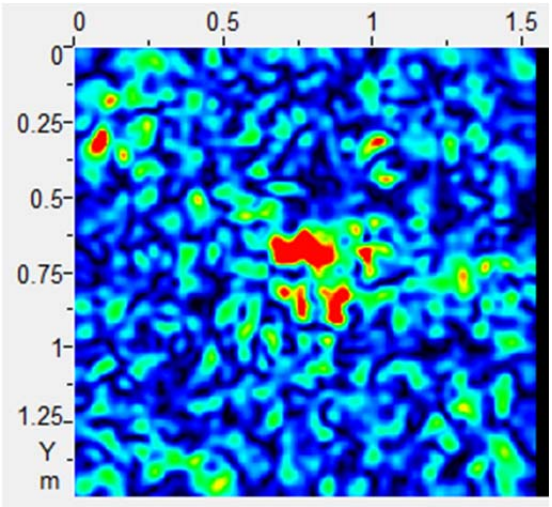

(d) Depth of 200 mm z =0.20 m.

Figure 75. C-Scans of Slab XI at Various Depths from 30 mm to 200 mm.

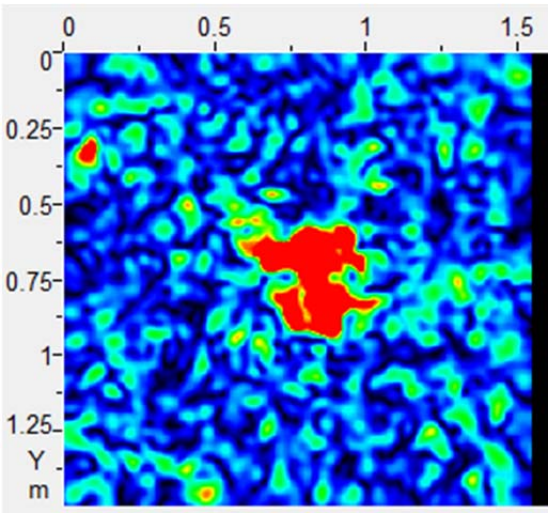

(a) Depth of 210 mm z =0.21 m.

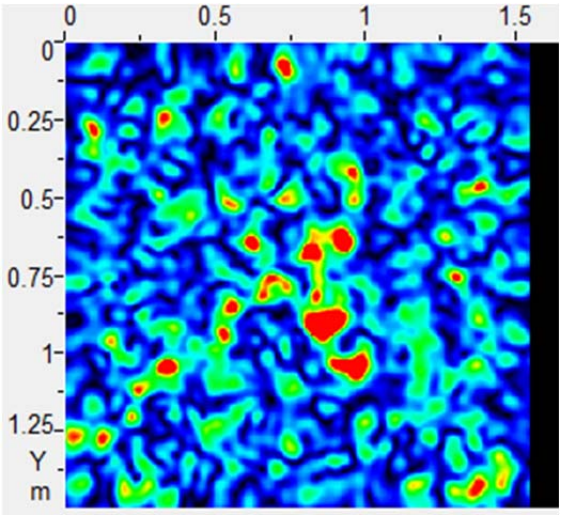

(b) Depth of 250 mm z =0.25 m.

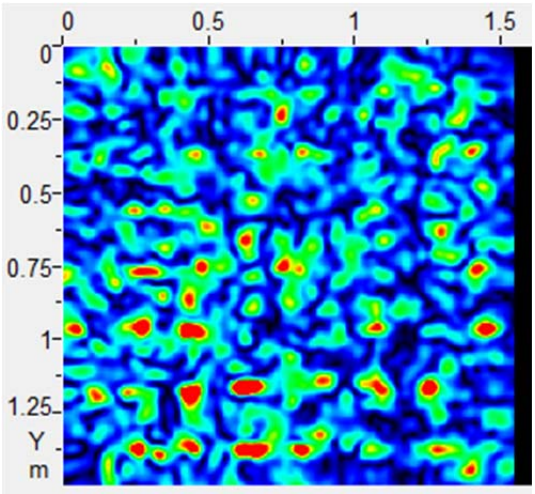

(c) Depth of 300 mm z =0.30 m.

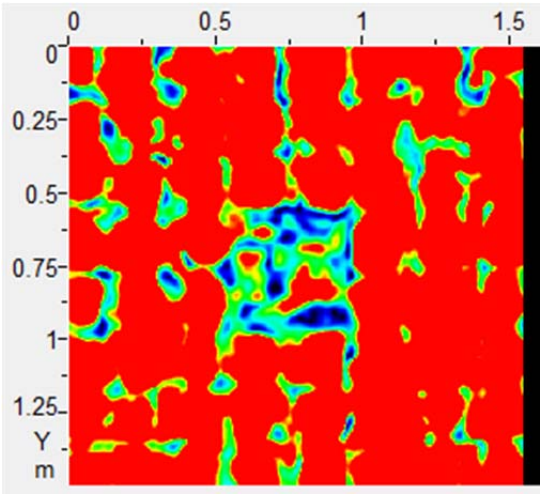

(d) Depth of 380 mm z =0.38 m.

Figure 76. C-Scans of Slab XI at Various Depths from 210 mm to 380 mm.

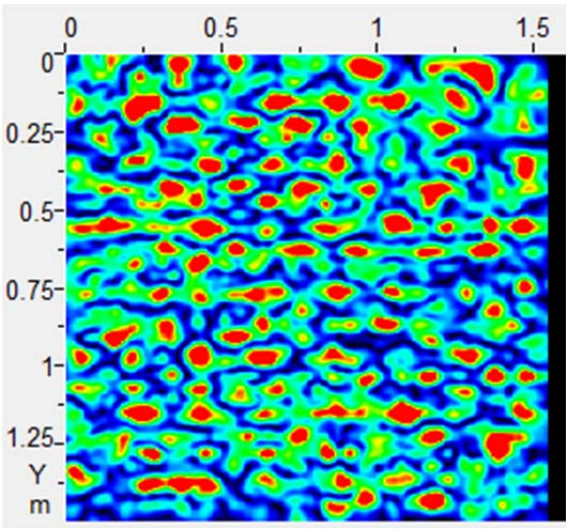

(a) Depth of 110 mm, Vertical Orientation.

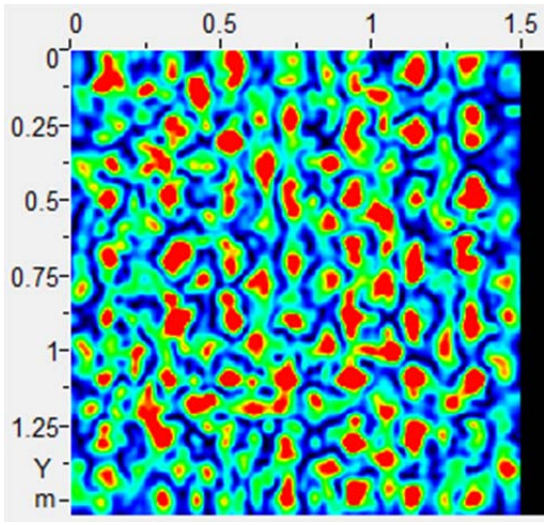

(b) Depth of 110 mm, Horizontal Orientation.

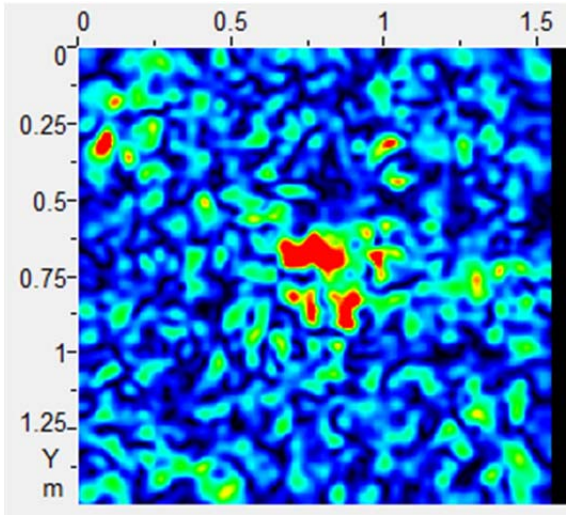

(c) Depth of 200 mm, Vertical Horizontal.

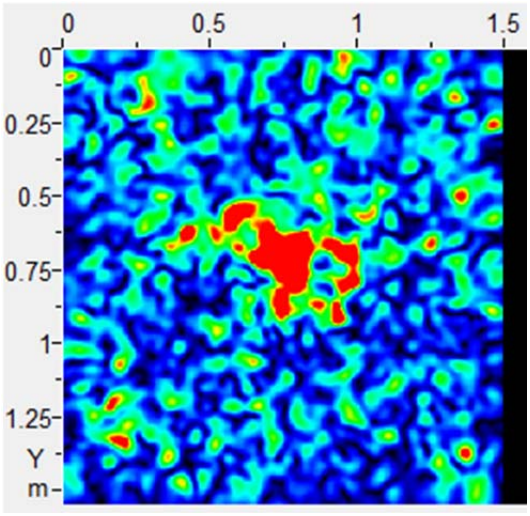

(d) Depth of 200 mm, Horizontal Orientation.

Figure 77. C-Scans of Slab XI with the Vertical (Left) and Horizontal (Right) Orientations at 110 mm and 200 mm.

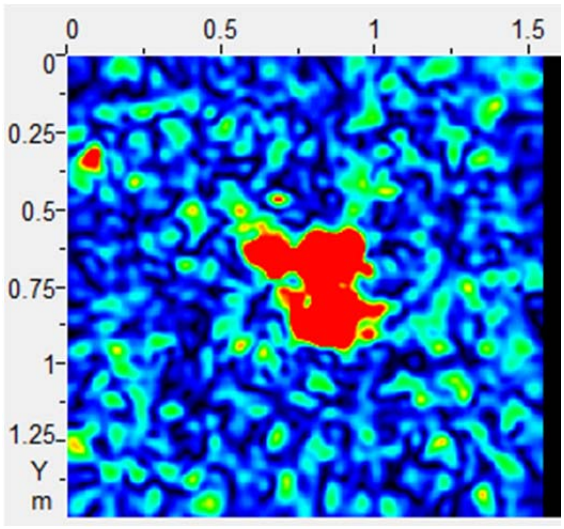

(a) Depth of 220 mm, Vertical Orientation.

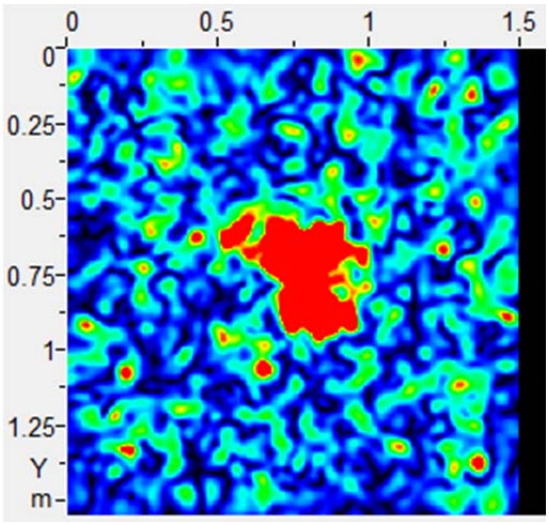

(b) Depth of 220 mm, Horizontal Orientation.

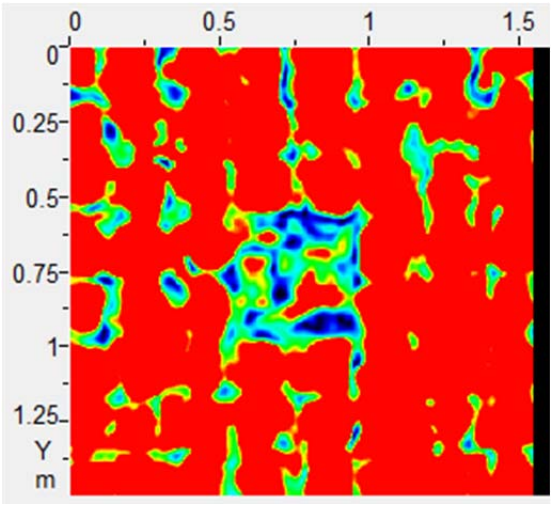

(c) Depth of 380 mm, Vertical Orientation.

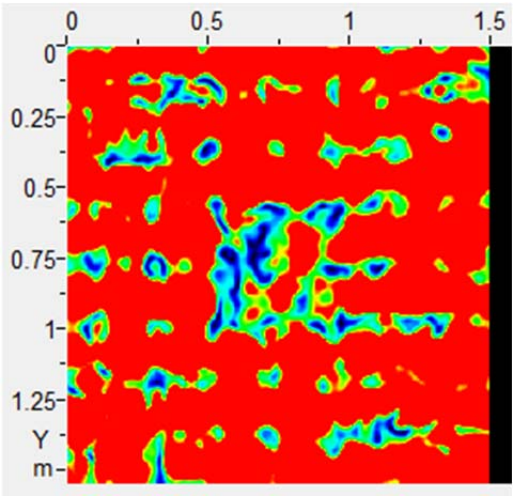

(d) Depth of 380 mm, Horizontal Orientation.

Figure 78. C-Scans of Slab XI with the Vertical (Left) and Horizontal (Right) Orientations at 220 mm and 380 mm.